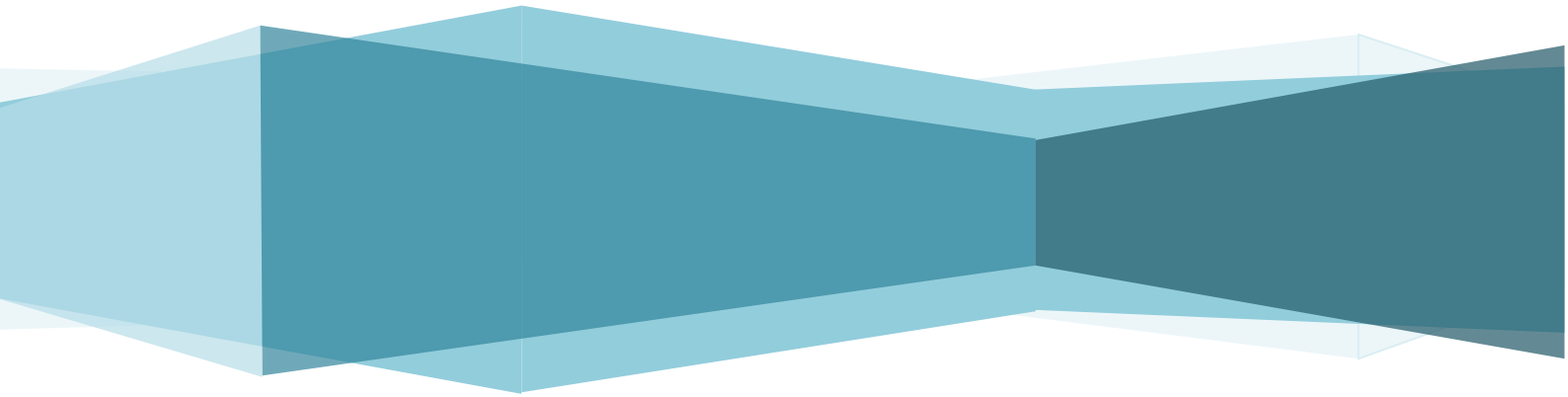

Universidad del País Vasco

Euskal Herriko Unibertsitatea

Makina eta Motor Termikoak Saila

Departamento de Máquinas y Motores Térmicos

Model Based Optimization of Thermal Management Systems for Electro-Mobility Applications

Presented by:

Leire Martín Martín

Supervised by:

Dr. Luis Alfonso del Portillo Valdés (UPV/ EHU)

Dr. Jon Gastelurrutia Roteta (IK4- Ikerlan)

2017

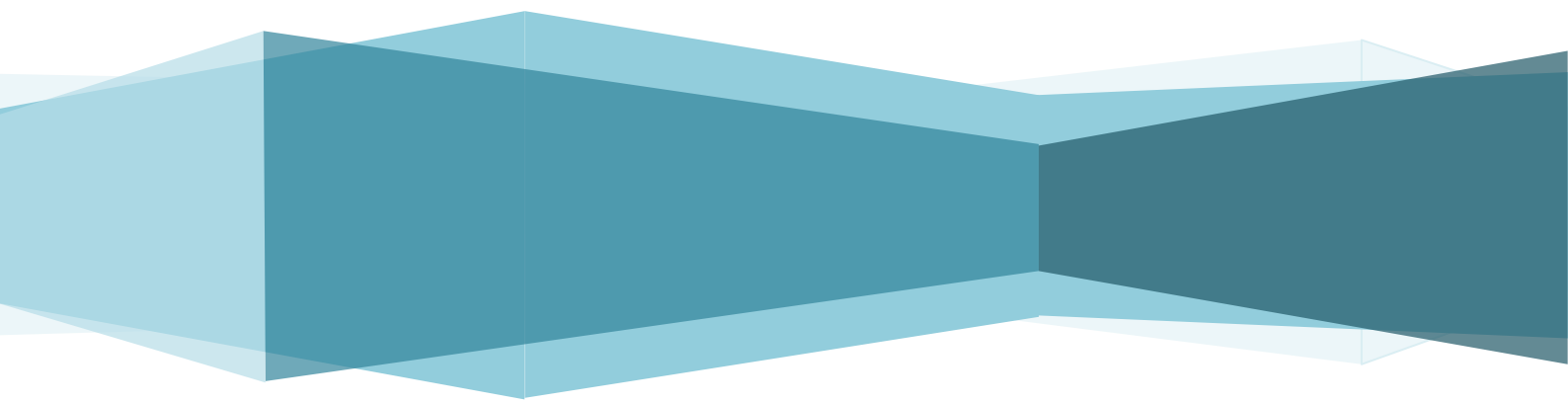

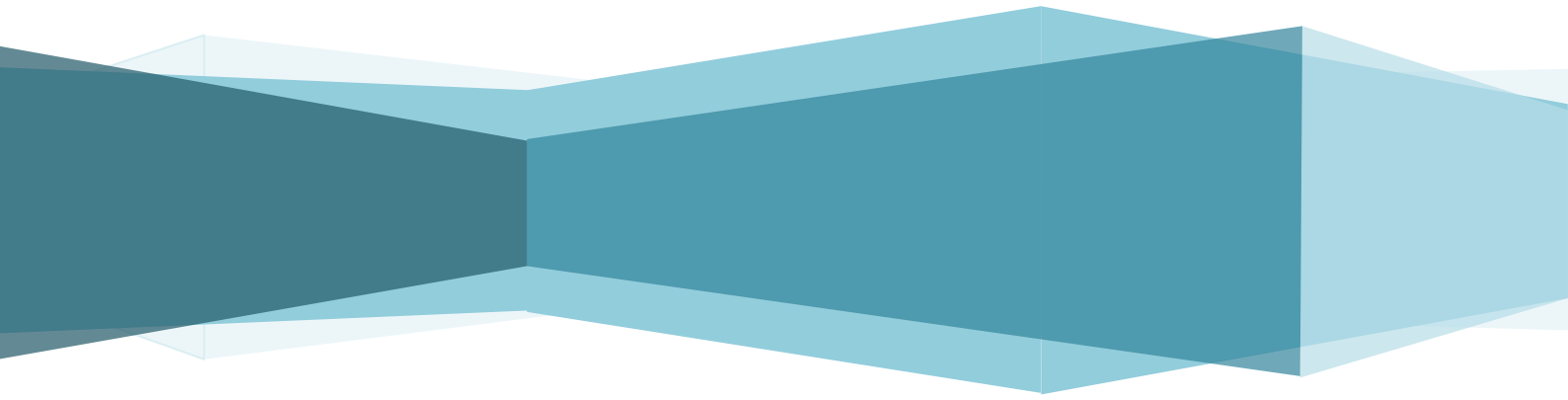

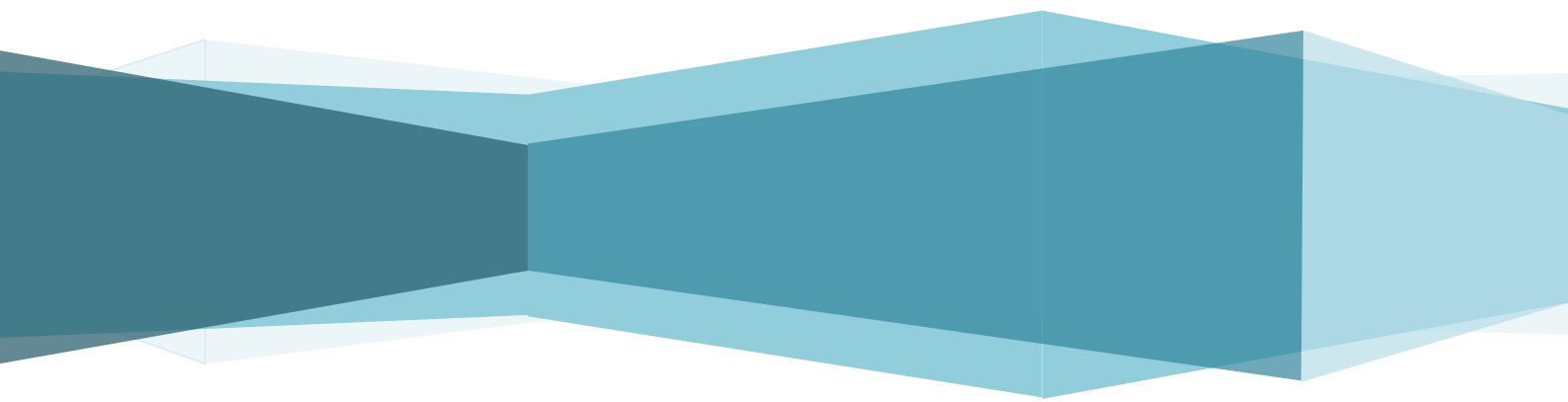

Makina eta Motor Termikoak Saila
Departamento de Máquinas y Motores Térmicos

Doctoral Thesis:

Model Based Optimization of Thermal Management Systems for Electro-Mobility Applications

Dissertation submitted to the University of the Basque Country (UPV/EHU) in fulfilment of the requirements for the degree of Doctor of the Thermal Engineering PhD program of the Department of Thermal Engineering

Leire Martín Martín

Supervised by

Dr. Luis Alfonso del Portillo Valdés

Dr. Jon Gastelurrutia Roteta

Bilbao, May 2017

The author gratefully acknowledge to IK4-IKERLAN Technology Research Centre for it supports.

En especial, a mi familia y a Ramón.

Agradecimientos

"Nadie logra el éxito sin la ayuda de los demás. El sabio y el confiado reconoce esta ayuda con gratitud" Alfred North Whitehead.

Presiento que va a ser complicado la redacción de las siguientes líneas, a pesar de tener una lista enorme de personas a las que tengo que agradecer todo el apoyo que me han ofrecido durante este tiempo. Ha sido un camino duro, con algunos baches importantes y otros no tanto, pero que gracias a la gente que he tenido al lado los he podido superar. Me vienen infinitos momentos vividos desde aquel 1 de Octubre del 2012 cuando entré por la puerta de Ikerlan con la ilusión y objetivo de dar un paso más en mi vida, tanto a nivel personal como profesional.

En primer lugar, me gustaría agradecer a mis directores Luis Alfonso del Portillo y Jon Gastelurrutia por su dedicación y ayuda sobre todo técnica, que me han aportado de manera incondicional. En especial a Jon le debo todo este trabajo que presento en este documento. Echando la vista atrás y con alguna lagrimilla en los ojos, me doy cuenta de la suerte que he tenido de tenerle como co-director y sobre todo como compañero y amigo. Espero que hayas podido aprender y disfrutar de mi trabajo al menos la cuarta parte de lo que he aprendido y he disfrutado yo, con eso me conformo.

La verdad que si he podido levantarme todas las veces que he tropezado en el camino ha sido gracias a la gente de la que he estado rodeada: Mi querida y mi gran apoyo Mai, de esas personas que sin saber por qué eres compatible al 100%. Ego(itz), mi compi que durante este último largo sprint ha estado a mi lado sin dudarlo. Genelva, Ruth, Mikel,

Luis, Itsaso por aguantar mis lloros, alegrías y siempre estar dispuestos a escuchar y apoyarme cuando lo he necesitado. A todos los demás con los que he compartido hamaiketakos y comidas en Domolab, como Nerea, Jaio, Iñigo, Eli, Isabel, Bakartxo, Fernando, Vicente, Carlos, Pedro, a todos y a cada uno de vosotros: MILA ESKER!! Creo que no hace falta decirlo, pero el día que esta etapa llegue a su fin estaréis todos invitados a una "galleta de la felicidad".

Also, I would like to express my gratitude to those special people that I knew during my short but intensive stage in Dresden. People that even without knowing me, they accepted me as one of them, integrating me in their work and friends group. They trusted on me from the first second and for this reason, I would like to mention them in these lines in the same way that I did on 1st of June of 2016 when I left Dresden: Sven, *my orange beard man*; Kevin, *my little bird*; Ronny, *the mexican-german man*; Alex, *my Bubu*, Lutz, *the ice cream man* and Mathis, *the Majorcan man*. All of you: Vielen Dank!

Por último y no por ello menos importante, es el agradecimiento infinito que les debo a mi familia y a Ramón. Sin ellos seguramente emocionalmente no hubiese podido llevar adelante todos los altibajos, que no han sido pocos, que he tenido sobre todo a lo largo del último año. A mi familia sobre todo me gustaría dedicarles simbólicamente este trabajo como resultado del esfuerzo que han realizado desde que era pequeña por darme la mejor educación y los mejores estudios posibles. A mi Ramoncin...*"¿Qué te puedo decir?"*... simplemente, muchísimas gracias por tener fuerza y aguantar este camino junto a mí de principio a fin.

A todos los demás amigos, amigas, cuadrilla y demás que sin poder evitarlo he dejado algo abandonados durante estos últimos meses, prometo dedicaros tiempo a partir de ahora.

Cierro con mucha ilusión esta etapa de mi vida con todos los momentos buenos vividos en ella, pero abro la siguiente con mucha más fuerza e ilusión esperando con muchas ganas todos esos momentos que están por llegar.

A todos, muchísimas gracias.

"*Todo es muy difícil antes de ser sencillo*"

Thomas Fuller

Resumen

La presente Tesis Doctoral desarrolla una metodología de diseño y optimización energética enfocada a sistemas de gestión térmica para aplicaciones que se engloban dentro del campo de la Electro-Movilidad. Se concretan procedimientos y ciertos tipos de cálculo que permiten tomar decisiones no arbitrarias en cada etapa de diseño, acelerando y haciendo más robusto el proceso de desarrollo. Esta metodología conlleva el desarrollo de modelos matemáticos avanzados, que independientemente de la herramienta de simulación que se utilice, aseguran la optimización del diseño final.

El interés de esta Tesis está motivado por el gran crecimiento experimentado durante los últimos años de aplicaciones tales como ascensores, aparatos de electrónica de potencia, sistemas de generación basados en energías renovables, vehículos eléctricos y vehículos híbridos. Muchos de estos elementos requieren de sistemas de almacenamiento de energía eléctrica de alta densidad de energía y potencia para su funcionamiento. El dimensionamiento eléctrico y térmico de estos sistemas de almacenamiento no es trivial.

Existe una amplia variedad de tecnologías referidas a sistemas de almacenamiento de energía entre las cuales, la tecnología de baterías de Litio-Ion y el concepto de *Battery Pack* se está imponiendo y tiene mayor perspectiva de futuro, especialmente para este tipo de aplicaciones de interés. Estos sistemas de almacenamiento de grandes dimensiones requieren un adecuado sistema de control y gestión denominado *Battery Management System*, que garantice bajo cualquier condición de operación, un correcto funcionamiento y una durabilidad aceptable para este tipo de sistemas. En este contexto

la gestión térmica juega un papel esencial ya que el comportamiento eléctrico del sistema de almacenamiento está influenciado directamente por la temperatura de operación y dispersión térmica que exista entre las diferentes celdas de Litio-Ion que lo conforman. Por ello, el software y hardware que constituye el denominado *Battery Thermal Management System*; parte del *Battery Management System* que gestiona la parte térmica, debe controlar y regular el sistema de enfriamiento o calentamiento que se considere en función de las condiciones de operación de las celdas. Su objetivo se centra en mantener estás dentro del rango de operación establecido como ideal; o al menos, dentro del rango de funcionamiento definido como admisible. De esta manera se intenta evitar cualquier situación de mal funcionamiento, deterioro acelerado o, incluso, un problema de seguridad.

En ciertas aplicaciones, no existe ningún tipo de restricciones relacionadas con el peso, espacio o consumo, por lo que generalmente en estos casos se asegura el correcto funcionamiento térmico de este tipo de sistemas implementando un sistema de gestión térmica sin ninguna otra preocupación que la de mantener la temperatura de las celdas lo más cerca posible de su temperatura óptima de funcionamiento. Sin embargo, en aplicaciones dentro del campo de la Electro-Movilidad los parámetros de diseño anteriormente mencionados suelen estar muy limitados y ser influyentes en el funcionamiento general de sistema, por lo que es importante plantear un sistema optimizado de gestión térmica. El proceso de optimización se debe llevar a cabo tanto a nivel de componente como a nivel de sistema, con el objetivo de minimizar aspectos tales como el coste inicial y de mantenimiento del sistema, tamaño, peso e incluso, el consumo de los auxiliares. Dichos aspectos pueden afectar de manera negativa directamente en la autonomía de la aplicación o incluso, pueden suponer la necesidad de tener que implementar un sistema de almacenamiento de mayores dimensiones.

La metodología propuesta consta de varios pasos secuenciales pero recursivos que serán completamente desarrollados en el presente documento. Se podría decir que el aporte principal de la tesis se centra en el último paso, concretamente en la tarea de optimización, por lo que se explicará más en profundidad.

El primer paso de la metodología propuesta consiste en definir las especificaciones de diseño que pueden involucrar aspectos térmicos, eléctricos y/o mecánicos así como, estéticos. Estos criterios de diseño pueden ser definidos por el cliente o por el propio

diseñador. En definitiva, independientemente del tipo de criterios de diseño que se definan y/o de quién los imponga, dicha metodología asegura el cumplimiento de los mismos bajo cualquier condición de operación para la aplicación de interés seleccionada.

El segundo paso se compone principalmente de dos tareas. La primera de ellas se refiere al pre-dimensionamiento del sistema de almacenamiento, considerando el dimensionamiento térmico del mismo, mientras que la segunda tarea supone la preselección de los componentes necesarios para el sistema de gestión térmica. El dimensionamiento térmico del sistema de almacenamiento se lleva a cabo teniendo en cuenta su funcionamiento en la máxima solicitación de potencia con el objetivo de mantener la temperatura del sistema de almacenamiento dentro de un rango adecuado de operación. Como resultado de dicha tarea, se obtiene el calor que debe ser disipado por el sistema de gestión térmica para cada una de las aplicaciones, en base al cual se procede a preseleccionar los componentes del mismo. Para ello, se realizan cálculos ingenieriles en condiciones estacionarias mediante una Hoja de Cálculo y se asumen ciertas suposiciones que facilitan los cálculos referidos especialmente a balances térmicos, hidráulicos y/o neumáticos. Consecuentemente, se obtiene tal y como es de esperar, un sistema de gestión térmica sobredimensionado, entendiendo como tal un sistema diseñado para las operaciones más exigentes posibles de funcionamiento con la única y exclusiva preocupación de cumplir los requisitos de diseño definidos.

Una vez dimensionado el sistema de almacenamiento y el sistema de gestión térmica, el tercer paso de la metodología propuesta se basa en desarrollar modelos matemáticos detallados de los mismos. En este paso se desarrollan varios modelos, tanto del sistema completo, como en base al concepto de escalabilidad, un subsistema de tamaño inferior siendo representativo del comportamiento real del sistema completo. El objetivo de este tercer paso es verificar numéricamente el cumplimiento estricto de dichos criterios de diseño definiendo para ello una matriz de ensayo basada en la técnica de Diseño de Experimentos. Mediante ella, se abarcan unas condiciones de operación lo más amplias y diversas posibles realizando para ello el menor número de simulaciones posibles. Para cada aplicación se define la herramienta de modelización numérica de diseño adecuada, mostrando de esta manera la aplicabilidad y versatilidad de la metodología no únicamente en cuanto a la aplicación, sino también en cuanto a la herramienta

empleada. Los modelos matemáticos se desarrollan mediante herramientas de simulación de *Dinámica de Fluidos Computacional* y *Sistemas de Ecuaciones Diferenciales, Algebraicas y Discretas* y se hacen simulaciones transitorias detalladas. Como resultado de esta tarea se obtienen los planos de diseño para construir el eventual prototipo si se verifica, al menos teóricamente, el cumplimiento de los objetivos fijados.

El cuarto y penúltimo paso a llevar a cabo mediante los modelos detallados desarrollados, es la validación experimental de los mismos. Para ello, se construyen prototipos en base a la escalabilidad aplicada del sistema en el paso anterior y se realizan los mismos ensayos experimentales correspondientes a la matriz definida en el paso anterior. De esta manera se chequea el cumplimiento de los criterios de diseño experimentalmente. Las medidas experimentales obtenidas se comparan directamente con los resultados numéricos obtenidos anteriormente, evaluando de esta manera el error y asegurando la fiabilidad de los modelos desarrollados en términos de ser representativos de la realidad.

Finalmente, el quinto paso corresponde a la optimización del sistema de gestión térmica. Antes de proceder con esta tarea es imprescindible chequear el margen de mejora que existe en el sistema diseñado en referencia a los criterios de diseño establecidos en el primer paso. En el presente trabajo prevalece la importancia de los aspectos térmicos y por ello, se fija el objetivo de minimizar el consumo y coste del sistema auxiliar del sistema de gestión térmica, manteniendo en todo momento la temperatura máxima del sistema de almacenamiento dentro de un rango de operación ideal y aceptable, junto con la minimización de la dispersión térmica en él. En ambas aplicaciones se lleva a cabo un proceso de optimización basado en simulaciones numéricas transitorias que se realizan en cada una de las herramientas de simulación seleccionadas. Debido al alto coste computacional referido a la simulación transitoria mediante la herramienta *Dinámica de Fluidos Computacional*, se introduce un nuevo concepto denominado *False Steady*, mediante el cual es posible superar esta limitación, sin prescindir de la exactitud de los resultados obtenidos. Como resultado de este paso se obtiene para cada caso un sistema de gestión térmica optimizado, evaluando por ejemplo la necesidad o no de utilizar diferentes componentes o reduciendo el consumo eléctrico requerido en función de las condiciones de trabajo.

A lo largo de la Tesis, la metodología descrita se ha implementado en dos aplicaciones concretas dentro del campo de la Electro-Movilidad: un ascensor residencial y un minibús eléctrico urbano. En ambos casos se han obtenido resultados satisfactorios. De esta manera se demuestra la versatilidad de la misma para ser aplicada en diferentes aplicaciones dentro del campo de la Electro- Movilidad con el fin de optimizar el sistemas de almacenamiento eléctrico y su correspondiente sistema de gestión térmica.

Abstract

This Thesis deals with the development of a design and optimization methodology which is focused on the Thermal Management Systems for applications within the Electro- Mobility framework. Procedures and certain sort of calculations have been established which allow taking non-arbitrary decisions at each design step, in order to speed up and to make more robust the development process. This methodology involves the development of advanced mathematical models, which independently of the simulation tool that is used, ensure the obtainment of an optimized final design.

The interest of this Thesis was awoken by the current progress today´s electrical powered applications such as elevators, tramways, household, electrical grids, full, hybrid and plug hybrid electric vehicles. These applications require improved Energy Storage Systems with high energy and power densities, in order to power them. The electrical and thermal sizing of these Energy Storage Systems is not trivial.

There is a wide variety of technologies related to Energy Storage Systems among which, Lithium-ion battery technology is becoming the most promising future technology for this type of applications. These large dimension systems require an adequate control system named Battery Management System, which ensures the correct performance and long lifetime of the Energy Storage System under any operating condition. In this context, the thermal issues are one of the major aspects that must bear in mind because the electric performance of the cells is directly influenced by the operating temperature and the thermal dispersion that exists between the Lithium-ion cells that comprised the Battery Pack. Therefore, the software and hardware that

constitutes the so-called Battery Thermal Management System, part of Battery Management System which manages the thermal issues, should control and regulate the performance of the cooling and heating system in order to keep the temperature of cells within an ideal or, at least, admissible operation range. In that way, it will be avoided any malfunction, accelerated degradation or any security problem.

In certain applications, there are no restrictions related to the weight, available space or consumption. In these cases, the correct thermal performance is ensured by means of a Thermal Management System, with no other concern than to keep the cells as close as possible to them optimal operation temperature. However, for applications within the Electro- Mobility scope, the previously mentioned design criteria are often limited and are influential in the overall performance of the system. Therefore, it is crucial to design and implement an optimized Thermal Management System. The optimization process must be carried out at component and at system level with the objective to minimize as far as possible aspects such as the compactness and complexity, weight, consumption, initial investment and maintenance of the overall system.

The proposed methodology is comprised of five steps which are described and completely developed in the present document. Some of these steps involve closed-back-loops that should be solved prior to proceed with the next step. The first four steps correspond to a standard design- and modeling-methodology, while the fifth step which is related to optimization process constitutes the main contribution of this research work.

The first step of this methodology is related to the definition of the design criteria which they can involve thermal, electrical and/or mechanical aspects, as well as aesthetical. These design criteria can be defined by the customer or by the designer. Definitely, regardless of type of criteria and/or who impose them, this methodology ensures the compliance of them under any operation conditions for the selected applications.

The second step is comprised primarily of two tasks. The first task is referred to the thermal sizing of the Energy Storage System, whereas the second one is related to the selection of the components of the Thermal Management System. The thermal sizing of the Energy Storage System is carried out taking into account the worst electrical

operation conditions in terms of power requirements with the objective to maintain the temperature of the Energy Storage System within the defined optimal operation range for this restrictive operation conditions. As a result of this task, the amount of heat that must be dissipated by the Thermal Management System is achieved. On this basis, the preselection of the components of the Thermal Management System is conducted. For that purpose, some engineering calculations at steady state are performed by means of Worksheets. In addition, some assumptions and simplifications are considered which facilitate the calculations mainly related to thermal, hydraulical and pneumatical balances. Consequently as it is expected, an oversized Thermal Management System is obtained, meaning a system designed to overcome the most restrictive operation conditions, with the unique and exclusive concern to fulfil the defined design criteria in the first step of this methodology.

Once the Energy Storage System and its Thermal Management System are predesigned, the third step of this proposed methodology is based on the development of the detailed models of them. In this step, several models are developed in both the complete system level and, based on the scalability concept, a lower subsystem level which is representative of the real performance of the complete system. The aim of this third step is to verify numerically the strict fulfilment of the design criteria, defining for that purpose a test matrix based on *DoE* technique. It covers as wide as possible operation conditions carrying out the minimum number of simulations. For each application the most suitable simulation tool is defined and in that way, not only is demonstrated the applicability and versatility of the methodology in terms of application, but also in the use of the most appropriate simulation tool. The mathematical models are developed by means of Computational Fluid Dynamics and Differential, Algebraic and Discrete Equation simulation tools. By means of them, detailed transient simulations are carried out. As a result of this step, design planes are obtained in order to construct the prototype, if it is verified, at least theoretically, the fulfilment of the established objectives.

The fourth and the penultimate step, on the basis of the developed detailed models, is the experimental validation of them. For that purpose, some prototypes are constructed in laboratory environment based on the scalability concept applied in the previous third step. Similarly, the same test matrix than in the previous step is conducted to check

experimentally the compliance of the defined design criteria. The experimental measurements are directly compared with the numerical results, evaluating the error and ensuring the reliability of the developed thermal models in terms of representation of the real performance.

At last, the fifth step corresponds to the optimization of the system. Before to proceed with this step is essential to check the optimization margin that exists in the designed Thermal Management System in reference to the design criteria established in the first step of this methodology. Particularly, in this present research work is predominated the importance of the thermal issues and therefore, it is defined the aim of minimizing the consumption of the auxiliary system keeping at all times the maximum temperature of the Energy Storage System within the ideal and admissible operation range, together to the minimization of the thermal dispersion within it.

In both applications, it is carried out the optimization process based on steady numerical simulations by means of each simulation tool selected for each application. Due to the high computational cost associated with the transient simulations by means of the Computational Fluid Dynamics simulation tool, issue which is not related to Differential, Algebraic and Discrete Equation simulation tool, a novel concept named as *False Steady* is introduced. *False Steady* concept makes possible to overcome this limitation, without expenses of the accuracy of the results obtained. As a result of this step, for each application an optimized Thermal Management System is obtained, evaluating for instance, the necessity or not of implement different components in the system or the appropriate rotational speed of the components in function of the actual operation conditions.

In the present Doctoral Thesis has been validated the developed methodology applying it to two particular application within the Electro- Mobility framework: a residential elevator and urban electric minibus. In both cases satisfactory results have been obtained. By this way, it is demonstrated the versatility and applicability of the developed methodology to design and optimize Energy Storage Systems together with its Thermal Management System for applications within the Electro- Mobility scope.

List of Symbols

The list corresponds to the symbols that appear along this document are defined below. These symbols are divided into latin characters, greek letters, subscripts and acronyms.

Latin Characters

A	[m^2]	area
C	[$J \cdot K^{-1}$]	thermal capacity
Cap	[$A \cdot h$]	nominal capacity
C_p	[$J \cdot g^{-1} \cdot K^{-1}$]	heat capacity at constant pressure
D	[m]	depth
E	[J; W·s]	energy
H	[mm]	height
h	[$J \cdot kg^{-1}$]	specific enthalpy
I	[A]	cell current, + for charge and - for discharge
$\dot{I}$	[$kg \cdot m \cdot s^{-2}$]	momentum flow
k	[$W \cdot m^{-1} \cdot K^{-1}$]	conduction heat transfer coefficient
L	[m]	characteristic length

$\dot{m}$	[kg·s^{-1}]	mass flow rate
M	[g]	total mass in the control volume
Nu	[-]	Nusselt number
P	[W]	power
p	[Pa]	static pressure
Pe	[m]	perimeter
P_{elec}	[W]	Electric consumption
Pr	[-]	Prandlt number
$\dot{q}$	[W]	heat generation rate
R	$[K \cdot W^{-1}]$	thermal resistance
Re	[-]	Reynolds number
R_{in}	[Ohm]	internal resistance
S_h	[W·m^{-3}]	volumetric heat source
t	[s]	time
T	[K]	absolute temperature
U	[J]	internal energy
w	[m·s^{-1}]	velocity
$\boldsymbol{v}$	[m^3]	volume
V	[V]	voltage
W	[mm]	width
V_{flow}	[lpm]	liquid mass flow rate
x	[m]	x- coordinate
x^*	[-]	flow steam quality

z	[m]	z- coordinate
Δp	[Pa]	pressure difference
Δp_f	[Pa]	friction pressure loss
ΔT	[°C]	temperature difference
$\partial U/\partial T$	$[\mathrm{V \cdot K^{-1}}]$	entropic heat coefficient

Greek Letter

ρ	$[\mathrm{kg \cdot m^{-3}}]$	density
λ	[-]	pipe friction factor
ν	$[\mathrm{m^2 \cdot s^{-1}}]$	kinematic molecular viscosity
ε	[-]	void fraction
ζ	[-]	friction factor
δ_{ij}	[-]	Kronecker delta
α	$[\mathrm{W \cdot m^{-2} \cdot K^{-1}}]$	heat transfer coefficient
τ_i	$[\mathrm{s^{-1}}]$	thermal time constant
τ_0	[Pa]	wall shear stress
μ	$[\mathrm{kg \cdot m^{-1} \cdot s^{-1}}]$	dynamic viscosity

Subscripts

$//$	parallel direction
$\perp$	normal direction
0	initial
amb	ambient
avg	average

CHA	charge
$cond$	condensation
DCH	discharge
$e$ff	effective
$e$vap	evaporation
$e$xp	experimental
dis	dissipation
gen	generation
in	inlet
cv	control volume
max	maximum
mid	middle
min	minimum
nom	nominal
out	outlet
ope	operation
sc	subcooling
sh	superheating
sto	storage
w	wall

Acronyms

AC	Active Cooling
A/C	Air Conditioning

BM	Battery Module
BMS	Battery Management System
BP	Battery Pack
CAES	Compressed Air Energy Storage
CEC	Cauer Equivalent Circuit
CFD	Computational Fluid Dynamic
COP	Coefficient of Performance
CPU	Central Processing Unit
C-rate	Current Rate
DAE	Differential Algebraic Equations
DoE	Design of Experiments
DOD	Depth of Discharge
EDLC	Electrochemical Double Layer Capacitor
eMOV	Electro- Mobility
ERA	European Research Area
ESS	Energy Storage System
EU	European Union
EV	Electric Vehicle
FC	Force Cooling
FCV	Fuel Cell Vehicle
FVM	Finite Volume Method
GWP	Global warning potential
HEV	Hybrid Electric Vehicle

HPC	High Performance Computing
LA	Lead Acid
LED	Light Emitting Diode
Li-Ion	Lithium- Ion
LTO	Lithium Titanate Oxide
MPET	Multi-Port Extruded Tubes
NC	Natural Convection
NTC	Negative Temperature Coefficient
ODP	Ozone Depletion Potential
PC	Passive Cooling
PCM	Phase Change Material
PHEV	Plug Hybrid Electric Vehicle
PHS	Pumped Hydro Storage
PI	Proportional- Integral
PTC	Positive Temperature Coefficient
PV	Photovoltaic
PWM	Pulse- Width Modulation
RFB	Redox Flow Batteries
RSM	Response Surface Methodology
SEI	Solid Electrolyte Interphase
SG	Smart Grid
SMES	Super Magnetic Energy Storage
SNG	Synthetic Natural Gas

SOC	State of Charge
TEC	Thermoelectricity
TIM	Thermal Interface Material
TMS	Thermal Management System
TRAIT	Thermal Resistance Analysis by Induced Transient
TXV	Thermal Expansion Valve
UDF	User Defined Function
UPS	Uninterruptible Power Supply
VCRC	Vapor Compression Refrigeration Cycle
WEG	Water- Ethylene Glycol

Contents

Chapter 1.

Introduction and Objectives

The goal of this chapter is to introduce the reader to the scenario in which this Doctoral Thesis is situated.

This introductory chapter is divided into two principal sections: The first one is devoted to describing the source of motivation for this research work together with the lack of knowledge that it has been detected in this field and therefore, in which this Thesis has been focused. In addition, the second part is dedicated to defining the main objective and the intermediate tasks developed in this research work, along with the description of the structure of the document explaining from an overall perspective the aim of each chapter.

The complete document is composed of 8 chapters, whereof in general terms, the first one is dedicated to introducing briefly this work. From the second to the fourth chapter some preliminary but important issues, are covered which are not strictly thermal tasks. The fifth one describes in depth the proposed methodology from a theoretical perspective. The sixth and seventh chapters are focused on the implementation of the methodology in the selected two real applications as test cases. At last, the eighth chapter deals with the description of the conclusions and future research lines based on this present research work.

1.1 MOTIVATION OF THE THESIS

Currently the focus of many companies is close to traction, elevation and renewable energy sectors applications which could require scalable *Energy Storage Systems* (*ESSs)* for novel applications such as trams without catenaries [1], regenerative elevators [2], e-bikes [3], *Hybrid Electric Vehicles* (*HEV*s) and full *Electric Vehicles* (*EV*s) [4], *Photovoltaic* (*PV)* integration and any *Smart Grid* (*SG*) applications [5, 6].

Nowadays a wide range of *ESS*s is available that could be implemented in this type of applications. However, it is important to have the knowledge in order to select the most suitable one in function of the particular specifications that the interest application required [7]. In general terms, these technologies are featured by high energy density, high power density, long life and environmental friendliness and therefore, they have been found wide applications to use them. Nevertheless, it should be paid especial attention to those technologies due to they provide high energy density coupled with such problems as safety, durability, uniformity and cost. Definitely, they impose technical limitations and restrictions around them.

The performance of these systems and their lifespan is directly influenced generally by operating conditions such as ambient temperature, power and energetic demands and the electrical and thermal configuration among others. As it has been pointed out in Abstract, it is essential to control the *ESS*s´ thermal performance within the optimal operation window. For that purpose, it is necessary to implement a suitable and appropriate *Battery Management System* (*BMS)* and in particular, a well sized *Thermal Management System* (*TMS)*.

Different *TMS* technologies have been analyzed by many authors in the literature. The tendency of many *TMS* designers is to oversize the selected *TMS* in order to guarantee thermal specifications compliance. In addition, no compromise is usually taken into consideration between aspects such as the maximum cell temperature, thermal dispersion between cells within the complete *ESS*s, weight, size, auxiliary power consumption and overall implementation and usage cost or even any esthetical aspect. Besides, an undersized *TMS* could affect negatively to the overall performance and lifespan of the *ESS*. The selection of the more suitable components, architectures,

and control strategies to build a specific *TMS* for a concrete application is not a trivial issue.

This research work resulted from the need to develop a methodology which ensures the implementation of an optimized *TMS* for a particular *ESS*, following non-arbitrary criteria. The attention is focused on *Electro- Mobility* (*eMOV)* applications, covering with this word any traction or elevation application, powered by an electric powertrain to transport people in a clean urban environment. The cooling or heating needs of other components apart from the *ESS*, that are used in these applications are out of the scope of this work, but they could be easily integrated into the proposed system level optimization methodology.

In the following section, it will be defined the main and intermediate objectives which have made possible to fulfil this lack of knowledge. In addition, the structure that has been followed in this PhD Thesis memory will be explained.

1.2 OBJECTIVE AND STRUCTURE OF THE THESIS

The main objective of this PhD Thesis is to propose and develop an improved methodology to design and optimize a *TMS* for any *Lithium-Ion (Li-Ion) ESS* intended to be used for *eMOV* applications. This methodology has been applied in two different applications which have been powered by this kind of *ESS*s. At each of these applications, a different simulation tool has been used in other to carry out this methodology. In Figure 1.1 is shown the schematic diagram of the structure of the Thesis which is described in the following paragraphs, together with the intermediate objectives that each chapter (indicated by red) has covered.

The specific task which has been carried out in each chapter, summarized in the final section of each one and named as "*Conclusion*", has contributed to achieving the final and main goal of this Thesis. The complete document has been composed of 8 chapters which are described from a general point of view in following to help the reader to have a clear view of the work and to serve as a guide to the understand better the structure of this document.

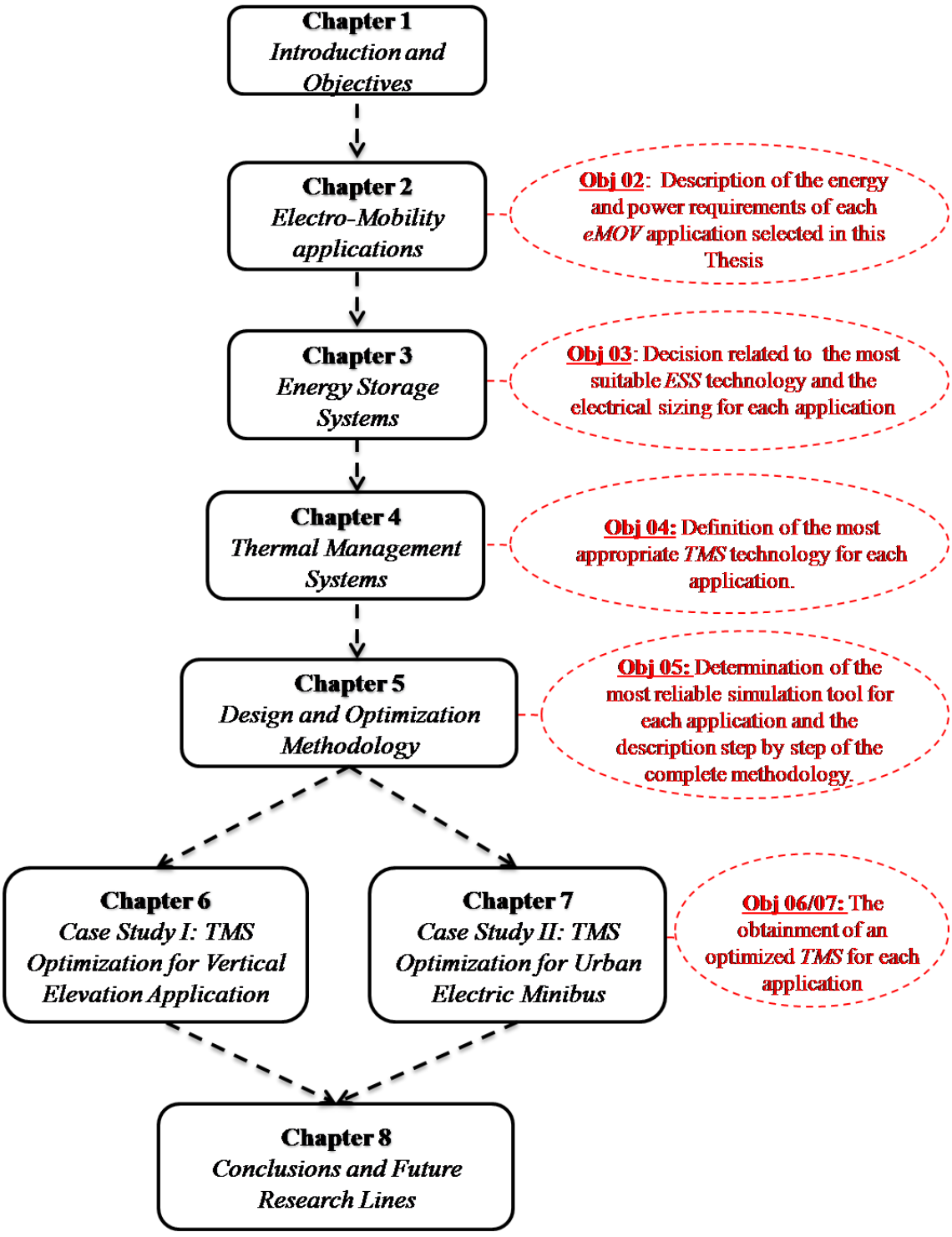

Figure 1.1 Schematic diagram of the structure of the Thesis together with the intermediate objectives of each chapter.

The aim of the current chapter, **Chapter 1**, is to introduce the reader to the general context of this research work. Besides, the motivation which led this work together with the objectives that have been defined and the structure that it has been followed along the present document are explained.

Chapter 2 is named *"Electro-Mobility applications"*. The goal of this chapter has been to describe the current scenario related to *eMOV* and the near future perspective mainly at European level in terms of boosting these applications to achieve some social, economical, environmental and political objectives. In this context, as a conclusion of this chapter, the two *eMOV* applications covered in this research work, in terms of energy and power requirements, have been presented (Obj. 02 in Figure 1.1).

Chapter 3 is named "*Energy Storage Systems"*. This chapter is focused on the description of the different available *ESS*s for *eMOV* applications, especially paying the attention on *Li-Ion* secondary batteries. In this chapter, the importance of the role played by the implementation of the *BMS* and mainly, of the *TMS* has been highlighted. This chapter is concluded by means of the electrical sizing of each *ESS* implemented in each interested application described in Chapter 2. (Obj. 03 in Figure 1.1).

"*Thermal Management Systems*" is the title of **Chapter 4**. Throughout this chapter, the description of the actually available cooling technologies is carried out concluding with the selection of the most suitable *TMS* technology for each application. For that purpose, the requirements and the electrical sizing which have been already carried out previously in the 2nd and 3rd chapters have bear in mind. Furthermore, the heating and insulation effects of each *ESS* are considered. (Obj. 04 in Figure 1.1).

The principal chapter of this Doctoral Thesis is **Chapter 5** titled as "*Design and Optimization Methodology*". This chapter is dedicated to describing step by step in detail, the methodology that it has been applied for both presented *eMOV* applications in order to mathematically model, design, implement and optimize their *TMS*. The first part of this chapter describes the different modeling tools to simulate the thermal performance of such complex systems. In that way, it is demonstrated the suitability and applicability of the methodology regardless of the application and simulation tool that it is used (Obj. 05 in Figure 1.1).

In **Chapter 6** and **Chapter** 7**,** the methodology is implemented for "*Case Study I*" and "*Case Study II*" considering the decisions that have been taken in the previous chapters related to each application such as, the energy and power requirements, the electrical sizing and the selected conceptual *TMS* architecture. The first case study is named "*Thermal Management System Optimization for Vertical Elevation Application*" and it is associated with a residential elevator application, whereas the second case study, "*Thermal Management System Optimization for Urban Electric Minibus*", is related to a full electric urban minibus. Based on the adopted decisions and following step by step the complete methodology that it has been described in Chapter 5, an optimized *TMS* is achieved. All the details of each intermediate steps are given such as the numerical models based design process description, simulation results and analysis of them and the prototypes which have been built for experimental validation purpose, among others (Obj. 06/07 in Figure 1.1).

Finally, **Chapter 8** "*Conclusions and Future Research Lines*", contains a summary of the main conclusions of this research work, a revision of the objectives fulfilment and a description of the future research lines in accordance with the present work.

Chapter 2.

Electro-Mobility applications

The goal of this chapter is to place the reader in the *Electro-Mobility* scenario in which this research work is situated and to introduce the specific problematic that it is going to be thoroughly analyzed in the next chapters.

Along this chapter the *Electro-Mobility* concept is presented, addressing issues related to its current situation at European level and the near future perspective in terms of boosting these applications to achieve some social, economic, environmental and political objectives. In addition, the solutions that are provided for some specific problems by the implementation of these applications are also briefly described, along with the barriers that must be solved in order to become competitive applications in comparison with the current applications. Finally, and with the objective to introduce both *Electro-Mobility* applications that will be studied in-depth in this Doctoral Thesis within this framework, their electrical demands are presented. These energetic and power requirements are necessary or crucial to take decisions in the next chapters.

Generally, the power profiles associated with the applications within the *eMOV* framework can be rather chaotic and/or intermittent. Nevertheless, they are often cyclical, due to the necessary repetitive process of the charge after the discharge. For a design process, as it has been carried out in this Thesis, it has been necessary to define or analyze particular profiles correspondent to the particular applications.

2.1 INTRODUCTION

Under *eMOV* concept can be grouped applications that can be defined such as clean and environmentally friendly urban mobility solutions. By means of them, it has been tried to minimize the use of hydrocarbons increasing the efficiency of the transport systems, as well as to reduce the contaminant emissions inside cities.

Due to the environmental and geopolitical concerns, in recent years there has been a push to increase the penetration of the renewable energy sources into the society in order to leave aside the use of fossil fuels. In this way, it will be possible to reduce the carbon gas emissions in generation points. One of the main negative issue related to the available renewable energies is their intermittent nature. They can present problems in applications in which are used for system stability, reliability and power quality purposes. The issue of sporadic availability of renewable resources can be addressed for instance, by implementing *ESS*s.

This technology, as it will be discussed below, apart from mitigate the previous mentioned effects can be also used in traction applications in order to improve aspects related to the growing actual problem of the urban mobility, the fulfilment of the sustainability specifications imposed by European guidelines, the enhancement of the energy demand management, the reduction of the dependence on petroleum or also, the application operation assurance under any possible fault on the supply system. In general trends, it can be said that these *eMOV* applications allow the use of a clean secondary energy source as electricity without any temporal restrictions.

2.2 CURRENT SITUATION

The *European Union* (*EU*) is aware of the importance of the opportunities that *eMOV* could bring in terms of a decarbonisation of the transport sector and the electrification of the European fleet. For this reason, in the last recent years, it has focused the attention on achieving the goals with regards to energy security, energy efficiency and a sustainable, low-carbon and climate-friendly economy.

For that purpose, the *EU* has defined some objectives for the near future related to the reduction the domestic greenhouse gas emissions by at least 40% below 1990 levels

by 2030 [8], the reduction the CO_2 emissions from the transport sector by 60% compared with respect to 1990 levels and the elimination the use of fossil fuels in vehicles by 2050 [9].

Over the last century, the *EU* has invested in the achievement of the previously cited objectives and it has defined various programs for research and development known as the Framework Programs for Research and Technological Development, also-called Framework Programs. They are abbreviated such as *FP* and they are funding programs created by the *EU* or European Commission to support and foster research in the *European Research Area* (*ERA*).

The 7th Framework Program for Research and Development was the *EU´*s main instrument for research in the period of 2007-2013. The objectives of this program were to promote safer, "greener" and "smarter" European transport systems that will benefit all citizens, take care of the environment, and increase the competitiveness of European industries in the global market [10]. Currently, the 8th Framework Program is being developed which is known as Horizon2020.

Horizon2020 is the world´s largest collaborative program proposed by *EU* for research and innovation until 2020. The four main priorities for transport research under Horizon 2020 program are [11]:

- Resource efficient transport that respects the environment: the aim is to minimize the transport systems' impact on climate and the environment (including noise and air pollution) by improving its efficiency in the use of natural resources, and by reducing its dependence on fossil fuels and energy imports.

- Better mobility, less congestion, more safety, and security: the aim is to reconcile the growing mobility needs with improved transport fluidity, through innovative solutions for seamless inclusive, affordable, safe, secure and robust transport systems which take advantage of the use of modern "Information and Communication Technologies" capabilities.

- Global leadership for the European transport industry: the aim is to reinforce the competitiveness and performance of European Transport manufacturing industries and related services on global markets.

- Socio-economic and behavioral research and forward-looking activities for policy making: The aim is to support improved policy making which is necessary to promote innovation and meet the challenges raised by transport, including the internalization of external costs, and the societal needs related to it. Socio-economic research is also an important instrument for reaching the objectives under this program.

These previous activities are addressed under this research program by three calls for proposal: *Mobility for Growth, Automated Road Transport* and *European Green Vehicles Initiative*.

Many are the efforts that have been made in order to impulse *eMOV* applications due to the advantages and improvements that they offer as a solution to a variety of current concerns and problems. Some of them will be described following.

2.3 FEASIBILITY OF ELECTRO-MOBILITY

The development and integration of applications within the *eMOV* framework in our society could suppose some solutions to various problems of concern to the global society nowadays. By means of these applications, it will be possible to propose a solution to issues related to the reduction of the CO_2 emissions, the improvement air quality and noise levels in cities, especially in city center, the integration of renewable energies, the enhancement the energy efficiency, the improvement the energy security, the boosting the sustainable growth and the reduction the cost of ownership.

- Reduce CO_2 emissions and Improve air quality and noise levels: regarding the reduction of the CO_2 emissions, it has to be considered that in 2013 the power sector generated the 54% of all *EU´*s electricity by means of low-carbon power and furthermore, currently it continues making efforts for decarbonisation by 2050. It is obvious that fuelling cars, vans, and buses with electric traction system would thus considerably reduce CO_2 emissions in the transport sector as well [12].

In addition and considering the effects of this type of applications in terms of improving air quality and noise levels in cities, it is clear that an electric motor does not release any waste gases or exhaust fumes and thereby, *EV*s can significantly mitigate the level of air pollutants in cities (especially particulate matter as dust or gaseous as NO_x). At the same time, the power sector has drastically reduced its own emissions during the last recent years that affect air quality reducing SO_2 and NO_x pollutants in 85% and 55% respectively. With regards to noise levels the electric motors generate significantly less noise compared with the conventional combustion engines, so in this sense, this problem would be also solved [12].

In this context, in Madrid since the end of the previous year, some corrective actions were taken into consideration in order to combat the atmospheric pollution, as it is shown in Figure 2.1. These decisions were based on establish a maximum velocity of 70 km/h in the zones identified such as M-30 and M-40 which are shown in Figure 2.1, prohibit parking in the center of the city with some exceptions such as for the residents and restrict the circulation of vehicles within M-30 zone in function on their plate number depending on the day of the month [13]. The *EV*´s was exempted from this regulation. Taking account these choices, the mayor of Madrid presented "Air Quality and Climate Change Plan" by means of which is boosted the pedestrian priority, the improvement of the urban cyclist- and buses path and the increase of incentives for a fleet of low-emissions for taxis, among others [14].

Figure 2.1 Pollution and distinguished zones where the corrective actions have been implemented in Madrid [13].

- Integrating renewable energies: the development of the *eMOV* applications will be another issue that will give more strength to the integration of the renewable energies. For instance, *eMOV* applications can play a dynamic part in the electricity system by acting as local storage connected to a smart home charged by means of the customers' own solar panels, that could be used to feed elevators or to charge *EVs*. This will also facilitate the integration of consumers in the electricity system while reducing the peak production exported to the grid and flattening the demand curve.

  Gamesa, for example, is a Spanish company which is focused on the *PV* sector together with the wind industry. Figure 2.2 (a) shows the wind generation park which is currently constructed and installed in Chile [15]. On the other hand, in Figure 2.2 (b) is shown the solar system developed by General Electric which it has been installed in California and it produces annually about 600 kW of energy.

(a) (b)

Figure 2.2(a) The wind generation park constructed in Chile by Gamesa[15] and (b) the solar system installed in California and developed by General Electric.

- Enhancing energy efficiency and energy security: considering the energy efficiency of an electric motor, in general terms, is inherently more energy efficient than other engines. Besides, in terms of the energy consumption, an *EV* can be three or four times more energy efficient than a conventional fuel vehicle. Moreover, solutions are provided as well to increase energy security when the current power source fails.

  To illustrate this, it can be mentioned that in a hypothetical full electrification scenario, electric cars would allow Europe to achieve considerable energy efficiency gains with a net reduction of 137 million tons

of oil equivalent per year in the *EU* by 2035 [16]. Moreover, the *EU´*s transport sector is 94% dependent on oil, with a bill of up to 1 billion € per day on oil imports. The scope of *eMOV* applications would help reduce those imports and thereby, a lower annual cost of the *EU´*s oil import bill [17]. In Figure 2.3 are shown the *EV*s that IAD institute of TU Dresden used to analyze and improve the performance of this type of vehicles.

Figure 2.3 EVs from IAD institute (TU Dresden).

- Boosting sustainable growth and lowering the cost of ownership: the deployment of charging infrastructure and the development of new business models, they could help to bolster jobs and growth creation in Europe. Also, the switch to electricity also could lead to a reduced personal cost for *EV* drives mainly due to cost savings on fuel. *EV* owners can end up paying three times less for their energy consumption over their vehicle´s lifetime than owners of a diesel or petrol car (including government incentives). The equal cost for *EV*s respect to conventional vehicles is expected by 2020 [18]. Figure 2.4 shows a fuel station against to charging station for an *EV*.

Figure 2.4 Fuel station against electric charging station.

These previously mentioned opportunities that *eMOV* applications can provide to the society have been and are currently limited by some economic, social and technological barriers that must be overcome to strengthen their use.

2.4 BARRIERS AND CHALLENGES OF ELECTRO-MOBILITY

Some are currently the barriers and challenges that must be overcome in order to extend the use of *eMOV* applications in our daily routine. Among them are the improvement related to batteries, availability, and preparedness of industry capacity, charging infrastructure, electrical grid capacity and connectivity, regulation and standardization issues and impacts on energy efficiency and greenhouse gas emissions. Following they will be explained individually.

- Batteries technological developments and challenges: the *eMOV* market is highly dependent on the availability of the battery technology that allows a reliable storage of the electric energy on-board. The key component for both performance characteristics and costs of an *eMOV* application is its *ESS*. Therefore, it is necessary to achieve the commercialization of these *ESS*s in order to reduce the cost related to this type of vehicles, besides with the increase of subsidies and incentives to foster the market introduction of these applications [19]. As an example, Figure 2.5 shows the evolution expected in terms of *Li-Ion Battery Pack* (*BP*) cost over the coming next years. Based on the study carried out by Patrick Hummel et al. [20], they enforced the idea that in the next years the price of the *ESS*s will be reduced. They estimate that by 2020 *Li-Ion BP* cost will drop by more than 50% compared to the price of 2013.

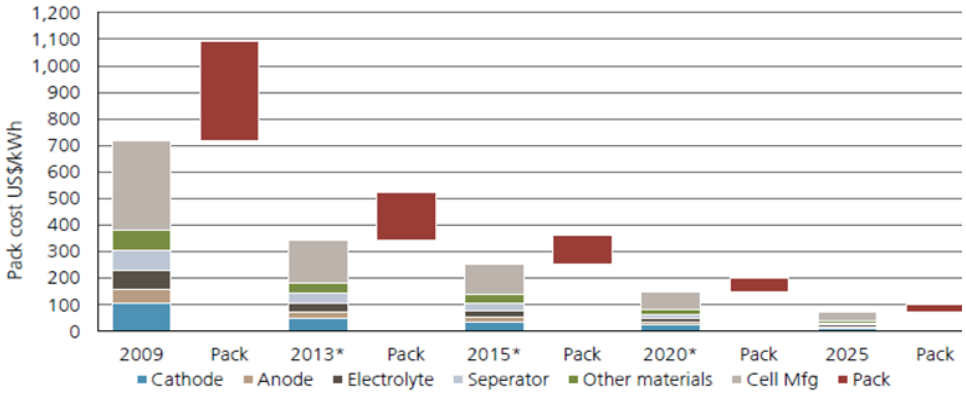

Figure 2.5Li-Ion BP cost evolution during the previous and following next year's[20].

It has to be taken into account that a battery system includes, besides the battery cells, components for interconnections and packaging as well as electrical and thermal management equipment. All these additional components have a significant influence on the overall volume, weight and cost of a battery system. Even although a lot of progress has been already made in terms of energy content related to volume and weight of a modern battery, the energy density remains about hundred times lower than that of fuels for combustion engines. This fact is one of the main challenges for *eMOV*, as it influences both costs and usability.

- Availability and preparedness of relevant industry capacity: the successful introduction and market penetration of electrically chargeable applications depend on many factors such as customer acceptance, market incentive systems, the attractiveness of alternative mobility solutions, *ESS*, etcetera [19].

Regarding the market penetration, it can be said that the most stakeholders assume a realistic market share for new, electrically powered vehicles in the range of 3 to 10% by 2020 to 2025. The market penetration will depend on the extent to which the tasks and requirements are addressed and fulfilled as well as on how fast the technology develops and in the way customers perceive/accept electric mobility. In fact, based on today´s *EV*s sales, it is expected between 450000 and 1500000 units of new *EV*s registrations between 2020 to 2025 [19].

Moreover, the commercial success of these applications could be fostered by new business models. For instance, high investment costs related to batteries could be managed by new leasing concepts, also battery exchange stations could be discussed as a viable choice in many cities. In addition, vehicle-to-grid interfaces may emerge in new grid management strategies resulting in more efficient the grid integration of the renewable energies. In Figure 2.6 can be seen the vehicle-to-grid concept shown in Minority Report film.

Figure 2.6 Urban vehicle-to-grid integration, futuristic concept art [21].

- Charging infrastructure: without appropriate recharging infrastructure, electrically chargeable vehicles cannot possible successfully be introduced in the market. The energy sector will have to build up a recharging infrastructure as a prerequisite for users' acceptance of electrically chargeable applications. For that purpose, it is necessary a combination of both private and public investments to overcome the current lack of a clear business model for public charging.

A suitable infrastructure should provide the availability and necessary density of recharging possibilities. The recharging places should be installed in parallel at strategic locations (e.g., homes, workplaces and truck or bus depots) and on main roads. In Figure 2.7 is shown a charging point installed in a community garage such as for example.

Figure 2.7 Charging point in a community garage.

On the other hand, from the customer point of view, it would be appropriate that they should have the free choice between different energy suppliers and access to all charging stations independent of the charging

station provider or energy provides (i.e. national/ international roaming). Furthermore, it would be suitable that a customer-friendly operation and billing systems are available at *EU* and global level. This includes different payment systems such as coin, credit card, prepaid card, etcetera [19].

- Electrical grid capacity and connectivity: in the future, it will be important to recharge vehicles in an intelligent manner in order to prevent charging at the peak loads for the power networks and to allow customers to recharge the *ESS* at low costs.

  Once a large volume of electrically chargeable vehicles will have reached the market, it is likely that some extra supply of electric energy will be needed. Also it will be necessary to develop and resolve some technological issues related to *ESS*s to ensure the durability of them, of the power grid and of the user convenience to could be used, among others thing, to feed energy back into the grid if the price for control energy or balancing energy is particularly high [19].

- Regulation and Standardization issues: comprehensive standards and norms have to be created to ensure the *eMOV* applications can be easily connected to the power network in order to recharge the *ESS*. The goal must be to establish worldwide standards in order to avoid market fragmentation and to reduce costs.

  Further improvements are needed in terms of cross-national compatibility / re-charging abroad should not be different to re-charging at home, data protection (personal, business), safety requirements for recharging places, charging cable at the vehicle or at the charging station, technical approval body for recharging places, periodic inspections and maintenance of recharging places and a convenient billing systems among others. Meanwhile, currently there is an intensive international standardization work running with regard to the relevant standards for connectors, charging stations and the communication interface [19].

- Impacts on energy efficiency and greenhouse gas emissions: while conventional vehicles with internal combustion engines create the largest

proportion of the fuel-cycle emissions during driving, full *EV*s do not produce any local air pollutants and greenhouse gas emissions during vehicle operations.

In contrary, electricity supply for *EV*s may cause considerably higher emissions at the power plant level (depending on the source of energy production) compare to only little emissions caused during production and distribution of conventional fuels. Overall, the environmental benefits of *EV*s significantly depend on what type of electricity (fossil, nuclear, renewable) is used for charging. In general terms and considering different average grid mixed, well-to-wheel greenhouse gas emissions of *EV*s are up to 70% lower compared to conventional vehicles but could be worse (10-20% higher) when electricity is based on coal-fired power plants.[19].

As an example, Figure 2.8 is shown the CO_2 footprint for different propulsion systems considering the effect of the electricity generation, fuel supply, vehicle usage and the production of the CO_2.

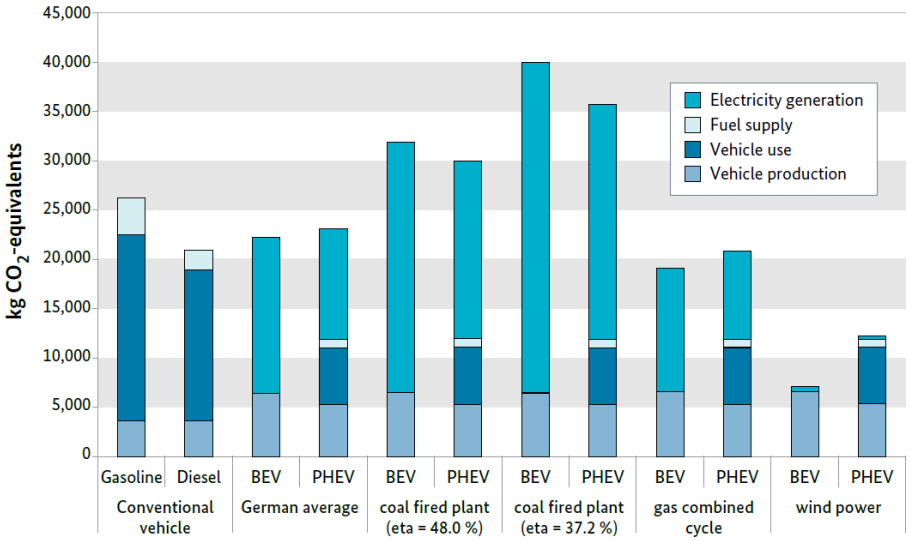

Figure 2.8 Comparison of the CO_2 footprint of passenger cars with different propulsion systems.

To sum up, the *eMOV* applications have the potential to be a sustainable long-term solution for mobility. Although significant progress has been already made over the last few years, some breakthroughs are still required in this field.

2.5 CONCLUSIONS

A quite wide range of applications, especially the ones related to the automotive and energy sectors can require an *ESS*. Many of them can be defined within the *eMOV* framework, such as any type of full *EV*s (bikes, motorcycles, cars, buses, minibuses, trams and elevators). Although the proposed thermal design and optimization methodology could be applied to any of them, the present work is mainly focused on two applications related to this scope. Figure 2.9 shows both selected applications: a residential elevator (a) and an urban electric minibus (b).

(a) (b)

Figure 2.9 Selected eMOV applications: (a) residential elevator and (b) urban electric minibus.

Regarding the residential elevator application, many manufacturing companies such as ORONA [2], use an *ESS* in their products in general terms to compensate for a sudden change in load, a line fault or a deficiency in the power generation avoiding a dip in the system voltage. However, for the case of an urban electric minibus, e.g., in companies as VECTIA [4], the implementation of the *ESS* is more focused on the development of a more sustainable urban transport in order to minimize the pollution and noise level problems, which are becoming crucial in some big cities. In both cases, the efficiency is increased by using suitable electric motors and by implementing operation strategies such as braking energy recovery or carrying out the charging process of the *ESS* during the night.

Three specific objectives should be covered with the proposed *ESS* installed in this residential elevator application. The first one is related to the reduction of the community power consumption allowing the use of single-phase motor, the second one is referred to the increase of the efficiency taking advantage of the regenerative energy obtained from the load favored trips and from charging the *ESS* at night and the third one, is based on the possibility to rescue people trapped inside the elevator using an autonomous mode even when the power supply in the building is not available.

The possible operation rides modes of the elevator are shown in Figure 2.10. The traction ride is referred when the elevator consumes energy from the *ESS*. This situation could happen when the elevator is heavily loaded by people and it goes up, or on the contrary, when it goes down empty. In contrast, the elevator operates in the regenerative mode when on the one hand, the elevator is full of people and goes down and on the other hand, when it is empty and goes up. The amount of discharging and charging power in the *ESS* depends on the number of people are in the elevator. As operation feature of this application, a great intermittency can be expected.

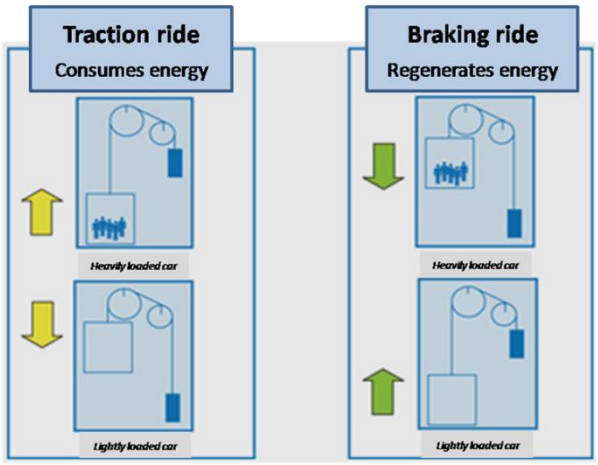

Figure 2.10 Elevator operation modes ride [2].

The particular analyzed elevator has been designed for a typical 7-floor building applied for the residential sector. This application has some energy and power requirements that must be fulfilled by the *ESS*.

In terms of power requirements at least three different operative conditions have to be supported by the *ESS* which is covered by a single-phase network of merely 2 kW: high load (Ride 1), medium load (Ride 2) and minimum load (Ride 3) indicated by red, green and blue lines in Figure 2.11 (a), (b) and (c), respectively. Each elevator ride

corresponds to a number of people inside it: 5, 3 and 1 people have been considered in Ride 1, Ride 2 and Ride 3, respectively. For every traction and braking process, the longest ride, i.e., from the 1st to the 7th floor, has been considered. Nevertheless, although it has been assumed the same number of people inside the elevator when it goes up and down, and the same trajectory in each defined ride, the required power for the traction process (discharge) is higher than for the equivalent braking process (charge). This effect can be seen in Figure 2.11 comparing the traction and braking operation power peaks for each ride.

Every profile shown in Figure 2.11 present the same structure: at first, a discharge process is carried out of 1 minute which corresponds to traction process in which the elevator goes up with corresponding people to each defined ride. Secondly, during an additional minute, the charging process is conducted which represents the braking process in which the elevator down with the same number of people than when it has gone up. At last, a recharging process of the *ESS* on-board is carried out at low current rate until it achieves the initial State of Charge (*SOC*) value of the discharge process. The recharging time for each operation condition varies and is function of the *SOC* jump that exists between the *SOC* value corresponded to the end of the braking process and to the initial of the traction process.

For all cases, it has been considered the repetitive and non-intermittent operation conditions. As it has been mentioned before in this section, one of the main feature related to this application is its intermittency, however these non-completely real load situations have been defined such as the most restrictive ones in terms of heat generation and dissipation.

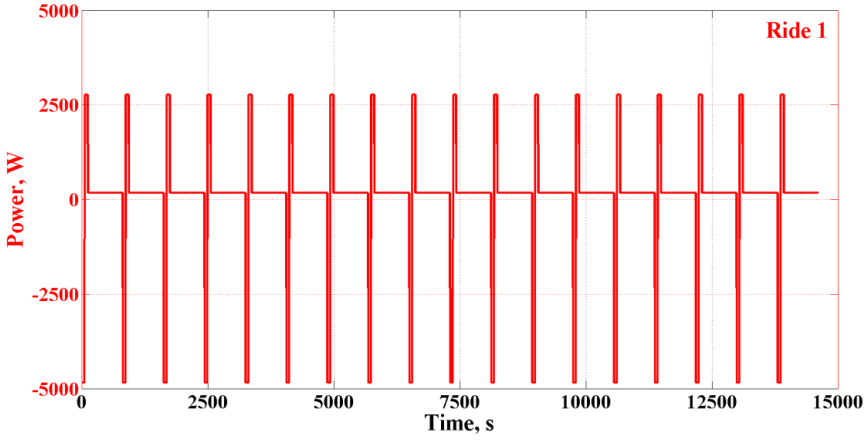

(a)

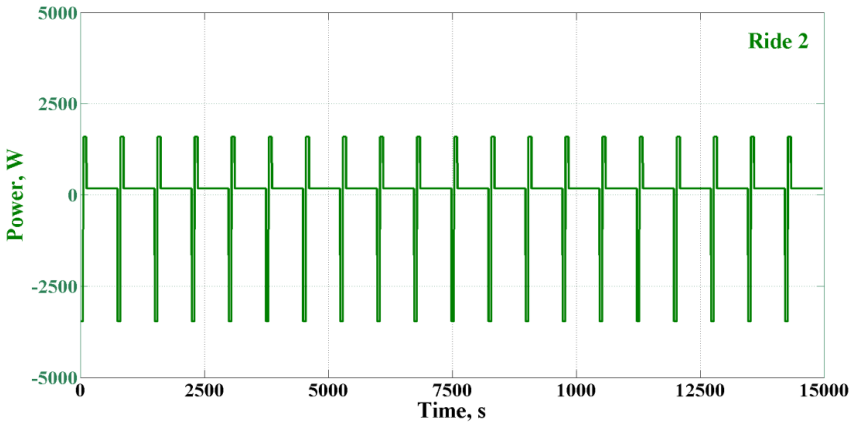

(b)

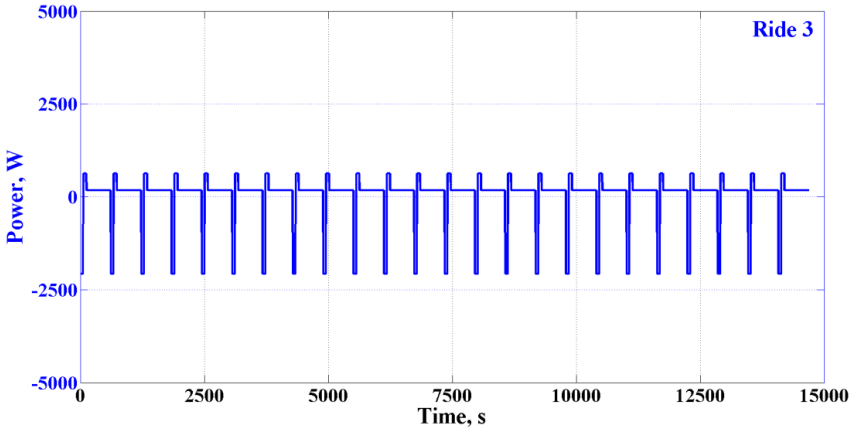

(c)

Figure 2.11 BP electrical power (W) requirements and SOC (%) evolution for the complete cycle for (a) Ride 1, (b) Ride 2 and (c) Ride 3.

In terms of energy requirements the application manufacturer established several criteria: the *ESS* should be able to supplement the single-phase network of 2 kW with up to a maximum of the longest 10 consecutive traction travels (discharge process), it should be able to store energy corresponding to the braking process of the longest 4 consecutive travels (charge process) and besides, an energetic requirement in terms of people rescue has been imposed. The manufacturer has provided the information regarding the energy correspondent to these three defined specifications which corresponded to a sum of 604 Wh. An oversized of 10% has been applied in the energy requirement in order to take into account the degradation effects which can produce capacity loss of the *BP*. Therefore, 664.4 Wh has been defined as energy requirement for this particular application.

In Table 2.1 are summarized the power and energy requirements related to the residential elevator application.

Table 2.1 Energy and power requirements related to residential elevator application at BP level.

Energy Requirement		Power Requirement		
$E_{on\text{-}board}$, Wh		$\hat{P}_{DCH}$, W	$\hat{P}_{CHA}$, W	$\hat{P}_{ReCHA}$, W
664.4	Ride 1	4765	2750	170
	Ride 2	3412	1535	170
	Ride 3	2020	616	170

Regarding the selected second application, the urban electric minibus, is nowadays the principal precursor for the electric mobility in urban areas. By means of the implementation of the *ESS* on this type of vehicles is promoted the reduction of the greenhouse gas emissions which affects negatively the life quality of the urban zones.

The analyzed urban electric minibus has been designed to circulate in a city center. In Figure 2.12 the three possible urban lines which have been defined by the manufacturer are shown. In function of the route of the urban electric minibus, it can be distinguished: the most restrictive route (Line 1, red line), the medium solicitations route (Line 2, green line) and the soft conditions route (Line 3, blue line). Although each bus line corresponds to a different route around the city, which involves different electrical, thermal and duration specifications for each one, the three lines start at the main station where the charge station is located. Line 1, Line 2 and Line 3 have around 6.2 km, 5.1 km and 4.4 km, respectively.

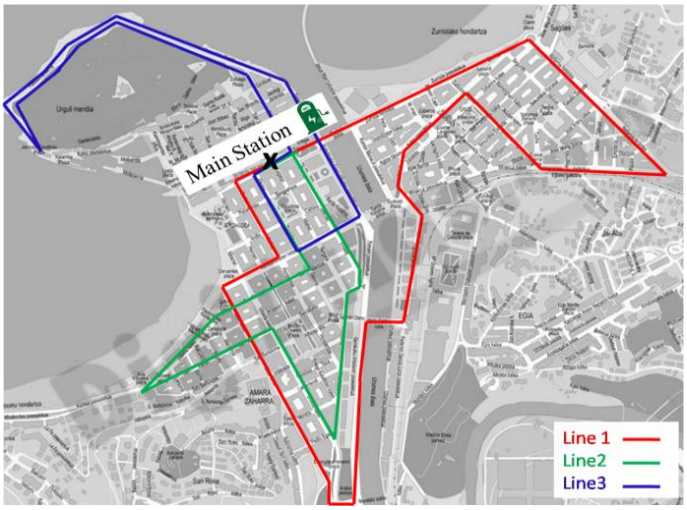

Figure 2.12 Urban electric minibus operation routes.

In Figure 2.13 are shown the power requirements at *ESS* level for each defined bus line: (a) Line 1, (b) Line 2 and (c) Line 3. As it can be seen in Figure 2.13 and compared with the residential elevator application ride profiles (Figure 2.11), it can be mentioned that there are clear differences related to the profile´s nature. It is evidence that the profiles correspondent to the electric minibus are more chaotic than previously mentioned ones. In addition, in these profiles two parts are distinguished. The first part corresponds to the chaotic current profile which refers to when the electric minibus is operating around the city. Although during this first operation part the *ESS* is also partially charging (positive values of power in each ride in Figure 2.13), probably due to regenerative braking process, the *ESS* is mainly discharging. Therefore, this part has been assumed as a discharge process stage. The second part, indicated by a flat power profile, is referred to the *ESS* charging process.

For all cases, repetitive and non-intermittent operation conditions have been considered. It has not been too realistic to consider a continuous operation of the urban electric minibus during the complete day, however it has been assumed this situation because it has been the most restrictive one regarding the heat generation and dissipation rate.

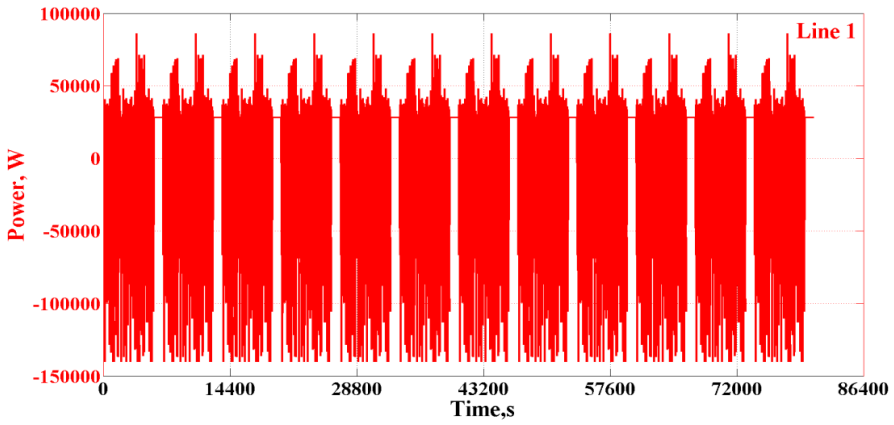

(a)

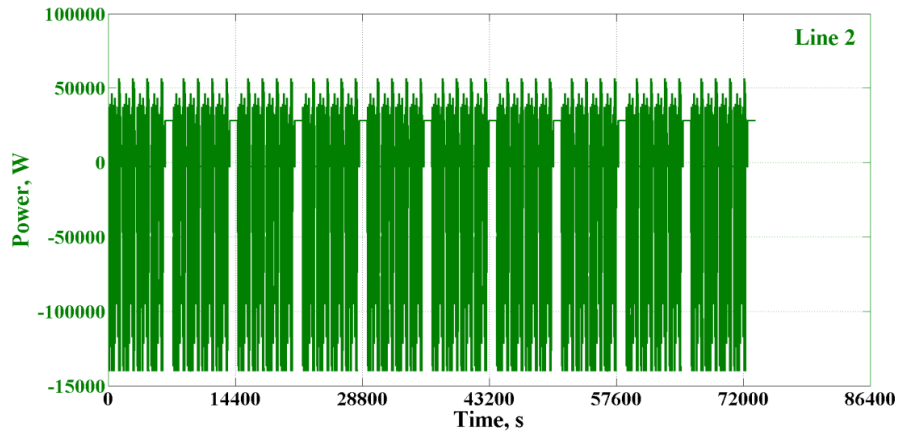

(b)

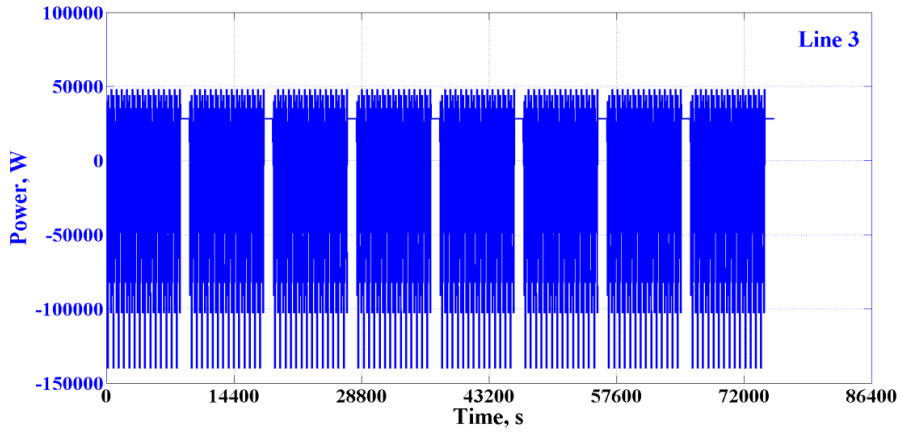

(c)

Figure 2.13 BP electrical power (W) requirements and SOC (%) evolution for the complete cycle for (a) Line 1, (b) Line 2 and (c) Line 3.

With regards to energy requirements, it has been imposed by the manufacturer that the *ESS* must be capable of performing at least two continuous complete round trips, returning to the departure point and provided with the possibility of recharging the *ESS* in the main station, regardless of the actual electric and thermal conditions. Considering the most restrictive bus route (Line 1) has been estimated a necessary energy on-board of 25.2 kWh in the *ESS* for this application. Similarly as for the residential elevator application an oversized of 10% has been applied to take into consideration the possible degradation effects and definitely, 27.7 kWh has been considered for the following electrical needs.

In Table 2.2 are summarized the power and energy requirements related to the urban electric minibus application.

Table 2.2 Energy and power requirements related to urban electric minibus application at BP level.

Energy Requirement		Power Requirement	
$E_{on\text{-}board}$, kWh		$\hat{P}_{DCH}$, W	$\hat{P}_{CHA}$, W
27.7	Line 1	139560	28380
	Line 2	138610	28380
	Line 3	131930	28380

The previously described background is in which this Doctoral Thesis has been developed.

Chapter 3.

Energy Storage Systems

After it has been placed the reader into the *Electro-Mobility* scenario in which this work is developed, the goal of this chapter is to describe different available *Energy Storage Systems*. This technology has been defined in the previous chapter as a crucial component to promote the penetration of the renewable energy sources in the society, providing stability, reliability and power quality to the application in which is implemented.

Throughout this chapter first of all, a short description of the different *Energy Storage Systems* is presented addressing issues related to technical characteristics, possible applications and future perspective of each of them. The interest is mainly focused on *Li-Ion* secondary batteries technology and its application to *Electro-Mobility* framework. The practical application of this technology requires *Battery Packs*, composed of several *Battery Modules*.

The importance of the role played by the implementation of *Battery Management System*, especially of *Thermal Management System*, is underlined as one of the main components for controlling and improving the *Li-Ion* battery thermal performance in order to ensure its lifespan. Finally, the electrical sizing of the *Battery Packs* related to the test cases of the present document is described.

3.1 INTRODUCTION

In order to achieve a totally "clean" and "green" urban environment, it is necessary to promote the growth of the renewable sources which in fact, are expected to have a fast growing currently. As it has been introduced in the previous chapter, the use of the *ESS*s could promote the integration of these renewable energies in the society using them for instance, to accumulate energy when it is cheap and make use of it freely when it is more expensive.

It is required to develop efficient *ESS*s to among other reasons, provide electricity which is reliably available 24 hours a day despite coming from intermittent sources and also, to mitigate short-term fluctuations of the power, which represents a major problem in the current electrical grid. Moreover, the improvement of the *ESS*s will be substantially important for the development of the *eMOV* applications themselves.

The stored energy in *ESS*s in applications within the framework of the *eMOV* could allow for example regarding *EV*s, to drive them without implementing a catenaries system providing them certain drive autonomy. On the other hand, it could be possible to install an *ESS* together with solar panels on the roof of a house in order to use the stored energy when is needed, e.g., for the elevator operation.

3.2 ELECTRIC STORAGE SYSTEMS

The *ESS* concept in general terms is understood such a device that makes possible the conversion of the electrical energy to some other form of energy than can be stored and released as needed. Strategically, the *ESS* stores the energy during low demand and low generation cost, and supplies during high demand, or when no effective generation is available.

The choice of the proper *ESS* is dependent on the application power and energy ratings, response time, weight, volume and operating temperature. An *ESS*s classification based on the form of storage energy used is shown in Figure 3.1. As it can be seen, they are classified into mechanical, chemical, electrical, thermal and electrochemical *ESS*s. Only a few of them are suitable and can be used in the practice

for *eMOV* applications. Sometimes the best option is a mix or combination of different *ESS*s taking the advantage of their different time scales.

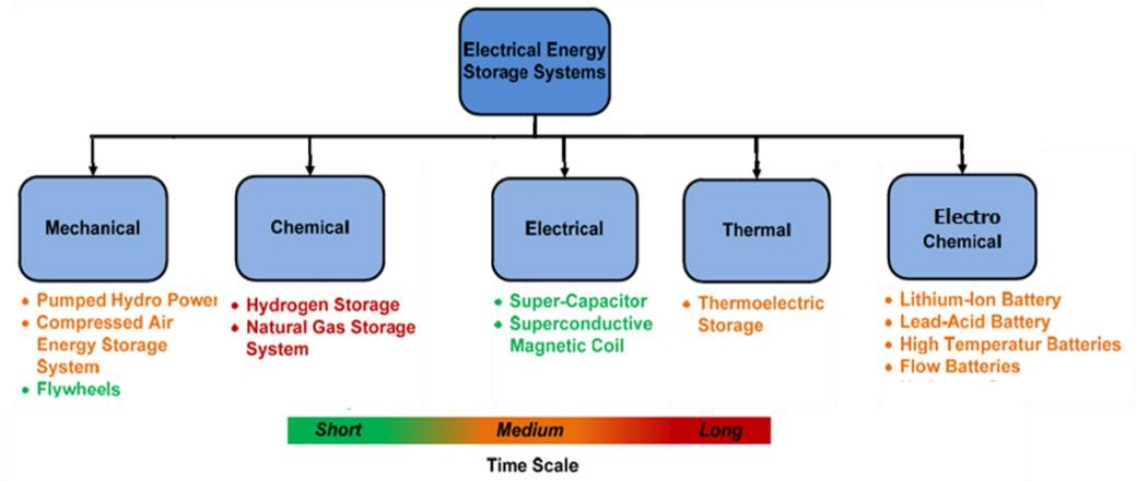

Figure 3.1 ESS classification according to energy form [22].

From a first preliminary review on the basis of the classification shown in Figure 3.1, the mechanical and thermal *ESS*s have been discarded first of all such as the possible option of *ESS* technology to be integrated into *eMOV* applications.

As an example of a mechanical *ESS*, in Figure 3.2 (a) is shown the scheme of a *Pumped Hydro Storage* (*PHS*) system which as it can be seen is composed of two interconnected water reservoirs. The amount of energy stored in this system is proportional to the product of the total water mass and the altitude difference between the reservoirs. Mechanical *ESS*s, such as the mentioned one, require high volume and weight installation that become unviable for these applications and also, the same can be said about the practical implementation of thermal *ESS*s.

The thermoelectric energy storage use is more focused on industrial and residential applications, such as space heating or cooling, hot water production or electricity generation. In Figure 3.2 (b) the scheme of a thermoelectric *ESS* is shown as an example. The main advantage of this technology is related to its large-scale storage, but however, it has high thermal losses and it is relatively low efficient. Considering the mechanical *ESS*s such as the pumped hydro and *Compressed Air Energy Storage* (*CAES*), the thermoelectric technology could be an alternative technology of both of them, because this latter technology does not require special site requirements, among other reasons.

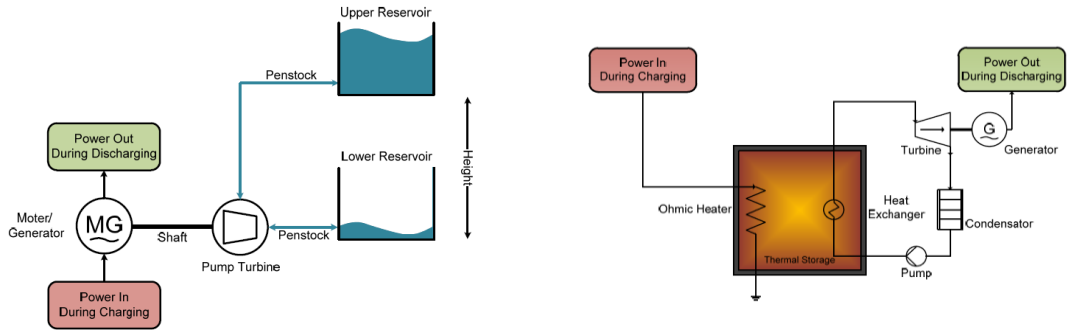

(a) (b)

Figure 3.2 Schematic diagram of (a) mechanical (pumped hydro storage system) and (b) thermal (thermoelectric energy storage) EESs [22].

Chemical *ESS*s are mainly focused on hydrogen and *Synthetic Natural Gas (SNG*) as secondary energy carriers since these could have a significant impact on the storage of electrical energy in large quantities. Figure 3.3 shows the schematic diagram of a hydrogen *ESS*. The main purpose of this technology is to use "excess" electricity to produce hydrogen via water electrolysis. The overall efficiency of hydrogen and *SNG* is low compared with storage technologies such as some of the secondary batteries. However, they allow storage a large amount of energy and it can use in different sectors such as transport, mobility, heating and chemical industry.

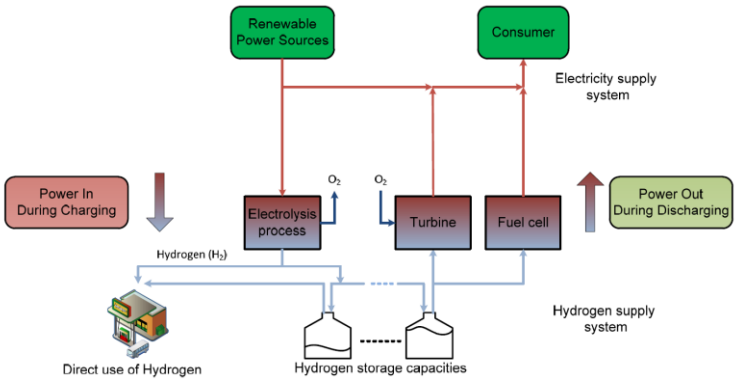

Figure 3.3 Schematic diagram of hydrogen ESS [22].

As it has been mentioned, this *ESS* technology is able to be implemented within *eMOV* applications but it must be considered some technical challenges that must be overcome before this technology will be a successful and competitive alternative in comparison with other *ESS*s. Currently it must decrease the cost for the fuel cell stack and hydrogen storage to be competitive with other *ESS*s technology; moreover, the current infrastructure for producing and getting hydrogen to consumers cannot yet

support the widespread adoption of *Fuel Cell Vehicles* (*FCVs*) and also, the performance of the Fuel Cells should be improved in terms of durability especially in some temperature and humidity ranges. These challenges make this technology already not cost- effective and appropriate to be selected for the chosen applications for this research work.

Regarding the electrical *ESSs*, the *electrochemical super- (double- layer) capacitors* (E*DLC*) and *super- conducting magnetic energy storages (SMES*) systems are fallen this category. One example of each schematic diagram is shown in Figure 3.4 (a) and (b) respectively.

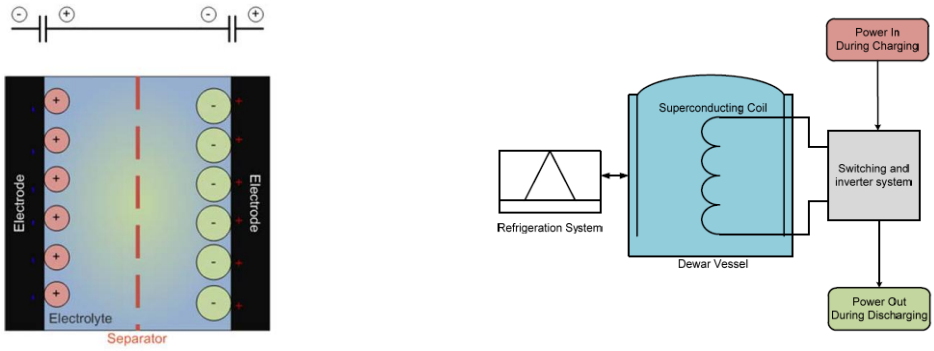

(a) (b)

Figure 3.4 Schematic diagram of (a) super-capacitor and (b) SMES ESSs [22].

The first group, *EDLC*, is also known as supercapacitors and comparing with the traditional capacitors they can provide unlimited cycle stability, extremely high power capability and many orders of magnitude higher energy storage capability. The two main features are the high capacitances values (order of many thousand farads) and the possibility of very fast charges and discharges due to low internal resistance (main difference with respect to conventional batteries). Moreover, durability, high reliability, no maintenance, long lifetime and operation over a wide temperature range are also other advantages. The efficiency is typically around 90% and discharge times are in the range of seconds to hours. The specific power density is around ten times higher than conventional electrochemical batteries but their specific energy density is about ten times lower. This technology since many years ago it has been widely applied in electronics and power electronics applications, and also as an *Uninterruptible Power Supply* (*UPS)* to bridge short voltage failures. Nowadays a deal of research is currently

conducted with the aim to impulse the use of this system as a buffer system for the acceleration process and regenerative braking in eMOV applications.

Considering *SMES* systems, the energy is stored in the magnetic field created by the flow of direct current in a superconducting coil, which is kept below its superconducting critical temperature. The main advantage of this technology is the very quick response time because the requested power is available almost instantaneously.

Definitely, due to the need to deepen investigation into these both technologies and the complexity of the system to be used in typical *eMOV* applications, this *ESS* technology was left out.

The last mentioned *ESS* in the classification shown in Figure 3.1 is the electrochemical storage system which can be divided into secondary batteries and flow batteries. The secondary battery storage technology is one of the oldest *ESS*s, which stores the electrical energy in form of chemical energy. Lead Acid (*LA*), Nickel Cadmium and Nickel Metal Hydride (NiCd/ NiMH), *Li-Ion*, Metal-air (Me-air), Sodium Sulphur (NaS) and Sodium Nickel Chloride (NaNiCl) are the six secondary batteries that are mainly known, while redox flow and hybrid flow batteries are the two sorts of flow batteries. In Figure 3.5 (a) is shown the schematic diagram of a *Li-Ion* battery as the representation of the secondary batteries and Figure 3.5 (b) is a conceptual example of a flow battery system.

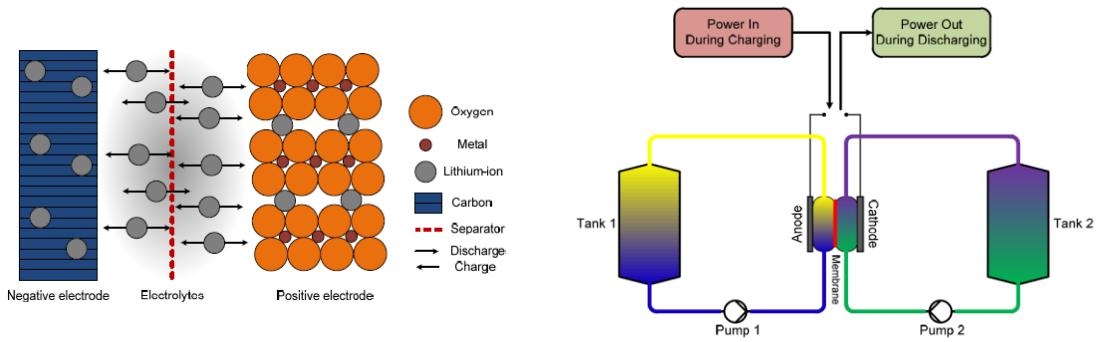

(a) (b)

Figure 3.5 Schematic diagram of (a) secondary battery (Li-Ion) and (b) flow battery system [22].

In both types of these electrochemical *ESS*s the energy is charged and discharged in the active mass of the electrodes, but in flow batteries, the energy is stored in one or

more electro-active species which are dissolved in liquid electrolytes. In this case, the electrolytes are stored externally in tanks and pumped through the electrochemical cell converting the chemical energy directly into electricity and vice versa, as it can be seen in Figure 3.5 (b). The power depends on the size and design of the electrochemical cell, whereas the energy is a function of the size of the tanks. The *redox flow batteries* (*RFB*), belonging the former mentioned electrochemical *ESS* group, is under discussion actually for mobile applications because the rechargeable ability within a few minutes by pumping out the discharged electrolyte and replacing it with recharged electrolyte. However, up to now the energy density of the electrolytes is too low for *EV*s.

A wide range of technologies exists within electrochemical batteries which are shown in Figure 3.6 considering their power density (per unit volume) against the energy density, along with other *ESSs* studied before. As it is indicated by arrows, the higher the power and energy density the lower the required volume for the storage system is. For instance, highly compact *ESS* technologies suitable for *eMOV* applications can be found at the top right, whereas large area and volume-consuming storage systems are located at the bottom left of this figure.

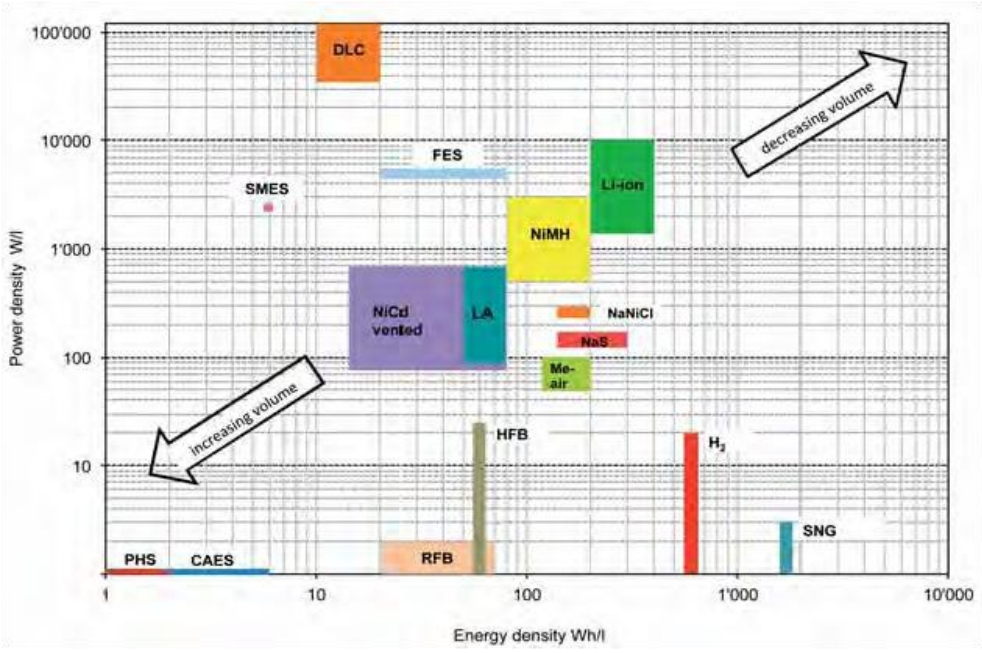

Figure 3.6 Comparison of power density and energy density (in relation to volume) ESS technologies [23].

Figure 3.6 reinforces aforementioned conclusion related to the previous mentioned *ESS*s: *PHS*, *CAES* and *RFB* have a low energy density compared to other storage

technologies, whereas *SMES* and *EDLC* have high power densities but low energy densities. Moreover, the main advantage of H_2 and *SNG* is the high energy density, superior to all other systems. Regarding the secondary batteries, NaS and NaNiCl have higher energy densities in comparison to the mature battery types such as *LA* and NiCd, but their power density is lower in comparison to NiMH and *Li-Ion*. Moreover, *Li-Ion* batteries, comparing with NiMH batteries, have both high energy and power density, which explains the broad range of applications where this type of battery is currently deployed. On the other hand, metal-air cells have the highest potential in terms of energy density and finally, flow batteries have a high potential for larger battery systems (MW/ MWh) but have only moderate energy densities.

In terms of maturity of the storage technologies, in Figure 3.7 is plotted the state of the art for each *ESS*s technology versus the power range. Thus, the suitability for different applications of the available technologies covered can be compared.

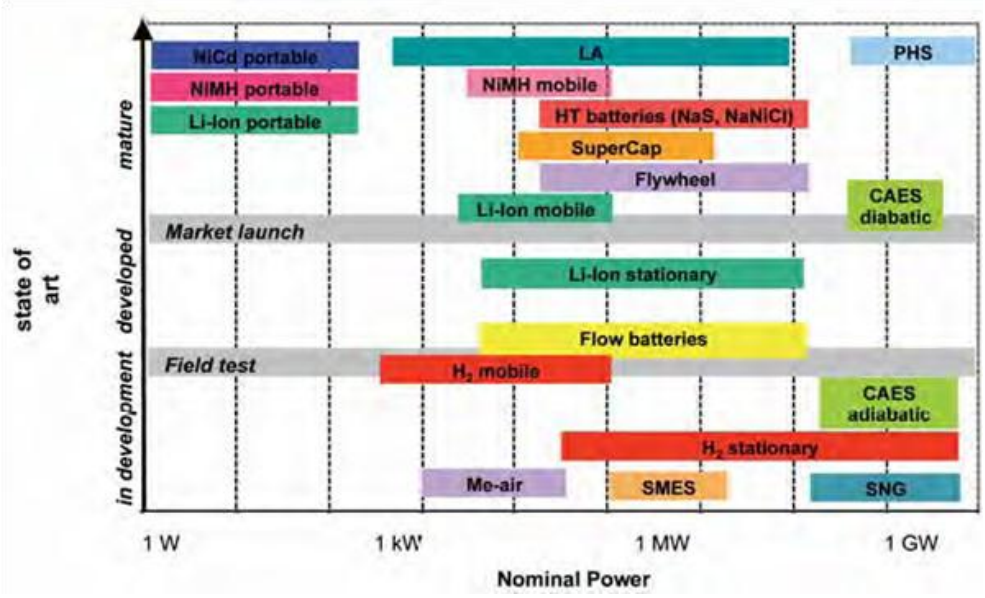

Figure 3.7 Maturity and state of the art of storage systems for electrical energy [23].

Finally, Figure 3.8 shows which *ESS* technology is or will become feasible for what applications, and where further research and development is necessary. From this figure, several conclusions could be drawn. On one side, it is obvious that it is expected that the potential market for *ESS*s in the future is much larger than the existing market, mainly driven by the extended use of the renewable energy sources and the transformation of the energy sector, including new applications such as *eMOV*. Moreover, if further cost reductions and technology improvements can be achieved, *ESS*s will be widely

implemented, for example, to shift the demand, smooth renewable energy output and improve the efficiency of existing power generation.

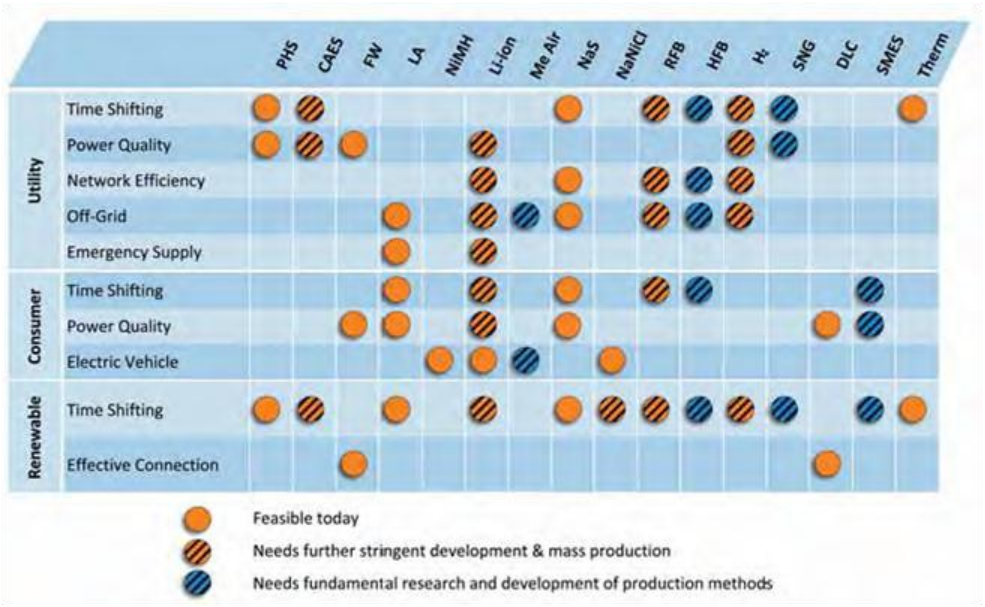

Figure 3.8 ESS present feasibility, future potential, need for further research and development [23].

At this point and discarding the rest of the *ESS* technologies, the secondary batteries within the electrochemical *ESS*s are concluded as the most suitable option for the *eMOV* applications analyzed in this research work. With the aim to conclude this section and in order to go to the following steps, due to its high energy density and high power density and because it is a mature and well-developed technology *Li-Ion* secondary batteries have been selected as a potential option to implement in the *eMOV* framework applications previously selected for this research work. Due to the further careful development and the future mass production of this technology, it will manage to become a cost effective product.

3.3 LITHIUM- ION BATTERY PACKS

Currently, *Li-Ion* batteries are the choice for portable electronic devices including cell phones, tablets, laptop computers, digital cameras, power tools and toys, due primarily to their durability, high specific energy (100 to 200 Wh/kg), and ability to operate at reasonably high power. Moreover, they are completely integrated at this time in the *eMOV* applications as bigger power packs for *HEV*s and full *EV*s. The *eMOV* market apart from the high specific energy of *Li-Ion* batteries, it also benefits from their

high power chemistry, efficiency, and long cycle life capability. As the automotive market drives the expansion of *Li-Ion* batteries production, these batteries may also be applied in stationary applications [24] as well, facilitating the implementation of renewable energy technologies such as solar and wind [25].

This section is divided into two parts. The first part is based on a brief description of *Li-Ion* cells considering aspects such as their structure and performance from a general point of view. Also in this first part, some commercial *BP*s are shown which are currently implemented in vertical and horizontal electric transport applications. The second part is more focused on the failure modes related to the thermal behavior of *Li-Ion BP*s highlighting the importance of the need of a *BMS.*

3.3.1 GENERAL OVERVIEW

From a general point of view and in the most basic sense, the term *Li-Ion* battery refers to a battery where the negative electrode (anode) and positive electrode (cathode) materials serve as a host for the lithium ion (Li^+). Lithium ions move from the anode to the cathode during the discharge and are intercalated into (inserted into voids in the crystallographic structure of) the cathode. The ions reverse the direction during the charging process. Since lithium ions are intercalated into host materials during charge and discharge, there is no free lithium metal within a *Li- Ion* cell, and thus, even if a cell does ignite due to external flame impingement, or an internal fault, metal fire suppression techniques are not appropriate for controlling the fire [26].

In a *Li-Ion* cell, the main components apart from the cathode and anode are the separator and electrolyte. The separator is a porous film which separates alternating layers of anode and cathode, whereas the electrolyte, composed of an organic solvent and dissolved lithium salt, provides the media for Li^+ transport.

Regarding the form factor of a *Li-Ion* cell, it can be constructed by stacking alternating layers of electrodes (typical for high- rate capability prismatic cells), or by winding long strips of electrodes into a "jelly roll" configuration typical for cylindrical cells. Electrode stacks or rolls can be inserted into hard cases that are sealed with gaskets (most commercial cylindrical cells, Figure 3.9 (a)), laser- welded hard cases (typical for prismatic cells, Figure 3.9 (b)), or enclosed in foil pouches with heat- sealed seams (commonly referred to as *Li-Ion* polymer pouch cells, Figure 3.9 (c))) [26].

(a) (b) (c)

Figure 3.9 Example of (a) cylindrical, (b) prismatic and (c) pouch cell.

Comparing the three mentioned types of battery cells, it must be stated that the cylindrical cell continues to be one of the most widely used packaging styles for primary and secondary batteries. The main advantages are the ease of manufacture and good mechanical stability and also, that it can withstand high internal pressures without deforming. This cell design has good cycling ability, offers a long calendar life, and is economical. Nevertheless, it is heavy and has low packaging density due to space cavities. However, the air cavities that result from side-by-side due to their placement can be used for an air-cooling system taking advantage of it, e.g., in an elevator application in where the air located in these gaps usually is the coldest of a building [27]. For these reasons, among other, this cell form factor could be appropriate for the proposed first application due to the small dimensions that it usually has and the feature to adapt easily to limited space.

Regarding prismatic cells, they can satisfy the demand for thinner sizes. They make optimal use of space by using a layered approach. Other designs are wound and flattened into a pseudo- prismatic jelly roll. These cells are predominantly found in mobile phones, tablets and low- profile laptops ranging from 800 mAh to 4000 mAh. Moreover, they are also available in large formats. Packaged in welded aluminum housings, the cell delivers capacities of 20- 50 Ah and are primarily used for electric powertrains in *HEV*s and *EV*s. In general, this type of cell improves space utilization and allows flexible design. However, it can be more expensive to manufacture, less efficient in thermal management and have a shorter cycle life than the cylindrical design [27]. Regarding the proposed urban electric minibus application, this type of cells could

be a possible option because of the favorable form factor in order to package them in a comprise way.

Pouch cells use conductive foil- tabs which are welded to the electrodes and brought to the outside in a fully sealed way. They make most efficient the use of space and achieve 90-95% of packing efficiency, the highest among *BP*s. To sum up, the pouch cell offers a simple, flexible and lightweight solution to big power battery design. This cell can deliver high load currents but it performs best under light loading conditions and with moderate charging [27]. From the mechanical point of view they need a packaging support and from the thermal point of view, because of their high compactness usually require water-cooling. In the same way as for the prismatic cells, the form factor of this latter type could be also suitable for the second proposed application in this study, being more packing efficiency than the previous one. Moreover, due to the feature of this type of cells to deliver high load currents which correspond with *EV*s driving specifications, it could be a potential option for the urban electric minibus application.

In terms of safety issues, each *Li-Ion* cell has a safe voltage range over which it can be cycled that will be determined by the specific cell chemistry. This safe voltage is understood such as the range in which the cell electrodes will not rapidly degrade due to lithium plating, copper dissolution or other undesirable reactions. For most commercial *Li-Ion* cells, the voltage range is approximately 2.0 V (discharged or 0% *SOC*) to 4.2 V (fully charged, or 100% *SOC*). Because of a relatively flat discharge profile, the nominal voltage of a typical *Li-Ion* cell is usually approximately 3.6 to 3.7 V. For most cells, discharged below 2.0 V can cause degradation of electrodes and thus, can lead to cell failure and cell thermal runaway. In the same way, for most cell charging significantly above 4.2 V can lead to rapid, exothermic degradation of the electrodes [26]. In order to protect the cells and batteries for this type of phenomena a *BMS* is required, which it will be discussed below.

Up to now along the document, the cell concept has been considered such as the smallest packaged form that a battery can have. Nevertheless from now on, a larger scalable unit will be referenced based on the minimal unit of a cell. A module which consists of several cells generally connected in either in series or parallel will be named as Battery Module (*BM*) and the assembly of some *BM*s together connected, again either

in series or parallel, will be called as *BP*. The scalability of these elements will permit along this research work to analyze the *BM* such as the minimal replicable element from the electrical, mechanical and thermal point of view and likewise, to consider the *BP* such as a scalable element based on the *BM* unit.

There are a lot of commercially available *BM*s and *BP*s that can be analyzed related to the interested applications of this work, but only a brief survey is given.

Regarding the elevator application, in Figure 3.10 are shown some real battery prototypes and commercial products that have been tested and implemented in this type of application. The aim of these *ESS*s in an elevator is to minimize the energetic consumption of the building and improve its efficiency. The *ESS*s which are shown in Figure 3.10 (a) and (b) have been developed by *IK4-IKERLAN* and have been tested in an elevator manufactured by Orona. The first *ESS*, Figure 3.10 (a), is comprised of ultracapacitors whereas the second one, Figure 3.10 (b), is composed of NiMH batteries. The *ESS* which is shown in Figure 3.10 (c) is currently integrated into an OTIS elevator and the *BP* technology is based on *LA*.

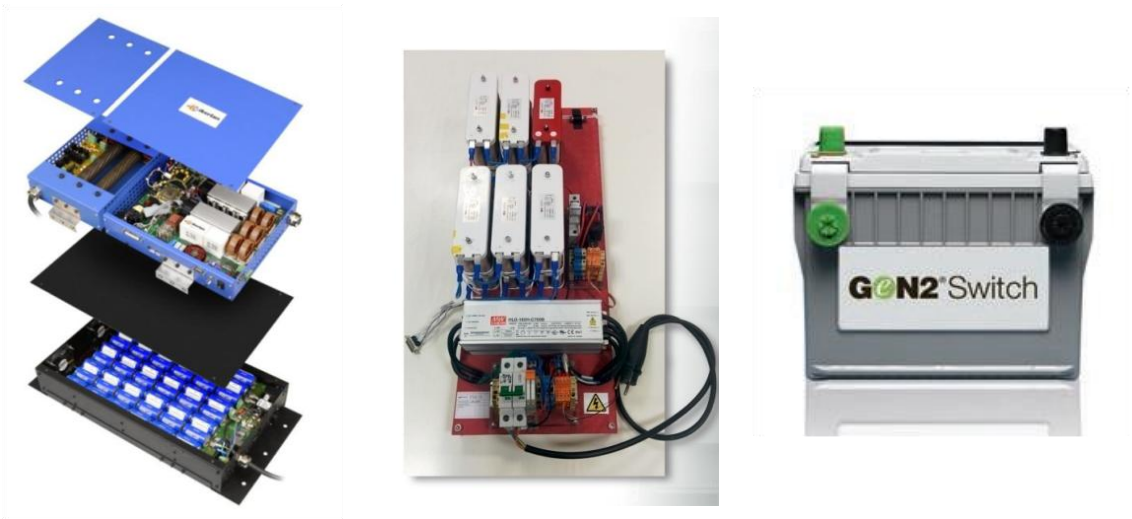

(a) (b) (c)

Figure 3.10 Real ESSs implemented in elevator applications.

*BM*s and *BP*s for urban electric bus applications are shown in Figure 3.11. On the left side of Figure 3.11, Solaris Urbino 12 urban electric bus is shown which is currently circulating in Dresden city. This electric bus has been developed by *IAD* institute (TU Dresden) and its *BP* has 200 kWh energy on-board and it is composed of 3120 *Li-Ion*

pouch cells. The complete system is comprised of 5 strings wherein each one there are 8 *BM*s. A *BM* is shown on the downside of the Figure 3.11 (a).

In the middle side, TOSA electric bus which, operates between Geneva airport and the city center, is shown. It has 38 kWh energy on board and its *BP* is located on the roof of the bus. The complete *BP* consists of 14 *BM*s in series as can be seen in Figure 3.11(b) and the lithium titanate oxide (*LTO*) technology has been selected for this specific application.

The third real example corresponds to Volvo Citybus which its *ESS* is composed of 7900 *Li-Ion* cells, 600 V 19 kW. Currently it runs on a city route and it has an estimated 20 km autonomy range.

(a) (b) (c)

Figure 3.11 Real ESSs implemented in urban electric bus application.

3.3.2 THERMAL BEHAVIOUR

Li-Ion batteries must operate within the safe and reliable operating conditions but their electrical performance is restricted mainly by temperature and voltage windows.

Exceeding the restrictions of these windows will lead to rapid attenuation of battery performance and even results in safety problem. According to the instructions of most battery manufacturers, the reliable operating temperatures required by a majority of current *Li-Ion* batteries (graphite/$LiMn_2O_4$ or C/LMO, C/$LiCo_xNi_yMn_zO_2$ or C/NCM, C/$LiFePO_4$ or C/LFP, C/ $LiNi_{0.8}Co_{0.15}Al_{0.05}O_2$ or C/NCA) are: discharging at -20 ºC to 55 ºC and charging at 0- 45 ºC and for *Li-Ion* battery with $Li_4Ti_5O_{12}$ or *LTO* negative

electrode, the minimum charge temperature can be -30 ºC [28]. In addition, the operating voltage range of the *Li-Ion* batteries is between 1.5 V and 4.2 V (C/LCO, C/NCA, C/NCM and C/LMO about 2.5- 4.2 V, LTO/LMO about 1.5- 2.7 V and C/LFP about 2.0- 3.7 V) [28]. Therefore, it can be concluded that the *Li-Ion* cells performance is dependent on both the operating temperature and voltage, as it is shown in Figure 3.12.

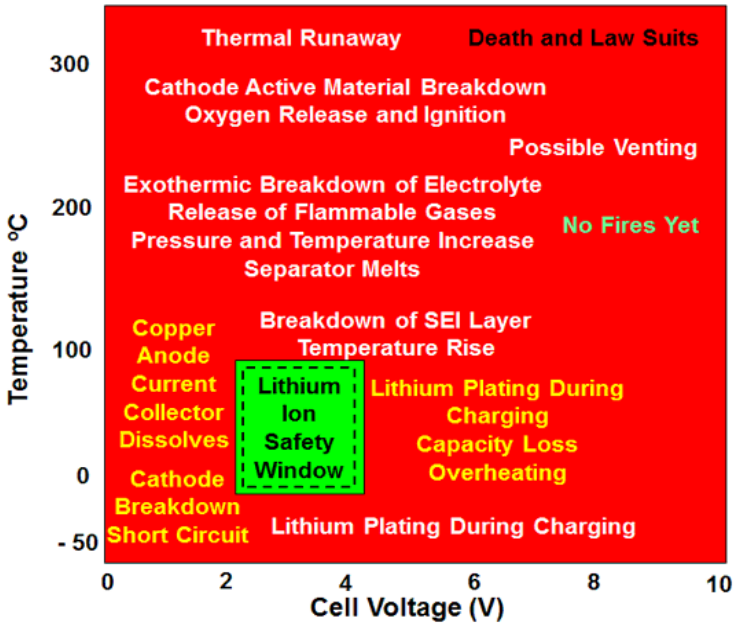

Figure 3.12 Li-Ion cells operating window[29].

As indicated in Figure 3.12, regarding the operating voltage range, if the charging voltage is increased beyond the recommended upper cell voltage, typically 4.2 V, excessive current flows giving rise to lithium plating and overheating problems [29]. It will lead the metallic lithium to be deposited on the surface of the negative electrode, which will accelerate the capacity fade, results in internal short circuits and safety problem, as well as the decomposition of the electrolyte [28].

Furthermore, when the if the voltage is too low (under- voltage) or the batteries are over-discharged, the phase change will lead to a progressive breakdown of the electrode materials and therefore, the performance of the batteries is influenced. In this voltage conditions, the negative electrode will dissolve in the electrolyte increasing the discharge rate of the cell. However, when the cells are recharged the copper ions which have been dispersed throughout the electrolyte are precipitated as metallic copper whenever (not necessarily back on the current collector foil) and consequently, it will

result in a short circuit between the electrodes [29]. Moreover, this situation can lead a gradual breakdown of the cathode over many cycles with the release of oxygen which will result in a permanent capacity loss.

The voltage is directly related to *SOC* of the battery. Taking into account the voltage operating restriction in Figure 3.13 can be seen the recommendation *SOC* operating range for this type of cells.

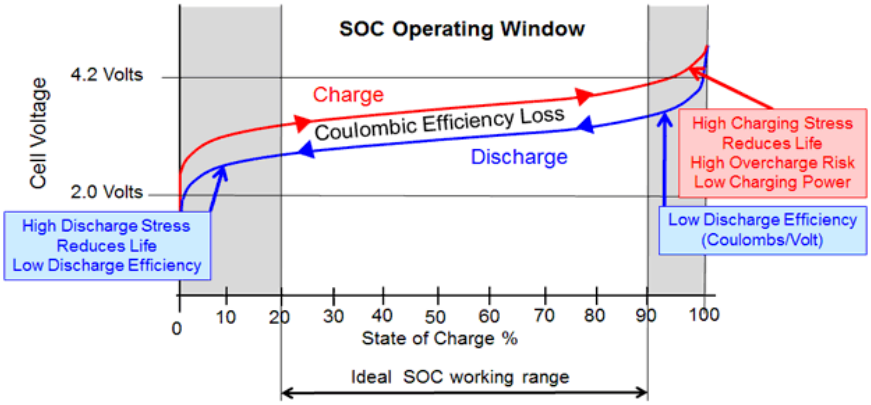

Figure 3.13 The recommended operating range of *SOC* for *Li-Ion* batteries[29].

Based on Figure 3.12, three operation temperature ranges can be distinguished: high temperature operation, low temperature operation and thermal runaway. When the operation temperature is high, around 90-120 ºC, the *Solid Electrolyte Interphase* (*SEI*) film will start exothermic decomposition, although some electrolyte systems will decompose at a lower temperature of about 69 ºC [28].

When the temperature exceeds 120 ºC, the *SEI* film after decomposition is unable to protect the negative carbon electrode from side reactions with the organic electrolyte and combustible gas would be produced. When the temperature is about 130 ºC, the separator will start melting and shut the cell down. Consequently, the pressure and temperature will start increasing. When the temperature becomes higher, the positive material will start decomposition and produce oxygen. As it can be seen in Figure 3.14 and depending on the material the positive material starts decomposing for different *Li-Ion* batteries, generally from 150 ºC to 310 ºC.

When the temperature is above 200 ºC, the electrolyte will decompose and produce combustion gas, and it will have a violent reaction with the oxygen produced by the

decomposition of the positive electrode and start to catch fire and lead to the irreversible situation of thermal runaway [28].

On the other hand, to charge *Li-Ion* batteries at low temperatures, below 0 ºC, it will lead the metallic lithium to deposit on the carbon negative electrode surface (lithium plating) and therefore reduce the cycle life of batteries. At extremely low temperatures, the cathode of batteries will break down and result in short circuit. Obviously, a more restrictive ideal temperature range is advised to avoid premature ageing of the cells [30, 31].

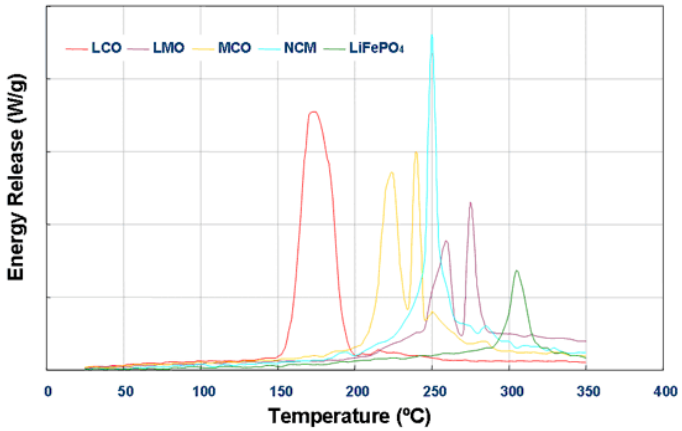

Figure 3.14 Temperature that the positive material will start decomposition for different Li-Ion batteries[29].

When big scalable *BP*s are taken into account, the thermal issue becomes even more challenging than at cell level. The effects due to the voltage and temperature tend to be immediately apparent in the cell. However, these effects on the *BP* level are less obvious but they are also important, mainly in terms of *BP* power and cycle life. At the same time, the temperature distribution among *BMs* and cells should be even to guarantee the *BP* performance and lifetime, avoiding problems with the electric equalization and balancing of the cells or a heterogeneous degradation of the system. That is the main reason why the *TMS* is necessary to almost each *BP* intended for *eMOV* applications. As it can be seen in Figure 3.15(a), the battery power reaches a maximum when the temperature range is between 20 and 40 ºC. Moreover, in Figure 3.15 (b) is shown that the cycle life goes down slowly below 10 ºC because of the anode plating and drops off quickly above 60 ºC due to the breakdown of electrode material.

Generally, the temperature must be controlled between 20 ºC and 40 ºC to ensure the performance and the cycle life. Moreover, the temperature distribution among different

*BM*s and even cells should be kept under 5 ºC to ensure the safety and lifetime of each of the cells inside the *BP* [32].

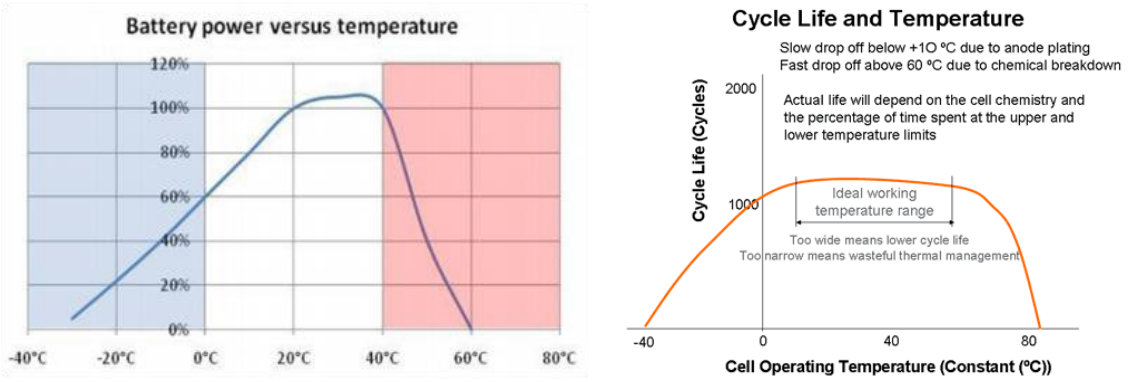

(a) (b)

Figure 3.15 The influence of the cell operating temperature on (a) battery power and (b) the cycle life.

3.3.3 BATTERY MANAGEMENT SYSTEM

The maintenance of the tight temperature and voltage values become a problem when people are trying to develop new battery systems that could be working under very extreme conditions. In addition, it must be considered that it is really different to consider a unique cell, which involves a capacity and voltage relatively small or to consider a *BP* which is comprised of hundreds or thousands of single cells. For those reasons, it is very important to manage all the cells by a *BMS*.

BMS means different things to different people, but according to references, it is defined such as any system that manages the battery and in any case and independently the application. It has three main tasks:

- protect the cells and *BP*s from being damaged.
- make the batteries operate within the proper voltage and temperature interval, guarantee the safety and prolong their service life as long as possible.
- maintain the batteries to operate in a state that the batteries could fulfil the application requirements.

To achieve these objectives, a *BMS* needs to monitor and control the battery based on the safety circuitry incorporated within the *BP*s. Whenever any abnormal conditions,

such as over-voltage or overheating, are detected, the *BMS* should notify the user and execute the preset correction procedure. In addition to these functions, the *BMS* also monitors the system temperature to provide a better power consumption scheme and communicates with individual components and operators. In other words, a *BMS* should include the following functions:

- Data acquisition.
- Safety protection.
- Ability to determine and predict the state of the battery.
- Ability to control charging and discharging.
- Cell balancing.
- Thermal Management.
- Delivery of battery status and authentication to a user interface.
- Communication with all battery components.
- Prolonged battery life.

Figure 3.16 shows a generic *BMS* structure with the basic functions. Various sensors are installed in the *BP* for data acquisition at the monitoring layer. The real-time collected data is used to maintain the system safety and to determine the battery state. The battery state refers to the charge time, discharge strategy, cell equalization and thermal management among the cells, while the state will be passed to the user interface as well [33].

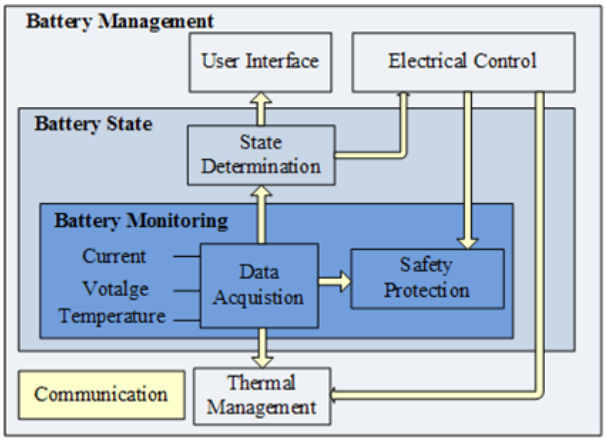

Figure 3.16 Scheme of a BMS [33].

A *BMS* in order to carry out the functions it should contain the components which are shown in Figure 3.17. The main components can be divided into hardware and software

group. Although all components are crucial to ensure a safety and reliable performance of the complete *BP*, in this research work only the thermal management system (*TMS*) will be analyzed more in detail.

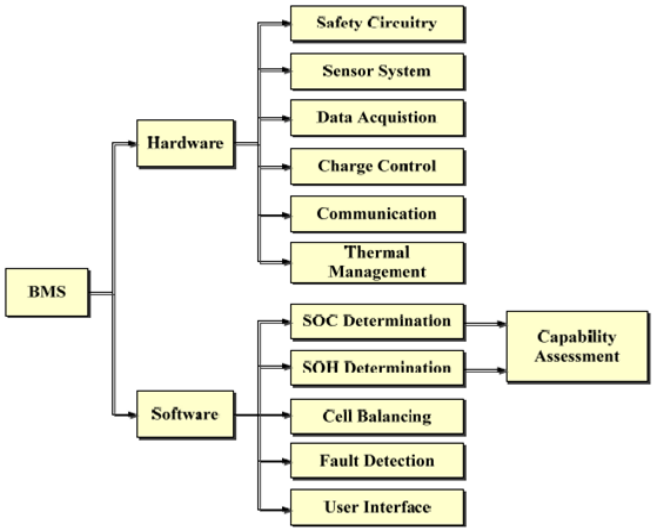

Figure 3.17 Components of a generic BMS[33].

Specific and well-sized hardware for *TMS* is critical because temperature differences have an impact on cell imbalance, reliability and performance. Thus, Pesaran [32] pointed out that it is important to reduce the temperature difference among cells, which must be monitored and operated under proper temperature conditions.

3.4 CONCLUSIONS

Focusing the attention on the particular applications of this Doctoral Thesis and considering the requirements defined in terms of power and energy for each application in Section 2.5 of Chapter 2, the electric sizing is carried following. The objective of the electrical sizing is to determinate how is the *BP* composed of, knowing the particular cell that it will be used in each application and ensuring the fulfillment of the specifications in terms of energy and power.

Throughout this chapter, it has been decided to implement *Li-Ion* secondary batteries in the both residential elevator and urban electric minibus applications, due to the suitable features, such as high energy density and power density, that they provide.

In both applications, the form and class of the cell implemented in the *BP* have been imposed by the manufacturer. Accordingly to which has been stated in this chapter, the

manufacturer has suggested using cylindrical cells for the residential elevator application due to the small dimensions and the feature to adapt easily into limited spaced that this type of cells provides. On the other hand related to the urban electric minibus, the manufacturer has proposed the implementation of pouch type cells primarily because of the capability that they offer to deliver high load currents.

Regarding the residential elevator application, the selected cells have been provided by A123 SYSTEMS manufacturer and they are based on lithium-ion-phosphate ($LiFePO_4$, *LFP*) with a nominal voltage and capacity of 3.3 V and 2.5 Ah, respectively. The properties of the used cell type are summarized in Table 3.1. Besides, the complete datasheet of this cell can be seen in Appendix 1A.

A minimal entity of a *BM* comprised of 12 cells in serial has been defined, which means an energy on-board in each *BM* of 99 Wh $\left(\frac{3.3\ V}{1\ cell} \cdot \frac{12\ cell\ serie}{1\ BM} \cdot \frac{2.5\ Ah}{1\ cell}\right)$.

Table 3.1 Properties of cylindrical A123 SYSTEMS cell.

	A123 SYSTEMS
Cathode	*LFP*
Anode	Graphite
Electrolyte	Carbonate-based, Li salt (LiPF6)
Dimensions, mm	26 Ø x 65 height
Cap_{nom}, Ah	2.5
V_{nom}, V	3.3
$I_{CHA/\ DCH}$, A	11 (5C)/ 22 (10C)
T_{ope}, ºC	-30 to 55
T_{sto}, ºC	-30 to 60

Once the cell has been selected and taking into account the power and energy requirements defined for this application, the electrical sizing of the *BP* has been carried out. To simplify the electrical sizing some assumptions such as a constant nominal voltage and capacity has been considered.

The proposed *BP* in terms of energy and according to the specifications defined for the application by the manufacturer, it should have 604 Wh. Nevertheless, because of an oversizing of 10% explained in section 2.5, an energy on-board of 664.4 Wh (Table

2.1) has been defined for the electrical sizing. Moreover and with regards to power requirements, comparing the three cyclic profiles defined in Figure 2.11, the first ride (Ride 1) has been considered as reference ride for this purpose because it has been the most restrictive one (indicated by asterisks in Table 3.2).

Table 3.2 shows the proposed different electrical configurations (defined as eConfig) for the three elevator possible travels. As a clarification, *7s* is referred to 7 *BM*s connected in serial in a unique string, *4s2p* to 2 strings connected in parallel and each string with 4 *BM*s connected in serial, whereas *2s4p* means that 4 strings are connected in parallel with 2 *BM*s connected in serial in each string.

The on-board energy in a *BP* is related to the number of cells that it is composed of. On this basis, it has been calculated that at least 7 *BMs* are needed in order to have enough energy for the application. Effectively, a *BP* composed of 6 *BM*s connected in serial will suppose 594 Wh which is insufficient energy according to the defined application specifications. Apart from serial configurations, as it can be seen in Table 3.2, different parallel configurations have been also imposed, i.e. *4s2p* and *2s4p*. As a condition, the same number of *BM*s connected in serial in each string has been proposed in order to avoid situation such as to have strings within a *BP* with different voltage level in each one. Consequently, the parallel configurations proposed are comprised of 8 *BM*s, which correspond to an energy on-board of 792 Wh.

The *BP* voltage level depends on the number of cells connected in serial: higher number of cells connected in serial, higher voltage level in the *BP*. The calculation of the voltage level of the *BP* is calculated multiplying the number of cells connected in serial in each proposed configuration by the cell voltage. Consequently and bearing in mind that each *BM* is composed of 12 cells connected in serial, for the *7s, 4s2p* and *2s4p* electrical configurations the voltage at *BP* level has corresponded to 277.2 V, 158.4 V and 79.2 V, respectively.

With regards to the current, it depends on the parallel strings that the *BP* is composed of, in contrast to occurs with the voltage. The current at *BP* level has been obtained considering the power requirements defined in Table 2.1 for each line divided by the voltage level of each electrical proposed configuration. The *BM* current level has been obtained dividing the voltage correspondent to the *BP* level by the parallel strings

defined for each electrical proposed configurations. In this case and due to the cells within the *BM* are connected in serial, the current at *BM* level is equal to the cell current level. The peak and *RMS* (Root Means Square) values in terms of current referred to the *BP* and *BM* are shown in Table 3.2.

Table 3.2 Electrical sizing of the BP installed in the residential elevator

				Discharge				Charge			
	eConfig	$\bar{E}_{BP}$, Wh	$\hat{V}_{BP}$, V	$\hat{I}_{BP}$, A	$I_{RMS_{BP}}$, A	$\hat{I}_{BM}$, A	$I_{RMS_{BM}}$, A	$\hat{I}_{BP}$, A	$I_{RMS_{BP}}$, A	$\hat{I}_{BM}$, A	$I_{RMS_{BM}}$, A
Ride 1*	***7s***	**693.0**	**277.2**	**-17.2**	**-17.2**	**-17.2**	**-17.2**	**9.9**	**9.9**	**9.9**	**9.9**
Ride 1*	*4s2p*	792.0	158.4	-30.1	-30.1	-15.0	-15.0	17.4	17.4	8.7	8.7
Ride 1*	*2s4p*	792.0	79.2	-60.2	-60.2	-15.0	-15.0	34.7	34.7	8.7	8.7
Ride 2	*7s*	693.0	277.2	-12.3	-12.3	-12.3	-12.3	5.5	5.5	5.5	5.5
Ride 3	*7s*	693.0	277.2	-7.3	-7.3	-7.3	-7.3	2.2	2.2	2.2	2.2

* Reference route for thermal and electrical sizing

Table 3.2 (continued) Electrical sizing of the BP installed in the residential elevator

				Recharge			
	eConfig	$\bar{E}_{BP}$, Wh	$\hat{V}_{BP}$, V	$\hat{I}_{BP}$, A	$I_{RMS_{BP}}$, A	$\hat{I}_{BM}$, A	$I_{RMS_{BM}}$, A
Ride 1*	***7s***	**693.0**	**277.2**	**0.6**	**0.6**	**0.6**	**0.6**
Ride 1*	*4s2p*	792.0	158.4	1.1	1.1	0.5	0.5
Ride 1*	*2s4p*	792.0	79.2	2.1	2.1	0.5	0.5
Ride 2	*7s*	693.0	277.2	0.6	0.6	0.6	0.6
Ride 3	*7s*	693.0	277.2	0.6	0.6	0.6	0.6

* Reference route for thermal and electrical sizing

With the purpose of choosing the most suitable electrical configuration, the aspects related to the energy, current and voltage must take into account. Based on Table 2.1, it can be concluded that in terms of energy every configuration proposed, fulfills the energy requirements. Regarding the current and especially, focused on the peak current values related to the *BM* and cell level, it can be mentioned that the cell selected is able to withstand the current level of charge and discharge process for any electrical

configuration. At last, the voltage level is related to the converter that it is used in the application. Mainly because of it and based on the commercial converters used in this type of *eMOV* applications, around 250-400 V, it has been decided to choose the *7s* electrical configuration to connected the *BM*s electrically within the *BP* in the residential application.

On the other hand and considering the urban electric minibus application, a *BP* comprised of *Li-Ion* pouch cells has been designed. The manufacturer, the cell provided from KOKAM (model SLPB100216216H) has selected, where its properties are summarized in Table 3.3. Besides, the complete datasheet of this cell can be seen in Appendix 1B.

The minimal entity of a *BM* comprised of 12 cells connected in serial has been defined, which suppose a voltage and a current at *BM* level of 44.4 V and 40 A, respectively and consequently an energy on board at *BM* level of 1776 Wh $\left(\frac{3.7\ V}{1\ cell} \cdot \frac{12\ cell\ serie}{1\ BM} \cdot \frac{40\ Ah}{1\ cell}\right)$.

Table 3.3 Properties of pouch KOKAM cells [34].

	KOKAM
Model	SLPB100216216H
Cathode	Lithium cobalt manganese nickel oxideLiMnNiCoO$_2$ (LMN)
Anode	Carbon
Electrolyte	Carbonate-based, Li salt (LiPF6)
Dimensions, mm	222.0 x 214.0 x 10.7
Cap_{nom}, Ah	40
V_{nom}, V	3.7
$I_{CHA/DCH}$, A	120 (3C)/ 320 (8C)
T_{ope}, ºC	10 to 45 (CHA) and -20 to 55 (DHC)
T_{sto}, ºC	-20 to 60

In the same way as for the previous application, the electric sizing for the urban electric minibus has been carried out assuming a constant nominal voltage and capacity in order to facilitate the calculation. For that purpose, the energy and power requirements defined for this application in Table 2.2. have been taken into consideration.

According to specifications in terms of energy, a *BP* with 27.7 kWh of energy on-board has been designed applying an oversizing of 10% respect to the requirements imposed by the manufacturer. In terms of power, the most restrictive bus line has been considered (identified such as Line1 in Table 2.2.) to carry out the electrical sizing of this *BP*.

As it has been mentioned for the residential elevator application, the energy on-board in a *ESS* is defined by means of the number of cells. On this basis and considering the energy on-board of 1776 Wh in a *BM*, *16 BMs* have been required in the *BP* to fulfil the defined energy specification of this application. The energy provided by means of this defined *ESS*, as it is indicated in Table 3.4, is around 28.4 kWh. Taking into consideration the defined 16 *BM*s, Table 3.4 shows the proposed different electrical configurations for the three possible bus lines of the urban electric minibus. A serial electrical configuration (*16s*) and several parallel electrical configurations (*8s2p* and *4s4p*) are proposed. Due to all the defined configurations have the same number of *BM*s, the energy on-board of them is equal.

Table 3.4 Electrical sizing of the BP installed in the urban electric minibus

				Discharge				Charge			
	eConfig	$\bar{E}_{BP}$, kWh	$\bar{V}_{BP}$, V	$\hat{I}_{BP}$, A	$I_{RMS_{BP}}$, A	$\hat{I}_{BM}$, A	$I_{RMS_{BM}}$, A	$\hat{I}_{BP}$, A	$I_{RMS_{BP}}$, A	$\hat{I}_{BM}$, A	$I_{RMS_{BM}}$, A
Line 1*	*16s*	28.4	710.4	-196.5	-45.6	-196.5	-45.6	40.0	40.0	40.0	40.0
Line 1*	***8s2p***	**28.4**	**355.2**	**-392.9**	**-91.2**	**-196.5**	**-45.6**	**80.0**	**80.0**	**40.0**	**40.0**
Line 1*	*4s4p*	28.4	177.6	-785.8	-182.4	-196.5	-45.6	160.0	160.0	40.0	40.0
Line 2	*8s2p*	28.4	355.2	-390.2	-83.9	-195.1	-41.9	80.0	80.0	40.0	40.0
Line 3	*8s2p*	28.4	355.2	-371.4	-65.4	-185.7	-32.7	80.0	80.0	40.0	40.0

* Reference route for thermal and electrical sizing

The voltage at *BP* level differs for each configuration because the number of *BM*s connected in serial is different in each proposed electrical configuration. As it has been expected, for the electrical configuration in which more *BM*s are in serial, higher is the voltage level. Regarding the current, following the same procedure as for the previous application, the peak and *RMS* current values at *BP* and *BM* level has been calculated,

which are shown in Table 3.5. Comparing these values with the maximum admissible current values at cell level (equal to *BM* level because of the serial connection between the cells within the *BM*) regarding the charge (120 A) and discharge process (320 A) shown in Table 3.3, it can be concluded that the selected cells are capable to withstanding any current level according to application requirements in terms of power.

With regards to voltage values at *BP* level, it has been decided to use an *8s2p* electrical configuration because this configuration provides a total *BP* voltage in the range of 300 to 400 V, as the typically implanted converter on commercial *EV*s (e.g. the BMW i3 [14]).

In order to summarize the results obtained in this chapter, in Table 3.5 are shown them. The current *RMS* values at *BM* level are shown again for the discharge and charge processes, which have been used to define cyclic current profiles for the use of them in following steps of the developed methodology. The approximated C-rate values have been calculated based on the nominal capacity of each cell used in each application.

For the residential elevator application, the *RMS* current value correspondent to the charge process has been estimated as *RMS* value of the current of the previously defined charge and recharge processes (Table 3.2).As it can be seen in Table 3.5, the cyclic current profiles related to the residential elevator application that will be used in the following developed methodology in the steps related to the thermal design and optimization, are asymmetrical: DCH 7C/ CHA 3C for Ride 1, DCH 5C/ CHA 2C for Ride 2 and DCH 3C/ CHA 1C for Ride 3.

On the contrary, for the urban electric minibus although the requirements according to the discharge process are more restrictive in the Line 1 in comparison with the defined Line 2 and Line 3, for the three defined bus lines the same C-rate values have been considered, defining a cyclic symmetrical current profile of DCH 1C/ CHA 1C.

Table 3.5 Electrical sizing for the residential elevator and urban electric minibus application.

	$\frac{\text{nº cells}}{BM}$	$\frac{\text{nº}BMs}{BP}$	$\bar{E}_{BP}$, Wh		$I_{RMS_{BM}}$, A (DCH/CHA)	≈C-rate (DCH/CHA)
Residential elevator	12 (A123)	7 (*7s*)	693	Ride 1	-17.2/ 7.3	7C/ 3C
				Ride 2	-12.3/ 4.6	5C/ 2C
				Ride 3	-7.3/ 2.5	3C/ 1C
Urban electric minibus	12 (KOKAM)	16 (*8s2p*)	28400	Line 1	-45.6/ 40.0	1C/ 1C
				Line 2	-41.9/ 40.0	1C/ 1C
				Line 3	-32.7/ 40.0	1C/ 1C

Once the electric sizing has been done and the requirements and specifications of each the applications have been known, the next step is related to the evaluation of the possible *TMS* that it could be implemented for each application.

Chapter 4.

Thermal Management Systems

Once the importance of implementing a *Thermal Management System* in *a Lithium-Ion Battery Pack* has been highlighted and the electrical sizing of the *BP* installed in each application has been carried out in Chapter 3, in this chapter a description of the different available cooling system technologies is done regarding the applications defined in this research work within the *Electro-Mobility* framework.

The first part of this chapter is dedicated to a description *of Thermal Management System* needs considering the cooling, the heating and the insulation effects. The second part is based on the analysis of the technologies and strategies that are currently implemented for *Lithium- Ion Battery Pack*s covering aspects related to the cooling, the heating and the insulation. At last, some real cases of the technologies analyzed that are already implemented in real *Electro-Mobility* applications are shown.

As a conclusion of this chapter, the most suitable *Thermal Management System* approach is selected for each application taking into account particularities and some preliminary design restrictions.

4.1 INTRODUCTION

On the basis of decisions related to interested applications, *Li-Ion* technology has been decided as the best choice to implement in the *ESS*s for the residential elevator and urban electric minibus applications. This decision has been taken for many reasons such as both a high energy density and power density and the broad range of available applications where *Li-Ion* technology is suitable to be used. However, further development is needed to increase its mass production, and consequently to achieve cost effectiveness.

Focusing the attention on the thermal issues related to *Li-Ion* technology, it is crucial to bear them in mind due to the influence that an inappropriate thermal performance could have on the lifespan, life-cycle cost and safety of *BP*s´[35]. In this context, the first concern is to evaluate the necessity of implementing a *TMS* or not, depending on the specifications of the interested application. Once this decision has been taken it is essential to implement non undersized or oversized thermal solutions to fulfil both thermal and efficiency requirements optimally.

A *TMS* must fulfil several general functions, which are listed below, in order to achieve an improved performance at *BM* or *BP* level:

- Optimum operating temperature range for every cell and all *BM*s inside the *BP*. Some authors such as R. Mahamud in [36] recommends to ensure the maximum *Li-Ion* cell temperature below 40 ºC. Moreover, A. Pesaran defined the desired operating temperature between 15 ºC and 35 ºC in [37] as it is shown in Figure 4.1. Obviously, the optimal temperature range depends on the selected cells.

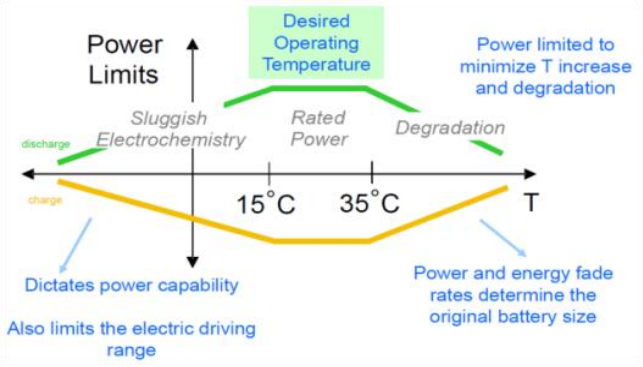

Figure 4.1 Recommendation operating temperature of Li- Ion cells [37] by Pesaran.

- Small temperature variations within a cell, between cells of a single *BM* and also between various *BMs* of a *BP*. R. Mahamud [36] as other authors such as C.S. Park et al.[38] recommended maintaining the cell temperature difference below 5 ºC for a full lifespan. The diminution of thermal anisotropies between single cells of a medium size *BP* requires a system level analysis.

- Compact and lightweight, easily packaged, reliable, low- cost and easy for service. It is logical the fact that an *eMOV* application should be used to transport people, not only batteries. This sentence can be applied as well as to the *BMSs* and all the auxiliary elements of the *BP*.

- Efficient use of the stored energy for cooling and heating in autonomous and mobile *BP* systems. These auxiliary but power consuming *TMSs* are usually characterized by a quite cyclic usage and high intermittency. An optimal thermal sizing at component level and smart control strategies become mandatory.

Although the cooling process along this chapter it will be developed more in-depth, the heating and insulation of the *BP* will be also studied for these particular *eMOV* applications.

4.2 THERMAL MANAGEMENT NEEDS

As it has been stated in the introductory section, it is crucial to control the *BP* temperature for safety, performance (both power and capacity) and lifespan reasons. Thus, the *TMS* should be equipped with three essential functions to ensure the right operation conditions of the *BP*: cooling, heating and insulation.

The cooling function is needed within a battery *TMS* in order to remove the heat generated by the *BP* and consequently, to achieve an optimum operation *BP* temperature. On other occasions however, in cold climates the *BP* temperature probably falls below the lower temperature limit and hence, a heating function is also required to assist the *BP* to reach the proper temperature range in a shorter time. Finally, as regards the insulation need, as far as possible must be prevented the *BP* from the temperature

difference between the inside and outside, especially in extreme cold or hot weather. This could affect for example to a vehicle that is parked outside along the night.

Following along this section, the different possibilities regarding cooling, heating and insulation process are analyzed.

4.2.1 COOLING

In general terms and regarding the cooling process from a *BP* to the surrounding environment, several classifications can be done.

Firstly, it can be distinguished between passive or active cooling (*PC* and *AC*) strategies. The *PC* mode takes advantage of a moving fluid but only at ambient temperature. In this case, no extra energy is used to cool down or heat up directly the cooling fluid. The *AC* mode uses a different kind of built-in sources that provide extra heating and/or cooling.

Inside the *PC* approach, a new subdivision can be established between the *natural and forced cooling* processes (*NC* and *FC*). In the *NC* case, the fluid motion is auto-generated by the heating up process itself and no extra mechanical power is needed. It is the cheapest cooling strategy but the heat power dissipation is very limited. Instead, if a mechanical element (fan or pump) is used to increase the fluid motion or velocity, *FC* mode is generated. In both cases, but especially in the *NC* mode, the heat exchanges by radiation can play a major role in the cooling of the whole *BP*.

Generally, it can be said that: the more restrictive are the specifications required by the application, the more complex and robust is the *TMS* which is needed. Figure 4.2 shows some real *BP*s cooled by *PC* as examples. In Figure 4.2 (a), a *BP* which has an aluminium plate placed on the lateral can be seen. This *BP* has been used in a stationary application with high intermittency. The aim of this aluminium plate has been to add thermal inertia to the system in order to absorb the heat when a power peak occurs and to evacuate it to surrounding afterwards [39]. On the other hand, in the *BP* shown in Figure 4.2 (b), instead of using an aluminium plate a heat sink has been placed. This *BP* has been used on an electric bike and, by means of bike´s movement together with the heat sinks, it has been taken benefit to the *NC* process [40].

(a) (b)

Figure 4.2 PC systems for (a) stationary application with an aluminum plate [39] and (b) mobile application using heat sinks [40].

The *AC* approach normally requires the use of heat exchangers between primary and secondary cooling fluids and bigger power consumptions. This strategy allows to maintain the cells of a *BP* below the ambient temperature which can be a key issue in hot and/or sunny environments. The best known and most mature active technology are the *vapor compression refrigeration cycles* (*VCRCs*). They require at least one mechanical compressor to increase the energy state of a refrigerant secondary fluid. This extra cooling power can be used directly in the so-called direct expansion systems, where the evaporator of the thermodynamic cycle is placed in direct contact with the cells of the *BP*. In other cases, compact heat exchangers can be used to transfer this cooling power to more suitable secondary fluids in more complex systems.

The other *AC* technology that can take advantage of the available electric energy of the *BP* of an *eMOV* application is the thermoelectricity (*TEC*). These *AC* systems can even reuse the waste heat of an *HEV* and they require less mechanical elements that the *VCRC*s, being less noisy. The main drawback of this technology is its poor efficiency.

A less generic classification can be done as well based on their primary cooling medium or fluid in direct contact with the *BP*, *BM* or cells themselves. The most common options are the heat pipe cooling technology, *phase change material* (*PCM*) cooling technology, air cooling and liquid cooling technologies. The latter two options are the most usual.

Regarding the *PC* system, which uses air as primary heat transfer medium or fluid, it is an available and a concurrent cooling option that many *TMS* designers often decide to implement this type of cooling system. For instance, in early vehicles and particularly in *EV*s, because of the cost, weight, space considerations and their use in mild climates,

*BP*s do not use heating or cooling units, and their thermal performance only depend on blowing ambient air for rejection of heat from these *BP*s, as it is shown in Figure 4.3 (a) 1). In more cooling/heating demanding cases the *BP* is thermally managed by cabin air which is heated and cooled by the vehicle air conditioning (*A/C*) or a heating system as can be seen in the scheme of Figure 4.3 (a) 2).

Among the passive *TMSs* which use liquid as primary cooling medium (Figure 4.3 (b) 4)), employ also ambient air for final heat rejection, i.e., the heat which is generated within the *BP* is evacuated from there by means of the liquid which circulates around the *BP*, possibly through some cold plates or by a liquid jacket. Via liquid, the heat is brought to a heat exchanger (liquid-air) in where the heat is transmitted to the outside air. For these systems, it is recommended that the ambient should have a mild temperature, between 10 ºC to 35 ºC, for the *TMS* could work properly; otherwise, the *BP* performance can suffer in very cold or very hot conditions.

Outside of these warm ambient conditions, for an extremely high and low environment temperatures, the use of *AC* components such as evaporator, compressor, condenser, engine coolant or even electric and fuel-fired heaters in order to keep the *BP* temperature within an ideal operating range are mandatory [41]. The main advantage of this type of cooling system is related to the possibility to control the *BP* temperature without dependency from the ambient temperature and electrical solicitation of the particular application, however at expense of a high consumption. In Figure 4.3 (a) 3) an *AC* and heating by air using an auxiliary or evaporator cores can be seen whereas, in Figure 4.3 (b) 5) and 6) two different active *TMS*s based on liquid circulation are shown.

The cooling system shown in Figure 4.3 (b) 5) which is defined such as active moderate, it is based on the similar cooling concept that in Figure 4.3 (b) 4). In both cases, a heat exchanger is used in order to reject the heat generated in the *BP*. The difference between them is that in the latter the secondary fluid through the heat exchanger is liquid, whereas in the former the air in. The heat from the *BP* is transmitted by the heat exchanger to the liquid coming from engine coolant which is impulsed by a hydraulic pump. The use of this extra pump leads to name of active moderate cooling system. The *AC* system shows in Figure 4.3 (b) 6) corresponds to the use an evaporator

or condenser with a secondary fluid that it can be air or refrigerant. In terms of cooling capacity, this last proposed cooling system is the most promising option.

Apart from the thermal point of view, when dealing with any kind of active *TMS* it must be bear in mind that its implementation can negatively affect the performance of the vehicle, especially in terms of the required space and the overall consumption at system level, which are features mainly important in *eMOV* applications scope. Equilibrium has to be reached between the increased cooling/heating power and the complexity of the *TMS*.

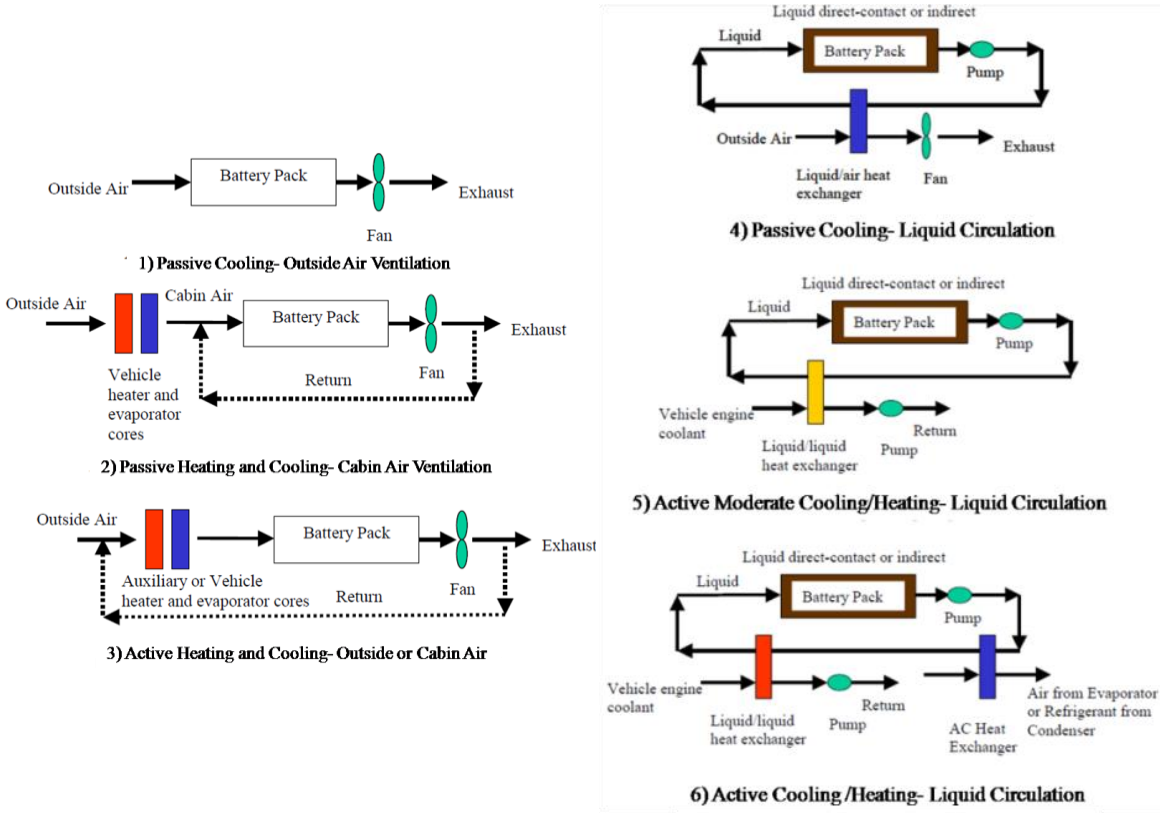

(a) (b)

Figure 4.3 General schematic of passive and active TMSs (a) using air and (b) using liquid [41] by Pesaran.

4.2.2 HEATING

The *BP* heating procedure is also important especially when it is exposed to very cold ambient temperatures of an urban environment. Nevertheless, and taking into account that the batteries heat up naturally themselves, it can be considered an auxiliary or secondary thermal management need. Attention must be paid anyway because as it has been explained before low temperatures lead to fast capacity degradation of the *BPs*.

The preheating of the *BP* temperature is an essential function of an effective battery *TMS*. The heating procedure can be carried out by direct (using electric heaters) or indirect (heating the battery coolant) heating process, applying both for the air and the liquid cooling system. Moreover, in *HEV*s it can be used the heat rejected from the combustion engine or from the heating system of the *A/C* system in order to preheat the *BP*.

With regards to direct heating procedure, it can be implemented using Positive Temperature Coefficient (*PTC*) resistance, electrical resistance or even, thermal blankets.

In Figure 4.4 (a) can be seen a *BP* which is heating by means of *PTC* method. As it can be seen in the schematic diagram, *PTC* resistance band is embedded in the slotted aluminium plates which are placed between each cell. By this way, the heat produced by *PTC* will be quickly transferred to the battery [42]. In addition, the *BP* which is shown Figure 4.4 (b) is heating up by several electric resistances located under the *BP* and also, a thermal blanket is placed around the *BP* in order to avoid thermal losses to the surrounding.

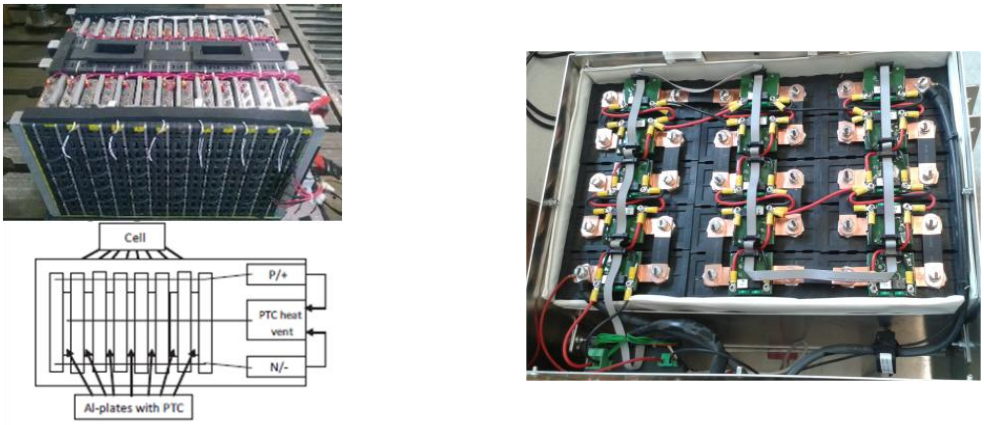

(a) (b)

Figure 4.4 Direct heating method by (a) PTC [42] and (b) electric resistance and thermal blankets.

In general terms, the indirect heating process is less efficient than the previously described method, due to the non-direct contact of the resistance with the *BP* makes the heating process more slowly for the same resistance.

Regarding an air cooling system, generally this cooling system is implemented when the ambient solicitations and electrical requirements of the application are not really restrictive. Consequently, it will be possible not need to implement a heating system. In either case, if it is needed a heating system in an air cooling system, a direct heating process should be sufficient, e.g., placing some resistances on the surface of the *BP* casing in the air admission zone. In that way, the air will enter from this side, heating itself up, and by means of *NC*, the air will warm the complete *BP*.

In contrast, for a liquid cooling system which usually uses in systems which operate in hot and cold extreme ambient conditions with restrictive electrical solicitations, indirect heating process would propose, which it is currently implemented in *EV*s such as Chevrolet. This indirect heating process consisted basically on a vessel in the liquid circuit with an electric resistance immersed on it. The resistance heats the liquid in the vessel and thanks to the pump, the liquid circulates through the complete system and also through the *BP*, heating it.

4.2.3 INSULATION

The insulation effects should bear in mind especially also, for the passive air cooled applications whose performance can be influenced by very low ambient temperatures or if there is risk of indirect excessive heating due to solar irradiation of the *BP* cooled by active water cooling systems. Obviously the insulation of the *BP* is a key issue if the *BP* temperature should be maintained below the ambient temperature.

In general terms when a system is insulated, theoretically it achieves the minimization of the influence of the external conditions on it. Therefore, it is important to evaluate when it will be useful to be used and when not.

The insulation of the *BP* is a key issue if the *BP* should be maintained below the ambient temperature. This casuistry mainly occurs when an *AC* is used that thanks to the compressor it is possible to drop the temperature of the *BP* below the ambient temperature. However, when a cooling system based on air as coolant is used the opposite happens, it is considered the ambient temperature as the lowest reference limit temperature that the *BP* could achieve.

In the hypothetical scenario in which the *BP* would be cooled by air and insulated, the cooling process would be more inefficient than normally is, i.e., the insulation would suppose a high resistance for the air to cool the *BP* and the cooling process would become slower. Moreover, the insulation could preclude the heat dissipation of the *BP* to surrounding.

As it has been mentioned in the previous section, a liquid cooling system normally is implemented in the cases when the electric and ambient solicitations are restrictive and it is necessary to keep the *BP* temperature below the ambient temperature. In that case, it will worth to insulate the *BP* in order to avoid mainly the influence of the high temperature and consequently, to improve the efficiency of the *TMS* reducing the consumption at system level. In Figure 4.5 can be seen the foil insulation used in the *BP* placed in Chevrolet Volt.

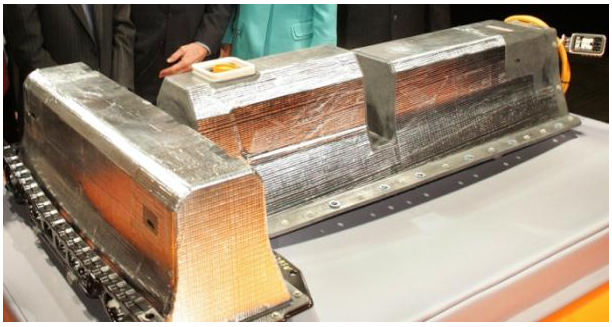

Figure 4.5 The foil insulation placed in Chevrolet Volt BP [43].

Currently, insulation blankets are used for insulation purpose but they present some drawbacks such as that they require large space and they result in higher weight and aerodynamic resistance. Aerogel material could be a promising substitute of common blankets due to its low density and thermal conductivity. The main problem is its current cost but is expected to go down in the next years.

Although at low ambient temperatures the opposite effect occurs, if the *BP* is insulated and it supposes a positive effect for the *TMS* because it would take advantage of the cool ambient temperature to cool passively the *BP*; this work is mainly focused on the cooling process for *BP* in situation that the ambient temperature is usually higher than its ideal operating temperature and must be cooled.

4.3 THERMAL MANAGEMENT TECHNOLOGIES

Following, a further in-depth analysis of the technologies that can be used to fulfil the previous thermal management needs are covered. Both primary (air and water) and secondary (refrigerants) cooling loops that can be used in the most common *TMSs* will be considered. This is carried out considering the main characteristics of each cooling medium, showing the principal components that can be used, describing the research work that other authors have done analyzing these solutions, and showing examples of implementation of this sort of *TMSs* in real *BP*s. At the end of this section, the most suitable *TMS* options for the *BP* of the residential elevator and urban electric minibus that are the subject of the present work will be decided.

4.3.1 HEAT PIPE COOLING

Heat pipe cooling technology, which makes use of the heat transfer provided by change-of-phase in liquids, was first suggested by R.S. Gaugler in 1942. This technology consists of a sealed container whose inner surfaces have a capillary wicking material to provide driving force to return the condensate to the evaporator. This cooling method has been taken more attention in recent years to apply in battery thermal management, due to its high effective conductivity (can reach 10^5 $W \cdot m^{-1} \cdot K^{-1}$) it has been widely used in industrial areas to cool electronic devices, light emitting diode (*LED*), desktop *PC-CPU* or laptops. In Figure 4.6 can be seen a heat pipe cooling system installed in a *Central Processing Unit (CPU)* with the aim to dissipate the heat generated in the *CPU* to the fins of the heat sink which it is cooled by a fan.

Figure 4.6 Heat pipe system used for cooling a CPU combined with heat sinks and air FC.

Many authors have already carried out research works related to this technology. Yan et al. in [44] analyzed experimentally the advantages of use of heat pipes´ bidirectional characteristic, which meant that the evaporator and the condenser of the heat pipe could be switched immediately according to actual cooling or heating needs. Moreover, Swanepoel [45] designed a pulsating heat pipe for the purpose of to manage the thermal management of *LA* batteries of an *HEV* using ammonia such as working fluid. Burban et al.[46] tested an unlooped pulsating heat pipe for cooling electronics components on a *HEV* and Rao et al. also examined heat pipe to cool a *BP* in an *EV* [47], in line with the research work presented by T. Tran et al. in [48], where they investigated the feasibility of the heat pipe cooling for a Li-Ion battery installed in HEV/EV, comparing its performance against to a conventional heat sink. Figure 4.7 shows the heat sink and heat pipe cooling diagram proposed by T. Tran et al.: (a) schematic of the experimented heat pipe, (b) tested both cooling systems and (c) experimental set-up.

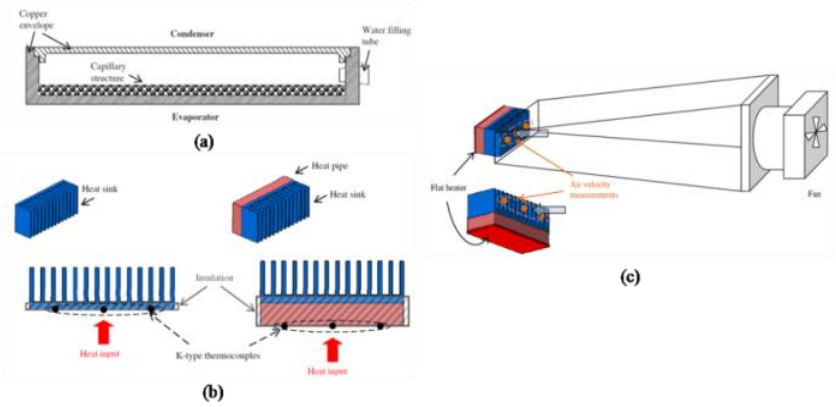

Figure 4.7 Schematic diagram of heat sink and heat pipe cooling system developed by T. Tran et al. [48].

Although many researchers as above have already carried out relevant research works related to battery thermal management with heat pipes in *eMOV* application, aspects such as weight and passive control limitation must still be needed to be investigated in the further, in order to become this technology more useful and competitive regarding more mature technologies. In addition, comparing with other cooling technologies, its initial investment cost is relatively high.

4.3.2 PHASE CHANGE MATERIAL COOLING

PCM has high fusion heat which stores and releases the amount of heat during melting and solidifying at a fixed point: when the temperature is lower than the melting point, *PCM* is solid and heat is absorbed as sensible heat and consequently, the

temperature increases. In contrast, when the temperature reaches the melting point, heat is absorbed and stored as latent heat. This latent heat is stored until the temperature keeps without increasing (at the same time PCM changes its phase from solid to liquid). After that, *PCM* becomes liquid and heat is absorbed by *PCM* and stored as sensible heat. The melting temperature of *PCM* is variable and can be chosen according to requirements of the system.

In recent years many researchers have proposed *PCM* cooling method such as a possible TMS for *BP*s related to *eMOV* applications. This cooling method was firstly introduced by Al- Hallaj and Selman in 2000 for 18650 cylindrical Li-Ion *BP* for an *EV* application [49]. They continued research in this field and in 2002 they carried out a research work in which they compared the *PCM* cooling system against an *AC* systems for batteries considering different cooling capacities [50]. The same research group that Al-Hallaj is belonged presented a work analyzing the possibility to use *PCM* cooling system for a *Li-Ion BP* on board of an electric scooter [51]. In this work they analyzed four heat dissipation modes: *NC*, presence of aluminium foam heat transfer matrix, use of *PCM* (Figure 4.8 (a)) and combination of aluminium foam and *PCM*.

Moreover, Javani et al. in [52] simulated the performance of n-octadecane based *PCM TMS*. They determined the least amount of *PCM* that could obtain a desirable maximum temperature for different tests varying the input values.

(a) (b)

Figure 4.8 Li-Ion BM filled with (a) PCM and (b) PCM and surrounded by Al-foam [51].

In that work, *PCM* cooling solution has been also discarded due to, although it is demonstrated by means of th*e* previous research works that is able to minimize the thermal gradient inside the *BP*, this passive *TMS* often suffers from the various

limitations that it makes an unviable option for these applications within practical *eMOV* scope.

Among the limitations, it can be mentioned that this cooling technology in general terms increases the volume and weight of the overall *BP* system, being more suitable for stationary applications. In addition, when the *PCM* is completely melted, the low thermal conductivity of the *PCM* creates an additional large thermal resistance between the cooling fluid and the batteries. Consequently, it causes not only the battery temperature to rise further due to the low heat dissipation, but also it generates an uneven heat distribution. In general, in both solid and liquid states, the specific heat capacity of the *PCM*s is low, which could lead to a dramatic rise in the temperature of the *BP* when the *PCM* temperature is below the melting range.

Another disadvantage of the *PCM TMS* is that it should only be used with batteries in which the discharge and charge processes are exothermic and endothermic, respectively, or vice versa. This is a quite improbable situation for the most common *eMOV* applications. The *PCM* would absorb the energy generated by the exothermic process and then release it during the endothermic process. If for example, both charge and discharge processes would be exothermic, the *PCM* would always absorb the energy generated during battery operation. Consequently, the melting point of the *PCM* could be exceeded and would no longer work properly since it would not be able to maintain a constant temperature. In such a case, the *PCM* would only release the accumulated energy when stopping the battery system.

4.3.3 AIR COOLING

As it has been pointed out previously, the passive air cooling method can be sub-classified into two particular categories, *NC* and *FC*, depending on whether cooling fan assists with the cooling operation or not. If the temperature of the air is taken below the ambient temperature using some kind of closed loops or devices an active air cooling is obtained.

Passive air cooling method is one of the most commonly adopted cooling strategy for *TMSs*, especially in *BP*s with low to moderate heat generation rates due to its relatively low specific heat power extraction capacity comparing with other cooling modes. However, advantages such as the no necessity of a separate cooling loop, no concern of

possible leakage, or electric short and the simple design, low cost and easy maintenance make it a really concurrent option. Nevertheless, because of the previous mentioned low heat transport capacity and the expected temperature variation within the *BP* may be higher than for example, with a liquid cooling system, make this option unviable for particular applications. Moreover, the usage of a fan in order to improve the thermal performance effectiveness of a *NC*, it could provide a high consumption and noise at a system level [41].

Primarily, two are the main types of fans that can be distinguished: axial (Figure 4.9 (a)) and centrifugal (Figure 4.9 (b)). The axial fans are named for the direction of the airflow they generate. Blades rotating around an axis draw air in parallel to that axis and force air out in the same direction. This type of fan creates a high air flow rate, but of low pressure. The main advantage of this type of fan is that it requires low power input in order to operate. On the other hand, the centrifugal fan as its name indicated, moves the air radially, i.e., the direction of the outward flowing air changes by 90 º respect to the direction of the incoming air. In contrast to the axial fans, centrifugal fans create a higher pressure airflow with a lower flow rate and require higher power input.

This component can operate continuously, under an ON/ OFF strategy or by a pulse width modulation (*PWM*) technique, adjusting the rotational speed of the fan to the current system solicitations.

In type of cooling system together with the fan, it is common to use a heat sink. The heat sink usually consists of a metal structure with one or more flat surfaces to ensure good thermal contact with the components to be cooled, and an array of protrusions called “fins” (that look like a hair comb) to increase the surface contact with the air, and thus the rate of heat dissipation.

(a) (b)

Figure 4.9 Type of fan: (a) axial and (b) centrifugal [53].

Active air cooling requires a loop with an *A/C* system to cool down the primary air flow. *A/C* system is a vapour-compression refrigeration system composed of evaporator, compressor, condenser and *thermal expansion valve (TXV)* which includes a reversing valve so that the direction of heat flow may be reversed. Therefore, the *A/C* system can heat or cool the cabin and in the same way, by means of this air the *BP* will be cooled or heated.

Considering *eMOV* framework, many authors have investigated about this technology and they demonstrated the feasibility of this technology for different practical cases such as Toyota Prius, Honda Civic or Nissan Leaf among others [54, 55].

Toyota Prius *HEV* has integrated a parallel passive air cooling system in which the conditioned air from the cabin is used to cool the *BP*. The Toyota Prius *BP*, which is shown in Figure 4.10, consists of 38 prismatic NiMH *BM*s connected in series and it delivers a nominal voltage of 273.6 Volts and has a 6.5 Ah capacity (around 1800 Wh energy) on board.

The Prius air cooling *TMS* consists of two fans, one to exhaust air from the cabin to the *BP* and the other one, to supply air to outside. To achieve a relatively uniform temperature distribution across the modules, a parallel airflow scheme is used rather than a series configuration. In a parallel configuration, each module is set up to receive the same amount of airflow and thus the same cooling.

Figure 4.10 Toyota Prius BP and its air cooling system [55].

Based on the results obtained from the research work show in [55] for different ambient temperatures and driving cycles of Toyota Prius *HEV*, the *BP* shows a good thermal performance for 25 ºC keeping its temperature below 45 ºC, whereas for an ambient temperature of 40 ºC the *BP* temperature reaches a maximum temperature of 52 ºC, which is not recommended to improve the lifespan of a *BP*.

The *BP* of Honda Civic *HEV* composed of *Li-Ion* prismatic cells with an on-board energy of 680 Wh is also cooled by air *FC* mode. The complete integrated system in shown in Figure 4.11 (a) and it is located on the back of the passengers´ seats [54].

The Nissan Leaf *BP* is also cooled by air *FC* system. The *BP* is located in the lower side on the *HEV*, it has on board 30 kWh and it is based on *Li-Ion* chemistry [56]. The *BP* can be seen in Figure 4.11 (b).

Figure 4.11 (a) Honda Civic BP located in the rear of the back seat [57] and (b) Nissan Leaf BP placed below the seats[56].

In contrast of Honda Civic and Nissan Leaf, Kia Soul *EV* has implemented an active air cooling system. The cabin air is heated or cooled using a heat pump and this air is used also to heat or cool the *BP*. The defined system is shown in Figure 4.12.

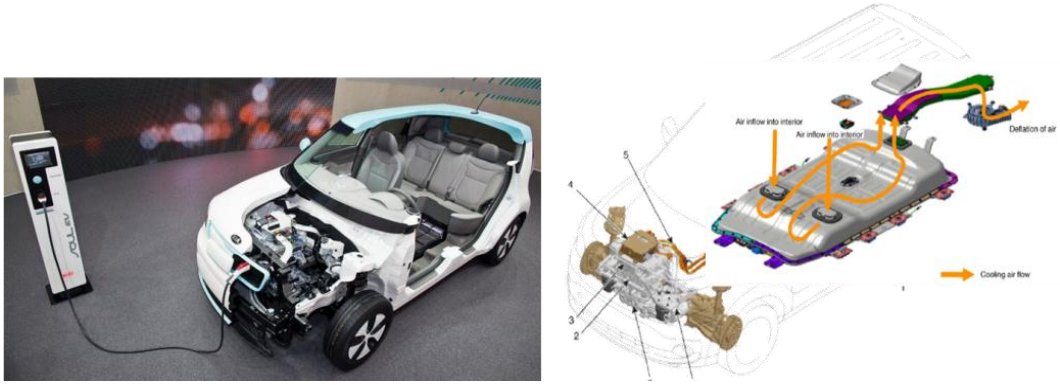

Figure 4.12 Kia Soul EV together with the air AC system implemented [58].

4.3.4 LIQUID COOLING

Passive or active liquid cooling, which has much higher specific heat power extraction capacity comparing with any air cooling system and it is more effective in sense of maintaining the operating temperature of the *BP* within a desirable range and a small thermal dispersion level. However, liquid cooling systems are more complex, even in the passive mode, because they need cold plates, external cooling circulatory system or piping, better sealing requirements, big weight and complex structure, and it also increased power requirements due to the necessity of more mechanical components.

Cold plates make possible to dissipate effectively heat from the *BM*s due to the direct contact that they have because they are placed on the surface of the *BM*s or *BP* directly. As it can be seen in Figure 4.13, a broad variety of cold plates are available in function of the form, material or also, of the circulated fluid which can be water, a mixture of glycol and water, oils or other fluid.

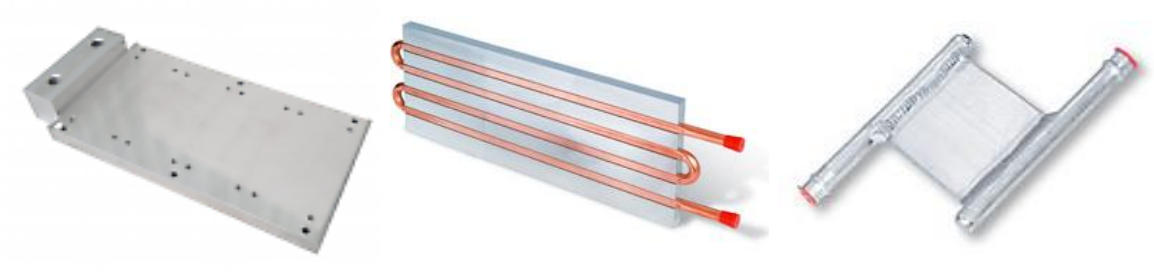

(a) (b) (c)

Figure 4.13 (a) Aluminum cold plates for glycol-water, (b) copper tubes pressed and locked into aluminum extruded plate and (c) header tubes welded aluminum cold plate.

Passive water cooling system is comprised of components such as hydraulic pump, liquid- air heat exchanger and fan.

The objective of the hydraulic pump in the liquid cooling system is to impulse the liquid through the complete circuit. Regarding the hydraulic pump, a wide range of the hydraulic pumps existed. Several classifications can be done in function of the power supplied, the usage or operating mode, among others. Considering that this research work is focused on *eMOV* applications and the auxiliary *TMS* would be powered from

the *BP* on- board in each application, the first mentioned classification has taken into account.

Considering the power supply, motor pump and electric pump can be distinguished. The main difference between them is that the first one is powered by a combustion engine, whereas the second one, is connected to a power outlet or is electrically charged. In Figure 4.14 can be seen the mentioned hydraulic pumps.

(a) (b)

Figure 4.14 Hydraulic pump: (a) motor pump and (b) electric pump.

The heat exchanger in the passive water cooling system is the component which makes possible the rejection of the heat from the *BP* to the surroundings. A wide range of heat exchangers can be found, but considering radiators where the liquid is the primary fluid and air the secondary fluid, the most common heat exchanger is which correspond to finned tube topology.

This type of heat exchanger are especially suited for work with air as secondary fluid, because the fins provide additional heat transfer area for the air which permitted to obtain relatively higher heat transfer coefficient. In this type of heat exchanger, the flow pattern is often crossflow, but it can also be counterflow or parallel flow. In general terms, the tubes and fins can be made of aluminum, copper- alloys and stainless steel, especially. Figure 4.15 shows aluminum and copper finned tube heat exchangers that could be installed for instance, in the front of a car.

Figure 4.15 Finned tube heat exchangers.

Besides, this component is usually complemented by a fan (Figure 4.9) in order to blow air through the fins and therefore, to improve the heat transfer phenomena.

Active water cooling requires a loop with a refrigeration cycle (*VCRC* or *TEC*) to cool down the primary water flow below ambient temperature. The primary and secondary flow circuits have to be separated by an intermediate heat exchanger. The primary fluid usually is liquid and the secondary, refrigerant.

The most well- known of refrigeration cycle, *VCRC*, uses a circulating refrigerant as the medium which absorbs and removes the heat from the space to be cooled and subsequently, rejects that heat. Figure 4.16 depicts a typical *VCRC* system and as it can be seen four are the main components that this system is comprised of: evaporator, compressor, condenser and *TXV*.

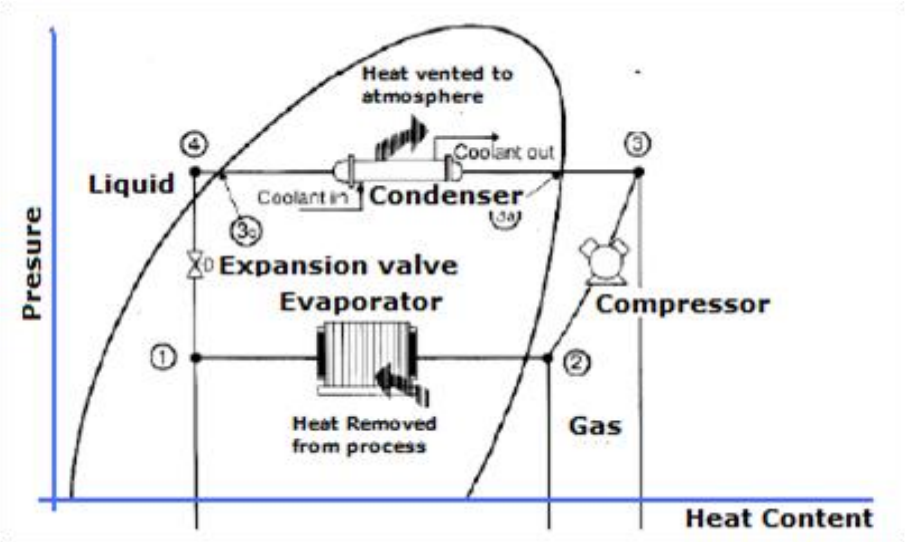

Figure 4.16 VCRC schematic diagram [59].

The aim of the evaporator is to remove the heat from the process, absorbing the heat that is in the liquid (primary fluid) and evaporating the refrigerant (secondary fluid). The saturated vapour of refrigerant, (Figure 4.16, point 2), enters the compressor and it is compressed to a higher pressure, resulting in a higher temperature as well (Figure 4.16, point 3). Afterwards, the high pressure refrigerant in vapour state enters the condenser where the heat is transferred to the secondary fluid, that usually it is air ambient. The refrigerant in a constant pressure process is converted to liquid state (Figure 4.16, point 4) due to the rejection of the heat in the condenser and it goes to the

expansion device, where the pressure and temperature drops until the appropriate conditions to enter again in the evaporator (Figure 4.16, point 1).

Among the components that this circuit is composed of the heat exchangers (evaporator and condenser) and electro-mechanical (compressor and expansion device) components can be distinguished.

The evaporator, which generally has liquid as primary fluid and refrigerant as secondary fluid, based on their construction can be categorized mainly into plate (Figure 4.17 (a)) and shell and tube heat exchangers (Figure 4.17 (b)). Regarding plate heat exchangers, due to the fluid spreads out over the plates their surface area is larger comparing with the conventional heat exchangers, their main advantage. Under this type of evaporator can be distinguished brazed (Figure 4.17 (a) left) and gasket (Figure 4.17 (a) right) plate evaporator, depending on the connection between the plates. On the other hand and related to shell and tube heat exchangers, as its name implies consists of a shell (a large pressure vessel) with a bundle of tubes inside it, and they are especially suited to use in high- pressure applications such as in oil refineries or other chemical processes.

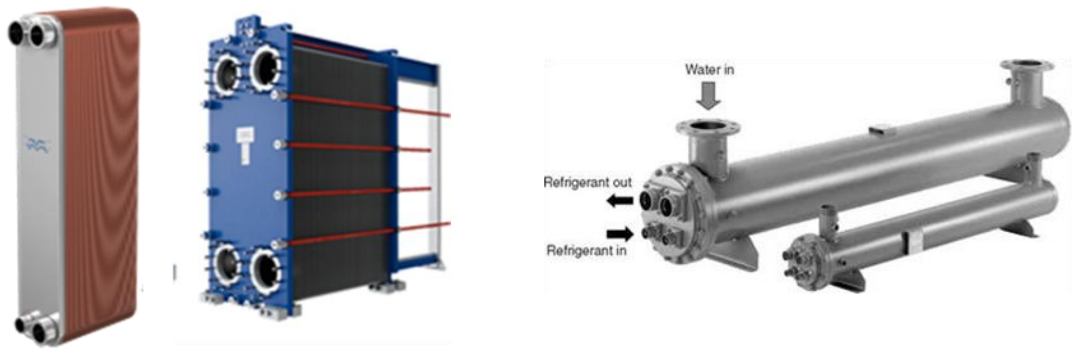

(a) (b)

Figure 4.17 (a) plate and (b) shell and tube evaporator.

In contrast and considering the condensers, can be categorized into finned tube or multi-port extruded tubes heat exchanger. The former corresponds to the same topology of previously mentioned radiator (Figure 4.15), whereas the multi-port extruded tubes, known as micro-channel tubes and it is shown in Figure 4.18, provide a large internal surface area, which yields more efficient heat transfer.

Figure 4.18 Multi-port extruded heat exchanger

Regarding the compressor, it circulates the refrigerant through the system and increases refrigerant vapour pressure to create the pressure differential between the condenser and evaporator. There are two broad categories of compressors in function of how they apply the pressure on the fluid, used in refrigeration systems: positive displacement compressor and rotatory compressor. Positive displacement compressors increases refrigerant vapour pressure by reducing the volume of the compression chamber through work applied to the compressor´s mechanism, whereas dynamic compressors increase the refrigerant vapour pressure by transfer of kinetic energy from the rotating component to the vapour, followed by the conversion of this energy into a pressure rise [60].

Nevertheless in terms of operation conditions, compressors with fixed and variable speed can be distinguished. The fixed speed compressor, the motor runs constant, at one speed, whereas a variable speed compressor uses a variable speed which allows the motor to control its rotational speed, permitting for energy savings which it has been an important issue related to *eMOV* applications.

For instance, Masterflux manufacturer provides some variety of compressor which can be operated at fixed and at variable speed with AC or DC voltage supply. In Figure 4.19 can be seen some of their product.

Figure 4.19 Compressor provided by Masterflux manufacturer which can operate at fixed and variable speed.

The last component which is necessary for *VCRC* is the *TXV*, which is located in the refrigeration circuit between the condenser and evaporator. Three are the main functions related to this component: Reduce the pressure of the refrigerant from the condenser working pressure to evaporator working pressure by means of closing more or less the valve orifice; keep the evaporator active controlling the refrigerant flow in function of the cooling load inside the evaporator, i.e., at higher load, the flow of the refrigerant is increased and vice versa. Related to the second function, the *TXV* also prevents the flooding of the liquid refrigerant to the compressor and improves the efficient performance of the evaporator and compressor and in general, all the whole system.

With regards to the *TXVs* two are the main types: internally or externally equalized. The difference between them is that the first one uses the evaporator inlet pressure to control the position of the valve, and the second one considered the evaporator outlet pressure, in both cases compensating any pressure drop that could happen within the evaporator. Generally, the external equalized *TXV* is more used, mainly because it does no present any inconvenient to be used regarding any type of variation of the architecture of the system (medium or big-size equipment, systems which work at high pressure level or at thermal load variation).

Figure 4.20 An externally equalized a TXV in a refrigeration system.

Currently, this type of *TMS* is implemented within *eMOV* framework in Chevrolet Volt and Tesla Model S *EV*s, among others.

The *BP* located in Chevrolet Volt which is shown in Figure 4.21 (a), has around 16.5 kWh on board and it is comprised of 200 cells based on *Li-Ion* technology. The temperature of the *BP* is controlled with an active liquid cooling system based on the scheme shown in Figure 4.21 (b). Inside the battery housing, there are thermal passages

in form of cold plates that permit coolant flow between the cells and these passages permit to cool or heat the *BP* depending on the operational requirements [61, 62].

This cooling system performance is regulated by a 3-way coolant flow control valve which has three positions: position A) permits the heating of the *BP* to attain a desirable operating temperature in cold weather, position B) allows to cool the *BP* when it is too hot by operating the compressor using R-134a refrigerant and position C), is used during more temperature stable operating conditions circulating the coolant flow (glycol) of the *BP* through the radiator and the pump.

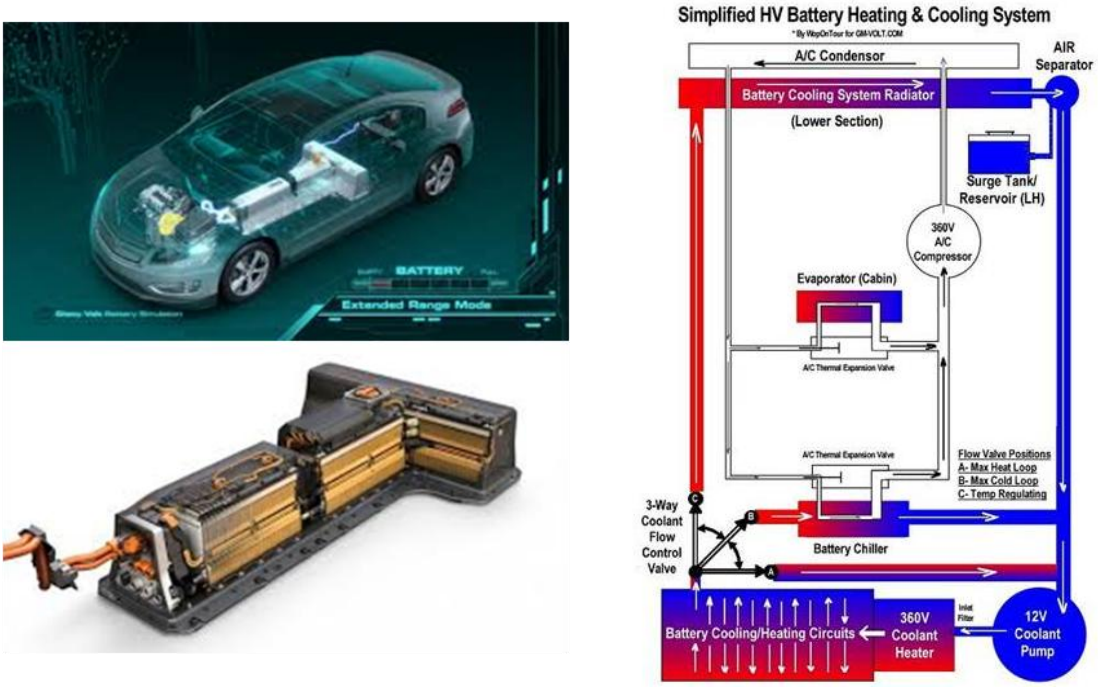

(a) (b)

Figure 4.21 Chevrolet Volt EV [63] (a) BP and (b) active liquid cooling system [64].

On the other hand, the *BP* of Tesla S is composed of 7000 Li-based cylindrical cells and the complete system is shown in Figure 4.22 (a). The *BP* has 85 kWh energy on board and that it is located in the car underneath the floor. The liquid cooling system performance, which is shown in Figure 4.22 (b), is similar than in Chrevolet Volt *EV* and it is explained in detail in [65]. The special feature of this cooling system is that instead of using cold plates as in the previous case, it uses a ribbon shaped metallic cooling tube that snakes through the cells of the *BP*, as it can be seen in Figure 4.22 (c).

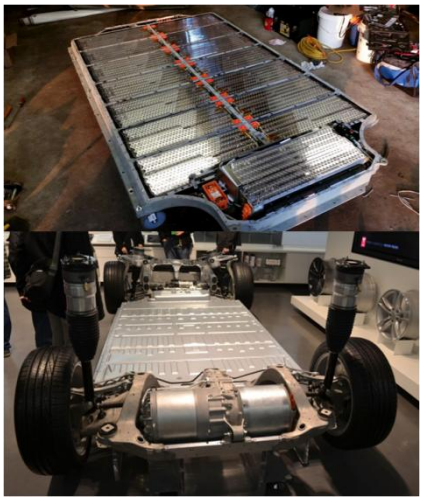

(a)

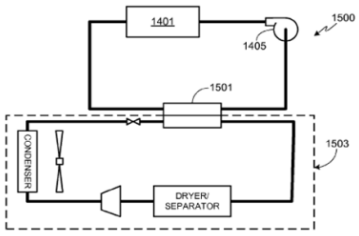

(b)

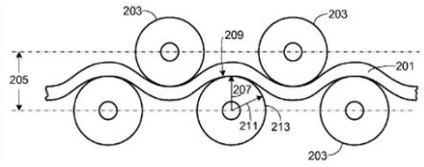

(c)

Figure 4.22 Tesla Model S (a) BP and the scheme of (b) TMS and (c) ribbon shaped metallic cooling tubes [65] by P.T. Tennessen.

In addition several electric buses can be found which its *BP* is cooled by liquid *TMS*. Nova electric bus (Figure 4.23), manufactured by Hybridrive propulsion systems, has installed on the roof of the bus a cooling package which is indicated schematically in Figure 4.23 (b) and more in detail in Figure 4.23 (c). The cooling system is based on liquid passive cooling composed of pump, fan and a radiator [66].

(a)

(b)

(c)

Figure 4.23 (a) Nova Bus manufactured by Hydridrive schematic and (b) cooling package installed on the roof [66].

4.4 CONCLUSIONS

The objective of this chapter has been to introduce the cooling, heating and insulation process for *BP*s implemented in *eMOV* applications in order to afterwards, take decisions related to the applications in which is focused this Thesis.

Regarding the cooling system, the manufacturer has imposed which thermal management technology has to be used in each application: air cooling system for residential elevator and liquid cooling for urban electric minibus application. On this basis, specific cooling system in terms of passive or active concept, has been proposed for each application.

Although the mandatory use of air cooling system in the residential elevator application has been predefined by manufacturer, the relatively soft electrical solicitations in real situations and the cold location in which the *BP* will be in the building, have made suitable the option to implement this simple and inexpensive air cooling system.

It is obvious that a *NC* will be more efficient to implement than a *FC*, that requires the implementation of a fan in the system, however, by means of this electro-mechanical component the thermal performance of the *BP* will be more ensured. Therefore and taking advantage of the intermittency that this application provides, in the next steps a control strategy will be proposed in order to combine the *NC* and *FC* operation modes in function of the actual system needs, i.e., the fan only will be turned on when the *BP* temperature and the thermal dispersion within the *BP* exceed the defined limits. In that way, it will be possible to guarantee a suitable and proper thermal performance of the *BP* minimizing as far as possible the auxiliary components consumption.

On the contrary, due to the restrictive requirements regarding the electric and thermal specifications of the urban electric minibus application, the option to implement a liquid cooling system has been a priori an adequate choice by the manufacturer.

In this case, the decision related to the type of the liquid cooling system has been totally influenced by the ambient conditions. It can be possible that with a passive liquid cooling composed of a pump, radiator and a fan, will be enough to keep the *BP* within

an appropriate thermal performance range when the ambient is below to a mild temperature as 25-30 ºC. However, when the ambient temperature is higher a passive liquid cooling system probably could be unviable. For this scenario in which is necessary to keep a huge *BP* at a temperature below the ambient temperature to ensure its lifetime, it will be required to implement an active liquid cooling system composed by evaporator, compressor, condenser and *TXV*. In the same way that for the first application and with the aim to minimize the system consumption of this proposed liquid cooling system, a dual architecture which combines passive and active liquid cooling system, in function of the actual electrical and ambient solicitations, has been defined, permitting the performance of each mode by means of changing the position of a directional valve.

With regards to heating process and firstly referring to the elevator application, it can be stated that because of the *BP* will be kept within the elevator shaft in a building, it has been considered that the auxiliary heating could discard a priori. Nevertheless, for the case in which the *BP* should be heated up, some electrical resistances will be included in the admission zone of the air, placed them on *BP* casing surface. In that way, the cells will warm by means of the air will rise circulating around the cells taking advantage of the *NC* effect.

For the urban electric minibus and because the cold ambient temperature that it can occur mainly at night when the vehicle is parked in the depot, it has been decided to implement an electric resistance within a reservoir. The electric resistance heats up the liquid impulsed by the pump in the reservoir and consequently, the *BP*.

At last, the third issue related to the *TMS* has been the insulation. For the case of the residential elevator application where the *BP* will place in the lift shaft and it will be cooled by a forced air cooling, it is no effective to insulate the *BP* because in that way the cooling system will become totally inefficient. For this particular case, the insulation will suppose a high resistance for the air that it will try to cool the *BP* and the cooling system will become slower than it normally is.

On the other hand, for the application of the electric minibus it is worth insulating the *BP* in order to avoid especially the influence of high ambient temperature and consequently, to improve the efficiency of the *TMS*. Due to the fact, the heat flows from

the hotter side to the colder side, if the *BP* is not insulated some undesired effects could occur that affect negatively on the system thermal performance. When the ambient temperature is high, 45 ºC at extreme condition, the active liquid cooling system will try to keep the *BP* temperature within an optimal operating range, around 25 ºC, surely at expense of a high auxiliary consumption. Nevertheless, if the *BP* is not insulated, at the same time that the *TMS* is working to ensure a correct thermal performance of it, the ambient temperature is providing extra heat to the *BP* by its surrounding that the *TMS* must evacuate from the *BP*. This supposes an extra consumption that it can be prevented insulating the *BP*. Depending on the location of the *BP* in the minibus, the solar irradiation could also become a critical issue. The insulation is mandatory for these case too.

Chapter 5.

Design and Optimization Methodology

In the previous three chapters of the present document, a brief introduction to the context of the *Electro-Mobility* is given, the electrical sizing of two different *BPs* to be used in specific applications is shown and the preferred TMS concept has been chosen for both cases. This fifth chapter is the core of this Doctoral Thesis and it is devoted to describing, step-by-step in detail, the methodology that has been followed in order to mathematically model, design, implement and optimize *Thermal Management Systems* for real applications within *Electro-Mobility* scope.

The first essential task, before carrying out this virtual modeling based methodology, has been to select the most suitable and appropriate modeling tools for each case because its selection is not arbitrary. In this way, the versatility in terms of applicability of the developed methodology has been demonstrated carrying out the same sequential steps for each application independently of the simulation tool that has been used.

This optimization methodology is comprised of five steps which are described in detail along this chapter. Some of these steps involve closed-back-loops that should be solved prior to proceed with the next step. The first four steps correspond to a standard design- and modeling-methodology [67], while the fifth step which is related to optimization process constitutes the main contribution of this research work.

5.1 INTRODUCTION

Along this chapter the thermal design process that has been followed to materialize the best possible *TMSs* is described conceptually. The detailed numerical results that have been obtained are explained later as test cases of the proposed methodology in chapters Chapter 6 and Chapter 7. The aim of this complete methodology is to design, model and lastly, optimize the *TMS* of any *Li-Ion BP* constrained to some restrictions. The main contribution of this methodology is focused on the optimization step, which is based on the minimization of the overall cost, weight, volume, auxiliary consumption and complexity of the *TMS* which have a dramatic impact on *eMOV* applications. Nevertheless, this is done ensuring at all times a suitable thermal performance of the *BP* in terms of maximum cell temperature and thermal dispersion within the *BP*. This methodology is focused only on thermal aspects, although it must bear in mind that the design process of the complete *BP* is a multidisciplinary task.

The general tendency of the engineers when are dimensioning any sort of new systems is to guarantee a high-security level in terms of correct performance in the proposed solution. In these cases the overall trend is to oversize the management system by a little factor in order to ensure the fulfilment of the established requirements such as way of a precaution. Definitely, it is usually considered such as "definitive design" the one which only is able to fulfil the design criteria without considering any other interest or transversal issues. However, in applications within the *eMOV* framework, as well as in many other applications in which the weight and efficiency of the auxiliaries is a key issue, an optimization process which will involve a reduction of the cost, consumption and complexity at system level could have significant positive effects on the overall performance.

This is why a great effort has been made in this work in order to develop specific knowledge to get a consistent optimization procedure to finally implement it in a complete standard design and modeling methodology.

Prior to the optimization task, some previous steps related to system design and modeling have been done. For that purpose, it has been necessary to analyze and select the proper modeling tools for thermal design for each particular case.

5.2 MODELING TOOLS FOR THERMAL DESIGN

Once the most suitable cooling medium has been selected and a specific *TMS* architecture has been sketched at least at conceptual level, the selection of the best modeling tool is mandatory in order to develop a reliable and accurate mathematical model to predict the thermal response of the complete *BP*. As far as possible, it is crucial to select a good enough simulation tool to study the performance at system level or only a part of it, but with the essential spatial and time resolution. Not always the most sophisticated tool is the best option in terms of development time.

The thermal performance of each cell of a bigger *BM* or *BP* is inherently transient, interdependent and highly nonlinear [68]. It is time dependent because the heat generation in each cell changes with the instantaneous charge/discharge current load demand, *SOC* and *SOH (State of Health)* states and even their absolute temperature [69]. The heat that releases one of the cells can affect the others dynamically depending on their spatial localization and cooling method [70, 71]. In this context, smart simulation approaches become necessary by means of which, the computational time can be greatly reduced without losing the required accuracy.

Two conceptually different modeling approaches and simulation tools will be assessed: detailed 3D differential equation models, implemented in *Computational Fluid Dynamics (CFD)* simulation tools, and spatially lumped *differential, algebraic and discrete equation* (*DAE*) models, implemented in fluid oriented physical system simulation tools. A short introduction is given in the following paragraphs.

5.2.1 COMPUTATIONAL FLUID DYNAMICS (CFD) SIMULATION TOOL

CFD is a branch of fluid mechanics that uses numerical analysis and complex data structures to solve and analyze problems that involve fluid flows. This simulation tool provides a detailed spatial and temporal quantitative prediction of fluid flows by means of mathematical modeling. Partial differential equations describing the basic fluid flow physics (Navier-Stokes), turbulence effects (models of different degree of closure and complexity) and energy transfer by conduction, convection and radiation are applied in a 3D domain. This physical domain is spatially and temporally discretized (mesh and time stepping) and iterative numerical methods are used to solve the sparse problem. Different software tools (solvers, pre- and post-processing utilities) can be used to

implement such models and obtain the desired simulation solutions restrained by some boundary and initial conditions.

The most common *CFD* simulation programs implement the *Eulerian Finite Volume Method* (*FVM*) in the frame of unstructured codes. *OpenFOAM* [72], *Ansys/ FLUENT* [73] and *Siemens/ STAR CCM+* [74] are the most known free and commercial *CFD* codes. There are less known approaches like the *Lagrangian Laticce-Boltzman Methods* (*LBM*) implemented in software like *Dassault Systemes*/ *X-Flow* that won´t be covered in the present work.

Although *CFD* enables users to perform the so-called "numerical experiments" in a "virtual prototype", that does not mean that this simulation tool replaces the experimental measurements. Once the developed model is validated by experimental results, a limited number of numerical tests can be performed and the overall cost of the design process can be significantly reduced. The experiments could be expensive, slow, and sequential with normally a single purpose, while the simulations could be cheaper, faster, and parallel covering multiple purposes. Another advantage of this type of numerical approaches is the fact that they can yield a very good level of accuracy in the solution even with some physical and geometrical simplifications [70, 71]. The main disadvantage of these simulation tools is the required computational effort in terms of result obtaining time and High Performance Computing (*HPC*) hardware requirements to study a complete *BP* at system level. Depending on the case, it can be an infeasible task. In order to minimize this last effect and therefore, reduce the computational effort, it can be used tips such as consider the same effects on both symmetrical sides of a *BP* model or to consider uniform flow conditions for each *BM* that comprises the system. The transient nature of the *BP* thermal performance is a great deal that has to be overcome in order to afford any optimization task.

When a system with fluid is modelled by *CFD* simulation tool, partial differential equations are discretized by applying conservation principles in each of the infinitesimal control volumes of the mesh. The equations raise a systematic count of mass, momentum and energy changes due to the flow of the fluid through the boundaries of a fluid element, the presences of walls or a possible surface and/or volume source terms that may exist. For that purpose, the fundamental equations related to mass, momentum and energy have been taken into consideration which in fluid mechanics are also

referred to Navier-Stokes equations. All of the following equations present magnitudes expressed per unit volume.

The law of conservation of mass is expressed by Eq.(5.1). The first term on the left represents the ratio of density change with time (transient term), while the second term describes the net mass flow which enters or leaves the element through its boundaries (convective term).

$$\frac{\partial p}{\partial t} + \frac{\partial}{\partial x_i}(\rho \cdot u_i) = 0 \tag{5.1}$$

For the momentum conservation, the equation (5.2) is the most general form of it. This law holds that equilibrium must exist between the ratio of momentum change in a particle and all the forces which act on it. The first term of the left side, as for the mass conservation equation, is referred to the transient term while the second one described the convective term. The terms in the right- hand side of the equation is called stress tensor. S_{Mi} term is referred to the flotation forces especially for *NC* cases.

$$\frac{\partial}{\partial t}(\rho \cdot u_i) + \frac{\partial}{\partial x_i}\left(\rho \cdot u_i \cdot u_j\right) = -\frac{\partial p}{\partial x_i} + \frac{\partial x_{ij}}{\partial x_j} + S_{Mi} \tag{5.2}$$

The energy conservation law holds that the ratio of energy change in a particle must be equal to the sum of the work ratio done to the particle and the energy ratio added in form of heat.

In the same way than for the mass and momentum equation, the first term of the equation (5.3) describes the transient variation of the energy, while the second term represents the energy transferred due to the fluid movement (convective term). In the right side of the equation, it can be seen four terms. The first two terms are referred to the energy ratio dissipated in the form of work done to the fluid particle by the superficial forces. However, the third and fourth terms recount the net ratio of the heat absorbed by the particle.

$$\frac{\partial(\rho \cdot e)}{\partial t} + \frac{\partial(\rho \cdot E \cdot u_i)}{\partial x_i} = -\frac{\partial(p \cdot u_i)}{\partial x_i} + \frac{\partial\left(\tau_{ij} \cdot u_i\right)}{\partial x_j} + \frac{\partial}{\partial x_i}\left(k\frac{\partial T}{\partial x_i}\right) + S_h \tag{5.3}$$

The heat generation model has been defined following the Eq.(5.11) and it has been applied as a uniform volumetric heat generation in the cell zones, S_h, by means of a user-defined function (*UDF*) which made possible to model each cell variable heat

generation rate as a function of the instantaneous cell temperature, *SOC* and current values. The *UDF* code is shown in Appendix 2A.

In general trend, the fluid flow could be laminar or turbulent. In this work the turbulence phenomena has been considered in all the cases taking into account the characteristic *Reynolds* (Re) and *Rayleigh* (Ra) numbers for *FC* and *NC* cases, respectively. For that purpose, Reynolds Average approach of the Navier-Stokes (*RANS*) equations, Eqs.(5.4) and (5.5), and the Energy equation, Eq.(5.6), have been used to include turbulence effects in the mean flow variables of the fluid region. The turbulence phenomena has been modelled using the RNG k-ε turbulence model [75] and a two layer near wall treatment [76] to obtain a precise description of the hydrodynamic and convective heat transfer phenomena (y+<2.7).

$$\frac{\partial}{\partial x_i}(\rho \cdot U_i) = 0 \tag{5.4}$$

$$\frac{\partial}{\partial x_j}\left(\rho \cdot U_i \cdot U_j\right) = -\frac{\partial p}{\partial x_i} + \frac{\partial}{\partial x_j}\left[(\mu + \mu_T) \cdot \left(\frac{\partial U_i}{\partial x_j} + \frac{\partial U_j}{\partial x_i}\right) - \frac{2}{3} \cdot \rho \cdot \lambda \cdot \delta_{ij}\right] \tag{5.5}$$

$$\frac{\partial}{\partial x_i}(\rho \cdot U_i \cdot C_P \cdot T) = \frac{\partial}{\partial x_i}\left[(k + k_T) \cdot \frac{\partial T}{\partial x_i}\right] \tag{5.6}$$

In general heat transfer can be occurred by conduction, convection or by radiation phenomena. The radiation phenomena between surfaces is expected to be an important factor especially at *NC* cases and an additional equation is solved to take into account this phenomena in the global heat balance [DO].

Many research works can be found in the literature in which this powerful numerical tool has been used to simulate *TMS* of *BPs* at system level, in both air and liquid cooling systems.

Regarding *BP*s cooled by air cooling system, most of the published works have the aim of improving the *BP* design in terms of the cell layout and the cell spacing, trying to minimize the maximum temperature and also, the temperature dispersion across the *BP* with minimum energy consumption.

For instance, in the work of L. Fan et al. [77] *CFD* code *ANSYS Fluent* has been applied to simulate the temperature distribution within a *BM* composed of eight prismatic cells surrounded by a passive forced convection air cooling applying a time-averaged heat generation rate correspondent to a US06 standard cycle for a *plug-in hybrid electric vehicle* (*PHEV*) application. The influence over the cell temperature of different cells arrangements, with different gap spacing between them, with several cooling strategies and using various values of volumetric air flow rates has been analyzed as it can be seen in Figure 5.1.

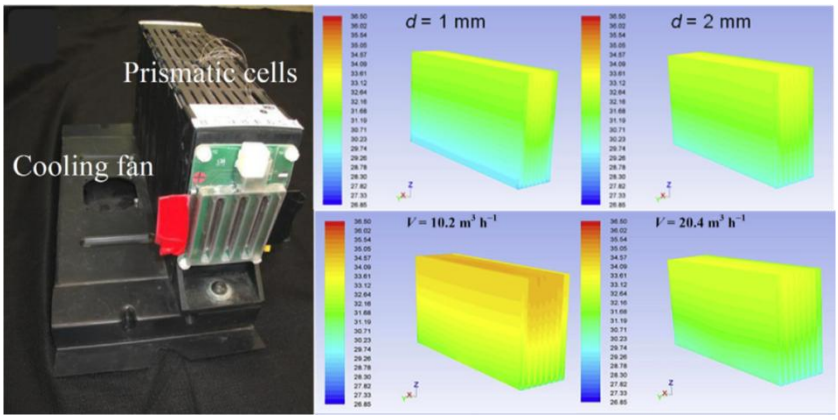

Figure 5.1 Air cooled module composed of prismatic cells and CFD results in terms of cell temperature considering the influence of gap spacing between cells (top) and air flow rate (bottom) developed by L. Fan [77].

Moreover, L. H. Saw et al. in proposed a *BP* composed of 24 38120 cylindrical cells and cooled by a passive forced convection flow of air [78]. They carried out steady state simulations with various air mass flow rates. In order to validate the results, an experimental testing of the *BP* at different charging rates was conducted. In Figure 5.2 can be seen the overview of the *BP* and as an example, the air flow path into the *BP* and the temperature distribution of the cells as a result of one of the simulated tests.

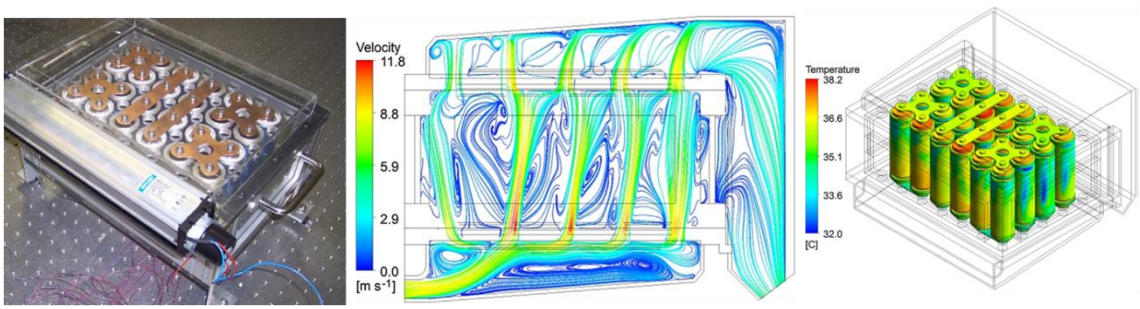

Figure 5.2 The overview of the BP (left), the air flow path (middle) and temperature distribution within the BP (right), developed by L. H. Saw [78].

The arrangements of cylindrical *Li-Ion* cells have also been explored in references [79, 80]. Yang et al. inspected the behaviors of aligned and staggered 6 x 10 cell *BP*s during discharge process [79]. Furthermore, in the second work five different pack geometries with 18-25 battery cells were compared in terms of thermal performance, wherein the best position for fan positioning and air mass flow rate were suggested for each geometry [80].

Other authors, such as R. Mahamud in proposed a reciprocating air flow system, switching the air flow direction after certain time interval in order to avoid the temperature non-uniformity between the cells [36]. A 72% drop in temperature difference was attained in their model with a switching time interval of 120 seconds.

Considering liquid cooled *BP*s there are also many authors that have used this simulation tool in order to study the thermal performance of the complete system.

A. Jarret designed thin metal battery cooling plates, which include serpentine-channels as it can be seen in Figure 5.3 (left) [81]. Different cold plate designs were proposed defining an objective function in terms of pressure drop, average temperature and temperature uniformity allowing the variation of channel width and position. Based on the *CFD* optimization results obtained, the optimized design can satisfy both pressure and average temperature objectives, but at the expense of temperature uniformity.

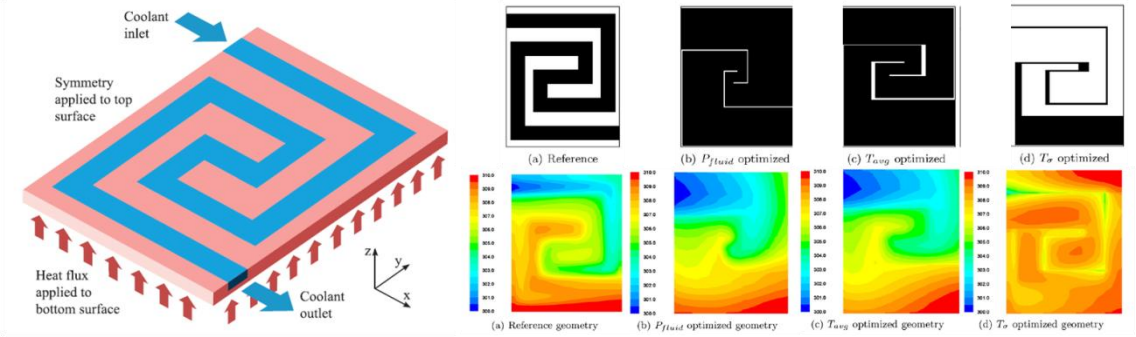

Figure 5.3 Schematic of CFD cold plate model developed by A. Jarrett (left), proposed optimized designs (middle) and the temperature distribution for the proposed cooling plate designs (right) [81].

Huo et al. in a three-dimensional thermal model developed to examine the performance of the cold plate with straight channels and with water as the cooling

medium [82]. By adjusting the number of channels, the liquid mass flow rate, and the flow directions inside the channel, the optimal parameter values were specified, e.g., the cold plate with 6 channels (4 mm spacing) and a mass flow rate of 0.5 $g \cdot s^{-1}$ was most favourable for the battery with a width of 63 mm.

N. Nieto et al. analyzed the thermal performance of a single compact *BM* composed of 12 KOKAM (model SLPB100216216H) pouch cells, with two symmetrically placed cold plates based on water liquid cooling [70]. Some mathematical models were developed to predict more accurately the heat generation of each of the cells (Figure 5.4) using *CFD* techniques to predict the transient *BM* thermal behaviour for different operating conditions. Finally, these models were experimentally validated and they ensured the correct thermal performance of the *Li-Ion BM* to be used in bigger systems. In Figure 5.4 is shown the contours of temperature for several tests carried out. It was possible to keep the maximum cell temperature below 35 ºC with a liquid flow rate of 2.375 $l \cdot min^{-1}$ and an inlet temperature of 25 ºC, maintaining the maximum module thermal dispersion below 2 ºC for moderate cycling *C-rates.*

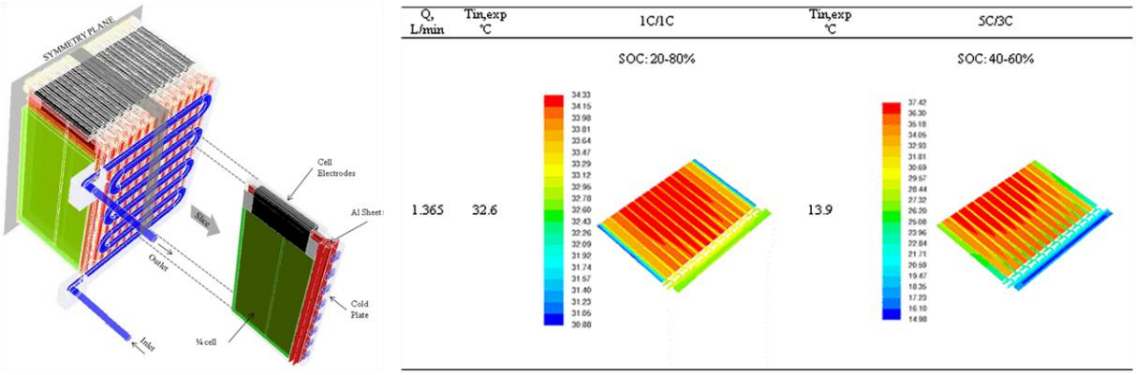

Figure 5.4 Schematic of TMS developed by N. Nieto for Li-Ion pouch cells BM (left) and temperature contours of several tests carried out (right) [70].

5.2.2 Differential, Algebraic and Discrete Equation (DAE) Simulation Tool

DAE simulation tools are based on a lumped physical representation of the flow and thermal phenomena using diverse differential algebraic and discrete equations and an object-oriented acausal or event oriented causal modeling approach. In this type of software, a hybrid approach between general-purpose programming language and domain-specific modeling language is applied. By means of these simulation tools can be solved initial value problems of implicit form described by a system of linear,

nonlinear or even differential algebraic equations. In this way, different one-dimensional flow and thermal problems can be solved by means of lumped or partially distributed parameters. Simple steady simulations or complex dynamic simulations can be performed, including even event driven dynamic state changes (i.e., discontinuous equations, state transition networks and discrete events).

There are many works in the literature carried out by different authors which have used different simulation software based on *DAE* tools in order to study the thermal performance of *BP´*s *TMS.*

Examples of event oriented simulation software libraries that can be used to analyze flow and thermal lumped problems are: Matlab-Simulink customized flow and thermal toolboxes like CoolSim [83], CARNOT [84], Thermolib [85]. Examples of object-oriented modeling simulation tools and libraries are: Modelica-*Dymola/TIL* Suite [86], KULI [87], MapleSim [88].

This object-oriented simulation tool provides some advantages such as the modularity, extensibility and reusability. The modularity is referred to the possibility that this simulation tool offers in terms of combination or interaction between different components in order to build a complete and complex system, although each component has different performance properties. The extensibility is related to the possibility to extend the components in order to include or change new attributes and behaviors of each component, and the reusability corresponds to the ability to duplicate and reuse the components in different systems. In addition, the lumped or compact character of these kinds of models allows very fast dynamic simulations to be performed, even in very complex *AC* thermodynamic systems, with reasonable computational requirements depending on the selected physical and thermal resolution level. Nevertheless, this simulation tool is not adequate to analyze some detailed performance such as it could be the air distribution within a system in contrast to the previous defined *CFD* simulation tool.

As for the previously analyzed simulation tool, for fluid oriented *DAE* simulation tool the conservation laws of energy, mass and momentum have been the starting point for the formulation which describes these mathematical models.

One of the main approaches or assumptions which is implemented in this simulation tool is related to the treatment of the fluid flow. This simulation tool is especially suited for conducted fluid flows because its dimensional resolution is lumped. In simple words it could be said that the *3D* fluid flows are treated as *1D* flows. Based on the lumped control volume that is shown in Figure 5.5 the formulation of the mass and energy balance have been defined. This control volume represent a so-called "fluid flow cell". As for the *CFD* case, these cells could be surrounded by walls.

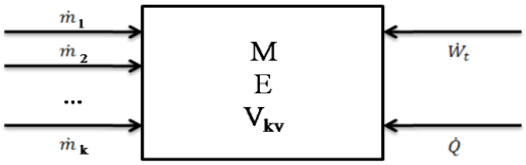

Figure 5.5 Control volume for the formulation of the mass and energy balances.

The mass balance can be written by Eq. (5.7).

$$\frac{dM}{dt} = \sum_k \dot{m}_k \tag{5.7}$$

where M is the total mass of the control volume, t time and $\dot{m}_k$ are k mass flow rate entering and leaving the control volume.

Considering negligible the influence of kinetic and potential energies, the energy conservation law can be defined as it can be seen in Eq. (5.8).

$$\frac{dh}{dt} = \frac{1}{M}\left\{\sum_k [\dot{m}_k(h_k - h)] + \dot{Q} + \dot{W}_t - V_{cv}\frac{dp}{dt}\right\} \tag{5.8}$$

The momentum equation is most difficult equation to solve and different approaches can be found in the literature. For the derivation of the momentum balance, only two mass flow rates, $\dot{m}_{in}$ and $\dot{m}_{out}$, have been considered as it is shown in Figure 5.6.

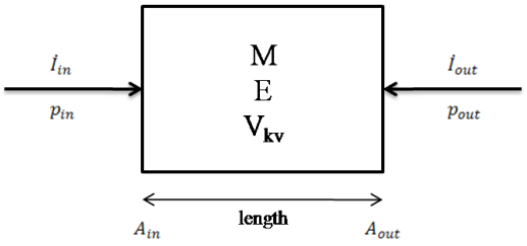

Figure 5.6 Control volume used for the formulation of the momentum balance.

Assuming that the two areas A_{in} and A_{out} are equal, the momentum equation can be written as it is shown in Eq. (5.9) [89]:

$$\frac{dI}{dt} = \dot{I}_{in} + \dot{I}_{out} + (p_{in} - p_{out})A - \Delta p_f A \tag{5.9}$$

where I is the momentum in the control volume (Figure 5.6), $\dot{I}_{in}$ and $\dot{I}_{out}$ are the momentum flows, and Δp_f is the friction pressure loss. Because the difference between the two momentum flows has assumed to be zero and the time derivative of the pressure has treated as constant along the direction of flow [90], the Eq. (5.9) can be written as in Eq. (5.10) is shown.

$$\Delta p = -\Delta p_f \quad \rightarrow \quad \frac{dp_{in}}{dt} = \frac{dp_{out}}{dt} \tag{5.10}$$

These mass, energy and momentum equations have been implemented in this simulation tool together with the heat and pressure drop equations which describe the thermal and hydraulic performance of the different components in the defined system [91].

A research group from NREL in 2013 developed a new automotive *A/C* system simulation toolbox called CoolSim using MATLAB/Simulink platform. The developed model consisted of a detailed cooling circuit model and a relative simple cabin model. By means of this model can be handled the fast transients that happen in the automotive *A/C* system [92]. The same research group led by Tibor Kiss in 2015 presented a research work in which they added liquid coolant loops to the previous developed *A/C* model to enable integrated system simulation of the entire *EV´*s *TMS*, including the *BP´*s *TMS* [93]. They demonstrated that this modeling method can be effectively used to evaluate various options that may be available for configurations of *EV* thermal systems. Also, it was useful for evaluating the possible operating modes that may be possible in a given complex *TMS*, thereby aiding the pairing of the most effective and efficient operating mode for any given driving and ambient conditions.

In top side of Figure 5.7 (a) can be seen the schematic of the *TMS* test bench developed by *NREL* which allowed for testing a wide range of advanced *A/C*, heat pump and cooling loop configurations. A refrigerant circuit (light green lines) operating on the vapor compression cycle was used as both an *A/C* unit, providing cooling, and as

a heat pump, providing heating. The refrigerant loop heat exchange with the liquid coolant was in the chiller and in the condenser. The liquid coolant, water-ethylene glycol (*WEG*, orange lines), was used to provide cooling and heating to the cabin, power electronics, electric motor and to the *ESS*. Particularly in this study by means of the developed model, they investigated the optimal location of the power electronics and electric motor in the condenser coolant loop or in the chiller coolant loop. They resulted in lower thermal system operation power, placing these components in the condenser loop. Some results are shown in Figure 5.7 (b).

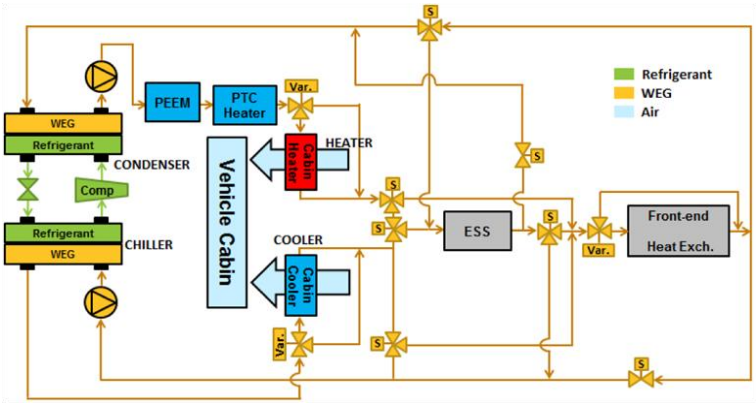

(a)

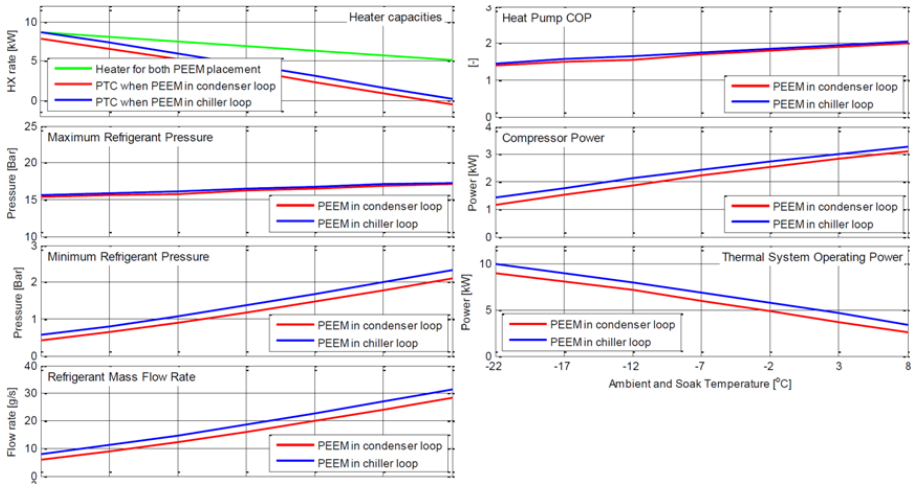

(b)

Figure 5.7(a) Developed TMS model by T. Kiss et al and (b) the results obtained at system level by MATLAB/Simulink A/C modeling toolset [93].

From the RWTH Aachen University, C. Bouvy et al. developed a new holistic vehicle library using *Modelica* programming language [94]. They considered all relevant sections of a vehicle development process, such as longitudinal and lateral dynamics, *TMS* and the power supply. They applied this newly developed library

exemplarily on an innovative architecture considering the traction battery as thermal storage device. The aim of this paper is to determine the potential of such design on the overall efficiency and to analyze different operational strategies. They only are concerned with the energetic point of view at system level.

In addition, J. Batteh et al. from Modelon Inc. used a coordinated suite of Modelica libraries such as Vehicle Dynamics Library, Liquid Cooling Library and Heat Exchanger Library to boost up the physical resolution of their numerical analysis [95]. They developed an integrated vehicle thermal management model, which is shown in Figure 5.8, to use to highlight complex, multi-domain interactions between physical and control systems over drive cycles for combined thermal and fuel efficiency studies. In addition, in this work also illustrate the use of Functional Mock-up Interface (*FMI*) to couple the developed vehicle thermal management model with controls in Matlab/Simulink and for use in robustness application in Excel.

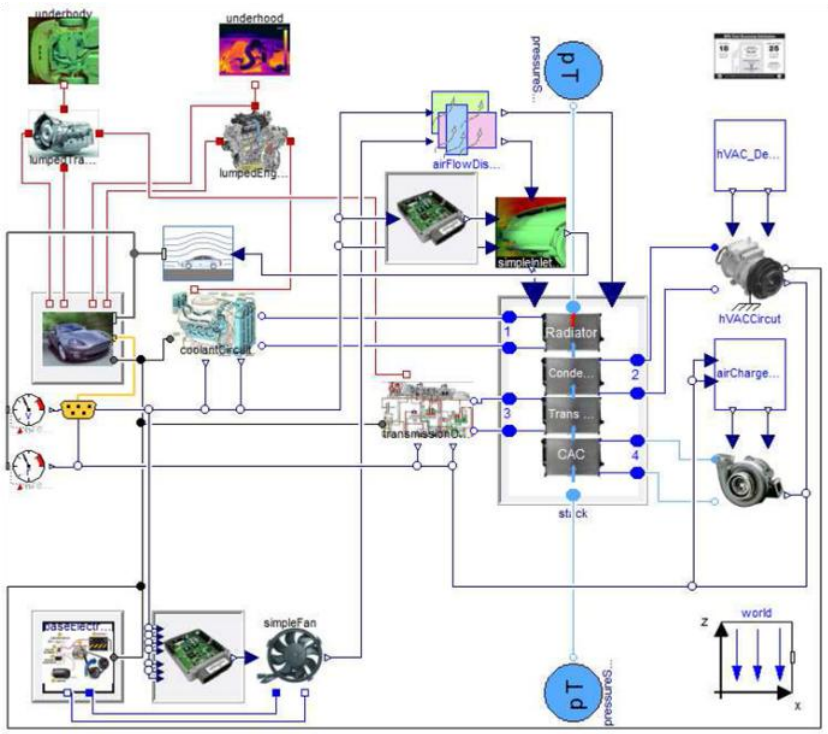

Figure 5.8 Developed integrated vehicle thermal management model by J. Batteh et al. [95].

Andreas et al. from TLK-Thermo GmbH company developed and validated a dynamic model for an automotive *A/C* cycle with an additional evaporator for battery cooling, as it can be seen in Figure 5.9 (a) [96]. In this work, an electric thermal battery

model library was developed as an add-on to the component library *TIL* providing models for battery, modules and systems. This work it was mainly focused on describing temperatures, waste heats and different cooling approaches.

Torben used an AUDI A1 Sportback as a technology demonstrator with an entirely electric powertrain, completed to a serial hybrid by a fuel cell range extender [97]. The main focus of this paper was the *TMS* of the car, which had to deal with different temperature levels and must be designed for zero emissions and energy efficiency. The models were built using as it is previously mentioned *TIL* Suite library and also, the commercial Powertrain Library. Figure 5.9 (b) shows the electrical battery model based on equivalent circuit composed of *RC* elements and the *TMS* model developed in Torben´s work.

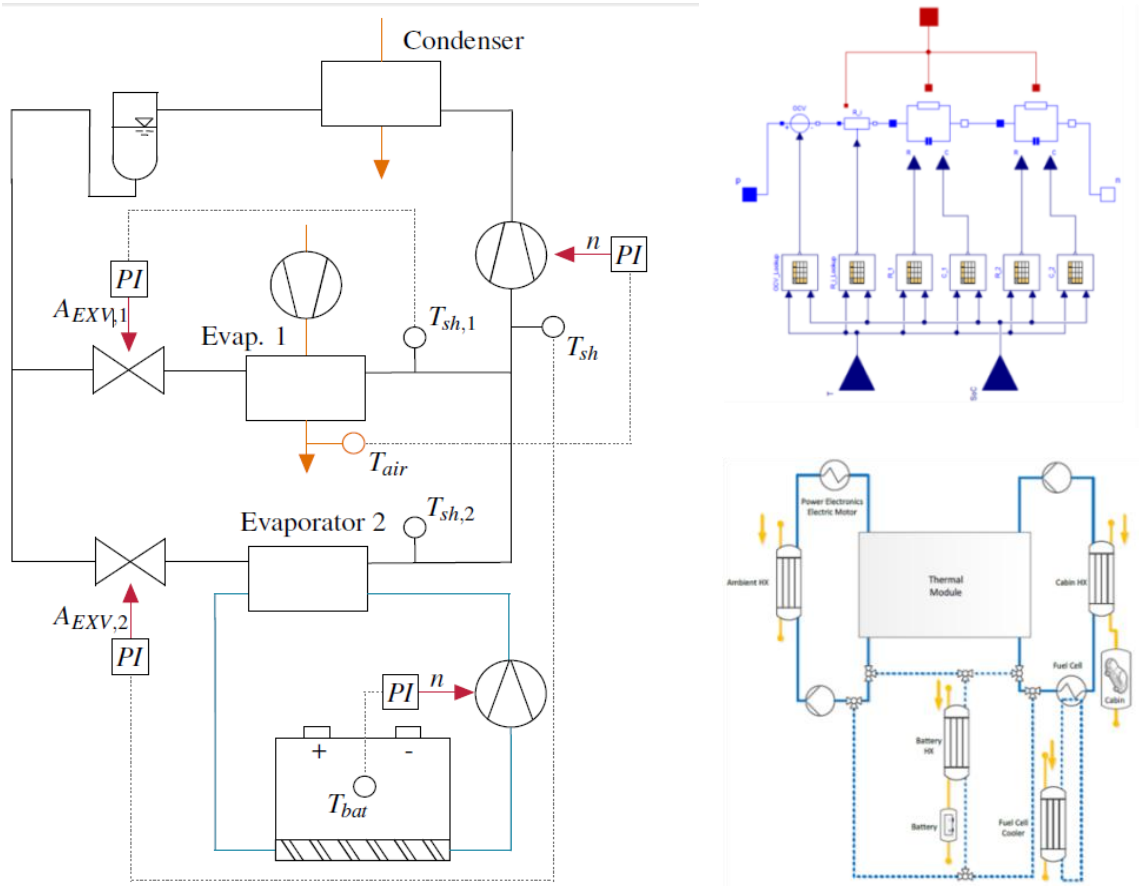

(a) *(b)*

Figure 5.9 (a) Vapor Compression Cycle for a Battery Electric vehicle including battery cooling developed by Andrea et. al [96] and (b) electrical battery (left) and the TMS (right) models developed by Torben et al. [97].

5.3 DESING AND OPTIMIZATION METHODOLOGY

The methodology developed in this research work has been comprised of five consecutive main steps which will be thoroughly explained in detail along this chapter, focusing the attention on the fifth step. A detailed complete flow diagram showing these steps can be seen in Figure 5.10. As it can be observed, some of these steps involve closed-back-loops that should be solved prior to continue with the next step. Different figures and lines have been used in order to make reference to different tasks, and it is important to know them to clearly understand the established methodology.

Firstly and as it is shown in Figure 5.10, the 5 steps are indicated by the correspondent number. Regarding the figures used, it can be observed rectangles, ovals and rhombuses. The rectangles are referred to the specific tasks that have to be fulfilled in each step along this methodology, while the ovals indicate the results obtained in one of each task. Besides, the rhombus figures indicate a question by means of which, it will be evaluated if the assumptions, decisions or the developments considered until this point are reliable and accurate or not.

These previous figures are linked between them by means of different type of lines as it is shown in Figure 5.10. The continuous green lines indicate progression in the design process, while the discontinuous red lines always involve a backward or reverse movement or a reflexion in the design process. At last, the discontinuous blue lines are bidirectional and they imply the use of a medium (in this case, the developed models) in order to achieve a specific aim (defined tasks in the rectangles).

All the steps to be followed are listed below:

(1) Design Criteria Definition

(2) Predesign of the *BP* and its *TMS*

(3) Detailed Design of the *BP* and its *TMS*

(4) Thermal Models Validation

(5) Thermal Design Optimization

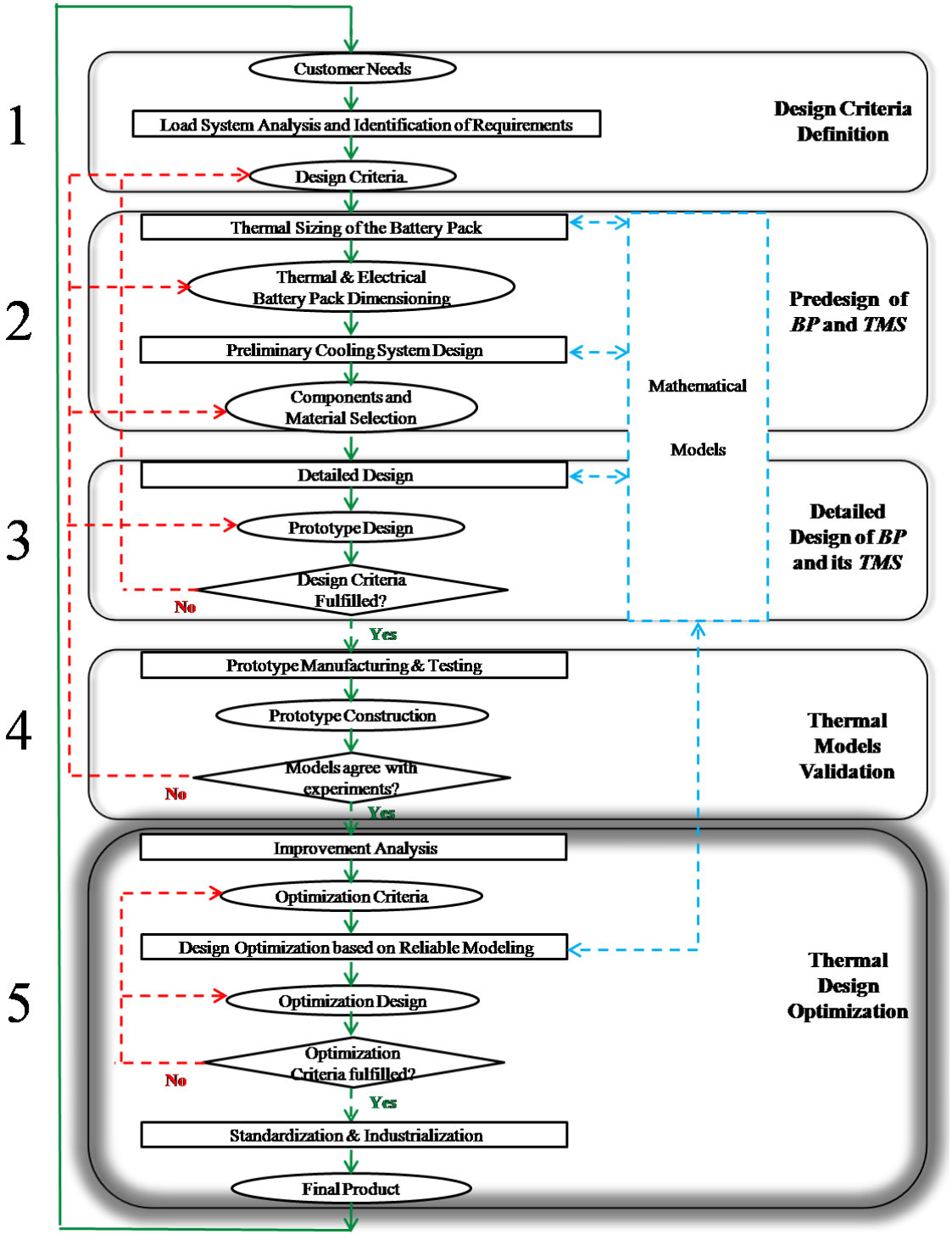

Figure 5.10 The developed complete methodology.

5.3.1 DESIGN CRITERIA DEFINITION

The main and unique task of this step, which it is shown in Figure 5.11., is related to the analysis of the load system and the identification of the requirements considering the customer needs. On this basis, the design criteria are defined which must be fulfilled at any step of this design and optimization methodology.

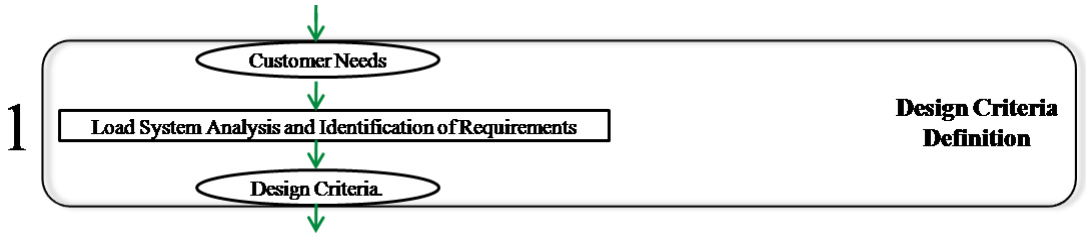

Figure 5.11. The step related to design criteria.

Some of the questions such as the ones mentioned below must be answered in this step:

"Which are the power, voltage and current requirements for the energy storage system in the application for which it is intended?"

"Which is the resulting charging and discharging behavior expected for the Li-Ion cells used in the battery system?"

"*Which are the requirements of the vehicle (compact, lightweight, etc)? Which is the available space to integrate the battery system in the vehicle?"*

"Which are the external conditions expected for the battery system (vibrations, ambient conditions such as humidity, etc)?"

"Which is the acceptable operating temperature range for the battery system? And the level of acceptable temperature variation for the modules and the pack?"

"Which is the priority when designing, battery uniformity and thus, extended lifetime, or reducing system complexity as much as possible?".

The needs or specifications that have to be fulfilled in any kind of application can be defined by the manufacturer itself or by the designer, and they can cover from thermal, electrical, consumption, initial cost, weight and compactness issues to even, aesthetic aspects. Independently that the requirements have been imposed by the manufacturer or

by the designer, this methodology should cover any involved limitation in this respect. Particularly, for the applications analyzed in this research work, the principal requirements have been defined by the manufacturer. For instance, the electrical solicitations that the applications must have in terms of energy and power (Chapter 2), the implemented specific cell type in each *ESS* (Chapter 3) and *TMS* technology (Chapter 4), have been imposed by the manufacturer. Nevertheless, other issues such as thermal criteria, have been defined by the designer based on the customer needs and on the identification of the load and requirements of each particular application.

In respect to the thermal criteria, an appropriate thermal performance of the *BP* it is really important in this type of applications especially to ensure *BP* lifetime since, among other things, it is one of the most expensive components of the *eMOV* application. For that reason and to avoid as far as possible for example the need of replacing the *BP*, a permissible maximum performance temperature and a thermal dispersion between cells and *BM*s in the overall system has been established in each case.

In this context, some operation ranges in terms of *BP* have been defined in order to control accurately its thermal performance. In Figure 5.12 are shown the defined operation temperature ranges. Ideally, it is preferable to keep the *BP* temperature as near as possible from the defined ideal temperature. A higher operation temperature than is recommended as the ideal temperature in the *BP*, could involve a set of problems which can result in a thermal runaway and the destruction of it in the worst case. In addition, it is important to establish a minimum operation temperature. A low operation temperature could generate a reduction of the power and lithium plating effect of the anode with an irreversible capacity loss at cell level and consequently, at *BP* level. Besides and related to the thermal dispersion between the cells and *BM*s within the complete *BP*, it should be measured and evaluated in order to take decisions about this issue, if it would be a real problem in the analyzed *BP*.

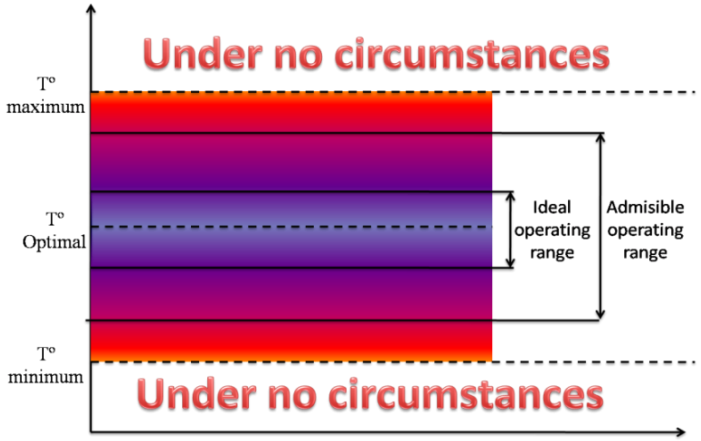

Figure 5.12 Thermal performance for a BP.

Apart from the thermal issues, the aspects related to the compactness and complexity, weight, consumption, initial investment and maintenance of the system should be minimized as far as possible, in order to reduce the overall cost of the system and not to affect negatively to essential features related to *eMOV* applications such it can be the autonomy.

5.3.2 PREDESIGN OF THE BATTERY PACK AND THERMAL MANAGEMENT SYSTEM

Once the design criteria and specifications that have to be met in each specific application have been identified, the next step, which is shown in Figure 5.13, has been defined such as the predesign of the *BP* and its *TMS*. The main two tasks of this preliminary design step have been to carry out the thermal sizing of the *BP*, evaluating the heat that must be dissipated by means of the designed *TMS*, and to predesign the *TMS* for each case selecting the components and materials needed. For that purpose, some simple calculations have been carried out based on thermal and hydraulic balances in order to at last, be able to take decisions in terms of design concept. The basic components that will be used to mount the *TMS* have been selected mainly based on their data sheets and considering the most restrictive operation conditions.

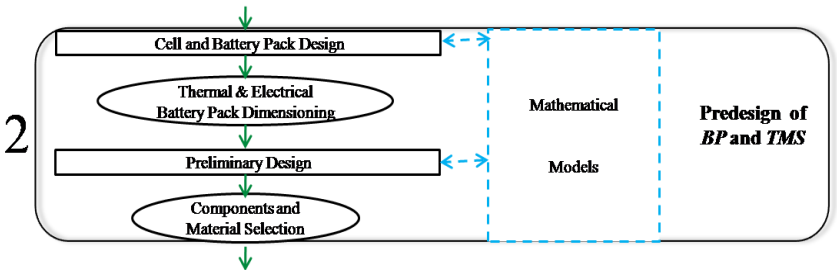

Figure 5.13. The second step related to the predesign of the Bp and TMS.

Based on the electrical sizing of the *BP* that it has been carried out in Chapter 3, has made possible to size the *BP* thermally, calculating the total mean heat generation rate generated within it. This thermal sizing gives a clear idea of the needed cooling capacity of the *TMS* to maintain the cells of the *BP* within the desired values for the worst ambient and operative circumstances. The procedure followed is explained in detail in the next paragraphs.

The first step to evaluate the total amount of heat that will be generated at *BM* or *BP* level is to characterize experimentally the thermal performance of a cell. In general terms, when some charge or discharge current is demanded to any *Li-Ion* cell some amount of heat is generated, which is accumulated and transmitted through its body. The instantaneous heat generation depends on the so-called thermo-chemical properties of a cell. The heat accumulation and transmission depend on the so-called thermo-physical parameters.

The internal resistance and entropy of reaction are the main important thermo-chemical parameters that must be known for dimensioning the *BP* system and therefore, the *TMS*. Regarding the internal resistance, the lower internal resistance the battery has, the lower the heat generation will be. The internal resistance is a parameter which depends on the thermal and chemical equilibriums, i.e., it is function of cell temperature and *SOC*. Besides, it is always inversely proportional to temperature and *SOC* in *Li-Ion* cells. In order to determine experimentally the internal resistance, the constant current discharge pulses have been used [68].

On the other hand, the most common method to determinate the entropic heat coefficient is the potentiometry, carrying out Open Circuit Potential (*OCP*) experiments. This parameter is obtained in function of *SOC*. Its tendency usually changes within the *SOC* range due to a phase change in the cathode or because of a structural change in the anode. For the same cell, this value can be positive for some *SOC* ranges and negative for others.

The developed heat generation model which it can be seen in Eq. (5.11) has been used along this research work. This formula is sensitive to the instantaneous current value and previously mentioned thermo-chemical parameters, the internal resistance,

R_{in}, which depends on the absolute cell and *SOC* variation, and the entropic heat coefficient, $\frac{\partial \mathrm{U}^{\mathrm{avg}}}{\partial \mathrm{T}}$, that only depends on the *SOC* value.

$$\mathrm{S_h} = \frac{\dot{\mathrm{q}}_{\mathrm{T}}}{\mathrm{V}} = \frac{\mathrm{I}^2 \cdot \mathrm{R_{in}}\left(SOC, \mathrm{T_{cell}}\right) + \mathrm{I} \cdot \mathrm{T_{cell}} \cdot \frac{\partial \mathrm{U}^{\mathrm{avg}}}{\partial \mathrm{T}}(SOC)}{\mathrm{V}} \tag{5.11}$$

The thermo-physical properties of a cell that have to bear in mind and must be determined in order to characterize it, are the heat capacity, Cp, and the thermal conductivity, k. Although a *Li-Ion* battery is a composite construction containing aluminum, copper and many other materials, along this research work has been assumed that the cells do not have a "distributed" heat capacity, but an average heat capacity influenced by the specific heats of each material that makes up the cell. By means of the adiabatic calorimetry has been determined this thermo-physical parameter. In terms of the thermal conductivity, due to the anisotropic structure layers of cylindrical cells, for instance, radial and axial thermal conductivities have been defined experimentally, using for that purpose the hot disk plane source technique [98]. Experimental validation of the heat generation model has been carried out by means of the accelerating rate calorimetry which is based on the direct measurement of the temperature change in a cell, inside a heat insulated and adiabatic system [68].

Once the heat generation model has been validated, the heat generation rate has been estimated using the formula shown by Eq. (5.11), for different invariable temperature values and cyclic electric load conditions. The instantaneous heat generation rate obtained at cell level has been averaged, obtaining the mean heat power value at cell level for different constant temperatures. This value can be easily scaled at *BM* level multiplying the cell level heat generation rate by the number of cells within the *BM*. The same philosophy related to the scalability has been followed in order to calculate the heat generation rate at *BP* level, i.e., based on the amount of heat that is generated on a single *BM*. This procedure can be applied to any previous electrical sizing.

As an example, in Figure 5.14 is shown the heat generation rate at *BP* level for a hypothetical case based on the heat generation estimation at cell level. This *BP* is composed of 6 *BM*s, comprised each one of 8 cells. An *Excel Worksheet* has been used for this purpose. As it can be concluded, the higher current rate and the lower

temperature, the greater heat generation rate. The current rate has been more influential than the temperature and *Depth of Discharge* (*DOD)* range.

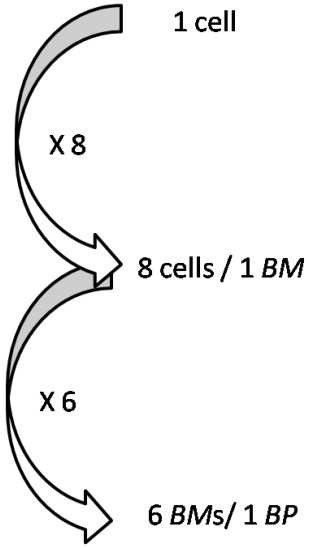

Tcell, °c	C-rate min			C-rate mid			C-rate max		
	DOD min	DOD mid	DOD max	DOD min	DOD mid	DOD max	DOD min	DOD mid	DOD max
10	-1,53	-1,54	-1,55	-2,78	-2,80	-2,84	-4,74	-4,78	-4,87
15	-1,42	-1,46	-1,47	-2,53	-2,54	-2,62	-4,21	-4,24	-4,31
20	-1,38	-1,39	-1,39	-2,28	-2,29	-2,31	-3,68	-3,70	-3,75
25	-1,29	-1,31	-1,31	-2,03	-2,03	-2,06	-3,16	-3,16	-3,19
30	-1,29	-1,29	-1,29	-1,95	-1,95	-1,96	-3,00	-3,00	-3,02
35	-1,25	-1,26	-1,26	-1,87	-1,87	-1,90	-2,84	-2,83	-2,85
40	-1,24	-1,24	-1,24	-1,80	-1,79	-1,80	-2,67	-2,67	-2,68
45	-1,21	-1,21	-1,22	-1,72	-1,72	-1,73	-2,51	-2,50	-2,51
50	-1,19	-1,19	-1,19	-1,64	-1,64	-1,64	-2,35	-2,34	-2,35

Tcell, °c	C-rate min			C-rate mid			C-rate max		
	DOD min	DOD mid	DOD max	DOD min	DOD mid	DOD max	DOD min	DOD mid	DOD max
10	-12,27	-12,32	-12,42	-22,24	-22,40	-22,75	-37,89	-38,24	-38,95
15	-11,34	-11,70	-11,78	-20,23	-20,34	-20,93	-33,68	-33,91	-34,47
20	-11,07	-11,09	-11,14	-18,23	-18,29	-18,47	-29,47	-29,61	-29,98
25	-10,28	-10,47	-10,50	-16,22	-16,23	-16,52	-25,25	-25,29	-25,50
30	-10,28	-10,28	-10,31	-15,61	-15,61	-15,69	-23,97	-23,98	-24,15
35	-9,96	-10,09	-10,12	-14,99	-14,98	-15,19	-22,68	-22,66	-22,80
40	-9,91	-9,91	-9,92	-14,38	-14,36	-14,41	-21,40	-21,35	-21,46
45	-9,65	-9,72	-9,73	-13,77	-13,73	-13,87	-20,11	-20,04	-20,11
50	-9,55	-9,53	-9,54	-13,16	-13,11	-13,13	-18,83	-18,73	-18,76

Tcell, °c	C-rate min			C-rate mid			C-rate max		
	DOD min	DOD mid	DOD max	DOD min	DOD mid	DOD max	DOD min	DOD mid	DOD max
10	-73,64	-73,92	-74,55	-133,46	-134,39	-136,50	-227,36	-229,44	-233,72
15	-68,03	-70,22	-70,70	-121,41	-122,06	-125,60	-202,07	-203,48	-206,81
20	-66,41	-66,52	-66,85	-109,36	-109,73	-110,84	-176,79	-177,66	-179,90
25	-61,69	-62,82	-63,00	-97,31	-97,40	-99,12	-151,50	-151,73	-152,99
30	-61,69	-61,70	-61,85	-93,64	-93,65	-94,16	-143,80	-143,89	-144,90
35	-59,78	-60,57	-60,69	-89,96	-89,90	-91,16	-136,09	-135,98	-136,82
40	-59,49	-59,44	-59,54	-86,29	-86,15	-86,45	-128,39	-128,13	-128,73
45	-57,87	-58,32	-58,38	-82,62	-82,40	-83,21	-120,68	-120,22	-120,65
50	-57,28	-57,19	-57,22	-78,95	-78,64	-78,75	-112,97	-112,37	-112,56

Figure 5.14 The calculation of the heat generation rate at cell, BM and BP level.

This initial approach assumes a null temperature dispersion within the cells of a *BP*. Nevertheless, this formula (Eq. (5.11)) has been defined and integrated into the simulation tool used for each application to make more advanced estimations based on preliminary or very basic models that will be upgraded in the next steps of the methodology. By this way, it will be possible to evaluate the thermal dispersion.

The estimation of the global heat generation rate at *BP* level has allowed the designer to determine the cooling capacity that will be required from the *TMS* for each specific application. The mean heat generation rate for the worst electrical conditions (permanent and cyclic load profiles) at the defined ideal operation temperature for the *BP*, has been considered for the purpose to carry out the dimensioning and the selection of the components and materials of the complete system. Basis on these assumptions, it is obvious that an oversized *TMS* will be predesigned as a result of this step of the methodology.

Considering the estimated heat generation rate that it should be dissipated by the *TMS* and based on the cooling technology previously selected for the analyzed applications, different *BP* structures and cooling architectures concepts have been

analyzed, resulting in the most suitable components selection. As this predesign step is a quite basic stage of this methodology, the idea is to use a simple modeling approach to analyze easily and by means of few computational and time resources, several different options in terms of *TMS* design.

One of the main simplification of this approach has been the approximate and lumped physical properties that have been considered to model the *BP*. With regards to the components that are part of the *TMS*, their performance curves provided by the manufacturer have been considered and implemented in the developed Worksheet. Based on them, thermal and hydraulic balances at stationary conditions are defined which implies the adoption of a lot of simplifications that should be improved and analyzed in the next design stages.

The generated nonlinear algebraic equation system is numerically solved using an efficient iterative resolution procedure. For that purpose, the *Microsoft Excel* spreadsheet has been selected, with its built-in *Solver*, to implement the mathematical model developed for each analyzed case of this research work. This widely-used software offers a user-friendly environment and includes a lot of programming options through use of the so-called *Visual Basic for Applications*. By this way, it has been demonstrated that the *Standard Solver* proved to be a useful tool for analyzing, in sense of predesign, systems and processes of medium complexity, expressed by means of linear or smooth nonlinear equation systems, with an acceptable compromise between the efficiency and the rapid obtainment of the results.

With the aim to explain in a simple way the procedure that has been followed in this step, a hypothetical case (different than the cases that will be analyzed following in Chapter 6 and Chapter 7) is explained as an example in the next paragraphs. The considered BP is cooled by an air cooling system and is composed of 3 strings (5 BMs in each string) which are connected electrically in parallel. The schematic layout of the described *BP* and *TMS* is shown in Figure 5.15.

Two fans have been placed in the rear part of the *BP* extracting the air from the system. Based on the requirements that the manufacturer could impose in terms of dimension or even consumption, several fans have been preselected and their performance curves have been introduced in this selected predesign tool. From the

hydraulic point of view ideally equilibrated air flows have been considered in each of the channels. The pressure loss depends directly on the magnitude of the air flow that can be achieved by the fan and it has been imposed an equilibrium that must be reached between this pressure loss and the fans hydraulic curve.

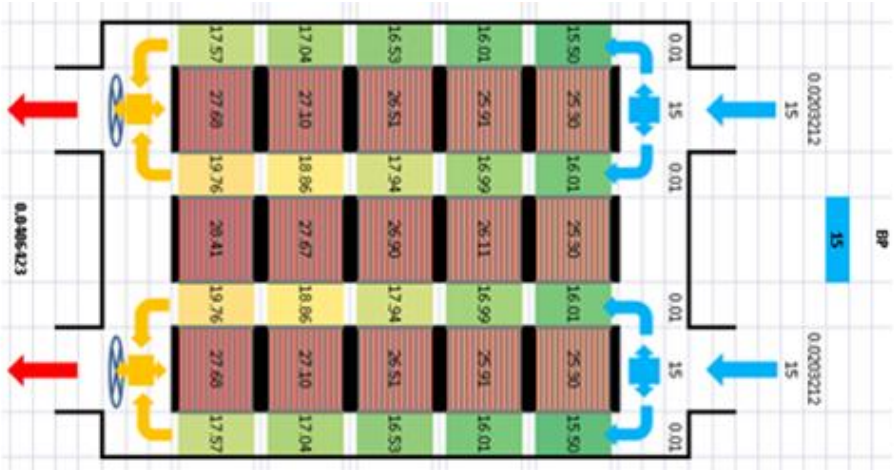

Figure 5.15 Schematic BP and TMS layout.

From the thermal point of view, it has been considered that all heat generated inside the *BP* has been transferred to the lateral face of the *BP* by thermal conduction. The external walls of it have been considered as adiabatic surfaces for simplicity. The thermal resistance of the *BP* has been approximately evaluated depending on the considered properties and sizes of the cells. The convective heat transfer inside the channel depends directly on the reached air flow. The air is heated as goes by through the channel due to the contribution of each of the modules generating different levels of thermal asymmetries and a thermal equilibrium should be reached by the total heat power that is generated in all *BM*s.

In Figure 5.16 (a) and (b) can be seen the hydraulic and thermal network example implemented in *Excel* of the previously explained case. All mathematical relations in terms of hydraulic and thermal balances have been easily implemented on *Excel* spreadsheet in order to check its real performance. For this purpose, the algebraic equations have been posed as a restricted problem in where air velocities and temperatures are tentatively modified to reach the global energetic balance. All the other possible relations hydraulic and thermal equations are posed as restrictions to the global problem.

(a)

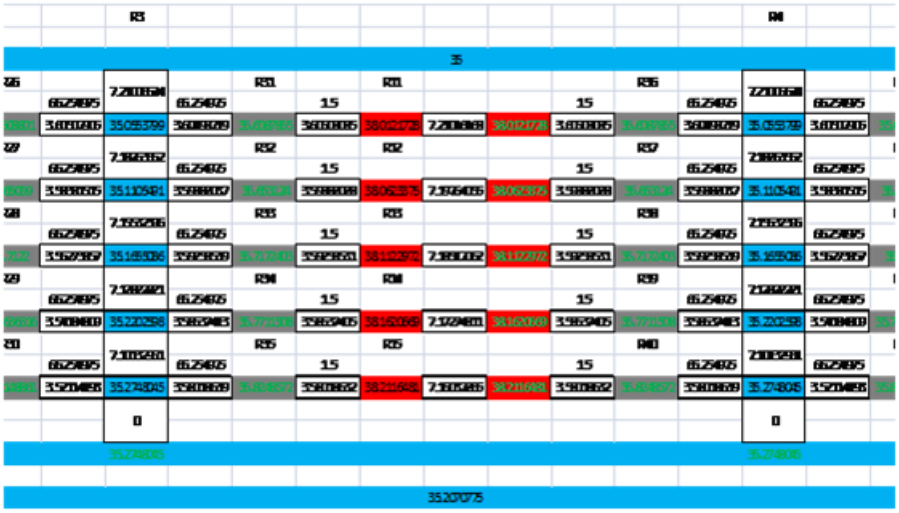

(b)

Figure 5.16 (a) Hydraulic and (b) thermal network in Excel for this example case.

Based on the previous results obtained it has been possible to select the most suitable fan for this particular case, considering the previously preselected and implemented fans in this predesign tool. Following the same procedure and philosophy, the selection of the components and materials for the *eMOV* applications analyzed in the present work has been carried out.

To conclude this section it can be stated that this second step of the methodology is the most conceptual one and leads normally to oversized designs due to the considered assumptions related mainly to thermal sizing of the *BP* and to thermal and hydraulic balances carried out in stationary states. Generally speaking, the selected components at this stage must guarantee an adequate thermal performance, even for the worst possible ambient and load conditions, but at expense of an elevated power consumption, volume or weight of the *TMS*. These considerations will be sequentially improved in the next steps.

5.3.3 Detailed Design of the Battery pack and Thermal Management System

The third main stage of this methodology corresponds to develop detailed numerical models of the both predesigned *BP* and *TMS* with the objective to check by means of them the fulfilment or not of the defined design criteria for broader ambient and load conditions and the eventual possible margin for improvement or not. In Figure 5.17 is shown the graphical description of this third step and the interactions that it has with the other previous steps.

The main task of this step is to obtain transient thermal results at *BM*, *BP* and *TMS* level to propose (or not) a complete or scaled prototype design with its detailed drawings. At the end of this step and before going on, it should be checked if the defined design criteria in the first step have been fulfilled or not. In the case they will be not achieved, it should be gone back in order to revise the previously defined design criteria, the thermal sizing of the *BP* and its *TMS*, the selection of the components and materials or even to propose an alternative conceptual design or architecture.

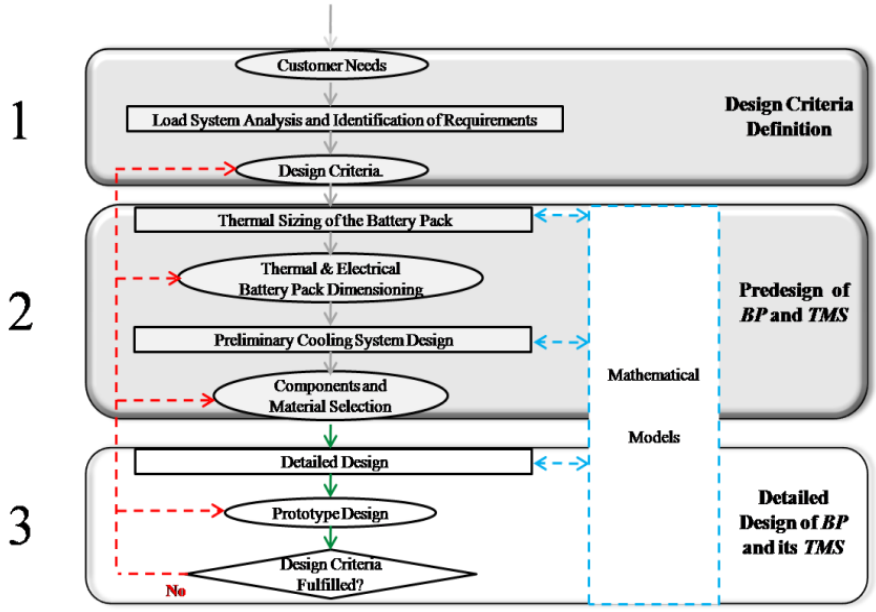

Figure 5.17. The third step related to the development of the detailed models.

The development of a detailed model forms the core of the engineering approach to a design of a *TMS* for a *BP*. In particular, for these both applications various have been the considerations that have been taken into account to make more effective modeling process.

The first consideration has been related to developing a model as simple as possible with an enough accurate predictions to address the set objectives, trying to minimize the possible high computational cost that could be implied on making a really detailed model.

Secondly, in each selected simulation tool has been considered the *BP* design specifications, the thermal properties and the electrical performance characteristics in order to predict accurately the transient temperature distribution and variation for different operating and ambient conditions of the complete system. Furthermore, the thermal model should take into account not only a distributed instantaneous heat generation rate for each cell, but also a more realistic heat dissipation to better understand how the *BP* design and operating variables could affect its thermal performance and also, to achieve a proper temperature control at cell, *BM* and *BP* level.

For both test cases, two models of the simplified but representative sample prototype have been developed: *BM* and *BP* models. These models have been developed based on the scalability concept that has been explained in the second step regarding the thermal sizing. At *BM* level the use of both proposed simulation tools would be reasonable and feasible especially for transient simulations. However, considering the *BP* level some simulations could become infeasible with this detail level. For instance, the analysis of the *NC* by means a *DAE* simulation tool would be unreasonable or very imprecise, whereas a *TMS* with phase change phenomena could be really complicated and unviable to model with a *CFD* simulation tool.

In this design step, the instantaneous heat generation model, Eq. (5.1) has been studied carrying out some real transient simulations at *BM* level using for that purpose, the cyclic *RMS* averaged current profiles defined for each application in the final section of Chapter 2. More details about the specific detailed models that have been developed both at *BM* or *BP* level and their *TMSs* will be shown when explaining the test cases.

At the end of this stage, it is essential to check whether the design criteria have been fulfilled or not by the proposed prototype by means of the developed detailed models prior to its construction. For that purpose a test matrix based on Design of Experiments (*DoE*) has been defined in order to study as wide as possible operation conditions range with the minimum numerical tests required. Different variables at different levels

(maximum, medium and minimum) have been defined to study their influence on the thermal responses such as maximum *BM* temperature or thermal dispersion between cells within the *BM*. The variables that have been considered have been the current rate, *SOC* range, ambient temperature and air or liquid mass flow rate among others. In this step, the model scaled at *BM* level is checked. However, the *BP* level models will be developed and used only after this detailed analysis.

Two options will be possible as it is indicated in Figure 5.17:

- Option A: if the design criteria have not been fulfilled with the selected design concept, steps (1) to (3) would have to be reviewed in order to find the reason and consequently, the solution. This option is indicated by red discontinuous lines in Figure 5.17. The specifications initially defined could turn out to be too demanding or even inconsistent and thus would have to redefine. If it were not the case, the proposed components and materials would have to be revised and modified. If it were still not enough, then a completely new design concept would have to be proposed in order to find a design solution which satisfies the initial design criteria established in the first step of the methodology.

- Option B: if the design criteria have been fulfilled accordingly to the decisions have been taken in the previous steps, it could be continued to the next steps in order to find a more adjusted design. The *BP* level models are developed for the next stages.

5.3.4 THERMAL MODELS VALIDATION

The fourth step as it is shown in Figure 5.18 is referred to the construction of a scaled system prototype for experimental validation purposes based on the previous developed detailed models. It is a quite complicated task or not a very practical approach to build up a prototype of the entire *BP* and its *TMS* in the laboratory environment. It is eventually impossible to load or cycle the complete *BP* emulating, for example, the regenerative braking of a full electric bus of medium size. For that reason, it is mandatory to use the thermal scalability at system level and only construct a prototype at *BM* level to check its performance experimentally.

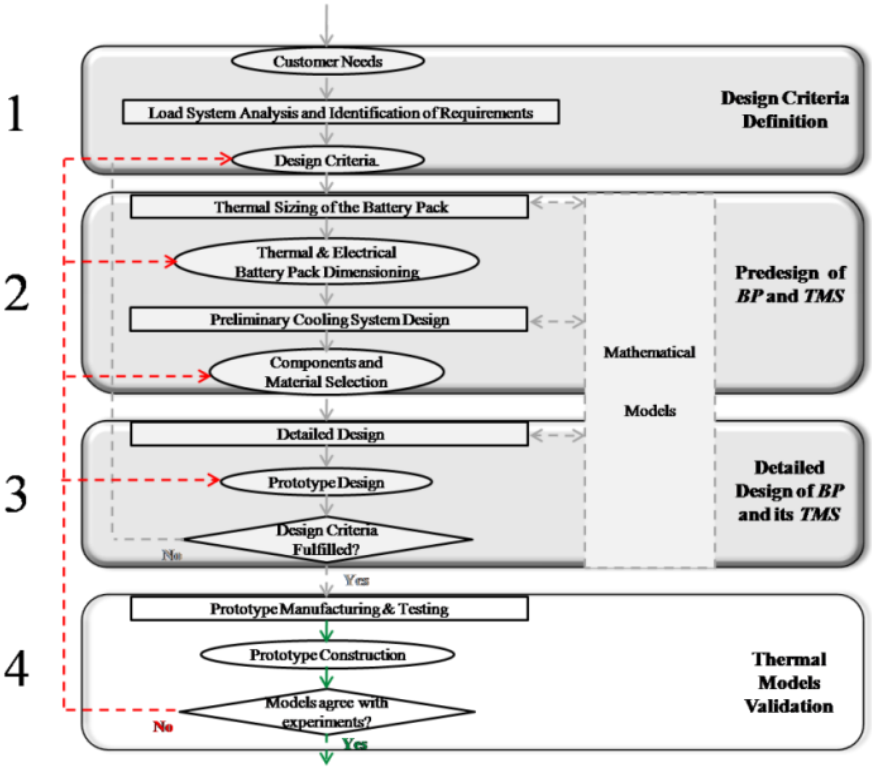

Figure 5.18 The fourth step related to the thermal models validation.

Although the designer trusts on the developed detailed mathematical thermal models described in the 3rd step, it has been necessary to carry out the validation of them through experimental tests to guarantee by means of real measurements, their reliability. In other words, the goal of the construction of the prototype is to check whether the equations, models and assumptions that have been used and applied during the development of the thermal model process represent well enough the reality in the validation process.

For both cases, a prototype to be tested in a laboratory environment has been constructed using a single *BM* such as a scaled unit of the complete *BP*. Regarding the *TMS*, for the first defined application it has been also considered its scalability at *BM* level, assuming the same scaled thermal performance of the *TMS* at *BM* and at *BP* level. Nevertheless, the contrary has occurred for the second studied *eMOV* application. In this case, it has been possible to scale the *BP* at *BM* level but not the associated complex *TMS*. Therefore, apart from a single *BM* an electric heater has been used to generate or emulate the extra heat that will be generated by the complete *BP*. By this way, it will be possible to carry out the validation of the complete *TMS* for the urban electric minibus application. It is important to add in the prototypes the necessary sensors to be possible

to measure variables regarding air and liquid mass flow rate and temperature, the pressure in different points of the system, the temperature of the cells, the electric solicitations and power consumption among others. All these experimental measurements must be compared with the predictions of the numerical models.

Once the prototypes have been constructed for both test cases, the next step correspond to carry out the experimental tests to determine and quantify afterwards, the numerical difference in terms of prediction of the thermal performance of the *BM*. The same test matrix than in the previous test has been carried out experimentally. In general terms the same procedure has been followed to perform all the tests: first, the air or liquid flow rate and ambient temperature have been set by potentiometer or valves. The ambient temperature of the climatic chamber has been regulated manually, until the objects have reached the same uniform initial temperature. Then, the cells of the *BM* have been completely charged (*SOC* 100%) and then discharged at the initial *SOC* value defined for the corresponding test. Once everything was ready for the test to be initiated, the *BM* has been continuously discharged and charged between defined *SOC* limits with the corresponding current rate for each process, until system has been established thermally.

The validation task has been performed comparing the experimental temperature measurements of the *BM* while it is cycling. In addition, to validate the *TMS* based on the dual architecture the thermodynamic variables and power consumption of the *TMS* have been studied. If these differences among simulated and measured variables are assumable, the developed model can be considered reliable and accurate. If it is not the case, the models should be adjusted or used sub-models checked. This task is shown in Figure 5.18 by means of the rhombus.

After carrying out the experimental tests defined for each case, two options are possible which are shown in Figure 5.18:

- Option A: if the experimental tests did not show agreement with numerical models and with design concept, it would mean that the thermal performance of the constructed prototype is not agreed with the developed thermal models. It could happen that the detailed models have overestimated or underestimated the reality; in any case the detailed

thermal model should be modified or adjusted searching for more accuracy. These options are indicated by red discontinuous line in Figure 5.18 meaning that each of the previous steps have to be checked searching for modeling errors (poor flow and thermal physics representability) or even scalability, architecture or component characterization errors.

- Option B: if the experimental tests showed agreement with numerical models and with design concept, it could be concluded that the detailed models are validated. This option is indicated by green discontinuous line in Figure 5.18.

If the modelling accuracy is good enough but the design has proved to be slightly undersized in the reality the design process could come into its end. If the improvement margin is still considerable reducing power consumptions or complexity of the prototype, a window is open for optimization.

5.3.5 THERMAL DESIGN OPTIMIZATION

Once the developed detailed thermal models have been experimentally validated, it is the moment to validate the thermal design itself and to evaluate the level of the compliance of the specifications or requirements defined in the first step. Accordingly, it has been defined the actual thermal margin of the *BP* or the eventual possibility to improve the *TMS* optimizing it at component and at system level in terms of simplicity, cost, weight, volume, power consumption and other less evident criteria. In other words, the aim of this last step is to analyze the degree of over sizing of the initially proposed prototype and to propose a definitive and optimized *BP* and *TMS*. This is an essential task to propose the most adequate thermal design for its industrialization.

Among the optimization methods that already exist and they have already been applied in different applications scopes, it has been decided to apply a non-arbitrary optimization method based on *DoE* technique and the analysis of response surfaces of several variables of interest. Minitab 17.0 software has been used for that purpose.

Several steps have been followed to achieve an optimized *TMS*. The first step is related to the selection of the response/s to be analyzed and the definition of the specific

objectives. It is called "objective function" to the variable or combination of variables to be measured as a result of the evaluated process.

The second step before selecting the most suitable and appropriate thermal design is the definition of the factors. These are the variables that affect significantly to the response and must be identified adequately. In this task, it is important to list all the possible factors that have to bear in mind in order to analyze the response and to discard the ones that they are not essential to the process after a first screening. The factors can be continuous numerical values such as temperature or the consumption of any component or discrete (categorical), such as the existence or not of a component or the use of a bigger or smaller component. It can be said that in the case studies of the present work the factors have been mostly continuous such as it can be the rotational speed of the fan, the pump or the compressor. On the contrary, for instance in the case of the elevator, it has been analyzed the influence of using or not heat sink or even different heat sinks, so in this case the factor has been discrete.

At last and as the third step, in order to select a suitable optimized design, it is mandatory to determine the order of the response surface for these factors to establish the number of levels. First-order or second-order models can be suitable to adjust the responses of these thermal simulations. First-order models are defined by Eq. (5.12), while the second-order models by Eq. (5.13) [100].

$$y = \beta_0 + \sum_{j=1}^{k} \beta_j x_j + \varepsilon \tag{5.12}$$

which can be written by

$$y(x) = \beta_0 + \beta' x + \varepsilon$$

$$y = \beta_0 + \sum_{j=1}^{k} \beta_j x_j + \sum_{j=1}^{k} \beta_{jj} x_j^2 + \sum_{i=1}^{j-1} \sum_{j=2}^{k} \beta_{ij} x_i x_j + \varepsilon \tag{5.13}$$

Which can be written by

$$y(x) = \beta_0 + \beta' x + x' E x + \varepsilon$$

where β's are the unknown parameters that must be estimated from numerical data from simulations and k the number of factors. β_{jj} parameters are called as "pure

quadratic" effects, to distinguish them from 2-factor interactions, which are also quadratic but due to the mixed effect of two factor. $\beta$and$x$ are $k \times 1$ vectors, while E is a symmetric $k \times k$ matrix that contains the β_{ii} parameters in the diagonals and $^1/_2\,\beta_{ij}$ in the (i, j) off- diagonal positions. $i$is the factor that is moved over two unit range, from -1 to 1 referring -1 to the minimum defined state and 1 to the maximum state of each parameter. Non-linear responses are expected in general taking into account the complexity of the developed models describing interrelated heating and cooling phenomena.

Response Surface Methodology (*RSM*) is a series of experimental design, analysis, and optimization technique that originated in the work by Box and Wilson in 1951 [101]. These experiments can be performed over real elements or processes or over previously validated virtual models. The main goal of *RSM* technique is to obtain an optimized process which could imply, for example, to minimize the cost of operation of a production process, to minimize the variability of a quality characteristic or to achieve desired specifications for a response. In many practical problems, multiple responses of interest are considered as it is in this particular case, for both selected *eMOV* applications.

RSM technique suggests estimating a second order polynomial when there is an evidence that the response is curved in the current region of interest, as it is shown in Figure 5.19, or when lack of fit tests point to an inadequacy of a first order model. In general, *RSM* is often used to refine models after the designer has determined important factors using previously factorial designs; especially if it is suspected a curvature in the surface response.

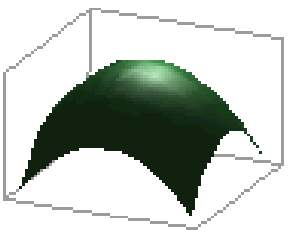

Figure 5.19 Response surface with curvature [102].

Within this optimization technique, there are two main types of response surface designs that are of special interest for their particular characteristics: Central Composite

Design (*CCD*) (Figure 5.20 (a)) and Box-Behnken designs (Figure 5.20 (b)). In this work, the *CCD* method has been selected to use because the Box-Behnken design is mainly used in the cases in where it does not contain an embedded factorial or fractional factorial design whereby involves that it is not suited for incremental number of experiments.

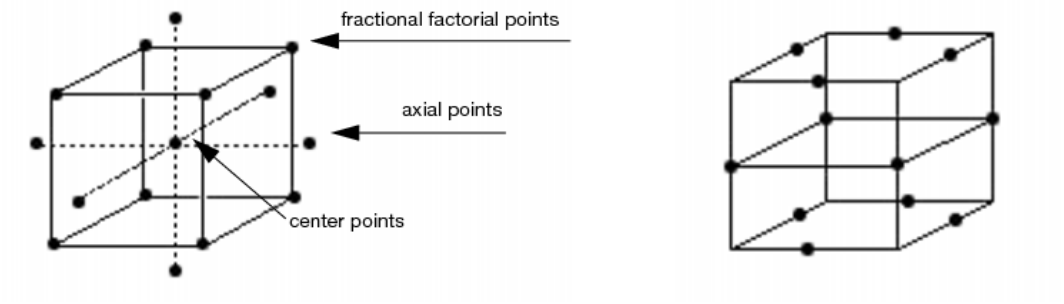

(a) *(b)*

Figure 5.20 Schematic of (a) Central Composite design (CCD) and (b) Box-Behnken design (Minitab 17.0 Support, [102]).

Moreover *CCD* is the most commonly used *RSM* design experiment. The second order designs which can be fit to Eq. (5.13), they must have at least three different levels in each defined factor and this is satisfied by *CCD*s, which can have up to five levels per variable.

CCD designs were first proposed by Box and Wilson [101] and they are composed of three parts [100]:

1) 2^k or $2_R^{k-r}\,(R \geq V)$ factorial experiment

2) 2k axial points

3) $n_0$replicates of the center point

They consist on a fractional factorial design of V (five in Roman number) resolution which allows clear estimations of all main effects and 2-factor interactions, and of the pure quadratic effects (curvature estimation) by means of axial points. Some center points can be designed to be run together with the factorial points and other ones can be designed to be run together with the axial points. In Figure 5.20 (a) are identified the fractional factorial, axial and center points.

The term "resolution" is referred to the concept that allows the user to "see" the effects clearly: a higher resolution, a better perception of the effects. In the limit, a full 2^k design has a full resolution to estimate in an impartial manner all effects in model defined by Eq.(5.13). It is crucial to keep in mind that the importance related to the effects usually decreases with the number of factors in the effects. Thus, main effects (i.e., single factor effects) are usually more important than 2-factor interactions which in turn are usually more important than 3-factor interactions, etcetera. As a definition it can be said that "*a design of resolution R is one in which no m-factor interactions effect is aliased with any other effect with less than R-m factors"*. Therefore and considering the previous definition, it can state that a V resolution has main effects confounded with 3-factor interactions, and 2-factor interactions are confounded with 3-factor interactions.

The rotatability and orthogonal blocks are both the desired properties of the *CCD*s. The orthogonal property is related to the independent estimation of each main effect and interaction and consequently, it makes the analysis of the results easier. This feature guarantees that the effect of one factor or interaction can be estimated separately from the effect of any other factor or interaction between various in the model.

On the other hand, the rotatability is defined such as "*an experimental design is said to be rotatable if* $Var(\hat{y}(x))$*is constant at all points x equidistant from the design center*" which means that rotatable designs provide constant prediction variance at all points that are equidistant from the design center. α is the parameter which is referred to the axial distance and it is related to the rotatability. This number depends on the number of experimental runs in the factorial portion of the *CCD* as it is shown in Eq. (5.14):

$$\alpha = [number\ of\ factorial\ runs]^{1/4} \tag{5.14}$$

A popular choice among *CCD* is called as *Face Centered CCD* and is featured by its axial distance (α) value of 1. As it is shown in Figure 5.21, an α value less than 1 puts the axial points in the cube; a value equal to 1 puts them on the faces of the cube and values greater than one puts them outside the cube. This variety of design requires only 3 levels of each factor and increasing an existing factorial or V resolution design with the appropriate axial points can also produce this design [102]. In this optimization step this design method has been used because it provides a complete overview of the effects of the factor on the responses with a reduce number of three levels for each factor

making easier the procedure. Moreover it allows the estimation of a quadratic model, frequently used with optimization objectives or when it is expected that the responses are not lineal.

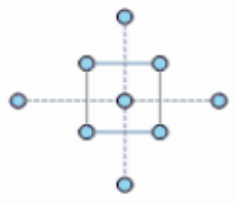

Figure 5.21. Axial points (α) in the cube [102].

Once the objective functions, factors and levels of the desired *DoE* design are identified and selected, the next step that has been carried out is to perform the needed simulations as numerical experiments. The objective function for both test cases has been, in general terms, the minimization of the auxiliary consumption and the involved cost of the system, ensuring the thermal defined requirements related to the maximum *BP* temperature and the thermal dispersion within the *BP*. For that purpose, it has been analyzed the influence of the use of heat sinks and the rotational speed of the fan on the previously mentioned variables for the residential elevator application, and in the same way, the performance of the compressor, fan and hydraulic pump for the urban electric minibus application. Similarly as for the complete methodology, in this step cyclic current profiles have been used in order to reach and evaluate the final steady state, i.e., once the *BP* has been stabilized thermally. In essence the same current cyclic profiles that have been previously used to validate the thermal models have been applied.

This optimization task has been carried out considering the complete performance at *BP* level. As aforementioned in Section 5.2.1, the main disadvantage related to *CFD* simulation tool is the high computational resources that are needed to analyze the performance of the complete *BP* at system level. Consequently and in order to avoid an unviable and infeasible task, a novel concept named *False Steady* has been introduced reducing significantly the simulation time cost and allowing the designer to carry out the optimization task with reasonable computational resources. On the other hand, in *DAE* simulation tool it has not been applied this concept due to pure transient simulations don´t generate any additional problem in terms of computational resources or required time.

The *False Steady* concept involves the use of an interpolation table which calculates the mean heat generation rate at cell level in function of a wide range of cyclic electrical solicitations (symmetric or asymmetric current profile of different *DoD* range) and possible cell temperatures, instead of using a heat generation model which calculates instantaneously the cell heat generation rate depending on the actual current profile, *SOC* value, internal resistance and entropic heat coefficient value (as it is defined in Eq.(5.11)). This way it is possible to perform steady simulations without considering prefixed and uniform heat power values for all the cells of the *BP*, obtaining realistic solutions of the final thermal state. In Figure 5.22 is graphically explained the *False Steady* concept.

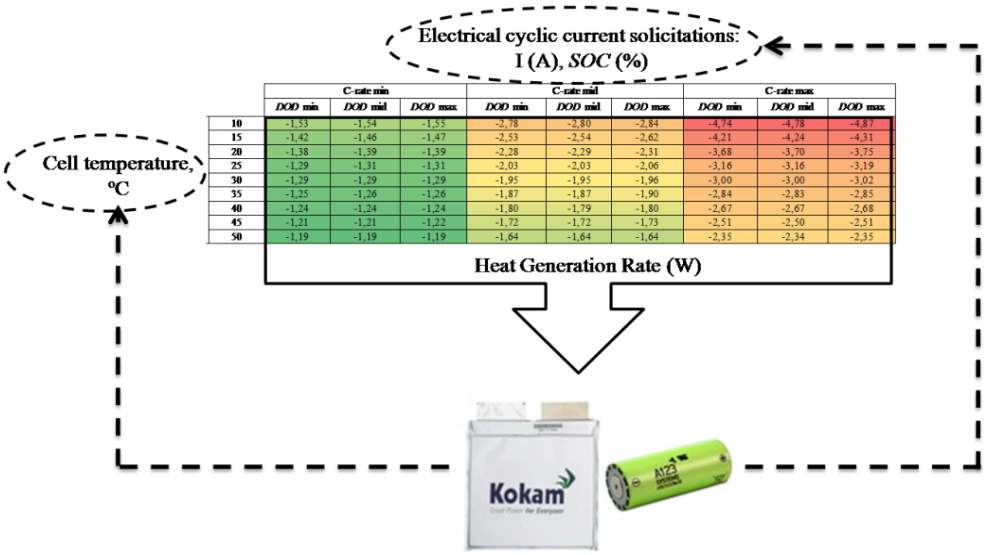

Figure 5.22 False Steady concept.

As an example, a heat generation rate at cell level which has been used is shown in Figure 5.14. As it can be seen the discontinuous lines indicated the inputs of the interpolation table (the actual cell temperature and the electrical solicitation at cell level) and by continuous black line is indicated the output, heat generation rate, which is applied in each cell.

At the expense of reducing the simulation time by means of this concept, it does not permit to exanimate the transient thermal evolution of the *BP* until the steady state is reached, but in this stage, this fact does not have much interest.

Once the simulation tests have been carried out following the *Face Centered CCD* design and the objective functions have been adjusted by means of Minitab and the

Surface Response Regression, the response surfaces can be thoroughly analyzed. By means of these surfaces responses, it is possible to understand the interactions and effects of the factors on the responses in an objective way. The last is of crucial importance in order to choose an optimized *TMS* which fulfilled the thermal requirements but with more suited characteristics.

In Figure 5.10 is shown the complete methodology emphasizing this fifth step. As it is indicated in Figure 5.10 before consider this step such as finished, it is necessary to check if this optimized product fulfils the design criteria and requirements previously defined in the first step.

Based on this situation, two options are possible:

- Option A: if by the proposed optimized design the requirements are not fulfilled, the optimization criteria and optimized design should be revised searching for new possible solutions. At this stage small modifications in the models could be expected.

- Option B: on the contrary, if the response is positive and every requirement defined at the beginning of the methodology is reached by the new improved *TMS*, the proposed design could be considered as optimized. These design modifications are included in the drawings of the prototype or in the improved control strategies.

Finally, once the complete system is optimized, the last step is related to the standardization and industrialization of the final product.

In the next chapters, this methodology has been applied to the design of a *TMS* for both applications presented along this Doctoral Thesis: the vertical residential elevator and full electric urban minibus. In that way, it is also demonstrated the versatility and applicability of this methodology in order to design, model and optimize quite different *BPs* and their *TMS*s. As it has been pointed out previously, this methodology can be easily implemented in a more general multidisciplinary approach to take into account other mechanical, electrical and electronical issues.

5.4 CONCLUSIONS

Several simulation tools exist in order to analyze the thermal performance of the *TMS* of a *BP*. Therefore, it is crucial to know them to select the most suitable and proper one to the case study of interest.

As it has been concluded in Chapter 4, the air cooling technology has been chosen as the *TMS* for the residential elevator, whereas for the urban electric minibus application a liquid cooling system based on a dual architecture (*FC + AC*) has been proposed such as *TMS*.

Considering the works carried out by other researchers and presented in Section 5.2, it is clear that the most research works which used *CFD* simulation tool has been used in the detailed simulations with the aim to obtain specific information related to air distribution around the cells within a *BM* or *BP*, and to predict the internal cell temperatures at system level. On contrast, the *CFD* models representing *BMs* cooled down using liquid flows are more concerned in the detail of the performance of the cold plates. Few reliable examples of liquid cooled complete *BP* cases have been analyzed in the literature using *CFD* tools.

Moreover, when the air is used such as cooling fluid, it is essential to analyze the air distribution around the cells within the *BP*, among other phenomena. This would be unviable with a *DAE* simulation tool due to the assumed simplifications. In addition, for the air cooling system the usage of *NC* and *FC* has been analyzed. It is impossible to study *NC* by means of *DAE* simulation tools with the minimum required accuracy. For these reasons, the option to use a *DAE* simulation tool for residential elevator case has been ruled out and it has been decided to use *CFD* simulation tool, exactly *Ansys/FLUENT* 14.5 *CFD* package.

In contrast, for the liquid cooling system, the proposed *TMS* is much more complex, composed of components such as hydraulic pump, compressor, fan and heat exchangers among others. Moreover, the evaporator and the condenser imply the need of taking into account the phase change phenomena which is unfeasible with *CFD* tools. In this case the *CFD* simulation tool would require too high computational cost even for steady simulations at *BP* level. Moreover, different control strategies for this cooling system

would be impossible to evaluate by means of *CFD* simulation tool. However, the *DAE* simulation tool provides the chance to carry out transient simulations of a complex system comprised of components with different inertia and also, to analyze phenomena such as the phase change (liquid/gas) and compression and expansion of the refrigerant, in a reasonable time.

Consequently, it is quite obvious that the *DAE* approach is much more reasonable than the *CFD* to afford problems related especially with liquid cooling at system level. An acausal object-oriented simulation tool is more suitable to afford complex, reversible and dynamic active liquid cooling problems. In particular, *Dymola/TIL* 3.4.1 simulation tool has been used.

An optimization methodology independent of the selected design and modeling simulation tool has been described step by step ensuring an optimized *TMS*, fulfilling the design criteria and constraints defined for a particular application. The methodology has been composed of five sequential steps and although, the first four steps correspond to a standard design- and modeling-methodology [67], the fifth step is related to optimization process which constitutes the main contribution of this research work.

The first step corresponds to the definition of the design criteria followed by the second step, which is related to the predesign of the *BP* and its *TMS*. The thermal sizing of the *BP* has been carried out as the first task of this step with the aim to design a proper *TMS* and selecting the suitable components and materials. This step has been carried out doing simple calculations related to thermal and hydraulic balances at steady state using *Excel Worksheets*. The obtained *TMS* should be oversized, because only the worst ambient and electrical conditions and a coarse modeling approach have been considered, i.e., a constant mean heat generation rate for a uniform ideal *BP* temperature and the worst electrical and ambient solicitations, constant boundary conditions, etcetera.

The third step, once the *BP* and its *TMS* are pre-designed, is referred to the development of detailed thermal models at cell, at *BM* and at *BP* level to be validated experimentally in transient conditions in the fourth step. For this purpose, the instantaneous heat generation model has been necessary to be implemented in each simulation tool. *DoE* technique has been used to define the minimal necessary

numerical tests in order to analyze and verify at as wide as possible conditions the fulfilment of the design criteria by means of the developed detailed numerical models.

Once it has been checked the virtual achievement of the design criteria by means of the developed detailed numerical models, the fourth step related to the construction of the prototype is carried out. Due to the impossibility of testing adequately a complete *BP* in a laboratory environment, the scalability of the systems at *BM* level has been taken into account to make viable the experimental validation of the detailed models. The same test matrix as in the previous step has been conducted experimentally to demonstrate the feasibility and reliability of the developed models. For that aim, the experimental results obtained have been compared with the numerical results achieved in the previous step.

The fifth and the most important step once the developed thermal models have been validated, is the optimization step, the core of this research work. An optimization procedure has been defined based on a numerical *DoE* technique and *RMS* methodology. The simulated thermal responses have been evaluated once the system has reached the thermal stabilization after applying cyclic current profiles. In this context and in order to avoid the limitation that the *CFD* simulation tools imply in terms of computational cost when simulations at *BP* level are carried out in a transient state, the novel concept of *False Steady* has been introduced and described. This advantageous numerical approach makes possible the optimization task by means of this type of simulation tool in a steady state. This limitation is less relevant for *DAE* simulation tools.

As a result of this methodology, an optimized *TMS* for the *BP* is obtained in terms of power consumption and initial cost of the system, among others, fulfilling all the design criteria with a more adjusted design. The versatility of this methodology in terms of applicability will be demonstrated in the next two chapters in where different simulation tools have been used to optimize very different *TMSs* for specific *eMOV* applications.

Chapter 6.

Case Study I: *TMS* optimization for Vertical Elevation Application

In the previous chapter, the proposed *Thermal Management System* optimization methodology has been theoretically described step by step.

In this chapter, this methodology has been applied to a *Battery Pack* placed in a residential elevator application. *Battery Pack* is comprised of 7 *Battery Modules* connected in serial, composed of 12 *Li-Ion* cylindrical cells each one. Because of the not so restrictive operation conditions together with the intermittency of the application, due to generally an elevator is not operating continuously, and the non-direct influence of the ambient conditions on the *Battery Pack,* due to usually it is located in one of the coldest places of a building, has been allowed to integrate an air cooling system in this application.

In this case, *Ansys/ FLUENT* simulation tool has been used. As a result, an optimized *Thermal Management System* has been proposed at component and at system level ensuring the fulfilment of the initial defined thermal requirements for the worst defined operation conditions, and at the same time allowing a more efficient operation mode when the circumstances are more favorable.

6.1 DESIGN CRITERIA DEFINITION

With regards to design criteria, and not considering all the electronic issues, electrical, mechanical and thermal and other design requirements can be distinguished.

According to electrical specifications, the energy and power solicitations explained in detail in Chapter 2 have been taken into account. In terms of energy, the complete *BP* should provide at least 664.4 Wh energy on-board in order to fulfil three design requirements defined by the manufacturer which supposed that it should be able to: (1) store energy from 4 braking regenerative rides reducing the net energy consumption, (2) supplement the single phase network of 2 kW by means of up to a maximum of the longest 10 consecutive traction travels and (3) rescue people in the most restrictive conditions permitting to use an autonomous mode. With regards to the power requirements, three current levels related to the people charge when the elevator goes up or down from the 1^{st} to 7^{th} floor have been defined (Figure 2.11): Ride 1, Ride 2 and Ride 3. Based on the current requirements related to the discharge and charge process of each defined ride, as it is shown in Table 3.5, cyclic current profiles have been defined. As it has been mentioned in Chapter 3, these cyclic profiles will be used in the following steps of this methodology for thermal modeling, validation and optimization purpose.

Regarding the mechanical issues, especially the limited space available in the elevator shaft has been considered: the *BP* should be entered in a volume space of 66 cm x 30 cm x 11.5 cm in terms of length, width and height, respectively. In contrast in terms of weight, because the *BP* does not move together with the elevator and it is maintained stationary, the weight will not be a problem in any case for this particular application.

At the same time, some thermal requirements must be fulfilled. As it has been highlighted along the complete document it is crucial to keep the *BP* temperature within an adequate operation range and to minimize the thermal dispersion within the *BP* in order to guarantee as much as it is possible its lifetime and to avoid some undesirable situations such as lithium plating, unbalanced between cells or even, the complete *BP*

destruction. Therefore, some ideal, admissible and limit operation range has been defined.

The ideal thermal operation range has been established between 20-30 ºC, although it has been considered a temperature range between 10 ºC and 40 ºC acceptable. Nevertheless, it has been considered unacceptable to reach a cell maximum temperature within the *BP* of 55 ºC and minimal operation limit temperature of 10 ºC. In these cases the elevator will be stopped. All the defined requirements for this application, it has been considered for an ambient temperature range between 10 ºC and 40 ºC, which means that even for the lowest defined ambient temperature (10 ºC) and due to the heat generation that the *BP* performance involves, the operation temperature of the *BP* will be always maintained above to this limit.

In terms of thermal dispersion, it has been defined a maximum temperature variation between the cells as maximum of 5 ºC under any operation conditions, trying to keep it below 3 ºC and ideally, minimizing it as far as possible.

As it has been mentioned in Chapter 5, the manufacturer has explicitly imposed the implementation of an air cooling system for this particular application among other reasons, due to the system simplicity and the low consumption that this type of cooling system usually implies in comparison with others, such as it could be a liquid cooling system. It will analyze the possibility to implement *NC* or *FC* system focusing the attention on the first option in order to minimize as far as possible the consumption of the system. In addition, if it will be demonstrated that a *FC* system is necessary to fulfil the defined design criteria, it will be intented to simplify as far as possible the system, evaluating the necessity of use components such as a heat sink or operate with the fan at the maximum *PWM* value. By means of a simple *TMS* it will be possible to reduce the mounting and installation requirements, simplifying and minimizing the initial costs associated with them.

To sum up, defined electrical and thermal requirements mentioned up to now are assembled in Table 6.1.

Table 6.1 Thermal and electrical requirements defined for this application

Electrical Requirements		**Mechanical Requirements**	
Energy on-board, Wh	664.4	Volume (H x W x H) cm	66 x 30 x 11.5
Thermal Requirements			
TMS technology		Air cooling	
Max Tº cell, ºC		55	
Admissible Tº cell range, ºC		10 - 40	
Ideal Tº cell range, ºC		20 - 30	
Ideal Tº cell, ºC		25	
Tº ambient, ºC		10 - 40	
Max. ΔT *BP*, ºC		5	
Ideal ΔT *BP*, ºC		Minimum	
Admissible ΔT *BP*, ºC		3	

6.2 PREDESIGN OF THE BATTERY PACK AND THERMAL MANAGEMENT SYSTEM

Once the electrical, mechanical and thermal design requirements have been defined, it has been possible to carry out the predesign of the complete *BP* and it *TMS*. This step involves the thermal sizing of the *BP* and the selection of the components and materials needed for the selected *TMS*.

6.2.1 THERMAL SIZING OF THE BATTERY PACK

As aforementioned in Chapter 3 where the electrical sizing has been carried out, it has been analyzed the required *BM*s to be implemented in the *BP* in order to provide the enough energy required by the application. It has been concluded that at least 7 *BM*s connected in serial or 8 *BM*s connected in parallel in different electrical configurations such as 4s2p or 2s4p have been needed. A *BP* composed of 6 *BM*s connected in serial which corresponds to an energy on-board of 594 Wh, it has been. insufficient compared with the electrical requirement defined in Table 6.1. At last, due to the simplicity regarding the connection between the *BM*s and the minimal number of *BM*s in the *BP* and due to the voltage level at *BP* level related to the converter that is needed, it has been decided to implement 7 *BM*s connected in serial which provide 693 Wh energy on-board.

As a result, a minimal entity of a *BM* comprised of 12 cylindrical cells (*LFP* chemistry) connected in serial, based on lithium-ion-phosphate ($LiFePO_4$, *LFP*) and provided by A123 SYSTEMS manufacturer has been considered. Definitely, the complete *BP* (7 *BM*s) has been composed of 84 cells. The nominal voltage and current level at the cell level have been around of 3.3 V and 2.5 A, respectively.

Once the electrical sizing at *BP* level has been defined, the next step, as it has been explained in Chapter 5, has corresponded to its thermal sizing. For this task, the model at cell level which has been developed considering its electro-chemical and electro-physical properties, experimentally determined in the Thesis developed by N. Nieto [68], has been used. By means of the heat generation model, the total amount of the heat that should be dissipated by the proposed *TMS* has been calculated. In Figure 6.1 is shown the internal resistance variation in function of the *SOC* and cell temperature and the entropic heat coefficient as a function of *SOC* in (a) and (b), respectively.

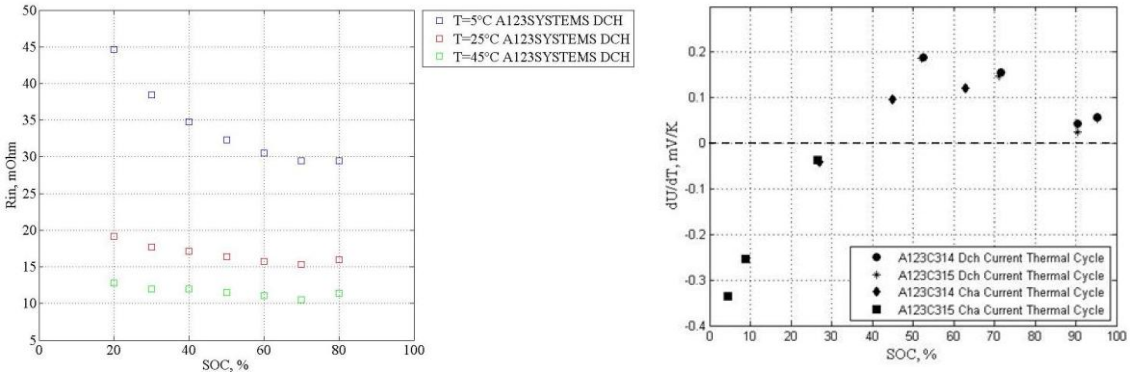

(a) (b)

Figure 6.1 (a) Variation of internal resistance with both SOC and temperature and (b) entropic heat coefficient as a function of SOC for A123 SYSTEMS cells

By means of the values referred to the thermo-chemical properties defined experimentally (Figure 6.1) and the procedure shown in Figure 6.2, the heat generation rate at cell, at *BM* $\left(HG_{cell} \cdot {}^{12\ cells}/_{BM}\right)$ and at *BP* $\left(HG_{BM} \cdot {}^{7\ BMs}/_{BP}\right)$ has been calculated.

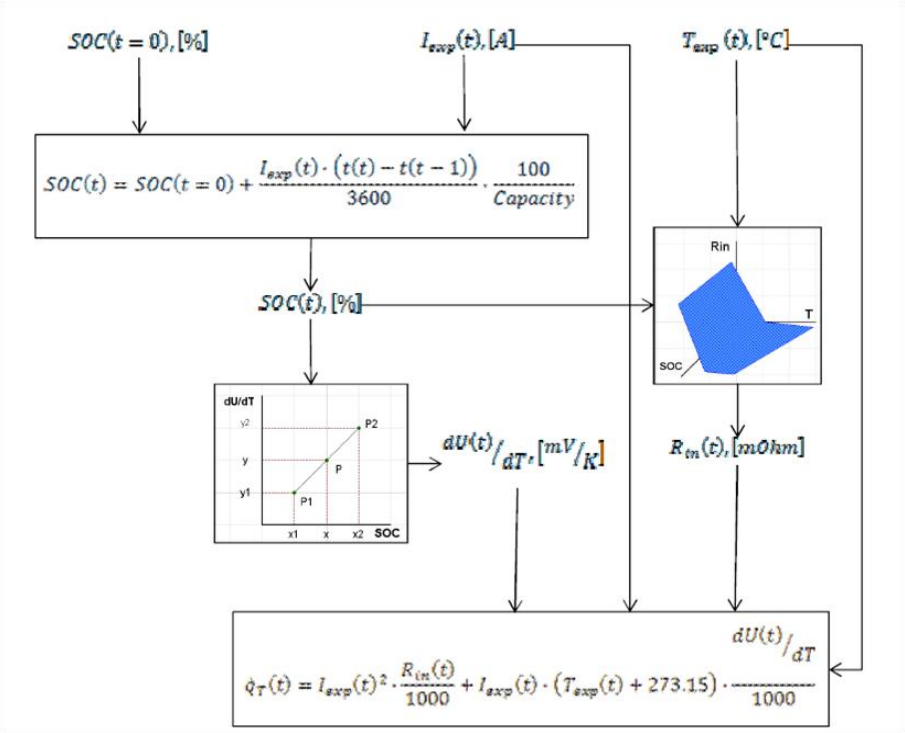

Figure 6.2 Procedure to determine the heat generation rate from experimental internal resistance and entropic heat coefficient data.

Figure 6.3 shows the mean heat generation rates at cell, *BM* and *BP* level for the three cyclic current levels defined (Table 3.5) for the application. For *SOC* range for each ride, a middle value of 50% has been considered. Consequently, *SOC* ranges of 56-44%, 54-46% and 52.5-47.5% have established for Ride 1, Ride 2 and Ride 3, respectively. In terms of thermal conditions, a complete sweep has been done from 10 ºC to 50 ºC, every 5 degrees.

At last considering the results shown in Figure 6.3, the heat generation rate has been defined based on the worst elevator travel (Ride 1) and the ideal mean *BP* temperature of 25 ºC have been considered, which it is highlighted by bold. Finally and considering an oversized of 10%, as in the electrical sizing, 202.1 W has been estimated that must be dissipated by the designed *TMS* for this application.

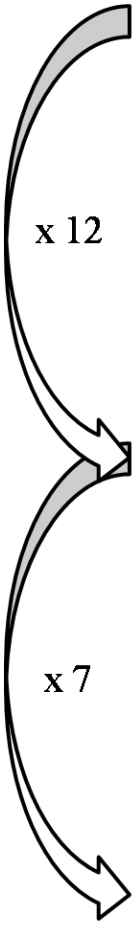

		Ride 1	Ride 2	Ride 3
		SOC 56-44%	SOC 54-46%	SOC 52.5-47.5%
Tcell, °C	10	-3.87	-1.80	-0.53
	15	-3.31	-1.54	-0.42
	20	-2.75	-1.29	-0.38
	25	**-2.19**	-1.03	-0.29
	30	-2.02	-0.95	-0.29
	35	-1.85	-0.87	-0.25
	40	-1.68	-0.79	-0.24
	45	-1.51	-0.72	-0.21
	50	-1.35	-0.64	-0.19

		Ride 1	Ride 2	Ride 3
		SOC 56-44%	SOC 54-46%	SOC 52.5-47.5%
Tcell, °C	10	-46.43	-21.60	-6.41
	15	-39.70	-18.51	-5.01
	20	-32.97	-15.43	-4.60
	25	**-26.25**	-12.35	-3.42
	30	-24.23	-11.41	-3.42
	35	-22.20	-10.47	-2.95
	40	-20.18	-9.54	-2.87
	45	-18.16	-8.60	-2.47
	50	-16.14	-7.66	-2.32

		Ride 1	Ride 2	Ride 3
		SOC 56-44%	SOC 54-46%	SOC 52.5-47.5%
Tcell, °C	10	-325.01	-151.18	-44.86
	15	-277.92	-129.60	-35.05
	20	-230.82	-108.03	-32.21
	25	**-183.73**	-86.46	-23.96
	30	-169.58	-79.89	-23.96
	35	-155.43	-73.32	-20.62
	40	-141.28	-66.76	-20.10
	45	-127.13	-60.19	-17.28
	50	-112.98	-53.63	-16.25

Figure 6.3 Thermal sizing for BP installed in the residential elevator.

To sum up, in Table 6.2 is shown the summary regarding the electrical and thermal sizing that it has been carried out in this section.

Table 6.2 The electrical and thermal sizing carried out for this application.

Electrical sizing		**Thermal sizing**	
BP	7 *BM*s in serial	Heat Generation at *BP* level, W	202.1
Energy on-board, Wh	693.0		

6.2.2 PRELIMINARY COOLING SYSTEM DESIGN

Once the amount of the heat generated within the *BP* has been determined, the proper cooling system has been selected and predesigned. As it has been mentioned in Chapter 4 and in the introduction of this chapter, an air cooling system has been proposed by the manufacturer as the best conceptual solution for this application.

Several calculations of thermal, hydraulic and pneumatic balances in a steady state have been carried out by means of *Excel Worksheet.* For that purpose, several assumptions and simplifications such as constant and maximum heat generation rate obtained from Figure 6.3 or simplified boundary conditions by means of approximate values of convective heat transfer have been considered. Due to all simplifications considered in this section, it has been expected an oversized *TMS* will be designed in terms of system design.

As it has been explained in Chapter 5 for this application, by means of this numerical tool only *FC* phenomena can be analyzed because of the thermal and hydraulic behaviors are decoupled, contrary that in a *NC* condition occurs. As a first approximation for this cooling mode and considering the best possible aspects in terms of cells thermal performance, some decisions have been taken in sense of design. In terms of insulation, it has been decided not use a complete closed plastic frame covering the cells. In fact, it has been determined to insulate them from the extreme parts and therefore, to ventilate them from the lateral side. In addition, it has been disposed to implement some aluminium heat sinks on the top and at the bottom of each *BM*. By this way, the heat sinks will provide to the system an increase in the total heat dissipation area and in the thermal inertia of the system. Moreover, it will make a more effective cooling process.

Focusing the attention on the heat sinks, it must be ensured the appropriate contact between the cells and heat sinks, because a wrong contact between them could cause an undesired increase in the temperature of the cells. For this effect, the usage of a specific Thermal Interface Material (*TIM)* between these two components has been considered. Three different *TIM*s have been preselected and analyzed: ProtectION^{+} DLP 3.0, ProtectION^{+} MPS and ProtectION^{+} PF40. The thermal conductivity values have been 3, 0.86 (with 50% compression) and 0.086 $W \cdot m^{-1} \cdot K^{-1}$, respectively. The selected *TIM* for this first design has been the first one mentioned because of its suitable thermal

properties. A mechanical compression has been used in order to benefit of the relatively high thermal conductivity of this type of cells in the axial direction.

Once the components that comprise the complete system design are identified, i.e., the fan and heat sinks, the specific components of this particular system have been preselected. These predesign calculations by means of *Excel* tool have been carried out assuming scalability at *BM* level, assuming the same thermal performance of the *BP* at *BM* level. In the same way, the air flow rate has been scaled in terms of the *TMS*. That means that in this particular case where the *BP* is comprised of 7 *BM*s and only a unique *BM* has been considered, the air flow rate supposed for the complete *BP* has been divided into 7 in order to refer only to one *BM*. Moreover, based on the symmetry planes of the *BM*, a quarter of a *BM* has been considered in order to make easier the calculations. Therefore, the overall air mass flow rate correspondent to the *BP* has been scaled to the quarter of the *BM* which it also depends on the final number of the fans that are defined in the complete *BP*. The air mass flow rate related to the quarter of the *BM* has been defined by (6.1).

$$Q_{air\_1/4BM} = \frac{Q_{air\_fan} \cdot nº\ fan}{4 \cdot 7} \tag{6.1}$$

With regards to cells properties and modeling process, the extreme thickness of each layer and complicated interfaces between different materials in the cylindrical cells [103] has not been considered, defining the non-homogeneous and anisotropic structure of the layers within the cell. The cell has been considered such as a single body, considering lumped properties in order to evaluate the cell thermal performance under normal conditions. The properties in terms of density, specific heat, and thermal conductivity defined in the cell can be found in Table 6.3. In respect to the thermal conductivity, different average values have been applied in the parallel and perpendicular direction to the layers in an orthotropic configuration. These properties within the cell have been kept constant during operation.

Table 6.3 Properties of the materials used in the thermal models.

Material	Type	ρ, kg m^{-3}	Cp, J kg^{-1} K^{-1}	k, W m^{-1} K^{-1}	μ, kg m^{-1} s^{-1}
Cell	Solid	1978	1016 ± 0.012	2.17 (axial) 0.434 (radial) ± 0.032	-

In Figure 6.4 is shown the schematic diagram that it has been used in order to carry out the thermal and hydraulic balances. The red arrows indicate the heat flow, i.e., it has been considered radial and axial heat flow. The green rectangles indicate the *BM* surface temperature, whereas the black rectangles are referred to the thermal resistance, distinguishing the axial and radial direction. Finally, the air temperature is indicated by the blue rectangles. In terms of hydraulic balance, the pressure drop around the *BM* and the heat sink must be considered. A thermal and hydraulic equilibrium state, in which the *BM* temperature is kept within the defined operation temperature range, must be obtained in order to determinate the required air flow rate.

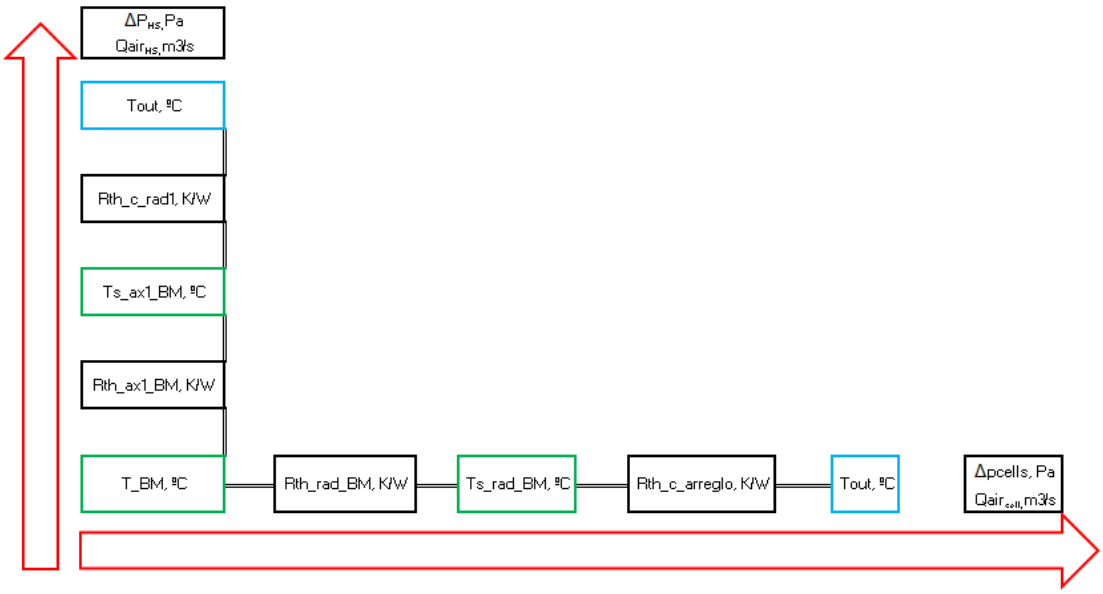

Figure 6.4 *Schematic diagram of the proposed air cooling system.*

As it has been mentioned before, in this section the heat sink and the fan have been selected. For both, three possible options have been preselected obtaining their performance data from the manufacturer, which have been implemented in the *Excel Worksheet.* In this particular case, the heat sink preselection has been conditioned by the width of the *BM*, i.e., it has been tried to adjust this dimension of the *BM* to the heat sinks. Moreover and referred to the fan, its dimension has been limited by the width of the case in which the complete *BP* will be introduced. As it has been indicated in Table 6.1, the fans length or height it cannot be bigger than 11.5 cm. In Figure 6.5 is shown the *Excel Worksheet* referred to the fans and the heat sinks preselected based on the datasheets provided by the manufacturers.

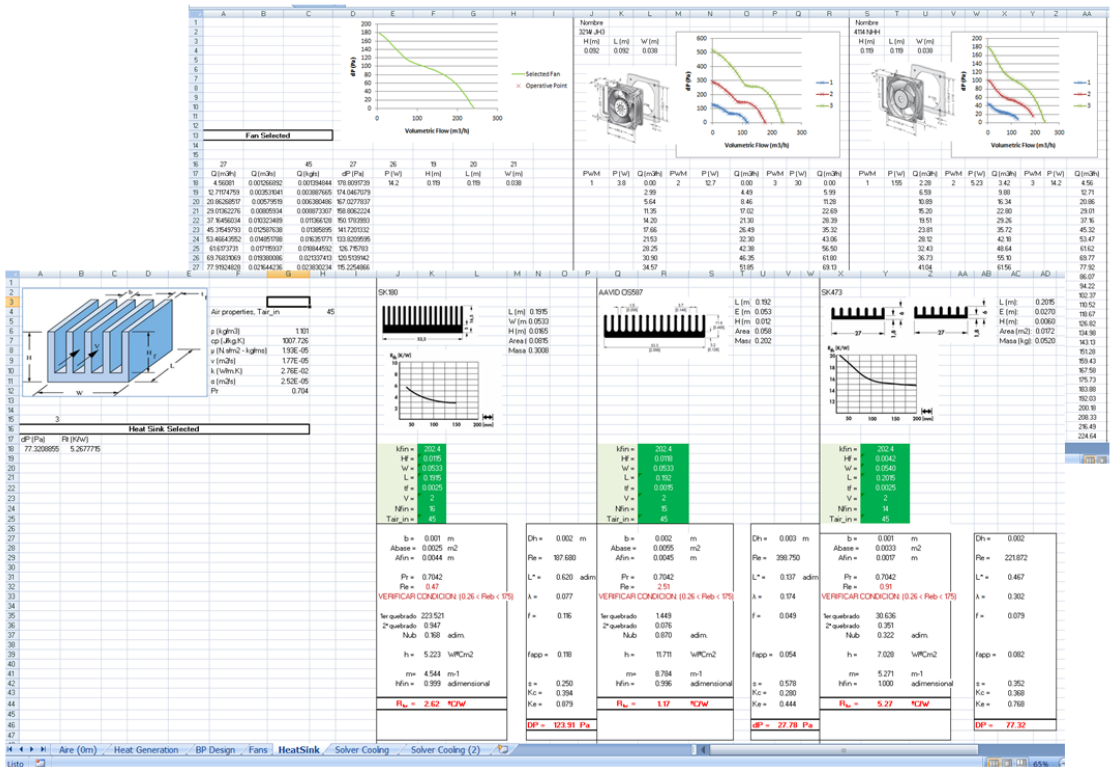

Figure 6.5 Components datasheet introduced in Excel Worksheet.

The developed *Worksheet* together with the Solver integrated into *Excel* tool has made possible the achievement of the most suitable components which fulfil all the defined thermal and hydraulical restrictions. On the one hand, it has been defined a restriction related to the heat generated within the *BM* that must be the same to the sum heat dissipated in the radial and axial direction. Moreover, hydraulically it has been defined that total air mass flow rate provided by the fan(s) must be the same to the sum of the air flow rate circulated around the cells and through the heat sinks. The air mass flow rate it must be sufficient to keep the *BM* temperature within in an acceptable operation range overcoming the total pressure drop supposed by the system. In addition, as aforementioned in this section, it must bear in mind the correct scalability of the air mass flow rate equivalent to a quarter of *BM*.

For the worst ambient conditions (40 ºC) and in order to dissipate the heat generation rate obtained from Figure 6.3, in Figure 6.6 is shown the results obtained. Based on this figure, it can be seen that for an ambient temperature of 40 ºC and provide an air mass flow rate of 0.031 m^3/s, it is possible to maintain the *BM* below 47 ºC. For that purpose, the best combination, in terms of operation conditions, of the fan and the heat sink has been obtained such as result.

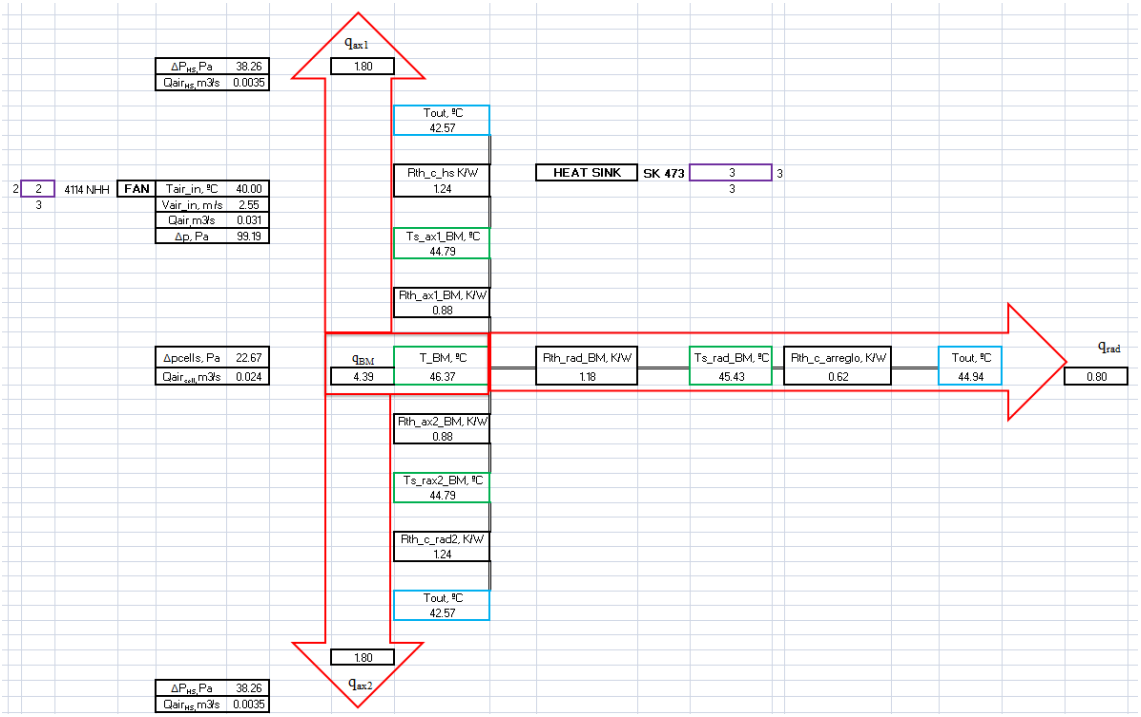

Figure 6.6 Schematic diagram of the Excel Worksheet developed for the air cooling system

Based on the results obtained from *Excel Worksheet*, the components tabulated in Table 6.4 have been selected.

Table 6.4 Selected components for the dual TMS for the urban electric minibus application.

	Components	Reference
1	Heat Sink	SK 473
2	Fan	4114 NHH

Following the selected components are shown individually taking into account the information that it has been obtained by the manufacturers.

- **<u>Heat Sink</u>**

The selected heat sink has been provided by Fischer manufacturer. In Figure 6.7 is shown the design and the performance curve related to thermal resistance. As it can be seen in Figure 6.7 the heat sink dimensions in terms of width has been just the middle of the total width of the *BM* and therefore, it must be placed two heat sinks in the top and other two in the bottom of each *BM*.

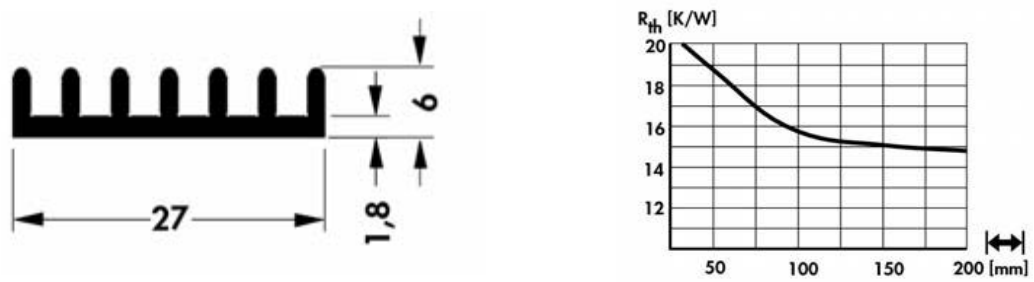

Figure 6.7 Selected SK 473 heat sink.

Comparing with the other two possibilities of heat sinks, this heat sink has been the smaller one, and so is the pressure drop that generates. However, its heat transfer coefficient has been the smaller compared with the other two options but in that sense, the hydraulically performance has been more relevant and it has influenced in terms of choosing a small fan, and consequently, with low consumption.

- **<u>Fan</u>**

The selected fan is shown in Figure 6.8. Considering the air mass flow rate needed at quarter *BM* level and based on the scalability of the *BP* which it is explained previously in this section, it has been decided to implement 3 fans of model 4114 NHH provided by EBM manufacturer at *BP* level. As it can be check in the Figure 6.8., the fan fulfils the requirement related to that its length or height not to be bigger than 12 cm. It has been decided to locate the fans in one lateral of the case in order to extract the air from there and to absorb from the front side by means of some grids.

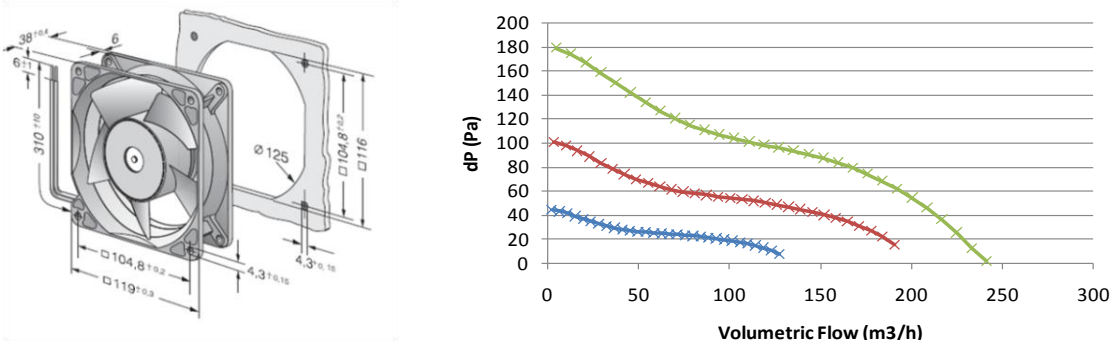

Figure 6.8 Design and performance curves related to the selected fan (4114 NHH).

Once the *BP* and the *TMS* have been predesigned, the detailed models have been developed to analyze deeply the transient thermal performance of it. It is worth underlining, although it has been mentioned before, that due to they have been taken assumptions in this step in a very roughly way, it has been assumed that the resulted *TMS* has been oversized.

6.3 DETAILED DESIGN OF THE BATTERY PACK AND THERMAL MANAGEMENT SYSTEM

Once the application design criteria have been defined and the *BP* and its *TMS* have been predesigned (Sections 6.1 and 6.2), more detailed *CFD* models have been developed which they will be necessary prior the construction of a sample prototype. The aim of this section is to develop detailed thermal models that by means of them, it could be possible to check if the previously defined design criteria are fulfilled by the predesigned system or not. Transient simulations have been carried out in this step of the methodology, by thermally coupling the heat generation model at cell level by means of the *UDF* implemented in the *CFD* simulation tool (Appendix 2A). As it has been explained deeply in Chapter 5, in this section at *BM* and at *BP* level have been developed detailed models, although the detailed thermal model at *BM* level has been only used to achieve the specific aim of this step. In Figure 6.9, (a) and (b), are shown the exploded drawings of the design at *BM* and *BP* level respectively, considering the decisions have been taken in the predesign step. As it can be seen in detail in Figure 6.9 (a), two heat sink of SK 473 have been placed on the top and on the bottom part of the *BM* using the *TIM* between the heat sinks and the cells to improve the good contact between them. In addition, in Figure 6.9 (b) can be observed the location of the selected fans, the complete *BP* (7 *BM*s) in the case and the grids placed in front of the fan in order to expel the air through them.

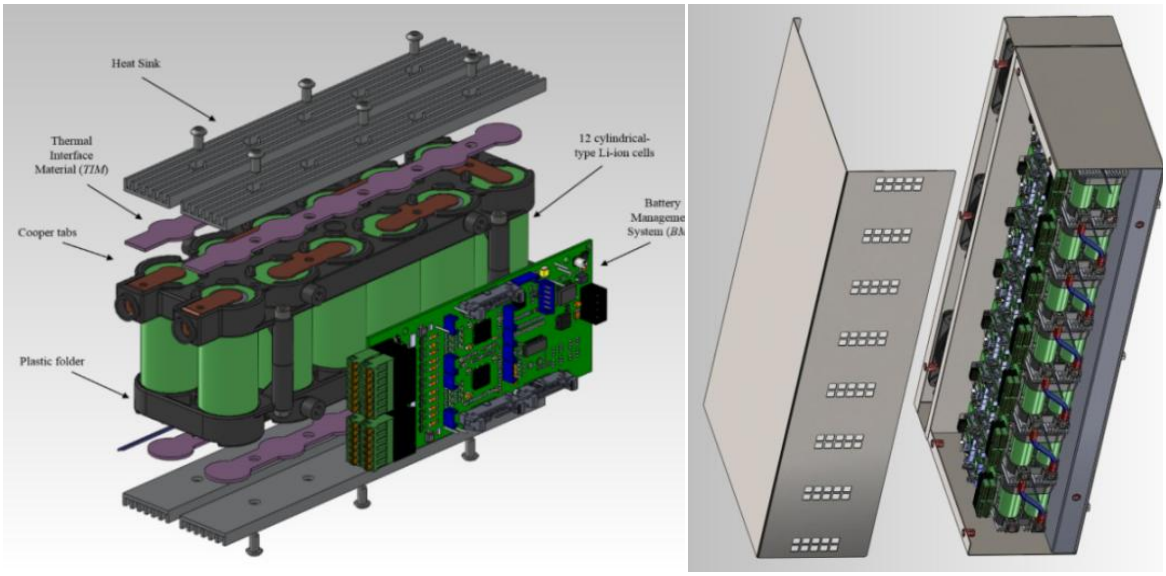

(a) (b)

Figure 6.9. Exploded drawing of the design at (a) BM and (b) BP level.

The models shown in Figure 6.9 have been made based on the cell model developed in Section 6.2. As it has been mentioned in the introductory paragraph of this step, transient simulations have been carried out with the model scaled at *BM* level integrating heat generation model at cell level in order to provide a realistic idea of the thermal diffusion through the cells in a transient state. In this way, it will be possible to analyze the thermal dispersion between the cells at *BM* level.

In terms of materials definition the same philosophy as in the cell modeling has been applied. In Table 6.5 are defined the thermophysical properties (density, specific heat, and thermal conductivity) of the rest solid and fluid zones that have been used in the *BM* and *BP* models. The cells properties in these models correspond to the same values that have been shown in Table 6.3.

Table 6.5 Properties of the materials used in the thermal models.

Material	Type	ρ, kg m^{-3}	Cp, J kg^{-1} K^{-1}	k, W m^{-1} K^{-1}	μ, kg m^{-1} s^{-1}
Aluminium	Solid	2719	871	202	-
TIM	Solid	2901	998	3	-
Air	Fluid	1.225	1006	0.024	1.79×10^{-5}

In these models apart from the previously mentioned assumptions regarding the cell level model, some other simplifications have been taken into account in order to simplify the models´ geometry and consequently, to minimize the computational cost.

Firstly, it has been decided to remove the *BMS* card from each *BM* in simulation models as well as experimentally, which it will be explained later, and secondly, it has been reduced the complete domain of developed models to a quarter considering the vertical and horizontal symmetry planes which are indicated in Figure 6.10. In addition, external heat transfer by radiation from the battery to the surroundings has not been neglected, especially due to the main effect that it has in the *BP* level model.

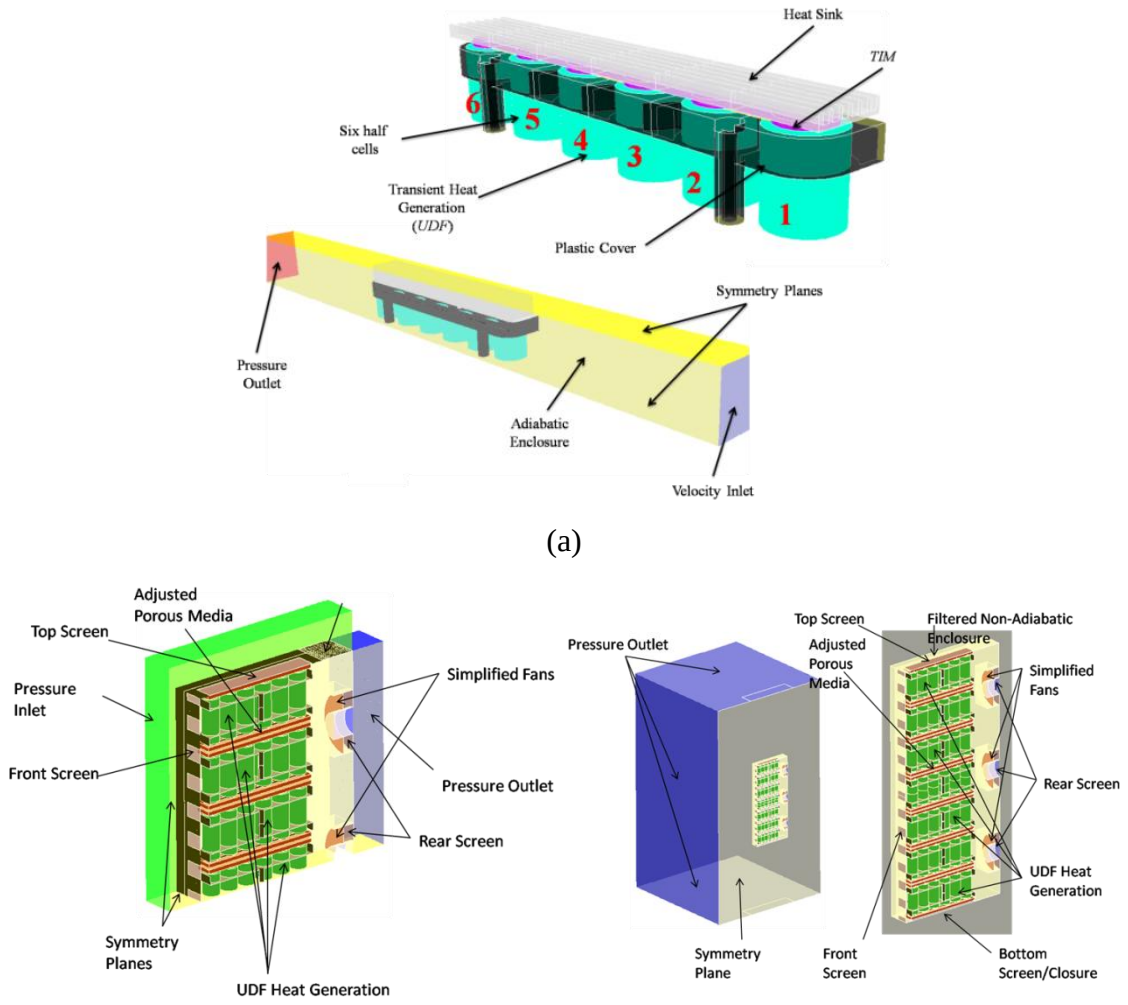

Figure 6.10 Transient designed model at (a) BM and (b) BP level.

Unlike with the simple thermal models developed in the predesign step, in these detailed models the fluid, air flow, has been modelled by means of partial differential equations with the aim to evaluate the changes of the fluid through the boundaries of a fluid element, the presences of walls or a possible surface and/or volume source terms.

With regards to the *BM* level model, as it can be seen in Figure 6.10 (a), a wind tunnel, which has been considered such as an adiabatic enclosure, has been modelled in which the *BM* has been located in the center. Inlet and outlet boundaries have been identified in the wind tunnel, defining in the former the air mass flow rate imposed for each test case and in the latter, the gauge pressure 0 Pa due to the exit is referred to the atmosphere. A quarter of *BM* has been modelled, i.e., six-half cells. Every component have been modelled in detail correspondent to each physical geometry and characteristics, such as, the *TIM* over the cells together with the heat sink and the plastic

cover that it covered the half of the cells. As it is indicated in Figure 6.10 (a) and it has been mentioned in this section, the instantaneous volumetric heat generation rate calculation has been imposed by *UDF*.

The detailed models at *BP* level are shown in Figure 6.10 (b) which of the left side is referred to *FC*, whereas the right side one has been developed in order to analyze the *BP* performance under *NC* conditions. In both models by means of the symmetry plane have been reduced and simplified the domain and in the same way that all of the detailed models developed in this step, the volumetric heat generation rate at cell level has been imposed by *UDF*.

As it can be seen in Figure 6.10 (b), the heat sinks at *BP* level have been modelled by adjusted porous media, i.e., the same thermal and hydraulic behavior that the real heat sink would have, it has been defined in this porous zone. For that purpose, superficial velocity and thermal equilibrium model have been implemented. These parameters have been defined by means of some other detailed simulations by which the inertial resistance and porosity has been obtained in order to model the heat sink by porous media hydraulically and the thermal effective conductivity for the thermal modeling. In Figure 6.11, as an example, the results obtained for an air inlet velocity of 3 $m \cdot s^{-1}$ are shown. Figure 6.11 (a) corresponds to the hydraulic performance in terms of pressure distribution, whereas Figure 6.11 (b) refers to the thermal performance considering the temperature distribution, in both cases along the detailed model heat sink and the porous media zone. This assumption has simplified the calculations and therefore, the computational cost which it is a very important requirement in a model as complex as this was, has been reduced.

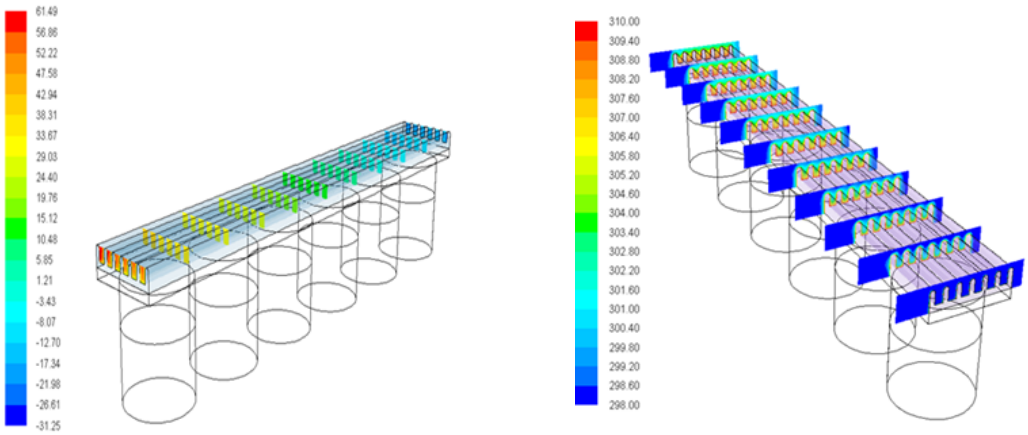

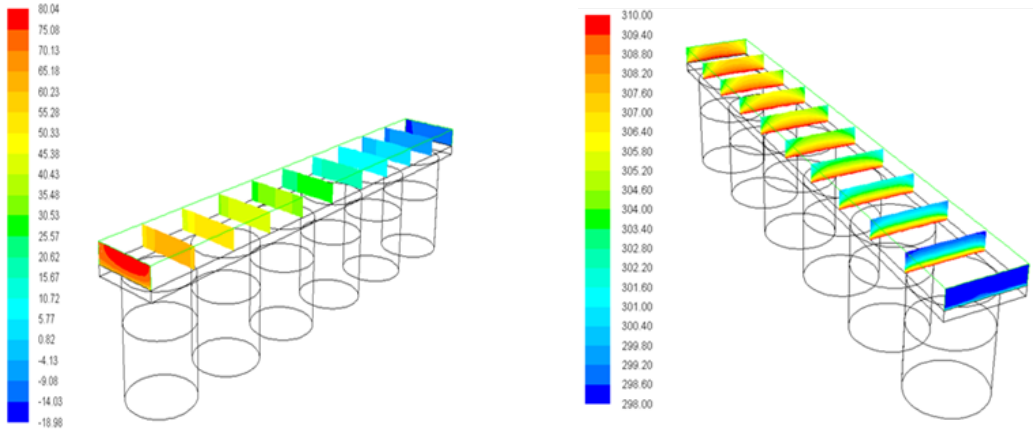

(a) (b)

Figure 6.11 (a) Pressure and (b) temperature distribution along the heat sink for the detailed (up) and porous (down) model for an air velocity of 3 m/s.

FC cooling at *BP* level, left side of Figure 6.10 (b), has modelled by means of simplified fans. The boundary conditions have been defined by means of the performance curve by which the air mass flow rate is calculated in function of the pressure drop of the system. In contrast, for *NC* system these boundaries are annulated, the right side of Figure 6.10 (b). In *NC* cooling conditions, the movement of the air is produced by little pressure forces in contrast to *FC* condition, where the air movement is determined by active forces. The radiation effect in the *NC* conditions has a crucial effect in the thermal performance evolution of the cells within the *BP*, which must be taken into consideration.

Given the importance of a fine mesh to accurately model the air flow and heat transfer through this particular geometry, a high-quality hybrid (mainly hexahedral) grid has been used to model the fluid zones [104]. The heat sink zone has been composed of 5.9 million of cells whereas 5 million of cells have been used in the area surrounding the cell. The grid refinement factor was higher in zones where the contact between the heat sink and the air was complete so as to capture the larger magnitude gradients that take place therein. Although the meshing requirements in solid regions are less restrictive that in the fluid zones, using 1.6 million of elements, in order to guarantee the grid independence of the results. The time step size used in these model has been for one second.

The Finite Volume Method *(FVM)* has been applied to discretize the differential equations of the mathematical models, using a segregated implicit solver to solve the

generated algebraic equation system. Therefore, equations have been linearised and then sequentially solved using the Gauss-Seidel algorithm accelerated by an Algebraic Multigrid method [105]. The pressure-velocity coupling has been achieved through the use of the SIMPLE algorithm [106]. Diffusive terms of the equations are discretized using a second-order centered scheme, and the convective terms are discretized using a second-order upwind scheme [107]. A body force weighted scheme [108] is chosen in the discretization of pressure to deal with this buoyancy-driven flow for *NC* conditions. All this numerical procedure has been implemented in the unstructured *CFD* code Fluent V.6.3 [109].

As it has been explained in Chapter 5, where the methodology is described in detail, the aim of this step is to check if the design criteria have been fulfilled by means of the developed detailed model. For that purpose, the *BM* level detailed model, Figure 6.10 (a), has been used because it makes possible by means of it to analyze the thermal dispersion and the maximum cell temperature within the *BM* in order to evaluate if there is margin and how is this margin regarding the design criteria defined in the first step. the *BP* level developed thermal model, Figure 6.10 (b), has been used in the following steps with the aim of optimizing the thermal proposed design in Section 6.2.

In order to check the fulfilment of the design criteria by means of the proposed predesign, the reduced test matrix which is shown in Table 6.6 has been proposed based on *DoE* technique. Variables such as the charge/ discharge *C-rate*, *SOC* range, the air inlet flow rate and temperature have been considered in order to analyze the thermal performance under a wide range of operation conditions. Regarding the *C-rate*, the electrical requirements of each ride defined for this application in terms of power have been considered. Instead of using the *SOC* ranges previously defined for each ride (Figure 6.3), they have been increased keeping a maximum *DOD* for Ride 1 and minimum *DOD* for Ride 3. On this basis, an operation *SOC* ranges have been defined for each ride: Ride 1 (DCH 7C/ CHA 3C) with SOC 20-80%, Ride 2 (DCH 5C/ CHA 2C) with SOC 30-70%, and Ride 3 (DCH 3C/ CHA 1C) with SOC 40-60%. The colours used to identify each ride, correspond with the same that have used in Chapter 2.

From 1 to 4 $m \cdot s^{-1}$ values have been taken such as references for the air flow rates to define the maximum and minimum air inlet flow rate for the experimental tests. The intermediate value has been fixed in 2 $m \cdot s^{-1}$. For the ambient temperature, a minimum

and maximum of 15 ºC and 35 ºC respectively have been defined. The intermediate temperature has been fixed considering the middle point between the both previous values (25 ºC).

Table 6.6 Test matrix for verification of the fulfillment of design criteria at BM level

	C-rate	***SOC*, %**	**w_{air}, m.s^{-1}**	**T_{air} inlet, ºC**	**Test n.º**
Ride 1:	7C/ 3C	80-20	1	15	2
			4	35	1
Ride 2:	5C/2C	70-30	2	25	5
Ride 3:	3C/1C	60-40	1	15	3
			4	35	4

In Table 6.7 are shown the results obtained for the different defined tests regarding the maximum cell temperature within the *BM*, the thermal dispersion between the cells, the temperature difference between the ambient temperature and cell maximum temperature, and at last the temperature difference between the peak temperature of charge and discharge process. The maximum *BM* temperature corresponded to the 6th cell, which is located on the opposite side of the air entrance, while the thermal dispersion within the *BM* has been calculated considering the temperature difference between the coldest (1st) and hottest (6th) cells. In addition, to evaluate the temperature difference between the peak temperature of charge and discharge process the temperature correspondent to the 6th cell has been considered.

Table 6.7 Simulation results obtained from the detailed thermal models for the test conditions defined in Table 6.6

	T_{BM}max, ºC	Thermal dispersion, ºC	Δ ($T_{ambient}$-T_{BM}max), ºC	ΔTº (CHA-DCH_{peak}), ºC
Test 1	39.26	0.83	4.26	3.46
Test 2	26.96	2.02	11.96	5.91
Test 3	17.33	0.41	2.33	1.01
Test 4	34.40	0.12	0.60	0.29
Test 5	28.92	0.77	3.92	2.18

As an example in Figure 6.12 is shown the temperature contour referred to the cell surface and heat sink surface regarding Test 2 defined in Table 6.6. This test

corresponds to the most restrictive electrical conditions (DCH 7C/ CHA 3C with SOC 20-80%) with an air mass flow rate of 1 $m \cdot s^{-1}$ at 15 ºC of ambient temperature. As it can be seen in Figure 6.12 (a) the maximum cell temperature is kept below 25 ºC, while the heat sink surface temperature is below 20 ºC (Figure 6.12 (b)).

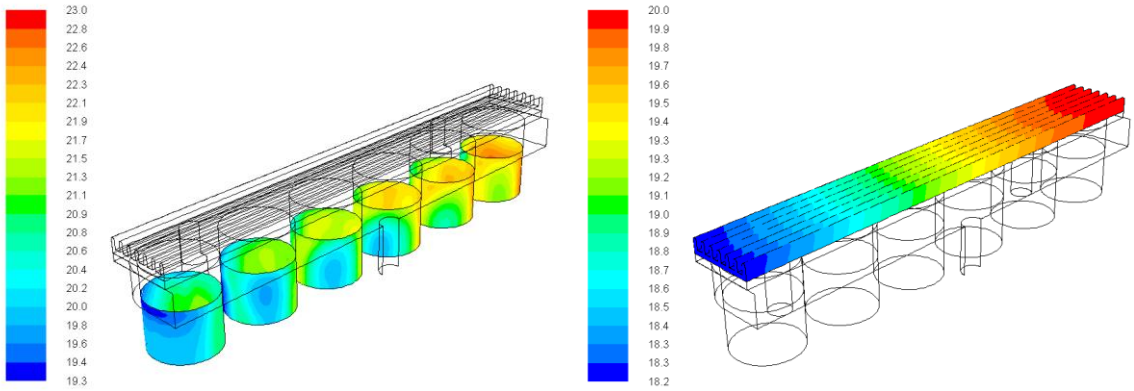

Figure 6.12 Temperature contours of the cell and heat sink surface for the Test 2 defined in Table 6.6

Moreover, variables as the heat generation and heat dissipation rate, which are only possible to evaluate by simulations, have been analyzed by means of these detailed models. In Figure 6.13 are shown the results obtained.

The red lines correspond to the simulated heat generation profiles for six-half cells, while the dark blue lines are the simulated heat dissipation profiles considering the heat released by the cell surface, the heat sink, the *TIM* and the cover. The convergence criterion has been met in both cases as the integral of the heat dissipation profiles equals the integral of the heat generation profiles. For each case the numeric data referred to the time- averaged heat generation and heat dissipation rate considering the last discharge-charge cycle is also included.

Considering Figure 6.13, it can be observed that when the air inlet temperature higher is (for the same other experimental conditions), the heat which needed to be dissipated from the cells is lower. In other words, heat generation rates were greatly increased at lower temperatures. The cell temperature has an import impact on the heat generation rate, especially on the internal resistance which depends on it. The internal resistance is the main cause of the irreversible heat generation. At low temperatures, the internal resistance of the battery increases and consequently, the amount of the irreversible heat generation. At high operating temperatures due to increased rates of

mass transport and reduced activation loss, the over potential during discharge decreased and therefore, the heat generation rate decreased.

Test 1		**Test 2**	
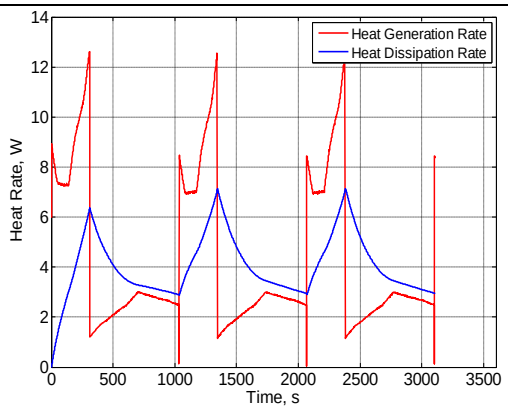		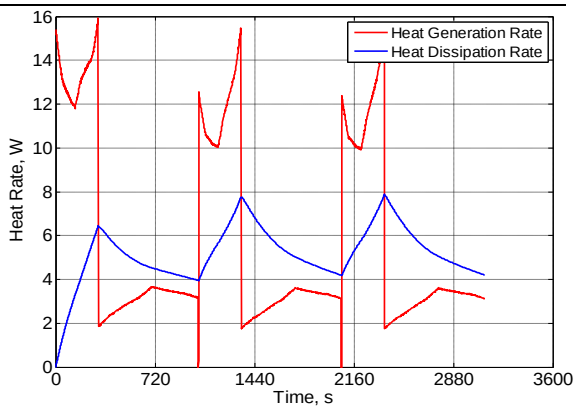	
$\dot{q}_{gen}$, W	4.25	$\dot{q}_{gen}$, W	5.54
$\dot{q}_{dis}$, W	4.27	$\dot{q}_{dis}$, W	5.56
Test 3		**Test 4**	
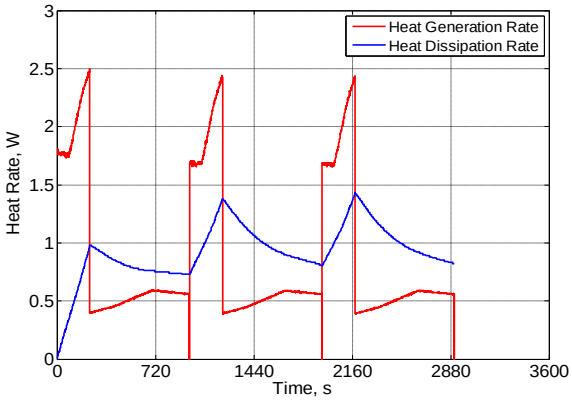		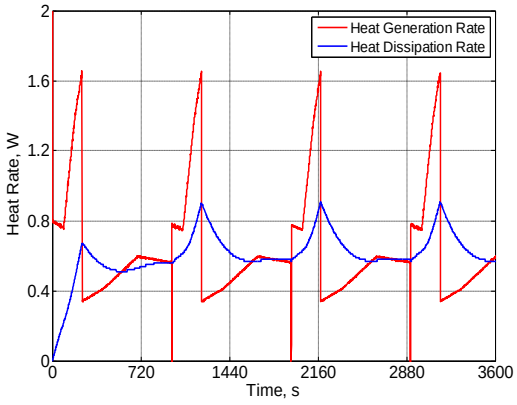	
$\dot{q}_{gen}$, W	4.18	$\dot{q}_{gen}$, W	0.61
$\dot{q}_{dis}$, W	4.22	$\dot{q}_{dis}$, W	0.64
Test 5			
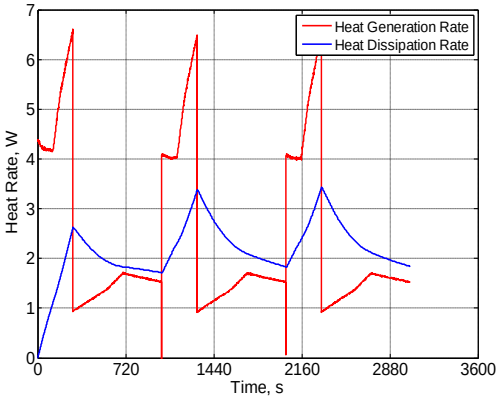			
$\dot{q}_{gen}$, W	2.28		
$\dot{q}_{dis}$, W	2.30		

Figure 6.13 Simulation heat generation and dissipation rate correspondent for tests defined in Table 6.10

This effect also can be seen in the same module comparing the temperature and the heat generation of each cell: colder cells will generate more heat than the hotter ones. Figure 6.14 shows the heat generation and temperature distribution for the 6th test from the Table 6.6. This test has been selected because it presented the highest thermal dispersion in the module comparing with other tests, so this effect will be seen more clearly.

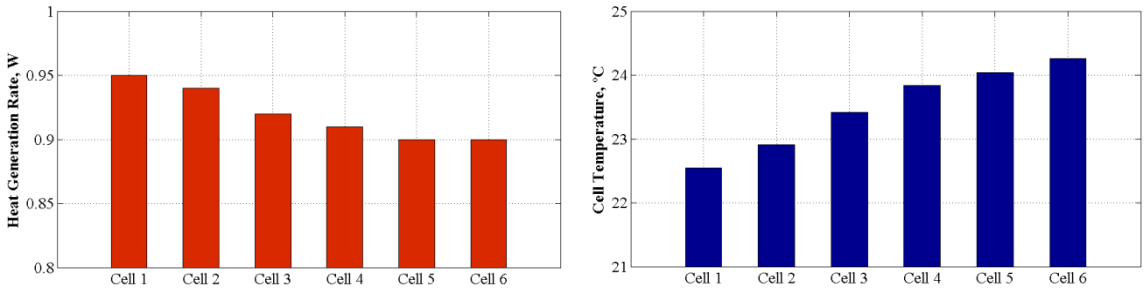

(a) (b)

Figure 6.14 Results from BM model corresponding to the Test 2 from the Table 6.6 (a) heat generation rate (W) distribution and (b) temperature distribution (ºC).

To concluded, and mainly based on results show in Table 6.7, it can be said that for any ambient and electrical conditions the thermal performance of the *BM* has been kept within the admissible operation range in terms of the maximum cell temperature and thermal dispersion between the cells within the *BM*. In addition, it can be specified that in terms of maximum temperature considering the maximum operation temperature defined in the first step of this methodology (Section 6.1) of 55 ºC and a maximum thermal dispersion of 5 ºC, it has been a margin of around 15.7 ºC and almost of 3 ºC regarding respectively the previous both variables. Consequently, it is obvious that the proposed *TMS* has been oversized as it has been expected, due to all the assumptions that have been considered during the predesign step (Section 6.2.).

6.4 THERMAL MODELS VALIDATION

The objective of the validation task has been to check whether the equations, models and assumptions made during thermal modeling process represent well enough, the reality which it has been intended to be emulated by means of the previously developed detailed simulation models. For that purpose, the main task of this step has been the construction of a prototype which is shown in Figure 6.15, i.e., on the left side it can be observed the prototype at *BP* level, whereas on the right side it can be seen the *BM*.

Figure 6.15 Constructed real prototype at BP and at BM level.

As it has been explained in Chapter 5 and it has been applied in the predesign step (Section 6.2), in order to validate the developed detailed thermal models by means of a real prototype, a unique *BM* has been used for several reasons: firstly, because it has been unviable to carry out experimental tests at *BP* level at reduced laboratory environment and secondly, due to it has been considered the scalability of the *BP* along with its *TMS*, i.e., it has been assumed the equivalent thermal performance analyzing only one *BM* instead of studying it at *BP* level, relativizing the air flow rate of the complete system to *BM* level.

The test set-up shown in Figure 6.16 has been defined in order to carry out experimental measurements on the constructed prototype. The *BM* which is shown on the right side of Figure 6.15, as it is indicated in the set- up scheme in Figure 6.16, has been placed into the wind tunnel that it has been constructed, exactly in the middle of the tunnel overall length. The wind tunnel has been made of wood and the height, width and length of it was about 107, 125 and 2000 mm, respectively, being the wall thickness of 10 mm.

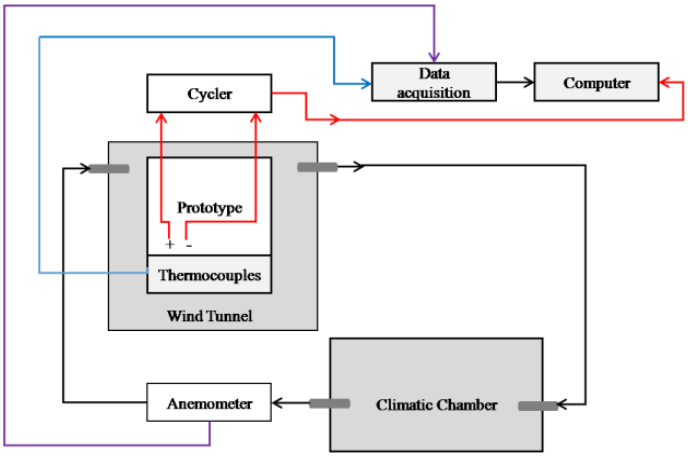

Figure 6.16Test set- up scheme of the constructed prototype.

16 type T thermocouples have made possible to analyze the temperature distribution in the *BM*. As it can be seen in Figure 6.17 (a) the location of the thermocouples were on the outside surface half- way up in each cell as well as in the inlet and outlet zones of the heat sink (symmetrically the opposite side were positioned similarly). The expected error of these temperature measurements has been of ±0.75%.

The air local velocity in the entrance of the wind tunnel has been measured by some anemometers (Accusense UAS 1200 XS) with a ± 5% of accuracy in the measured air velocity. As it can be seen in Figure 6.17 (b), the anemometers have been located one meter from the entrance of the wind tunnel in the medium height of the wind tunnel.

Table 6.8 Air flow velocity measured by means of the anemometers located in the entrance of the wind tunnel.

	$v_{air}\ Anemometer\ 1, \frac{m}{s}$	$v_{air}\ Anemometer\ 2, \frac{m}{s}$	$\bar{v}_{air}\ , \frac{m}{s}$
Test 1	4.06	4.14	4.10
Test 2	1.15	1.21	1.18
Test 3	1.15	1.25	1.20
Test 4	4.09	4.19	4.15
Test5	1.99	2.29	2.14

The cooling air circulated through the *BM* has been provided by an axial fan (ebmpapst, 4114 N/2H8P) placed on the outlet side of the wind tunnel. It has operated by a pulse- width modulation (*PWM)* control that has made possible to set air flow. As it can be seen in Figure 6.17 (c), the fan has been powered by OMRON S8VS- 12024 power supply and the fan velocity has been fixed manually by a potentiometer until the desired values are measured in the anemometers.

(a)

(b)

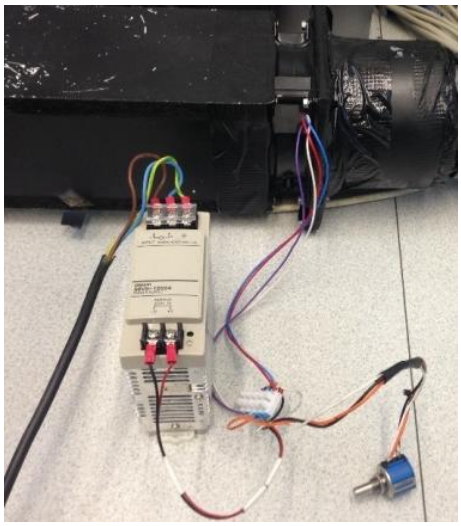

(c)

Figure 6.17 Location of (a) temperature sensors in the cells and heat sinks surface, (b) anemometers in the wind tunnel and (c) fan, its power supplier and potentiometer.

The wind tunnel where the *BM* has been placed has joined by the climatic chamber by some flexible tubes. The climatic chamber (CTS, Clima Temperatur Systeme) has been used to keep the desired inlet air temperature in the tunnel in all tests carried out. The climatic chamber can be seen in Figure 6.18 (a). It has maintained the desired temperature with a precision of ± 0.3 K and it has a test space capacity of 2000 liters.

As it has been mentioned in the section related to models description, the *BMS* card has been removed from the *BM*. As it is shown in Figure 6.18 (b), the programmable cycler (IBT, which runs with Digatron/Firing Circuits BTS600 software for data evaluation) has been connected to *BM* during the experiments to charge and discharge the cells and to measure in situ the current and voltage among other electrical variables. Moreover, the cycler has limited the cell voltages during charge/discharge, preventing overcharging/discharging. The accuracy of the current and voltage measurements has been 0.1% (full scale) in the range of 0.01-100 A and 0-6 V, respectively.

Finally, the *BM* has been also connected to a voltmeter (Agilent 34970A) to measure and record the temperature. Besides, the air flow rate has been also recorded. The voltmeter accuracy specifications have been ± (0.0035% of reading and + 0.0005% of range) for voltage and ±1 ºC for temperature. A multichannel Data Acquisition card and a computer have been used to record the temperature and air flow rate data taken during tests. These specifications include measurement error, switching error and transducer

conversion error. Apart from considering the accuracy of the measurement hardware, the inherent accuracy of the thermocouple has to be considered, too. Thermocouples used have been of type T. The maximum error permitted for this type of thermocouples in accordance with IEC 60 584-2:1995 has been of ± 0.5 ºC between -40 ºC and 125 ºC.

(a) (b) (c)

Figure 6.18 Experimental equipment used in the experimental tests: (a) climatic chamber, (b) cycler, and (c) voltmeter.

Figure 6.19 shows the real set- up that has been constructed in the laboratory environment with the *BM* and the previously mentioned equipment to carry out the experimental tests. The experimental tests have been carried out in the same conditions as it has been defined in *Table 6.6* in order to prove the correctness and reliability of the simulation results.

As it has been described in Chapter 5, the same procedure has been followed to perform all the experimental tests: first, the air flow rate and ambient temperature have set by a potentiometer and climatic chamber regulation manually, respectively. Cells of the *BM* have been completely charged (*SOC* 100%) and then discharged at the maximum *SOC* value defined for the corresponding test. Once everything was ready for the test to be initiated, the *BM* has been continuously discharged and charger between defined *SOC* limits with the corresponding current for each process. The cycler program that has been used for each experimental test can be seen in Appendix 3A.

Figure 6.19 Real test set- up.

Experimental temperature measurements obtained while cycling the *BM* have been used to validate especially the model at *BM* level. Figure 6.20 compare the experimental temperature measurements on the surface of the hottest (red lines) and coldest (green lines) cell and over the heat sink (blue lines) with the model developed at *BM* level for the tests defined in the test matrix shown in Table 6.6.

The hottest cell corresponds to the 6^{th} cell of the module, whereas the coldest is referred to de 1^{st} cell for all test carried out. The dashed and continuous lines are referred to the temperature profiles prediction by the model and measured in experimental tests. The difference in degrees Celsius between the experimental and predicted temperature profiles is also shown for each case using dotted lines with the same colours identification as previously. As regards shapes, both the thermal inertia and thermal resistances at module level seem to be very well represented by the developed model. The thermal performance could even be further adjusted taking into account a non-ideal thermal contact between the heat sink and *TIM* surfaces.

Test 1

C-rate: DCH 7C/CHA 3C, *SOC*: 80-20%, w_{air} : 4.10 m.s^{-1}, T_{air}inlet: 35 ºC

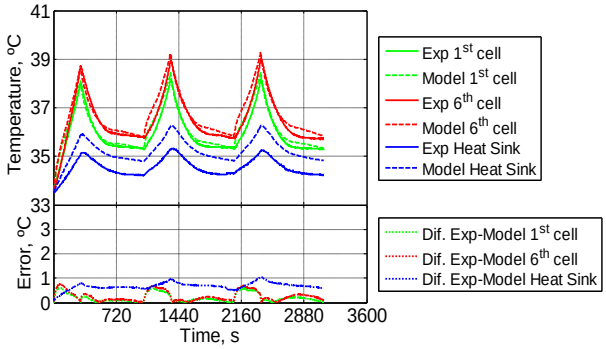

Test 2

C-rate: DCH 7C/CHA 3C, *SOC*: 80-20%, w_{air} : 1.18 m.s^{-1}, T_{air}inlet: 15 ºC

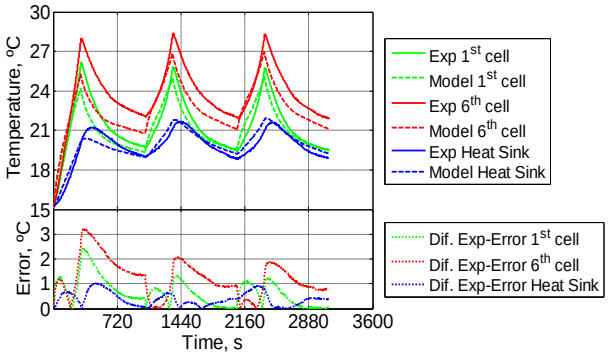

Test 3

C-rate: DCH 3C/CHA 1C, *SOC*: 60-40%, w_{air} : 1.18 m.s^{-1}, T_{air}inlet: 15 ºC

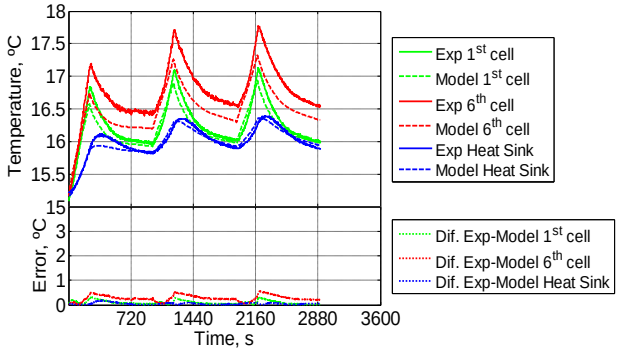

Test 4

C-rate: DCH 3C/CHA 1C, *SOC*: 60-40%, w_{air} : 4.15 m.s^{-1}, T_{air}inlet: 35 ºC

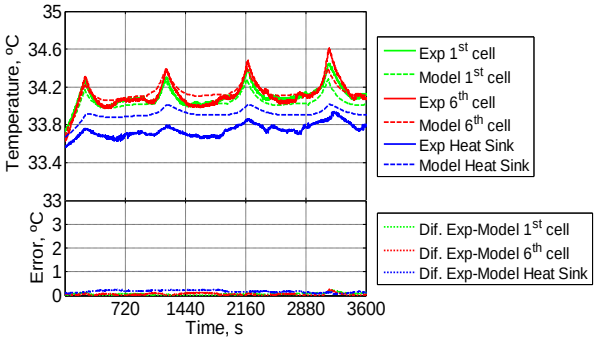

Test 5

C-rate: DCH 5C/CHA 2C, *SOC*: 70-30%, w_{air} : 2.14 m.s^{-1}, T_{air}inlet: 25 ºC

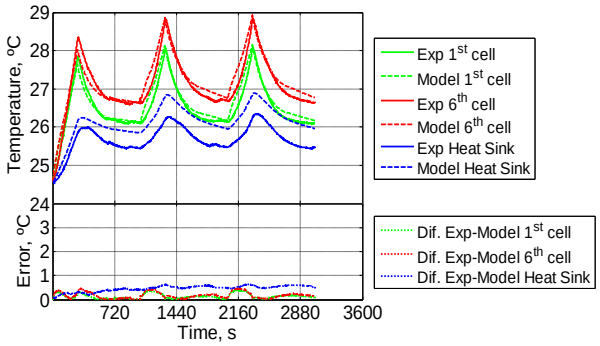

Figure 6.20 Measured and simulated hottest, coldest and heat sink temperature profiles (ºC) corresponding to the tests from Table 6.6. The error of each measurement is depicted by dotted lines.

Table 6.9 shows the numerical results obtained experimentally and numerically paying the attention especially on the maximum cell temperature and thermal dispersion between the cells, both thermal design criteria defined in the first step of this methodology. Similarly, as for the numerical results obtained, the maximum *BM* temperature corresponds to the 6th cell, which is located on the opposite side of the air entrance, while the thermal dispersion within the *BM* has been calculated considering the temperature difference between the coldest (1st) and hottest (6th) cells. These averaged values have been calculated considering the last discharge- charge cycle.

Table 6.9 Numerical, experimental and the difference between them regarding the maximum BM temperature and thermal dispersion between cells.

	T_{BM}max, ºC			Thermal dispersion, ºC		
	Numerical	Experimental	Difference	Numerical	Experimental	Difference
Test 1	39.26	39.03	0.23	0.83	0.90	0.07
Test 2	26.96	25.78	1.18	2.02	2.99	0.97
Test 3	17.33	17.18	0.45	0.41	0.72	0.31
Test 4	34.40	34.60	0.20	0.12	0.13	0.01
Test 5	28.87	28.87	0.05	0.77	0.84	0.07

As can be seen, model predictions closely follow the experimental measurements with a maximum time-averaged difference no higher than 1.2 ºC and 1.0 ºC for the tests shown regarding the maximum *BM* temperature referred to the 6th cell and the thermal dispersion within the *BM*, respectively. These errors have been occurred for the cases in

where the power requirements have been the most restrictive (Ride 1) and the air mass flow rate and the ambient temperature have been the lowest, i.e., 1 $m \cdot s^{-1}$ and 15 ºC, respectively.

To sum up, considering that the maximum error of the prediction the *BM* temperature and thermal dispersion between the cells of the *BM* for any electrical and ambient condition experimentally tested, it can be concluded that the developed models have been completely reliable and representative of the real thermal performance and they could be used confidently for validate the thermal design and to carry out the following optimization process.

6.5 THERMAL DESIGN OPTIMIZATION

Once the model at *BM* level has been validated, it has been carried out the process to check if the design criteria have been fulfilled by means of the defined first design and constructed prototype and/or even, if there is the possibility to optimize the system design at *BP* level.

Figure 6.21 shows the maximum temperatures corresponding to the 6th cell and the dispersion between the 1st and the 6th cell for the last discharge- charge cycle experimental measured together with the predictions of *BM* model.

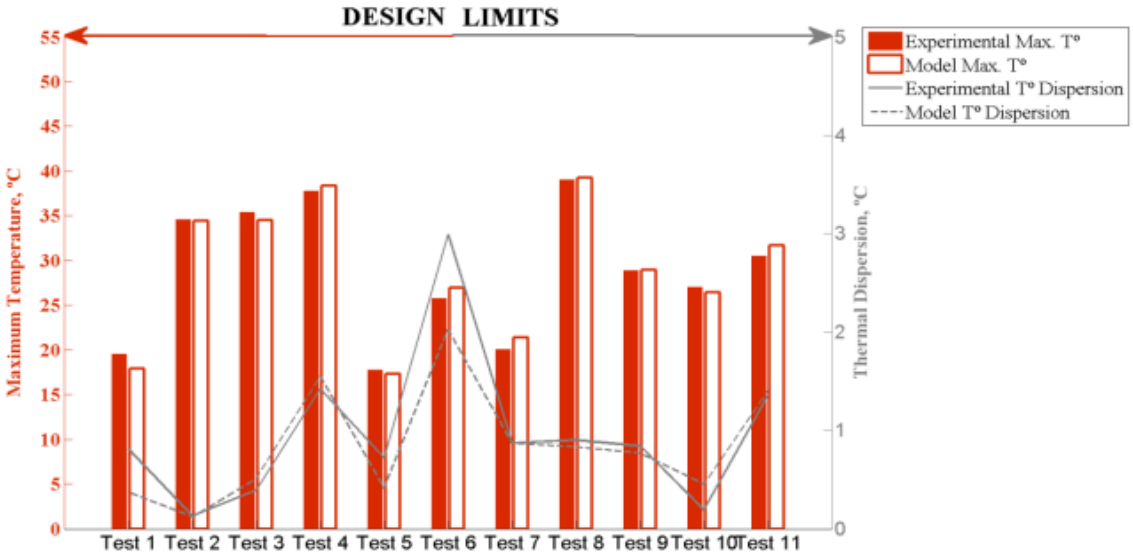

Figure 6.21 Experimental and numerical maximum temperatures (ºC) in the 6th cells and the thermal dispersion (ºC) between the hottest and the coldest cell for each test.

As it can be seen, Test 8 has been the test with the highest cell temperature due to its high current rate and ambient temperature, while Test 6 because of its electrical demanding conditions and low air velocity has presented the highest thermal dispersion in the *BM*. However, in both cases there has been a margin of almost 16 ºC and 2 ºC for the maximum cell temperature and thermal dispersion respectively, up to previously defined operation limits. Accordingly, the thermal constraints have been completely fulfilled opening a window for a future design optimization.

In this optimization step, design changes such as the possibility to remove or not the heat sinks or to work with a fan with a lower power (air velocity) have been analyzed. The aim of this step has been to allow the designer to define the optimal design choice fulfilling the established design constraints and criteria for the most restrictive conditions.

As it has been explained in Chapter 5, *False Steady* concept has been applied in the optimization process at system level in order to accelerate the transient simulations with the aim to get the steady state in each case. Before performing the optimization task, *False Steady* concept has been proved at *BM* level. For that purpose, several tests at diverse conditions in terms of electric solicitations and cooling conditions have been selected. In Figure 6.22 are shown the results obtained related to the temperature evolution considering Test 2, Test 4 and Test 5 defined in Table 6.6. The continuous lines are referred to the transient temperature evolution, whereas the discontinuous lines represent the temperature values obtained in the steady state using *False Steady* concept. The colour green and red represents the temperature regarding the 1st and the 6th cell, respectively. These obtained results permit to apply this concept at *BP* level for optimization purpose.

Test 2

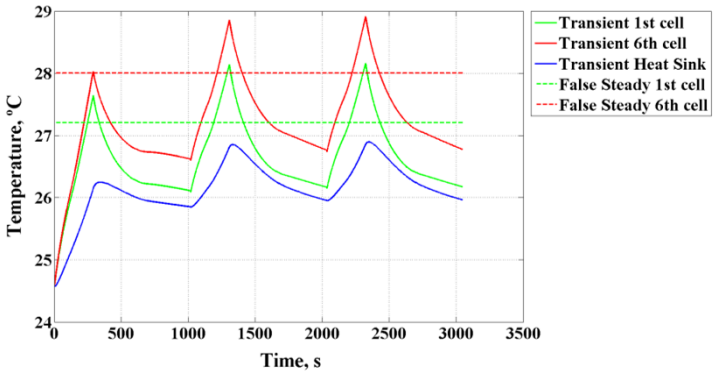

Test 4

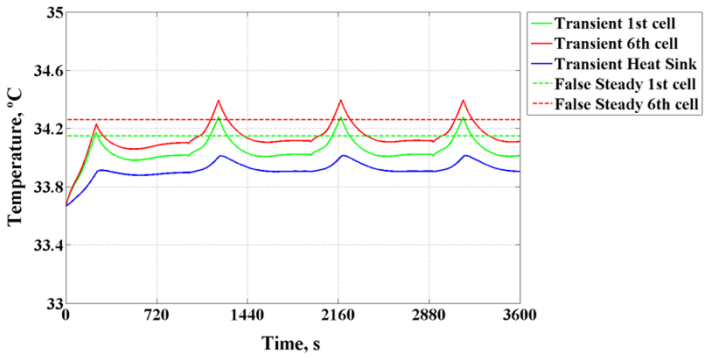

Test 5

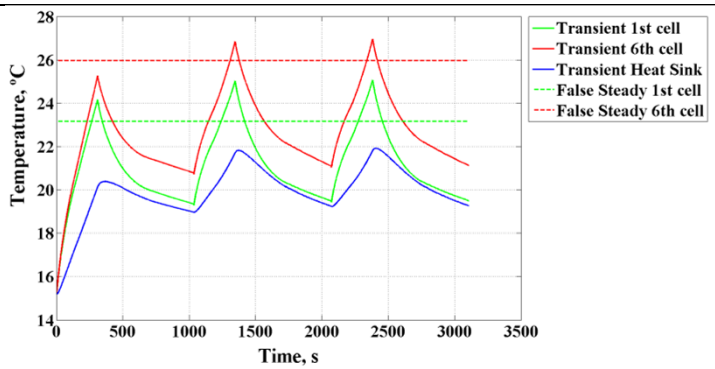

Figure 6.22 False Steady concept applied to Test 2, Test 4 and Test 5 defined in Table 6.6

Three different optimization cases have been defined: Optimization I, Optimization II, Optimization III. Optimization I has been focused on the evaluation of the necessity or not of implementing components such as heat sinks and fans based on *BM* level model (Figure 6.10 (a)), Optimization II has been applied to evaluate and define an adequate regulation of the fan *PWM* at *BP* level (left side of Figure 6.10 (b)) and the objective of Optimization III has been to check the limit of the *NC* performance at *BP* level (right side of Figure 6.10 (b))). It must be bear in mind that these optimization studies have been carried out in permanent conditions, too restrictive and non-realistic conditions for this application.

6.5.1 OPTIMIZATION I

The simulation tests defined in Table 6.10 have been carried out by means of the *DoE* technique.

Since it has been necessary for *Face Centered CCD*s, three levels have been defined for each factor coded them such as 1 (maximum level), 0 (medium level) and -1

(minimum level). The defined factors have been: the heat sink (without heat sink, medium heat sink SK473 and bigger heat sink SK180), the fan *PWM* (natural convection (*NC*) (5 W/m^{2}K), 50% *PWM* and 100% *PWM*), ambient temperature (10 ºC, 25 ºC and 40 ºC) and *C-rate* (Cmin: DCH 3C/ CHA 1C, Cmid: DCH 5C/ CHA 2C, Cmax: DCH 7C/ CHA 3C).

Table 6.10 DoE matrix at BM level

	Coded Value				UnCoded Value			
	Heat sink	Fan PWM	T amb	C-rate	Heat sink	Fan	T amb	C-rate
1	-1	1	1	1	NO	PWM 100%	40	Cmax
2	0	0	0	0	SK473	PWM 50%	25	Cmid
3	-1	1	-1	-1	NO	PWM 100%	10	Cmin
4	1	1	1	-1	SK180	PWM 100%	40	Cmin
5	-1	1	-1	1	NO	PWM 100%	10	Cmax
6	1	1	-1	1	SK180	PWM 100%	10	Cmax
7	1	-1	-1	-1	SK180	NC	10	Cmin
8	-1	-1	-1	1	NO	NC	10	Cmax
9	-1	1	1	-1	NO	PWM 100%	40	Cmin
10	1	-1	1	-1	SK180	NC	40	Cmin
11	-1	-1	1	-1	NO	NC	40	Cmin
12	1	1	1	1	SK180	PWM 100%	40	Cmax
13	-1	-1	1	1	NO	NC	40	Cmax
14	1	-1	1	1	SK180	NC	40	Cmax
15	-1	-1	-1	-1	NO	NC	10	Cmin
16	1	-1	-1	1	SK180	NC	10	Cmax
17	1	1	-1	-1	SK180	PWM 100%	10	Cmin
18	-1	0	0	0	NO	PWM 50%	25	Cmid
19	1	0	0	0	SK180	PWM 50%	25	Cmid
20	0	-1	0	0	SK473	NC	25	Cmid
21	0	1	0	0	SK473	PWM100	25	Cmid
22	0	0	-1	0	SK473	PWM 50%	10	Cmid
23	0	0	1	0	SK473	PWM 50%	40	Cmid
24	0	0	0	-1	SK473	PWM 50%	25	Cmin
25	0	0	0	1	SK473	PWM 50%	25	Cmax

In Table 6.11 are shown the numerical results have been obtained for each test that has been carried out. The maximum cell temperature and the thermal dispersion within the *BM* has been evaluated such as response variables in each test

Table 6.11 Numerical results of the DoE matrix at BM level

	Heat Sink	Fan *PWM*	Tamb	C-rate	Tmax, ºC	Dispersion *BM* , ºC
1	-1	1	1	1	47,5	1,74
2	0	0	0	0	30,5	1,21
3	-1	1	-1	-1	12,5	0,60
4	1	1	1	-1	40,8	0,16
5	-1	1	-1	1	22,8	2,34
6	1	1	-1	1	19,7	1,56
7	1	-1	-1	-1	15,1	0,01
8	-1	-1	-1	1	49,0	0,68
9	-1	1	1	-1	41,2	0,31
10	1	-1	1	-1	42,7	0,01
11	-1	-1	1	-1	45,8	0,16
12	1	1	1	1	45,2	0,98
13	-1	-1	1	1	64,4	0,43
14	1	-1	1	1	54,6	0,03
15	-1	-1	-1	-1	20,5	0,22
16	1	-1	-1	1	33,3	0,04
17	1	1	-1	-1	11,7	0,33
18	-1	0	0	0	33,9	3,15
19	1	0	0	0	29,6	1,15
20	0	-1	0	0	40,0	0,08
21	0	1	0	0	28,8	0,70
22	0	0	-1	0	18,1	1,61
23	0	0	1	0	44,2	0,94
24	0	0	0	-1	26,6	0,38
25	0	0	0	1	35,6	2,23

As an example, in Figure 6.23 are shown the temperature contours of the cells surface and the air fluid in the plane of symmetry correspondent to tests 2 (Figure 6.23 (a)), 18 (Figure 6.23 (b)) and 19 (Figure 6.23 (c)). These tests have been selected since they have the medium conditions regarding fan *PWM* (50%), ambient temperature (25 ºC) and electrical solicitations (DCH 5C/ CHA 2C) for the three possibilities of the heat sink.

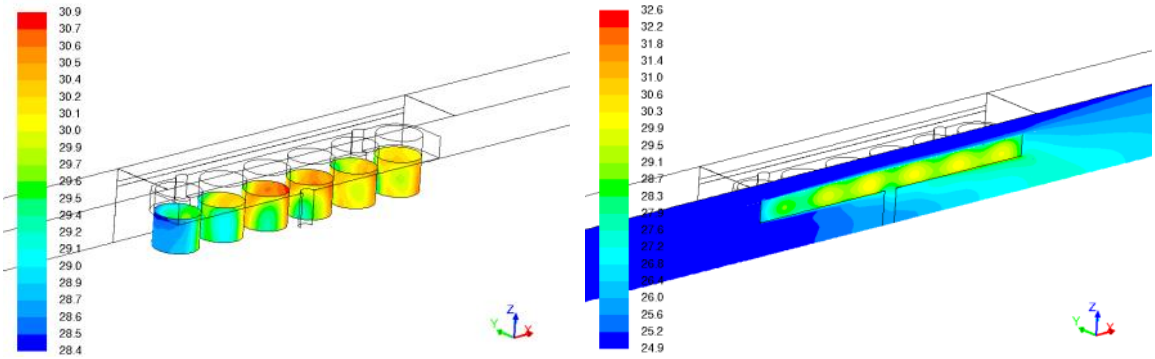

(a)

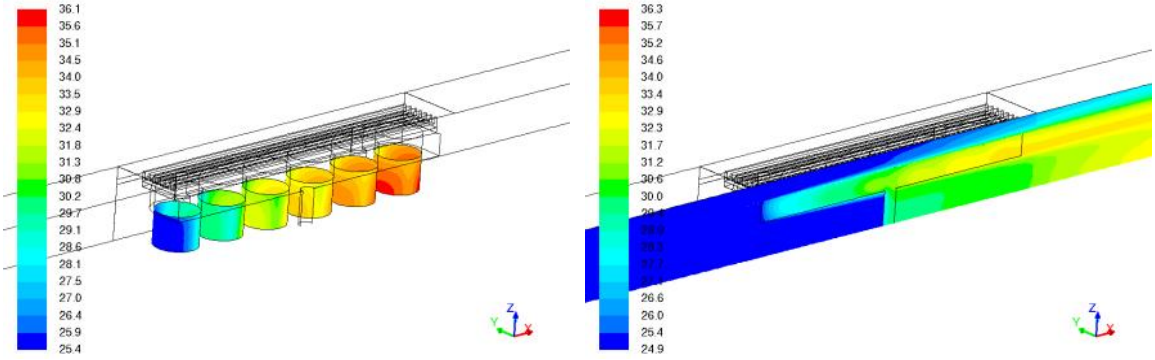

(b)

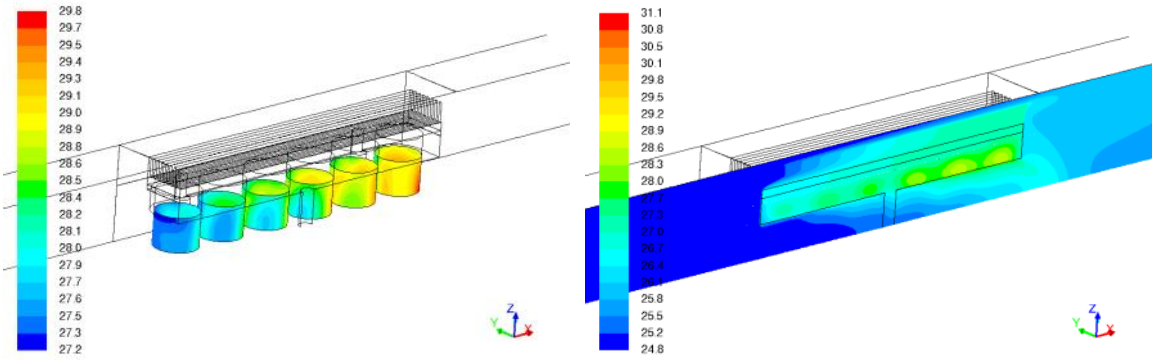

(c)

Figure 6.23 The temperature contours of the cells surface and air fluid in the plane of symmetry correspondent to test 2, 18 and 19.

Applying the *Face Centered CCD* the regression surface response of each variable has been obtained. The equation which defines the surface response regarding the cell maximum temperature and thermal dispersion has been defined by means of the coefficients tabulated in Table 6.12. The p-value of each term is also shown. It indicates how significant ($p<0.005$) or not is the effect of the variable on the response.

Table 6.12 Coefficients correspondent to the regression surface response of maximum cell temperature and thermal dispersion together with the p-values.

	Maximum *BM* temperature		Thermal Dispersion	
	Coefficients	p- value, [-]	Coefficients	p- value, [-]
Constant	30.9000	**0.000**	1.4514	**0.000**
Heat Sink	-2.4944	**0.000**	-0.2978	0.015
Fan *PWM*	-5.2889	**0.000**	0.3922	**0.003**
Tamb	12.4278	**0.000**	-0.1461	0.180
C-rate	6.4000	**0.000**	0.4361	**0.002**
Heat Sink*Heat Sink	0.7833	0.482	0.6584	0.035
Fan *PWM**Fan *PWM*	3.4333	**0.005**	-1.1016	**0.002**
Tamb*Tamb	0.1833	0.868	-0.2166	0.440
*C-rate*C-rate*	0.1333	0.903	-0.1866	0.505
Heat Sink*Fan *PWM*	1.7125	**0.002**	-0.0350	0.752
Heat Sink*Tamb	0.5875	0.199	0.0275	0.803
Heat Sink***C-rate*	-1.3250	0.011	-0.1125	0.320
Fan *PWM**Tamb	1.1500	0.023	-0.0825	0.461
Fan *PWM*C-rate*	-3.0125	**0.000**	0.2775	0.027
Tamb***C-rate*	-1.4875	0.009	-0.0575	0.605

Based on Table 6.12, it can be concluded that for the *BM* temperature lineal effects of heat sink, rotational speed of the fan, ambient temperature and *C-rate* have been important, together with quadratic effect of fan speed and interactions between heat sink and speed of the fan and at last, the *PWM* of the fan and *C-rate*. Regarding the thermal dispersion, the lineal effect of the rotational speed of the fan and *C-rate* have been significant along with fan speed quadratic effect. In this case, the interactions between the variables have had insignificant effects on the response.

R-square (R^2) is the percentage of response variable variation and when its value is higher, it means that the models better fits with the data. In this case for each analyzed response 99.35% and 91.26% has been obtained.

Figure 6.24 and Figure 6.25 show the surface response regarding the cell maximum temperature and thermal dispersion in the *BM* respectively, for the case in which SK473 heat sink has been used with the fan at rotational speed of *50% PWM*.

When the surface response is interpreted, it must has bear in mind that the colour of the response surface indicates how low (adequate) or high (inappropriate) is the value of each variable result, considering the established limits for each one. Besides, a black rectangle is in each surface response which includes the values of the responses within the defined design conditions, i.e., regarding the *C-rate* from Cmin (DCH 3C/ CHA 1C) to Cmax (DCH 7C/ CHA 3C) and ambient temperature from 10 ºC to 40 ºC. Also, the response values within the range defined as optimal are in bold.

With the aim to see more clearly the obtained previously results by means of the surface responses, in Table 6.13 are shown the numerical results related with them. Two design zones have been distinguished within the zone marked by a black rectangle: the first one is referred to a soft conditions where the ambient temperature is between 10-25 ºC and the current rate level is between previously defined minimum (DCH 3C/ CHA 1C) and medium (DCH 5C/ CHA 2C) conditions, whereas the second area corresponds to a more restrictive conditions where the ambient temperature is between 25-40 ºC and the current level is between an area previously defined such as medium (DCH 5C/ CHA 2C) and maximum (DCH 7C/ CHA 3C) rate.

It can be concluded that for the worst and more restrictive operating conditions in terms of ambient and electrical solicitations has not been possible to maintain the maximum cell temperature below 55 ºC with a natural convection, both for the case in which the heat sink has been used as for the case that it has not been used.

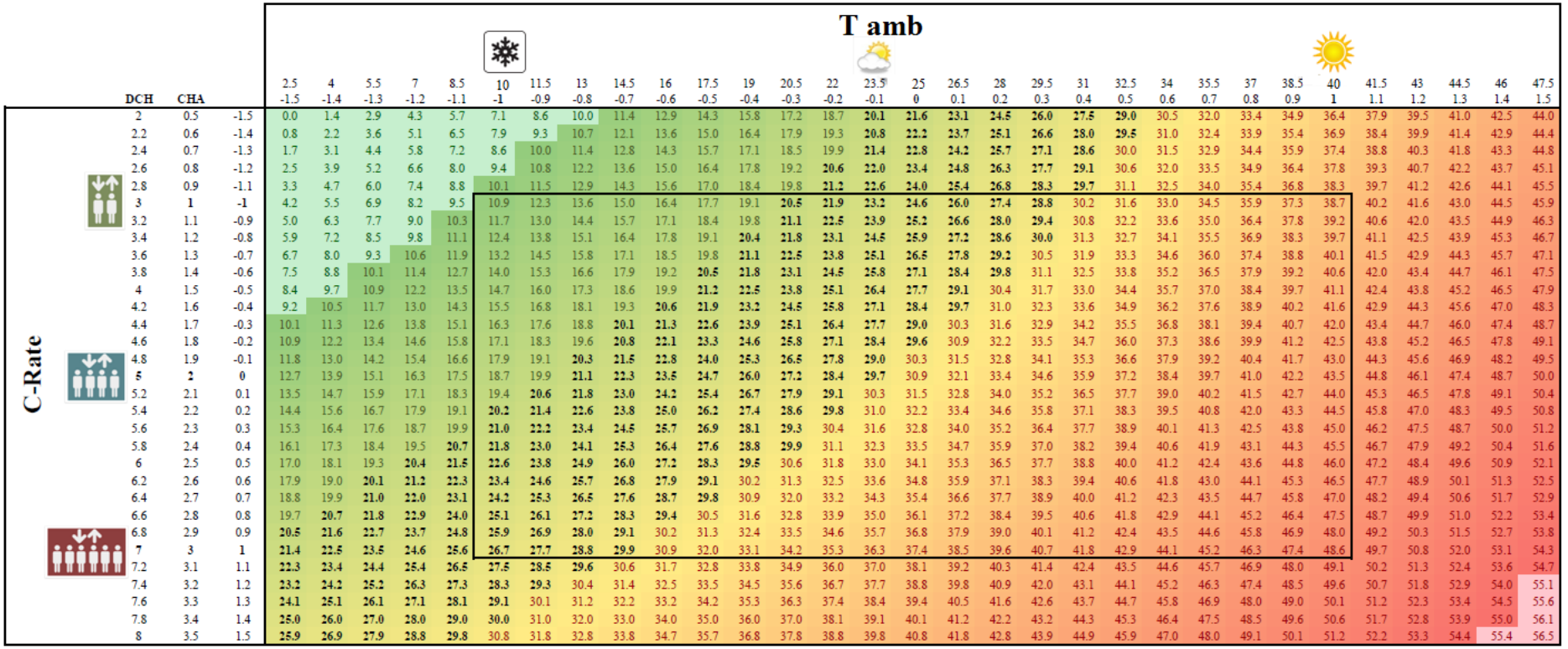

DCH	CHA		2.5	4	5.5	7	8.5	10	11.5	13	14.5	16	17.5	19	20.5	22	23.5	25	26.5	28	29.5	31	32.5	34	35.5	37	38.5	40	41.5	43	44.5	46	47.5
			-1.5	-1.4	-1.3	-1.2	-1.1	-1	-0.9	-0.8	-0.7	-0.6	-0.5	-0.4	-0.3	-0.2	-0.1	0	0.1	0.2	0.3	0.4	0.5	0.6	0.7	0.8	0.9	1	1.1	1.2	1.3	1.4	1.5
2	0.5	-1.5	0.0	1.4	2.9	4.3	5.7	7.1	8.6	10.0	11.4	12.9	14.3	15.8	17.2	18.7	20.1	21.6	23.1	24.5	26.0	27.5	29.0	30.5	32.0	33.4	34.9	36.4	37.9	39.5	41.0	42.5	44.0
2.2	0.6	-1.4	0.8	2.2	3.6	5.1	6.5	7.9	9.3	10.7	12.1	13.6	15.0	16.4	17.9	19.3	20.8	22.2	23.7	25.1	26.6	28.0	29.5	31.0	32.4	33.9	35.4	36.9	38.4	39.9	41.4	42.9	44.4
2.4	0.7	-1.3	1.7	3.1	4.4	5.8	7.2	8.6	10.0	11.4	12.8	14.3	15.7	17.1	18.5	19.9	21.4	22.8	24.2	25.7	27.1	28.6	30.0	31.5	32.9	34.4	35.9	37.4	38.8	40.3	41.8	43.3	44.8
2.6	0.8	-1.2	2.5	3.9	5.2	6.6	8.0	9.4	10.8	12.2	13.6	15.0	16.4	17.8	19.2	20.6	22.0	23.4	24.8	26.3	27.7	29.1	30.6	32.0	33.5	34.9	36.4	37.8	39.3	40.7	42.2	43.7	45.1
2.8	0.9	-1.1	3.3	4.7	6.0	7.4	8.8	10.1	11.5	12.9	14.3	15.6	17.0	18.4	19.8	21.2	22.6	24.0	25.4	26.8	28.3	29.7	31.1	32.5	34.0	35.4	36.8	38.3	39.7	41.2	42.6	44.1	45.5
3	1	-1	4.2	5.5	6.9	8.2	9.5	10.9	12.3	13.6	15.0	16.4	17.7	19.1	20.5	21.9	23.2	24.6	26.0	27.4	28.8	30.2	31.6	33.0	34.5	35.9	37.3	38.7	40.2	41.6	43.0	44.5	45.9
3.2	1.1	-0.9	5.0	6.3	7.7	9.0	10.3	11.7	13.0	14.4	15.7	17.1	18.4	19.8	21.1	22.5	23.9	25.2	26.6	28.0	29.4	30.8	32.2	33.6	35.0	36.4	37.8	39.2	40.6	42.0	43.5	44.9	46.3
3.4	1.2	-0.8	5.9	7.2	8.5	9.8	11.1	12.4	13.8	15.1	16.4	17.8	19.1	20.4	21.8	23.1	24.5	25.9	27.2	28.6	30.0	31.3	32.7	34.1	35.5	36.9	38.3	39.7	41.1	42.5	43.9	45.3	46.7
3.6	1.3	-0.7	6.7	8.0	9.3	10.6	11.9	13.2	14.5	15.8	17.1	18.5	19.8	21.1	22.5	23.8	25.1	26.5	27.8	29.2	30.5	31.9	33.3	34.6	36.0	37.4	38.8	40.1	41.5	42.9	44.3	45.7	47.1
3.8	1.4	-0.6	7.5	8.8	10.1	11.4	12.7	14.0	15.3	16.6	17.9	19.2	20.5	21.8	23.1	24.5	25.8	27.1	28.4	29.8	31.1	32.5	33.8	35.2	36.5	37.9	39.2	40.6	42.0	43.4	44.7	46.1	47.5
4	1.5	-0.5	8.4	9.7	10.9	12.2	13.5	14.7	16.0	17.3	18.6	19.9	21.2	22.5	23.8	25.1	26.4	27.7	29.1	30.4	31.7	33.0	34.4	35.7	37.0	38.4	39.7	41.1	42.4	43.8	45.2	46.5	47.9
4.2	1.6	-0.4	9.2	10.5	11.7	13.0	14.3	15.5	16.8	18.1	19.3	20.6	21.9	23.2	24.5	25.8	27.1	28.4	29.7	31.0	32.3	33.6	34.9	36.2	37.6	38.9	40.2	41.6	42.9	44.3	45.6	47.0	48.3
4.4	1.7	-0.3	10.1	11.3	12.6	13.8	15.1	16.3	17.6	18.8	20.1	21.3	22.6	23.9	25.1	26.4	27.7	29.0	30.3	31.6	32.9	34.2	35.5	36.8	38.1	39.4	40.7	42.0	43.4	44.7	46.0	47.4	48.7
4.6	1.8	-0.2	10.9	12.2	13.4	14.6	15.8	17.1	18.3	19.6	20.8	22.1	23.3	24.6	25.8	27.1	28.4	29.6	30.9	32.2	33.5	34.7	36.0	37.3	38.6	39.9	41.2	42.5	43.8	45.2	46.5	47.8	49.1
4.8	1.9	-0.1	11.8	13.0	14.2	15.4	16.6	17.9	19.1	20.3	21.5	22.8	24.0	25.3	26.5	27.8	29.0	30.3	31.5	32.8	34.1	35.3	36.6	37.9	39.2	40.4	41.7	43.0	44.3	45.6	46.9	48.2	49.5
5	2	0	12.7	13.9	15.1	16.3	17.5	18.7	19.9	21.1	22.3	23.5	24.7	26.0	27.2	28.4	29.7	30.9	32.1	33.4	34.6	35.9	37.2	38.4	39.7	41.0	42.2	43.5	44.8	46.1	47.4	48.7	50.0
5.2	2.1	0.1	13.5	14.7	15.9	17.1	18.3	19.4	20.6	21.8	23.0	24.2	25.4	26.7	27.9	29.1	30.3	31.5	32.8	34.0	35.2	36.5	37.7	39.0	40.2	41.5	42.7	44.0	45.3	46.5	47.8	49.1	50.4
5.4	2.2	0.2	14.4	15.6	16.7	17.9	19.1	20.2	21.4	22.6	23.8	25.0	26.2	27.4	28.6	29.8	31.0	32.2	33.4	34.6	35.8	37.1	38.3	39.5	40.8	42.0	43.3	44.5	45.8	47.0	48.3	49.5	50.8
5.6	2.3	0.3	15.3	16.4	17.6	18.7	19.9	21.0	22.2	23.4	24.5	25.7	26.9	28.1	29.3	30.4	31.6	32.8	34.0	35.2	36.4	37.7	38.9	40.1	41.3	42.5	43.8	45.0	46.2	47.5	48.7	50.0	51.2
5.8	2.4	0.4	16.1	17.3	18.4	19.5	20.7	21.8	23.0	24.1	25.3	26.4	27.6	28.8	29.9	31.1	32.3	33.5	34.7	35.9	37.0	38.2	39.4	40.6	41.9	43.1	44.3	45.5	46.7	47.9	49.2	50.4	51.6
6	2.5	0.5	17.0	18.1	19.3	20.4	21.5	22.6	23.8	24.9	26.0	27.2	28.3	29.5	30.6	31.8	33.0	34.1	35.3	36.5	37.7	38.8	40.0	41.2	42.4	43.6	44.8	46.0	47.2	48.4	49.6	50.9	52.1
6.2	2.6	0.6	17.9	19.0	20.1	21.2	22.3	23.4	24.6	25.7	26.8	27.9	29.1	30.2	31.3	32.5	33.6	34.8	35.9	37.1	38.3	39.4	40.6	41.8	43.0	44.1	45.3	46.5	47.7	48.9	50.1	51.3	52.5
6.4	2.7	0.7	18.8	19.9	21.0	22.0	23.1	24.2	25.3	26.5	27.6	28.7	29.8	30.9	32.0	33.2	34.3	35.4	36.6	37.7	38.9	40.0	41.2	42.3	43.5	44.7	45.8	47.0	48.2	49.4	50.6	51.7	52.9
6.6	2.8	0.8	19.7	20.7	21.8	22.9	24.0	25.1	26.1	27.2	28.3	29.4	30.5	31.6	32.8	33.9	35.0	36.1	37.2	38.4	39.5	40.6	41.8	42.9	44.1	45.2	46.4	47.5	48.7	49.9	51.0	52.2	53.4
6.8	2.9	0.9	20.5	21.6	22.7	23.7	24.8	25.9	26.9	28.0	29.1	30.2	31.3	32.4	33.5	34.6	35.7	36.8	37.9	39.0	40.1	41.2	42.4	43.5	44.6	45.8	46.9	48.0	49.2	50.3	51.5	52.7	53.8
7	3	1	21.4	22.5	23.5	24.6	25.6	26.7	27.7	28.8	29.9	30.9	32.0	33.1	34.2	35.3	36.3	37.4	38.5	39.6	40.7	41.8	42.9	44.1	45.2	46.3	47.4	48.6	49.7	50.8	52.0	53.1	54.3
7.2	3.1	1.1	22.3	23.4	24.4	25.4	26.5	27.5	28.5	29.6	30.6	31.7	32.8	33.8	34.9	36.0	37.0	38.1	39.2	40.3	41.4	42.4	43.5	44.6	45.7	46.9	48.0	49.1	50.2	51.3	52.4	53.6	54.7
7.4	3.2	1.2	23.2	24.2	25.2	26.3	27.3	28.3	29.3	30.4	31.4	32.5	33.5	34.5	35.6	36.7	37.7	38.8	39.8	40.9	42.0	43.1	44.1	45.2	46.3	47.4	48.5	49.6	50.7	51.8	52.9	54.0	55.1
7.6	3.3	1.3	24.1	25.1	26.1	27.1	28.1	29.1	30.1	31.2	32.2	33.2	34.2	35.3	36.3	37.4	38.4	39.4	40.5	41.6	42.6	43.7	44.7	45.8	46.9	48.0	49.0	50.1	51.2	52.3	53.4	54.5	55.6
7.8	3.4	1.4	25.0	26.0	27.0	28.0	29.0	30.0	31.0	32.0	33.0	34.0	35.0	36.0	37.0	38.1	39.1	40.1	41.2	42.2	43.2	44.3	45.3	46.4	47.5	48.5	49.6	50.6	51.7	52.8	53.9	55.0	56.1
8	3.5	1.5	25.9	26.9	27.9	28.8	29.8	30.8	31.8	32.8	33.8	34.7	35.7	36.8	37.8	38.8	39.8	40.8	41.8	42.8	43.9	44.9	45.9	47.0	48.0	49.1	50.1	51.2	52.2	53.3	54.4	55.4	56.5

Figure 6.24. The surface response correspondent to cell temperature with SK473 heat sink with at fan PWM 50%.

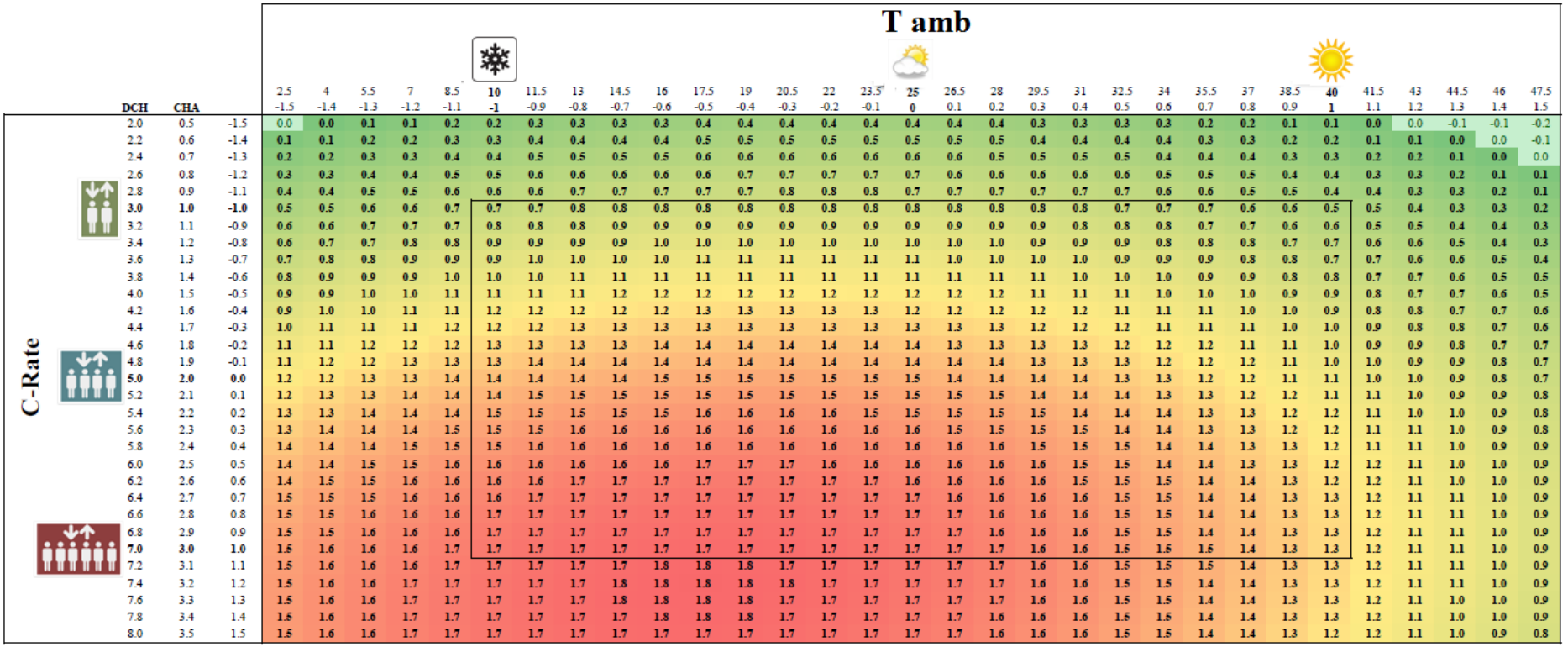

DCH	CHA		2.5	4	5.5	7	8.5	10	11.5	13	14.5	16	17.5	19	20.5	22	23.5	25	26.5	28	29.5	31	32.5	34	35.5	37	38.5	40	41.5	43	44.5	46	47.5
			-1.5	-1.4	-1.3	-1.2	-1.1	-1	-0.9	-0.8	-0.7	-0.6	-0.5	-0.4	-0.3	-0.2	-0.1	0	0.1	0.2	0.3	0.4	0.5	0.6	0.7	0.8	0.9	1	1.1	1.2	1.3	1.4	1.5
2.0	0.5	-1.5	0.0	0.0	0.1	0.1	0.2	0.2	0.3	0.3	0.3	0.3	0.4	0.4	0.4	0.4	0.4	0.4	0.4	0.4	0.3	0.3	0.3	0.3	0.2	0.2	0.1	0.1	0.0	0.0	-0.1	-0.1	-0.2
2.2	0.6	-1.4	0.1	0.1	0.2	0.2	0.3	0.3	0.4	0.4	0.4	0.4	0.5	0.5	0.5	0.5	0.5	0.5	0.5	0.5	0.4	0.4	0.4	0.4	0.3	0.3	0.2	0.2	0.1	0.1	0.0	0.0	-0.1
2.4	0.7	-1.3	0.2	0.2	0.3	0.3	0.4	0.4	0.5	0.5	0.5	0.5	0.6	0.6	0.6	0.6	0.6	0.6	0.6	0.5	0.5	0.5	0.5	0.4	0.4	0.4	0.3	0.3	0.2	0.2	0.1	0.0	0.0
2.6	0.8	-1.2	0.3	0.3	0.4	0.4	0.5	0.5	0.6	0.6	0.6	0.6	0.6	0.7	0.7	0.7	0.7	0.7	0.6	0.6	0.6	0.6	0.6	0.5	0.5	0.5	0.4	0.4	0.3	0.3	0.2	0.1	0.1
2.8	0.9	-1.1	0.4	0.4	0.5	0.5	0.6	0.6	0.6	0.7	0.7	0.7	0.7	0.7	0.8	0.8	0.8	0.7	0.7	0.7	0.7	0.7	0.7	0.6	0.6	0.5	0.5	0.4	0.4	0.3	0.3	0.2	0.1
3.0	**1.0**	**-1.0**	0.5	0.5	0.6	0.6	0.7	0.7	0.7	0.8	0.8	0.8	0.8	0.8	0.8	0.8	0.8	0.8	0.8	0.8	0.8	0.8	0.7	0.7	0.7	0.6	0.6	0.5	0.5	0.4	0.3	0.3	0.2
3.2	1.1	-0.9	0.6	0.6	0.7	0.7	0.7	0.8	0.8	0.8	0.9	0.9	0.9	0.9	0.9	0.9	0.9	0.9	0.9	0.9	0.9	0.8	0.8	0.8	0.7	0.7	0.6	0.6	0.5	0.5	0.4	0.4	0.3
3.4	1.2	-0.8	0.6	0.7	0.7	0.8	0.8	0.9	0.9	0.9	0.9	1.0	1.0	1.0	1.0	1.0	1.0	1.0	1.0	1.0	0.9	0.9	0.9	0.8	0.8	0.8	0.7	0.7	0.6	0.6	0.5	0.4	0.3
3.6	1.3	-0.7	0.7	0.8	0.8	0.9	0.9	0.9	1.0	1.0	1.0	1.0	1.1	1.1	1.1	1.1	1.1	1.1	1.0	1.0	1.0	1.0	0.9	0.9	0.9	0.8	0.8	0.7	0.7	0.6	0.6	0.5	0.4
3.8	1.4	-0.6	0.8	0.9	0.9	0.9	1.0	1.0	1.0	1.1	1.1	1.1	1.1	1.1	1.1	1.1	1.1	1.1	1.1	1.1	1.1	1.1	1.0	1.0	1.0	0.9	0.9	0.8	0.8	0.7	0.7	0.6	0.5
4.0	1.5	-0.5	0.9	0.9	1.0	1.0	1.1	1.1	1.1	1.1	1.2	1.2	1.2	1.2	1.2	1.2	1.2	1.2	1.2	1.2	1.2	1.1	1.1	1.1	1.0	1.0	1.0	0.9	0.9	0.8	0.7	0.7	0.6
4.2	1.6	-0.4	0.9	1.0	1.0	1.1	1.1	1.2	1.2	1.2	1.2	1.2	1.3	1.3	1.3	1.3	1.3	1.2	1.2	1.2	1.2	1.2	1.1	1.1	1.1	1.0	1.0	0.9	0.8	0.8	0.7	0.7	0.6
4.4	1.7	-0.3	1.0	1.1	1.1	1.1	1.2	1.2	1.2	1.3	1.3	1.3	1.3	1.3	1.3	1.3	1.3	1.3	1.3	1.3	1.2	1.2	1.2	1.1	1.1	1.1	1.0	1.0	0.9	0.8	0.8	0.7	0.6
4.6	1.8	-0.2	1.1	1.1	1.2	1.2	1.2	1.3	1.3	1.3	1.3	1.4	1.4	1.4	1.4	1.4	1.4	1.4	1.3	1.3	1.3	1.3	1.2	1.2	1.2	1.1	1.1	1.0	0.9	0.9	0.8	0.7	0.7
4.8	1.9	-0.1	1.1	1.2	1.2	1.3	1.3	1.3	1.4	1.4	1.4	1.4	1.4	1.4	1.4	1.4	1.4	1.4	1.4	1.4	1.3	1.3	1.3	1.2	1.2	1.2	1.1	1.0	1.0	0.9	0.9	0.8	0.7
5.0	**2.0**	**0.0**	1.2	1.2	1.3	1.3	1.4	1.4	1.4	1.4	1.4	1.5	1.5	1.5	1.5	1.5	1.5	1.5	1.4	1.4	1.4	1.4	1.3	1.3	1.2	1.2	1.1	1.1	1.0	1.0	0.9	0.8	0.7
5.2	2.1	0.1	1.2	1.3	1.3	1.4	1.4	1.4	1.5	1.5	1.5	1.5	1.5	1.5	1.5	1.5	1.5	1.5	1.5	1.5	1.4	1.4	1.4	1.3	1.3	1.2	1.2	1.1	1.1	1.0	0.9	0.9	0.8
5.4	2.2	0.2	1.3	1.3	1.4	1.4	1.4	1.5	1.5	1.5	1.5	1.5	1.6	1.6	1.6	1.6	1.5	1.5	1.5	1.5	1.5	1.4	1.4	1.4	1.3	1.3	1.2	1.2	1.1	1.0	1.0	0.9	0.8
5.6	2.3	0.3	1.3	1.4	1.4	1.4	1.5	1.5	1.5	1.6	1.6	1.6	1.6	1.6	1.6	1.6	1.6	1.6	1.5	1.5	1.5	1.5	1.4	1.4	1.3	1.3	1.2	1.2	1.1	1.1	1.0	0.9	0.8
5.8	2.4	0.4	1.4	1.4	1.4	1.5	1.5	1.5	1.6	1.6	1.6	1.6	1.6	1.6	1.6	1.6	1.6	1.6	1.6	1.6	1.5	1.5	1.5	1.4	1.4	1.3	1.3	1.2	1.1	1.1	1.0	0.9	0.9
6.0	2.5	0.5	1.4	1.4	1.5	1.5	1.6	1.6	1.6	1.6	1.6	1.6	1.7	1.7	1.7	1.6	1.6	1.6	1.6	1.6	1.6	1.5	1.5	1.4	1.4	1.3	1.3	1.2	1.2	1.1	1.0	1.0	0.9
6.2	2.6	0.6	1.4	1.5	1.5	1.6	1.6	1.6	1.6	1.7	1.7	1.7	1.7	1.7	1.7	1.7	1.7	1.6	1.6	1.6	1.6	1.5	1.5	1.5	1.4	1.4	1.3	1.2	1.2	1.1	1.0	1.0	0.9
6.4	2.7	0.7	1.5	1.5	1.5	1.6	1.6	1.6	1.7	1.7	1.7	1.7	1.7	1.7	1.7	1.7	1.7	1.7	1.6	1.6	1.6	1.6	1.5	1.5	1.4	1.4	1.3	1.3	1.2	1.1	1.1	1.0	0.9
6.6	2.8	0.8	1.5	1.5	1.6	1.6	1.6	1.7	1.7	1.7	1.7	1.7	1.7	1.7	1.7	1.7	1.7	1.7	1.7	1.6	1.6	1.6	1.5	1.5	1.4	1.4	1.3	1.3	1.2	1.1	1.1	1.0	0.9
6.8	2.9	0.9	1.5	1.5	1.6	1.6	1.6	1.7	1.7	1.7	1.7	1.7	1.7	1.7	1.7	1.7	1.7	1.7	1.7	1.6	1.6	1.6	1.5	1.5	1.4	1.4	1.3	1.3	1.2	1.1	1.1	1.0	0.9
7.0	**3.0**	**1.0**	1.5	1.6	1.6	1.6	1.7	1.7	1.7	1.7	1.7	1.7	1.7	1.7	1.7	1.7	1.7	1.7	1.7	1.7	1.6	1.6	1.5	1.5	1.5	1.4	1.3	1.3	1.2	1.1	1.1	1.0	0.9
7.2	3.1	1.1	1.5	1.6	1.6	1.6	1.7	1.7	1.7	1.7	1.7	1.8	1.8	1.8	1.8	1.7	1.7	1.7	1.7	1.7	1.7	1.6	1.6	1.5	1.5	1.5	1.4	1.3	1.3	1.2	1.1	1.1	1.0	0.9
7.4	3.2	1.2	1.5	1.6	1.6	1.7	1.7	1.7	1.7	1.7	1.8	1.8	1.8	1.8	1.8	1.7	1.7	1.7	1.7	1.7	1.7	1.6	1.6	1.5	1.5	1.4	1.4	1.3	1.3	1.2	1.1	1.1	1.0	0.9
7.6	3.3	1.3	1.5	1.6	1.6	1.7	1.7	1.7	1.7	1.7	1.8	1.8	1.8	1.8	1.7	1.7	1.7	1.7	1.7	1.7	1.7	1.6	1.6	1.5	1.5	1.4	1.4	1.3	1.3	1.2	1.1	1.0	1.0	0.9
7.8	3.4	1.4	1.5	1.6	1.6	1.7	1.7	1.7	1.7	1.7	1.7	1.8	1.8	1.8	1.7	1.7	1.7	1.7	1.7	1.7	1.6	1.6	1.6	1.5	1.5	1.4	1.4	1.3	1.3	1.2	1.1	1.0	1.0	0.9
8.0	3.5	1.5	1.5	1.6	1.6	1.7	1.7	1.7	1.7	1.7	1.7	1.7	1.7	1.7	1.7	1.7	1.7	1.7	1.7	1.7	1.6	1.6	1.6	1.5	1.5	1.4	1.4	1.3	1.2	1.2	1.1	1.0	0.9	0.8

Figure 6.25. The surface response correspondent to the thermal dispersion with SK473 heat sink with at fan PWM 50%.

Table 6.13 Numerical results obtained from the surface responses.

		Cell Temperature, ºC				**Thermal Dispersion, ºC**			
		Tamb: 10-25 ºC / Crate:min-mid		**Tamb: 25-40 ºC / Crate:mid-max**		**Tamb: 10-25 ºC / Crate:min-mid**		**Tamb: 25-40 ºC / Crate:mid-max**	
		Min	**Max**	**Min**	**Max**	**Min**	**Max**	**Min**	**Max**
Without Heat Sink	Natural Convection	22.0	44.6	44.6	64.9	0.2	0.9	0.6	1.0
	50% *PWM*	13.4	34.2	34.2	52.6	1.5	2.4	2.1	2.8
	100% *PWM*	11.7	30.6	30.6	47.1	0.7	1.8	1.3	2.4
SK 473	Natural Convection	17.8	39.6	39.6	59.1	-0.6	0.0	-0.4	0.0
	50% *PWM*	10.9	30.9	30.9	48.6	0.7	1.5	1.1	1.7
	100% *PWM*	10.9	29.0	29.0	44.8	-0.2	0.8	0.4	1.3
SK 180	Natural Convection	15.1	36.2	36.2	55.0	-0.2	0.4	0.0	0.4
	50% *PWM*	9.9	29.2	29.2	46.1	1.1	1.8	1.5	2.0
	100% *PWM*	11.6	29.0	29.0	44.1	0.2	1.1	0.7	1.5

In addition and based on the results shown in Table 6.13, it is evidenced that the main factor to keep the *BM* within an appropriate operation range has been the usage of *FC*. In fact, it is clear that although when a heat sink is used the obtained *BM* temperature has been slightly lower, has not been indispensable the implementation in the system of it, since for the cases without heat sink with forced convection the *BM* has been kept within the admissible operation range for the worst conditions. Moreover, the higher the *PWM* of the fan, the influence or use or not a heat sink is less on the temperature of the *BM*.

Regarding the thermal dispersion and considering the results tabulated in Table 6.13, it is obvious that at any conditions have been achieved to keep the temperature difference within the *BM* below 3 ºC. In natural convection conditions the thermal dispersion between the cells in smaller compared with the cases has been which forced convection has been used. Another effect that it is important to mention but it cannot observe by means of the surface responses has been, that when natural convection has been used the hottest cell at *BM* level has been the cell placed in the centre of the *BM*, whereas when the forced convection has been used the hottest cell has been which was located on the opposite side from the air exit.

Based on this study it has been decided to dispense with the heat sink reducing the initial cost and the simplicity in terms of the system mounting. Nevertheless, in order to consider if it is needed or not fan, once it has been decided not to use a heat sink, the time required for the cooling process at *BM* has been evaluated.

For that purpose, a *DoE* shows in Table 6.14 has been defined considering such as parameters the fan rotational speed (25% *PWM*, 50% *PWM* and 75% *PWM*), ambient temperature (10 ºC, 25 ºC and 40 ºC) and current rate (Cmin: DCH 3C/ CHA 1C, Cmid: DCH 5C/ CHA 2C, Cmax: DCH 7C/ CHA 3C).

Table 6.14 DoE matrix at BM level for cooling purpose.

	Coded Value			UnCoded Value		
	Fan *PWM*	T amb	C-rate	Fan *PWM*	T amb	C-rate
1	-1	-1	-1	PWM 25%	10	Cmin
2	-1	1	-1	PWM 25%	40	Cmin
3	-1	-1	1	PWM 25%	10	Cmax
4	-1	1	1	PWM 25%	40	Cmax
5	0	0	0	PWM 50%	25	Cmid
6	1	-1	0	PWM 75%	10	Cmin
7	1	1	0	PWM 75%	40	Cmin
8	1	-1	1	PWM 75%	10	Cmax
9	1	1	1	PWM 75%	40	Cmax
10	-1	0	0	PWM 25%	25	Cmid
11	0	0	1	PWM 50%	25	Cmax
12	1	0	0	PWM 75%	25	Cmid
13	0	0	-1	PWM 50%	25	Cmin
14	0	1	0	PWM 50%	40	Cmid
15	0	-1	0	PWM 50%	10	Cmid

Following the same procedure than in the previous case, in Table 6.15 are shown the numerical results obtained for each test that has been carried out. The cooling time has been evaluated considering that the temperature has been reached when the difference respect to the objective temperature was 0.1 ºC. The cooling time has been evaluated in second, minutes and hours in Table 6.15, although the response surface following has been defined in minutes only.

Applying the *Face Centered CCD* the regression surface responses of cooling time variable have been obtained by mean of the coefficients tabulated in *Table 6.16*. p-values associated to each variable are also shown. As aforementioned, the p-value lower than 0.005 means that the variable has a significant effect on the response.

Table 6.15Numerical results of the DoE matrix at BM level for cooling purpose.

	Fan *PWM*	T amb	C-rate	**Cooling time, s**	**Cooling time, min**	**Cooling time, h**
1	1	1	1	2210	36.8	0.6
2	1	-1	-1	1442	24.0	0.4
3	1	-1	1	2175	36.3	0.6
4	-1	-1	1	16306	271.8	4.5
5	1	1	-1	1118	18.6	0.3
6	-1	1	-1	9503	158.4	2.6
7	-1	1	1	12219	203.7	3.4
8	-1	-1	-1	11044	184.1	3.1
9	0	0	0	4915	81.9	1.4
10	-1	0	0	13756	229.3	3.8
11	1	0	0	1679	28.0	0.5
12	0	0	-1	3476	57.9	1.0
13	0	0	1	6275	104.6	1.7
14	0	-1	0	4123	68.7	1.1
15	0	1	0	5563	92.7	1.5

In this case and as it can be seen in *Table 6.16*, the rotational speed of the fan has a relevant lineal effect on the cooling time response, whereas the quadratic effects and the interactions between the factors have been insignificant. Nevertheless, among the quadratic effects, it can be said that the quadratic effect of the fan rotational speed has been the most important one (p=0.012).

Table 6.16 Coefficients correspondent to the regression surface response of BM cooling time with the p-values.

	Cooling time	
	Coefficient	p- value, [-]
Constant	85.487	**0.000**
Fan PWM	-90.360	**0.000**
Tamb	-7.47	0.236
C-rate	21.020	0.013
Fan PWM*Fan PWM	42.267	0.012
Tamb*Tamb	-5.683	0.625
*C-rate***C-rate*	-5.133	0.658
Fan PWM*Tamb	11.113	0.133
Fan PWM**C-rate*	-12.813	0.093
Tamb**C-rate*	-4.563	0.495

Moreover, the sign of the coefficients is related to whether the factor is directly or inversely proportional to the response, for instance, when the fan rotational speed increases the cooling time decreases, as it has been expected.

The R-square value corresponded for this adjustment has been 98.39%.

Figure 6.26 shows the surface responses regarding the cooling required time in minutes considering the *BM* without heat sink and with different convection alternatives: (a) natural convection, (b) 50% *PWM* and (c) 100% *PWM*.

Considering the results show in Figure 6.26 (b) and (c), for the less restrictive (10 ºC and DCH 3C/ CHA 1C) and the most severe (40 ºC and DCH 7C/ CHA 3C) operation conditions, the system has required 56 and 183 minutes respectively to cool down the *BM* with the fan working at 50% of *PWM*, while with the fan at 100% of *PWM* 10 and 33 minutes have been needed respectively.

Defined such as the optimal and limit cooling time range 75 and 120 minutes respectively, it can be seen that for the natural convection case the waiting time to cool the *BM* has made this option unviable. For instance, as it can be seen in Figure 6.26 (a) for the less restrictive conditions in terms of ambient and *C-rate* (10 ºC and DCH 3C/ CHA 1C), the *BM* has needed at least 188 minutes (little more than three hours).

As conclusion, it can be said that for the cooling process the forced convection has defined as completely necessary. To keep the cooling time range lower than 2 hours for the worst conditions (40 ºC and DCH 7C/ CHA 3C), a fan *PWM* of 32.5% has been required. However, with this rotational speed of the fan with an ambient temperature of 10 ºC and a current rate of DCH 3C/ CHA 1C, the *BM* has been cooled in 92 minutes, within the operation range defined such as acceptable. Nevertheless, in the strictest sense to achieve a cooling time below than 75 minutes (optimal range) for the harshest conditions, a *PWM* of 55% has been established.

C-Rate	DCH	CHA		T amb 2.5	4.0	5.5	7.0	8.5	10.0	11.5	13.0	14.5	16.0	17.5	19.0	20.5	22.0	23.5	25.0	26.5	28.0	29.5	31.0	32.5	34.0	35.5	37.0	38.5	40.0	41.5	43.0	44.5	46.0	47.5
				-1.5	-1.4	-1.3	-1.2	-1.1	-1.0	-0.9	-0.8	-0.7	-0.6	-0.5	-0.4	-0.3	-0.2	-0.1	0.0	0.1	0.2	0.3	0.4	0.5	0.6	0.7	0.8	0.9	1.0	1.1	1.2	1.3	1.4	1.5
	2.0	0.5	-1.5	168.3	167.9	167.3	166.7	166.1	165.3	164.4	163.5	162.5	161.3	160.2	158.9	157.5	156.1	154.5	152.9	151.2	149.5	147.6	145.6	143.6	141.5	139.3	137.0	134.7	132.2	129.7	127.0	124.3	121.6	123.3
	2.2	0.6	-1.4	174.3	173.8	173.3	172.6	171.9	171.1	170.2	169.2	168.1	167.0	165.7	164.4	163.0	161.5	159.9	158.3	156.5	154.7	152.8	150.8	148.7	146.6	144.3	142.0	139.6	137.1	134.5	131.8	129.1	126.3	123.3
	2.4	0.7	-1.3	180.2	179.7	179.1	178.4	177.6	176.7	175.8	174.8	173.6	172.4	171.2	169.8	168.3	166.8	165.2	163.5	161.7	159.8	157.9	155.8	153.7	151.5	149.2	146.8	144.4	141.8	139.2	136.5	133.7	130.8	127.9
	2.6	0.8	-1.2	186.0	185.4	184.7	184.0	183.2	182.3	181.3	180.2	179.0	177.8	176.5	175.0	173.5	172.0	170.3	168.5	166.7	164.8	162.8	160.7	158.5	156.3	154.0	151.5	149.0	146.4	143.8	141.0	138.2	135.3	132.2
	2.8	0.9	-1.1	191.6	191.0	190.3	189.5	188.6	187.6	186.6	185.5	184.3	183.0	181.6	180.1	178.6	177.0	175.3	173.5	171.6	169.6	167.6	165.5	163.2	160.9	158.6	156.1	153.5	150.9	148.2	145.4	142.5	139.5	136.5
	3.0	**1.0**	**-1.0**	197.0	196.4	195.6	194.8	193.9	192.9	191.8	190.6	189.4	188.0	186.6	185.1	183.5	181.9	180.1	178.3	176.3	174.3	172.2	170.1	167.8	165.5	163.0	160.5	157.9	155.2	152.5	149.6	146.7	143.7	140.6
	3.2	1.1	-0.9	202.4	201.7	200.9	200.0	199.0	198.0	196.9	195.6	194.3	193.0	191.5	189.9	188.3	186.6	184.8	182.9	180.9	178.9	176.7	174.5	172.2	169.8	167.4	164.8	162.2	159.4	156.6	153.7	150.8	147.7	144.6
	3.4	1.2	-0.8	207.6	206.8	206.0	205.0	204.0	202.9	201.8	200.5	199.2	197.7	196.2	194.6	192.9	191.2	189.3	187.4	185.4	183.3	181.1	178.8	176.5	174.1	171.5	168.9	166.2	163.5	160.6	157.7	154.7	151.6	148.4
	3.6	1.3	-0.7	212.6	211.8	210.9	210.0	208.9	207.8	206.5	205.2	203.8	202.4	200.8	199.2	197.5	195.6	193.7	191.8	189.7	187.6	185.3	183.0	180.6	178.1	175.6	172.9	170.2	167.4	164.5	161.5	158.4	155.3	152.1
	3.8	1.4	-0.6	217.5	216.7	215.7	214.7	213.6	212.4	211.2	209.8	208.4	206.9	205.3	203.6	201.8	200.0	198.0	196.0	193.9	191.7	189.4	187.1	184.6	182.1	179.5	176.8	174.0	171.2	168.2	165.2	162.1	158.9	155.6
	4.0	1.5	-0.5	222.3	221.4	220.4	219.4	218.2	217.0	215.7	214.3	212.8	211.2	209.6	207.9	206.0	204.1	202.2	200.1	197.9	195.7	193.4	191.0	188.5	185.9	183.3	180.5	177.7	174.8	171.8	168.7	165.6	162.3	159.0
	4.2	1.6	-0.4	226.9	226.0	225.0	223.9	222.7	221.4	220.0	218.6	217.1	215.5	213.8	212.0	210.1	208.2	206.1	204.0	201.8	199.5	197.2	194.7	192.2	189.6	186.9	184.1	181.2	178.3	175.2	172.1	168.9	165.6	162.3
	4.4	1.7	-0.3	231.4	230.4	229.4	228.2	227.0	225.7	224.2	222.8	221.2	219.5	217.8	216.0	214.1	212.1	210.0	207.8	205.6	203.3	200.9	198.4	195.8	193.1	190.4	187.5	184.6	181.6	178.5	175.4	172.1	168.8	165.4
	4.6	1.8	-0.2	235.8	234.7	233.6	232.4	231.1	229.8	228.3	226.8	225.2	223.5	221.7	219.8	217.9	215.8	213.7	211.5	209.2	206.8	204.4	201.8	199.2	196.5	193.7	190.8	187.9	184.8	181.7	178.5	175.2	171.8	168.4
	4.8	1.9	-0.1	240.0	238.9	237.7	236.5	235.2	233.8	232.3	230.7	229.0	227.3	225.4	223.5	221.5	219.4	217.3	215.0	212.7	210.3	207.8	205.2	202.5	199.8	196.9	194.0	191.0	187.9	184.7	181.5	178.1	174.7	171.2
	5.0	**2.0**	**0.0**	244.1	242.9	241.7	240.4	239.1	237.6	236.1	234.4	232.7	230.9	229.1	227.1	225.0	222.9	220.7	218.4	216.0	213.6	211.0	208.4	205.7	202.9	200.0	197.0	194.0	190.8	187.6	184.3	180.9	177.5	173.9
	5.2	2.1	0.1	248.0	246.8	245.6	244.2	242.8	241.3	239.7	238.0	236.3	234.5	232.5	230.5	228.4	226.3	224.0	221.7	219.2	216.7	214.1	211.5	208.7	205.8	202.9	199.9	196.8	193.6	190.4	187.0	183.6	180.1	176.5
	5.4	2.2	0.2	251.8	250.6	249.3	247.9	246.4	244.9	243.2	241.5	239.7	237.8	235.9	233.8	231.7	229.5	227.2	224.8	222.3	219.7	217.1	214.4	211.6	208.7	205.7	202.6	199.5	196.3	193.0	189.6	186.1	182.5	178.9
	5.6	2.3	0.3	255.4	254.2	252.8	251.4	249.9	248.3	246.6	244.8	243.0	241.1	239.1	237.0	234.8	232.5	230.2	227.7	225.2	222.6	219.9	217.2	214.3	211.4	208.3	205.2	202.1	198.8	195.4	192.0	188.5	184.9	181.2
	5.8	2.4	0.4	258.9	257.6	256.2	254.8	253.2	251.6	249.8	248.0	246.1	244.2	242.1	240.0	237.7	235.4	233.0	230.6	228.0	225.3	222.6	219.8	216.9	213.9	210.9	207.7	204.5	201.2	197.8	194.3	190.7	187.0	183.3
	6.0	2.5	0.5	262.3	261.0	259.5	258.0	256.4	254.7	252.9	251.1	249.2	247.1	245.0	242.8	240.6	238.2	235.8	233.2	230.6	227.9	225.2	222.3	219.4	216.3	213.2	210.0	206.7	203.4	199.9	196.4	192.8	189.1	185.3
	6.2	2.6	0.6	265.5	264.1	262.7	261.1	259.4	257.7	255.9	254.0	252.0	250.0	247.8	245.6	243.3	240.8	238.4	235.8	233.1	230.4	227.6	224.7	221.7	218.6	215.5	212.2	208.9	205.5	202.0	198.4	194.7	191.0	187.2
	6.4	2.7	0.7	268.6	267.2	265.7	264.1	262.4	260.6	258.7	256.8	254.7	252.6	250.4	248.2	245.8	243.3	240.8	238.2	235.5	232.7	229.8	226.9	223.9	220.7	217.5	214.3	210.9	207.4	203.9	200.3	196.6	192.8	188.9
	6.6	2.8	0.8	271.6	270.1	268.5	266.9	265.1	263.3	261.4	259.4	257.3	255.2	252.9	250.6	248.2	245.7	243.1	240.5	237.7	234.9	232.0	229.0	225.9	222.7	219.5	216.2	212.7	209.2	205.7	202.0	198.2	194.4	190.5
	6.8	2.9	0.9	274.4	272.9	271.2	269.5	267.8	265.9	263.9	261.9	259.8	257.6	255.3	252.9	250.5	247.9	245.3	242.6	239.8	236.9	234.0	230.9	227.8	224.6	221.3	217.9	214.5	210.9	207.3	203.6	199.8	195.9	191.9
	7.0	**3.0**	**1.0**	277.1	275.5	273.8	272.1	270.2	268.3	266.3	264.3	262.1	259.8	257.5	255.1	252.6	250.0	247.3	244.6	241.7	238.8	235.8	232.7	229.6	226.3	223.0	219.5	216.0	212.4	208.8	205.0	201.2	197.2	193.2
	7.2	3.1	1.1	279.6	278.0	276.3	274.5	272.6	270.6	268.6	266.5	264.3	262.0	259.6	257.1	254.6	251.9	249.2	246.4	243.5	240.6	237.5	234.4	231.2	227.9	224.5	221.0	217.5	213.8	210.1	206.3	202.4	198.4	194.4
	7.4	3.2	1.2	282.0	280.3	278.6	276.7	274.8	272.8	270.7	268.5	266.3	263.9	261.5	259.0	256.4	253.7	251.0	248.1	245.2	242.2	239.1	235.9	232.7	229.3	225.9	222.4	218.8	215.1	211.3	207.5	203.5	199.5	195.4
	7.6	3.3	1.3	284.2	282.5	280.7	278.8	276.9	274.8	272.7	270.5	268.2	265.8	263.3	260.8	258.1	255.4	252.6	249.7	246.7	243.7	240.5	237.3	234.0	230.6	227.1	223.6	219.9	216.2	212.4	208.5	204.5	200.4	196.3
	7.8	3.4	1.4	286.4	284.6	282.7	280.8	278.8	276.7	274.5	272.3	269.9	267.5	265.0	262.4	259.7	256.9	254.1	251.1	248.1	245.0	241.8	238.6	235.2	231.8	228.2	224.6	220.9	217.2	213.3	209.4	205.3	201.2	197.0
	8.0	3.5	1.5	288.3	286.5	284.6	282.7	280.6	278.5	276.2	273.9	271.5	269.0	266.5	263.8	261.1	258.3	255.4	252.4	249.4	246.2	243.0	239.7	236.3	232.8	229.2	225.6	221.8	218.0	214.1	210.1	206.0	201.9	197.6

(a)

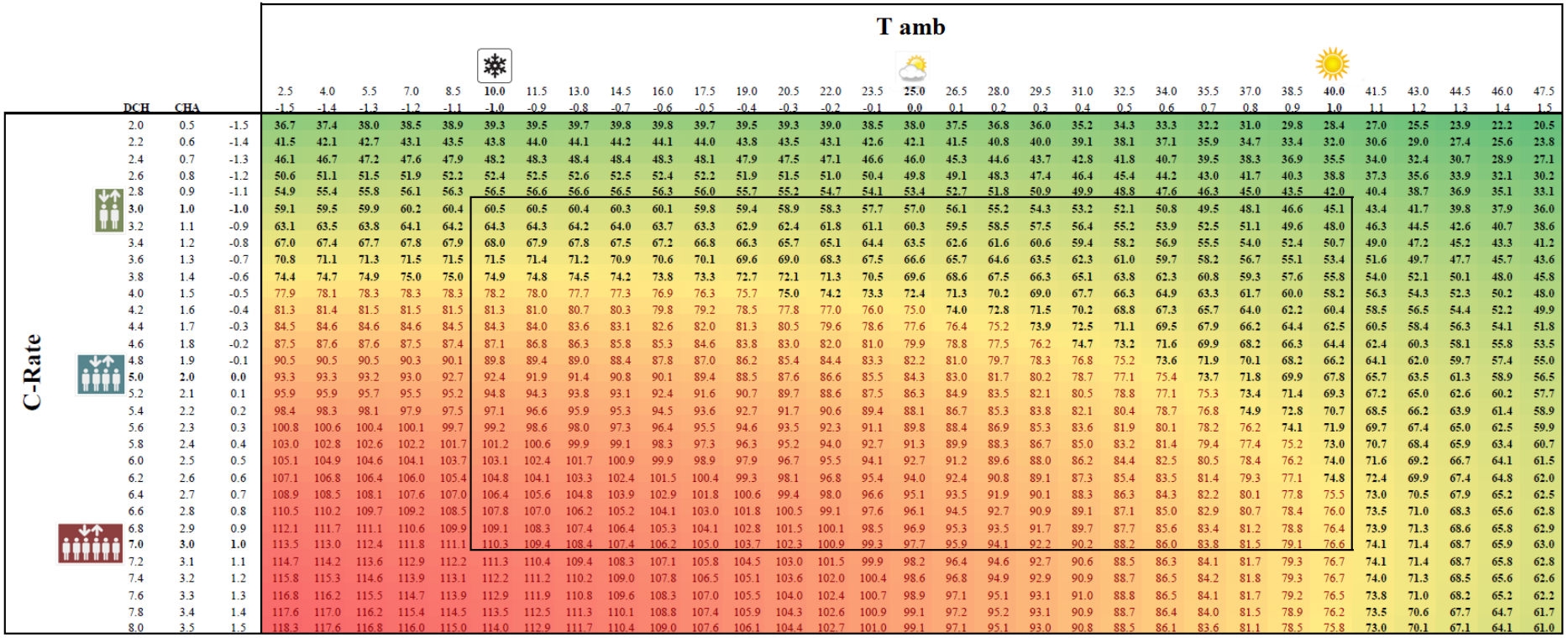

C-Rate			T amb																														
			2.5	4.0	5.5	7.0	8.5	10.0	11.5	13.0	14.5	16.0	17.5	19.0	20.5	22.0	23.5	25.0	26.5	28.0	29.5	31.0	32.5	34.0	35.5	37.0	38.5	40.0	41.5	43.0	44.5	46.0	47.5
DCH	CHA		-1.5	-1.4	-1.3	-1.2	-1.1	-1.0	-0.9	-0.8	-0.7	-0.6	-0.5	-0.4	-0.3	-0.2	-0.1	0.0	0.1	0.2	0.3	0.4	0.5	0.6	0.7	0.8	0.9	1.0	1.1	1.2	1.3	1.4	1.5
2.0	0.5	-1.5	36.7	37.4	38.0	38.5	38.9	39.3	39.5	39.7	39.8	39.8	39.7	39.5	39.3	39.0	38.5	38.0	37.5	36.8	36.0	35.2	34.3	33.3	32.2	31.0	29.8	28.4	27.0	25.5	23.9	22.2	20.5
2.2	0.6	-1.4	41.5	42.1	42.7	43.1	43.5	43.8	44.0	44.1	44.2	44.1	44.0	43.8	43.5	43.1	42.6	42.1	41.5	40.8	40.0	39.1	38.1	37.1	35.9	34.7	33.4	32.0	30.6	29.0	27.4	25.6	23.8
2.4	0.7	-1.3	46.1	46.7	47.2	47.6	47.9	48.2	48.3	48.4	48.4	48.3	48.1	47.9	47.5	47.1	46.6	46.0	45.3	44.6	43.7	42.8	41.8	40.7	39.5	38.3	36.9	35.5	34.0	32.4	30.7	28.9	27.1
2.6	0.8	-1.2	50.6	51.1	51.5	51.9	52.2	52.4	52.5	52.6	52.5	52.4	52.2	51.9	51.5	51.0	50.4	49.8	49.1	48.3	47.4	46.4	45.4	44.2	43.0	41.7	40.3	38.8	37.3	35.6	33.9	32.1	30.2
2.8	0.9	-1.1	54.9	55.4	55.8	56.1	56.3	56.5	56.6	56.6	56.5	56.3	56.0	55.7	55.2	54.7	54.1	53.4	52.7	51.8	50.9	49.9	48.8	47.6	46.3	45.0	43.5	42.0	40.4	38.7	36.9	35.1	33.1
3.0	1.0	-1.0	59.1	59.5	59.9	60.2	60.4	60.5	60.5	60.4	60.3	60.1	59.8	59.4	58.9	58.3	57.7	57.0	56.1	55.2	54.3	53.2	52.1	50.8	49.5	48.1	46.6	45.1	43.4	41.7	39.8	37.9	36.0
3.2	1.1	-0.9	63.1	63.5	63.8	64.1	64.2	64.3	64.3	64.2	64.0	63.7	63.3	62.9	62.4	61.8	61.1	60.3	59.5	58.5	57.5	56.4	55.2	53.9	52.5	51.1	49.6	48.0	46.3	44.5	42.6	40.7	38.6
3.4	1.2	-0.8	67.0	67.4	67.7	67.8	67.9	68.0	67.9	67.8	67.5	67.2	66.8	66.3	65.7	65.1	64.4	63.5	62.6	61.6	60.6	59.4	58.2	56.9	55.5	54.0	52.4	50.7	49.0	47.2	45.2	43.3	41.2
3.6	1.3	-0.7	70.8	71.1	71.3	71.5	71.5	71.5	71.4	71.2	70.9	70.6	70.1	69.6	69.0	68.3	67.5	66.6	65.7	64.6	63.5	62.3	61.0	59.7	58.2	56.7	55.1	53.4	51.6	49.7	47.7	45.7	43.6
3.8	1.4	-0.6	74.4	74.7	74.9	75.0	75.0	74.9	74.8	74.5	74.2	73.8	73.3	72.7	72.1	71.3	70.5	69.6	68.6	67.5	66.3	65.1	63.8	62.3	60.8	59.3	57.6	55.8	54.0	52.1	50.1	48.0	45.8
4.0	1.5	-0.5	77.9	78.1	78.3	78.3	78.3	78.2	78.0	77.7	77.3	76.9	76.3	75.7	75.0	74.2	73.3	72.4	71.3	70.2	69.0	67.7	66.3	64.9	63.3	61.7	60.0	58.2	56.3	54.3	52.3	50.2	48.0
4.2	1.6	-0.4	81.3	81.4	81.5	81.5	81.5	81.3	81.0	80.7	80.3	79.8	79.2	78.5	77.8	77.0	76.0	75.0	74.0	72.8	71.5	70.2	68.8	67.3	65.7	64.0	62.2	60.4	58.5	56.5	54.4	52.2	49.9
4.4	1.7	-0.3	84.5	84.6	84.6	84.6	84.5	84.3	84.0	83.6	83.1	82.6	82.0	81.3	80.5	79.6	78.6	77.6	76.4	75.2	73.9	72.5	71.1	69.5	67.9	66.2	64.4	62.5	60.5	58.4	56.3	54.1	51.8
4.6	1.8	-0.2	87.5	87.6	87.6	87.5	87.4	87.1	86.8	86.3	85.8	85.3	84.6	83.8	83.0	82.0	81.0	79.9	78.8	77.5	76.2	74.7	73.2	71.6	69.9	68.2	66.3	64.4	62.4	60.3	58.1	55.8	53.5
4.8	1.9	-0.1	90.5	90.5	90.5	90.3	90.1	89.8	89.4	89.0	88.4	87.8	87.0	86.2	85.4	84.4	83.3	82.2	81.0	79.7	78.3	76.8	75.2	73.6	71.9	70.1	68.2	66.2	64.1	62.0	59.7	57.4	55.0
5.0	2.0	0.0	93.3	93.3	93.2	93.0	92.7	92.4	91.9	91.4	90.8	90.1	89.4	88.5	87.6	86.6	85.5	84.3	83.0	81.7	80.2	78.7	77.1	75.4	73.7	71.8	69.9	67.8	65.7	63.5	61.3	58.9	56.5
5.2	2.1	0.1	95.9	95.9	95.7	95.5	95.2	94.8	94.3	93.8	93.1	92.4	91.6	90.7	89.7	88.6	87.5	86.3	84.9	83.5	82.1	80.5	78.8	77.1	75.3	73.4	71.4	69.3	67.2	65.0	62.6	60.2	57.7
5.4	2.2	0.2	98.4	98.3	98.1	97.9	97.5	97.1	96.6	95.9	95.3	94.5	93.6	92.7	91.7	90.6	89.4	88.1	86.7	85.3	83.8	82.1	80.4	78.7	76.8	74.9	72.8	70.7	68.5	66.2	63.9	61.4	58.9
5.6	2.3	0.3	100.8	100.6	100.4	100.1	99.7	99.2	98.6	98.0	97.3	96.4	95.5	94.6	93.5	92.3	91.1	89.8	88.4	86.9	85.3	83.6	81.9	80.1	78.2	76.2	74.1	71.9	69.7	67.4	65.0	62.5	59.9
5.8	2.4	0.4	103.0	102.8	102.6	102.2	101.7	101.2	100.6	99.9	99.1	98.3	97.3	96.3	95.2	94.0	92.7	91.3	89.9	88.3	86.7	85.0	83.2	81.4	79.4	77.4	75.2	73.0	70.7	68.4	65.9	63.4	60.7
6.0	2.5	0.5	105.1	104.9	104.6	104.1	103.7	103.1	102.4	101.7	100.9	99.9	98.9	97.9	96.7	95.5	94.1	92.7	91.2	89.6	88.0	86.2	84.4	82.5	80.5	78.4	76.2	74.0	71.6	69.2	66.7	64.1	61.5
6.2	2.6	0.6	107.1	106.8	106.4	106.0	105.4	104.8	104.1	103.3	102.4	101.5	100.4	99.3	98.1	96.8	95.4	94.0	92.4	90.8	89.1	87.3	85.4	83.5	81.4	79.3	77.1	74.8	72.4	69.9	67.4	64.8	62.0
6.4	2.7	0.7	108.9	108.5	108.1	107.6	107.0	106.4	105.6	104.8	103.9	102.9	101.8	100.6	99.4	98.0	96.6	95.1	93.5	91.9	90.1	88.3	86.3	84.3	82.2	80.1	77.8	75.5	73.0	70.5	67.9	65.2	62.5
6.6	2.8	0.8	110.5	110.2	109.7	109.2	108.5	107.8	107.0	106.2	105.2	104.1	103.0	101.8	100.5	99.1	97.6	96.1	94.5	92.7	90.9	89.1	87.1	85.0	82.9	80.7	78.4	76.0	73.5	71.0	68.3	65.6	62.8
6.8	2.9	0.9	112.1	111.7	111.1	110.6	109.9	109.1	108.3	107.4	106.4	105.3	104.1	102.8	101.5	100.1	98.5	96.9	95.3	93.5	91.7	89.7	87.7	85.6	83.4	81.2	78.8	76.4	73.9	71.3	68.6	65.8	62.9
7.0	3.0	1.0	113.5	113.0	112.4	111.8	111.1	110.3	109.4	108.4	107.4	106.2	105.0	103.7	102.3	100.9	99.3	97.7	95.9	94.1	92.2	90.2	88.2	86.0	83.8	81.5	79.1	76.6	74.1	71.4	68.7	65.9	63.0
7.2	3.1	1.1	114.7	114.2	113.6	112.9	112.2	111.3	110.4	109.4	108.3	107.1	105.8	104.5	103.0	101.5	99.9	98.2	96.4	94.6	92.7	90.6	88.5	86.3	84.1	81.7	79.3	76.7	74.1	71.4	68.7	65.8	62.8
7.4	3.2	1.2	115.8	115.3	114.6	113.9	113.1	112.2	111.2	110.2	109.0	107.8	106.5	105.1	103.6	102.0	100.4	98.6	96.8	94.9	92.9	90.9	88.7	86.5	84.2	81.8	79.3	76.7	74.0	71.3	68.5	65.6	62.6
7.6	3.3	1.3	116.8	116.2	115.5	114.7	113.9	112.9	111.9	110.8	109.6	108.3	107.0	105.5	104.0	102.4	100.7	98.9	97.1	95.1	93.1	91.0	88.8	86.5	84.1	81.7	79.2	76.5	73.8	71.0	68.2	65.2	62.2
7.8	3.4	1.4	117.6	117.0	116.2	115.4	114.5	113.5	112.5	111.3	110.1	108.8	107.4	105.9	104.3	102.6	100.9	99.1	97.2	95.2	93.1	90.9	88.7	86.4	84.0	81.5	78.9	76.2	73.5	70.6	67.7	64.7	61.7
8.0	3.5	1.5	118.3	117.6	116.8	116.0	115.0	114.0	112.9	111.7	110.4	109.0	107.6	106.1	104.4	102.7	101.0	99.1	97.1	95.1	93.0	90.8	88.5	86.1	83.6	81.1	78.5	75.8	73.0	70.1	67.1	64.1	61.0

(b)

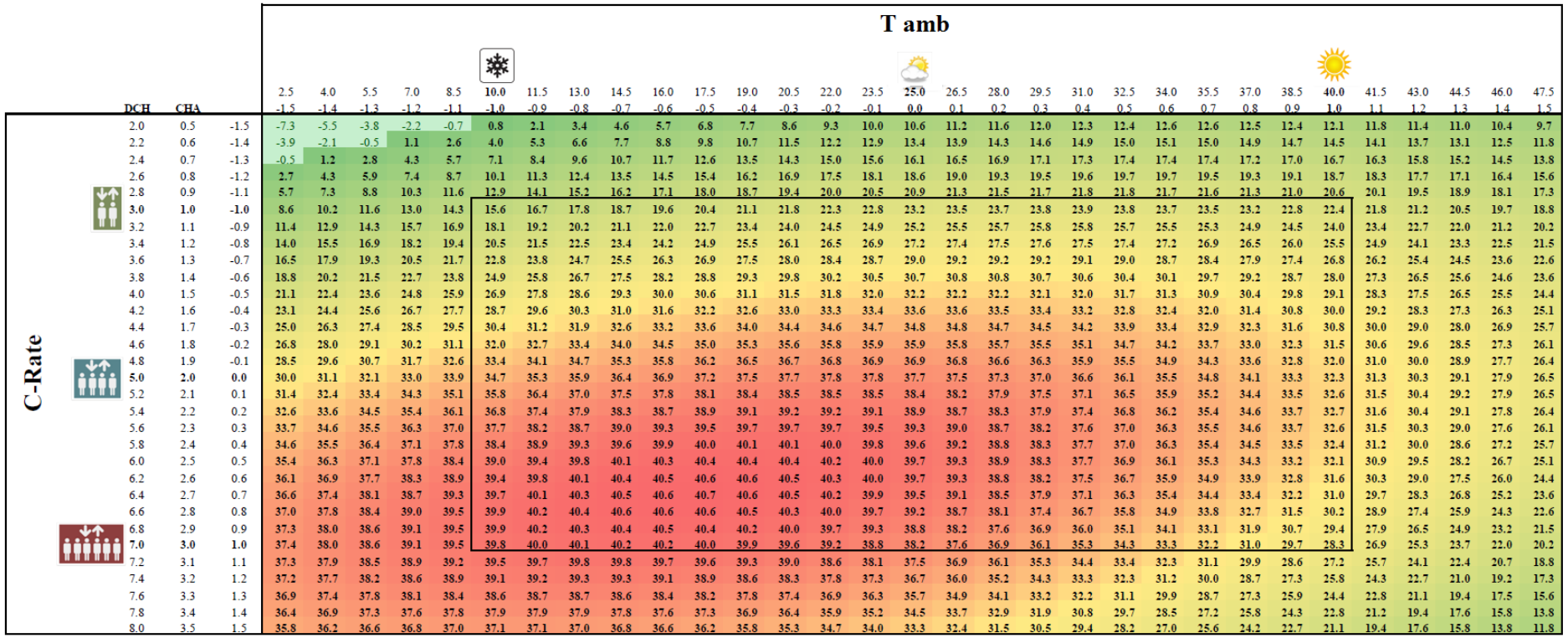

C-Rate			T amb																																
			2.5	4.0	5.5	7.0	8.5	10.0	11.5	13.0	14.5	16.0	17.5	19.0	20.5	22.0	23.5	25.0	26.5	28.0	29.5	31.0	32.5	34.0	35.5	37.0	38.5	40.0	41.5	43.0	44.5	46.0	47.5
			-1.5	-1.4	-1.3	-1.2	-1.1	-1.0	-0.9	-0.8	-0.7	-0.6	-0.5	-0.4	-0.3	-0.2	-0.1	0.0	0.1	0.2	0.3	0.4	0.5	0.6	0.7	0.8	0.9	1.0	1.1	1.2	1.3	1.4	1.5
DCH	CHA																																		
2.0	0.5	-1.5	-7.3	-5.5	-3.8	-2.2	-0.7	0.8	2.1	3.4	4.6	5.7	6.8	7.7	8.6	9.3	10.0	10.6	11.2	11.6	12.0	12.3	12.4	12.6	12.6	12.5	12.4	12.1	11.8	11.4	11.0	10.4	9.7
2.2	0.6	-1.4	-3.9	-2.1	-0.5	1.1	2.6	4.0	5.3	6.6	7.7	8.8	9.8	10.7	11.5	12.2	12.9	13.4	13.9	14.3	14.6	14.9	15.0	15.1	15.0	14.9	14.7	14.5	14.1	13.7	13.1	12.5	11.8
2.4	0.7	-1.3	-0.5	1.2	2.8	4.3	5.7	7.1	8.4	9.6	10.7	11.7	12.6	13.5	14.3	15.0	15.6	16.1	16.5	16.9	17.1	17.3	17.4	17.4	17.4	17.2	17.0	16.7	16.3	15.8	15.2	14.5	13.8
2.6	0.8	-1.2	2.7	4.3	5.9	7.4	8.7	10.1	11.3	12.4	13.5	14.5	15.4	16.2	16.9	17.5	18.1	18.6	19.0	19.3	19.5	19.6	19.7	19.7	19.5	19.3	19.1	18.7	18.3	17.7	17.1	16.4	15.6
2.8	0.9	-1.1	5.7	7.3	8.8	10.3	11.6	12.9	14.1	15.2	16.2	17.1	18.0	18.7	19.4	20.0	20.5	20.9	21.3	21.5	21.7	21.8	21.8	21.7	21.6	21.3	21.0	20.6	20.1	19.5	18.9	18.1	17.3
3.0	1.0	-1.0	8.6	10.2	11.6	13.0	14.3	15.6	16.7	17.8	18.7	19.6	20.4	21.1	21.8	22.3	22.8	23.2	23.5	23.7	23.8	23.9	23.8	23.7	23.5	23.2	22.8	22.4	21.8	21.2	20.5	19.7	18.8
3.2	1.1	-0.9	11.4	12.9	14.3	15.7	16.9	18.1	19.2	20.2	21.1	22.0	22.7	23.4	24.0	24.5	24.9	25.2	25.5	25.7	25.8	25.8	25.7	25.5	25.3	24.9	24.5	24.0	23.4	22.7	22.0	21.2	20.2
3.4	1.2	-0.8	14.0	15.5	16.9	18.2	19.4	20.5	21.5	22.5	23.4	24.2	24.9	25.5	26.1	26.5	26.9	27.2	27.4	27.5	27.6	27.5	27.4	27.2	26.9	26.5	26.0	25.5	24.9	24.1	23.3	22.5	21.5
3.6	1.3	-0.7	16.5	17.9	19.3	20.5	21.7	22.8	23.8	24.7	25.5	26.3	26.9	27.5	28.0	28.4	28.7	29.0	29.2	29.2	29.2	29.1	29.0	28.7	28.4	27.9	27.4	26.8	26.2	25.4	24.5	23.6	22.6
3.8	1.4	-0.6	18.8	20.2	21.5	22.7	23.8	24.9	25.8	26.7	27.5	28.2	28.8	29.3	29.8	30.2	30.5	30.7	30.8	30.8	30.7	30.6	30.4	30.1	29.7	29.2	28.7	28.0	27.3	26.5	25.6	24.6	23.6
4.0	1.5	-0.5	21.1	22.4	23.6	24.8	25.9	26.9	27.8	28.6	29.3	30.0	30.6	31.1	31.5	31.8	32.0	32.2	32.2	32.2	32.1	32.0	31.7	31.3	30.9	30.4	29.8	29.1	28.3	27.5	26.5	25.5	24.4
4.2	1.6	-0.4	23.1	24.4	25.6	26.7	27.7	28.7	29.6	30.3	31.0	31.6	32.2	32.6	33.0	33.3	33.4	33.6	33.6	33.5	33.4	33.2	32.8	32.4	32.0	31.4	30.8	30.0	29.2	28.3	27.3	26.3	25.1
4.4	1.7	-0.3	25.0	26.3	27.4	28.5	29.5	30.4	31.2	31.9	32.6	33.2	33.6	34.0	34.4	34.6	34.7	34.8	34.8	34.7	34.5	34.2	33.9	33.4	32.9	32.3	31.6	30.8	30.0	29.0	28.0	26.9	25.7
4.6	1.8	-0.2	26.8	28.0	29.1	30.2	31.1	32.0	32.7	33.4	34.0	34.5	35.0	35.3	35.6	35.8	35.9	35.9	35.8	35.7	35.5	35.1	34.7	34.2	33.7	33.0	32.3	31.5	30.6	29.6	28.5	27.3	26.1
4.8	1.9	-0.1	28.5	29.6	30.7	31.7	32.6	33.4	34.1	34.7	35.3	35.8	36.2	36.5	36.7	36.8	36.9	36.9	36.8	36.6	36.3	35.9	35.5	34.9	34.3	33.6	32.8	32.0	31.0	30.0	28.9	27.7	26.4
5.0	2.0	0.0	30.0	31.1	32.1	33.0	33.9	34.7	35.3	35.9	36.4	36.9	37.2	37.5	37.7	37.8	37.8	37.7	37.5	37.3	37.0	36.6	36.1	35.5	34.8	34.1	33.3	32.3	31.3	30.3	29.1	27.9	26.5
5.2	2.1	0.1	31.4	32.4	33.4	34.3	35.1	35.8	36.4	37.0	37.5	37.8	38.1	38.4	38.5	38.5	38.5	38.4	38.2	37.9	37.5	37.1	36.5	35.9	35.2	34.4	33.5	32.6	31.5	30.4	29.2	27.9	26.5
5.4	2.2	0.2	32.6	33.6	34.5	35.4	36.1	36.8	37.4	37.9	38.3	38.7	38.9	39.1	39.2	39.2	39.1	38.9	38.7	38.3	37.9	37.4	36.8	36.2	35.4	34.6	33.7	32.7	31.6	30.4	29.1	27.8	26.4
5.6	2.3	0.3	33.7	34.6	35.5	36.3	37.0	37.7	38.2	38.7	39.0	39.3	39.5	39.7	39.7	39.7	39.5	39.3	39.0	38.7	38.2	37.6	37.0	36.3	35.5	34.6	33.7	32.6	31.5	30.3	29.0	27.6	26.1
5.8	2.4	0.4	34.6	35.5	36.4	37.1	37.8	38.4	38.9	39.3	39.6	39.9	40.0	40.1	40.1	40.0	39.8	39.6	39.2	38.8	38.3	37.7	37.0	36.3	35.4	34.5	33.5	32.4	31.2	30.0	28.6	27.2	25.7
6.0	2.5	0.5	35.4	36.3	37.1	37.8	38.4	39.0	39.4	39.8	40.1	40.3	40.4	40.4	40.4	40.2	40.0	39.7	39.3	38.9	38.3	37.7	36.9	36.1	35.3	34.3	33.2	32.1	30.9	29.5	28.2	26.7	25.1
6.2	2.6	0.6	36.1	36.9	37.7	38.3	38.9	39.4	39.8	40.1	40.4	40.5	40.6	40.6	40.5	40.3	40.0	39.7	39.3	38.8	38.2	37.5	36.7	35.9	34.9	33.9	32.8	31.6	30.3	29.0	27.5	26.0	24.4
6.4	2.7	0.7	36.6	37.4	38.1	38.7	39.3	39.7	40.1	40.3	40.5	40.6	40.7	40.6	40.5	40.2	39.9	39.5	39.1	38.5	37.9	37.1	36.3	35.4	34.4	33.4	32.2	31.0	29.7	28.3	26.8	25.2	23.6
6.6	2.8	0.8	37.0	37.8	38.4	39.0	39.5	39.9	40.2	40.4	40.6	40.6	40.6	40.5	40.3	40.0	39.7	39.2	38.7	38.1	37.4	36.7	35.8	34.9	33.8	32.7	31.5	30.2	28.9	27.4	25.9	24.3	22.6
6.8	2.9	0.9	37.3	38.0	38.6	39.1	39.5	39.9	40.2	40.3	40.4	40.5	40.4	40.2	40.0	39.7	39.3	38.8	38.2	37.6	36.9	36.0	35.1	34.1	33.1	31.9	30.7	29.4	27.9	26.5	24.9	23.2	21.5
7.0	3.0	1.0	37.4	38.0	38.6	39.1	39.5	39.8	40.0	40.1	40.2	40.2	40.0	39.9	39.6	39.2	38.8	38.2	37.6	36.9	36.1	35.3	34.3	33.3	32.2	31.0	29.7	28.3	26.9	25.3	23.7	22.0	20.2
7.2	3.1	1.1	37.3	37.9	38.5	38.9	39.2	39.5	39.7	39.8	39.8	39.7	39.6	39.3	39.0	38.6	38.1	37.5	36.9	36.1	35.3	34.4	33.4	32.3	31.1	29.9	28.6	27.2	25.7	24.1	22.4	20.7	18.8
7.4	3.2	1.2	37.2	37.7	38.2	38.6	38.9	39.1	39.2	39.3	39.3	39.1	38.9	38.6	38.3	37.8	37.3	36.7	36.0	35.2	34.3	33.3	32.3	31.2	30.0	28.7	27.3	25.8	24.3	22.7	21.0	19.2	17.3
7.6	3.3	1.3	36.9	37.4	37.8	38.1	38.4	38.6	38.7	38.7	38.6	38.4	38.2	37.8	37.4	36.9	36.3	35.7	34.9	34.1	33.2	32.2	31.1	29.9	28.7	27.3	25.9	24.4	22.8	21.1	19.4	17.5	15.6
7.8	3.4	1.4	36.4	36.9	37.3	37.6	37.8	37.9	37.9	37.9	37.8	37.6	37.3	36.9	36.4	35.9	35.2	34.5	33.7	32.9	31.9	30.8	29.7	28.5	27.2	25.8	24.3	22.8	21.2	19.4	17.6	15.8	13.8
8.0	3.5	1.5	35.8	36.2	36.6	36.8	37.0	37.1	37.1	37.0	36.8	36.6	36.2	35.8	35.3	34.7	34.0	33.3	32.4	31.5	30.5	29.4	28.2	27.0	25.6	24.2	22.7	21.1	19.4	17.6	15.8	13.8	11.8

(c)

Figure 6.26 The surface response correspondent to cooling time without heat sink and (a) NC, (b) fan PWM 50% and (c) fan PWM 100%

6.5.2 OPTIMIZATION II

Based on the optimization results obtained from the previous optimization study at *BM* level, the decisions referred to not to use heat sink and to implement a forced convection has been applied at *BP* level. In order to minimize the consumption of the system that it is implicitly related to fan performance, it has been important to know how much was the required power that in the fan to keep the complete system within the ideal operation range in thermal sense.

For that purpose, the same procedure than in the previous study has been followed and applying the *False Steady* concept. The *DoE* which is shown in Table 6.17 has been defined in function of rotational speed of the fan (25% *PWM*, 50% *PWM* and 75% *PWM*), ambient temperature (10 ºC, 25 ºC and 40 ºC) and current rate (Cmin: DCH 3C/ CHA 1C, Cmid: DCH 5C/ CHA 2C, Cmax: DCH 7C/ CHA 3C). The *Complete model* developed for integration purpose has been used in this step.

Table 6.17 DoE matrix at BP level for fan PWM adjust purpose.

	Coded Value			UnCoded Value		
	Fan *PWM*	T amb	C-rate	Fan *PWM*	T amb	C-rate
1	-1	-1	-1	PWM 25%	10	Cmin
2	-1	1	-1	PWM 25%	40	Cmin
3	-1	-1	1	PWM 25%	10	Cmax
4	-1	1	1	PWM 25%	40	Cmax
5	0	0	0	PWM 50%	25	Cmid
6	1	-1	0	PWM 75%	10	Cmin
7	1	1	0	PWM 75%	40	Cmin
8	1	-1	1	PWM 75%	10	Cmax
9	1	1	1	PWM 75%	40	Cmax
10	-1	0	0	PWM 25%	25	Cmid
11	0	0	1	PWM 50%	25	Cmax
12	1	0	0	PWM 75%	25	Cmid
13	0	0	-1	PWM 50%	25	Cmin
14	0	1	0	PWM 50%	40	Cmid
15	0	-1	0	PWM 50%	10	Cmid

The numerical results for each defined test regarding the maximum cell temperature and thermal dispersion within the complete *BP* are shown in Table 6.18.

Table 6.18 Numerical results of DoE matrix at BP level

	Fan *PWM*	T amb	C-rate	Tmax, ºC	Dispersion *BP* , ºC
1	-1	-1	-1	15.42	2.28
2	-1	-1	1	42.32	1.80
3	-1	1	-1	34.00	9.60
4	-1	1	1	54.70	6.60
5	0	0	0	32.23	3.02
6	1	-1	-1	12.80	1.10
7	1	-1	1	41.30	0.60
8	1	1	-1	24.18	4.14
9	1	1	1	48.46	3.06
10	-1	0	0	34.20	6.02
11	0	1	0	38.73	5.36
12	1	0	0	30.07	1.67
13	0	-1	0	26.90	0.81
14	0	0	1	45.53	2.33
15	0	0	-1	20.26	3.78

By means of Table 6.18 it is possible to have an insight about the effects of the selected parameters on the responses. For instance, if they are chosen three representative tests: test 1, test 5 and test 9. All factors in each test have been in the minimum (-1, -1, -1), medium (0, 0, 0) and in the maximum (1, 1, 1) level respectively. Besides, in Figure 6.27 are shown the temperature contours of the surface of the cells and of the air fluid in the plane of symmetry in the *Complete model* for the previous tests. It can be seen that the influence between the *BMs* it has been important in terms of heat transfer and as it has been expected, the hottest cell has been located in the *BM* which was placed in the middle of the complete system and on the opposite side from the air exits.

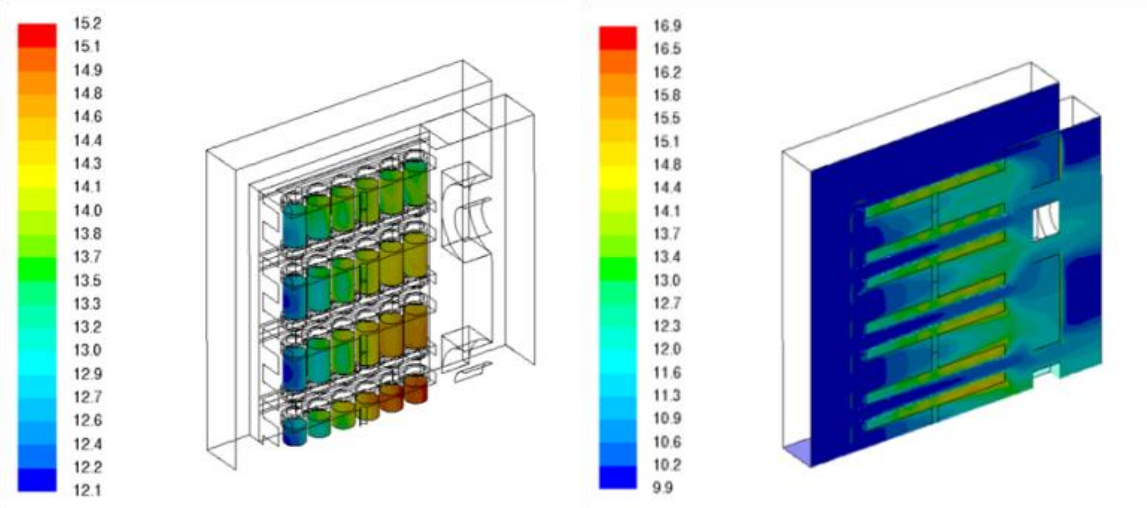

(a)

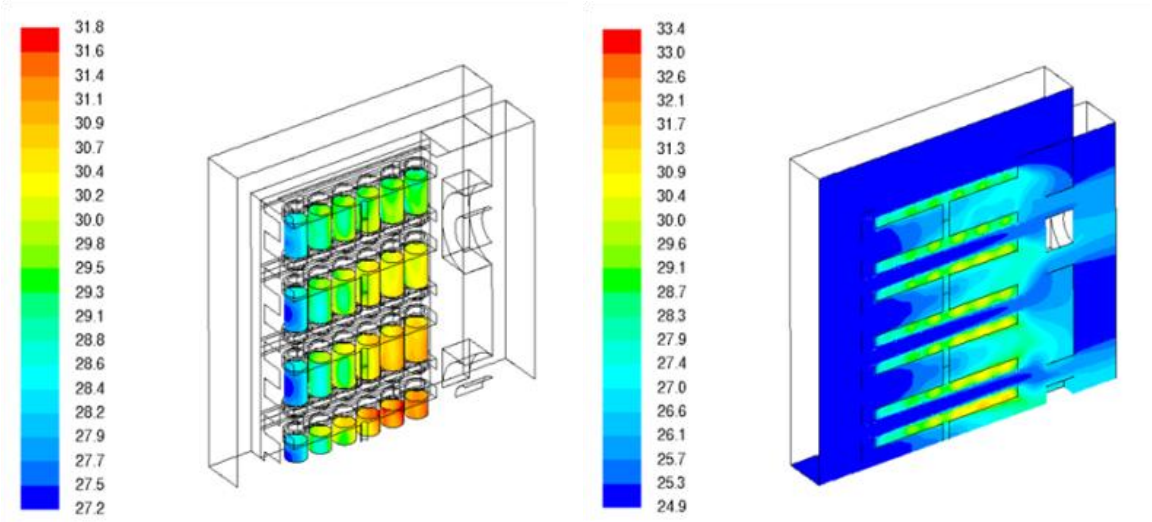

(b)

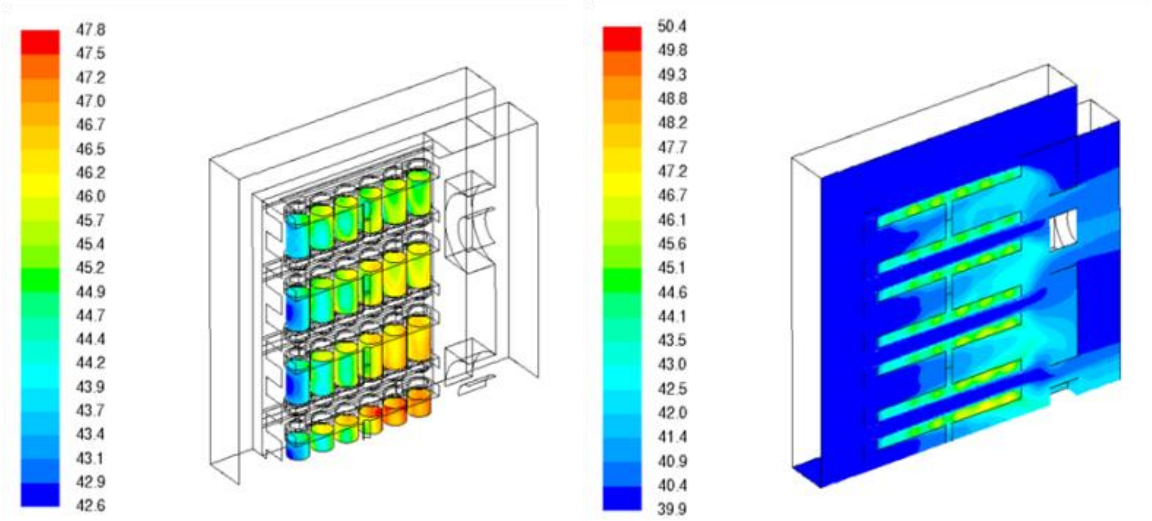

(c)

Figure 6.27.The temperature contours of the cells surface and air fluid in the plane of symmetry correspondent to test (a) 1, (b) 5 and (c) 9.

Applying the *Face Centered CCD* the regression surface responses of each variable have been obtained. In Table 6.19 are listed the coefficients and p-values for maximum temperature and thermal dispersion within the complete *BP*. In both the lineal effects have been significant and also, the effect of the interactions between rotational speed of the fan and ambient temperature. The R^2 value for both cases has been 99.95% and 98.39%, respectively.

In Figure 6.28-Figure 6.29 are shown the response surfaces obtained regarding the maximum cell temperature and thermal dispersion within the *BP* for the cases in where the fan *PWM* has been at 50%, such as an example.

Table 6.19 Coefficients correspondent to the regression surface response of maximum cell temperature and thermal dispersion.

	Maximum *BP* temperature		Thermal Dispersion	
	Coefficient	p- value, [-]	Coefficient	p- value, [-]
Constant	31.9511	**0.000**	3.1244	**0.000**
Fan PWM	-2.37	**0.000**	-1.57	**0.000**
C-rate	6.14	**0.000**	2.22	**0.000**
Tamb	12.56	**0.000**	-0.65	0.012
Fan PWM*Fan PWM	0.2611	0.417	0.6944	0.091
*C-rate***C-rate*	0.9111	0.020	-0.056	0.847
Tamb*Tamb	1.0111	0.015	-0.1056	0.781
Fan PWM*Tamb	-1.55	**0.000**	-0.825	**0.007**
Fan PWM**C-rate*	0.65	0.009	0.25	0.262
Tamb**C-rate*	-1.3	0.009	-0.375	0.094

In Table 6.20 are shown the numerical results related to previously simulated tests for this optimization task. Based on Table 6.20, for the worst thermal and electrical conditions has not been possible to keep the *BP* operating within the ideal and admissible operation range in terms of maximum cell temperature and thermal dispersion at once. However, the maximum cell temperature has been always kept below 55 ºC even with the less power of the fan.

Table 6.20Numerical results obtained from the surface responses at BP level.

		Cell Temperature, ºC			
		Tamb: 10-25 ºC / Crate:min-mid		**Tamb: 25-40 ºC / Crate:mid-max**	
		Min	**Max**	**Min**	**Max**
Fan *PWM*	25%	15.6	34.6	34.6	54.8
	50%	13.9	32.0	32.0	51.3
	75%	12.7	29.8	29.8	48.3

		Thermal Dispersion, ºC			
		Tamb: 10-25 ºC / Crate:min-mid		**Tamb: 25-40 ºC / Crate:mid-max**	
		Min	**Max**	**Min**	**Max**
Fan *PWM*	25%	2.3	6.2	4.4	8.4
	50%	0.8	3.7	2.4	5.3
	75%	0.7	2.5	1.7	3.6

C-Rate			T amb																														
	DCH	CHA		2.5	4.0	5.5	7.0	8.5	10.0	11.5	13.0	14.5	16.0	17.5	19.0	20.5	22.0	23.5	25.0	26.5	28.0	29.5	31.0	32.5	34.0	35.5	37.0	38.5	40.0	41.5	43.0	44.5	46.0	47.5
				-1.5	-1.4	-1.3	-1.2	-1.1	-1.0	-0.9	-0.8	-0.7	-0.6	-0.5	-0.4	-0.3	-0.2	-0.1	0.0	0.1	0.2	0.3	0.4	0.5	0.6	0.7	0.8	0.9	1.0	1.1	1.2	1.3	1.4	1.5
	2.0	0.5	-1.5	5.3	6.5	7.6	8.8	10.1	11.3	12.6	13.8	15.1	16.4	17.8	19.1	**20.5**	**21.9**	**23.4**	**24.8**	**26.3**	**27.7**	**29.2**	30.8	32.3	33.9	35.4	37.0	38.7	40.3	42.0	43.7	45.4	47.1	48.8
	2.2	0.6	-1.4	5.8	7.0	8.2	9.3	10.5	11.8	13.0	14.3	15.6	16.9	18.2	19.6	**20.9**	**22.3**	**23.7**	**25.1**	**26.6**	**28.1**	**29.5**	31.1	32.6	34.1	35.7	37.3	38.9	40.5	42.2	43.9	45.5	47.3	49.0
	2.4	0.7	-1.3	6.4	7.5	8.7	9.9	11.1	12.3	13.5	14.8	16.0	17.3	18.6	20.0	**21.3**	**22.7**	**24.1**	**25.5**	**26.9**	**28.4**	**29.9**	31.4	32.9	34.4	36.0	37.6	39.2	40.8	42.4	44.1	45.7	47.4	49.2
	2.6	0.8	-1.2	7.0	8.1	9.2	10.4	11.6	12.8	14.0	15.2	16.5	17.8	19.1	**20.4**	**21.8**	**23.1**	**24.5**	**25.9**	**27.3**	**28.8**	30.2	31.7	33.2	34.7	36.3	37.8	39.4	41.0	42.7	44.3	46.0	47.6	49.4
	2.8	0.9	-1.1	7.6	8.7	9.8	11.0	12.1	13.3	14.5	15.8	17.0	18.3	19.6	**20.9**	**22.2**	**23.5**	**24.9**	**26.3**	**27.7**	**29.1**	30.6	32.1	33.5	35.1	36.6	38.1	39.7	41.3	42.9	44.5	46.2	47.9	49.6
	3.0	**1.0**	**-1.0**	8.2	9.3	10.4	11.5	12.7	13.9	15.1	16.3	17.5	18.8	**20.0**	**21.3**	**22.7**	**24.0**	**25.3**	**26.7**	**28.1**	**29.5**	31.0	32.4	33.9	35.4	36.9	38.5	40.0	41.6	43.2	44.8	46.4	48.1	49.8
	3.2	1.1	-0.9	8.8	9.9	11.0	12.1	13.3	14.4	15.6	16.8	18.0	19.3	**20.6**	**21.8**	**23.1**	**24.5**	**25.8**	**27.2**	**28.5**	**29.9**	31.4	32.8	34.3	35.8	37.3	38.8	40.3	41.9	43.5	45.1	46.7	48.4	50.0
	3.4	1.2	-0.8	9.5	10.6	11.7	12.8	13.9	15.0	16.2	17.4	18.6	19.8	**21.1**	**22.3**	**23.6**	**24.9**	**26.3**	**27.6**	**29.0**	30.4	31.8	33.2	34.7	36.1	37.6	39.1	40.7	42.2	43.8	45.4	47.0	48.6	50.3
	3.6	1.3	-0.7	10.2	11.2	12.3	13.4	14.5	15.6	16.8	18.0	19.2	**20.4**	**21.6**	**22.9**	**24.1**	**25.4**	**26.8**	**28.1**	**29.5**	30.8	32.2	33.6	35.1	36.5	38.0	39.5	41.0	42.6	44.1	45.7	47.3	48.9	50.6
	3.8	1.4	-0.6	10.9	11.9	13.0	14.0	15.1	16.3	17.4	18.6	19.8	**21.0**	**22.2**	**23.4**	**24.7**	**26.0**	**27.3**	**28.6**	**29.9**	31.3	32.7	34.1	35.5	37.0	38.4	39.9	41.4	42.9	44.5	46.1	47.6	49.3	50.9
	4.0	1.5	-0.5	11.6	12.6	13.6	14.7	15.8	16.9	18.0	19.2	**20.4**	**21.5**	**22.8**	**24.0**	**25.2**	**26.5**	**27.8**	**29.1**	30.4	31.8	33.2	34.6	36.0	37.4	38.9	40.3	41.8	43.3	44.9	46.4	48.0	49.6	51.2
	4.2	1.6	-0.4	12.3	13.3	14.3	15.4	16.5	17.6	18.7	19.8	**21.0**	**22.2**	**23.4**	**24.6**	**25.8**	**27.1**	**28.3**	**29.6**	31.0	32.3	33.7	35.0	36.4	37.9	39.3	40.8	42.2	43.7	45.3	46.8	48.4	49.9	51.5
	4.4	1.7	-0.3	13.0	14.0	15.1	16.1	17.2	18.3	19.4	**20.5**	**21.6**	**22.8**	**24.0**	**25.2**	**26.4**	**27.6**	**28.9**	30.2	31.5	32.8	34.2	35.5	36.9	38.3	39.8	41.2	42.7	44.2	45.7	47.2	48.7	50.3	51.9
	4.6	1.8	-0.2	13.8	14.8	15.8	16.8	17.9	19.0	**20.0**	**21.2**	**22.3**	**23.4**	**24.6**	**25.8**	**27.0**	**28.2**	**29.5**	30.8	32.1	33.4	34.7	36.0	37.4	38.8	40.2	41.7	43.1	44.6	46.1	47.6	49.1	50.7	52.3
	4.8	1.9	-0.1	14.6	15.6	16.6	17.6	18.6	19.7	**20.7**	**21.8**	**23.0**	**24.1**	**25.3**	**26.4**	**27.6**	**28.8**	30.1	31.3	32.6	33.9	35.2	36.6	37.9	39.3	40.7	42.1	43.6	45.0	46.5	48.0	49.6	51.1	52.7
	5.0	**2.0**	**0.0**	15.4	16.3	17.3	18.3	19.4	**20.4**	**21.5**	**22.6**	**23.7**	**24.8**	**25.9**	**27.1**	**28.3**	**29.5**	30.7	32.0	33.2	34.5	35.8	37.1	38.5	39.9	41.2	42.6	44.1	45.5	47.0	48.5	50.0	51.5	53.1
	5.2	2.1	0.1	16.2	17.2	18.1	19.1	**20.1**	**21.2**	**22.2**	**23.3**	**24.4**	**25.5**	**26.6**	**27.8**	**28.9**	30.1	31.3	32.6	33.8	35.1	36.4	37.7	39.0	40.4	41.8	43.2	44.6	46.0	47.5	48.9	50.4	52.0	53.5
	5.4	2.2	0.2	17.0	18.0	18.9	19.9	**20.9**	**21.9**	**23.0**	**24.0**	**25.1**	**26.2**	**27.3**	**28.5**	**29.6**	30.8	32.0	33.2	34.5	35.7	37.0	38.3	39.6	41.0	42.3	43.7	45.1	46.5	48.0	49.4	50.9	52.4	53.9
	5.6	2.3	0.3	17.9	18.8	19.8	**20.7**	**21.7**	**22.7**	**23.7**	**24.8**	**25.9**	**26.9**	**28.0**	**29.2**	30.3	31.5	32.7	33.9	35.1	36.3	37.6	38.9	40.2	41.5	42.9	44.3	45.6	47.1	48.5	49.9	51.4	52.9	54.4
	5.8	2.4	0.4	18.8	19.7	**20.6**	**21.6**	**22.5**	**23.5**	**24.5**	**25.6**	**26.6**	**27.7**	**28.8**	**29.9**	31.0	32.2	33.4	34.6	35.8	37.0	38.3	39.5	40.8	42.1	43.5	44.8	46.2	47.6	49.0	50.5	51.9	53.4	54.9
	6.0	2.5	0.5	19.7	**20.6**	**21.5**	**22.4**	**23.4**	**24.3**	**25.3**	**26.4**	**27.4**	**28.5**	**29.5**	30.6	31.8	32.9	34.1	35.2	36.4	37.7	38.9	40.2	41.5	42.8	44.1	45.4	46.8	48.2	49.6	51.0	52.4	53.9	55.4
	6.2	2.6	0.6	**20.6**	**21.5**	**22.4**	**23.3**	**24.2**	**25.2**	**26.2**	**27.2**	**28.2**	**29.3**	30.3	31.4	32.5	33.6	34.8	36.0	37.2	38.4	39.6	40.8	42.1	43.4	44.7	46.0	47.4	48.8	50.1	51.6	53.0	54.4	55.9
	6.4	2.7	0.7	**21.5**	**22.4**	**23.3**	**24.2**	**25.1**	**26.1**	**27.0**	**28.0**	**29.0**	30.1	31.1	32.2	33.3	34.4	35.5	36.7	37.9	39.1	40.3	41.5	42.8	44.0	45.3	46.7	48.0	49.4	50.7	52.1	53.5	55.0	56.4
	6.6	2.8	0.8	**22.4**	**23.3**	**24.2**	**25.1**	**26.0**	**26.9**	**27.9**	**28.9**	**29.9**	30.9	31.9	33.0	34.1	35.2	36.3	37.4	38.6	39.8	41.0	42.2	43.5	44.7	46.0	47.3	48.6	50.0	51.3	52.7	54.1	55.6	57.0
	6.8	2.9	0.9	**23.4**	**24.3**	**25.1**	**26.0**	**26.9**	**27.8**	**28.8**	**29.8**	30.7	31.7	32.8	33.8	34.9	36.0	37.1	38.2	39.4	40.5	41.7	42.9	44.2	45.4	46.7	48.0	49.3	50.6	52.0	53.3	54.7	56.1	57.6
	7.0	**3.0**	**1.0**	**24.4**	**25.2**	**26.1**	**26.9**	**27.8**	**28.8**	**29.7**	30.6	31.6	32.6	33.6	34.7	35.7	36.8	37.9	39.0	40.1	41.3	42.5	43.7	44.9	46.1	47.4	48.7	50.0	51.3	52.6	54.0	55.3	56.7	58.2
	7.2	3.1	1.1	**25.4**	**26.2**	**27.0**	**27.9**	**28.8**	**29.7**	30.6	31.6	32.5	33.5	34.5	35.5	36.6	37.6	38.7	39.8	40.9	42.1	43.2	44.4	45.6	46.8	48.1	49.4	50.6	51.9	53.3	54.6	56.0	57.4	58.8
	7.4	3.2	1.2	**26.4**	**27.2**	**28.0**	**28.9**	**29.8**	30.6	31.6	32.5	33.4	34.4	35.4	36.4	37.4	38.5	39.5	40.6	41.7	42.9	44.0	45.2	46.4	47.6	48.8	50.1	51.4	52.6	54.0	55.3	56.6	58.0	59.4
	7.6	3.3	1.3	**27.4**	**28.2**	**29.1**	**29.9**	30.7	31.6	32.5	33.4	34.4	35.3	36.3	37.3	38.3	39.3	40.4	41.5	42.6	43.7	44.8	46.0	47.2	48.4	49.6	50.8	52.1	53.4	54.7	56.0	57.3	58.7	60.1
	7.8	3.4	1.4	**28.5**	**29.3**	30.1	30.9	31.7	32.6	33.5	34.4	35.3	36.3	37.2	38.2	39.2	40.2	41.3	42.3	43.4	44.5	45.6	46.8	48.0	49.1	50.3	51.6	52.8	54.1	55.4	56.7	58.0	59.4	60.7
	8.0	3.5	1.5	**29.6**	30.3	31.1	31.9	32.8	33.6	34.5	35.4	36.3	37.2	38.2	39.1	40.1	41.1	42.2	43.2	44.3	45.4	46.5	47.6	48.8	49.9	51.1	52.3	53.6	54.8	56.1	57.4	58.7	60.0	61.4

Figure 6.28 The surface response correspondent to cell temperature with a fan PWM of 50%.

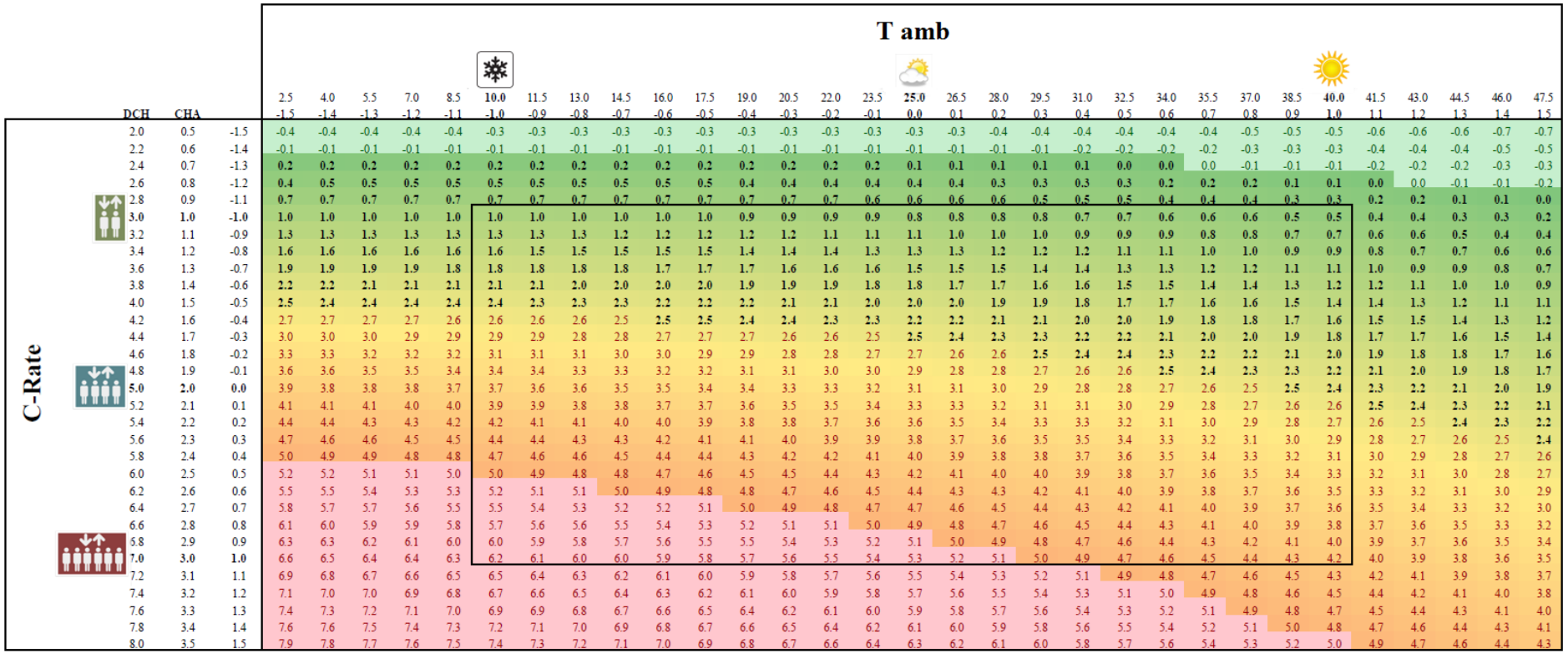

DCH	CHA		2.5	4.0	5.5	7.0	8.5	10.0	11.5	13.0	14.5	16.0	17.5	19.0	20.5	22.0	23.5	25.0	26.5	28.0	29.5	31.0	32.5	34.0	35.5	37.0	38.5	40.0	41.5	43.0	44.5	46.0	47.5
			-1.5	-1.4	-1.3	-1.2	-1.1	-1.0	-0.9	-0.8	-0.7	-0.6	-0.5	-0.4	-0.3	-0.2	-0.1	0.0	0.1	0.2	0.3	0.4	0.5	0.6	0.7	0.8	0.9	1.0	1.1	1.2	1.3	1.4	1.5
2.0	0.5	-1.5	-0.4	-0.4	-0.4	-0.4	-0.4	-0.3	-0.3	-0.3	-0.3	-0.3	-0.3	-0.3	-0.3	-0.3	-0.3	-0.3	-0.3	-0.4	-0.4	-0.4	-0.4	-0.4	-0.4	-0.5	-0.5	-0.5	-0.6	-0.6	-0.6	-0.7	-0.7
2.2	0.6	-1.4	-0.1	-0.1	-0.1	-0.1	-0.1	-0.1	-0.1	-0.1	-0.1	-0.1	-0.1	-0.1	-0.1	-0.1	-0.1	-0.1	-0.1	-0.1	-0.1	-0.2	-0.2	-0.2	-0.2	-0.3	-0.3	-0.3	-0.4	-0.4	-0.4	-0.5	-0.5
2.4	0.7	-1.3	0.2	0.2	0.2	0.2	0.2	0.2	0.2	0.2	0.2	0.2	0.2	0.2	0.2	0.2	0.2	0.1	0.1	0.1	0.1	0.1	0.0	0.0	0.0	-0.1	-0.1	-0.1	-0.2	-0.2	-0.2	-0.3	-0.3
2.6	0.8	-1.2	0.4	0.5	0.5	0.5	0.5	0.5	0.5	0.5	0.5	0.5	0.5	0.4	0.4	0.4	0.4	0.4	0.4	0.3	0.3	0.3	0.3	0.2	0.2	0.2	0.1	0.1	0.0	0.0	-0.1	-0.1	-0.2
2.8	0.9	-1.1	0.7	0.7	0.7	0.7	0.7	0.7	0.7	0.7	0.7	0.7	0.7	0.7	0.7	0.7	0.6	0.6	0.6	0.6	0.5	0.5	0.5	0.4	0.4	0.4	0.3	0.3	0.2	0.2	0.1	0.1	0.0
3.0	1.0	-1.0	1.0	1.0	1.0	1.0	1.0	1.0	1.0	1.0	1.0	1.0	1.0	0.9	0.9	0.9	0.9	0.8	0.8	0.8	0.8	0.7	0.7	0.6	0.6	0.6	0.5	0.5	0.4	0.4	0.3	0.3	0.2
3.2	1.1	-0.9	1.3	1.3	1.3	1.3	1.3	1.3	1.3	1.3	1.2	1.2	1.2	1.2	1.2	1.1	1.1	1.1	1.0	1.0	1.0	0.9	0.9	0.9	0.8	0.8	0.7	0.7	0.6	0.6	0.5	0.4	0.4
3.4	1.2	-0.8	1.6	1.6	1.6	1.6	1.6	1.6	1.5	1.5	1.5	1.5	1.5	1.4	1.4	1.4	1.3	1.3	1.3	1.2	1.2	1.2	1.1	1.1	1.0	1.0	0.9	0.9	0.8	0.7	0.7	0.6	0.6
3.6	1.3	-0.7	1.9	1.9	1.9	1.9	1.8	1.8	1.8	1.8	1.8	1.7	1.7	1.7	1.6	1.6	1.6	1.5	1.5	1.5	1.4	1.4	1.3	1.3	1.2	1.2	1.1	1.1	1.0	0.9	0.9	0.8	0.7
3.8	1.4	-0.6	2.2	2.2	2.1	2.1	2.1	2.1	2.1	2.0	2.0	2.0	2.0	1.9	1.9	1.9	1.8	1.8	1.7	1.7	1.6	1.6	1.5	1.5	1.4	1.4	1.3	1.2	1.2	1.1	1.0	1.0	0.9
4.0	1.5	-0.5	2.5	2.4	2.4	2.4	2.4	2.4	2.3	2.3	2.3	2.2	2.2	2.2	2.1	2.1	2.0	2.0	2.0	1.9	1.9	1.8	1.7	1.7	1.6	1.6	1.5	1.4	1.4	1.3	1.2	1.1	1.1
4.2	1.6	-0.4	2.7	2.7	2.7	2.7	2.6	2.6	2.6	2.6	2.5	2.5	2.5	2.4	2.4	2.3	2.3	2.2	2.2	2.1	2.1	2.0	2.0	1.9	1.8	1.8	1.7	1.6	1.5	1.5	1.4	1.3	1.2
4.4	1.7	-0.3	3.0	3.0	3.0	2.9	2.9	2.9	2.9	2.8	2.8	2.7	2.7	2.7	2.6	2.6	2.5	2.5	2.4	2.3	2.3	2.2	2.2	2.1	2.0	2.0	1.9	1.8	1.7	1.7	1.6	1.5	1.4
4.6	1.8	-0.2	3.3	3.3	3.2	3.2	3.2	3.1	3.1	3.1	3.0	3.0	2.9	2.9	2.8	2.8	2.7	2.7	2.6	2.6	2.5	2.4	2.4	2.3	2.2	2.2	2.1	2.0	1.9	1.8	1.8	1.7	1.6
4.8	1.9	-0.1	3.6	3.6	3.5	3.5	3.4	3.4	3.4	3.3	3.3	3.2	3.2	3.1	3.1	3.0	3.0	2.9	2.8	2.8	2.7	2.6	2.6	2.5	2.4	2.3	2.3	2.2	2.1	2.0	1.9	1.8	1.7
5.0	2.0	0.0	3.9	3.8	3.8	3.8	3.7	3.7	3.6	3.6	3.5	3.5	3.4	3.4	3.3	3.3	3.2	3.1	3.1	3.0	2.9	2.8	2.8	2.7	2.6	2.5	2.5	2.4	2.3	2.2	2.1	2.0	1.9
5.2	2.1	0.1	4.1	4.1	4.1	4.0	4.0	3.9	3.9	3.8	3.8	3.7	3.7	3.6	3.5	3.5	3.4	3.3	3.3	3.2	3.1	3.1	3.0	2.9	2.8	2.7	2.6	2.6	2.5	2.4	2.3	2.2	2.1
5.4	2.2	0.2	4.4	4.4	4.3	4.3	4.2	4.2	4.1	4.1	4.0	4.0	3.9	3.8	3.8	3.7	3.6	3.6	3.5	3.4	3.3	3.3	3.2	3.1	3.0	2.9	2.8	2.7	2.6	2.5	2.4	2.3	2.2
5.6	2.3	0.3	4.7	4.6	4.6	4.5	4.5	4.4	4.4	4.3	4.3	4.2	4.1	4.1	4.0	3.9	3.9	3.8	3.7	3.6	3.5	3.5	3.4	3.3	3.2	3.1	3.0	2.9	2.8	2.7	2.6	2.5	2.4
5.8	2.4	0.4	5.0	4.9	4.9	4.8	4.8	4.7	4.6	4.6	4.5	4.4	4.4	4.3	4.2	4.2	4.1	4.0	3.9	3.8	3.8	3.7	3.6	3.5	3.4	3.3	3.2	3.1	3.0	2.9	2.8	2.7	2.6
6.0	2.5	0.5	5.2	5.2	5.1	5.1	5.0	5.0	4.9	4.8	4.8	4.7	4.6	4.5	4.5	4.4	4.3	4.2	4.1	4.0	4.0	3.9	3.8	3.7	3.6	3.5	3.4	3.3	3.2	3.1	3.0	2.8	2.7
6.2	2.6	0.6	5.5	5.5	5.4	5.3	5.3	5.2	5.1	5.1	5.0	4.9	4.8	4.8	4.7	4.6	4.5	4.4	4.3	4.3	4.2	4.1	4.0	3.9	3.8	3.7	3.6	3.5	3.3	3.2	3.1	3.0	2.9
6.4	2.7	0.7	5.8	5.7	5.7	5.6	5.5	5.5	5.4	5.3	5.2	5.2	5.1	5.0	4.9	4.8	4.7	4.7	4.6	4.5	4.4	4.3	4.2	4.1	4.0	3.9	3.7	3.6	3.5	3.4	3.3	3.2	3.0
6.6	2.8	0.8	6.1	6.0	5.9	5.9	5.8	5.7	5.6	5.6	5.5	5.4	5.3	5.2	5.1	5.1	5.0	4.9	4.8	4.7	4.6	4.5	4.4	4.3	4.1	4.0	3.9	3.8	3.7	3.6	3.5	3.3	3.2
5.8	2.9	0.9	6.3	6.3	6.2	6.1	6.0	6.0	5.9	5.8	5.7	5.6	5.5	5.5	5.4	5.3	5.2	5.1	5.0	4.9	4.8	4.7	4.6	4.4	4.3	4.2	4.1	4.0	3.9	3.7	3.6	3.5	3.4
7.0	3.0	1.0	6.6	6.5	6.4	6.4	6.3	6.2	6.1	6.0	6.0	5.9	5.8	5.7	5.6	5.5	5.4	5.3	5.2	5.1	5.0	4.9	4.7	4.6	4.5	4.4	4.3	4.2	4.0	3.9	3.8	3.6	3.5
7.2	3.1	1.1	6.9	6.8	6.7	6.6	6.5	6.5	6.4	6.3	6.2	6.1	6.0	5.9	5.8	5.7	5.6	5.5	5.4	5.3	5.2	5.1	4.9	4.8	4.7	4.6	4.5	4.3	4.2	4.1	3.9	3.8	3.7
7.4	3.2	1.2	7.1	7.0	7.0	6.9	6.8	6.7	6.6	6.5	6.4	6.3	6.2	6.1	6.0	5.9	5.8	5.7	5.6	5.5	5.4	5.3	5.1	5.0	4.9	4.8	4.6	4.5	4.4	4.2	4.1	4.0	3.8
7.6	3.3	1.3	7.4	7.3	7.2	7.1	7.0	6.9	6.9	6.8	6.7	6.6	6.5	6.4	6.2	6.1	6.0	5.9	5.8	5.7	5.6	5.4	5.3	5.2	5.1	4.9	4.8	4.7	4.5	4.4	4.3	4.1	4.0
7.8	3.4	1.4	7.6	7.6	7.5	7.4	7.3	7.2	7.1	7.0	6.9	6.8	6.7	6.6	6.5	6.4	6.2	6.1	6.0	5.9	5.8	5.6	5.5	5.4	5.2	5.1	5.0	4.8	4.7	4.6	4.4	4.3	4.1
8.0	3.5	1.5	7.9	7.8	7.7	7.6	7.5	7.4	7.3	7.2	7.1	7.0	6.9	6.8	6.7	6.6	6.4	6.3	6.2	6.1	6.0	5.8	5.7	5.6	5.4	5.3	5.2	5.0	4.9	4.7	4.6	4.4	4.3

Figure 6.29The surface response correspondent to the thermal dispersion with a fan PWM of 50%.

In order to determine the adequate power of the fan for a suitable performance of the *BP*, it has been important to consider at the same time the fulfilment of both thermal requirements at any possible conditions that have been defined in the first step of this methodology. Therefore, an adequate *PWM* rate has been defined for each current rate level paying special attention to the requirement of the thermal dispersion variable.

It has been defined a *PWM* of 10%, 40% and 67.5% for Cmin, Cmid and Cmax current rates respectively, ensuring a maximum cell temperature and a thermal dispersion below 55 ºC and 5 ºC, respectively.

Table 6.21 Results obtained referred to fan PWM for different C-rate levels.

		Tamb, ºC	Cell Temperature, ºC	Thermal Dispersion, ºC
Fan *PWM* 10%	Cmin	10	16.9	4.4
		25	28.7	3.8
		40	42.5	3.0
Fan *PWM* 40%	Cmid	10	21.7	4.5
		25	32.9	3.9
		40	46.2	3.0
Fan *PWM* 67.5%	Cmax	10	25.7	4.7
		25	36.4	3.9
		40	49.1	3.0

6.5.3 OPTIMIZATION III

With the aim to conclude the complete study of this application, the last optimization case has been proposed. The objective of this optimization study has been to analyze the thermal performance at *BP* level under *NC* conditions considering the operation limit parameters in terms of maximum cell and thermal dispersion admissible at *BP* level. Based on the results that will be obtained, it will be determined a control strategy which defines the conditions it will be possible to use *NC* or in contrary, the fans will switch on.

Because of lack of time to carry out the simulations involve in this optimization step, this task will be explained more in detail in the section named "Future Research Line" in Chapter 8.

6.6 CONCLUSIONS

The systematic methodology described in Chapter 5 for designing and optimizing a *TMS* of a *BP* has been applied in a residential elevator application obtaining an optimized *TMS* which ensures a suitable thermal performance related to the maximum operation temperature and the thermal dispersion within the *BP*, by means of a *TMS* as cheapest as possible and with a minimum consumption.

The main conclusions drawn from this chapter are summarized in the following bullets:

- The developed methodology has been adjusted to the design criteria imposed in the first step (Section 6.1). Electrical, thermal and mechanical design criteria have been defined which have been fulfilled in every step of this methodology. The cooling system technology that it has been implemented in this application, it has been imposed by the manufacturer. However, it has not been a problematic condition in order to follow the complete methodology and therefore, to achieve an optimized *TMS*. **Three possible rides** for the residential elevator have been defined. These rides requirements in terms of power have been defined by the manufacturer and the have been directly related to the people that were inside and with the direction of the residential elevator. For any power condition, the *BP* must fulfil some thermal imposed requirements. **An ideal operation window between 20-30 ºC** has been defined, although it has been considered a **temperature range between 10 ºC and 40 ºC admissible**. If the *BP* reaches an operation temperature higher than **55 ºC, the residential elevator will stop**. Regarding the **thermal dispersion within the *BP***, it should manage to keep this value **below 3 ºC** in the most of the time. A thermal dispersion higher than **5 ºC will be unacceptable.** These thermal requirements must be fulfilled for an **ambient temperature range between 10 ºC and 40 ºC**.

- The predesign step which it has been described in Section 6.2 has been comprised of two main tasks: the thermal sizing of the *BP* and the selection of the components for the *TMS* at system level.

The thermal sizing (Section 6.2.1) has been carried out based on the electrical sizing that it has been performed in Chapter 3. By means of the electrical sizing, for this application **a *BP* composed of 7 *BM*s** connected in serial with an **energy on-board of 693 Wh** has been defined. Each ***BM* has been comprised of 12 cylindrical cells (A123)** connected in serial and therefore, it has been possible to calculate that the complete *BP* has been composed of 84 cells.

On this basis and by means of the cell heat generation model developed in Doctoral Thesis of N. Nieto [68], the heat generation rate has been calculated in order to estimate how much heat must be dissipated by the *TMS*. The scalability at cell, *BM* and *BP* level has been applied in terms of heat generated, multiplying the heat generated at cell level by the number of cells that are in the *BM* and *BP*. For the purpose to design a *TMS* for this application, the heat generated in the most restrictive ride of the residential elevator in terms of power and the thermal requirement related to the ideal temperature that the *BP* must be kept by means of the *TMS* (25 ºC) have been taken into consideration. At last, **a *TMS* that could dissipate 202.1 W has been predesigned.**

The preselection of the components (Section 6.2.2) of **the air cooling system imposed by the manufacturer** has been carried out by means of some **simple calculations in terms of thermal and hydraulic balances in *Excel Worksheet***. Several assumptions and simplifications have been considered in this step in order to simplicity as far as possible the calculations. Based on the scalability of the *BP* and the complete *TMS*, in the *Excel Worksheet* a quarter of a *BM* has been considered. Also, the influence of the air mass flow rate on the complete *BP* has been scaled to this specific part of the *BM*.

As a results of this section, **it has been decided to place two heat sinks in the top and other two in the bottom of each *BM*.** The selected heat sink has been **SK 473**, provided by Fisher manufacturer. In addition, in order to ensure an appropriate contact between the cells and the heat sink, it has been decided to use ***TIM*,** particularly for this case **ProtecION^{+} DLP 3.0** has been decided

to implement because the adequate thermal conductivity (3 $W \cdot m^{-1} \cdot K^{-1}$) that it provides. At last, **it has been determined the implementation of three fans provided by EBM manufacturer of model 4114 NHH.** They have been placed on one lateral of the case in order to extract the air from there and to absorb from the front side by means of some grids.

As a result, due to all general assumptions and considerations that they have been assumed in this predesign step, an **oversized *TMS*** has been obtained.

- Once the *BP* and the *TMS* have been predesigned, the next step has been to develop **detailed models** (Section 6.3) of them in order to check if the design criteria defined in Section 6.1 have been fulfilled or not, prior the construction of a sample prototype. As it has been explained in detail in Chapter 5, in this application ***Ansys/ FLUENT* simulation tool** has been chosen for modeling purpose. This decision has been carried out because this simulation tool provides the opportunity to analyze the air distribution around the cells within the *BP*, among other phenomena, that with a *DAE* simulation tool, for instance, would be unviable. By means of this tool, several high-fidelity detailed numerical thermal models have been developed improving the efficiency of the design process relative to a trial- and- error determination of the *BP* cooling system design concept.

  Detailed models at *BM* and *BP* level have been developed. As in the previous step, the scalability at *BM* level in terms of *BP* and *TMS* has been applied in this step of the methodology. The *BM* level thermal model has been used in this and in the following step with the aim to check and validate the thermal performance of the system in transient state, whereas the *BP* level thermal model has been used for optimization purpose.

  Once the detailed models have been completely modelled, **a test matrix has been defined in order to check the thermal performance** of the system at as wide as possible operation conditions with a minimum number of numerical tests. Based on the results obtained, which have been shown in Table 6.7, it can be observed that for the worst electrical conditions tested the

BM temperature is below the temperature defined as acceptable (40 ºC). The maximum *BM* temperature has been reached in the test in which the most restrictive electrical conditions have been applied with the maximum air velocity and ambient temperature (Test 1 in Table 6.6). Moreover, the thermal dispersion within the *BM* has been lower than 3 ºC for every operation conditions. Unlike the maximum *BM* temperature, the maximum thermal dispersion has been obtained for the case that the minimum air velocity and ambient temperature has been applied, with the most restrictive electrical conditions (Test 2 in Table 6.6).

Therefore, it has been concluded that by means of **the proposed thermal design have been fulfilled the defined design criteria.** In addition, it is clear that the possibility to optimize the *TMS* existed, due to the considerable margin that it has been related to both *BM* temperature and thermal dispersion, considering the limit values that have been defined in the Section 6.1.

- The fourth step of the methodology, once they have been checked the design criteria numerically, is based on the **experimental validation of the developed thermal models by means of a construction of a prototype** in the laboratory environment.

  Following the same philosophy, a prototype based on a unique *BM* has been constructed. A wind tunnel has been designed placing the *BM* in the middle of it. In the entrance of the tunnel a fan has been placed by means of which the necessary air flow rate has provided. The same test matrix as for numerical simulations (Table 6.6) has been carried out experimentally to validate the thermal models. Different measurement instruments have been used in order to measure variables such as the air inlet velocity and temperature, *BM* and heat sink surface temperature and the fan *PWM*. These measured variables have been compared directly against the numerical data, quantifying in that way the accuracy of the developed models for validation purpose.

Although the thermal resolution inside the cell has not been fully realistic due to the assumptions and simplifications that have been considered, it has proved to be valid as **the maximum time- averaged prediction error has been below than 1.5 ºC.**

This result has underscored the importance of using a large testing matrix to investigate and validate thermal modeling of *Li-Ion BP*. In addition, it has been also concluded that ***Ansys/ FLUENT* simulation tool has been an adequate and an appropriate tool to analyze the thermal performance of this type of air cooled systems**.

- Once the developed thermal models have been validated, they have made possible to verify the fulfilment of the thermal requirements related to the maximum cell temperature and thermal dispersion for the worst operation conditions by means of the first designed *TMS.* Also, **they have proved the possibility of optimization of the *TMS*.**

The optimization process has been based on numerical **steady simulations using *DoE* technique**. In this application and due to the high computational cost that transient simulations supposed in *CFD* simulation tool especially regarding the developed *BP* level model, the ***False Steady* novel concept** has been introduced and applied. The aim of this technique has been **to accelerate the achievement of the steady state of a cyclic transient profile**, without losing accuracy. ***RSM* analysis has been supported by Minitab 17.0 software.**

Three optimization processes have been carried out: Optimization I, Optimization II and Optimization III.

- **Optimization I** analysis has been focused on the optimization at component level, analyzing the influence of use *NC* or *FC* and on the evaluation of the possibility to dispense with the heat sink or not. For this purpose the detailed thermal developed model at *BM* level has been used.

Based on the results obtained for this optimization step, Table 6.13, it has been evidenced that the main factor to keep the *BM* within an appropriate operation range has been the usage of *FC*. In fact, it is clear that although when a heat sink is used the obtained *BM* temperature has been slightly lower, has not been indispensable the implementation in the system of it, since for the cases without heat sink with *FC* the *BM* has been kept within the admissible operation range for the worst conditions. Regarding the thermal dispersion, it has been obvious that at any conditions have been achieved to keep the temperature difference within the *BM* below 3 ºC. In *NC* conditions the thermal dispersion between the cells has been smaller compared with the cases in which *FC* has been used.

Not using heat sink has supposed a saving of 226 €. For this calculation, it has been considered on the one side that each *BM* has 4 SK473 heat sinks and on the other hand, the costs related to per unit (5.085 €/unit) and mounting (3 €/unit).

In addition, the cooling mode has been evaluated considering the required time for the cooling process of the *BM* level. As a conclusion of this analysis it can be stated that a *FC* system has been necessary. In order to **keep the cooling time range lower than 2 hours** for the worst conditions (40 ºC and DCH 7C/ CHA 3C), **a fan *PWM* of 32.5%** has been required. However, with this rotational speed of the fan with an ambient temperature of 10 ºC and a current rate of DCH 3C/ CHA 1C, the *BM* has been cooled in 92 minutes. Nevertheless, in the strictest sense to achieve a **cooling time below than 75 minutes** (defined such as optimal range) for the harshest conditions, **a *PWM* of 55%** has been established.

- **Optimization II** analysis has been focused on the optimization at *BP* level with the aim to determinate an optimize rotational speed of the fan to keep the *BM* within an acceptable operation range. For this analysis has been considered the non-necessity of the heat sinks.

For an ambient temperature of 40 ºC and:

- a minimum *C-rate* level (DCH 3C/ CHA 1C) with a *PWM* of 10%, it has been possible to keep the maximum cell temperature at 42.5 ºC and a thermal dispersion of 3 ºC.
- a medium *C-rate* level (DCH 5C/ CHA 2C) with a *PWM* of 40% it has been possible to keep the maximum cell temperature at 46.2 ºC and a thermal dispersion of 3 ºC.
- a maximum *C-rate* level (DCH 7C/ CHA 3C) with a *PWM* of 67.5% it has been possible to keep the maximum cell temperature at 49.1 ºC and a thermal dispersion of 3 ºC.

For an ambient temperature of 25 ºC and:

- a minimum *C-rate* level (DCH 3C/ CHA 1C) with a *PWM* of 17.5%, it has been possible to keep the maximum cell temperature at 28.2 ºC and a thermal dispersion of 3 ºC.
- a medium *C-rate* level (DCH 5C/ CHA 2C) with a *PWM* of 52.5% it has been possible to keep the maximum cell temperature at 31.7 ºC and a thermal dispersion of 3 ºC.
- a maximum *C-rate* level (DCH 7C/ CHA 3C) with a *PWM* of 92.5 % it has been possible to keep the maximum cell temperature at 33.1 ºC and a thermal dispersion of 3.2 ºC.

For an ambient temperature of 10 ºC and:

- a minimum *C-rate* level (DCH 3C/ CHA 1C) with a *PWM* of 22.5%, it has been possible to keep the maximum cell temperature at 15.8 ºC and a thermal dispersion of 3 ºC.
- a medium *C-rate* level (DCH 5C/ CHA 2C) with a *PWM* of 61.25% it has been possible to keep the maximum cell temperature at 19.1 ºC and a thermal dispersion of 3 ºC.
- a maximum *C-rate* level (DCH 7C/ CHA 3C) with a *PWM* of 100% it has been possible to keep the maximum cell temperature at 20.7 ºC and a thermal dispersion of 3.7 ºC.

Based on the actual electrical requirements and ambient conditions, the rotational speed of the fan will be regulated in order to optimize the system consumption. As it can be seen, the main factor to establish the required fan *PWM* value has been the thermal dispersion within the *BM* and although it might seem paradoxical, the lower is the ambient temperature, the higher is the *PWM* needed value.

For **the worst operation conditions** in terms of ambient and electrical solicitations in which a ***PWM* of 67.5%** has been defined as optimized operation point, the consumption has been **11.44 Wh** which correspond to a **69.2% less** in terms of consumption than the reference proposed first design.

- **Optimization III** analysis, which is in progress at the moment, is focused on the **evaluation of the use of *NC* at *BP* level. Based on the results that will be obtained, it will be determined a control strategy.** This strategy will define the ambient and electrical conditions that would allow the advantageous use of the *NC*. When the measured conditions are unfavourable the fans will switch on with the previously defined *PWM* levels depending on the measured current and ambient temperatures. A dramatic reduction of the use of the fans is expected when parameters like intermittency are taken into account in the analysis.

- The complete previous optimization procedure has been carried out considering cyclic and permanent electrical conditions for this specific application imposed by the manufacturer. Consequently, **the conclusions obtained are valid for these previously defined operation conditions.**

  However, these **specifications are not too realistic** for a real residential elevator, because **high intermittency is expected** in the use of the application. Therefore, **it will be probable that the fans could remain inactive** and furthermore, that by means of *NC* should be enough to fulfil the thermal design criteria. **On this basis and for a future research work, it has been proposed to define a control strategy** related to the fans operation based on the control of the maximum cell temperature and the thermal dispersion within the *BP* by means of the *BMS*.

Chapter 7.

Case Study II: *TMS* Optimization for Urban Electric Minibus

Along this chapter the methodology proposed in Chapter 5 has been applied to an urban electric minibus application.

In this particular case, the on-board *Battery Pack* has been composed of 16 *Battery Modules* where each one has been comprised of 12 *Li-Ion* pouch cells connected in a serial configuration. Regarding the necessity to keep the *Battery Pack* temperature below the ambient temperature, it has been decided to implement a liquid cooling system based on a dual architecture which combines F*orced and Active Cooling* modes, keeping the *Battery Pack* within an admissible operating range. Moreover, the compactness and the weight of the complete system, as well as the insulation of the *Battery Pack* have been taken into consideration, in order to avoid as far as possible the influence for instance, of the direct sun exposure.

In this case, *Dymola/TIL* simulation tool has been used with the aim to optimize the *Thermal Management System* at component and at system level ensuring the fulfilment of the established requirements even for the worst ambient and electrical solicitations.

7.1 DESIGN CRITERIA DEFINITION

Such as for the residential elevator, for the urban electric minibus some criteria have been defined considering electrical, mechanical, thermal and other design aspects.

With regards to the electrical solicitations, some energy and power requirements have been taken into account according to the application which it has been explained in Chapter 2. In terms of energy, the complete *BP* should provide at least 27.7 kWh energy on-board in order to be able to perform one requirement defined by the manufacturer: the urban electric minibus at least should be able to round two full cycles of any bus line until its stored energy has been fully depleted. In referenced to power requirements, in the same way as for the residential elevator application, three possible bus lines around the city have been considered. Based on them and similarly as for the previous test case, current cyclic profiles have been defined considering the *RMS* current value of the charge and discharge process of each bus line. For this particular case and as it can be seen in Table 3.5, the estimated *RMS* current value for the three bus lines has been equal. Consequently, in the following task related to thermal modeling, validation and optimization a cycle of 1C/1C will be used as the unique current rate profile. In contrast, for the thermal sizing of the *BP* the real current profile of each line will be used in order to estimate a realistic heat generation rate.

Unlike for the residential elevator case, for this application and regarding the mechanical aspects, the weight of the complete *BP* must be minimized, mainly because in this case the complete *BP* is moving together with the electric minibus. The overweight can affect the autonomy of this vehicle. Along with this requirement, the *BP* should be as compact as possible. Furthermore, defined by the manufacturer the *BP* has been located in the rear of the electric minibus and the *TMS* must be entered in a space no bigger than 60 cm x 50 cm x 50 cm in terms of length, width and height, respectively.

At the same time, some thermal requirements must be fulfilled. Primarily in transport applications, special attention must be paid to the combination of ambient conditions together with the possible restrictive solicitations related to the application. Therefore, mainly in *EVs* scope is crucial to integrate a battery *TMS* to maintain the *BP* at an optimum average operation range even for the worst ambient conditions. By means of

the *TMS* it must be possible to keep the *BP* between 20-30 ºC (ideally 25 ºC), although it has been considered a temperature range between 10 ºC and 40 ºC acceptable. Nevertheless, it has been considered unacceptable to reach a cell maximum temperature within the *BP* of 55 ºC and the urban electric minibus could not operate whether the *BP* temperature is lower than 10 ºC. In terms of thermal dispersion, it has been defined a maximum temperature variation between the cells as maximum of 5 ºC under any operation conditions, trying to keep it below 3 ºC and ideally, minimizing it as far as possible. All these thermal requirements must be achieved for an ambient temperature range between 10 ºC and 45 ºC.

As it has been mentioned in Chapter 5, the manufacturer has been selected a liquid cooling system in order to fulfil the previously mentioned requirements, but without expenses to achieve an efficient system in terms of consumption. Moreover, the manufacturer has been requested a *TMS* able to withstand the possible ambient temperature fluctuations. For that purpose, it has been proposed a dual architecture that when the ambient temperature is warm, around 25 ºC, uses a *FC* mode by means of a radiator and a fan and whereas, the ambient temperature is higher, around 45 ºC, an *AC* mode operates to ensure using a compressor to keep the *BP* within the ideal operation range.

To sum up, defined requirements mentioned up to now are assembled in Table 7.1.

Table 7.1 Thermal and electrical requirements defined for this application

Electrical Requirements		**Mechanical Requirements**	
Energy on-board, kWh	27.7	Volume (H x W x H) cm	60 x 50 x 50
Thermal Requirements			
TMS technology		Liquid cooling: Dual (*FC* + *AC*)	
Max Tº cell, ºC		55	
Admissible Tº cell range, ºC		10 - 40	
Ideal Tº cell range, ºC		20 - 30	
Ideal Tº cell, ºC		25	
Tº ambient, ºC		10 - 45	
Max. ΔT *BP*, ºC		5	
Ideal ΔT *BP*, ºC		Minimum	
Admissible ΔT *BP*, ºC		3	

7.2 PREDESIGN OF THE BATTERY PACK AND THERMAL MANAGEMENT SYSTEM

Regarding the electrical, mechanical and thermal design requirements that have been defined in the previous section; the thermal sizing of the *BP* and the selection of the components and materials needed for the defined *TMS* has been carried out in following.

7.2.1 THERMAL SIZING OF THE BATTERY PACK

In Chapter 3 the electrical sizing has been carried out by means of which, the required *BM*s in the *BP* have been defined. As a result, the complete *BP* installed in the urban electric minibus has been comprised of 16 *BM*s connected in serial with an associated energy on- board of 28.4 kWh, which it is sufficient to achieve the energy requirement imposed by the manufacturer for this application. Effectively, a *BP* composed of 15 *BM*s, it will not have enough energy on-board (26.6 kWh) in order to fulfil the defined energy requirement defined in Table 3.5. Furthermore, different parallel configurations have been also analyzed. At last, mainly because the voltage at *BP* level which is related to the converter needed it has been decided to implement *8s2p* electrical configuration.

Each *BM,* as it has been defined before, has been composed of 12 *Li-Ion* pouch type cells (*NMC* chemistry) from KOKAM (model SLPB100216216H) connected in serial electrical configuration. The nominal voltage and current level at the cell level have been around 3.7 V and 40 A, respectively.

Once the electrical sizing has been done, the next step before design and construct a suitable *TMS* has been to calculate the heat generated in the *BP* for diverse operation conditions. In the same way as for the previous case study, the minimal entity identification for the thermal sizing has considered a cell. For that objective, a cell model has been developed considering its thermo-chemical and thermo-physical properties which have been experimentally determined in the N. Nieto Thesis [68]. In Figure 6.1 is shown the internal resistance variation in function of the *SOC* and cell temperature and the entropic heat coefficient as a function of *SOC* in (a) and (b), respectively.

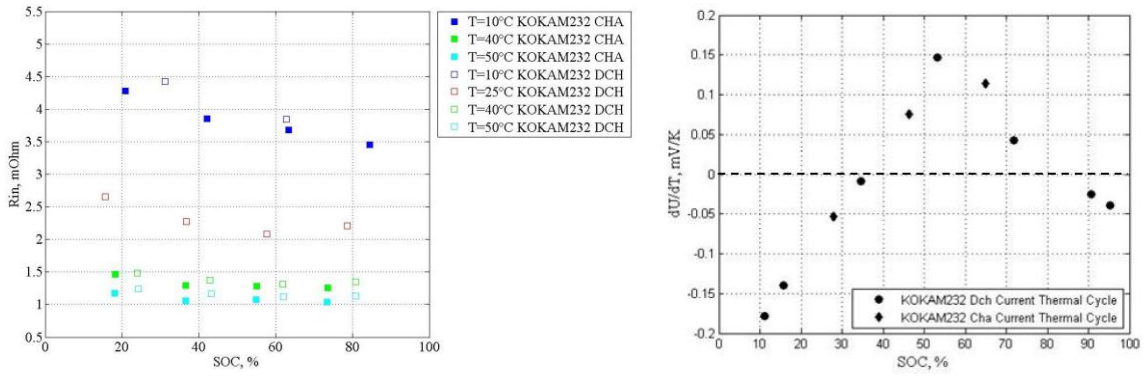

(a) (b)

Figure 7.1 (a) Variation of internal resistance with both SOC and temperature and (b) entropic heat coefficient as a function of SOC for KOKAM cells

By means of these values referred to the thermo-chemical properties defined experimentally (Figure 7.1), and the procedure shown in Figure 7.2 in order to calculate the heat generated, the heat generation rate at cell, at *BM* $\left(HG_{cell} \cdot {}^{12\ cells}/_{BM}\right)$ and at *BP* $\left(HG_{BM} \cdot {}^{16\ BMs}/_{BP}\right)$ level has been calculated.

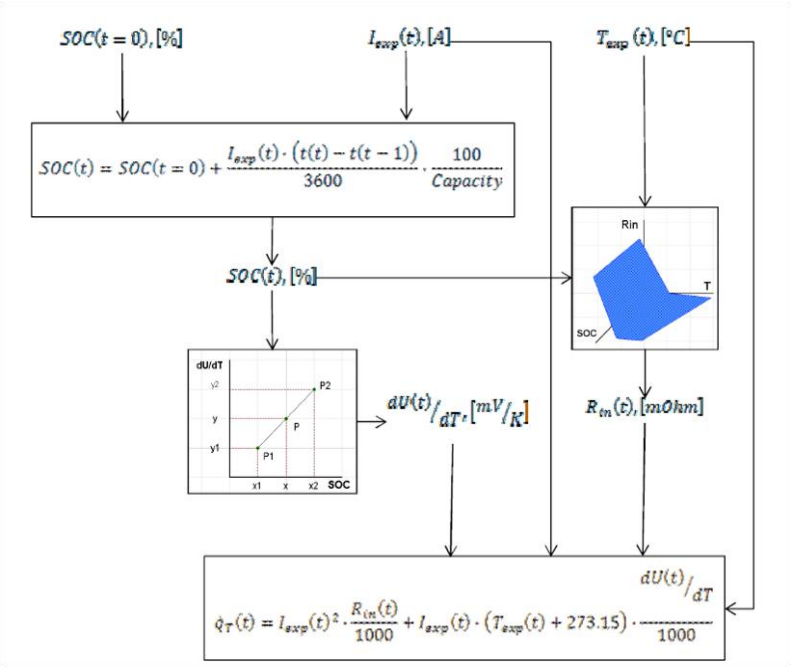

Figure 7.2 Procedure to determine the heat generation rate from experimental internal resistance and entropic heat coefficient data.

In that way, the total amount of heat that should be dissipated by the proposed *TMS* has been calculated, multiplying the heat from a single cell by the number of the cells within the *BP*. This *BP* has been comprised of 192 cells.

Figure 7.3 shows the heat generation rate considering a unique cell, a *BM* and the complete *BP* for a wide range of operation conditions: different *SOC* ranges (*SOC* 40-60%, *SOC* 30-70% and *SOC* 20-80%) for the three possible minibus lines (Line 1, Line 2 and Line 3). Depending on the *SOC* drop required for each line, it would be possible to operate within specific range, e.g., due to Line 1 needed 54.4% *DOD* range to complete an entire route, it has been impossible to operate within *SOC* 70-30% (*DOD* 40%) or *SOC* 60-40% (*DOD* 20%) range. Regarding the temperature of the cells a complete sweep has been carried out from 10 ºC to 50 ºC, every 5 degrees.

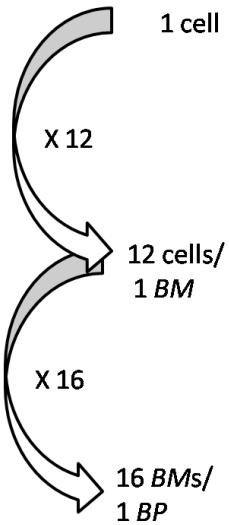

		Line 1	Line 2		Line 3		
		SOC 80-20%	SOC 70-30%	SOC 80-20%	SOC 60-40%	SOC 70-30%	SOC 80-20%
Tcell, ºC	10	-7,58	-6,34	-6,39	-4,38	-4,37	-4,46
	15	-6,46	-5,40	-5,45	-3,73	-3,72	-3,82
	20	-5,34	-4,46	-4,52	-3,08	-3,07	-3,17
	25	**-4,22**	-3,53	-3,58	-2,44	-2,42	-2,52
	30	-3,68	-3,10	-3,13	-2,16	-2,13	-2,20
	35	-3,15	-2,70	-2,69	-1,90	-1,86	-1,89
	40	-2,63	-2,29	-2,26	-1,64	-1,59	-1,58
	45	-2,43	-2,12	-2,08	-1,53	-1,48	-1,46
	50	-2,24	-1,95	-1,92	-1,43	-1,38	-1,35

		Line 1	Line 2		Line 3		
		SOC 80-20%	SOC 70-30%	SOC 80-20%	SOC 60-40%	SOC 70-30%	SOC 80-20%
Tcell, ºC	10	-91,02	-76,07	-76,69	-52,53	-52,45	-53,58
	15	-77,55	-64,80	-65,44	-44,76	-44,62	-45,79
	20	-64,09	-53,54	-54,20	-37,00	-36,81	-38,01
	25	**-50,65**	-42,31	-42,98	-29,29	-29,04	-30,26
	30	-44,14	-37,23	-37,56	-25,96	-25,61	-26,40
	35	-37,86	-32,36	-32,33	-22,81	-22,34	-22,67
	40	-31,60	-27,53	-27,12	-19,74	-19,12	-18,98
	45	-29,15	-25,44	-25,01	-18,38	-17,77	-17,56
	50	-26,84	-23,45	-23,00	-17,10	-16,51	-16,22

		Line 1	Line 2		Line 3		
		SOC 80-20%	SOC 70-30%	SOC 80-20%	SOC 60-40%	SOC 70-30%	SOC 80-20%
Tcell, ºC	10	-1456,24	-1217,19	-1227,04	-840,53	-839,17	-857,23
	15	-1240,76	-1036,80	-1047,02	-716,09	-713,92	-732,61
	20	-1025,43	-856,63	-867,18	-592,02	-589,00	-608,21
	25	**-810,33**	-676,91	-687,69	-468,65	-464,61	-484,13
	30	-706,20	-595,66	-600,96	-415,44	-409,74	-422,35
	35	-605,70	-517,80	-517,26	-365,00	-357,46	-362,78
	40	-505,52	-440,55	-433,88	-315,81	-305,89	-303,70
	45	-466,44	-407,11	-400,10	-294,00	-284,37	-280,90
	50	-429,40	-375,21	-367,98	-273,65	-264,10	-259,47

Figure 7.3 Thermal sizing for BP installed in the urban electric minibus.

In order to evaluate the thermal sizing of the *TMS* for the whole *BP*, the values referred to the worst bus line (Line 1) and an ideal *BP* temperature of 25 ºC have been considered. Besides, an oversizing of 10% has been assumed to take into account the increase in the *BP* of the internal resistance due to ageing effect during the first life of the *BP*. Consequently, a heat generation around 891.3 W has been estimated in the whole *BP* to be dissipated by the *TMS*.

To sum up, in Table 7.2 is shown the summary regarding the electrical and thermal sizing that it has been carried out in this section.

Table 7.2 The electrical and thermal sizing carried out for this application.

Electrical sizing		**Thermal sizing**	
Battery Pack	16 *BM*s in serial	Heat Generation at	891.3
Energy on board, kWh	28.4	*BP* level, W	

7.2.2 PRELIMINARY COOLING SYSTEM DESIGN

As it has been explained in detail in Chapter 5, the preliminary thermal sizing of the *TMS* is done to overcome the worst possible thermal situation. This coarse analysis is done using an *Excel Worksheet.* Because of the assumptions and overall suppositions that have been considered, oversized results are obviously expected at this design stage.

Once the amount of the heat generated within the *BP* has been determined, the proper cooling system has been selected and predesigned. As it has been mentioned in Chapter 4 and in the introduction of this chapter, a liquid cooling based on dual architecture which combines *FC* and *AC* has been proposed as the best conceptual solution for this application, mainly to keep the *BM* within acceptable thermal conditions when the ambient temperature is high. Unlike to the previous test case, for this urban electric minibus application the scalability in terms of the *BP* and *TMS* has not been applied in this step. The total amount of heat generated within the *BP* has been considered to select the components of the proposed *TMS*.

In Figure 7.4 can be seen the schematic diagram of this dual architecture *TMS*. Red, blue, green and orange lines can be distinguished which represent the heat, the liquid, the refrigerant and the air through the system, respectively. Regarding the liquid, a mixture of 50% *WEG* has been considered due to the excellent properties that this coolant fluid provides in terms of anti-freezing. R134a refrigerant, the most commonly used currently in automotive applications, has been utilized. In the last years authorities and researchers are working on the decision related to the replacement of R134a in favour of more environmentally benign refrigerants [110]. The main candidate to replace R134a is R1234yf because its similar thermo-physical properties [111] although, the R1234yf provides lower cooling capacity for the same thermodynamic conditions. However, it does not contain chlorine and therefore, its *Ozone Depletion Potential* (*ODP)* is zero, and its *Global Warning Potential* (*GWP)* is as low as 4. Nevertheless, for this research work it has been decided to use R134a because little

amount of components can be found nowadays for R1234yf refrigerant to handle this cooling capacity.

In general terms, based on Figure 7.4 two circuits can be defined: the primary and secondary circuit. The first one is referred to the *FC* system where the cold plates (1), hydraulic pump (2), radiator (3) and fan (8) are integrated, whereas in the second one, the *AC* system, the evaporator (4), condenser (5), compressor (6), *TXV* (7) and fan (8) can be found. The link between the primary and secondary circuit, as it can be seen in Figure 7.4, is by means of the evaporator which is indicated by discontinuous blue lines. The *FC* and *AC* modes operate in function of several directional valves. Moreover, as it can be observed, all the components have been considered as a lumped elements without evaluating any discretization within them, uniquely inputs and output signals. Regarding the *BP*, for both cooling modes, it has been supposed in this step that the 16 *BM*s have been configured in a hydraulic configuration of 4 strings in parallel composed each one of 4 *BM*s, because a priori the connection of the 16 *BM*s in serial will suppose a high-pressure drop and on the other hand, a configuration connected 16 *BM*s in parallel requires a very complex piping. However, 4s4p (s: serial, p: parallel) configuration has been considered as commitment configuration between thermal and hydraulic compromises from a general overview.

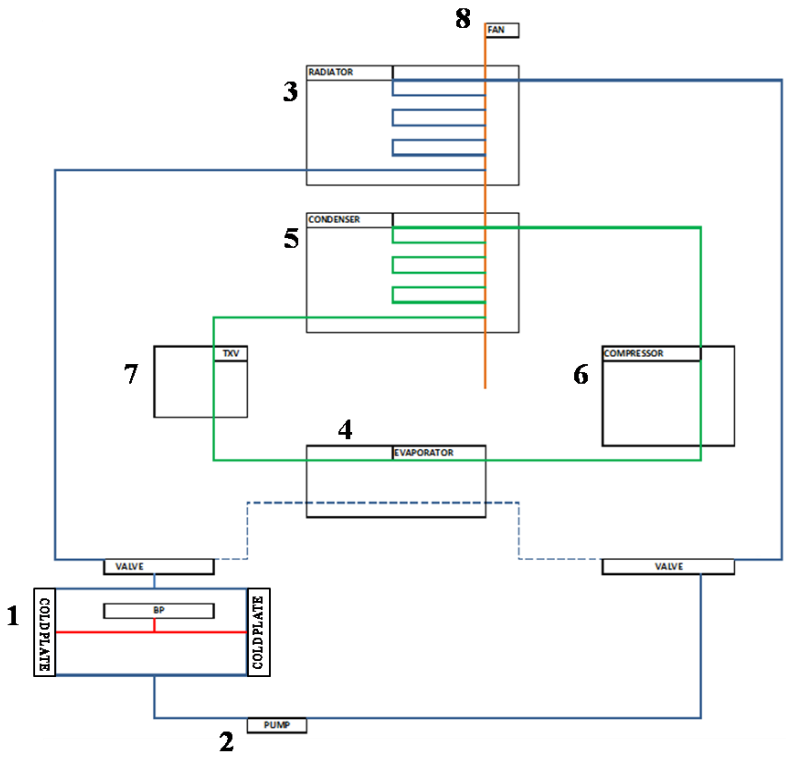

Figure 7.4 Schematic diagram of the proposed dual TMS: AC+FC.

In this step *FC* and *AC* systems have been analyzed separately, firstly the *FC* has been studied and secondly, the *AC* system. The *BP* for both cooling modes has been modelled using lumped properties, considering the total amount of the cells, as a unique component. Therefore, a unique heat capacity value and thermal conductance has been calculated based on the physical properties of the cells. The first general task for both operating modes has been to preselect the possible suitable components (cold plates, hydraulic pumps, radiator, evaporator, condenser, compressor, *TXV*) for each system based on the estimation of the approximated heat generation rate that must be dissipated by the *TMS*. An aspect that it must be bear in mind when preselecting the components for this *eMOV* application, it is that a voltage supply of 24 VDC is required. On this basis, the components have been chosen and their performance data has been introduced in the *Excel Worksheet*. As an example, in Figure 7.5 is shown the *Excel Worksheet* referred to cold plates and hydraulic pumps that have been used for this work.

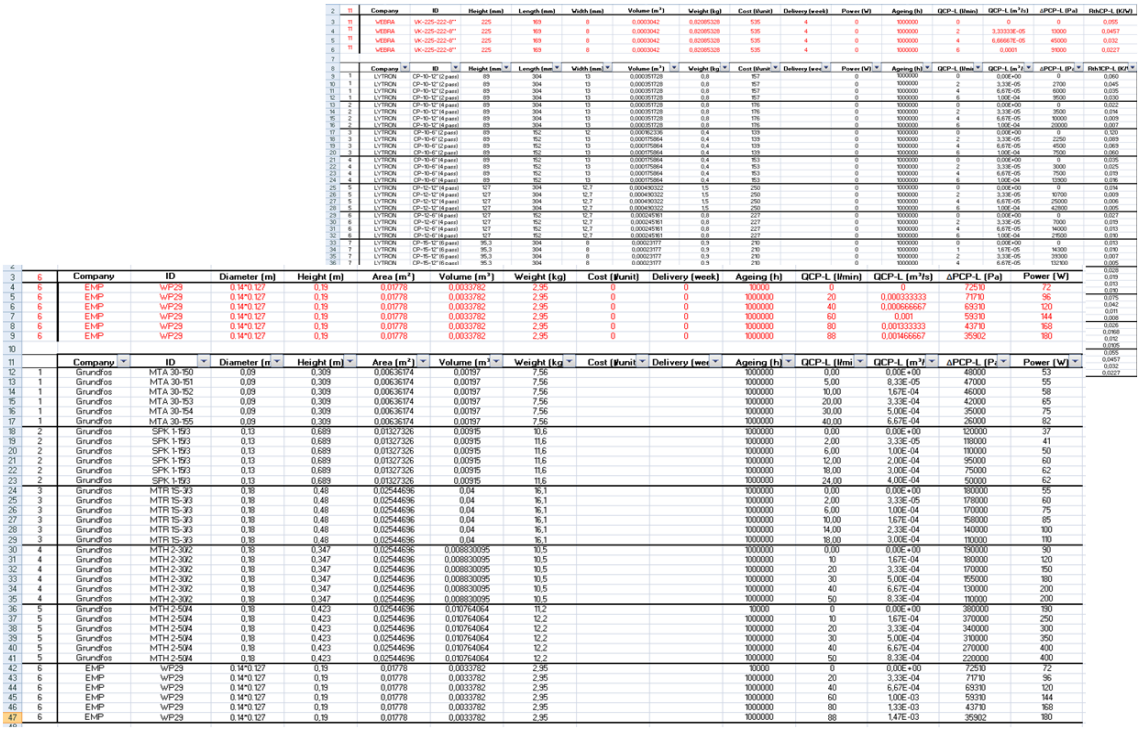

Figure 7.5 Components datasheet introduced in Excel Worksheet.

The developed *Excel Worksheet* together with the Solver integrated into Excel tool has been able to achieve solutions for diverse component combinations which fulfil the entire thermal, hydraulic and pneumatic restrictions defined in Table 7.1. The simple models developed for each cooling mode are shown in Figure 7.6 (a) and (b), respectively.

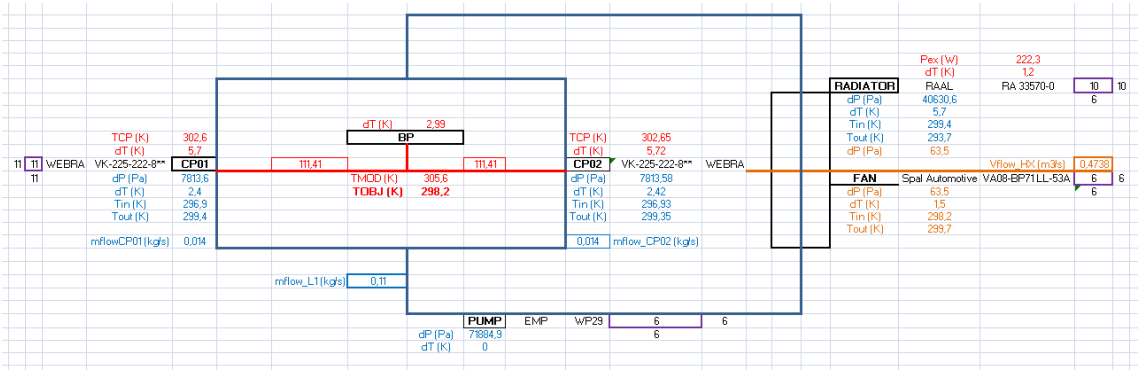

(a)

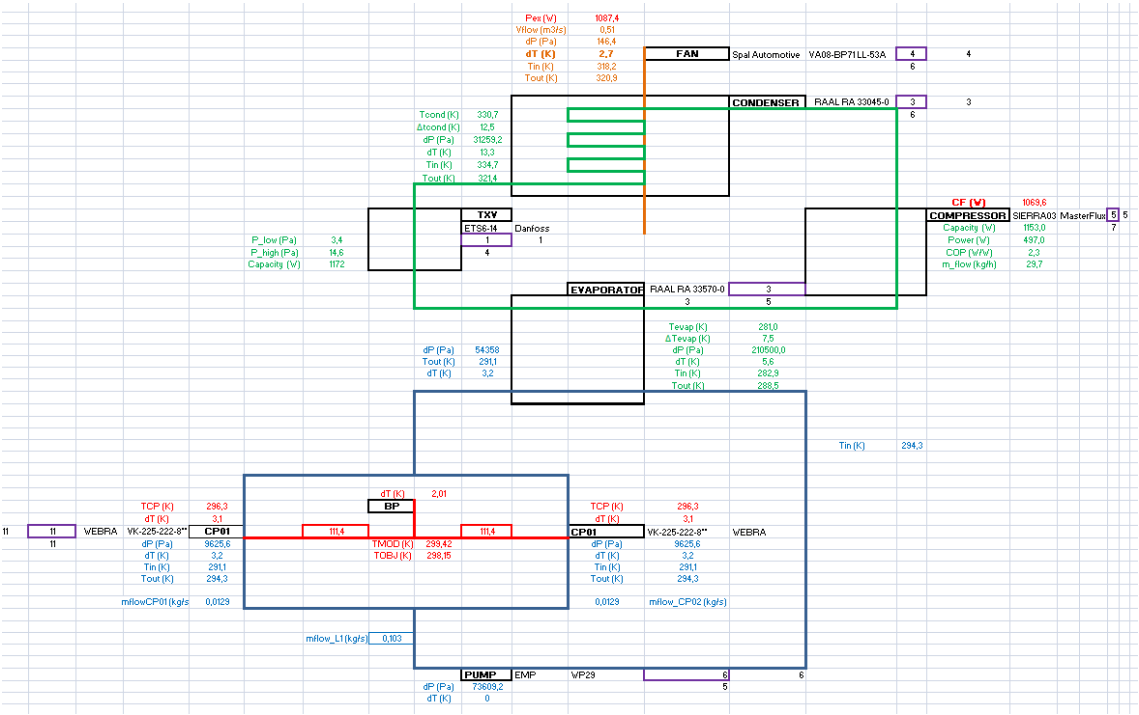

(b)

Figure 7.6 Schematic diagram of the Excel Worksheet developed for (a) FC and (b) AC system

As a result of this second step of the methodology the preselected components of the proposed *TMS* have been obtained. In Table 7.3 are tabulated the components that have been selected with the help of this *Excel* tool and which will be used to develop the detailed models in the next step of the methodology. The same identification number that is used in Figure 7.4 has been used here too.

Table 7.3 Selected components for the dual TMS for the urban electric minibus application.

	Components	Reference
1	Cold Plates	VK-225-222-8**
2	Hydraulic pump	EMP electric pump, WP29
3	Radiator	RAAL, RA 33570-0
4	Evaporator	RAAL, RA 33046-0
5	Condenser	RAAL, RA 33045-0
6	Compressor	Masterflux, SIERRA03-0982Y3
7	Thermal Expansion Valve	Danfoss, ETS 6-14
8	Fan	Spal Automotive, VA08-BP71 LL-53A

The selected components are shown individually taking into account the information that it has been obtained by the manufacturers in the following paragraphs.

- **Cold Plate**

The selected cold plates have been provided by AMS technologies and they have been manufactured by Webra Industry [112]. In Figure 7.7 is shown the design of Webra VK-225-222-8** liquid cooler together with its performance curves related to thermal resistance and the pressure drop in function of the liquid mass flow rate. As it can be seen in Figure 7.7, the pressure drop increases and the thermal resistance decreases when the liquid mass flow rate increases.

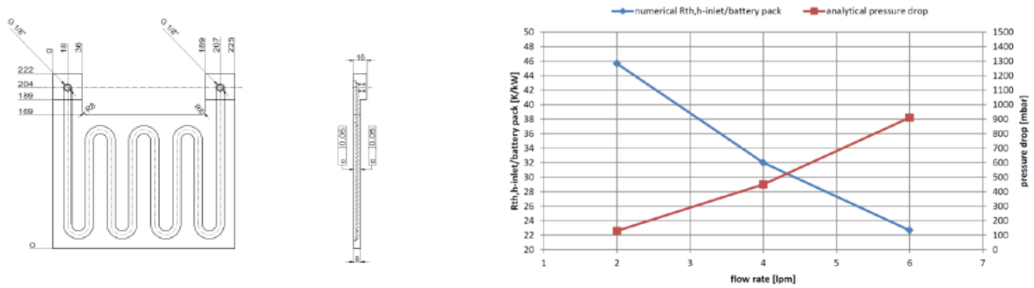

Figure 7.7 Selected Webra cold plate along with its performance curves [111].

- **Hydraulic Pump**

The 24 VDC electric pump has been provided by *EMP* manufacturer [113]. Figure 7.8 shows the pump together with the pressure drop curve in function of the liquid mass flow rate for different possible rotational speed in rpm.

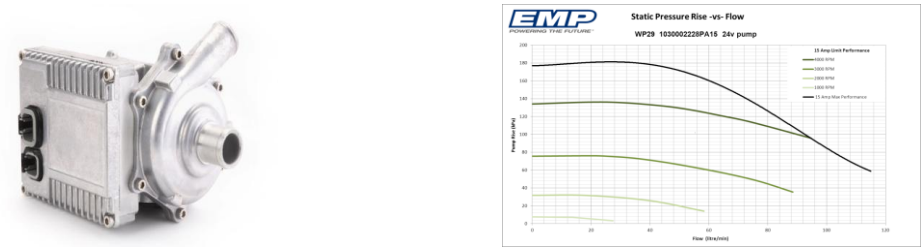

Figure 7.8 The selected electric hydraulic pump [112].

- **<u>Heat Exchangers (Radiator, Evaporator, Condenser)</u>**

Three heat exchangers have been provided by *RAAL* manufacturer [114]. In *Figure 7.9* (a), (b) and (c) can be observed the drawings correspondent to liquid-air radiator, refrigerant-air condenser and liquid- refrigerant evaporator. The manufacturer has not allowed publishing the thermal and hydraulic performance curves related to these heat exchangers.

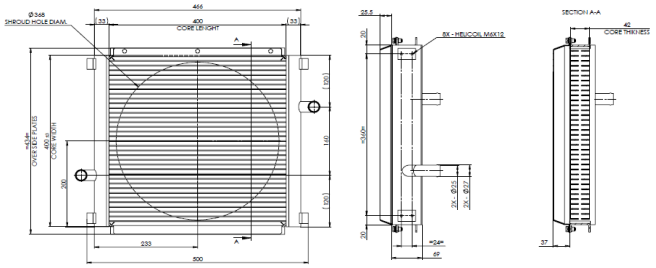

(a)

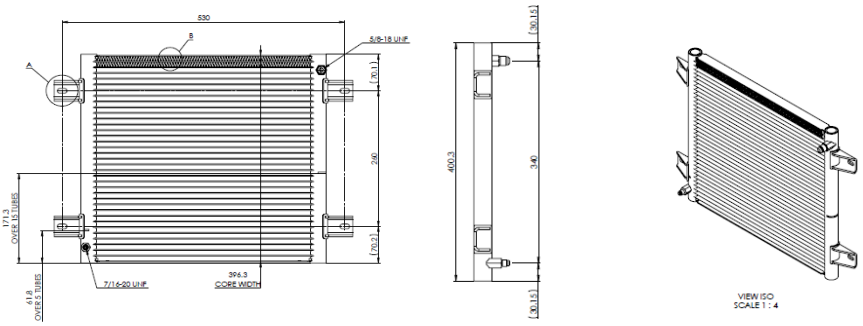

(b)

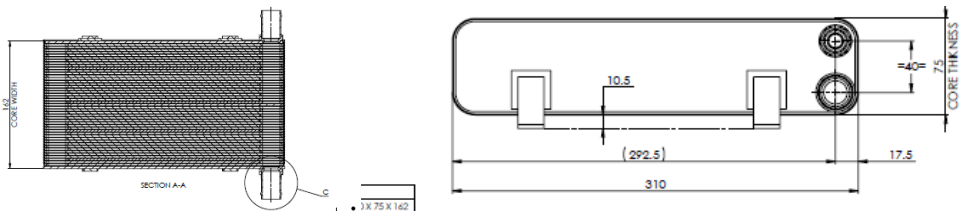

(c)

Figure 7.9 The selected heat exchangers:(a) radiator,(b) evaporator and (c)condenser [113].

- **Compressor**

As for the hydraulic pump, a 24 VDC compressor has been chosen which can operate at variable speed. The compressor has been provided by Masterflux [115]. Figure 7.10 shows the performance curves that have been used to select the most suitable option among different compressors. The cooling capacity, power consumption and efficiency data is given in function of evaporation and condensation temperature.

Analyzing the tendency of each variable in general terms, it can be stated that all the parameters increase proportionally to the rotational speed of the compressor. In addition, the higher evaporation temperature is, the higher is the cooling capacity, the consumption and the efficiency of this component.

Cooling Capacity (24V) - ARI HBP — BTU/hr (Watt)

Evaporator Temperature

RPM	-10°F	(-23°C)	10°F	(-12°C)	20°F	(-7°C)	30°F	(-1°C)	40°F	(4°C)	45°F	(7°C)	55°F	(13°C)
1800	1046	(306)	1955	(573)	2309	(676)	2725	(798)	3301	(967)	3680	(1078)	4678	(1370)
2400	1648	(483)	2824	(827)	3363	(985)	3999	(1171)	4830	(1414)	5348	(1566)	6652	(1948)
3000	2100	(615)	3545	(1038)	4270	(1251)	5127	(1502)	6213	(1820)	6872	(2013)	8484	(2485)
3600	2443	(716)	4159	(1218)	5071	(1485)	6150	(1801)	7492	(2194)	8293	(2429)	10212	(2991)

Power Consumption (24V) - ARI HBP — Watt

Evaporator Temperature

RPM	-10°F	10°F	20°F	30°F	40°F	45°F	55°F
1800	270	355	415	465	488	485	439
2400	397	451	505	556	587	590	561
3000	522	550	601	656	697	708	700
3600	647	655	706	767	822	842	857

Current (24V) - ARI HBP — Amp

Evaporator Temperature

-10°F	10°F	20°F	30°F	40°F	45°F	55°F
11.24	14.80	17.30	19.37	20.35	20.22	18.29
16.56	18.80	21.05	23.16	24.46	24.58	23.38
21.76	22.93	25.06	27.33	29.06	29.51	29.16
26.95	27.29	29.43	31.98	34.27	35.10	35.73

Efficiency (24V) - ARI HBP — BTU/hr/W (W/W)

Evaporator Temperature

RPM	-10°F	(-23°C)	10°F	(-12°C)	20°F	(-7°C)	30°F	(-1°C)	40°F	(4°C)	45°F	(7°C)	55°F	(13°C)
1800	3.88	(1.13)	5.50	(1.61)	5.56	(1.63)	5.86	(1.72)	6.76	(1.98)	7.58	(2.22)	10.66	(3.12)
2400	4.15	(1.21)	6.26	(1.83)	6.65	(1.95)	7.19	(2.11)	8.23	(2.41)	9.06	(2.65)	11.85	(3.47)
3000	4.02	(1.18)	6.44	(1.89)	7.10	(2.08)	7.82	(2.29)	8.91	(2.61)	9.70	(2.84)	12.12	(3.55)
3600	3.78	(1.11)	6.35	(1.86)	7.18	(2.10)	8.01	(2.35)	9.11	(2.67)	9.84	(2.88)	11.91	(3.49)

* all points are at 35°C (95°F) ambient temperature, 18.33°C (65°F) suction, 8.33°C (15°F) subcooling, 55.4°C (130°F) condenser

Figure 7.10 Selected compressor provided by Masterflux [114].

- **Thermal Expansion Valve**

The *TXV* has been provided by Danfoss. In Figure 7.11 can be seen, as for the compressor, the performance data in terms of cooling capacity of the expansion valve in function of evaporation and condensation temperature. As for the previously mentioned component, the cooling capacity of the *TXV* is higher when the evaporation and condensation temperature arise.

Rated Capacity (kW)

	Condensing temperature (°C)	ETS 6-14 Evaporation temperature (°C)						
		10	5	0	-5	-10	-20	-30
R134a	30	3.82	4.08	4.27	4.40	4.49	4.56	4.53
	35	4.17	4.37	4.51	4.60	4.65	4.67	4.60
	38	4.35	4.51	4.62	4.69	4.73	4.72	4.63
	40	4.45	4.59	4.69	4.74	4.77	4.74	4.64
	45	4.65	4.75	4.81	4.84	4.84	4.77	4.63
	50	4.79	4.85	4.88	4.88	4.86	4.75	4.59

Figure 7.11 Selected TXV provided by Danfoss.

- **Fan**

With regards to the fan, an axial fan has been chosen for this *TMS*. The performance data, which is shown in Figure 7.12, has been implemented in the *Excel Worksheet* used in this predesign step. The fan has to overcome the pressure drop of the air side of two heat exchangers in series in the proposed dual architecture which makes quite tricky its selection. By means of the performance curve, it has been possible to determine the necessary air mass flow rate for the specific pressure drop.

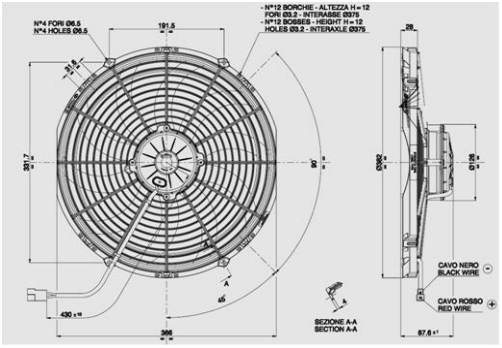

Static pressure *Pressione statica* mm H_2O	Airflow *Portata* m^3/h
0	3120
2,5	2900
5	2690
7,5	2450
10	1930
12,5	1550
15	1290
17,5	960
20	660
22,5	260
25	0

Figure 7.12 Selected fan provided by Spal Automotive.

Once the *BP* and the *TMS* have been predesigned, the detailed models have been developed to analyze deeply the transient thermal performance of it. It is worth underlining, although it has been mentioned before, that due to the assumptions that have been considered in this step in a very roughly way, it has been assumed that the *TMS* has been oversized.

7.3 DETAILED DESIGN OF THE BATTERY PACK AND THERMAL MANAGEMENT SYSTEM

Once the application design criteria have been defined and the *BP* and its *TMS* have been predesigned (Sections 7.1 and 7.2), detailed models of the complete system have been developed to verify the proposed design. The aim of this section is to develop detailed thermal models that by means of them, it could be possible to check if the previously defined design criteria are fulfilled by the predesigned system or not prior the construction of a sample prototype. This objective has been achieved carrying out transient simulations of the scaled complete system at *BM* level, together with its complete *TMS*. Moreover, as in the previous case, the heat generation model has been thermally coupling in the selected simulation tool by means of a Modelica subroutine

which is shown in Appendix 2B. Although for the objective of this step only the thermal model at *BM* level has been used, in Figure 7.13, up and down, are shown the exploded drawings of the design at *BM* and *BP* level respectively, considering the decisions that have been taken in the previous predesign step.

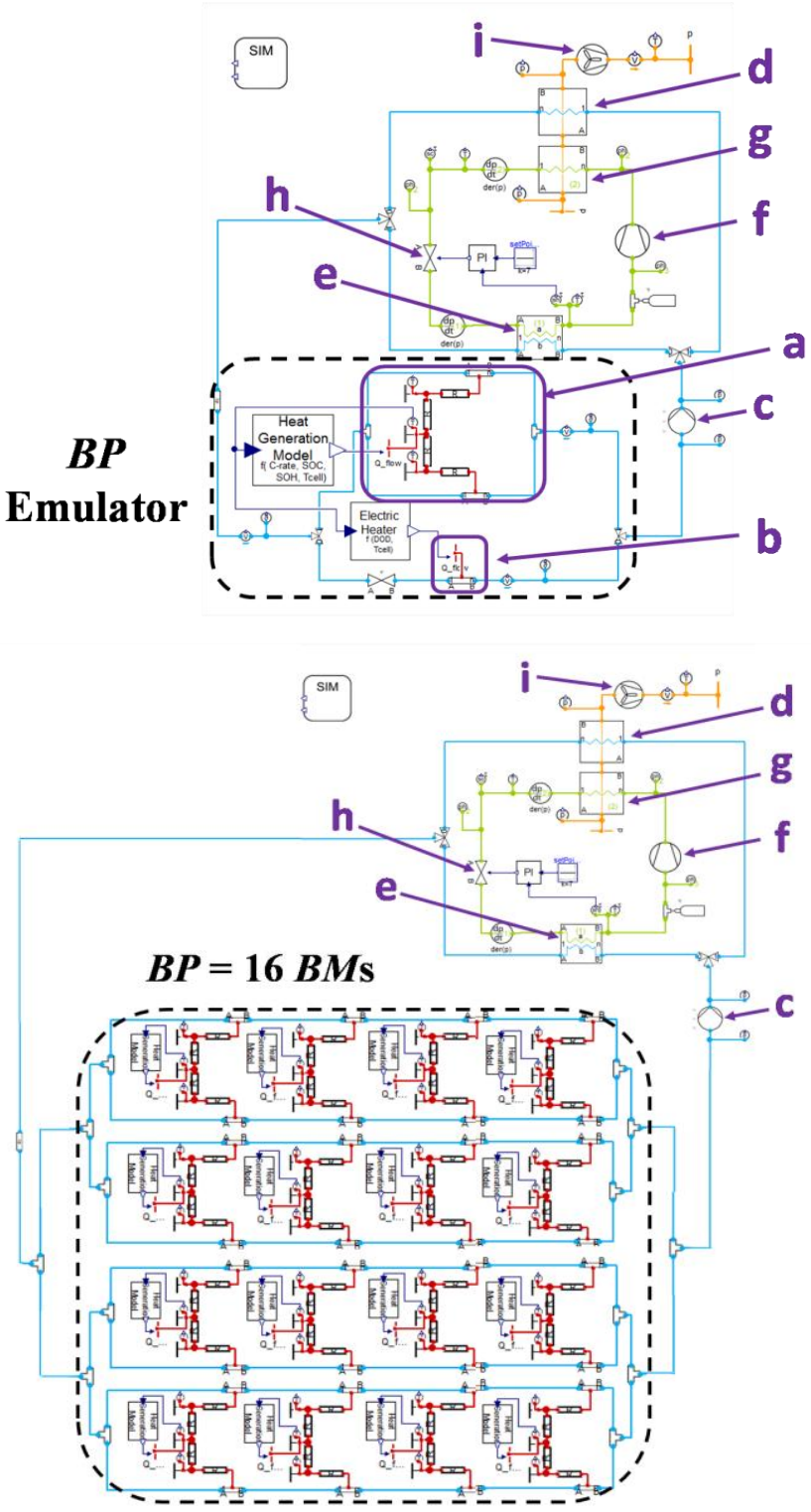

Figure 7.13 Developed thermal model at BM (up) and at BP (down) level.

As it is shown in Figure 7.13 (up), the *BP emulator* is modelled by means of 1D-lumped *Cauer Equivalent Circuit*, (*CEC*) based on a circuit composed of thermal capacities and resistances. The *BP emulator* is comprised of unique *BM* with its cold plates (Figure 7.13 (a)) together with the electric heater (Figure 7.13 (b)), which emulates the heat provided by the other 15 *BM*s of the complete *BP*. Nevertheless, in Figure 7.13 down, each *BM* is modelled allowing the numerical analysis of the thermal dispersion between *BM*s within the complete *BP*.

The *BM* and the cold plates which are shown in Figure 7.13 (a), have been modelled based on the research work carried out by N. Nieto in [68] using for that purpose *CFD* simulation tool. In Figure 7.14 (a) and (b) are shown the models related to the cell and *BM*, and the cold plate, respectively.

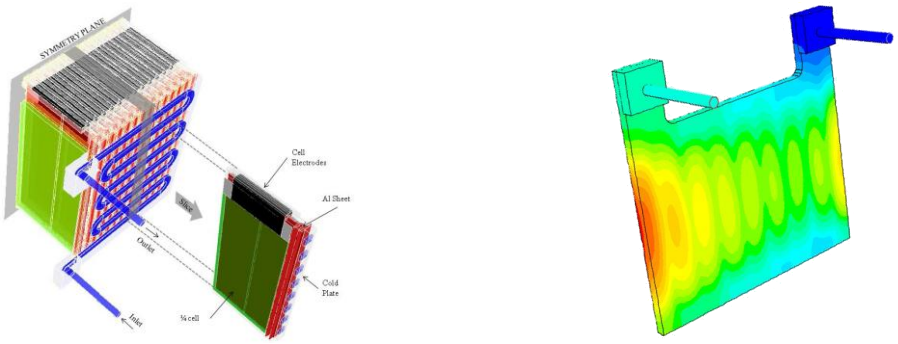

(a) (b)

Figure 7.14 Detailed thermal models of the cell, BM and cold plates developed in CFD simulation tool by N.Nieto [68]

N. Nieto by means of her research work has been demonstrated that for a flow rate no higher than 1 lpm and for similar electrical requirements than for the bus lines proposed for the urban electric minibus in this research work, the thermal dispersion within the *BM* is lower than 1 ºC [68]. Based on this statement, in the lumped model developed in *Dymola/TIL* at *BM* level, it has been assumed a null thermal dispersion among the 12 cells of the *BM*. Therefore, a unique characteristic temperature has been considered, in the same way as for the solid part of the cold plate. These temperatures will be compared later against the experimentally measured mean temperatures.

The thermal capacities and resistances of these components, *BM* and its cold plates, have been determined using the "Thermal Resistance Analysis by Induced Transient" (*TRAIT*) method [116, 117]. The methodology employed is graphically illustrated schematically in Figure 7.15 which is composed of three principal steps. The first step has consisted of applying a constant heat power by means of the developed experimentally validated *3D CFD* models (Figure 7.14), separately both for regarding the *BM* and the cold plates. Once the steady state of the temperature of each component has been reached, the heat power has been shutdown instantaneously and the transient thermal relaxation of both *BM* and cols plate has been registered. That is the basis of the second step. As an example, in Figure 7.15 the obtained curves for different tested conditions related to heat power, temperature or even, liquid mass flow rate can be observed. From these curves the representative and simplified lumped *1D* thermal impedances are obtained. That is the third and the last step of this methodology.

It is worth mentioning that as it can be observed in Figure 7.15, the *3D CFD BM* model only represented half of the real system, assuming a symmetric cooling power on both cold plates. Therefore, the thermal capacity of the *BM*, C_{BM}, that it has been included on the thermal equivalent circuit was double that obtained directly from this analysis.

The *BM* thermal capacity and resistance values, C_{BM} and $R_{1/2BM}$ respectively, are constant values that provide a simplified representation of its heat diffusion, whereas the values obtained related to the thermal capacity and resistance for the cold plates, C_{CP} and R_{CP}, depend on the liquid volumetric flow rates (V_{flow} in lpm) that circulate through it, as can be seen in Figure 7.15. The heat generated in *BM* is transferred to the liquid cooling loop of the *TMS* using a variable heat port, connected to a nude Liquid Tube model that represents each of the cold plates. The hydraulic performance of each cold plate, ΔP, has been likewise obtained from the *CFD* simulations for variable volumetric flow rates. The equation which defines this performance is defined in Figure 7.15.

These both models, as it can be seen in Figure 7.13 (a) which have been used to analyze the *BM* temperature evolution due to instantaneous heat generation. The instantaneous heat power generated in the *BM*, as in the same way than in the previous case study, has implemented in Modelica language as a specific subroutine (Appendix 2B).

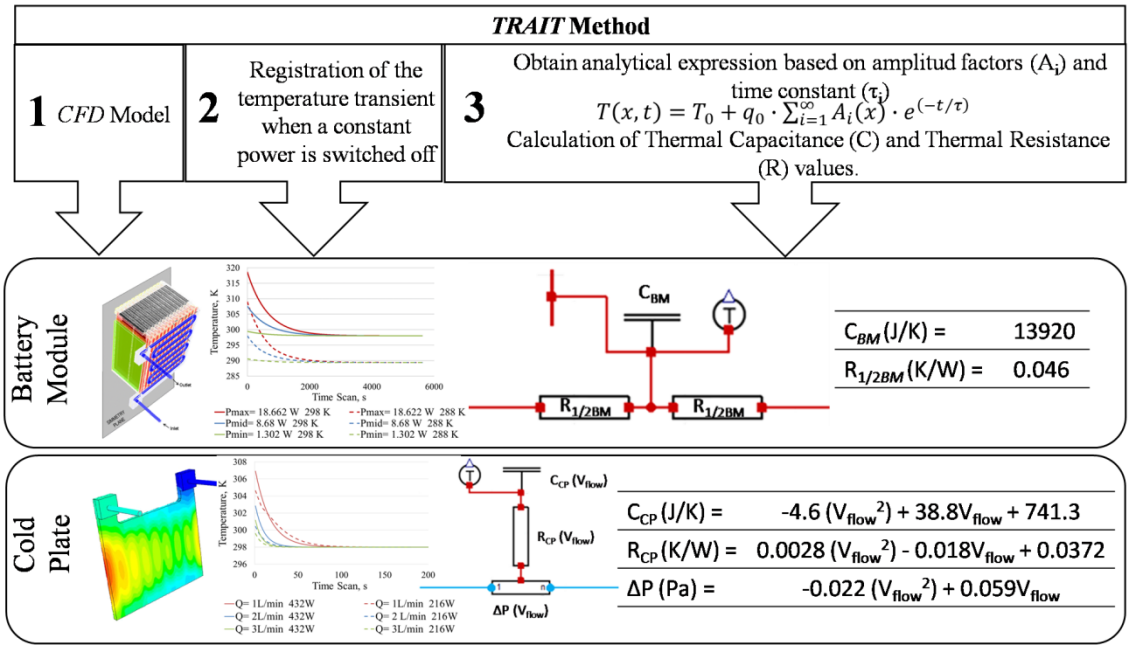

Figure 7.15 Thermal characterization methodology carried out to obtain CEC for BM and cold plates.

The electric heater, which as it has been explained before, it has been used to emulate the heat that would generate 15 *BM*s, has been modelled by a variable heat port which introduced the extra heat amount in a common liquid tube model, as it can be seen in Figure 7.13 (b). Another subroutine has generated in Modelica that generates the heat for the electric heater model in the same way as in the experimental validation, but using simulated *BM* temperature readings instead of real temperature measurements. The *SOC* range used in each experimental test has defined such as input and, by t he look-up table which is shown in Figure 7.16, the heat that would be provided by the electric resistance has interpolated in function of the instantaneous cell temperature.

		SOC, %								
		80-60	60-40	40-20	80-50	70-40	65-35	80-40	70-30	60-20
BM Temperature, K	278.2	-1194.0	-1263.4	-1415.2	-1216.6	-1251.4	-1278.4	-1228.8	-1288.9	-1339.3
	283.2	-1046.6	-1094.7	-1232.9	-1062.7	-1085.8	-1107.6	-1070.7	-1118.1	-1163.8
	288.2	-899.1	-925.9	-1050.6	-908.8	-920.2	-936.7	-912.6	-947.3	-988.3
	293.2	-751.7	-757.2	-868.3	-754.9	-754.6	-765.9	-754.5	-776.5	-812.8
	298.2	-604.3	-588.4	-686.1	-601.0	-589.0	-595.1	-596.4	-605.7	-637.3
	303.2	-526.9	-519.5	-591.0	-525.0	-519.1	-523.5	-523.2	-530.5	-555.3
	308.2	-449.6	-450.6	-495.9	-449.0	-449.1	-451.8	-450.1	-455.4	-473.3
	313.2	-372.2	-381.7	-400.8	-373.0	-379.1	-380.2	-377.0	-380.2	-391.3
	318.2	-342.4	-350.5	-371.2	-342.9	-348.7	-350.5	-346.5	-350.8	-360.9
	323.2	-312.5	-319.3	-341.7	-312.8	-318.2	-320.8	-315.9	-321.5	-330.5
	328.2	-241.9	-251.3	-272.6	-243.4	-249.2	-252.3	-246.6	-252.9	-262.0

T_{cell}, K

Heat

Figure 7.16 Interpolation table data for the heat (W) must be provided by the electrical heater.

With regards to the *TMS*, the proposed dual architecture has been comprised of electromechanical and heat exchange components. The first group includes the hydraulic pump (Figure 7.13 (c)), the fan (Figure 7.13 (i)), the compressor (Figure 7.13 (f)) and the expansion valve (Figure 7.13 (h)); whereas the second group would include all of the heat exchangers such as the *FC* radiator (Figure 7.13 (d)), *AC* evaporator (Figure 7.13 (e)) and *AC* condenser (Figure 7.13 (g)).

As it can be seen in Figure 7.13, two control valves make possible the use of *FC* loop (blue line) or *AC* loop (green line) system to cool down the *BP* and ultimately to dissipate the heat to the surrounding air (orange line) in both scenarios.

The electro- mechanical components have been mainly modelled by their performance characteristics vs. power consumption curves provided by the manufacturers. Whereas the heat exchanger components have been modelled taking into consideration their specific geometry and suitable correlations in order to predict their thermal and hydraulic performance correctly.

The fan (Figure 7.13 (i)) and the pump (Figure 7.13 (c)) have modelled as fixed velocity components. Their performance has based on the conversion of mechanical power into pressure increase in an incompressible fluid. The fan supplied air mass flow rate in function of the combined pressure drop of the air side of the *AC* condenser and *FC* radiator simultaneously. This pressure drop value has been evaluated using some air pressure sensors, as it can be seen in Figure 7.17. By the performance curves provided by the manufacturer the mass flow rate has been calculated and also, the power consumption (Figure 7.17).

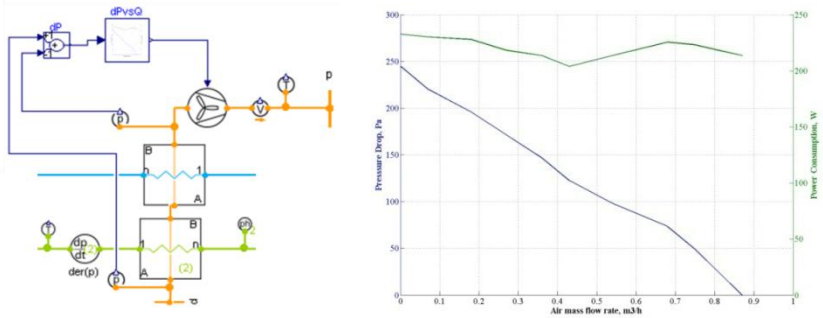

Figure 7.17 Developed fan model in TIL library with its corresponding performance curves.

In the same way it has defined the liquid mass flow rate that the hydraulic pump should supply. Pressure drop in the liquid circuit has been evaluated by means of some liquid pressure sensors which are shown in Figure 7.18. The pump performance curves related to the liquid flow rate vs. pressure drop and the power consumption are shown in Figure 7.18.

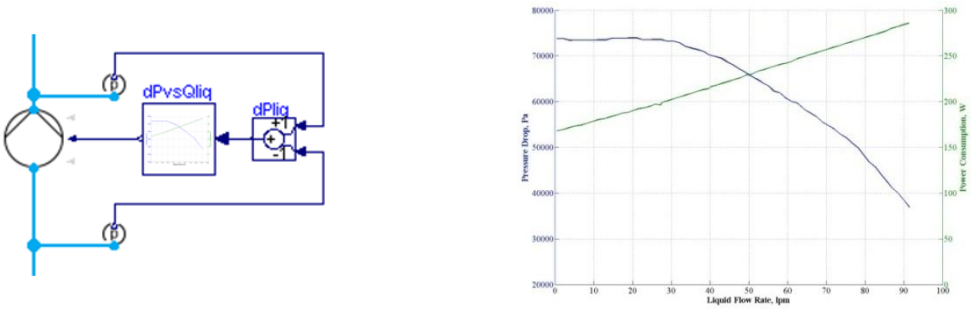

Figure 7.18 Developed pump model in TIL with its corresponding performance curves.

With regards to the compressor, (Figure 7.13 (f)), a variable speed compressor has modelled using its data sheet provided by the manufacturer. In Figure 7.19 is shown the compressor developed model using TIL library. The required rotational speed and power consumption of the compressor has been calculated by means of several complex polynomial functions adjusted by a set of coefficients. These defined coefficients, ci and cj, for the estimation of the rotational speed and power consumption respectively are provided by the manufacturer. As it is indicated by Eq. (7.1), the compressor rotational speed, ω, is function of the heat that must be dissipated from the *BP* ,Q_{Dis}, of the suction dew point temperature calculated from the suction pressure, *Tevap*, and the discharge dew point temperature calculated from the discharge pressure, *Tcond*. The power consumption, P, apart from the influence of the *Tevap* and *Tcond* as it is indicated in Eq. (7.2), also it depends of the rotational speed, ω, previously defined.

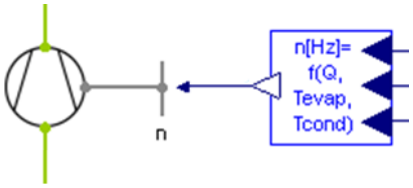

Figure 7.19 Developed compressor model in TIL.

$$\omega = f\left(Q_{Dis}, T_{evap}, T_{cond}\right) \tag{7.1}$$

$$P = f\left(\omega, T_{evap}, T_{cond}\right) \tag{7.2}$$

The actual *TXV* has 1.4 mm orifice and it has been controlled by a Proportional-Integral (*PI)* controller with a proportional gain of 0.3 and with a time constant of 120 s. The dynamics of the valve have been dominated by the response of the sensing bulb which has been modelled usually using the first-order element with a time constant of 1 s. In this model it has assumed that there has no transient mass storage across the *TXV*. Moreover, the throttling process has considered isenthalpic, i.e.., $h_{in} = h_{out}$ and the mass flow rate was calculated by an approach based on Bernoulli´s equation using Eq. (7.3).

$$\dot{m}_{in} = \dot{m}_{out} = A_{eff}\sqrt{2 \cdot \rho_{in}(p_{in} - p_{out})} \tag{7.3}$$

Where $\dot{m}_{in}$ and $\dot{m}_{out}$ are the inlet and outlet mass flow rates, respectively, A_{eff} is the effective flow area of the valve, ρ_{in} is the inlet refrigerant density and p_{in} and p_{out} are the inlet and outlet pressures, respectively.

Heat exchangers have been the more complex component to model in this selected design tool and they have developed mainly considering the work and the experience of Kossel [118] and Ahlbrink [119]. All the heat exchanger models have based on 1D Finite Volume Method (*FVM*) which means that they are composed using fluid cells to model the fluids flows and the wall [120].

The evaporator has modelled by a parallel flow, whereas the condenser and the radiator were modelled by a cross flow configuration. For all heat exchanger models a discretization of 5 cells has been used, defining this number considering a compromise between simulation time and results accuracy. Physical geometry description and material definition of each heat exchanger have been used to calculate the external and the internal heat exchange surfaces, and the internal and external cross-sectional flow areas. This information has been used in each fluid, refrigerant, gas and wall cell to calculate the internal and external heat transfer coefficients and heat flow at each time step based on the implemented heat transfer correlations [121]. Pressure drop is modelled in the same way using the correlation implemented in the *Dymola*/*TIL* simulation tool. The pressure drop correlations that have been used for this particular case are defined in Table 7.4 and Table 7.5.

The *FC* radiator and *AC* condenser have been heat exchangers composed of multi-port extruded tubes, *MPET*. The *FC* radiator has been a liquid- air heat exchanger,

whereas the *AC* condenser has been a refrigerant-air heat exchanger. In the former, the primary fluid was a mixture of a 50/50 *WEG*, whereas in the latter it was R-134a refrigerant. In both cases incompressible air has used as a secondary fluid, releasing the heat out of the system.

The detailed geometry values together with the correlations used to fully define the *FC* radiator and *AC* condenser are summarized in Table 7.4.

Apart from the electro-mechanical and heat exchanger components previously described, there were other components that they should be defined, the pressure states. As it is explained by M. Gräber et al. in [122], these components in a compressive system only are referred to a system pressure level and they provide the benefit of improving the numerical speed because it has considered the term dp/dt (time derivative of pressure) in the balance equation as constant along the direction of flow for each pressure level of the system. Gräber [122] also highlighted that it does not mean that it was constant over the time. Moreover, Lemke [90] demonstrated that this approach is appropriate for processes that are not characterized by fast dynamics such in this particular case

In the developed both models a convergence criterion has been defined in order to determine when the numerical procedures described have converged to a solution in the thermal models. As it is proper to an effective thermal cyclic state, the defined convergence criterion has been to ensure that, in all cases, integral values of the heat dissipation profiles have been equal to the integral values of the heat generation profiles.

The simulations have carried out by means of Dassl algorithm with a tolerance of 0.001. Dassl is one of the most used simulation code on the today market and also, in *Dymola* problems. *Dymola* was designed to be used in a large-scale system modeling with complex models are almost stiff related to simultaneously at phenomena with different time constants. Generally, *Dymola* users don´t know whether their models are stiff or nor and in this situation, it is preferred to use a stiff-system solver which is capable of dealing with non-stiff models as well, and not vice versa. Dassl is stiff-system solver which provide this feature. Also, there are another stiff-system solvers such as Radau II but it is currently as robust and well tested as the Dassl code.

.

Table 7.4 Description of radiator and condenser parameters in Dymola/ TIL.

			Radiator	**Condenser**	
Geometry	General	HxWxD, mm	400 x 400 x 42	396.3 x 430.1 x 25.4	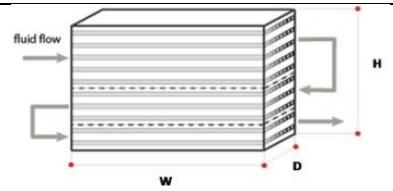
		Passes	70	3 (20/ 10/ 5)	
	Tube Side	Material	Aluminium		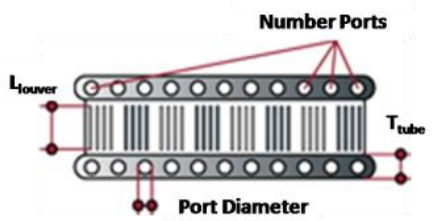
		Ports/ tube	1	13	
		A_{port}, mm^2	36.9	2.13	
		P_{port}, mm	40.1	5.84	
		T_{tube}, mm	2	2	
	Fin Side	T_{Fin}, mm	0.14	0.14	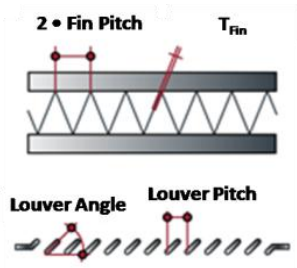
		Pitch, mm	5	5	
		Louver Pitch, mm	1.21	1.1	
		Louver Angle, °	27	27	
Correlations	Liquid/ Refrigerant Side	*HTM*	Gniesliski DittusBoelter [123, 124]	Steiner and Shah [125, 126]/ DittusBoelter [124]	
		PDM	Swamme Jain [124]		
	Air Side	*HTM*	Chang and Wang [126]		
		PDM	Kim and Bullard [127]		

Table 7.5 Description of evaporator parameters in Dymola/ TIL.

			Evaporator	
Geometry	Outside	Nº Plates	46	
		L, mm	292.5	
		W, mm	75	
		phi	35	
	Inside	T_{wall}, mm	0.2	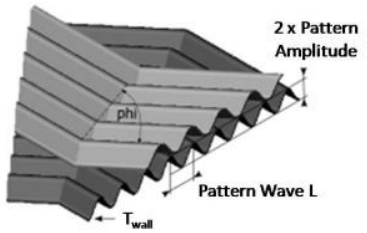
		Pattern Amplitude, mm	2.5	
		Pattern Wave L, mm	0.14	
Correlations	Liquid Side	*HTM*	VDI plate alpha for one phase fluid [128]	
		PDM	for Chevron Plates and one phase fluid [129]	
	Refrigerant Side	*HTM*	Steiner and Shah [124, 125]/ Dittus Boelter [123]	
		PDM	for Chevron Plates and one phase fluid[129]	

Once detailed models have been defined and developed, some transient simulations have been carried out in order to check numerically if the design criteria will be fulfilled or not with the proposed first design. For that purpose, the representative cyclic current profile (1C/1C) defined in Table 3.5 has been used.

Three different *DOD* ranges (*SOC* 60-40%, SOC 65-35 and *SOC* 70-30%) have been taken into account with a middle *SOC* value of 50%. In addition, tree different ambient temperatures have been considered that differ depending on the selected cooling mode: for the *FC* mode an ambient temperature range from 15 ºC to 35 ºC has been defined, whereas for *AC* mode from 25 ºC to 45 ºC. The reduced test matrix is shown in Table 7.6.

Table 7.6 Test matrix for verification of the fulfilment of design criteria at BM level

	C-rate	***SOC, %***	***DOD, %***	**T_{amb}, ºC**	**Test**
FC	1C/1C	60-40	20	15	1
		65-35	30	25	2
		70-30	40	35	3
AC	1C/ 1C	60-40	20	25	4
		65-35	30	35	5
		70-30	40	45	6

The verification of the fulfilment of the design thermal criteria by means of the model at *BM* level which is shown in Figure 7.13 (up), has been focused on the thermal performance of the *BM*, evaluating the averaged temperature of the thermal capacitance which represents the complete *BM* (Figure 7.13 (a)), of the last two discharge- charge cycles for each test. In contrast to the previous analyzed application, in that case it has not been possible to analyze the thermal dispersion between the cells because of the *1D* lumped model that it has been modelled the *BM*. In Table 6.7 are shown the simulation results obtained for the previous defined six tests.

It is worth mentioning, although it is stated above, that the thermal performance of the electric heater has not assessed because it has only used with the aim to generate the extra heat that should generate the designed complete *BP* and should be dissipated by the *TMS*.

Table 7.7 Simulation results obtained from the detailed thermal models for the test conditions defined in Table 7.6

		T_{BM}avg, ºC
FC	Test 1	21.7
	Test 2	30.0
	Test 3	38.8
AC	Test 4	17.6
	Test 5	20.2
	Test 6	20.7

As it can be concluded, the *AC* mode enables *BM* temperature to be kept below the ambient temperature and close to the ideal temperature defined in the specifications. This is possible thanks to the compressor, but in exchange leads to higher system power consumption than *FC* mode. Nevertheless, with the *FC* system, the *BM* temperature is kept higher than ambient temperature, but in all cases studied it is below the limit temperature defined in thermal requirements in Section 6.1.

Moreover and considering the thermal performance of the *TMS*, in Figure 7.20 are shown the *P-h* and *T-s* diagrams related to the tests carried out with *AC* mode at (a) 25 ºC (Test 4), (b) 35 ºC (Test 5) and (c) 45 ºC (Test 6) of ambient temperature. They represent an arbitrary state of the refrigeration cycle at each ambient condition. In *P-h* and *T-s* diagrams four points could be distinguished in the cycle which are coloured by green. The point number 1 is related to the outlet zone of the evaporator, point number 2 represents the outlet zone of the compressor, point number 3 corresponds to the outlet zone of the condenser and the point number 4 is referred to the outlet zone of the expansion valve. Red lines of the *P-h* diagram corresponds to isothermal lines, highlighted by dashed blue lines the refrigerant temperature in the evaporator and in the condenser. On the other hand, in *T-h* diagram pink lines are the isobaric lines.

These diagrams make possible an easier understanding of the refrigeration cycle. It is clearly seen that the state change of the refrigerant in the evaporator (liquid to gas) and also in the condenser (gas to liquid), has been carried out in a constant pressure state. Moreover, it can be concluded that when the ambient temperature increases the mechanical work that must be done by the compressor has been higher. This effect can be seen considering the pressure difference between point 1 and 4 in each diagram: 5.6,

9.2 and 12.9 bar for the refrigerant cycle with an ambient temperature of 25, 35 and 45 ºC, respectively.

The cooling capacity has been evaluated by the enthalpy difference between the point 4 and 1 displaced through the isobaric line until the saturation curve. The difference between this previous point and the actual position of the point 1 is representing the overheating of the refrigerant at the end of the evaporator. In this type of system, it is recommendable to have enough overheating which ensures that the refrigerant that enters into the evaporator is in gas state. On contrary, from the refrigeration cycle point of view it was ideally to keep this point on the saturation line in order not to increase the work that compressor should do, and therefore its consumption. Regarding the point 3 of the refrigeration cycle and the distance until the saturation liquid line is representing the subcooling phenomena. The subcooling is advantageous from the point of view that it increases the cooling capacity of the refrigeration cycle, but in the negative view, it supposes an oversizing of the condenser.

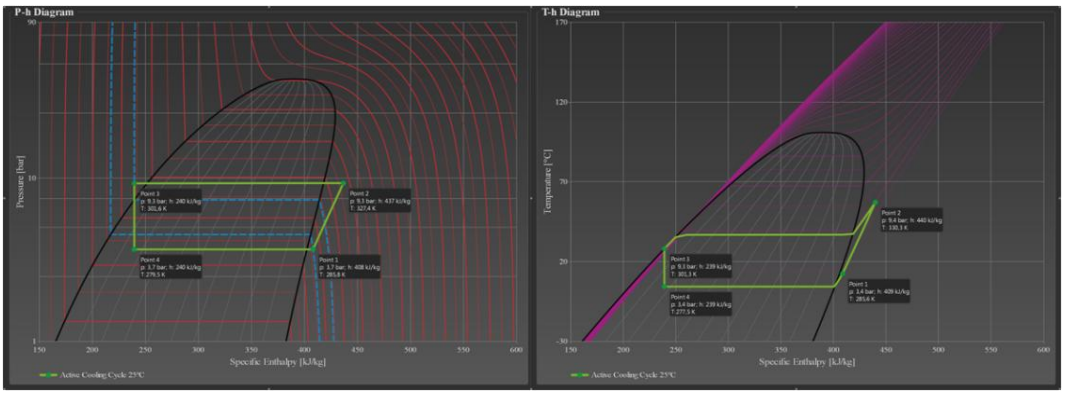

(a)

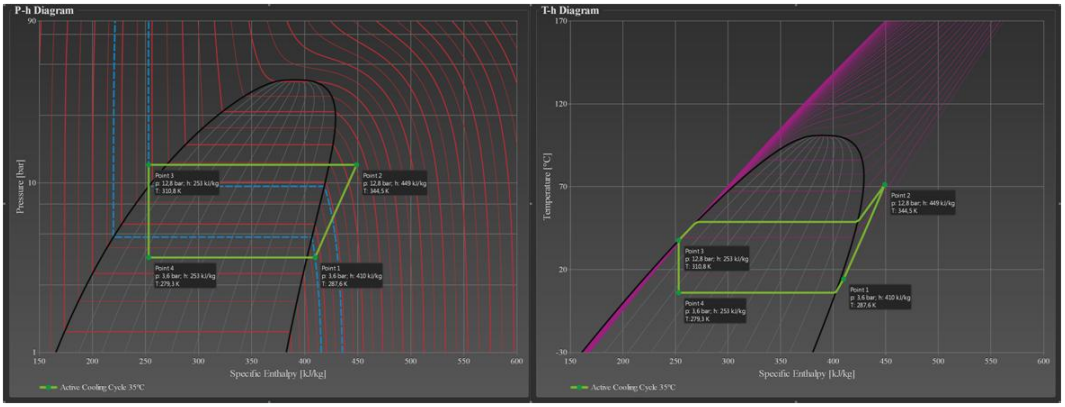

(b)

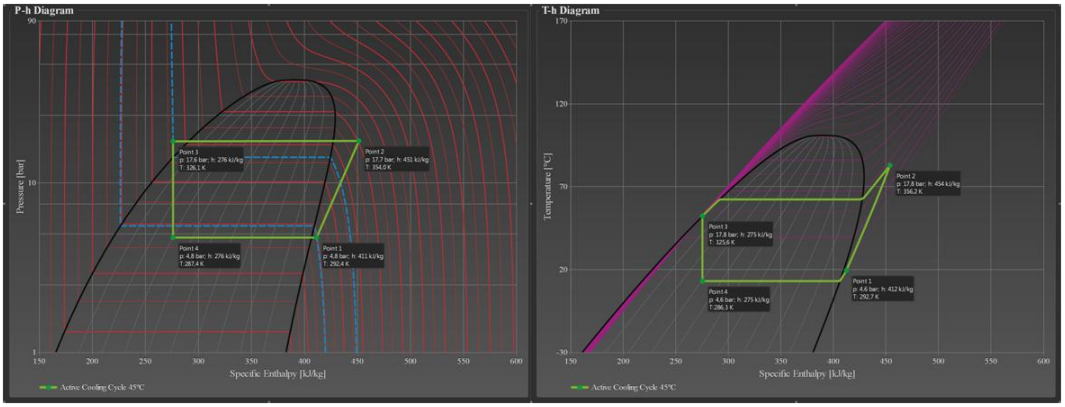

(c)

Figure 7.20 P-h diagram (up) and T-h diagram (down) referred to AC mode for (a) 25 ºC, (b) 35 ºC and (c) 45 ºC ambient temperatures.

To concluded, and mainly based on the results show in Table 6.7, it can be said that the representative *BM* temperature has been maintained for any cooling mode, any ambient and electrical conditions within the admissible operation range considering the temperature range defined in Section 7.1 in Table 7.1. Considering the results obtained firstly related to *FC* mode, it can be said that even for the maximum tested ambient temperature (35 ºC) that it has been a margin of around 16 ºC, whereas for *AC* mode for any operating conditions, the *TMS* has been able to keep the *BM* near the ideal operation range, between 20 ºC and 30 ºC. Consequently, it has been obvious that the proposed *TMS* in this predesign step has been oversized as it was expected due to all the assumptions have been considered during the predesign. This statement has opened the window to the possibility to optimize the *TMS* in the next steps of this methodology.

7.4 THERMAL MODELS VALIDATION

The objective of the validation step has been to check if the assumptions that have been considered during the thermal modeling process represent well enough the real performance which it has been intended to be emulated by means of the developed detailed simulation models. For that purpose the construction of the system prototype has been carried out. In Figure 7.21 is shown the constructed prototype in the laboratory environment, i.e., on the left side it can be seen the *BP* emulator (*BM* + electrical heater) and on the right side it can be seen the constructed prototype of the *TMS*.

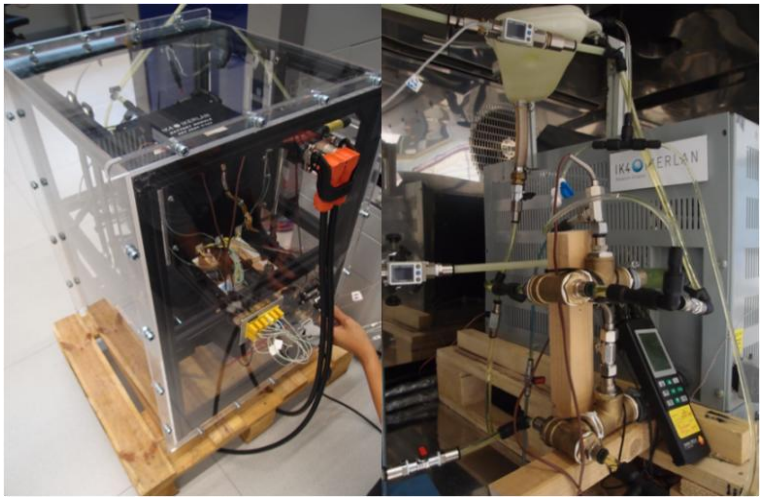

Figure 7.21 Constructed real prototype at BM level.

The test set-up which is shown in Figure 7.22 has been defined to carry out the experimental tests.

As it has been explained in Chapter 5, in order to validate the developed detailed thermal models by means of a real prototype, a unique *BM* has been used because on the one hand, it has been unviable to construct the complete *BP* at reduced laboratory environment and on the other hand, due to it has not been the appropriate facilities in terms of cyclers to operate with the complete *BP*. In contrast to the previous test case, in this case not only a single *BM* has been used, as it has been explained in the predesign section (Section 7.2), an electric heater has been used to simulate the complete heat generated by the other 15 *BM*s. The *BM* that has been used, it has been developed in IKERLAN and it is indicated by letter a in Figure 7.22, whereas the selected electric heater of 2 kW is indicated by letter b in Figure 7.22.

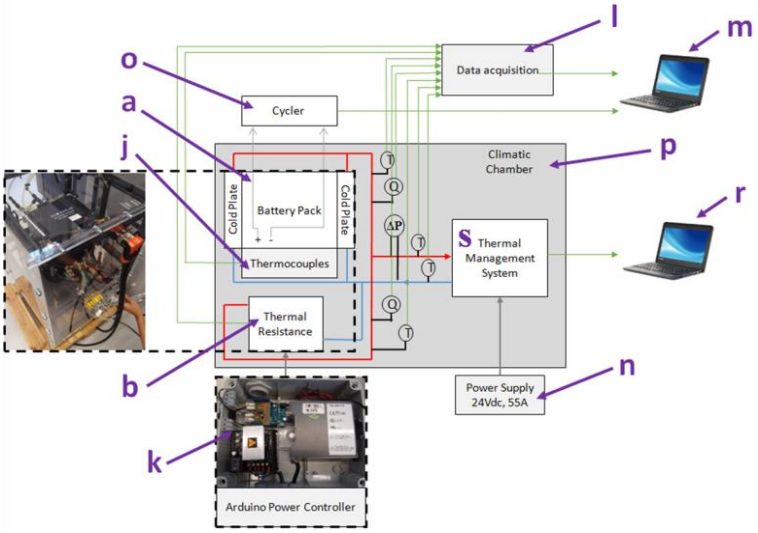

Figure 7.22 Test set- up for the experimental measurements on prototype constructed.

Regarding the electric heater performance, it has been dynamically controlled by a specific controller which used a Arduino card (Figure 7.22 (k)). The heater must operate in the same electric solicitations placed on the single *BM* during the validation process. For that purpose, the controller has been capable of reading the actual mean temperature on the *BM* every second by Negative Temperature Coefficient (*NTC*) places in the interior of the *BM* and of providing an adequate supply value of heat to the electric heater by a calibrated power regulator, interpolating linearly from the matrix showed in Figure 7.16. In Figure 7.23 can be seen the components of the control system: Arduino Leonard card, power supply of 12V and power regulator.

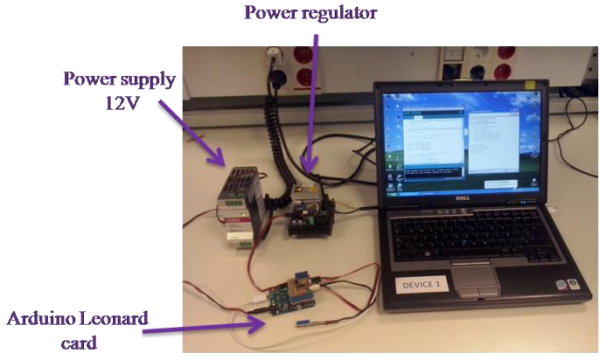

Figure 7.23 Components of the control system.

The *TMS* is indicated by s in Figure 7.22. and more in detail is shown in Figure 7.24. All components have been identified in the same manner as in the Figure 7.13: the hydraulic pump (c), fan (i), the compressor (f), the expansion valve (h), radiator (d), *AC* evaporator (e) and *AC* condenser (g).

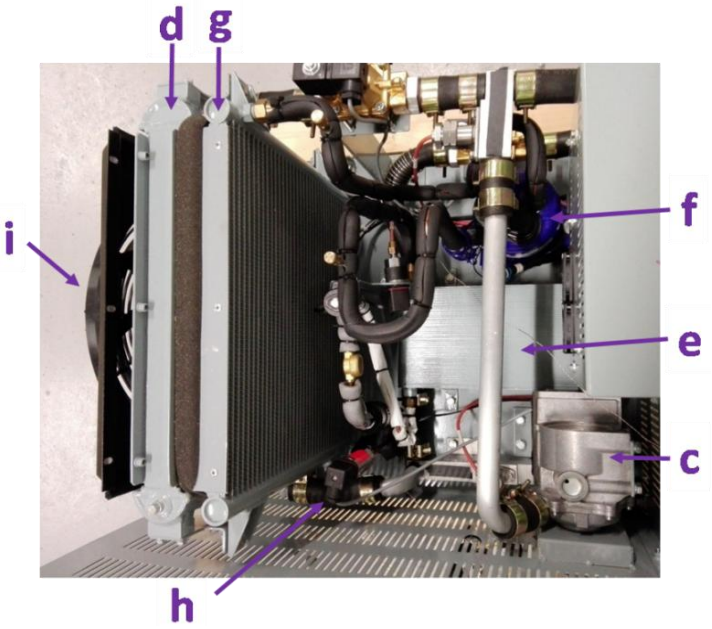

Figure 7.24 TMS with its different components (c-i).

In respect of measuring the representative mean temperature of the *BM*, 8 type K thermocouples located inside of it have been used (Figure 7.22 (j)).The measurement accuracy of this type of thermocouple has been of ± 1.5 ºC. On the other hand, the temperature of the liquid has been measured using 4 type T thermocouples, both of them located in the outlet zone of the cold plates and the electric resistance and the other two, at the *TMS* inlet and outlet zones. In Figure 7.22 are indicated by T. This type of thermocouple has a measurement accuracy of ± 0.2 ºC.

TESTO 312-4 electronic differential pressure gauge which made possible to measure the *TMS* pressure difference considering the liquid side. Its accuracy has been around ± 0.5% for a variable full scale, ranging from 0 to 25 bar. The points between which the pressure different has been measured are represented in Figure 7.22 by means of P .

Finally, regarding the volumetric flow rate measurement two flowmeters have been used to measure the liquid flow rate in the outlet zone of the cold plates (SMC PF3W740-F03-DT-M) and at the exit of the electric resistance (SMC PF3W720- F03-DT-M). The expected error of these flowmeters has been of ± 3% of the full scale, ranging from 0.5- 4 lpm and 2-16 lpm respectively. Both flowmeters are indicated in Figure 7.22 by Q.

These measures, as well as *TMS* power consumption, have been recorded during the tests using a multichannel Data Acquisition card (Figure 7.22 (l)) and a computer (Figure 7.22 (m)). The *TMS* has been connected and monitored by an N8737A Power Supply (Figure 7.22 (n)). The refrigerant circuit variables, such as evaporating and condensing temperature and pressure, compressor and pump speed, and ambient temperature have been monitored by the *TMS* control software developed in LabVIEW (Figure 7.22 (r)). In Figure 7.25 is shown the software interface.

On the other hand, the *BM* has been connected to an IBT programmable cycle running Digatron/ Firing Circuits BTS600 software for data evaluation and for cell charging and discharging (Figure 7.22 (o)). This has enabled in situ *BM* current and voltage value measurements to be conducted, amongst other electrical variables. Moreover, the cycler has limited the cell voltage during charge/ discharge, preventing overcharging/ discharging.

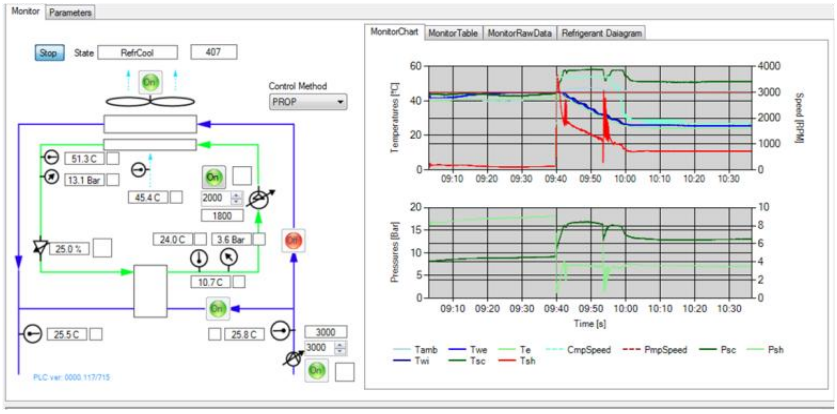

Figure 7.25 Programmed LabVIEW software for the TMS performance.

All tests have been carried out using the same CTS climatic chamber (Figure 7.22 (p)) with a precision of ± 0.3 K to maintain the desired ambient temperature for each test.

The *TMS* has been into the climatic chamber, whereas the *BM* and the heater have been thermally isolated by a methacrylate enclosure keeping outside of the climatic chamber, as it can be seen in Figure 7.21.

Once the experimental prototype has been completely constructed, the experimental tests have been carried out considering the same conditions defined in Table 7.6 in order to prove the correctness and reliability of the simulation results.

As it has been described in Chapter 5, the same procedure has been followed to perform all the experimental tests: first, the ambient temperature has been set for the climatic chamber until all objects have reached the same uniform temperature. Then, the cells of the *BM* have been fully charged (*SOC* 100%) and then have discharged to the initial *SOC* value defined for the corresponding test. Finally, the *TMS* has turned on in the desired cooling mode, *FC* or *AC*. Once everything has been ready for the test to be initiated, the *BM* has continuously discharged and charged between the defined *SOC* limits, until system has been stabilized thermally. The cycler program that has been used for each experimental test can be seen in Appendix 3B.

The validation task by means of these experimental tests has divided into two steps, in the first one the dynamic thermal performance of *BP* emulator has analyzed focusing the attention on the *BM*, whereas in the second step the thermodynamic variables and power consumption of the *TMS* have studied.

For the first step defined, the transient experimental temperature measurements obtained while the *BM* was cycling has considered. It is worth mentioning, although it is stated above, that the thermal performance of the electric heater has not assessed, because it has only used with the aim to generate the extra heat that should generate the designed complete *BP* and should be dissipated by the *TMS*.

Figure 7.26 and Figure 7.27 compare the experimental mean temperature measurements over the *BM* cells (red lines) with the temperature of the heat capacitor that represents this component in the developed model (red dashed lines) for the 6 tests defined in the test matrix shown in Table 7.6. The experimental temperature profiles have calculated as a mean of the different temperatures measured with the sensors located inside the *BM*, as it has observed that temperature differences over the surface of the cells have not exceeded 2 ºC. As clarification, Figure 7.26 results are referred *FC* system whereas the results shown in Figure 7.27 are related to *AC* mode. Considering the curves shapes of temperature variations, it can be concluded that the model predictions closely follow the experimental measurements and it seemed that both thermal inertia and thermal resistance at *BM* level have accurately represented.

Moreover, the secondary y-axis of Figure 7.26 and Figure 7.27 represent the dissipated and generated heat for *FC* and *AC* modes, respectively. The *BM* experimental and numerical instantaneous heat dissipation profiles have plotted by dark and light blue lines respectively, while simulated heat generation profiles have charted by green dashed lines. It is obvious that the experimental heat generation rate could not be plotted because it has no possible to measure it directly. The rate of heat released from the *BM* has calculated by Eq. (5.1) and it has implemented in *Dymola* environment using the experimental current and *SOC* profiles as inputs. Moreover, the numerical and experimental heat dissipation profiles have calculated using Eq.(7.4) considering the heat released from the inside of the *BM* to the liquid via cold plates.

$$\dot{q}_{dis} = Cp \cdot \dot{m} \left(T_{out\_CP} - T_{in\_CP} \right) \tag{7.4}$$

Considering the temperature and heat power results profiles together, *Figure 7.26* and *Figure 7.27*, it can be observed that when the liquid inlet temperature is higher, the heat which is needed to be dissipated from the *BM* is lower. This effect can be easily seen considering the results of the *FC* mode, Figure 7.26, where the liquid temperature

increases with the ambient temperature. On contrary, when *AC* mode is used (Figure 7.27), this effect is not possible to concluded because due to the influence of the compressor the liquid temperature is kept more or less at the same temperature without dependency of the ambient temperature and therefore, the generated heat rate of the *BM* is in general terms the same. As it was explained for the previous case study, this effect between the liquid temperature and heat generation rate is consequence of the influence that the temperature has on the internal resistance and hence, on the heat generation rate. At low temperatures, the internal resistance of the battery increases and consequently, the amount of the heat generation; while at high temperature the opposite occurs.

In addition to both figures can be observed, Figure 7.26 and Figure 7.27, that temperature increases during the discharge time intervals, when heat generation exceeds heat dissipation. Likewise, temperature decreases during charge time intervals, when heat generation is less than the heat dissipation. The amplitude of the temperature variation in each of the discharge-charge cycle has also well captured.

Considering the last two discharge-charge cycles for each test, the maximum time-averaged difference between the experimental and predicted temperature profiles have calculated in **¡Error! No se encuentra el origen de la referencia.**. For the *FC* mode this difference has been no higher than 0.4 ºC, while for the *AC* mode it has maintained below 0.7 ºC.

Table 7.8 Numerical, experimental and the difference between them regarding the average BM temperature.

		T_{BM}max, ºC		
		Numerical	Experimental	Difference
FC	Test 1	21.7	21.3	0.4
	Test 2	30.0	29.8	0.2
	Test 3	38.8	39.0	0.2
AC	Test 4	17.6	18.3	0.7
	Test 5	20.2	20.7	0.5
	Test6	20.7	21.1	0.4

FC
Test 1
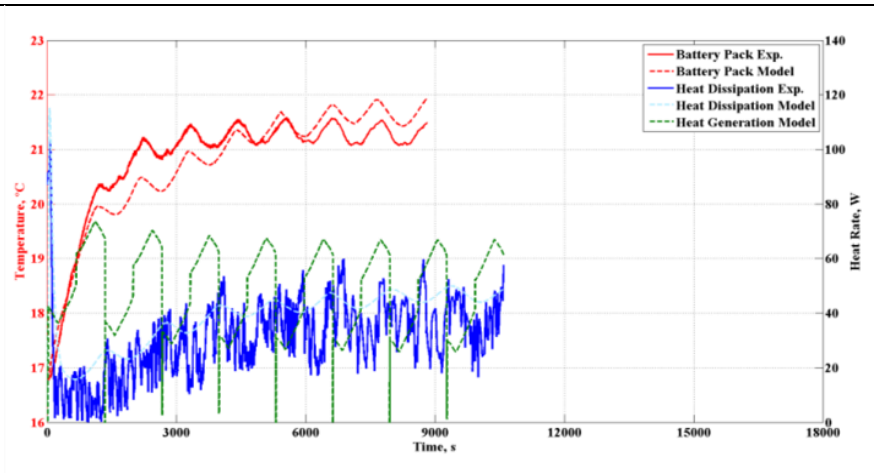
Test 2
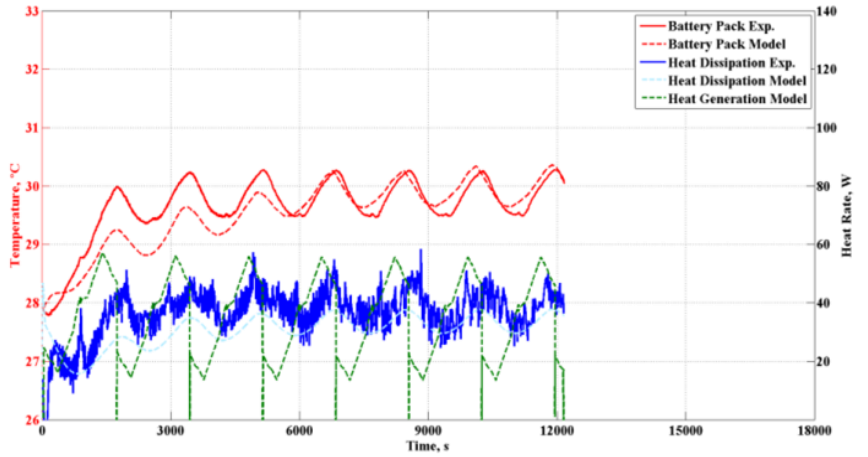
Test 3
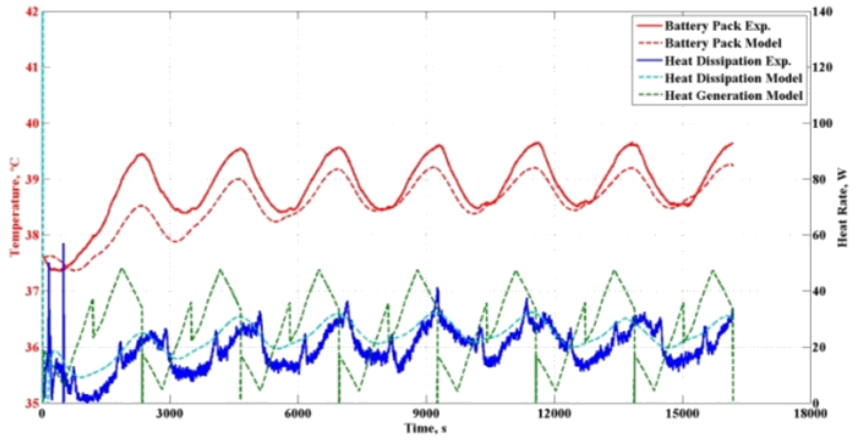

Figure 7.26 Transient thermal (ºC) and heat power (W) results for experimental tests in FC mode.

AC

Test 4

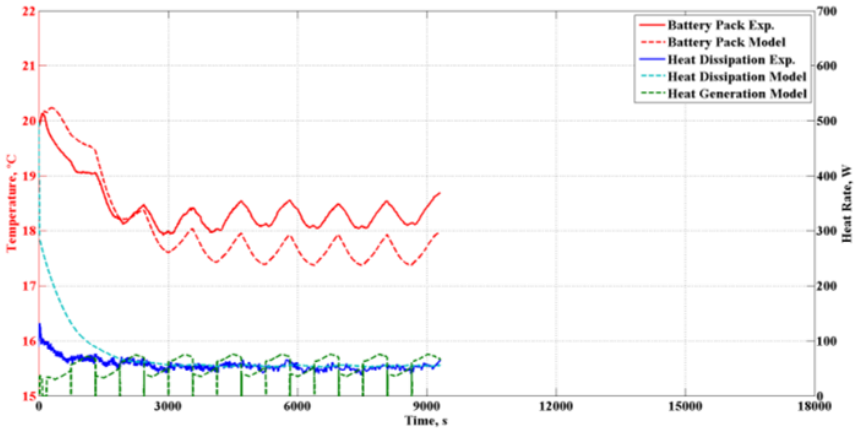

Test 5

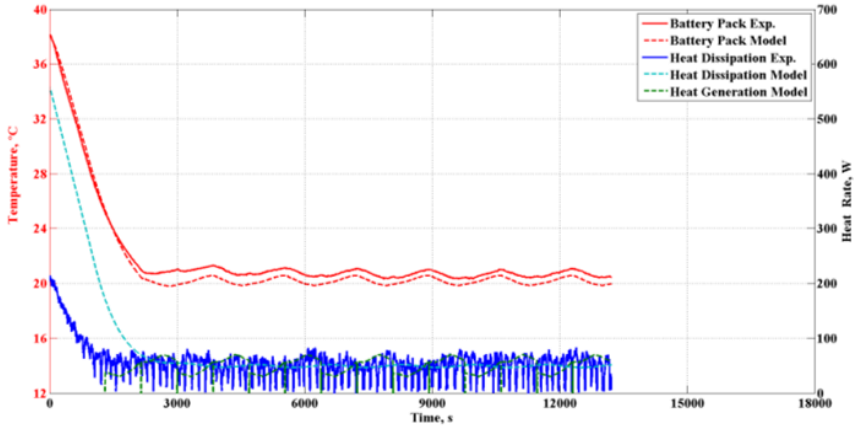

Test 6

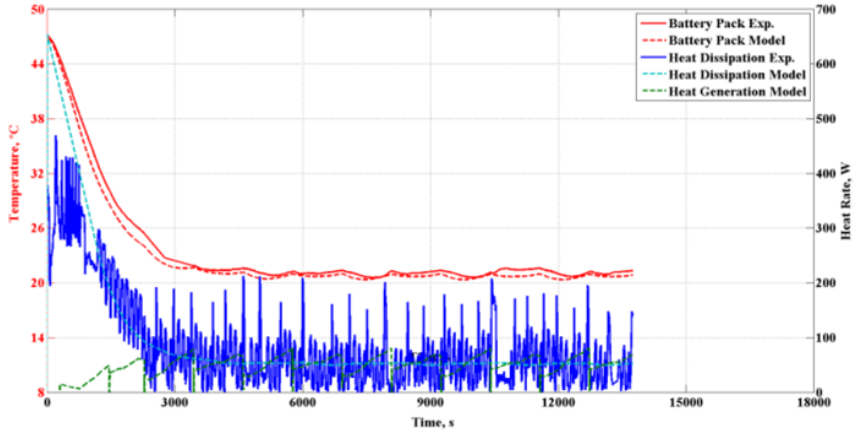

Figure 7.27 Transient thermal (ºC) and heat power (W) results for experimental tests in AC mode.

Therefore, and taking into account all previous validation analysis, the first task of the model validation process could be considered to be entirely reliable and representative of the real thermal performance at *BM* and *BP* level.

For the second step of the thermal models validation task, mean values for several experimental measurements obtained of thermodynamic variables, dissipated total heat power and power consumption have used for each of the experimental tests defined in Table 7.6. These calculated mean values correspond to an average value for the last two discharge- charge cycles, when it has considered that the system is completely thermally stable.

Table 7.9 shows the differences between the numerical and experimental values for all of the variables used to validate the steady performance of the model representing *FC* and *AC* modes of the Dual *TMS*. Both cooling modes have assessed by comparing hydraulic, energy and thermal measurements.

From a hydraulic point of view, the pressure loss has been very similar in the coolant loop for both cooling modes, being slightly higher in *AC* mode due to the evaporator. Volumetric flow rates have been close to the experimentally measured values with differences no higher than 0.2 lpm as can be seen in Table 7.9. This error is totally admissible considering the measuring error of the flowmeters (3% of each full scale).

Regarding the energy perspective, the total amount of heat generated, dissipated and the consumed electric energy) has been calculated. It can be concluded observing these values, in the same way as analyzing Figure 7.26 and Figure 7.27, that the model captures the non-linear heat generation behaviour in the *BM* due to the influence of its temperature on its internal resistance. However, in *AC* mode because the system has been able to keep the *BM* in the same level of the operating temperature, approximately the same amount of heat has dissipated during the latter cycles of tests 4, 5 and 6. The difference between the model and the experimentally evaluated heat power dissipation has been less than 190 W and 286 W for *FC* and *AC* modes, respectively.

The total power that has been consumed by the system in each of the tests carried out is also shown in Table 7.9. Power consumption has been quite stable during all tests due to the non-variable nature of the most electro-mechanical components. In *FC* mode, the pump and the fan were the components responsible for the consumption of the whole

system, whereas in *AC* mode, in addition to the aforementioned two components, the compressor has been which caused a notable increase in the overall consumption of the system. Power consumption in *FC* mode has been hardly related to the ambient temperature, whereas the opposite has occurred in *AC* mode. This has been principally due to the performance of the variable velocity compressor. The differences between experimentally measured and modelled consumptions have been slightly higher in *AC* mode, with a maximum difference of 126 W in the worst case.

At last, regarding the refrigeration cycle variables, both high and low-pressure levels have been compared and evaluated. For the worst ambient conditions tested (45 ºC), the evaporation and condensation pressure has been around 16 bar and 4 bar, respectively, with a model prediction difference lower than 1 bar for each parameter. The difference between the saturation temperature at the evaporation and condensation pressure respectively, with the temperature measured at the end of the evaporator (T_{sh}) and the condenser (T_{sc}) provided the superheating and subcooling temperature.

To sum up, considering that the maximum error of the prediction the *BM* temperature profiles for any electrical and ambient condition experimentally tested has been lower than 0.7 ºC for both cooling modes, it can be concluded that the developed model for validation has been completely reliable and representative of the real thermal performance and it could be used confidently for validate the thermal design and to carry out the following optimization process to achieve at equilibrium between optimal power consumption and consequently, cost and the *BP* lifetime expectancy.

This validated thermal model enabled the designer to check the individual performance of the *BM* in a complete *BP* (its dynamic thermal response and the thermal dispersion between *BM*s), and its interaction with the complex *TMS* at system level that by experimental via it would not be possible.

Table 7.9 Experimental and model predicted variables values for TMS performance validation.

		FC								
		Test 1			Test 2			Test 3		
		Exp.	Model	Diff.	Exp.	Model	Diff.	Exp.	Model	Diff.
Hydraulic	V_{flow_BM},lpm	2.1	2.0	+0.1	2.1	1.9	+0.2	2.1	1.9	+0.1
	V_{flow_system},lpm	8.1	8.0	+0.1	8.2	8.0	+0.2	8.1	8.0	+0.1
	ΔP, mbar	640.0	660.0	-20.0	640.0	659.3	-19.3	640.0	658.6	-18.6
Energy	$\dot{q}_{gen\_BM}$,W	*	46.3	-	*	33.8	-	*	26.5	-
	$\dot{q}_{dis\_system}$, W	949.0	762.7	+186.3	646.6	572.0	+74.6	530.3	438.2	+92.1
	$C_{Elec\text{-}FC}$, W	348.8	397.0	-48.2	340.3	397.0	-56.7	331.5	397.0	-65.5
	COP, [-]	2.7	1.9	+0.8	1.9	1.5	+0.4	1.6	1.1	+0.5
		AC								
		Test 4			Test 5			Test 6		
		Exp.	Model	Diff.	Exp.	Model	Diff.	Exp.	Model	Diff.
Hydraulic	V_{flow_BM}, lpm	2.0	2.0	+0.0	1.9	2.0	-0.1	2.0	2.0	+0.0
	V_{flow_system},lpm	8.1	8.0	+0.1	8.0	8.0	+0.0	8.1	8.0	+0.1
	ΔP, mbar	680.0	712.2	-32.2	680.0	714.7	-34.7	680.0	717.9	-37.9
Thermal	$\dot{q}_{Gen\_BM}$,W	*	55.6	-	*	50.5	-	*	54.0	-
	$\dot{q}_{Dis\_system}$, W	1086.1	956.7	+129.4	1084.6	920.4	+164.2	1325.2	1039.3	+285.9
	$P_{Elec\text{-}AC}$, W	611.5	737.1	-125.6	740.3	800.5	-60.2	1152.4	1117.2	+35.2
	COP, [-]	1.8	1.3	+0.5	1.5	1.1	+0.4	1.1	0.9	+0.2
Energy	P_{cond}, bar	8.6	9.1	-0.5	11.5	12.4	-0.9	15.9	16.9	-1.0
	P_{evap}, bar	4.1	4.2	-0.1	4.4	4.2	+0.2	4.3	3.8	+0.5
	T_{cond}, ºC	33.9	35.9	-2.0	44.6	47.5	-2.9	57.6	60.1	-2.5
	T_{evap}, ºC	9.7	10.1	-0.4	12.1	10.5	1.6	11.5	7.4	+4.1
	T_{sc}, ºC	30.1	32.0	-1.9	41.2	38.9	+2.3	52.1	50.8	+1.3
	T_{sh}, ºC	16.2	14.1	+2.1	19.3	14.1	+5.2	23.1	14.1	+9.0

* Variables that cannot be measured experimentally.

7.5 THERMAL DESIGN OPTIMIZATION

Once the developed thermal model which is shown in Figure 7.13 (up), has been validated by experimental measurements, it has been carried out the process to check if the design criteria have been fulfilled by means of the defined first design and constructed prototype and/or even, if there is the possibility to optimize the system design.

Previously, by means of Table 6.7, it has been advanced the possibility to optimize the predesigned *TMS*, but with the results that are shown in Figure 7.28 that supposition has been ascertained. In Figure 7.28 can be seen as a summary of the results obtained in the previous section, the average *BM* temperature considering the last two discharge-charge cycles related to (a) *FC* and (b) *AC* system. It is obvious that for the *FC* system already exists a margin in terms to achieve the maximum defined operation temperature of the *BM*. Furthermore, related to *AC* system and based on the results shown in Figure 7.28 (b) it can be said that with this *TMS* is possible to keep the *BM* within the ideal thermal operation range. Consequently, in order to reduce the consumption the designer can be decided to relax the constraints in terms of *BM* temperature set-point or on the other hand, to use smaller components with less consumption. This decision will be in the designer hands.

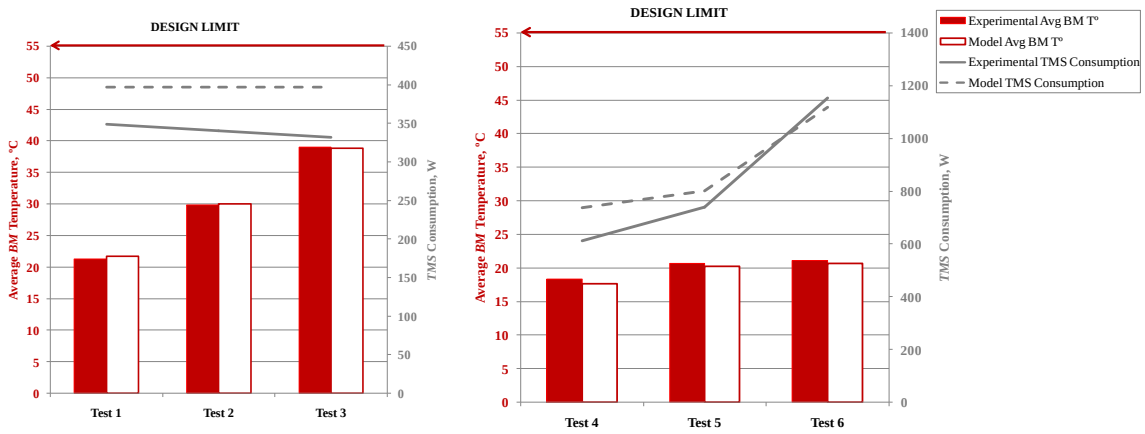

(a) (b)

Figure 7.28 Experimental and numerical average BM temperature for (a) FC and (b) AC system.

For optimization task the model developed at *BP* level, which is shown in Figure 7.13 (down) has been used. Every proposed variations in this optimization step should

meet the initially defined specifications (Table 7.1), especially the thermal requirements related to maximum performance temperature and the thermal dispersion. In every following optimization cases the similar working conditions of the urban electric minibus have been considered in terms of current profile, operation time and the component operation strategy. In the same way and because of the same reasons such as for the thermal model development task (Section 7.3), a cyclic profile of DCH 1C/ CHA 1C has been used. A 10-hour working day has been considered and as it has explained in the description of the application the urban minibus should be capable of performing at least two complete round trips, returning to the departure point, and provided with the possibility of recharging the *BP* (at 40 A current rate at *BM* level). The *SOC* range has fixed between 80-20%. Considering the performance of the auxiliary components for this thermal design optimization task, for both cooling modes, *FC* and *AC*, every components (pump, fan and compressor) have operated at different prefixed speeds. The pump has operated continuously whereas the fan and the compressor have worked according to ON/OFF control, with a set point of 25 ºC and bandwidth of 4 ºC.

The first step before proceeding with the optimization task has been to validate the design in terms of hydraulic architecture. In the previous predesign step (Section 7.2) a hydraulic configuration of *4s4p* has been decided mainly because of its lower pressure drop and simplicity of assembly comparing with the other proposed hydraulic configurations (*16s* and *8s2p*), as it is shown in Figure 7.29. At this point and due to that the system model has been already validated, it has been possible to analyze the thermal performance regarding the different configurations at system level.

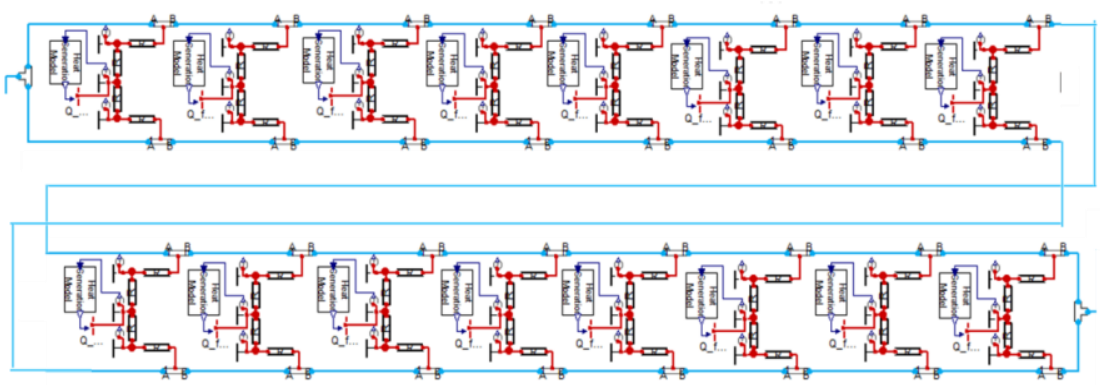

(a)

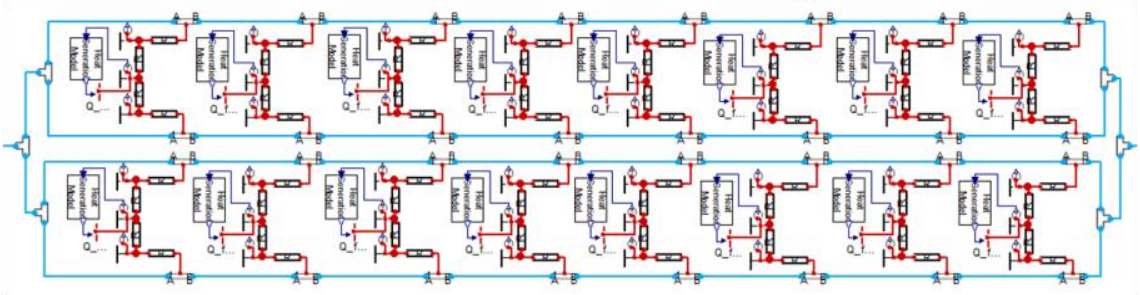

(b)

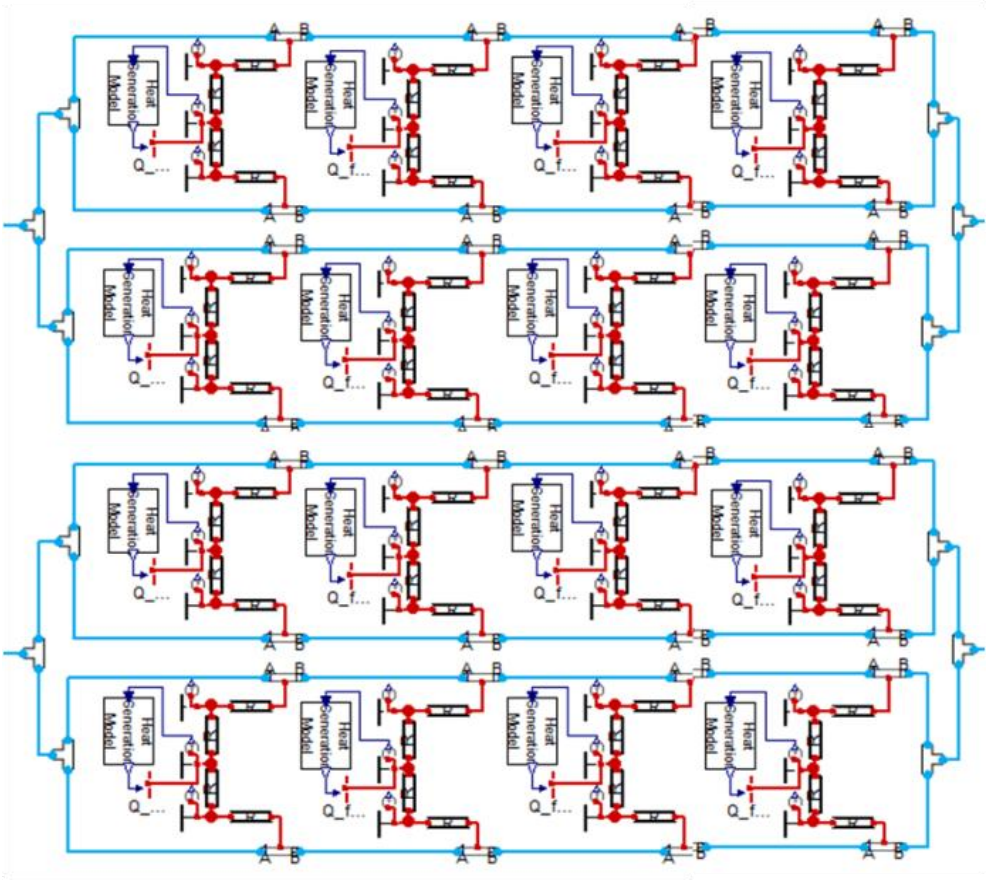

(c)

Figure 7.29 Hydraulic configurations (a) 16s, (b) 8s2p and (c) 4s4p.

In Figure 7.30 is shown the results obtained regarding *BP* temperature, thermal dispersion and auxiliary consumption of the *TMS* for the different hydraulic architectures proposed considering an ambient temperature of 20 ºC and both cooling modes, *FC* and *AC*.

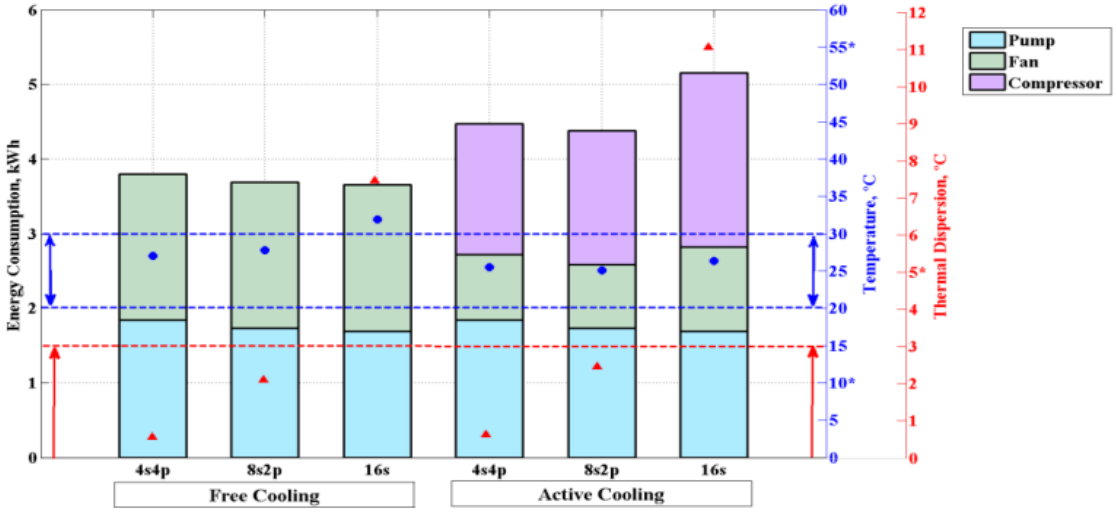

Figure 7.30 BP temperature (ºC), thermal dispersion (ºC) and auxiliary consumption (kWh) for the different hydraulic architectures studied.

As it can be observed in Figure 7.30, the 16s hydraulic configuration has ruled out mainly because it has not met the two thermal requirements previously defined for the three electric minibus lines, in particular which is related to thermal dispersion. Both *4s4p* and *8s2p* hydraulic configurations have fulfilled the thermal requirements. Nevertheless, given the more complex piping connection required by the *4s4p* configuration, the *8s2p* hydraulic connection has been selected as it has deemed to be the most suitable for the final design.

Once the most suitable hydraulic configuration has been selected the optimization task has been carried out. This case study, unlike that in the previous test case, it has not been necessary to apply *False Steady* concept because as it has mentioned before in this type of simulation tool the transient simulations have not supposed a computational cost problem and *ON/OFF* dynamics are involved.

As in the case for the residential elevator, two different optimization cases have been defined: Optimization I and Optimization II. Optimization I has been focused on the evaluation an adequate regulation speed for the components in function of the cooling mode, *FC* and *AC*, whereas Optimization II has applied in order to determinate an adequate electrical resistance in other to warm up the *BP* in cold ambient conditions.

7.5.1 OPTIMIZATION I

The aim of the Optimization I task has been to define an adequate rotational speed of the electromechanical components of each cooling system mode ensuring an adequate thermal performance of the *BP*. Based on the hydraulic configuration that has been selected, 2 strings in parallel with 8 *BM*s placed in serial in each one, the maximum *BM* temperature will be correspondent to the last *BM* located in each string and the thermal dispersion will be calculated considering the difference temperature between the first and the last *BM* in each string.

The same procedure base on *DoE* technique has been followed in these both cases, which they will be analyzed independently in depth following.

Forced Cooling

For the *FC* system, three were the factors that have been defined as it is shown in Table 7.10: the pump rotational speed (2000 rpm, 3000 rpm and 4000 rpm), the fan *PWM* (70% *PWM*, 85% *PWM* and 100% *PWM*) and ambient temperature (10 ºC, 17.5 ºC and 25 ºC).

Table 7.10 DoE matrix for FC system

	Coded Value			UnCoded Value		
	Pump	Fan	T amb	Pump Speed, rpm	Fan PWM, %	T amb, ºC
1	1	1	1	4000	100	25
2	-1	-1	1	2000	70	25
3	1	-1	1	4000	70	25
4	1	-1	-1	4000	70	10
5	-1	-1	-1	2000	70	10
6	0	0	0	3000	85	17.5
7	1	1	-1	4000	100	10
8	-1	1	-1	2000	100	10
9	-1	1	1	2000	100	25
10	0	0	-1	3000	85	10
11	0	0	1	3000	85	25
12	-1	0	0	2000	85	17.5
13	1	0	0	4000	85	17.5
14	0	1	0	3000	100	17.5
15	0	-1	0	3000	70	17.5

In Table 7.11 are shown the numerical results have been obtained for each test that has been carried out. The maximum temperature and the thermal dispersion within the BP has been evaluated such as response variables in each test.

Table 7.11 Numerical results correspondent to the DoE matrix related to FC system

	Pump	Fan	T amb	Tmax, ºC	Dispersion *BM* , ºC
1	1	1	1	28.68	1.18
2	-1	-1	1	32.65	3.71
3	1	-1	1	31.47	1.11
4	1	-1	-1	25.44	0.48
5	-1	-1	-1	24.61	4.56
6	0	0	0	24.32	2.00
7	1	1	-1	26.49	0.14
8	-1	1	-1	24.85	2.18
9	-1	1	1	31.53	4.08
10	0	0	-1	25.14	0.74
11	0	0	1	30.04	1.99
12	-1	0	0	25.65	4.69
13	1	0	0	24.91	0.68
14	0	1	0	25.52	0.41
15	0	-1	0	26.02	2.16

Applying the *Face Centered CCD* the regression surface response of each variable has been obtained. The equation which defines the surface response regarding the cell maximum temperature and thermal dispersion has been defined by means of the coefficients tabulated in Table 7.12.The p-value of each term is also shown. It indicates how significant ($p<0.005$) or not is the effect of the variable on the response.

Based on Table 7.12, it can be concluded that for the *BP* temperature the lineal and quadratic effect of the ambient temperature has been significant for this *FC* system. As it has been expected, the sign of the coefficients related to the ambient lineal and quadratic parameters have indicated that this factor has been directly proportional to the *BP* temperature, i.e., when the ambient temperature has increased, the *BP* temperature also. On the other hand and related to the thermal dispersion within the *BP*, the lineal effect of the pump speed which has involved more or less liquid mass flow rate in the system, has been the main significant effect.

R-square (R^2) is the percentage of response variable variation and when its value is higher, it means that the models better fits with the data. In this case for each analyzed response 98.57% and 94.14% has been obtained, so it can be said that the obtained surface response model has been representative of the simulation results obtained.

As an example, Figure 7.31 and Figure 7.32 show the surface response regarding the maximum *BP* temperature and thermal dispersion within the *BP* for pump rotational speed of values 3000 rpm for *FC* mode. In every surface responses in the horizontal axis the ambient temperature has indicated whereas in the vertical axis the fan rotational speed (*PWM*).

Table 7.12 Coefficients correspondent to the regression surface response of maximum temperature and thermal dispersion within the BP together with the p-values.

	Maximum *BP* temperature		Thermal Dispersion	
	Coefficients	p- value, [-]	Coefficients	p- value, [-]
Constant	24.9547	0.000	1.6996	0.004
Pump Speed	-0.2300	0.264	-1.5630	**0.001**
Fan *PWM*	-0.3120	0.149	-0.4030	0.099
Tamb	2.7840	**0.000**	0.3970	0.103
Pump Speed * Pump Speed	0.1667	0.663	1.0606	0.043
Fan *PWM* * Fan *PWM*	0.6567	0.128	-0.3394	0.427
Tamb*Tamb	2.4767	**0.001**	-0.2595	0.538
Pump Speed *Fan *PWM*	-0.1075	0.622	0.2175	0.374
Pump Speed * Tamb	-0.8125	0.011	0.078	0.742
Fan *PWM* * Tamb	-0.6500	0.025	0.3950	0.137

In Table 7.13 are tabulated the numerical results obtained from Figure 7.31 and Figure 7.32, in order to take conclusion easier. In Table 7.13 two design zones have been distinguished within the zone marked by black rectangle in Figure 7.31 and Figure 7.32: the first one is referred to soft conditions where the ambient temperature is between 10-17.5 ºC and the fan *PWM* is between 70-85 % (minimum and medium conditions). The second zone corresponds to a more abusive condition where the ambient temperature is between 17.5-25 ºC and the Fan *PWM* is between the range defined such as medium (85% *PWM*) and maximum (100% *PWM*) range.

Based on the results obtained in Figure 7.31, Figure 7.32 and Table 7.13, it can be concluded that even for the worst ambient conditions the maximum BP temperature has been kept within the acceptable operation range. In fact, for the most operation conditions, except for the cases when the pump has operated at 2000 and 3000 rpm, the maximum *BP* temperature has been maintained within the ideal operation range. Regarding the thermal dispersion, for the defined minimum rotational speed of the pump, 2000 rpm, this variable response has reached values out of the operational range. While for the rest analyzed operation conditions have been obtained acceptable thermal dispersion values within the *BP*.

Fan PWM	m3/s	PWM		T amb																											
				6.3	7.0	7.8	8.5	9.3	10.0	10.8	11.5	12.3	13.0	13.8	14.5	15.3	16.0	16.8	17.5	18.3	19.0	19.8	20.5	21.3	22.0	22.8	23.5	24.3	25.0	25.8	26.5	27.3	28.0	28.8
				-1.5	-1.4	-1.3	-1.2	-1.1	-1.0	-0.9	-0.8	-0.7	-0.6	-0.5	-0.4	-0.3	-0.2	-0.1	0.0	0.1	0.2	0.3	0.4	0.5	0.6	0.7	0.8	0.9	1.0	1.1	1.2	1.3	1.4	1.5
	0.02	62.5	-1.5	26.8	26.5	26.2	26.0	25.8	25.6	25.5	25.5	25.5	25.5	25.6	25.8	26.0	26.2	26.5	26.9	27.3	27.8	28.3	28.8	29.4	30.0	30.7	31.5	32.3	33.1	34.0	35.0	36.0	37.0	38.1
	0.04	64.0	-1.4	26.7	26.4	26.1	25.8	25.6	25.5	25.4	25.3	25.3	25.4	25.5	25.6	25.8	26.0	26.3	26.7	27.1	27.5	28.0	28.6	29.1	29.8	30.5	31.2	32.0	32.8	33.7	34.7	35.7	36.7	37.8
	0.07	65.5	-1.3	26.6	26.2	25.9	25.7	25.5	25.3	25.2	25.2	25.1	25.2	25.3	25.4	25.6	25.8	26.1	26.5	26.9	27.3	27.8	28.3	28.9	29.5	30.2	31.0	31.7	32.6	33.5	34.4	35.4	36.4	37.5
	0.09	67.0	-1.2	26.5	26.1	25.8	25.6	25.4	25.2	25.1	25.0	25.0	25.0	25.1	25.2	25.4	25.7	25.9	26.3	26.7	27.1	27.6	28.1	28.7	29.3	30.0	30.7	31.5	32.3	33.2	34.1	35.1	36.1	37.2
	0.11	68.5	-1.1	26.4	26.0	25.7	25.5	25.2	25.1	24.9	24.9	24.9	24.9	25.0	25.1	25.3	25.5	25.8	26.1	26.5	26.9	27.4	27.9	28.5	29.1	29.8	30.5	31.2	32.1	32.9	33.9	34.8	35.8	36.9
	0.14	70.0	-1.0	26.3	26.0	25.6	25.4	25.1	25.0	24.8	24.8	24.7	24.8	24.8	24.9	25.1	25.3	25.6	25.9	26.3	26.7	27.2	27.7	28.3	28.9	29.5	30.3	31.0	31.8	32.7	33.6	34.6	35.6	36.6
	0.16	71.5	-0.9	26.3	25.9	25.6	25.3	25.1	24.9	24.7	24.7	24.6	24.6	24.7	24.8	25.0	25.2	25.5	25.8	26.1	26.5	27.0	27.5	28.1	28.7	29.3	30.0	30.8	31.6	32.5	33.4	34.3	35.3	36.4
	0.18	73.0	-0.8	26.2	25.9	25.5	25.2	25.0	24.8	24.7	24.6	24.5	24.5	24.6	24.7	24.9	25.1	25.3	25.6	26.0	26.4	26.8	27.3	27.9	28.5	29.2	29.9	30.6	31.4	32.3	33.2	34.1	35.1	36.2
	0.21	74.5	-0.7	26.2	25.8	25.5	25.2	24.9	24.7	24.6	24.5	24.4	24.4	24.5	24.6	24.7	24.9	25.2	25.5	25.8	26.2	26.7	27.2	27.7	28.3	29.0	29.7	30.4	31.2	32.1	32.9	33.9	34.9	35.9
	0.23	76.0	-0.6	26.2	25.8	25.4	25.1	24.9	24.7	24.5	24.4	24.4	24.4	24.4	24.5	24.6	24.8	25.1	25.4	25.7	26.1	26.6	27.0	27.6	28.2	28.8	29.5	30.2	31.0	31.9	32.8	33.7	34.7	35.7
	0.25	77.5	-0.5	26.2	25.8	25.4	25.1	24.9	24.6	24.5	24.4	24.3	24.3	24.3	24.4	24.6	24.8	25.0	25.3	25.6	26.0	26.4	26.9	27.4	28.0	28.7	29.3	30.1	30.9	31.7	32.6	33.5	34.5	35.5
	0.27	79.0	-0.4	26.2	25.8	25.4	25.1	24.8	24.6	24.5	24.3	24.3	24.2	24.3	24.4	24.5	24.7	24.9	25.2	25.5	25.9	26.3	26.8	27.3	27.9	28.5	29.2	29.9	30.7	31.5	32.4	33.3	34.3	35.3
	0.30	80.5	-0.3	26.2	25.8	25.4	25.1	24.8	24.6	24.4	24.3	24.2	24.2	24.2	24.3	24.4	24.6	24.8	25.1	25.4	25.8	26.2	26.7	27.2	27.8	28.4	29.1	29.8	30.6	31.4	32.2	33.2	34.1	35.1
	0.32	82.0	-0.2	26.2	25.8	25.4	25.1	24.8	24.6	24.4	24.3	24.2	24.2	24.2	24.3	24.4	24.6	24.8	25.0	25.4	25.7	26.1	26.6	27.1	27.7	28.3	29.0	29.7	30.4	31.2	32.1	33.0	34.0	35.0
	0.34	83.5	-0.1	26.3	25.9	25.5	25.1	24.9	24.6	24.4	24.3	24.2	24.2	24.2	24.2	24.4	24.5	24.7	25.0	25.3	25.7	26.1	26.5	27.0	27.6	28.2	28.9	29.6	30.3	31.1	32.0	32.9	33.8	34.8
	0.37	85.0	0.0	26.4	25.9	25.5	25.2	24.9	24.6	24.5	24.3	24.2	24.2	24.2	24.2	24.3	24.5	24.7	25.0	25.3	25.6	26.0	26.5	27.0	27.5	28.1	28.8	29.5	30.2	31.0	31.9	32.8	33.7	34.7
	0.39	86.5	0.1	26.4	26.0	25.6	25.2	24.9	24.7	24.5	24.3	24.2	24.2	24.2	24.2	24.3	24.5	24.7	24.9	25.2	25.6	26.0	26.4	26.9	27.5	28.0	28.7	29.4	30.1	30.9	31.8	32.7	33.6	34.6
	0.41	88.0	0.2	26.5	26.1	25.7	25.3	25.0	24.7	24.5	24.4	24.3	24.2	24.2	24.3	24.3	24.5	24.7	24.9	25.2	25.5	25.9	26.4	26.9	27.4	28.0	28.6	29.3	30.0	30.8	31.7	32.6	33.5	34.5
	0.44	89.5	0.3	26.6	26.1	25.7	25.4	25.1	24.8	24.6	24.4	24.3	24.3	24.2	24.3	24.4	24.5	24.7	24.9	25.2	25.5	25.9	26.4	26.8	27.4	27.9	28.6	29.3	30.0	30.8	31.6	32.5	33.4	34.4
	0.46	91.0	0.4	26.7	26.3	25.8	25.5	25.2	24.9	24.7	24.5	24.4	24.3	24.3	24.3	24.4	24.5	24.7	24.9	25.2	25.5	25.9	26.3	26.8	27.3	27.9	28.5	29.2	29.9	30.7	31.5	32.4	33.3	34.3
	0.48	92.5	0.5	26.8	26.4	26.0	25.6	25.3	25.0	24.8	24.6	24.5	24.4	24.4	24.4	24.4	24.6	24.7	25.0	25.2	25.6	25.9	26.3	26.8	27.3	27.9	28.5	29.2	29.9	30.7	31.5	32.3	33.3	34.2
	0.50	94.0	0.6	27.0	26.5	26.1	25.7	25.4	25.1	24.9	24.7	24.5	24.5	24.4	24.4	24.5	24.6	24.8	25.0	25.3	25.6	25.9	26.4	26.8	27.3	27.9	28.5	29.2	29.9	30.6	31.4	32.3	33.2	34.2
	0.53	95.5	0.7	27.1	26.7	26.2	25.8	25.5	25.2	25.0	24.8	24.6	24.6	24.5	24.5	24.6	24.7	24.8	25.1	25.3	25.6	26.0	26.4	26.8	27.3	27.9	28.5	29.2	29.9	30.6	31.4	32.3	33.2	34.1
	0.55	97.0	0.8	27.3	26.8	26.4	26.0	25.6	25.3	25.1	24.9	24.8	24.7	24.6	24.6	24.7	24.8	24.9	25.1	25.4	25.7	26.0	26.4	26.9	27.4	27.9	28.5	29.2	29.9	30.6	31.4	32.3	33.1	34.1
	0.57	98.5	0.9	27.5	27.0	26.5	26.1	25.8	25.5	25.2	25.0	24.9	24.8	24.7	24.7	24.8	24.9	25.0	25.2	25.5	25.7	26.1	26.5	26.9	27.4	28.0	28.6	29.2	29.9	30.6	31.4	32.3	33.1	34.1
	0.60	100.0	1.0	27.7	27.2	26.7	26.3	25.9	25.6	25.4	25.2	25.0	24.9	24.9	24.8	24.9	25.0	25.1	25.3	25.5	25.8	26.2	26.5	27.0	27.5	28.0	28.6	29.2	29.9	30.6	31.4	32.3	33.1	34.1
	0.62	101.5	1.1	27.9	27.4	26.9	26.5	26.1	25.8	25.6	25.3	25.2	25.1	25.0	25.0	25.0	25.1	25.2	25.4	25.6	25.9	26.2	26.6	27.1	27.5	28.1	28.6	29.3	30.0	30.7	31.5	32.3	33.2	34.1
	0.64	103.0	1.2	28.1	27.6	27.1	26.7	26.3	26.0	25.7	25.5	25.3	25.2	25.1	25.1	25.1	25.2	25.4	25.5	25.8	26.0	26.4	26.7	27.1	27.6	28.1	28.7	29.3	30.0	30.7	31.5	32.3	33.2	34.1
	0.67	104.5	1.3	28.3	27.8	27.3	26.9	26.5	26.2	25.9	25.7	25.5	25.4	25.3	25.3	25.3	25.4	25.5	25.7	25.9	26.1	26.5	26.8	27.2	27.7	28.2	28.8	29.4	30.1	30.8	31.6	32.4	33.2	34.1
	0.69	106.0	1.4	28.6	28.0	27.6	27.1	26.7	26.4	26.1	25.9	25.7	25.6	25.5	25.5	25.5	25.5	25.6	25.8	26.0	26.3	26.6	27.0	27.4	27.8	28.3	28.9	29.5	30.2	30.9	31.6	32.4	33.3	34.2
	0.71	107.5	1.5	28.8	28.3	27.8	27.4	27.0	26.6	26.3	26.1	25.9	25.8	25.7	25.6	25.6	25.7	25.8	26.0	26.2	26.4	26.7	27.1	27.5	27.9	28.4	29.0	29.6	30.2	31.0	31.7	32.5	33.4	34.3

Figure 7.31 The surface response correspondent to maximum BP temperature with a pump speed of 3000 rpm.

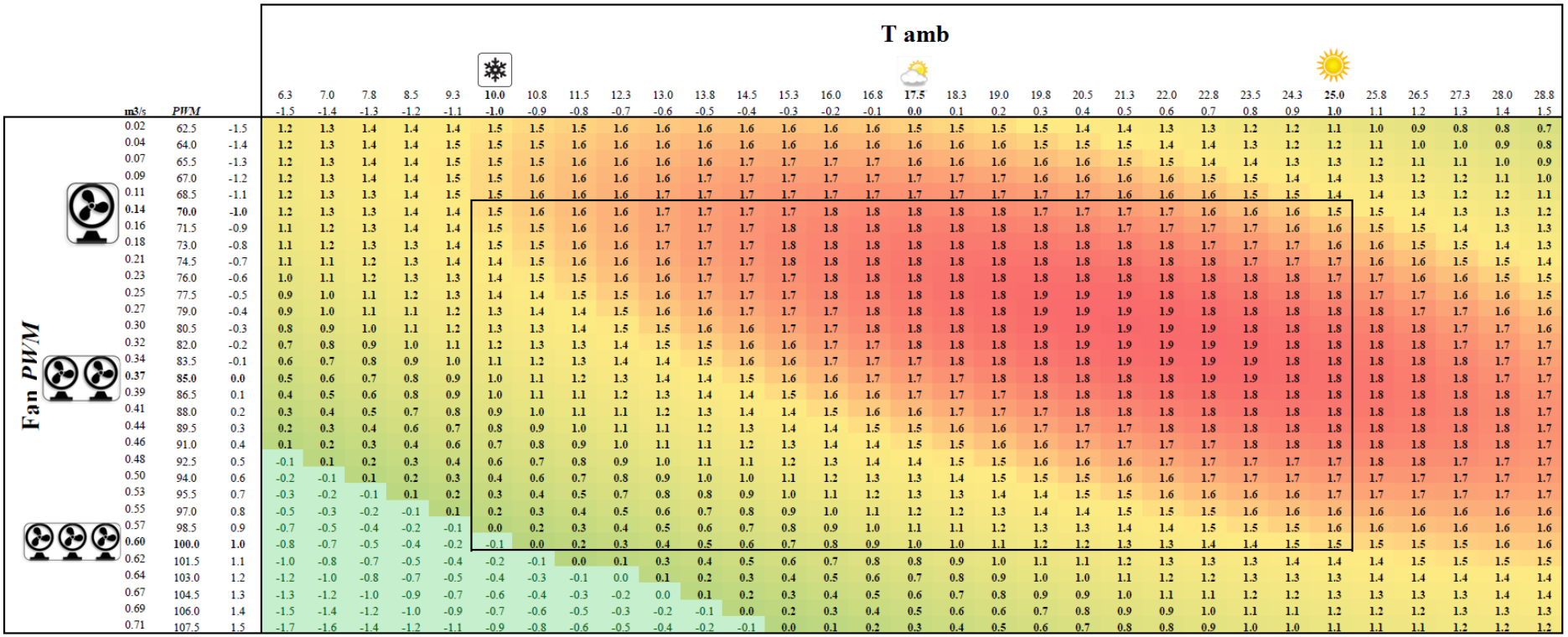

m3/s	PWM		6.3	7.0	7.8	8.5	9.3	10.0	10.8	11.5	12.3	13.0	13.8	14.5	15.3	16.0	16.8	17.5	18.3	19.0	19.8	20.5	21.3	22.0	22.8	23.5	24.3	25.0	25.8	26.5	27.3	28.0	28.8
			-1.5	-1.4	-1.3	-1.2	-1.1	-1.0	-0.9	-0.8	-0.7	-0.6	-0.5	-0.4	-0.3	-0.2	-0.1	0.0	0.1	0.2	0.3	0.4	0.5	0.6	0.7	0.8	0.9	1.0	1.1	1.2	1.3	1.4	1.5
0.02	62.5	-1.5	1.2	1.3	1.4	1.4	1.4	1.5	1.5	1.5	1.6	1.6	1.6	1.6	1.6	1.6	1.6	1.5	1.5	1.5	1.5	1.4	1.4	1.3	1.3	1.2	1.2	1.1	1.0	0.9	0.8	0.8	0.7
0.04	64.0	-1.4	1.2	1.3	1.4	1.4	1.5	1.5	1.5	1.6	1.6	1.6	1.6	1.6	1.6	1.6	1.6	1.6	1.6	1.6	1.5	1.5	1.5	1.4	1.4	1.3	1.2	1.2	1.1	1.0	1.0	0.9	0.8
0.07	65.5	-1.3	1.2	1.3	1.4	1.4	1.5	1.5	1.5	1.6	1.6	1.6	1.6	1.7	1.7	1.7	1.7	1.6	1.6	1.6	1.6	1.6	1.5	1.5	1.4	1.4	1.3	1.3	1.2	1.1	1.1	1.0	0.9
0.09	67.0	-1.2	1.2	1.3	1.4	1.4	1.5	1.5	1.6	1.6	1.6	1.6	1.7	1.7	1.7	1.7	1.7	1.7	1.7	1.7	1.6	1.6	1.6	1.6	1.5	1.5	1.4	1.4	1.3	1.2	1.2	1.1	1.0
0.11	68.5	-1.1	1.2	1.3	1.3	1.4	1.5	1.5	1.6	1.6	1.6	1.7	1.7	1.7	1.7	1.7	1.7	1.7	1.7	1.7	1.7	1.7	1.6	1.6	1.6	1.5	1.5	1.4	1.4	1.3	1.2	1.2	1.1
0.14	70.0	-1.0	1.2	1.3	1.3	1.4	1.4	1.5	1.6	1.6	1.6	1.7	1.7	1.7	1.7	1.8	1.8	1.8	1.8	1.8	1.7	1.7	1.7	1.7	1.6	1.6	1.6	1.5	1.5	1.4	1.3	1.3	1.2
0.16	71.5	-0.9	1.1	1.2	1.3	1.4	1.4	1.5	1.5	1.6	1.6	1.7	1.7	1.7	1.8	1.8	1.8	1.8	1.8	1.8	1.8	1.8	1.7	1.7	1.7	1.7	1.6	1.6	1.5	1.5	1.4	1.3	1.3
0.18	73.0	-0.8	1.1	1.2	1.3	1.3	1.4	1.5	1.5	1.6	1.6	1.7	1.7	1.7	1.8	1.8	1.8	1.8	1.8	1.8	1.8	1.8	1.8	1.8	1.7	1.7	1.7	1.6	1.6	1.5	1.5	1.4	1.3
0.21	74.5	-0.7	1.1	1.1	1.2	1.3	1.4	1.4	1.5	1.6	1.6	1.7	1.7	1.8	1.8	1.8	1.8	1.8	1.8	1.8	1.8	1.8	1.8	1.8	1.7	1.7	1.7	1.7	1.6	1.6	1.5	1.5	1.4
0.23	76.0	-0.6	1.0	1.1	1.2	1.3	1.3	1.4	1.5	1.5	1.6	1.6	1.7	1.7	1.7	1.8	1.8	1.8	1.8	1.8	1.8	1.8	1.8	1.8	1.8	1.8	1.8	1.7	1.7	1.6	1.6	1.5	1.5
0.25	77.5	-0.5	0.9	1.0	1.1	1.2	1.3	1.4	1.4	1.5	1.5	1.6	1.7	1.7	1.7	1.8	1.8	1.8	1.8	1.8	1.9	1.9	1.9	1.8	1.8	1.8	1.8	1.8	1.7	1.7	1.6	1.6	1.5
0.27	79.0	-0.4	0.9	1.0	1.1	1.1	1.2	1.3	1.4	1.4	1.5	1.6	1.6	1.7	1.7	1.7	1.8	1.8	1.8	1.8	1.9	1.9	1.9	1.9	1.8	1.8	1.8	1.8	1.8	1.7	1.7	1.6	1.6
0.30	80.5	-0.3	0.8	0.9	1.0	1.1	1.2	1.3	1.3	1.4	1.5	1.5	1.6	1.6	1.7	1.7	1.8	1.8	1.8	1.8	1.9	1.9	1.9	1.9	1.8	1.8	1.8	1.8	1.8	1.8	1.7	1.7	1.6
0.32	82.0	-0.2	0.7	0.8	0.9	1.0	1.1	1.2	1.3	1.3	1.4	1.5	1.5	1.6	1.6	1.7	1.7	1.8	1.8	1.8	1.8	1.9	1.9	1.9	1.9	1.9	1.8	1.8	1.8	1.8	1.7	1.7	1.7
0.34	83.5	-0.1	0.6	0.7	0.8	0.9	1.0	1.1	1.2	1.3	1.4	1.4	1.5	1.6	1.6	1.7	1.7	1.7	1.8	1.8	1.8	1.8	1.9	1.9	1.9	1.9	1.8	1.8	1.8	1.8	1.8	1.7	1.7
0.37	85.0	0.0	0.5	0.6	0.7	0.8	0.9	1.0	1.1	1.2	1.3	1.4	1.4	1.5	1.6	1.6	1.7	1.7	1.7	1.8	1.8	1.8	1.8	1.8	1.9	1.9	1.8	1.8	1.8	1.8	1.8	1.7	1.7
0.39	86.5	0.1	0.4	0.5	0.6	0.8	0.9	1.0	1.1	1.1	1.2	1.3	1.4	1.4	1.5	1.6	1.6	1.7	1.7	1.7	1.8	1.8	1.8	1.8	1.8	1.8	1.8	1.8	1.8	1.8	1.8	1.8	1.7
0.41	88.0	0.2	0.3	0.4	0.5	0.7	0.8	0.9	1.0	1.1	1.1	1.2	1.3	1.4	1.4	1.5	1.6	1.6	1.7	1.7	1.7	1.8	1.8	1.8	1.8	1.8	1.8	1.8	1.8	1.8	1.8	1.8	1.7
0.44	89.5	0.3	0.2	0.3	0.4	0.6	0.7	0.8	0.9	1.0	1.1	1.1	1.2	1.3	1.4	1.4	1.5	1.5	1.6	1.6	1.7	1.7	1.7	1.8	1.8	1.8	1.8	1.8	1.8	1.8	1.8	1.8	1.7
0.46	91.0	0.4	0.1	0.2	0.3	0.4	0.6	0.7	0.8	0.9	1.0	1.1	1.1	1.2	1.3	1.4	1.4	1.5	1.5	1.6	1.6	1.7	1.7	1.7	1.7	1.8	1.8	1.8	1.8	1.8	1.8	1.8	1.7
0.48	92.5	0.5	-0.1	0.1	0.2	0.3	0.4	0.6	0.7	0.8	0.9	1.0	1.1	1.1	1.2	1.3	1.4	1.4	1.5	1.5	1.6	1.6	1.6	1.7	1.7	1.7	1.7	1.7	1.8	1.8	1.7	1.7	1.7
0.50	94.0	0.6	-0.2	-0.1	0.1	0.2	0.3	0.4	0.6	0.7	0.8	0.9	1.0	1.0	1.1	1.2	1.3	1.3	1.4	1.5	1.5	1.5	1.6	1.6	1.7	1.7	1.7	1.7	1.7	1.7	1.7	1.7	1.7
0.53	95.5	0.7	-0.3	-0.2	-0.1	0.1	0.2	0.3	0.4	0.5	0.7	0.8	0.8	0.9	1.0	1.1	1.2	1.3	1.3	1.4	1.4	1.5	1.5	1.6	1.6	1.6	1.7	1.7	1.7	1.7	1.7	1.7	1.7
0.55	97.0	0.8	-0.5	-0.3	-0.2	-0.1	0.1	0.2	0.3	0.4	0.5	0.6	0.7	0.8	0.9	1.0	1.1	1.2	1.2	1.3	1.4	1.4	1.5	1.5	1.5	1.6	1.6	1.6	1.6	1.6	1.6	1.6	1.6
0.57	98.5	0.9	-0.7	-0.5	-0.4	-0.2	-0.1	0.0	0.2	0.3	0.4	0.5	0.6	0.7	0.8	0.9	1.0	1.1	1.1	1.2	1.3	1.3	1.4	1.4	1.5	1.5	1.5	1.6	1.6	1.6	1.6	1.6	1.6
0.60	100.0	1.0	-0.8	-0.7	-0.5	-0.4	-0.2	-0.1	0.0	0.2	0.3	0.4	0.5	0.6	0.7	0.8	0.9	1.0	1.0	1.1	1.2	1.2	1.3	1.3	1.4	1.4	1.5	1.5	1.5	1.5	1.5	1.6	1.6
0.62	101.5	1.1	-1.0	-0.8	-0.7	-0.5	-0.4	-0.2	-0.1	0.0	0.1	0.3	0.4	0.5	0.6	0.7	0.8	0.8	0.9	1.0	1.1	1.1	1.2	1.3	1.3	1.3	1.4	1.4	1.4	1.5	1.5	1.5	1.5
0.64	103.0	1.2	-1.2	-1.0	-0.8	-0.7	-0.5	-0.4	-0.3	-0.1	0.0	0.1	0.2	0.3	0.4	0.5	0.6	0.7	0.8	0.9	1.0	1.0	1.1	1.2	1.2	1.3	1.3	1.3	1.4	1.4	1.4	1.4	1.4
0.67	104.5	1.3	-1.3	-1.2	-1.0	-0.9	-0.7	-0.6	-0.4	-0.3	-0.2	0.0	0.1	0.2	0.3	0.4	0.5	0.6	0.7	0.8	0.9	0.9	1.0	1.1	1.1	1.2	1.2	1.3	1.3	1.3	1.3	1.4	1.4
0.69	106.0	1.4	-1.5	-1.4	-1.2	-1.0	-0.9	-0.7	-0.6	-0.5	-0.3	-0.2	-0.1	0.0	0.2	0.3	0.4	0.5	0.6	0.6	0.7	0.8	0.9	0.9	1.0	1.1	1.1	1.2	1.2	1.2	1.3	1.3	1.3
0.71	107.5	1.5	-1.7	-1.6	-1.4	-1.2	-1.1	-0.9	-0.8	-0.6	-0.5	-0.4	-0.2	-0.1	0.0	0.1	0.2	0.3	0.4	0.5	0.6	0.7	0.8	0.8	0.9	1.0	1.0	1.1	1.1	1.1	1.2	1.2	1.2

Figure 7.32 The surface response correspondent to thermal dispersion with a pump speed of 3000 rpm.

Table 7.13 Numerical results obtained from the surface responses related to FC system.

		Cell Temperature, °C				**Thermal Dispersion, °C**			
		Tamb: 10-17.5 °C / Fan *PWM: 70-85%*		**Tamb: 17.5-25 °C / Fan *PWM: 85-100%***		**Tamb: 10-17.5 °C / Fan *PWM: 70-85%***		**Tamb: 17.5-25 °C / Fan *PWM: 85-100%***	
		Min	**Max**	**Min**	**Max**	**Min**	**Max**	**Min**	**Max**
Pump Speed	2000 rpm	24,0	26,2	25,3	31,4	**3,7**	**4,6**	**3,4**	**4,4**
	3000 rpm	24,2	25,9	24,9	30,2	1,0	1,8	1,0	1,9
	4000 rpm	24,5	26,0	24,8	29,3	0,5	1,2	0,7	1,4

By means of these figures and table, it has been verified the conclusions obtained from the Table 7.12 referring to the p-values. It has been evidenced that the *BP* maximum temperature has changed mainly because of the influence of ambient temperature, while the thermal dispersion has been especially influenced by pump rotational speed: greater rotational speed of the pump, the lower thermal dispersion within the *BP*.

On the basis of this study, it has been defined a pump rotational speed and a fan *PWM* of 2300 rpm and 98% respectively, to keep the maximum temperature and thermal dispersion within the *BP* for the maximum tested ambient temperature of 25 ºC for *FC* mode at 31.2ºC and 3.0 ºC, respectively. This rotational speed of the pump and fan correspond to a total liquid flow rate in the system of 2.95 lpm (0.74 lpm through each cold plate) and 0.573 $m^3 \cdot s^{-1}$ air flow rate. Moreover, for soft ambient conditions, such as 10 ºC and 17.5 ºC, for the same pump rotational speed it should be enough to keep the fan *PWM* at 92.5% and 80.5%, respectively for each ambient temperature.

In conclusion, it can be said that with smaller components regarding the pump and the fan would be enough to keep the *BP* of this urban electric minibus within adequate thermal operation conditions for at maximum ambient temperature of 25 ºC by means of a *FC* system.

Active Cooling

The same procedure as for the *FC* system has been carried out in order to optimize the *AC* system. For this system four factors have been defined as it can be seen in Table 7.14 : the pump rotational speed (2000 rpm, 3000 rpm and 4000 rpm), the fan *PWM* (70% *PWM*, 85% *PWM* and 100% *PWM*), the compressor rotational speed (1800 rpm, 2400 rpm and 3600 rpm) and ambient temperature (25 ºC, 35 ºC and 45 ºC).

Table 7.14. DoE matrix for AC system

	Coded Value				UnCoded Value			
	Pump	Fan	Compressor	Tamb	Pump Speed, rpm	Fan *PWM* , %	Compressor Speed, rpm	Tamb, ºC
1	-1	1	1	1	2000	100	3000	45
2	0	0	0	0	3000	85	2400	35
3	-1	1	-1	-1	2000	100	1800	25
4	1	1	1	-1	4000	100	3000	25
5	-1	1	-1	1	2000	100	1800	45
6	1	1	-1	1	4000	100	1800	45
7	1	-1	-1	-1	4000	70	1800	25
8	-1	-1	-1	1	2000	70	1800	45
9	-1	1	1	-1	2000	100	3000	25
10	1	-1	1	-1	4000	70	3000	25
11	-1	-1	1	-1	2000	70	3000	25
12	1	1	1	1	4000	100	3000	45
13	-1	-1	1	1	2000	70	3000	45
14	1	-1	1	1	4000	70	3000	45
15	-1	-1	-1	-1	2000	70	1800	25
16	1	-1	-1	1	4000	70	1800	45
17	1	1	-1	-1	4000	100	1800	25
18	0	-1	0	0	3000	70	2400	35
19	0	1	0	0	3000	100	2400	35
20	-1	0	0	0	2000	85	2400	35
21	1	0	0	0	4000	85	2400	35
22	0	0	-1	0	3000	85	1800	35
23	0	0	1	0	3000	85	3000	35
24	0	0	0	-1	3000	85	2400	25
25	0	0	0	1	3000	85	2400	45

In Table 7.15 are shown the numerical results have been obtained for each test that has been carried out. The maximum temperature and the thermal dispersion within the *BP* has been evaluated such as response variables in each test.

Table 7.15 Numerical results correspondent to the DoE matrix related to AC system

	Pump	Fan	Compressor	Tamb	Tmax *BP* , ºC	Dispersion *BP* , ºC
1	-1	1	1	1	25.73	5.32
2	0	0	0	0	24.91	2.91
3	-1	1	-1	-1	25.25	4.95
4	1	1	1	-1	25.28	1.79
5	-1	1	-1	1	24.31	4.39
6	1	1	-1	1	24.96	1.52
7	1	-1	-1	-1	25.33	1.70
8	-1	-1	-1	1	25.58	4.88
9	-1	1	1	-1	25.74	5.24
10	1	-1	1	-1	25.48	1.76
11	-1	-1	1	-1	25.45	5.63
12	1	1	1	1	24.85	1.88
13	-1	-1	1	1	25.56	5.42
14	1	-1	1	1	25.45	1.76
15	-1	-1	-1	-1	25.53	4.92
16	1	-1	-1	1	25.31	1.47
17	1	1	-1	-1	24.84	1.69
18	0	-1	0	0	25.67	2.41
19	0	1	0	0	24.97	2.83
20	-1	0	0	0	25.66	5.28
21	1	0	0	0	25.37	1.65
22	0	0	-1	0	25.79	2.30
23	0	0	1	0	25.16	2.98
24	0	0	0	-1	25.09	2.89
25	0	0	0	1	25.44	2.60

Applying the *Face Centered CCD* the regression surface response of each variable has been obtained. The equation which defines the surface response regarding the cell maximum temperature and thermal dispersion has been defined by means of the coefficients tabulated in Table 7.16. The p-value of each term is also shown. It indicates how significant ($p<0.005$) or not is the effect of the variable on the response.

Based on the results obtained in Table 7.16 it can be seen that the maximum temperature of the *BP* has been independent to any factor, the same conclusion that it be drawn based on the results obtained in Table 7.15. However, the thermal dispersion has been especially influenced by pump and compressor speed lineally and by the quadratic effect of the hydraulic pump rotational speed.

Table 7.16 Coefficients correspondent to the regression surface response of maximum temperature and thermal dispersion within the BP together with the p-values.

	Maximum *BP* temperature		Thermal Dispersion	
	Coefficients	p- value, [-]	Coefficients	p- value, [-]
Constant	25.3315	0.000	2.7323	0.000
Pump Speed	-0.1078	0.241	-1.7117	**0.000**
Fan *PWM*	-0.1906	0.052	-0.0189	0.662
Compressor	0.1000	0.274	0.2200	**0.000**
Tamb	-0.044	0.618	-0.0739	0.109
Pump Speed * Pump Speed	0.1132	0.633	0.7622	**0.000**
Fan PWM * Fan *PWM*	-0.0818	0.729	-0.0827	0.475
Compressor * Compressor	0.0732	0.756	-0.0628	0.586
Tamb*Tamb	-0.1368	0.565	0.0422	0.713
Pump Speed *Fan *PWM*	-0.0344	0.715	0.0712	0.140
Pump Speed * Compressor	-0.0744	0.436	-0.1037	0.042
Pump Speed * Tamb	0.0269	0.775	0.0262	0.568
Fan *PWM* * Compressor	0.1281	0.192	0.0050	0.913
Fan *PWM* * Tamb	-0.0856	0.372	-0.0050	0.913
Compressor * Tamb	0.0269	0.775	0.0600	0.207

Because the non-influence of any parameter on the *BM* temperature with the *AC* system, it has been decided not to analyze this parameter following by the surface responses. It is obvious that this effect is thanked the compressor, even if at the

minimum rotational speed or even, at maximum ambient conditions. Evidently, at the higher rotational speed of the compressor, faster it can reach the fixed temperature, which it will be analyzed following. This statement is also an evidence of the oversized *TMS*.

The R-square (R^2) value related to the surface response of the thermal dispersion for this *AC* system has been of 99.44%, so it can be said that the obtained surface response model has been representative of the simulation results obtained.

With regards to thermal dispersion, as an example in Figure *7.33* are shown the response surfaces correspondent the thermal dispersion for different rotational speed of the pump ((a) 2000 rpm, (b) 3000 rpm and (c) 4000 rpm) for a fan intermediate *PWM* value of 85%. As it can be seen, when the rotational speed of the pump has increased the thermal dispersion within the *BP* decreased. In fact, it can be concluded that by means of the established minimal rotational speed of the pump, no admissible thermal dispersion values have been obtained. In addition, Table 7.17 in are summarized the results obtained in this study.

Based on the numerical results show in Table 7.17, it can be seen effectively that when the pump has worked at 2000 rpm the thermal dispersion has been higher than the maximum limit (5ºC). Also, it can be observed a little effect of the fan, that when its *PWM* values increased, the *BP* temperature slightly decreased.

For the worst ambient conditions, 45 ºC, and considering the objective to minimize the overall system consumption it can be concluded that when a rotational speed of the pump has been at 2950 rpm, which has supposed a total liquid flow rate of 4.5 lpm (1.13 lpm for each cold plate), a *PWM* in the fan of 70% and a rotational speed at the compressor of 1800 rpm, it has been possible to reach a *BP* temperature of 25.5 ºC and a thermal dispersion of 3.0 ºC. For the same conditions it would be possible to increase the compressor rotational speed in order to drop the temperature faster from the initial 45 ºC to the fixed 25 ºC, but in exchange for a higher consumption.

Compressor speed		T amb																														
		20.0	21.0	22.0	23.0	24.0	**25.0**	26.0	27.0	28.0	29.0	30.0	31.0	32.0	33.0	34.0	**35.0**	36.0	37.0	38.0	39.0	40.0	41.0	42.0	43.0	44.0	**45.0**	46.0	47.0	48.0	49.0	50.0
rpm		-1.5	-1.4	-1.3	-1.2	-1.1	**-1.0**	-0.9	-0.8	-0.7	-0.6	-0.5	-0.4	-0.3	-0.2	-0.1	**0.0**	0.1	0.2	0.3	0.4	0.5	0.6	0.7	0.8	0.9	**1.0**	1.1	1.2	1.3	1.4	1.5
1500	-1.5	5.0	5.0	5.0	5.1	5.1	5.2	5.2	5.2	5.3	5.3	5.3	5.3	5.4	5.4	5.4	5.5	5.5	5.5	5.5	5.5	5.6	5.6	5.6	5.6	5.6	5.6	5.6	5.6	5.6	5.7	5.7
1560	-1.4	4.9	5.0	5.0	5.1	5.1	5.1	5.2	5.2	5.2	5.3	5.3	5.3	5.4	5.4	5.4	5.4	5.5	5.5	5.5	5.5	5.5	5.6	5.6	5.6	5.6	5.6	5.6	5.6	5.6	5.6	5.6
1620	-1.3	4.9	4.9	5.0	5.0	5.1	5.1	5.1	5.2	5.2	5.2	5.3	5.3	5.3	5.4	5.4	5.4	5.4	5.5	5.5	5.5	5.5	5.5	5.5	5.5	5.6	5.6	5.6	5.6	5.6	5.6	5.6
1680	-1.2	4.9	4.9	5.0	5.0	5.0	5.1	5.1	5.1	5.2	5.2	5.2	5.3	5.3	5.3	5.4	5.4	5.4	5.4	5.5	5.5	5.5	5.5	5.5	5.5	5.6	5.6	5.6	5.6	5.6	5.6	5.6
1740	-1.1	4.8	4.9	4.9	5.0	5.0	5.0	5.1	5.1	5.2	5.2	5.2	5.3	5.3	5.3	5.3	5.4	5.4	5.4	5.4	5.5	5.5	5.5	5.5	5.5	5.5	5.6	5.6	5.6	5.6	5.6	5.6
1800	**-1.0**	4.8	4.9	4.9	4.9	5.0	5.0	5.1	5.1	5.1	5.2	5.2	5.2	5.3	5.3	5.3	5.3	5.4	5.4	5.4	5.4	5.5	5.5	5.5	5.5	5.5	5.5	5.6	5.6	5.6	5.6	5.6
1860	-0.9	4.8	4.8	4.9	4.9	5.0	5.0	5.0	5.1	5.1	5.1	5.2	5.2	5.2	5.3	5.3	5.3	5.4	5.4	5.4	5.4	5.4	5.5	5.5	5.5	5.5	5.5	5.6	5.6	5.6	5.6	5.6
1920	-0.8	4.8	4.8	4.8	4.9	4.9	5.0	5.0	5.1	5.1	5.1	5.2	5.2	5.2	5.3	5.3	5.3	5.3	5.4	5.4	5.4	5.4	5.5	5.5	5.5	5.5	5.5	5.5	5.6	5.6	5.6	5.6
1980	-0.7	4.7	4.8	4.8	4.9	4.9	5.0	5.0	5.0	5.1	5.1	5.1	5.2	5.2	5.2	5.3	5.3	5.3	5.4	5.4	5.4	5.4	5.4	5.5	5.5	5.5	5.5	5.5	5.5	5.6	5.6	5.6
2040	-0.6	4.7	4.8	4.8	4.8	4.9	4.9	5.0	5.0	5.0	5.1	5.1	5.2	5.2	5.2	5.3	5.3	5.3	5.3	5.4	5.4	5.4	5.5	5.5	5.5	5.5	5.5	5.5	5.5	5.6	5.6	5.6
2100	-0.5	4.7	4.7	4.8	4.8	4.9	4.9	5.0	5.0	5.0	5.1	5.1	5.1	5.2	5.2	5.2	5.3	5.3	5.3	5.3	5.4	5.4	5.4	5.4	5.5	5.5	5.5	5.5	5.5	5.5	5.6	5.6
2160	-0.4	4.7	4.7	4.8	4.8	4.8	4.9	4.9	5.0	5.0	5.1	5.1	5.1	5.2	5.2	5.2	5.3	5.3	5.3	5.3	5.4	5.4	5.4	5.4	5.5	5.5	5.5	5.5	5.5	5.5	5.5	5.6
2220	-0.3	4.6	4.7	4.7	4.8	4.8	4.9	4.9	5.0	5.0	5.0	5.1	5.1	5.1	5.2	5.2	5.2	5.3	5.3	5.3	5.4	5.4	5.4	5.4	5.4	5.5	5.5	5.5	5.5	5.5	5.5	5.6
2280	-0.2	4.6	4.7	4.7	4.8	4.8	4.9	4.9	4.9	5.0	5.0	5.1	5.1	5.1	5.2	5.2	5.2	5.3	5.3	5.3	5.3	5.4	5.4	5.4	5.4	5.5	5.5	5.5	5.5	5.5	5.5	5.6
2340	-0.1	4.6	4.6	4.7	4.7	4.8	4.8	4.9	4.9	5.0	5.0	5.0	5.1	5.1	5.2	5.2	5.2	5.2	5.3	5.3	5.3	5.4	5.4	5.4	5.4	5.5	5.5	5.5	5.5	5.5	5.5	5.6
2400	**0.0**	4.6	4.6	4.7	4.7	4.8	4.8	4.9	4.9	4.9	5.0	5.0	5.1	5.1	5.1	5.2	5.2	5.2	5.3	5.3	5.3	5.4	5.4	5.4	5.4	5.4	5.5	5.5	5.5	5.5	5.5	5.6
2460	0.1	4.6	4.6	4.7	4.7	4.8	4.8	4.8	4.9	4.9	5.0	5.0	5.1	5.1	5.1	5.2	5.2	5.2	5.3	5.3	5.3	5.3	5.4	5.4	5.4	5.4	5.5	5.5	5.5	5.5	5.5	5.6
2520	0.2	4.5	4.6	4.6	4.7	4.7	4.8	4.8	4.9	4.9	5.0	5.0	5.0	5.1	5.1	5.2	5.2	5.2	5.3	5.3	5.3	5.3	5.4	5.4	5.4	5.4	5.5	5.5	5.5	5.5	5.5	5.6
2580	0.3	4.5	4.6	4.6	4.7	4.7	4.8	4.8	4.9	4.9	5.0	5.0	5.0	5.1	5.1	5.1	5.2	5.2	5.2	5.3	5.3	5.3	5.4	5.4	5.4	5.4	5.5	5.5	5.5	5.5	5.5	5.6
2640	0.4	4.5	4.6	4.6	4.7	4.7	4.8	4.8	4.9	4.9	4.9	5.0	5.0	5.1	5.1	5.1	5.2	5.2	5.2	5.3	5.3	5.3	5.4	5.4	5.4	5.4	5.5	5.5	5.5	5.5	5.5	5.6
2700	0.5	4.5	4.5	4.6	4.7	4.7	4.8	4.8	4.8	4.9	4.9	5.0	5.0	5.1	5.1	5.1	5.2	5.2	5.2	5.3	5.3	5.3	5.4	5.4	5.4	5.4	5.5	5.5	5.5	5.5	5.5	5.6
2760	0.6	4.5	4.5	4.6	4.6	4.7	4.7	4.8	4.8	4.9	4.9	5.0	5.0	5.0	5.1	5.1	5.2	5.2	5.2	5.3	5.3	5.3	5.4	5.4	5.4	5.4	5.5	5.5	5.5	5.5	5.5	5.6
2820	0.7	4.5	4.5	4.6	4.6	4.7	4.7	4.8	4.8	4.9	4.9	5.0	5.0	5.0	5.1	5.1	5.2	5.2	5.2	5.3	5.3	5.3	5.4	5.4	5.4	5.4	5.5	5.5	5.5	5.5	5.5	5.6
2880	0.8	4.5	4.5	4.6	4.6	4.7	4.7	4.8	4.8	4.9	4.9	5.0	5.0	5.0	5.1	5.1	5.2	5.2	5.2	5.3	5.3	5.3	5.4	5.4	5.4	5.4	5.5	5.5	5.5	5.5	5.6	5.6
2940	0.9	4.4	4.5	4.6	4.6	4.7	4.7	4.8	4.8	4.9	4.9	4.9	5.0	5.0	5.1	5.1	5.2	5.2	5.2	5.3	5.3	5.3	5.4	5.4	5.4	5.4	5.5	5.5	5.5	5.5	5.6	5.6
3000	**1.0**	4.4	4.5	4.5	4.6	4.7	4.7	4.8	4.8	4.8	4.9	4.9	5.0	5.0	5.1	5.1	5.1	5.2	5.2	5.3	5.3	5.3	5.4	5.4	5.4	5.4	5.5	5.5	5.5	5.5	5.6	5.6
3060	1.1	4.4	4.5	4.5	4.6	4.6	4.7	4.7	4.8	4.8	4.9	4.9	5.0	5.0	5.1	5.1	5.1	5.2	5.2	5.3	5.3	5.3	5.4	5.4	5.4	5.4	5.5	5.5	5.5	5.5	5.6	5.6
3120	1.2	4.4	4.5	4.5	4.6	4.6	4.7	4.7	4.8	4.8	4.9	4.9	5.0	5.0	5.1	5.1	5.1	5.2	5.2	5.3	5.3	5.3	5.4	5.4	5.4	5.5	5.5	5.5	5.5	5.6	5.6	5.6
3180	1.3	4.4	4.5	4.5	4.6	4.6	4.7	4.7	4.8	4.8	4.9	4.9	5.0	5.0	5.1	5.1	5.1	5.2	5.2	5.3	5.3	5.3	5.4	5.4	5.4	5.5	5.5	5.5	5.5	5.6	5.6	5.6
3240	1.4	4.4	4.5	4.5	4.6	4.6	4.7	4.7	4.8	4.8	4.9	4.9	5.0	5.0	5.1	5.1	5.1	5.2	5.2	5.3	5.3	5.3	5.4	5.4	5.4	5.5	5.5	5.5	5.5	5.6	5.6	5.6
3300	1.5	4.4	4.4	4.5	4.6	4.6	4.7	4.7	4.8	4.8	4.9	4.9	5.0	5.0	5.1	5.1	5.2	5.2	5.2	5.3	5.3	5.3	5.4	5.4	5.4	5.5	5.5	5.5	5.6	5.6	5.6	5.6

(a)

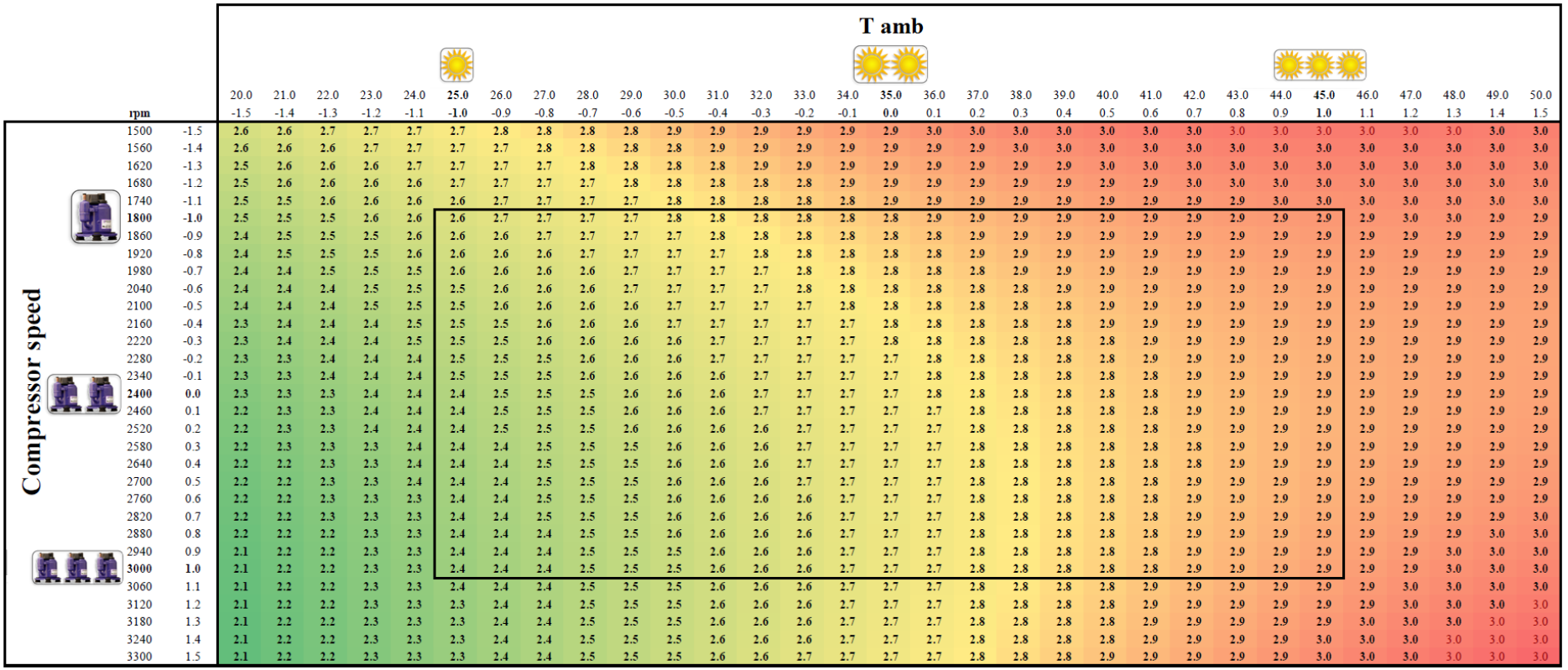

Compressor speed			T amb																																
			20.0	21.0	22.0	23.0	24.0	**25.0**	26.0	27.0	28.0	29.0	30.0	31.0	32.0	33.0	34.0	**35.0**	36.0	37.0	38.0	39.0	40.0	41.0	42.0	43.0	44.0	**45.0**	46.0	47.0	48.0	49.0	50.0
	rpm		-1.5	-1.4	-1.3	-1.2	-1.1	**-1.0**	-0.9	-0.8	-0.7	-0.6	-0.5	-0.4	-0.3	-0.2	-0.1	**0.0**	0.1	0.2	0.3	0.4	0.5	0.6	0.7	0.8	0.9	**1.0**	1.1	1.2	1.3	1.4	1.5
	1500	-1.5	2.6	2.6	2.7	2.7	2.7	2.7	2.8	2.8	2.8	2.8	2.9	2.9	2.9	2.9	2.9	2.9	3.0	3.0	3.0	3.0	3.0	3.0	3.0	3.0	3.0	3.0	3.0	3.0	3.0	3.0	3.0	3.0	3.0
	1560	-1.4	2.6	2.6	2.6	2.7	2.7	2.7	2.7	2.8	2.8	2.8	2.8	2.9	2.9	2.9	2.9	2.9	2.9	2.9	3.0	3.0	3.0	3.0	3.0	3.0	3.0	3.0	3.0	3.0	3.0	3.0	3.0	3.0	3.0
	1620	-1.3	2.5	2.6	2.6	2.6	2.7	2.7	2.7	2.7	2.8	2.8	2.8	2.8	2.9	2.9	2.9	2.9	2.9	2.9	2.9	2.9	3.0	3.0	3.0	3.0	3.0	3.0	3.0	3.0	3.0	3.0	3.0	3.0	3.0
	1680	-1.2	2.5	2.6	2.6	2.6	2.6	2.7	2.7	2.7	2.7	2.8	2.8	2.8	2.8	2.8	2.9	2.9	2.9	2.9	2.9	2.9	2.9	2.9	3.0	3.0	3.0	3.0	3.0	3.0	3.0	3.0	3.0	3.0	3.0
	1740	-1.1	2.5	2.5	2.6	2.6	2.6	2.6	2.7	2.7	2.7	2.7	2.8	2.8	2.8	2.8	2.8	2.9	2.9	2.9	2.9	2.9	2.9	2.9	2.9	2.9	3.0	3.0	3.0	3.0	3.0	3.0	3.0	3.0	3.0
	1800	**-1.0**	2.5	2.5	2.5	2.6	2.6	2.6	2.7	2.7	2.7	2.7	2.8	2.8	2.8	2.8	2.8	2.8	2.9	2.9	2.9	2.9	2.9	2.9	2.9	2.9	2.9	2.9	2.9	3.0	3.0	2.9	2.9	2.9	2.9
	1860	-0.9	2.4	2.5	2.5	2.5	2.6	2.6	2.6	2.7	2.7	2.7	2.7	2.8	2.8	2.8	2.8	2.8	2.8	2.9	2.9	2.9	2.9	2.9	2.9	2.9	2.9	2.9	2.9	2.9	2.9	2.9	2.9	2.9	2.9
	1920	-0.8	2.4	2.5	2.5	2.5	2.6	2.6	2.6	2.6	2.7	2.7	2.7	2.7	2.8	2.8	2.8	2.8	2.8	2.8	2.9	2.9	2.9	2.9	2.9	2.9	2.9	2.9	2.9	2.9	2.9	2.9	2.9	2.9	2.9
	1980	-0.7	2.4	2.4	2.5	2.5	2.5	2.6	2.6	2.6	2.6	2.7	2.7	2.7	2.7	2.8	2.8	2.8	2.8	2.8	2.9	2.9	2.9	2.9	2.9	2.9	2.9	2.9	2.9	2.9	2.9	2.9	2.9	2.9	2.9
	2040	-0.6	2.4	2.4	2.4	2.5	2.5	2.5	2.6	2.6	2.6	2.7	2.7	2.7	2.7	2.8	2.8	2.8	2.8	2.8	2.8	2.9	2.9	2.9	2.9	2.9	2.9	2.9	2.9	2.9	2.9	2.9	2.9	2.9	2.9
	2100	-0.5	2.4	2.4	2.4	2.5	2.5	2.5	2.6	2.6	2.6	2.6	2.7	2.7	2.7	2.7	2.8	2.8	2.8	2.8	2.8	2.8	2.9	2.9	2.9	2.9	2.9	2.9	2.9	2.9	2.9	2.9	2.9	2.9	2.9
	2160	-0.4	2.3	2.4	2.4	2.4	2.5	2.5	2.5	2.6	2.6	2.6	2.7	2.7	2.7	2.7	2.7	2.8	2.8	2.8	2.8	2.8	2.8	2.9	2.9	2.9	2.9	2.9	2.9	2.9	2.9	2.9	2.9	2.9	2.9
	2220	-0.3	2.3	2.4	2.4	2.4	2.5	2.5	2.5	2.6	2.6	2.6	2.6	2.7	2.7	2.7	2.7	2.8	2.8	2.8	2.8	2.8	2.8	2.9	2.9	2.9	2.9	2.9	2.9	2.9	2.9	2.9	2.9	2.9	2.9
	2280	-0.2	2.3	2.3	2.4	2.4	2.4	2.5	2.5	2.5	2.6	2.6	2.6	2.7	2.7	2.7	2.7	2.7	2.8	2.8	2.8	2.8	2.8	2.9	2.9	2.9	2.9	2.9	2.9	2.9	2.9	2.9	2.9	2.9	2.9
	2340	-0.1	2.3	2.3	2.4	2.4	2.4	2.5	2.5	2.5	2.6	2.6	2.6	2.6	2.7	2.7	2.7	2.7	2.8	2.8	2.8	2.8	2.8	2.8	2.9	2.9	2.9	2.9	2.9	2.9	2.9	2.9	2.9	2.9	2.9
	2400	**0.0**	2.3	2.3	2.3	2.4	2.4	2.4	2.5	2.5	2.5	2.6	2.6	2.6	2.7	2.7	2.7	2.7	2.8	2.8	2.8	2.8	2.8	2.8	2.9	2.9	2.9	2.9	2.9	2.9	2.9	2.9	2.9	2.9	2.9
	2460	0.1	2.2	2.3	2.3	2.4	2.4	2.4	2.5	2.5	2.5	2.6	2.6	2.6	2.7	2.7	2.7	2.7	2.7	2.8	2.8	2.8	2.8	2.8	2.9	2.9	2.9	2.9	2.9	2.9	2.9	2.9	2.9	2.9	2.9
	2520	0.2	2.2	2.3	2.3	2.4	2.4	2.4	2.5	2.5	2.5	2.6	2.6	2.6	2.6	2.7	2.7	2.7	2.7	2.8	2.8	2.8	2.8	2.8	2.9	2.9	2.9	2.9	2.9	2.9	2.9	2.9	2.9	2.9	2.9
	2580	0.3	2.2	2.3	2.3	2.3	2.4	2.4	2.4	2.5	2.5	2.5	2.6	2.6	2.6	2.7	2.7	2.7	2.7	2.8	2.8	2.8	2.8	2.8	2.8	2.9	2.9	2.9	2.9	2.9	2.9	2.9	2.9	2.9	2.9
	2640	0.4	2.2	2.2	2.3	2.3	2.4	2.4	2.4	2.5	2.5	2.5	2.6	2.6	2.6	2.7	2.7	2.7	2.7	2.8	2.8	2.8	2.8	2.8	2.8	2.9	2.9	2.9	2.9	2.9	2.9	2.9	2.9	2.9	2.9
	2700	0.5	2.2	2.2	2.3	2.3	2.4	2.4	2.4	2.5	2.5	2.5	2.6	2.6	2.6	2.7	2.7	2.7	2.7	2.8	2.8	2.8	2.8	2.8	2.8	2.9	2.9	2.9	2.9	2.9	2.9	2.9	2.9	2.9	2.9
	2760	0.6	2.2	2.2	2.3	2.3	2.3	2.4	2.4	2.5	2.5	2.5	2.6	2.6	2.6	2.6	2.7	2.7	2.7	2.8	2.8	2.8	2.8	2.8	2.8	2.9	2.9	2.9	2.9	2.9	2.9	2.9	2.9	2.9	2.9
	2820	0.7	2.2	2.2	2.3	2.3	2.3	2.4	2.4	2.5	2.5	2.5	2.6	2.6	2.6	2.6	2.7	2.7	2.7	2.8	2.8	2.8	2.8	2.8	2.8	2.9	2.9	2.9	2.9	2.9	2.9	2.9	2.9	2.9	3.0
	2880	0.8	2.2	2.2	2.2	2.3	2.3	2.4	2.4	2.4	2.5	2.5	2.6	2.6	2.6	2.6	2.7	2.7	2.7	2.8	2.8	2.8	2.8	2.8	2.8	2.9	2.9	2.9	2.9	2.9	2.9	2.9	3.0	3.0	3.0
	2940	0.9	2.1	2.2	2.2	2.3	2.3	2.4	2.4	2.4	2.5	2.5	2.5	2.6	2.6	2.6	2.7	2.7	2.7	2.8	2.8	2.8	2.8	2.8	2.9	2.9	2.9	2.9	2.9	2.9	2.9	3.0	3.0	3.0	3.0
	3000	**1.0**	2.1	2.2	2.2	2.3	2.3	2.4	2.4	2.4	2.5	2.5	2.5	2.6	2.6	2.6	2.7	2.7	2.7	2.8	2.8	2.8	2.8	2.8	2.9	2.9	2.9	2.9	2.9	2.9	2.9	3.0	3.0	3.0	3.0
	3060	1.1	2.1	2.2	2.2	2.3	2.3	2.4	2.4	2.4	2.5	2.5	2.5	2.6	2.6	2.6	2.7	2.7	2.7	2.8	2.8	2.8	2.8	2.9	2.9	2.9	2.9	2.9	2.9	3.0	3.0	3.0	3.0	3.0	3.0
	3120	1.2	2.1	2.2	2.2	2.3	2.3	2.3	2.4	2.4	2.5	2.5	2.5	2.6	2.6	2.6	2.7	2.7	2.7	2.8	2.8	2.8	2.8	2.9	2.9	2.9	2.9	2.9	2.9	3.0	3.0	3.0	3.0	3.0	3.0
	3180	1.3	2.1	2.2	2.2	2.3	2.3	2.3	2.4	2.4	2.5	2.5	2.5	2.6	2.6	2.6	2.7	2.7	2.7	2.8	2.8	2.8	2.8	2.9	2.9	2.9	2.9	2.9	3.0	3.0	3.0	3.0	3.0	3.0	3.0
	3240	1.4	2.1	2.2	2.2	2.3	2.3	2.3	2.4	2.4	2.5	2.5	2.5	2.6	2.6	2.6	2.7	2.7	2.7	2.8	2.8	2.8	2.8	2.9	2.9	2.9	2.9	3.0	3.0	3.0	3.0	3.0	3.0	3.0	3.0
	3300	1.5	2.1	2.2	2.2	2.3	2.3	2.3	2.4	2.4	2.5	2.5	2.5	2.6	2.6	2.7	2.7	2.7	2.7	2.8	2.8	2.8	2.9	2.9	2.9	2.9	2.9	3.0	3.0	3.0	3.0	3.0	3.0	3.0	3.0

(b)

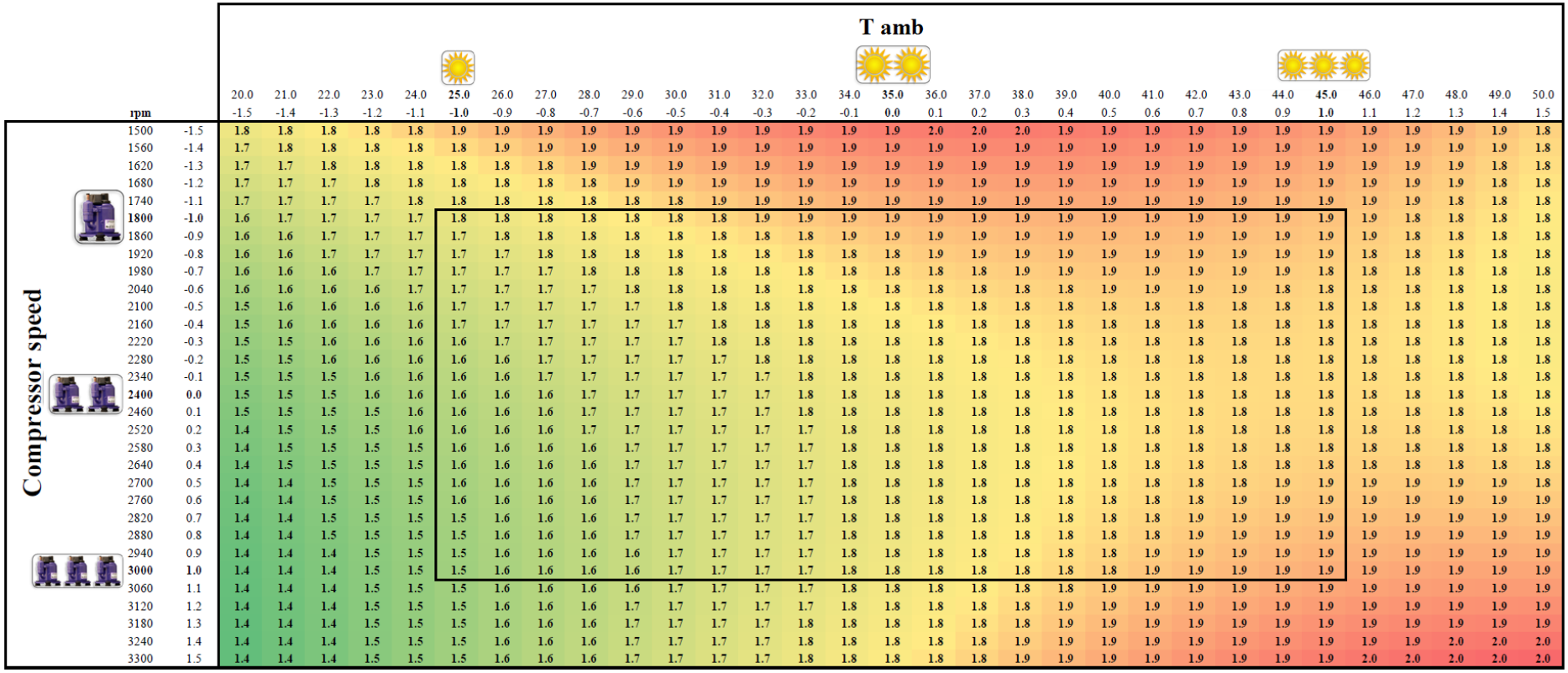

rpm		20.0	21.0	22.0	23.0	24.0	25.0	26.0	27.0	28.0	29.0	30.0	31.0	32.0	33.0	34.0	35.0	36.0	37.0	38.0	39.0	40.0	41.0	42.0	43.0	44.0	45.0	46.0	47.0	48.0	49.0	50.0
		-1.5	-1.4	-1.3	-1.2	-1.1	-1.0	-0.9	-0.8	-0.7	-0.6	-0.5	-0.4	-0.3	-0.2	-0.1	0.0	0.1	0.2	0.3	0.4	0.5	0.6	0.7	0.8	0.9	1.0	1.1	1.2	1.3	1.4	1.5
1500	-1.5	1.8	1.8	1.8	1.8	1.8	1.9	1.9	1.9	1.9	1.9	1.9	1.9	1.9	1.9	1.9	1.9	2.0	2.0	2.0	1.9	1.9	1.9	1.9	1.9	1.9	1.9	1.9	1.9	1.9	1.9	1.8
1560	-1.4	1.7	1.8	1.8	1.8	1.8	1.8	1.9	1.9	1.9	1.9	1.9	1.9	1.9	1.9	1.9	1.9	1.9	1.9	1.9	1.9	1.9	1.9	1.9	1.9	1.9	1.9	1.9	1.9	1.9	1.9	1.8
1620	-1.3	1.7	1.7	1.8	1.8	1.8	1.8	1.8	1.8	1.9	1.9	1.9	1.9	1.9	1.9	1.9	1.9	1.9	1.9	1.9	1.9	1.9	1.9	1.9	1.9	1.9	1.9	1.9	1.9	1.9	1.8	1.8
1680	-1.2	1.7	1.7	1.7	1.8	1.8	1.8	1.8	1.8	1.8	1.9	1.9	1.9	1.9	1.9	1.9	1.9	1.9	1.9	1.9	1.9	1.9	1.9	1.9	1.9	1.9	1.9	1.9	1.9	1.9	1.8	1.8
1740	-1.1	1.7	1.7	1.7	1.7	1.8	1.8	1.8	1.8	1.8	1.8	1.8	1.9	1.9	1.9	1.9	1.9	1.9	1.9	1.9	1.9	1.9	1.9	1.9	1.9	1.9	1.9	1.9	1.9	1.8	1.8	1.8
1800	**-1.0**	1.6	1.7	1.7	1.7	1.7	1.8	1.8	1.8	1.8	1.8	1.8	1.8	1.9	1.9	1.9	1.9	1.9	1.9	1.9	1.9	1.9	1.9	1.9	1.9	1.9	1.9	1.9	1.8	1.8	1.8	1.8
1860	-0.9	1.6	1.6	1.7	1.7	1.7	1.7	1.8	1.8	1.8	1.8	1.8	1.8	1.8	1.8	1.9	1.9	1.9	1.9	1.9	1.9	1.9	1.9	1.9	1.9	1.9	1.9	1.9	1.8	1.8	1.8	1.8
1920	-0.8	1.6	1.6	1.7	1.7	1.7	1.7	1.7	1.8	1.8	1.8	1.8	1.8	1.8	1.8	1.8	1.8	1.9	1.9	1.9	1.9	1.9	1.9	1.9	1.9	1.9	1.9	1.8	1.8	1.8	1.8	1.8
1980	-0.7	1.6	1.6	1.6	1.7	1.7	1.7	1.7	1.7	1.8	1.8	1.8	1.8	1.8	1.8	1.8	1.8	1.8	1.8	1.9	1.9	1.9	1.9	1.9	1.9	1.9	1.8	1.8	1.8	1.8	1.8	1.8
2040	-0.6	1.6	1.6	1.6	1.6	1.7	1.7	1.7	1.7	1.7	1.8	1.8	1.8	1.8	1.8	1.8	1.8	1.8	1.8	1.8	1.8	1.9	1.9	1.9	1.9	1.8	1.8	1.8	1.8	1.8	1.8	1.8
2100	-0.5	1.5	1.6	1.6	1.6	1.6	1.7	1.7	1.7	1.7	1.7	1.8	1.8	1.8	1.8	1.8	1.8	1.8	1.8	1.8	1.8	1.8	1.8	1.8	1.8	1.8	1.8	1.8	1.8	1.8	1.8	1.8
2160	-0.4	1.5	1.6	1.6	1.6	1.6	1.7	1.7	1.7	1.7	1.7	1.7	1.8	1.8	1.8	1.8	1.8	1.8	1.8	1.8	1.8	1.8	1.8	1.8	1.8	1.8	1.8	1.8	1.8	1.8	1.8	1.8
2220	-0.3	1.5	1.5	1.6	1.6	1.6	1.6	1.7	1.7	1.7	1.7	1.7	1.8	1.8	1.8	1.8	1.8	1.8	1.8	1.8	1.8	1.8	1.8	1.8	1.8	1.8	1.8	1.8	1.8	1.8	1.8	1.8
2280	-0.2	1.5	1.5	1.6	1.6	1.6	1.6	1.6	1.7	1.7	1.7	1.7	1.7	1.8	1.8	1.8	1.8	1.8	1.8	1.8	1.8	1.8	1.8	1.8	1.8	1.8	1.8	1.8	1.8	1.8	1.8	1.8
2340	-0.1	1.5	1.5	1.5	1.6	1.6	1.6	1.6	1.7	1.7	1.7	1.7	1.7	1.7	1.8	1.8	1.8	1.8	1.8	1.8	1.8	1.8	1.8	1.8	1.8	1.8	1.8	1.8	1.8	1.8	1.8	1.8
2400	**0.0**	1.5	1.5	1.5	1.6	1.6	1.6	1.6	1.6	1.7	1.7	1.7	1.7	1.7	1.8	1.8	1.8	1.8	1.8	1.8	1.8	1.8	1.8	1.8	1.8	1.8	1.8	1.8	1.8	1.8	1.8	1.8
2460	0.1	1.5	1.5	1.5	1.5	1.6	1.6	1.6	1.6	1.7	1.7	1.7	1.7	1.7	1.8	1.8	1.8	1.8	1.8	1.8	1.8	1.8	1.8	1.8	1.8	1.8	1.8	1.8	1.8	1.8	1.8	1.8
2520	0.2	1.4	1.5	1.5	1.5	1.6	1.6	1.6	1.6	1.7	1.7	1.7	1.7	1.7	1.7	1.8	1.8	1.8	1.8	1.8	1.8	1.8	1.8	1.8	1.8	1.8	1.8	1.8	1.8	1.8	1.8	1.8
2580	0.3	1.4	1.5	1.5	1.5	1.5	1.6	1.6	1.6	1.6	1.7	1.7	1.7	1.7	1.7	1.8	1.8	1.8	1.8	1.8	1.8	1.8	1.8	1.8	1.8	1.8	1.8	1.8	1.8	1.8	1.8	1.8
2640	0.4	1.4	1.5	1.5	1.5	1.5	1.6	1.6	1.6	1.6	1.7	1.7	1.7	1.7	1.7	1.8	1.8	1.8	1.8	1.8	1.8	1.8	1.8	1.8	1.8	1.8	1.8	1.8	1.8	1.8	1.8	1.8
2700	0.5	1.4	1.4	1.5	1.5	1.5	1.6	1.6	1.6	1.6	1.7	1.7	1.7	1.7	1.7	1.8	1.8	1.8	1.8	1.8	1.8	1.8	1.8	1.8	1.8	1.9	1.9	1.9	1.9	1.9	1.9	1.8
2760	0.6	1.4	1.4	1.5	1.5	1.5	1.6	1.6	1.6	1.6	1.7	1.7	1.7	1.7	1.7	1.8	1.8	1.8	1.8	1.8	1.8	1.8	1.8	1.8	1.9	1.9	1.9	1.9	1.9	1.9	1.9	1.9
2820	0.7	1.4	1.4	1.5	1.5	1.5	1.5	1.6	1.6	1.6	1.7	1.7	1.7	1.7	1.7	1.8	1.8	1.8	1.8	1.8	1.8	1.8	1.8	1.8	1.9	1.9	1.9	1.9	1.9	1.9	1.9	1.9
2880	0.8	1.4	1.4	1.5	1.5	1.5	1.5	1.6	1.6	1.6	1.7	1.7	1.7	1.7	1.7	1.8	1.8	1.8	1.8	1.8	1.8	1.8	1.8	1.8	1.9	1.9	1.9	1.9	1.9	1.9	1.9	1.9
2940	0.9	1.4	1.4	1.4	1.5	1.5	1.5	1.6	1.6	1.6	1.6	1.7	1.7	1.7	1.7	1.8	1.8	1.8	1.8	1.8	1.8	1.8	1.8	1.9	1.9	1.9	1.9	1.9	1.9	1.9	1.9	1.9
3000	**1.0**	1.4	1.4	1.4	1.5	1.5	1.5	1.6	1.6	1.6	1.6	1.7	1.7	1.7	1.7	1.8	1.8	1.8	1.8	1.8	1.8	1.8	1.8	1.9	1.9	1.9	1.9	1.9	1.9	1.9	1.9	1.9
3060	1.1	1.4	1.4	1.4	1.5	1.5	1.5	1.6	1.6	1.6	1.6	1.7	1.7	1.7	1.7	1.8	1.8	1.8	1.8	1.8	1.8	1.8	1.9	1.9	1.9	1.9	1.9	1.9	1.9	1.9	1.9	1.9
3120	1.2	1.4	1.4	1.4	1.5	1.5	1.5	1.6	1.6	1.6	1.7	1.7	1.7	1.7	1.7	1.8	1.8	1.8	1.8	1.8	1.8	1.9	1.9	1.9	1.9	1.9	1.9	1.9	1.9	1.9	1.9	1.9
3180	1.3	1.4	1.4	1.4	1.5	1.5	1.5	1.6	1.6	1.6	1.7	1.7	1.7	1.7	1.8	1.8	1.8	1.8	1.8	1.8	1.9	1.9	1.9	1.9	1.9	1.9	1.9	1.9	1.9	1.9	1.9	1.9
3240	1.4	1.4	1.4	1.4	1.5	1.5	1.5	1.6	1.6	1.6	1.7	1.7	1.7	1.7	1.8	1.8	1.8	1.8	1.8	1.9	1.9	1.9	1.9	1.9	1.9	1.9	1.9	1.9	1.9	2.0	2.0	2.0
3300	1.5	1.4	1.4	1.4	1.5	1.5	1.5	1.6	1.6	1.6	1.7	1.7	1.7	1.7	1.8	1.8	1.8	1.8	1.8	1.9	1.9	1.9	1.9	1.9	1.9	1.9	1.9	2.0	2.0	2.0	2.0	2.0

(c)

Figure 7.33 The surface response correspondent to thermal dispersion at (a) 2000 (b) 3000 and (c) 4000 rpm of pump speed and fan PWM 85%.

Table 7.17 Results obtained for the surface responses correspondent to AC system

		***BP* Temperature, ºC**				**Thermal Dispersion *BP*, ºC**			
		Tamb: 25-35 ºC / Compressor: 1800-2400 rpm		**Tamb: 35-45 ºC / Compressor: 2400-3000 rpm**		**Tamb: 25-35 ºC / Compressor: 1800-2400 rpm**		**Tamb: 35-45 ºC / Compressor: 2400-3000 rpm**	
		Min	**Max**	**Min**	**Max**	**Min**	**Max**	**Min**	**Max**
Pump Speed									
2000 rpm	70% *PWM*	25.5	25.7	25.5	25.7	4.8	5.2	5.0	5.4
	85% *PWM*	25.4	25.6	25.3	25.8	4.8	5.2	5.0	5.4
	100% *PWM*	25.1	25.4	2.0	25.7	4.6	5.1	4.8	5.2
3000 rpm	70% *PWM*	25.3	25.5	25.3	25.5	2.4	2.7	2.6	2.8
	85% *PWM*	25.2	25.3	25.2	25.5	2.4	2.8	2.6	2.9
	100% *PWM*	24.9	25.1	24.8	25.4	2.3	2.7	2.5	2.8
4000 rpm	70% *PWM*	25.3	25.7	25.4	25.5	1.5	1.7	1.6	1.8
	85% *PWM*	25.2	25.4	25.2	25.4	1.6	1.8	1.7	1.9
	100% *PWM*	24.9	25.0	24.8	25.3	1.6	1.8	1.7	1.9

7.5.2 OPTIMIZATION II

Following, the optimization procedure has been applied in order to analyze the thermal resistance in the system for heating purpose for the cases that the ambient temperature is lower than 10 ºC (lower admissible operation temperature limit of the BP). For that purpose, an electric resistance inserted in a vessel placed in the liquid circuit has been proposed. The *BP* has been warmed at the main station and the electric resistor has been powered from the grid. In addition, it is worth mentioning that when the heater was on, simultaneously only the pump has been also working to push the liquid through entire system.

Consequently, the next three factors have been defined as it can be seen in Table 7.18: the pump rotational speed (2000 rpm, 3000 rpm and 4000 rpm), the electric resistance power (500 W, 1500 W and 2500 W)m) and ambient temperature (5 ºC, -5 ºC and -15 ºC).

Table 7.18. DoE matrix for heating process

	Coded Value			UnCoded Value		
	Pump	Resistance	T amb	Pump Speed, rpm	Resistance, W	T amb, ºC
1	1	1	1	4000	2500	5
2	-1	-1	1	2000	500	5
3	1	-1	1	4000	500	5
4	1	-1	-1	4000	500	-15
5	-1	-1	-1	2000	500	-15
6	0	0	0	3000	1500	-5
7	1	1	-1	4000	2500	-15
8	-1	1	-1	2000	2500	-15
9	-1	1	1	2000	2500	5
10	0	0	-1	3000	1500	-15
11	0	0	1	3000	1500	5
12	-1	0	0	2000	1500	-5
13	1	0	0	4000	1500	-5
14	0	1	0	3000	2500	-5
15	0	-1	0	3000	500	-5

In Table 7.19 are shown the numerical results have been obtained for each test that has been carried out. The heating time required by the *BP* to reach 10 ºC, it has been evaluated such as response variable in each test.

Applying the *Face Centered CCD* the regression surface response of each variable has been obtained. The equation which defines the surface response regarding the cell maximum temperature and thermal dispersion has been defined by means of the coefficients tabulated in Table 7.16. The p-value of each term is also shown. It indicates how significant ($p<0.005$) or not is the effect of the variable on the response.

Table 7.19 Numerical results correspondent to the DoE matrix related to heating process of the BP.

	Pump	Resistance	T amb	Time, s	Time, min
1	1	1	1	372.0	6.2
2	-1	-1	1	2369.0	39.5
3	1	-1	1	2302.0	38.4
4	1	-1	-1	14421.0	240.4
5	-1	-1	-1	10966.0	182.8
6	0	0	0	2650.0	44.2
7	1	1	-1	2738.0	45.6
8	-1	1	-1	3257.0	54.3
9	-1	1	1	863.0	14.4
10	0	0	-1	4808.0	80.1
11	0	0	1	818.0	13.6
12	-1	0	0	3134.0	52.2
13	1	0	0	2586.0	43.1
14	0	1	0	1706.0	28.4
15	0	-1	0	7526.0	125.4

Based on the results obtained in Table 7.20, the electric resistance power and ambient temperature have significant effect on the time required to warm the *BP*, and particularly this effect has been inversely proportional to the variable response. The last statement means that, as it has been expected, when the ambient temperature has been higher and also, the power of the thermal resistance, the time required to warm the *BP* has been less. Moreover, the interaction between ambient temperature and electric resistance power has been identified such as significant effect on the response. Besides, pump speed seems not to affect warming time.

Table 7.20 Coefficients correspondent to the regression surface response of maximum temperature and thermal dispersion within the BP together with the p-values.

	Maximum *BP* temperature	
	Coefficients	p- value, [-]
Constant	46.0844	**0.003**
Pump Speed	3.0500	0.564
Resistance	-47.7600	**0.000**
Tamb	-49.1100	**0.000**
Pump Speed * Pump Speed	1.0944	0.915
Resistance * Resistance	30.3444	0.026
Tamb*Tamb	0.2944	0.977
Pump Speed *Resistance	-9.1750	0.157
Pump Speed * Tamb	-7.275	0.244
Resistance * Tamb	33.2500	**0.002**

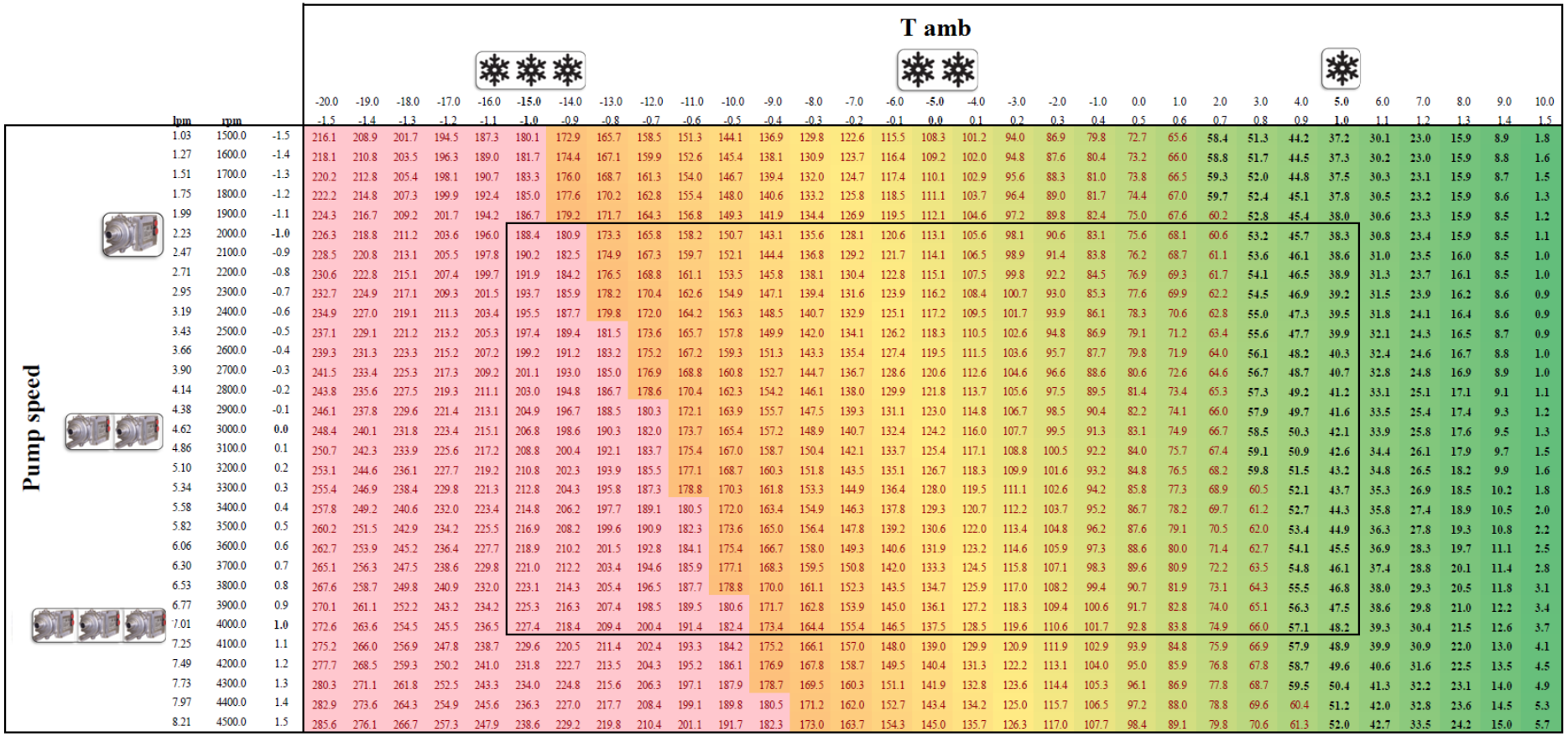

Pump speed	lpm	rpm		T amb																														
				-20.0	-19.0	-18.0	-17.0	-16.0	-15.0	-14.0	-13.0	-12.0	-11.0	-10.0	-9.0	-8.0	-7.0	-6.0	-5.0	-4.0	-3.0	-2.0	-1.0	0.0	1.0	2.0	3.0	4.0	5.0	6.0	7.0	8.0	9.0	10.0
				-1.5	-1.4	-1.3	-1.2	-1.1	-1.0	-0.9	-0.8	-0.7	-0.6	-0.5	-0.4	-0.3	-0.2	-0.1	0.0	0.1	0.2	0.3	0.4	0.5	0.6	0.7	0.8	0.9	1.0	1.1	1.2	1.3	1.4	1.5
	1.03	1500.0	-1.5	216.1	208.9	201.7	194.5	187.3	180.1	172.9	165.7	158.5	151.3	144.1	136.9	129.8	122.6	115.5	108.3	101.2	94.0	86.9	79.8	72.7	65.6	58.4	51.3	44.2	37.2	30.1	23.0	15.9	8.9	1.8
	1.27	1600.0	-1.4	218.1	210.8	203.5	196.3	189.0	181.7	174.4	167.1	159.9	152.6	145.4	138.1	130.9	123.7	116.4	109.2	102.0	94.8	87.6	80.4	73.2	66.0	58.8	51.7	44.5	37.3	30.2	23.0	15.9	8.8	1.6
	1.51	1700.0	-1.3	220.2	212.8	205.4	198.1	190.7	183.3	176.0	168.7	161.3	154.0	146.7	139.4	132.0	124.7	117.4	110.1	102.9	95.6	88.3	81.0	73.8	66.5	59.3	52.0	44.8	37.5	30.3	23.1	15.9	8.7	1.5
	1.75	1800.0	-1.2	222.2	214.8	207.3	199.9	192.4	185.0	177.6	170.2	162.8	155.4	148.0	140.6	133.2	125.8	118.5	111.1	103.7	96.4	89.0	81.7	74.4	67.0	59.7	52.4	45.1	37.8	30.5	23.2	15.9	8.6	1.3
	1.99	1900.0	-1.1	224.3	216.7	209.2	201.7	194.2	186.7	179.2	171.7	164.3	156.8	149.3	141.9	134.4	126.9	119.5	112.1	104.6	97.2	89.8	82.4	75.0	67.6	60.2	52.8	45.4	38.0	30.6	23.3	15.9	8.5	1.2
	2.23	2000.0	**-1.0**	226.3	218.8	211.2	203.6	196.0	188.4	180.9	173.3	165.8	158.2	150.7	143.1	135.6	128.1	120.6	113.1	105.6	98.1	90.6	83.1	75.6	68.1	60.6	53.2	45.7	38.3	30.8	23.4	15.9	8.5	1.1
	2.47	2100.0	-0.9	228.5	220.8	213.1	205.5	197.8	190.2	182.5	174.9	167.3	159.7	152.1	144.4	136.8	129.2	121.7	114.1	106.5	98.9	91.4	83.8	76.2	68.7	61.1	53.6	46.1	38.6	31.0	23.5	16.0	8.5	1.0
	2.71	2200.0	-0.8	230.6	222.8	215.1	207.4	199.7	191.9	184.2	176.5	168.8	161.1	153.5	145.8	138.1	130.4	122.8	115.1	107.5	99.8	92.2	84.5	76.9	69.3	61.7	54.1	46.5	38.9	31.3	23.7	16.1	8.5	1.0
	2.95	2300.0	-0.7	232.7	224.9	217.1	209.3	201.5	193.7	185.9	178.2	170.4	162.6	154.9	147.1	139.4	131.6	123.9	116.2	108.4	100.7	93.0	85.3	77.6	69.9	62.2	54.5	46.9	39.2	31.5	23.9	16.2	8.6	0.9
	3.19	2400.0	-0.6	234.9	227.0	219.1	211.3	203.4	195.5	187.7	179.8	172.0	164.2	156.3	148.5	140.7	132.9	125.1	117.2	109.5	101.7	93.9	86.1	78.3	70.6	62.8	55.0	47.3	39.5	31.8	24.1	16.4	8.6	0.9
	3.43	2500.0	-0.5	237.1	229.1	221.2	213.2	205.3	197.4	189.4	181.5	173.6	165.7	157.8	149.9	142.0	134.1	126.2	118.3	110.5	102.6	94.8	86.9	79.1	71.2	63.4	55.6	47.7	39.9	32.1	24.3	16.5	8.7	0.9
	3.66	2600.0	-0.4	239.3	231.3	223.3	215.2	207.2	199.2	191.2	183.2	175.2	167.2	159.3	151.3	143.3	135.4	127.4	119.5	111.5	103.6	95.7	87.7	79.8	71.9	64.0	56.1	48.2	40.3	32.4	24.6	16.7	8.8	1.0
	3.90	2700.0	-0.3	241.5	233.4	225.3	217.3	209.2	201.1	193.0	185.0	176.9	168.8	160.8	152.7	144.7	136.7	128.6	120.6	112.6	104.6	96.6	88.6	80.6	72.6	64.6	56.7	48.7	40.7	32.8	24.8	16.9	8.9	1.0
	4.14	2800.0	-0.2	243.8	235.6	227.5	219.3	211.1	203.0	194.8	186.7	178.6	170.4	162.3	154.2	146.1	138.0	129.9	121.8	113.7	105.6	97.5	89.5	81.4	73.4	65.3	57.3	49.2	41.2	33.1	25.1	17.1	9.1	1.1
	4.38	2900.0	-0.1	246.1	237.8	229.6	221.4	213.1	204.9	196.7	188.5	180.3	172.1	163.9	155.7	147.5	139.3	131.1	123.0	114.8	106.7	98.5	90.4	82.2	74.1	66.0	57.9	49.7	41.6	33.5	25.4	17.4	9.3	1.2
	4.62	3000.0	**0.0**	248.4	240.1	231.8	223.4	215.1	206.8	198.6	190.3	182.0	173.7	165.4	157.2	148.9	140.7	132.4	124.2	116.0	107.7	99.5	91.3	83.1	74.9	66.7	58.5	50.3	42.1	33.9	25.8	17.6	9.5	1.3
	4.86	3100.0	0.1	250.7	242.3	233.9	225.6	217.2	208.8	200.4	192.1	183.7	175.4	167.0	158.7	150.4	142.1	133.7	125.4	117.1	108.8	100.5	92.2	84.0	75.7	67.4	59.1	50.9	42.6	34.4	26.1	17.9	9.7	1.5
	5.10	3200.0	0.2	253.1	244.6	236.1	227.7	219.2	210.8	202.3	193.9	185.5	177.1	168.7	160.3	151.8	143.5	135.1	126.7	118.3	109.9	101.6	93.2	84.8	76.5	68.2	59.8	51.5	43.2	34.8	26.5	18.2	9.9	1.6
	5.34	3300.0	0.3	255.4	246.9	238.4	229.8	221.3	212.8	204.3	195.8	187.3	178.8	170.3	161.8	153.3	144.9	136.4	128.0	119.5	111.1	102.6	94.2	85.8	77.3	68.9	60.5	52.1	43.7	35.3	26.9	18.5	10.2	1.8
	5.58	3400.0	0.4	257.8	249.2	240.6	232.0	223.4	214.8	206.2	197.7	189.1	180.5	172.0	163.4	154.9	146.3	137.8	129.3	120.7	112.2	103.7	95.2	86.7	78.2	69.7	61.2	52.7	44.3	35.8	27.4	18.9	10.5	2.0
	5.82	3500.0	0.5	260.2	251.5	242.9	234.2	225.5	216.9	208.2	199.6	190.9	182.3	173.6	165.0	156.4	147.8	139.2	130.6	122.0	113.4	104.8	96.2	87.6	79.1	70.5	62.0	53.4	44.9	36.3	27.8	19.3	10.8	2.2
	6.06	3600.0	0.6	262.7	253.9	245.2	236.4	227.7	218.9	210.2	201.5	192.8	184.1	175.4	166.7	158.0	149.3	140.6	131.9	123.2	114.6	105.9	97.3	88.6	80.0	71.4	62.7	54.1	45.5	36.9	28.3	19.7	11.1	2.5
	6.30	3700.0	0.7	265.1	256.3	247.5	238.6	229.8	221.0	212.2	203.4	194.6	185.9	177.1	168.3	159.5	150.8	142.0	133.3	124.5	115.8	107.1	98.3	89.6	80.9	72.2	63.5	54.8	46.1	37.4	28.8	20.1	11.4	2.8
	6.53	3800.0	0.8	267.6	258.7	249.8	240.9	232.0	223.1	214.3	205.4	196.5	187.7	178.8	170.0	161.1	152.3	143.5	134.7	125.9	117.0	108.2	99.4	90.7	81.9	73.1	64.3	55.5	46.8	38.0	29.3	20.5	11.8	3.1
	6.77	3900.0	0.9	270.1	261.1	252.2	243.2	234.2	225.3	216.3	207.4	198.5	189.5	180.6	171.7	162.8	153.9	145.0	136.1	127.2	118.3	109.4	100.6	91.7	82.8	74.0	65.1	56.3	47.5	38.6	29.8	21.0	12.2	3.4
	7.01	4000.0	**1.0**	272.6	263.6	254.5	245.5	236.5	227.4	218.4	209.4	200.4	191.4	182.4	173.4	164.4	155.4	146.5	137.5	128.5	119.6	110.6	101.7	92.8	83.8	74.9	66.0	57.1	48.2	39.3	30.4	21.5	12.6	3.7
	7.25	4100.0	1.1	275.2	266.0	256.9	247.8	238.7	229.6	220.5	211.4	202.4	193.3	184.2	175.2	166.1	157.0	148.0	139.0	129.9	120.9	111.9	102.9	93.9	84.8	75.9	66.9	57.9	48.9	39.9	30.9	22.0	13.0	4.1
	7.49	4200.0	1.2	277.7	268.5	259.3	250.2	241.0	231.8	222.7	213.5	204.3	195.2	186.1	176.9	167.8	158.7	149.5	140.4	131.3	122.2	113.1	104.0	95.0	85.9	76.8	67.8	58.7	49.6	40.6	31.6	22.5	13.5	4.5
	7.73	4300.0	1.3	280.3	271.1	261.8	252.5	243.3	234.0	224.8	215.6	206.3	197.1	187.9	178.7	169.5	160.3	151.1	141.9	132.8	123.6	114.4	105.3	96.1	86.9	77.8	68.7	59.5	50.4	41.3	32.2	23.1	14.0	4.9
	7.97	4400.0	1.4	282.9	273.6	264.3	254.9	245.6	236.3	227.0	217.7	208.4	199.1	189.8	180.5	171.2	162.0	152.7	143.4	134.2	125.0	115.7	106.5	97.2	88.0	78.8	69.6	60.4	51.2	42.0	32.8	23.6	14.5	5.3
	8.21	4500.0	1.5	285.6	276.1	266.7	257.3	247.9	238.6	229.2	219.8	210.4	201.1	191.7	182.3	173.0	163.7	154.3	145.0	135.7	126.3	117.0	107.7	98.4	89.1	79.8	70.6	61.3	52.0	42.7	33.5	24.2	15.0	5.7

(a)

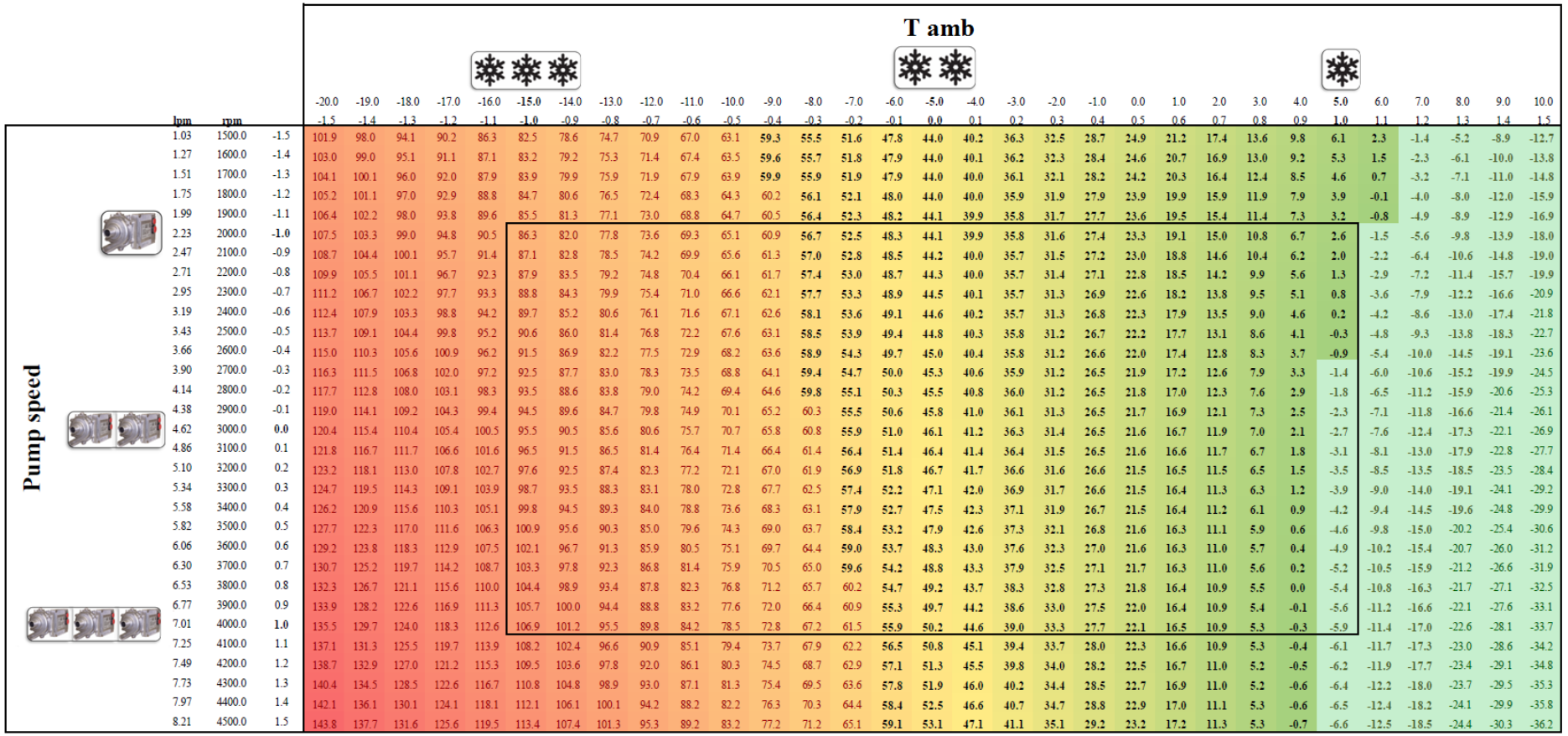

Pump speed	lpm	rpm		T amb																														
				-20.0	-19.0	-18.0	-17.0	-16.0	-15.0	-14.0	-13.0	-12.0	-11.0	-10.0	-9.0	-8.0	-7.0	-6.0	-5.0	-4.0	-3.0	-2.0	-1.0	0.0	1.0	2.0	3.0	4.0	5.0	6.0	7.0	8.0	9.0	10.0
				-1.5	-1.4	-1.3	-1.2	-1.1	-1.0	-0.9	-0.8	-0.7	-0.6	-0.5	-0.4	-0.3	-0.2	-0.1	0.0	0.1	0.2	0.3	0.4	0.5	0.6	0.7	0.8	0.9	1.0	1.1	1.2	1.3	1.4	1.5
	1.03	1500.0	-1.5	101.9	98.0	94.1	90.2	86.3	82.5	78.6	74.7	70.9	67.0	63.1	59.3	55.5	51.6	47.8	44.0	40.2	36.3	32.5	28.7	24.9	21.2	17.4	13.6	9.8	6.1	2.3	-1.4	-5.2	-8.9	-12.7
	1.27	1600.0	-1.4	103.0	99.0	95.1	91.1	87.1	83.2	79.2	75.3	71.4	67.4	63.5	59.6	55.7	51.8	47.9	44.0	40.1	36.2	32.3	28.4	24.6	20.7	16.9	13.0	9.2	5.3	1.5	-2.3	-6.1	-10.0	-13.8
	1.51	1700.0	-1.3	104.1	100.1	96.0	92.0	87.9	83.9	79.9	75.9	71.9	67.9	63.9	59.9	55.9	51.9	47.9	44.0	40.0	36.1	32.1	28.2	24.2	20.3	16.4	12.4	8.5	4.6	0.7	-3.2	-7.1	-11.0	-14.8
	1.75	1800.0	-1.2	105.2	101.1	97.0	92.9	88.8	84.7	80.6	76.5	72.4	68.3	64.3	60.2	56.1	52.1	48.0	44.0	40.0	35.9	31.9	27.9	23.9	19.9	15.9	11.9	7.9	3.9	-0.1	-4.0	-8.0	-12.0	-15.9
	1.99	1900.0	-1.1	106.4	102.2	98.0	93.8	89.6	85.5	81.3	77.1	73.0	68.8	64.7	60.5	56.4	52.3	48.2	44.1	39.9	35.8	31.7	27.7	23.6	19.5	15.4	11.4	7.3	3.2	-0.8	-4.9	-8.9	-12.9	-16.9
	2.23	2000.0	-1.0	107.5	103.3	99.0	94.8	90.5	86.3	82.0	77.8	73.6	69.3	65.1	60.9	56.7	52.5	48.3	44.1	39.9	35.8	31.6	27.4	23.3	19.1	15.0	10.8	6.7	2.6	-1.5	-5.6	-9.8	-13.9	-18.0
	2.47	2100.0	-0.9	108.7	104.4	100.1	95.7	91.4	87.1	82.8	78.5	74.2	69.9	65.6	61.3	57.0	52.8	48.5	44.2	40.0	35.7	31.5	27.2	23.0	18.8	14.6	10.4	6.2	2.0	-2.2	-6.4	-10.6	-14.8	-19.0
	2.71	2200.0	-0.8	109.9	105.5	101.1	96.7	92.3	87.9	83.5	79.2	74.8	70.4	66.1	61.7	57.4	53.0	48.7	44.3	40.0	35.7	31.4	27.1	22.8	18.5	14.2	9.9	5.6	1.3	-2.9	-7.2	-11.4	-15.7	-19.9
	2.95	2300.0	-0.7	111.2	106.7	102.2	97.7	93.3	88.8	84.3	79.9	75.4	71.0	66.6	62.1	57.7	53.3	48.9	44.5	40.1	35.7	31.3	26.9	22.6	18.2	13.8	9.5	5.1	0.8	-3.6	-7.9	-12.2	-16.6	-20.9
	3.19	2400.0	-0.6	112.4	107.9	103.3	98.8	94.2	89.7	85.2	80.6	76.1	71.6	67.1	62.6	58.1	53.6	49.1	44.6	40.2	35.7	31.3	26.8	22.3	17.9	13.5	9.0	4.6	0.2	-4.2	-8.6	-13.0	-17.4	-21.8
	3.43	2500.0	-0.5	113.7	109.1	104.4	99.8	95.2	90.6	86.0	81.4	76.8	72.2	67.6	63.1	58.5	53.9	49.4	44.8	40.3	35.8	31.2	26.7	22.2	17.7	13.1	8.6	4.1	-0.3	-4.8	-9.3	-13.8	-18.3	-22.7
	3.66	2600.0	-0.4	115.0	110.3	105.6	100.9	96.2	91.5	86.9	82.2	77.5	72.9	68.2	63.6	58.9	54.3	49.7	45.0	40.4	35.8	31.2	26.6	22.0	17.4	12.8	8.3	3.7	-0.9	-5.4	-10.0	-14.5	-19.1	-23.6
	3.90	2700.0	-0.3	116.3	111.5	106.8	102.0	97.2	92.5	87.7	83.0	78.3	73.5	68.8	64.1	59.4	54.7	50.0	45.3	40.6	35.9	31.2	26.5	21.9	17.2	12.6	7.9	3.3	-1.4	-6.0	-10.6	-15.2	-19.9	-24.5
	4.14	2800.0	-0.2	117.7	112.8	108.0	103.1	98.3	93.5	88.6	83.8	79.0	74.2	69.4	64.6	59.8	55.1	50.3	45.5	40.8	36.0	31.2	26.5	21.8	17.0	12.3	7.6	2.9	-1.8	-6.5	-11.2	-15.9	-20.6	-25.3
	4.38	2900.0	-0.1	119.0	114.1	109.2	104.3	99.4	94.5	89.6	84.7	79.8	74.9	70.1	65.2	60.3	55.5	50.6	45.8	41.0	36.1	31.3	26.5	21.7	16.9	12.1	7.3	2.5	-2.3	-7.1	-11.8	-16.6	-21.4	-26.1
	4.62	3000.0	0.0	120.4	115.4	110.4	105.4	100.5	95.5	90.5	85.6	80.6	75.7	70.7	65.8	60.8	55.9	51.0	46.1	41.2	36.3	31.4	26.5	21.6	16.7	11.9	7.0	2.1	-2.7	-7.6	-12.4	-17.3	-22.1	-26.9
	4.86	3100.0	0.1	121.8	116.7	111.7	106.6	101.6	96.5	91.5	86.5	81.4	76.4	71.4	66.4	61.4	56.4	51.4	46.4	41.4	36.4	31.5	26.5	21.6	16.6	11.7	6.7	1.8	-3.1	-8.1	-13.0	-17.9	-22.8	-27.7
	5.10	3200.0	0.2	123.2	118.1	113.0	107.8	102.7	97.6	92.5	87.4	82.3	77.2	72.1	67.0	61.9	56.9	51.8	46.7	41.7	36.6	31.6	26.6	21.5	16.5	11.5	6.5	1.5	-3.5	-8.5	-13.5	-18.5	-23.5	-28.4
	5.34	3300.0	0.3	124.7	119.5	114.3	109.1	103.9	98.7	93.5	88.3	83.1	78.0	72.8	67.7	62.5	57.4	52.2	47.1	42.0	36.9	31.7	26.6	21.5	16.4	11.3	6.3	1.2	-3.9	-9.0	-14.0	-19.1	-24.1	-29.2
	5.58	3400.0	0.4	126.2	120.9	115.6	110.3	105.1	99.8	94.5	89.3	84.0	78.8	73.6	68.3	63.1	57.9	52.7	47.5	42.3	37.1	31.9	26.7	21.5	16.4	11.2	6.1	0.9	-4.2	-9.4	-14.5	-19.6	-24.8	-29.9
	5.82	3500.0	0.5	127.7	122.3	117.0	111.6	106.3	100.9	95.6	90.3	85.0	79.6	74.3	69.0	63.7	58.4	53.2	47.9	42.6	37.3	32.1	26.8	21.6	16.3	11.1	5.9	0.6	-4.6	-9.8	-15.0	-20.2	-25.4	-30.6
	6.06	3600.0	0.6	129.2	123.8	118.3	112.9	107.5	102.1	96.7	91.3	85.9	80.5	75.1	69.7	64.4	59.0	53.7	48.3	43.0	37.6	32.3	27.0	21.6	16.3	11.0	5.7	0.4	-4.9	-10.2	-15.4	-20.7	-26.0	-31.2
	6.30	3700.0	0.7	130.7	125.2	119.7	114.2	108.7	103.3	97.8	92.3	86.8	81.4	75.9	70.5	65.0	59.6	54.2	48.8	43.3	37.9	32.5	27.1	21.7	16.3	11.0	5.6	0.2	-5.2	-10.5	-15.9	-21.2	-26.6	-31.9
	6.53	3800.0	0.8	132.3	126.7	121.1	115.6	110.0	104.4	98.9	93.4	87.8	82.3	76.8	71.2	65.7	60.2	54.7	49.2	43.7	38.3	32.8	27.3	21.8	16.4	10.9	5.5	0.0	-5.4	-10.8	-16.3	-21.7	-27.1	-32.5
	6.77	3900.0	0.9	133.9	128.2	122.6	116.9	111.3	105.7	100.0	94.4	88.8	83.2	77.6	72.0	66.4	60.9	55.3	49.7	44.2	38.6	33.0	27.5	22.0	16.4	10.9	5.4	-0.1	-5.6	-11.2	-16.6	-22.1	-27.6	-33.1
	7.01	4000.0	1.0	135.5	129.7	124.0	118.3	112.6	106.9	101.2	95.5	89.8	84.2	78.5	72.8	67.2	61.5	55.9	50.2	44.6	39.0	33.3	27.7	22.1	16.5	10.9	5.3	-0.3	-5.9	-11.4	-17.0	-22.6	-28.1	-33.7
	7.25	4100.0	1.1	137.1	131.3	125.5	119.7	113.9	108.2	102.4	96.6	90.9	85.1	79.4	73.7	67.9	62.2	56.5	50.8	45.1	39.4	33.7	28.0	22.3	16.6	10.9	5.3	-0.4	-6.1	-11.7	-17.3	-23.0	-28.6	-34.2
	7.49	4200.0	1.2	138.7	132.9	127.0	121.2	115.3	109.5	103.6	97.8	92.0	86.1	80.3	74.5	68.7	62.9	57.1	51.3	45.5	39.8	34.0	28.2	22.5	16.7	11.0	5.2	-0.5	-6.2	-11.9	-17.7	-23.4	-29.1	-34.8
	7.73	4300.0	1.3	140.4	134.5	128.5	122.6	116.7	110.8	104.8	98.9	93.0	87.1	81.3	75.4	69.5	63.6	57.8	51.9	46.0	40.2	34.4	28.5	22.7	16.9	11.0	5.2	-0.6	-6.4	-12.2	-18.0	-23.7	-29.5	-35.3
	7.97	4400.0	1.4	142.1	136.1	130.1	124.1	118.1	112.1	106.1	100.1	94.2	88.2	82.2	76.3	70.3	64.4	58.4	52.5	46.6	40.7	34.7	28.8	22.9	17.0	11.1	5.3	-0.6	-6.5	-12.4	-18.2	-24.1	-29.9	-35.8
	8.21	4500.0	1.5	143.8	137.7	131.6	125.6	119.5	113.4	107.4	101.3	95.3	89.2	83.2	77.2	71.2	65.1	59.1	53.1	47.1	41.1	35.1	29.2	23.2	17.2	11.3	5.3	-0.7	-6.6	-12.5	-18.5	-24.4	-30.3	-36.2

(b)

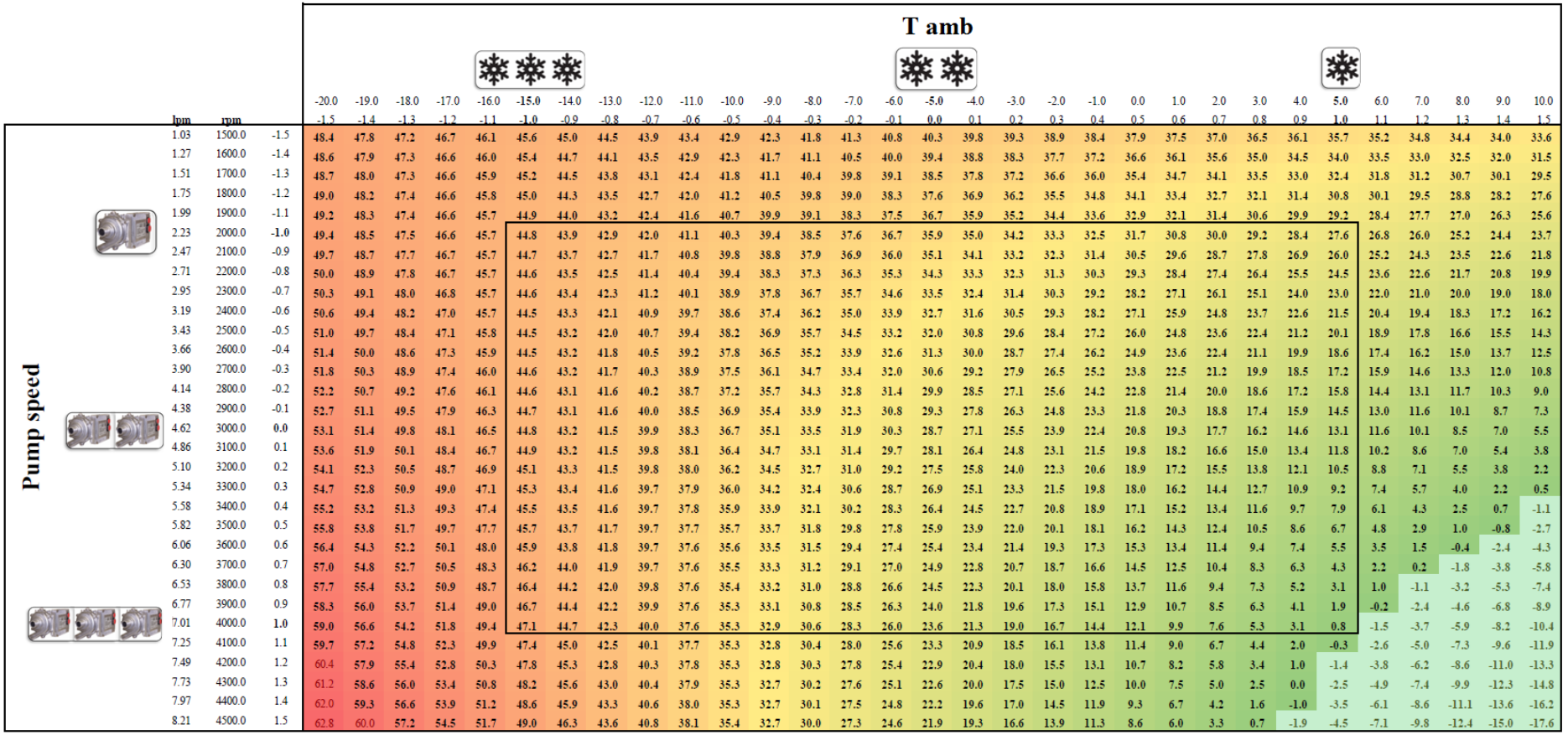

lpm	rpm		-20.0	-19.0	-18.0	-17.0	-16.0	-15.0	-14.0	-13.0	-12.0	-11.0	-10.0	-9.0	-8.0	-7.0	-6.0	-5.0	-4.0	-3.0	-2.0	-1.0	0.0	1.0	2.0	3.0	4.0	5.0	6.0	7.0	8.0	9.0	10.0
			-1.5	-1.4	-1.3	-1.2	-1.1	-1.0	-0.9	-0.8	-0.7	-0.6	-0.5	-0.4	-0.3	-0.2	-0.1	0.0	0.1	0.2	0.3	0.4	0.5	0.6	0.7	0.8	0.9	1.0	1.1	1.2	1.3	1.4	1.5
1.03	1500.0	-1.5	48.4	47.8	47.2	46.7	46.1	45.6	45.0	44.5	43.9	43.4	42.9	42.3	41.8	41.3	40.8	40.3	39.8	39.3	38.9	38.4	37.9	37.5	37.0	36.5	36.1	35.7	35.2	34.8	34.4	34.0	33.6
1.27	1600.0	-1.4	48.6	47.9	47.3	46.6	46.0	45.4	44.7	44.1	43.5	42.9	42.3	41.7	41.1	40.5	40.0	39.4	38.8	38.3	37.7	37.2	36.6	36.1	35.6	35.0	34.5	34.0	33.5	33.0	32.5	32.0	31.5
1.51	1700.0	-1.3	48.7	48.0	47.3	46.6	45.9	45.2	44.5	43.8	43.1	42.4	41.8	41.1	40.4	39.8	39.1	38.5	37.8	37.2	36.6	36.0	35.4	34.7	34.1	33.5	33.0	32.4	31.8	31.2	30.7	30.1	29.5
1.75	1800.0	-1.2	49.0	48.2	47.4	46.6	45.8	45.0	44.3	43.5	42.7	42.0	41.2	40.5	39.8	39.0	38.3	37.6	36.9	36.2	35.5	34.8	34.1	33.4	32.7	32.1	31.4	30.8	30.1	29.5	28.8	28.2	27.6
1.99	1900.0	-1.1	49.2	48.3	47.4	46.6	45.7	44.9	44.0	43.2	42.4	41.6	40.7	39.9	39.1	38.3	37.5	36.7	35.9	35.2	34.4	33.6	32.9	32.1	31.4	30.6	29.9	29.2	28.4	27.7	27.0	26.3	25.6
2.23	2000.0	-1.0	49.4	48.5	47.5	46.6	45.7	44.8	43.9	42.9	42.0	41.1	40.3	39.4	38.5	37.6	36.7	35.9	35.0	34.2	33.3	32.5	31.7	30.8	30.0	29.2	28.4	27.6	26.8	26.0	25.2	24.4	23.7
2.47	2100.0	-0.9	49.7	48.7	47.7	46.7	45.7	44.7	43.7	42.7	41.7	40.8	39.8	38.8	37.9	36.9	36.0	35.1	34.1	33.2	32.3	31.4	30.5	29.6	28.7	27.8	26.9	26.0	25.2	24.3	23.5	22.6	21.8
2.71	2200.0	-0.8	50.0	48.9	47.8	46.7	45.7	44.6	43.5	42.5	41.4	40.4	39.4	38.3	37.3	36.3	35.3	34.3	33.3	32.3	31.3	30.3	29.3	28.4	27.4	26.4	25.5	24.5	23.6	22.6	21.7	20.8	19.9
2.95	2300.0	-0.7	50.3	49.1	48.0	46.8	45.7	44.6	43.4	42.3	41.2	40.1	38.9	37.8	36.7	35.7	34.6	33.5	32.4	31.4	30.3	29.2	28.2	27.1	26.1	25.1	24.0	23.0	22.0	21.0	20.0	19.0	18.0
3.19	2400.0	-0.6	50.6	49.4	48.2	47.0	45.7	44.5	43.3	42.1	40.9	39.7	38.6	37.4	36.2	35.0	33.9	32.7	31.6	30.5	29.3	28.2	27.1	25.9	24.8	23.7	22.6	21.5	20.4	19.4	18.3	17.2	16.2
3.43	2500.0	-0.5	51.0	49.7	48.4	47.1	45.8	44.5	43.2	42.0	40.7	39.4	38.2	36.9	35.7	34.5	33.2	32.0	30.8	29.6	28.4	27.2	26.0	24.8	23.6	22.4	21.2	20.1	18.9	17.8	16.6	15.5	14.3
3.66	2600.0	-0.4	51.4	50.0	48.6	47.3	45.9	44.5	43.2	41.8	40.5	39.2	37.8	36.5	35.2	33.9	32.6	31.3	30.0	28.7	27.4	26.2	24.9	23.6	22.4	21.1	19.9	18.6	17.4	16.2	15.0	13.7	12.5
3.90	2700.0	-0.3	51.8	50.3	48.9	47.4	46.0	44.6	43.2	41.7	40.3	38.9	37.5	36.1	34.7	33.4	32.0	30.6	29.2	27.9	26.5	25.2	23.8	22.5	21.2	19.9	18.5	17.2	15.9	14.6	13.3	12.0	10.8
4.14	2800.0	-0.2	52.2	50.7	49.2	47.6	46.1	44.6	43.1	41.6	40.2	38.7	37.2	35.7	34.3	32.8	31.4	29.9	28.5	27.1	25.6	24.2	22.8	21.4	20.0	18.6	17.2	15.8	14.4	13.1	11.7	10.3	9.0
4.38	2900.0	-0.1	52.7	51.1	49.5	47.9	46.3	44.7	43.1	41.6	40.0	38.5	36.9	35.4	33.9	32.3	30.8	29.3	27.8	26.3	24.8	23.3	21.8	20.3	18.8	17.4	15.9	14.5	13.0	11.6	10.1	8.7	7.3
4.62	3000.0	0.0	53.1	51.4	49.8	48.1	46.5	44.8	43.2	41.5	39.9	38.3	36.7	35.1	33.5	31.9	30.3	28.7	27.1	25.5	23.9	22.4	20.8	19.3	17.7	16.2	14.6	13.1	11.6	10.1	8.5	7.0	5.5
4.86	3100.0	0.1	53.6	51.9	50.1	48.4	46.7	44.9	43.2	41.5	39.8	38.1	36.4	34.7	33.1	31.4	29.7	28.1	26.4	24.8	23.1	21.5	19.8	18.2	16.6	15.0	13.4	11.8	10.2	8.6	7.0	5.4	3.8
5.10	3200.0	0.2	54.1	52.3	50.5	48.7	46.9	45.1	43.3	41.5	39.8	38.0	36.2	34.5	32.7	31.0	29.2	27.5	25.8	24.0	22.3	20.6	18.9	17.2	15.5	13.8	12.1	10.5	8.8	7.1	5.5	3.8	2.2
5.34	3300.0	0.3	54.7	52.8	50.9	49.0	47.1	45.3	43.4	41.6	39.7	37.9	36.0	34.2	32.4	30.6	28.7	26.9	25.1	23.3	21.5	19.8	18.0	16.2	14.4	12.7	10.9	9.2	7.4	5.7	4.0	2.2	0.5
5.58	3400.0	0.4	55.2	53.2	51.3	49.3	47.4	45.5	43.5	41.6	39.7	37.8	35.9	33.9	32.1	30.2	28.3	26.4	24.5	22.7	20.8	18.9	17.1	15.2	13.4	11.6	9.7	7.9	6.1	4.3	2.5	0.7	-1.1
5.82	3500.0	0.5	55.8	53.8	51.7	49.7	47.7	45.7	43.7	41.7	39.7	37.7	35.7	33.7	31.8	29.8	27.8	25.9	23.9	22.0	20.1	18.1	16.2	14.3	12.4	10.5	8.6	6.7	4.8	2.9	1.0	-0.8	-2.7
6.06	3600.0	0.6	56.4	54.3	52.2	50.1	48.0	45.9	43.8	41.8	39.7	37.6	35.6	33.5	31.5	29.4	27.4	25.4	23.4	21.4	19.3	17.3	15.3	13.4	11.4	9.4	7.4	5.5	3.5	1.5	-0.4	-2.4	-4.3
6.30	3700.0	0.7	57.0	54.8	52.7	50.5	48.3	46.2	44.0	41.9	39.7	37.6	35.5	33.3	31.2	29.1	27.0	24.9	22.8	20.7	18.7	16.6	14.5	12.5	10.4	8.3	6.3	4.3	2.2	0.2	-1.8	-3.8	-5.8
6.53	3800.0	0.8	57.7	55.4	53.2	50.9	48.7	46.4	44.2	42.0	39.8	37.6	35.4	33.2	31.0	28.8	26.6	24.5	22.3	20.1	18.0	15.8	13.7	11.6	9.4	7.3	5.2	3.1	1.0	-1.1	-3.2	-5.3	-7.4
6.77	3900.0	0.9	58.3	56.0	53.7	51.4	49.0	46.7	44.4	42.2	39.9	37.6	35.3	33.1	30.8	28.5	26.3	24.0	21.8	19.6	17.3	15.1	12.9	10.7	8.5	6.3	4.1	1.9	-0.2	-2.4	-4.6	-6.8	-8.9
7.01	4000.0	1.0	59.0	56.6	54.2	51.8	49.4	47.1	44.7	42.3	40.0	37.6	35.3	32.9	30.6	28.3	26.0	23.6	21.3	19.0	16.7	14.4	12.1	9.9	7.6	5.3	3.1	0.8	-1.5	-3.7	-5.9	-8.2	-10.4
7.25	4100.0	1.1	59.7	57.2	54.8	52.3	49.9	47.4	45.0	42.5	40.1	37.7	35.3	32.8	30.4	28.0	25.6	23.3	20.9	18.5	16.1	13.8	11.4	9.0	6.7	4.4	2.0	-0.3	-2.6	-5.0	-7.3	-9.6	-11.9
7.49	4200.0	1.2	60.4	57.9	55.4	52.8	50.3	47.8	45.3	42.8	40.3	37.8	35.3	32.8	30.3	27.8	25.4	22.9	20.4	18.0	15.5	13.1	10.7	8.2	5.8	3.4	1.0	-1.4	-3.8	-6.2	-8.6	-11.0	-13.3
7.73	4300.0	1.3	61.2	58.6	56.0	53.4	50.8	48.2	45.6	43.0	40.4	37.9	35.3	32.7	30.2	27.6	25.1	22.6	20.0	17.5	15.0	12.5	10.0	7.5	5.0	2.5	0.0	-2.5	-4.9	-7.4	-9.9	-12.3	-14.8
7.97	4400.0	1.4	62.0	59.3	56.6	53.9	51.2	48.6	45.9	43.3	40.6	38.0	35.3	32.7	30.1	27.5	24.8	22.2	19.6	17.0	14.5	11.9	9.3	6.7	4.2	1.6	-1.0	-3.5	-6.1	-8.6	-11.1	-13.6	-16.2
8.21	4500.0	1.5	62.8	60.0	57.2	54.5	51.7	49.0	46.3	43.6	40.8	38.1	35.4	32.7	30.0	27.3	24.6	21.9	19.3	16.6	13.9	11.3	8.6	6.0	3.3	0.7	-1.9	-4.5	-7.1	-9.8	-12.4	-15.0	-17.6

(c)

Figure 7.34 The surface response correspondent to heating time required when an electric resistance of (a) 500 W (b) 1500 W and (c) 2500 W is used.

Figure 7.34 shows the surface responses regarding the heating time required of the *BP* to reach 10 ºC when the initial temperature is lower, considering different electric resistance power values: (a) 500 W, (b) 1500 W and (c) 2500 W.

Considering the results based on Figure 7.34, with the higher tested electrical resistance for the most restrictive conditions, -15 ºC and the lower rotational speed of the pump, the minimum time required to reach the minimum admissible limit is less than 45 minutes. However, for the medium power of the electric resistance analyzed, for the same restrictive conditions, around 106 minutes have been needed to warm the *BP* until 10ºC. Furthermore, considering the results obtained for 500 W of electric resistance, the minimum level, the waiting time has been higher than 3 hours and a half.

Regarding a maximum required time of an hour for the defined worst conditions in the previous paragraph, an electric resistance of 2000 W has been needed. With this resistance and with an ambient temperature of -5 ºC in 30 minutes the urban electric minibus was ready and with ambient temperature of 5 ºC in less than 8 minutes.

7.6 CONCLUSIONS

The applicability of the developed systematic methodology has already been demonstrated with the objective of optimizing a *TMS* for a *Li-Ion* battery system for an urban electric minibus. The optimization of the designed *TMS* has been based on achieving a compromise related to the thermal response of *BP* and thermal dispersion within the *BM*s, ensuring the minimum consumption of the auxiliary system.

The main conclusions drawn from this chapter are summarized in the following bullets:

- The developed methodology has been adjusted to the design criteria imposed in the first step (Section 7.1). Electrical, thermal and mechanical design criteria have been defined which have been fulfilled in every steps of this methodology. Some of those, such as the cooling system technology, have been imposed by the manufacturer and even so, it has not been an obstacle to carry out the complete process until to achieve an optimized *TMS*. In addition, the power requirements of this urban electric minibus in terms of urban city routes (3 bus lines) have been defined by the manufacturer.

For any power condition, the *BP* must fulfil some thermal imposed requirements. **An ideal operation window between 20-30 ºC** has been defined, although it has been considered a **temperature range between 10 ºC and 40 ºC admissible**. If the *BP* reaches an operation temperature higher than **55 ºC, the urban electric minibus will stop**. Regarding the **thermal dispersion within the *BP***, it should manage to keep this value **below 3 ºC** at most time. A thermal dispersion higher than **5 ºC will be unacceptable.** These thermal requirements must be fulfilled for an **ambient temperature range between 10 ºC and 45 ºC**.

- The predesign step (Section 7.2) has been composed of two main tasks, i.e., the thermal sizing of the *BP* and the preselection of the components of the proposed *TMS*.

  The thermal sizing (Section 7.2.1) has been carried out based on the electrical sizing that has been performed for this particular case in Chapter 3. The complete ***BP* has been composed of 16 *BM*s** connected in two parallel strings with 8 *BM*s in serial in each one and with **28.4 kWh of energy on-board.** Moreover, considering that each *BM* has been comprised of **12 pouch type cells (KOKAM)** connected in serial, it has been calculated that the complete *BP* has been composed of 192 cells.

  On this basis and by means of the cell heat generation model developed at cell level, the total mean heat that must be dissipated by the *TMS* has been estimated. Scalability between cell and *BP* level has been defined in terms of heat generated, multiplying the heat generated associated to a cell by the number of cells that are in the complete *BP* (192 cells for this particular case). At last, ***TMS* that could dissipate 891.3 W has been predesigned.**

  A **liquid cooling system has been imposed by the manufacturer**. On this basis, a *TMS* which based on **a combination of a *FC* and *AC* system has been proposed (dual architecture)** to be implemented in this application mainly in order to manage the not so restrictive but variable electrical solicitations that this application requires and also, because of the high influence of the ambient conditions in the cooling process.

The preselection of the components (Section 7.2.2) of this system have been carried out considering **simple and coarse calculations by means of an *Excel Worksheet*.** The components have been modeled in a lumped way, based on their data sheets. Hydraulic and thermal balances have been considered for different component combinations in steady state and taking into account the most restrictive ambient conditions. Constant thermo-physical properties have been considered for the different fluids (air, 50/50 *WEG* and R-134a refrigerant), considering an approximate temperature of 25 ºC.

As a result of this section, the necessary components of the proposed *TMS* have been selected. With regards to the components of the primary circuit, **Webra VK-225-222-8** cold plates from AMS Technologies**, WP29 electric pump provided by EMP** and **RA 33570-0 radiator from RAAL** manufacturer have been chosen. On the other hand and related to the components of the secondary fluid, **RA 33046-0 evaporator and RA 33045-0 condenser both provided by RAAL** manufacturer, **SIERRA03-0982Y3 variable speed compressor from Masterflux** manufacturer and **ETS 6-14 thermal expansion valve from Danfoss** have been implemented. In addition, the **fan, VA08-BP71 LL-53A, has been provided by Spal Automotive** manufacturer.

Due to all the general assumptions and considerations that they have been assumed **in this predesign step an oversized *TMS*** has been obtained.

- Once the *BP* and the *TMS* have been predesigned, the next step has been to **develop detailed models** (Section 7.3) of them in order to check if the design criteria defined in Section 7.1 have been fulfilled or not, prior the construction of a sample prototype. As it has been explained in Chapter 5, for that purpose the ***Dymola/TIL* simulation tool** has been chosen especially due to its capacity to analyze the transient response of complex components combinations at system level. By means of this tool, several high-fidelity detailed numerical thermal models have been developed improving the efficiency of the design process relative to a trial- and- error determination of the *BP* cooling system design concept.

In this step detailed models at *BM* and at *BP* level have been developed. The *BM* level thermal model has been used with the aim to check and experimentally validate the thermal performance of the system in transient state, whereas a more complete *BP* level thermal model has been used later for optimization purposes. In this case it is not possible to scale the *TMS* at *BM* level for experimental validation purposes as it was done for the other test case. Therefore, a unique *BM* has been modeled but an electrical heater has been introduced in the model as *BP* thermal emulator; i.e., to include the heat that is generated by the rest of the 15 *BMs*.

The *BM* along with its cold plates has been modeled based on 1D-lumped *Cauer Equivalent Circuit* composed of thermal capacities and resistances, assuming a null thermal dispersion among the 12 cells of the *BM* and also, in the solid part of the cold plate. By doing this a characteristic temperature is obtained for both lumped objects. The rest of the components that comprised the overall *TMS* have been modeled based on the geometrical features and performance curves provided by the manufacturers.

A test matrix has been defined in order to check the thermal performance of the system at as wide as possible operating conditions for *FC* and *AC* modes. As a results and evaluating the *BM* temperature for each cooling mode individually, several conclusions can be extracted. For *FC* mode for the maximum tested ambient temperature (35 ºC) a margin of around 16 ºC below the limit temperature (55 ºC) has been found, whereas for *AC* mode the *TMS* has been able to keep the *BM* near the ideal operation range, between 20 ºC and 30 ºC, but with a relatively high power consumption for moderate ambient temperatures. Consequently, the **design criteria have been fulfilled by means of the proposed initial design**. As the proposed *TMS* for this urban electric minibus application is slightly oversized, a window has been opened for the possibility of optimizing the *TMS* in the next steps.

- After the checking of the fulfilment of the design criteria by means of the proposed predesign *TMS*, **the validation of the developed thermal models**

has been carried out by means of a prototype construction in the laboratory environment.

Based on the same philosophy that in the previous step, a *BP* emulator based on a unique *BM* and a heater has been constructed. The *TMS* has been tested in a climatic chamber in order to analyze the performance of each cooling mode in function of ambient conditions, whereas the BP emulator has been insulated by means of methacrylate case in order to emulate the non-influence of the ambient temperature on it. Different measurement instruments have been used in order to measure variables such as the temperature in the *BM*, in the liquid at different location in the *TMS* and in the ambient, the pressure states at different points of the *TMS* and the consumption of the system. These measurements have been compared against the simulation results obtained previously in the developed detailed thermal models.

A maximum time-averaged prediction error for the mean temperature of the *BM* of merely 0.4 ºC has been obtained for the *FC* mode, whereas for the *AC* mode this value has maintained below 0.7 ºC. As it was expected in general terms, the power consumption related to *FC* system has been higher than for the *AC* system, especially mainly due to the compressor. For *FC* mode because of the electro-mechanical components such as the hydraulic pump and fan have operated continuously the consumption has been more or less invariable around 340 W. However, for *AC* mode where the compressor performance has been related to the ambient temperature, the system consumption has changed in function of the ambient temperature: for an ambient temperature of 25 ºC, 35 ºC and 45 ºC the mean power consumption has been 611.5 W, 740.3 W and 1152.4 W, respectively. **The maximum difference respect to the model regarding the system consumption has been of 125 W for the case** at lowest tested ambient temperature (25 ºC) of the *AC* mode.

As a conclusion of this fourth step of the methodology it can be said that a reliable and accurate thermal model has been obtained which simulated in a realistic way the real performance of the complete *BP* and its *TMS*. Moreover,

it has been also concluded that the ***Dymola/TIL* simulation tool has been an adequate and an appropriate tool to analyze the thermal performance of this type of complex system.**

- Once the developed models have been validated it has been possible to use them to **optimize the *TMS* at *BP* level**, therefore for that purpose the thermal detailed model developed at *BP* level has been used.

  Prior to carry out the optimization task, the influence of the hydraulic configurations between the *BM*s on the average temperature and thermal dispersion within the *BP* has been analyzed. Three hydraulic configurations **(*4s4p*, *8s2p* and *16s*)** have been studied for each cooling mode. The first two proposed configurations have fulfilled the defined thermal specification for both cooling modes, whereas the ***16s* hydraulic configurations supposed a high thermal dispersion** (up to 7.5 ºC and 10 ºC for *FC* and *AC* respectively), out of the limit established in the design criteria.

  Finally, ***8s2p* hydraulic configuration has been proposed** for the final optimized design in order to avoid **the complex piping connection required by *4s4p*** hydraulic configuration.

  The ***FC* and *AC* modes have been optimized separately**. A numerical *DoE* has been used to analyze the final steady state of several transient simulations. **Minitab 17.0** has been used to obtain the adequate response surfaces in order to optimize the cooling circuits of the proposed dual architecture.

  - **Optimization I** analysis, which has been focused on the **power consumption reduction** for both cooling processes has concluded that:

    FC: for the worst ambient conditions considered for this cooling mode, 25 ºC, and keeping the fan *PWM* between 85-100%:

    - with the hydraulic pump at 2000 rpm, it has been possible to keep the maximum *BP* temperature at 31.4 ºC and a thermal dispersion of 4.4 ºC.

- with the hydraulic pump at 3000 rpm, it has been possible to keep the maximum *BP* temperature at 30.2 ºC and a thermal dispersion of 1.9 ºC.
- with the hydraulic pump at 4000 rpm, it has been possible to keep the maximum *BP* temperature at 29.3 ºC and a thermal dispersion of 1.4 ºC.

It can be concluded that keeping **the pump rotational speed of 2370 rpm with fan at minimum *PWM* value of 70%, a maximum *BP* temperature of 32.5 ºC and a thermal dispersion of 3.0 ºC** can be maintained. This pump speed allows a total 3.11 lpm liquid flow rate in system, which corresponds to 0.78 lpm per each cold plate for the selected hydraulic configuration.

***AC*:** for the worst ambient conditions considered for this cooling mode, 45 ºC, and keeping the compressor between 2400-3000 rpm:

- with the hydraulic pump at 2000 rpm and the fan *PWM* at 100%, it has been possible to keep the maximum *BP* temperature at 25.7 ºC and a thermal dispersion of 5.2 ºC.
- with the hydraulic pump at 3000 rpm and the fan *PWM* at 100%, it has been possible to keep the maximum *BP* temperature at 25.4 ºC and a thermal dispersion of 2.8 ºC.
- with the hydraulic pump at 4000 rpm and the fan *PWM* at 100%, it has been possible to keep the maximum *BP* temperature at 24.8 ºC and a thermal dispersion of 1.9 ºC.

It can be concluded that keeping **the pump rotational speed at 2950 rpm with fan at minimum *PWM* value of 70% and the compressor rotational speed of 1800 rpm, a maximum *BP* temperature of 25.5 ºC and a thermal dispersion of 3.0 ºC** can be maintained. This pump speed allows a total of 4.5 lpm liquid flow rate in system, which corresponds to 1.13 lpm per each cold plate for the selected hydraulic configuration.

- **Optimization II** analysis has been focused **on the power reduction of the heating or warm-up process**. It has been concluded that when the ambient temperature is lower than 10 ºC, the admissible minimum operation temperature of the *BP*, an **electric resistance inside a vessel in the liquid circuit of at least 2000 W** is needed to reach secure temperatures at a reasonable time lapse. By means of this resistance it is possible to **reach the 10 ºC in the *BP* starting from an initial and ambient temperatures of -15 ºC in 59 minutes, from -5 ºC in 30 minutes and from 5 ºC in less than 8 minutes.**

  Moreover, in order not to reduce the autonomy of this urban electric minibus, it has been decided to feed this electric resistance only from the grid in the station during the night. It is assumed that the *BP* will maintain its warm temperature during the working day due to its high thermal capacity and the considered isolation level.

Chapter 8.

Conclusions and Future Research Lines

Throughout this Thesis, the steps for systematically design and optimize *Thermal Management Systems* for *Energy Storage Systems* for applications within the *Electro-Mobility* framework have been provided. Particularly this Thesis has been focused on a residential elevator and an urban electric minibus application.

Although each chapter included a section with its corresponding conclusions, this chapter highlights the main conclusions and contributions of this research work, including the compliance of the objectives that have been defined in the first chapter.

In addition, the main future lines of research are presented based on the work that has been described along this document.

8.1 CONCLUSIONS

As mentioned in Chapter 1, this research work has been motivated by the need to develop a procedure which ensures the implementation of the best possible *TMS* for a particular *ESS* installed in an *eMOV* application, following for that purpose non-arbitrary criteria.

This led us to define the main objective of this Thesis as the design and optimization of a *TMS* for any *Li-Ion BP* intended to be used for *eMOV* application by means of an improved methodology, i.e., by using numerical modelling. It can be said that this method has been based on the smart implementation of different versions of the same heat generation model on the most adequate thermal simulation tool.

Throughout the chapters of this document, the sequence of steps to be followed for the design and optimization of a *TMS* has been described. Cooling, heating and the insulation of the *BP* have been taken into account.

The applicability of the methodology, one of the main objectives of this research work, has been demonstrated applying this procedure to two different applications, both within the *eMOV* scope: a residential elevator and an urban electric minibus. As it is described in Chapter 5, five main steps have been defined which have to be followed to achieve an optimized *TMS*. Apart from them, some other issues have to bear in mind before carrying out the complete methodology:

- As it has been covered in Chapter 2, it is essential to understand the application´s requirements in terms of energy and power solicitations. This point will affect to the following issue related to the electrical sizing of the installed *ESS*. The specifications of the applications analyzed throughout this document have been defined by the manufacturer.

  For the residential elevator an *ESS* with 664.4Wh energy on board has been defined, whereas for the urban electric minibus a system with 27.7 kWh is needed. In terms of power requirements, the installed *ESS* in the first application must withstand power peaks of around 4.77 kW and 2.75 kW for the discharge and charge process, respectively. The power requirements for the second application, the urban electric minibus, have been more restrictive

defining power peaks for the discharge and charge process of 139.56 kW and 28.38 kW, respectively. Some cyclic power profiles can be defined for both cases for thermal design purposes.

- The in-depth analysis regarding different and available *ESS* technologies has been carried out in Chapter 3, in order to have the appropriate criteria to choose the most suitable one for the interested applications. The election of it must be based on criteria such as the maturity and availability of the technology and the energy and power density that the technology offers, among others. On this basis, for these both applications it has been decided to implement a *Li-Ion ESS*. In addition, due to the limited space in the residential elevator application and the high peak load currents solicitations by the urban electric minibus, it has been proposed to use cylindrical and pouch cells respectively in each application.

  The electrical sizing of the *BP* has been made in this chapter, defining how many cells and *BM*s were in the *BP*, together with the electrical configuration and connection between them.

  The *BP* of the residential elevator application has been composed of 7 *BM*s connected in serial between them. Each *BM* has been comprised of 12 cylindrical *Li-Ion* cells connected in serial, which have been provided by A123 manufacturer. The installed *BP* in the urban electric minibus has been composed of 16 *BM*s, connected 8 *BM*s in serial into 2 strings connected in parallel. Each *BM* has been comprised of 12 pouch *Li-Ion* cells connected in serial, which have been provided by KOKAM manufacturer. Both *BPs* have been completely designed, mounted and tested at *IK4-IKERLAN* working in a bigger multidisciplinary group.

- A detailed study related to different cooling technologies has been carried out. In addition, the insulation and the auxiliary heating processes have also been analyzed in Chapter 4.

  With regards to the first studied application, a direct air cooling system composed of fan and heat sinks, an air heater system based on some electrical resistances placed in the bottom of the case of the *BP* and a non-insulated

system has been implemented. This *TMS* allows taking advantage of the natural convection when the ambient and load conditions are favourable. For the urban electric minibus, it has been decided to install a more complex *TMS* composed of a first liquid cooling loop that transfers the heat to a secondary loop based on a dual architecture. This dual architecture combines *FC* and *AC* modes in terms of cooling process, a liquid heater system based on a resistance submerged in a vessel and an insulated system in order to protect the *BP* of the external environmental effects.

These previous steps have been treated out of the developed methodology, but they are crucial and necessary steps to achieve the final objective. As aforementioned, 5 steps have been defined in the developed methodology. Each step has been defined in Chapter 5 from a theoretical point of view. In Chapter 6 and Chapter 7 each step has been applied and completely developed for two different test cases using the most adequate simulation tools. The main conclusions that have been obtained are listed following:

- The developed methodology is valid and independent of the specific application and the numerical simulation tool that has been used for modeling and optimization process.

  One of the main issue when a novel methodology is defined, in this case in terms of optimization process, is related to its applicability, i.e., know if it could be extended to other application or in contrast, it must be only applied to a particular application. By means of this work not only has been demonstrated the validity of the methodology in order to construct a specific optimized *TMS*, it has been also shown its applicability to two different *eMOV* cases. Both applications require quite different specifications and solicitations and they have diverse *BP*s installed on it.

  In addition, different simulation tools have been used in each case, so it has been proved that the developed methodology is totally independent of the numerical tool that is used. The efficiency is searched in terms of the required time to fulfil each step of the methodology to boost up, in that way, the design

process. Specific and not arbitrary calculations and mathematical approaches, like the numerical *DoEs*, are mandatory in that sense.

The *TMS* design process has been improved as compared to a trial-and error determination of the battery cooling system design parameters and operation conditions. In addition, the simulations provided insights about the effects that are of interest in practice but hard to study experimentally.

- After selecting the most suitable components for the proposed *TMSs* some detailed and reliable thermal models have been developed at cell, at *BM* and at *BP* level for each application.

  This is done implementing different versions of the heat generation model by means of *UDF*s or embedded codes, depending on the simulation tool. Based on the thermal and hydraulic scalability, different models correspondent to *BM* and *BP* level have been developed.

  For the case of the residential elevator application, these models have been developed exclusively by means of *CFD (Ansys /FLUENT*) simulation tool due to the complexity of describing the physics of the air as direct cooling media both for *NC* and *FC* modes. Different simplifications related to the domain to be modelled, symmetry planes, etcetera have been applied in order to minimize the computational cost, that it is the main drawback of this simulation tool.

  Regarding the urban electric minibus, based on the work developed previously by N. Nieto in her Thesis, the cell, *BM* and cold plate *CFD* models have been used to obtain the 1D-lumped circuit composed of thermal capacitances and resistances to be used in *DAE (Dymola/TIL)* simulation tool. This is done to study at system level the primary and secondary loops of the proposed *TMS*, and taking into account especially the particularities of the *AC* cycles. Although this *DAE* model assumes a null thermal dispersion within the *BM*, it has been selected a suitable minimal liquid flow rate from the *CFD* model to avoid any problem in that sense. Doing so, the analysis is only focused on the thermal dispersion among the *BMs* of the *BP*.

Finally, both developed detailed models have been validated in a laboratory environment with a maximum time-averaged difference no higher than 1.3 ºC and 0.7 ºC regarding *BM´*s temperature for each application respectively. Besides, in both test cases a margin in terms of maximum temperature and dispersion within the *BMs* or cells has been checked which has opened the window to optimize the system design.

- The *False Steady* concept has been demonstrated such as a reliable method to accelerate the *CFD* transient simulations in order to reach valid results in reasonable time frames.

  The *False Steady* concept has been applied in the optimization task in order to boost up the transient cyclic simulations carried out by means of *Ansys/FLUENT* simulation tool for residential elevator case. This method only can be applied when cyclic current profiles have been used, e.i., when a steady state is reached after a certain time period. These types of load cycles are characteristic of the electrical performance of these *ESSs*.

  By means of this novel technique the simulation time has been reduced at minute level comparing with several hours or even days that a "real" transient simulation could take for *FC* flows. It has been a really important improvement in this methodology because it makes the usage of this simulation tool viable for this purpose. Simulation times are radically reduced for *NC* flows as well.

- An improved thermal design method based on the study of surface responses has been presented in this research work. For this purpose Minitab 17.0 software has been used as analysis tool. By means of this tool, the linear and quadratic effects and interactions between the parameters defined in each case have been analyzed with a small number of simulation runs. In many cases is really difficult to understand the cooling phenomena only plotting discrete results.

- For both applications the most suitable *TMS* has been proposed in the optimization stage. The main benefits that will be obtained can be shortly listed for each application:

Residential elevator application:

For this application *NC* and *FC* modes have been analyzed separately. The conclusions obtained are listed below:

- The thermal performance of the proposed *TMS* depends specially on the current level in the *BP*. Paradoxically the thermal dispersion at *BP* level arises as a problem when the ambient temperature is low, especially for the *NC* cooling mode.

- At component level it has been decided to remove the heat sinks from the final system design due to the low impact that they had in terms of thermal performance. This decision involved a slight reduction regarding the cost at *BP* level (around of 226 €) but primarily, it simplifies the manufacturing and industrialization of the complete *BP*.

- Although it is not expected, the required cooling time could become another important issue when the intermittency of the application is especially low. If the *FC* is considered a *PWM* of 67.5% has been defined as optimized operation point, even for the worst operation conditions in terms of ambient and electrical solicitations. In this case the diary energy consumption can be reduced at least in 69.2% if the original design is taken as a reference.

- More efficient *PWM* operating points can be defined depending on the situation. Due to the expected high intermittency of the application the selected fans will remain inactive until they are necessary. If the maximum temperature or the dispersion monitored by the *BMS* reaches their operational limits the fans will be activated. The *PWM* level of the fans defined for each situation will be controlled by the measured instantaneous current level and the ambient temperature.

Urban electric minibus:

For this application *FC* and *AC* modes have been analyzed separately. The conclusions obtained for each cooling mode of the dual system are listed below:

- The thermal performance of the proposed *TMS* depends specially on the ambient temperature in this case. As far as the *RMS* current level in the *BP* for the different routes is similar no active regulation of the *TMS* is proposed as in the previous case.

- For the *FC* mode it is enough keeping the pump rotational speed at 2370 rpm and the fan at a minimum *PWM* value of 70%, to achieve a maximum *BP* temperature of 32.5 ºC and a thermal dispersion of 3.0 ºC, even for the worst conditions. This pump speed corresponded to a total of 3.11 lpm liquid flow rate in system, which means considering 0.78 lpm per each cold plate for the selected hydraulic configuration (*8s2p*).

- For the AC cooling mode it is enough a pump rotational speed of 2950 rpm, a fan at minimum *PWM* value of 70% and a compressor rotational speed of merely 1800 rpm, to achieve a maximum *BP* temperature of 25.5 ºC and a thermal dispersion of 3.0 ºC for the worst operative case. This pump speed corresponded to a total of 4.5 lpm liquid flow rate in system, which means considering 1.13 lpm per each cold plate for the selected hydraulic configuration (*8s2p*).The selection of the *FC* or *AC* mode for the secondary loop will depend at first stage on the ambient temperature. In any case, if the maximum temperature or the dispersion monitored by the *BMS* reaches their operational limits the *AC* mode will be activated for security reason.

8.2 DIFUSSION OF THE RESULTS

The main relevant contributions to the dissemination of the results at international level are subsequently listed:

- International Journal

  - Martín-Martín L., Gastelurrutia J., Nieto N., Ramos J.C., Rivas A., Gil I. Modeling based on design of thermal management systems for vertical elevation applications powered by lithium-ion batteries. Applied Thermal Engineering 102 (2016) 1081-1094.

  - Martín-Martín L., Gastelurrutia J., del Portillo L.A., Försterling S. Modeling based design of a dual thermal management system for the battery pack of a full electric minibus. Applied Thermal Engineering (accepted with minor changes).

- International Conferences

  - Martín-Martín L., Gastelurrutia J., Nieto N. del Portillo L.A. 1D thermal modeling of lithium-ion battery packs for transport applications. ModVal11, March 17^{th}-19^{th} , 2014. Winterthur (Switzerland).

  - Martín-Martín L., Gastelurrutia J., Nieto N. del Portillo L.A. Adjusted sizing of an Electric Vehicle´s battery pack thermal management system based on a cost effective heat generation model. Advanced Battery Power Conference, April 28^{th}-29^{th}, 2015. Aachen (Germany).

  - Thermal management for EV/HEV Conference. February 16^{th}- 18^{th}, 2015. Berlin (Germany). Attended as listener.

  - New Mobility Conference. April 12^{th}-13^{th}, 2016. Leipzig (Germany). Attended in a stand in collaboration with IAD-TU Dresden.

8.3 FUTURE RESEARCH LINES

Although this Thesis finishes here, the research work could be still improved. Different directions have been identified to carry on with it:

- Analyze and define an optimized control strategy at system level considering the co-simulation choice regarding the residential elevator case study.

  Based on the results obtained in this research work for this application it has been defined a particular *PWM* value for the worst operative conditions. However, and as it has been explained, these worst conditions have been defined not considering an intermittency of the application which is not a very realistic condition in the practice (apart from the design requirements). An active control strategy for the fan performance is needed in order to reduce drastically its power consumption. This regulation will be based principally on the measured electrical conditions.

  The analysis of an active dynamic control strategy in *CFD* simulations is not a really easy and intuitive task and also, it involves high computational cost, which makes this option unfeasible nowadays. Therefore, a co-simulation is proposed between the *CFD* model and a control model implemented in another tool to check more realistic performance curves. Moreover, a *Reduced Order Model* (*ROM*) could be generated from the original *CFD* model and implemented in *Matlab/Simulink* together with the control strategy model. This will open the door even for more complex level of analysis.

- Analyze and define an optimized control strategy at system level regarding the urban electric minibus case study.

  The *TMS* for the urban electric minibus could be further optimized defining a control strategy in terms of component active regulation.

  In the present optimization work different prefixed velocities have been considered for the auxiliary components of the *TMS.* The pump has been always running whereof fan and the compressor have operated according to

an ON/OFF control strategy. Nevertheless, it could be more efficient to define a control strategy based on variable speeds components. In other words, components which could adjust their rotational speed in function of the actual solicitations in terms of ambient temperature or electrical requirements and only consuming what it would be necessary.

- Develop and experimentally adjust a hybrid electro-thermal model to analyze the electric and thermal coupled behaviour of the cells within a *BP* increasing the accuracy and taking into account the degradation effects in a very efficient way.

  In the heat generation model used in the thermal models developed in this research work, only the thermal effects in new cells have been considered. No accumulative effect of the degradation due to electrical and thermal operative conditions on the heat generation rate itself has been considered. This makes unviable a long term analysis to evaluate the real impact of the designed *TMS* in the life of the *BP*.

  By means of this hybrid electro-thermal model it would be possible to obtain a more accurate approach, taking into account more realistic electric and thermal performance of the *BP* with the time and the usage of the application. This way the process of designing and optimizing the *TMS* would be more reliable and precise, obtaining an improved insight not only to the actual system thermal performance but to the future evolution of it.

Appendix 1

Cells Data Sheet

Two different type of cells have been used in order to design the BP for each interested application.

For residential elevator application cylindrical cells provided by A123 SYSTEMS manufacturer have been used to design the complete *BP*, whereas for the urban electric minibus the pouch cells that have been implemented in the BP have been provided by KOKAM manufacturer.

Following the detailed datasheet of each one can be seen.

1.A CYLINDRICAL CELLS PROVIDED BY A123 SYSTEMS

Nanophosphate® High Power Lithium Ion Cell ANR26650*m1-B*

A123 SYSTEMS

KEY FEATURES AND BENEFITS

- Excellent abuse tolerance and superior cycle life from A123's patented Nanophosphate® lithium ion chemistry
- High power with over 2,600 W/kg and 5,800 W/L, 10 seconds, 50% SOC
- High usable energy over a wide state of charge (SOC) range

ANR26650*m1-B* Cell Specifications	
Cell Dimensions (mm)	ø26 x 65
Cell Weight (g)	76
Cell Capacity (nominal/minimum, Ah)	2.5/2.4
Voltage (nominal, V)	3.3
Internal Impedance (1kHz AC typical, mΩ)	6
HPPC 10 Sec Discharge Pulse Power 50% SOC	200 W
Recommended Standard Charge Method	1C to 3.6V CCCV, 45 min
Recommended Fast Charge Method to 80% SOC	4C to 3.6V CC, 12 min
Maximum Continuous Discharge (A)	70
Maximum Pulse Discharge (10 seconds, A)	120
Cycle Life at 10C Discharge, 100% DOD	>1,000 cycles
Operating Temperature	-30°C to 55°C
Storage Temperature	-40°C to 60°C

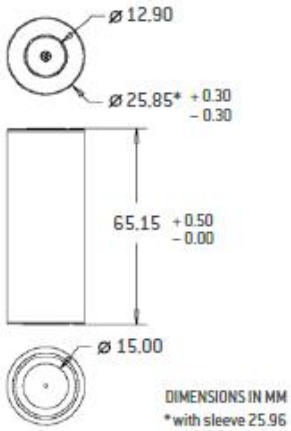

APPLICATIONS

Transportation

Advanced energy storage for electric drive vehicles

Commercial

Enabling next-generation commercial products

Electric Grid

Dynamic energy solutions for a smarter grid

www.a123systems.com

Nanophosphate® High Power Lithium Ion Cell

ANR26650*m1-B*

1C Discharge Characteristics at High and Low Temperatures

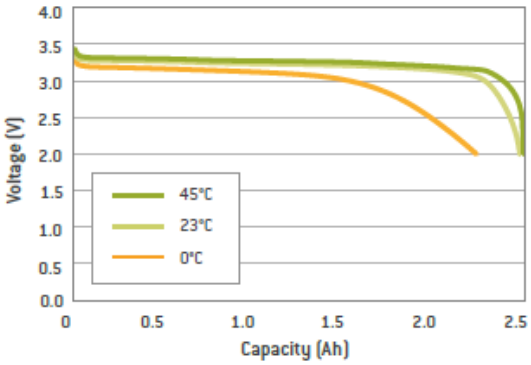

Discharge Characteristics at 23°C

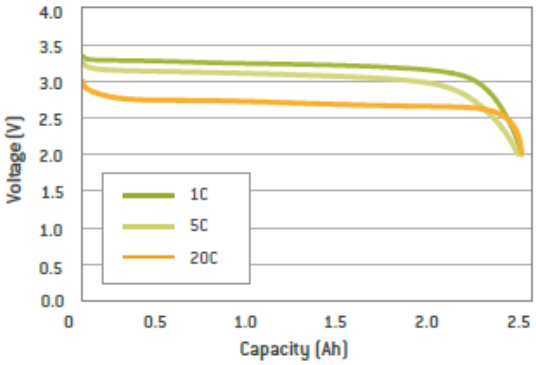

Cycle Life Performance, 100% DOD, Various Temperatures and Discharge Rates

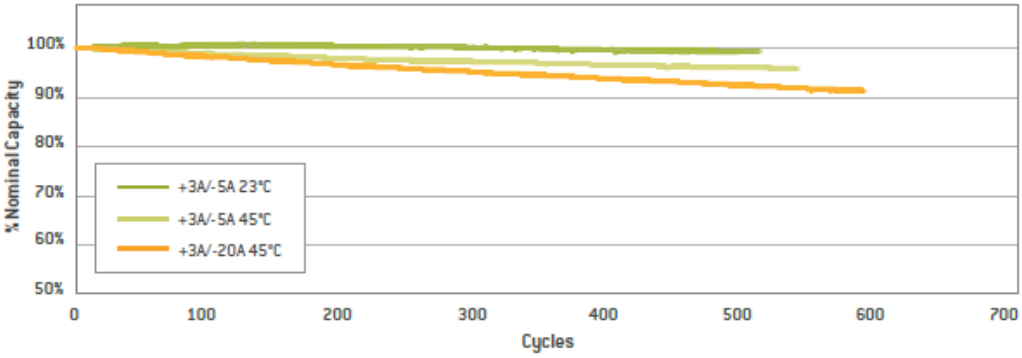

Preliminary Specifications. Performance may vary depending on use conditions and application.
A123 Systems makes no warranty explicit or implied with this datasheet. Contents subject to change without notice.

CORPORATE HEADQUARTERS
A123 Systems, Inc.
200 West Street
Waltham, MA 02451
(617) 778-5700
www.a123systems.com

A123 SYSTEMS

1.B POUCH CELLS PROVIDED BY KOKAM

Kokam Great Power for Everyone	Technical Specification	Document # : KD07-RC23-01 Issued date : March. 23, 2009 Revision : A0

2. Technical Specification

2.1 General Information

No.	ITEM	VALUE	REMARK
1	Rated Capacity	Typ. 41.0Ah Min. 40.0Ah	Charge@0.2C(8.0A) Discharge@0.5C(20A)
2	Nominal Voltage	3.7V	
	End Of Discharge	3.0V	
	Max. Charge Voltage	4.15 ±0.03V	
3	Max. Conti. Charge Current	120A	CC-CV charging is required End Condition: 0.05C(2.0A) or 5Hr Temperature: 23±3℃
4	Max. Conti. Discharge Current	320A	
5	Operation Temperature Range	Charge: 10 ~ 45°C	@60±25% R.H.
		Discharge: -20 ~ 55°C	
6	Storage Temperature Range	1 YEAR -20 ~ 25°C	@60±25% R.H. SOC 50 ±5%
		3 MONTH 25 ~ 40°C	
		1 WEEK 40 ~ 60°C	
7	Weight	Max. 1,030.0g	
8	Cell Dimension	Length : Max.222.0mm	Except for tab length
		Width : Max.214.0mm	
		Thickness : Max.10.7mm	Initial full charge

Kokam	Technical Specification	Document # : KD07-RC23-01 Issued date : March. 23, 2009 Revision : A0

2.2 Drawing

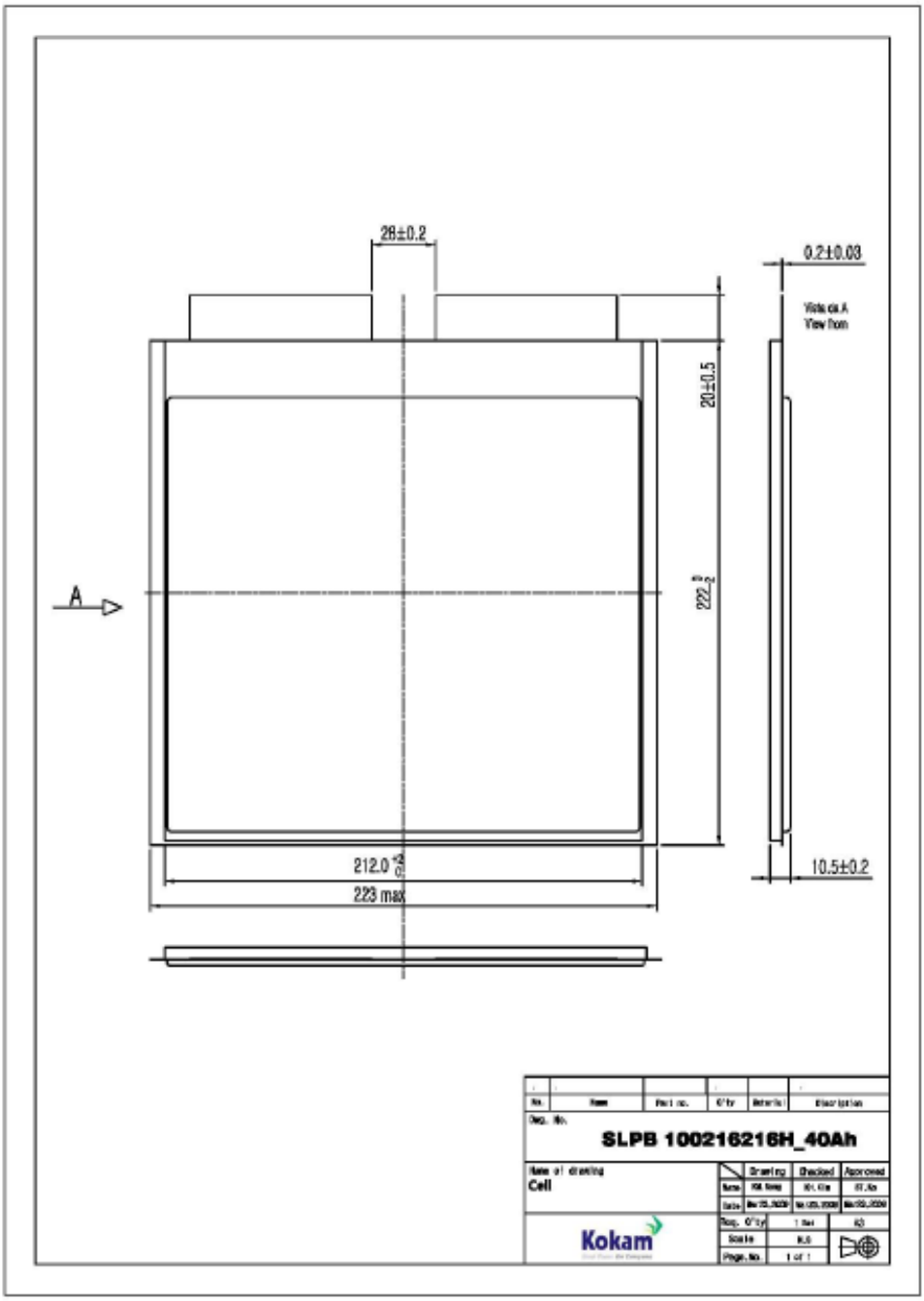

Kokam	Technical Specification	Document # : KD07-RC23-01 Issued date : March. 23, 2009 Revision : A0

2.3 Electrical Performance

.No	ITEM	CRITERIA						TESTING CONDITIONS
1	Outside Appearance	No abnormal strain, Deformation nor damage						Visual check
2	External Dimension	According to the attached drawing						Use caliper (0.05mm a division) specified in ISO 3599
3	Discharge Time	More than the time Mentioned hereunder						Measure capacity by holding at various temperatures for 1Hr after standard charging.
	Discharge Rate	0.5C	1.0C	2.0C	3.0C	5.0C	8.0C	
	Capacity (%)	100%	> 95%	> 92%	> 92%	> 90%	> 85%	
	Discharge Temperature	-20℃	-10℃	0℃	25℃	40℃	55℃	
	Capacity (%)	>70%	>75%	> 85%	100%	> 97%	> 97%	
4	Charge Time	More than the rates Mentioned hereunder						Measure time elapsed till end charge current at the charge conditions mentioned hereunder after standard discharge
	Charge Current	Less than 5.0 hrs						0.5C
		Less than 2.0 hrs						1.0C
5	Initial Internal Impedance	Less than 0.8mΩ						Measure by alternate current (1kHz) within 6hr after charge. (23±3°C)
6	Cycle Life	Above 32.0Ah						Carry out 1000cycles charging/discharging in the below condition. ■ Charge : CC/CV, 1.0C(40A), 4.15V, 0.05C(2A)(5Hr)-END ■ Discharge : 1.0C(40A) to 3.0V ■ Rest Time between charge/discharge : 10min. ■ Temperature : 23±3°C
7	Storage Performance	Above 36.0Ah						After full charge at 60±3°C, then leave 1 week. After storage, measure discharge capacity at 23±3°C
8	Leakage-Proof	No leakage [visual inspection]						After full charge, stand at 60±3°C, 60±10%RH for 1month.

Kokam	Technical Specification	Document # : KD07-RC23-01 Issued date : March. 23, 2009 Revision : A0

◆Discharge profiles at RT

❖ Charge : CC-CV, 1.0C, 4.2V, 0.05C cut-off @23℃±2℃
❖ Discharge : CC, 0.3 ~ 8.0C, 2.7V cut-off @23℃±2℃

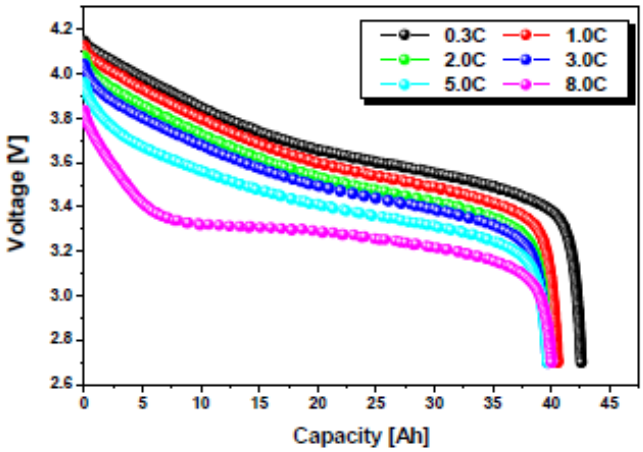

◆Temperature characteristics

❖ Charge : CC-CV, 0.5C, 4.2V, 0.05C cut-off @25℃±2℃
❖ Discharge : CC, 0.5C, 2.7V cut-off @ each temperature
❖ Soaking time : 2hr

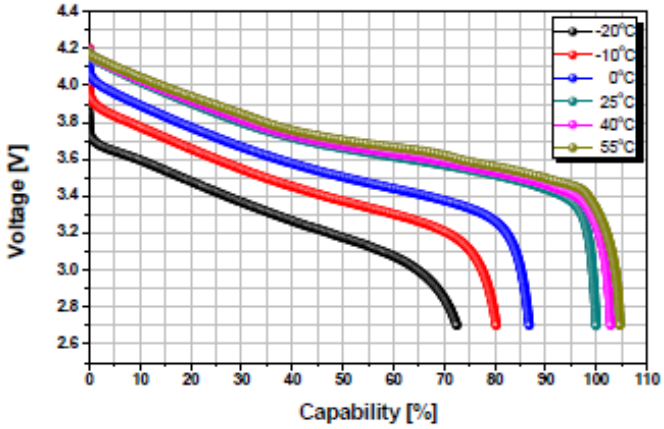

Kokam	Technical Specification	Document # : KD07-RC23-01 Issued date : March. 23, 2009 Revision : A0

Charge profiles at RT

❖ Charge : CC-CV, 0.5C ~ 3.0C, 4.2V, 0.05C cut off @23℃±2℃

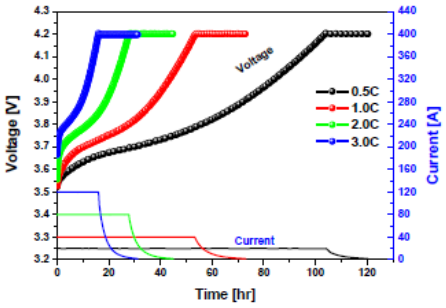

2.5 Life Performance

Cycle characteristics at RT

❖ Charge : CC-CV, 1.0C, 4.15V, 0.05C cut-off @23℃±2℃
❖ Discharge : CC, 1C, 3.0V cut-off @23℃±2℃

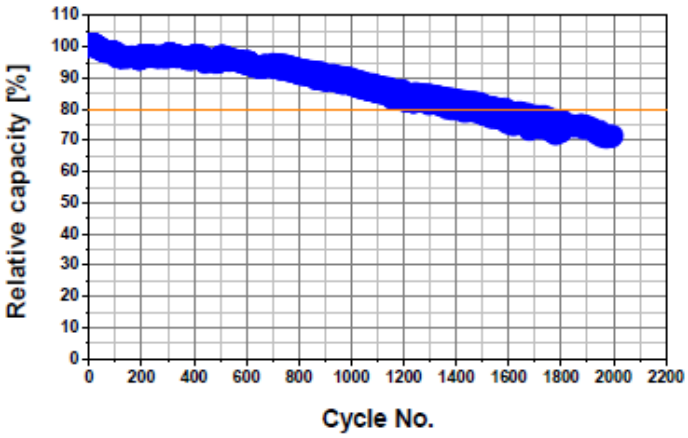

2.4 Environmental Performance

- **Operating condition**
  Charging : 10~45℃
  Discharging : -20~55℃

- **Storage condition**
  SOC 40~60% at -20~60℃
  Recommend condition : SOC 40~60% at 25±3℃

- **Self discharging rate**
  <2% for Month at Room temperature

Appendix 2

Heat Generation Subroutine

The heat generation rate in this Thesis has been calculated based on the Eq.(A2.2.1) as it has been explained in Chapter 5.

This formula, as it can be observed, is sensitive to the instantaneous current value, the internal resistance, R_{in}, and the entropic heat coefficient , $\frac{\partial U^{avg}}{\partial T}$, considering the absolute cell and *SOC* variation.

$$S_h = \frac{\dot{q}_T}{V} = \frac{I^2 \cdot R_{in}(SOC, T_{cell}) + I \cdot T_{cell} \cdot \frac{\partial U^{avg}}{\partial T}(SOC)}{V} \qquad \text{(A2.2.1)}$$

This heat generation model has been validated experimentally based on direct heat generation measurements by means of the accelerating rate calorimeter (THT, EV Standard Calorimeter) adiabatically.

In the following section, the subroutine that it has been used to implement this generation model in *CFD* (*Ansys/ Fluent*) simulation tool for residential elevator application and in *DAE* (*Dymola/TIL*) simulation tool for the urban electric minibus application it is explained.

2.A COMPUTATIONA FLUID DYNAMICS (CFD) SIMULATION TOOL

The generation model subroutine implement in *Ansys/Fluent* simulation tool is shown along this section.

The code which is shown below, it has been used to calculate the volumetric heat generation rate in the cell zones for the residential elevator application. This subroutine has been implemented in the detailed models developed in the third step of the methodology in the Chapter 6.

The entropic heat coefficient and the internal resistance are defined such as an array. As it can be seen in the following code, the entropic heat generation coefficient is defined as "*Coeftxt*" (indicated by purple), whereas the internal resistance as "*Data*" (indicated by blue).

```
#include "udf.h"
#include <stdio.h>
#define n_CELL 50
#define n_DATA 100000
real ID[n_CELL]=[21];
real HEAT[n_CELL]=[21];
int ID_i;
int ID_size;
int ID_value;
real CURR[n_DATA][2]={{0}};
int CURR_i, CURR_j;
int CURR_size_i, CURR_size_j;
float CURR_value;
real SOC[n_DATA][2]={{0}};
int SOC_i, SOC_j;
int SOC_size_i, SOC_size_j;
float SOC_value;
float Coeftxt[8][2]={{4.4419,-0.3365},{8.8837,-0.2543},{26.9006,-
0.0417},{44.8343,0.0954},{52.5186,0.1885},{71.5111,0.1547},{90.5037,0.0441},{95.2519,0.0
571}};

int size_j=8;
float
DATA[3][9]={{55.0480,44.6480,38.4240,34.7280,32.3200,30.5600,29.4400,29.4720,28.3280},{22.
384,19.2,17.728,17.144,16.4,15.752,15.336,16,14.944},{14.184,12.816,11.968,12.016,11.52,11.064,
10.48,11.392,10.656}};
float SOCrow[9]={10,20,30,40,50,60,70,80,90};
real Tcolumn[3]={5,25,45};
int size_m=3;
int size_n=9;
DEFINE_ADJUST(ID_input,d)
{
```

```
	#if !RP_NODE
		FILE *ID_file;
	#endif
	#if !RP_NODE
		ID_file= fopen("ID.txt","r");
		fscanf(ID_file,"%d\n",&ID_size);
		for (ID_i=0; ID_i<ID_size; ID_i++)
		{
			fscanf(ID_file,"%d\n",&ID_value);
			ID[ID_i]=ID_value;
		}
		fclose(ID_file);
	#endif
	host_to_node_int_1(ID_size);
	host_to_node_real(ID,n_CELL);
}
DEFINE_ADJUST(input_corriente,d)
{
	#if !RP_NODE
		FILE *CURR_file;
	#endif
	#if !RP_NODE
		CURR_file= fopen("CURR.txt","r");
		fscanf(CURR_file,"%d\n",&CURR_size_i);
		fscanf(CURR_file,"%d\n",&CURR_size_j);
		for (CURR_i=0; CURR_i<CURR_size_i; CURR_i++)
		{
			for (CURR_j=0; CURR_j<CURR_size_j; CURR_j++)
			{
			fscanf(CURR_file,"%f",&CURR_value);
			CURR[CURR_i][CURR_j]=CURR_value;
			}
		}
		fclose(CURR_file);
	#endif
	host_to_node_int_2(CURR_size_i,CURR_size_j);
	host_to_node_real(CURR,(2*n_DATA));
}
DEFINE_ADJUST(input_soc,d)
{
	#if !RP_NODE
		FILE *SOC_file;
	#endif
	#if !RP_NODE
		SOC_file= fopen("SOC.txt","r");
		fscanf(SOC_file,"%d\n",&SOC_size_i);
		fscanf(SOC_file,"%d\n",&SOC_size_j);
		for (SOC_i=0; SOC_i<SOC_size_i; SOC_i++)
		{
			for (SOC_j=0; SOC_j<SOC_size_j; SOC_j++)
			{
			fscanf(SOC_file,"%f",&SOC_value);
			SOC[SOC_i][SOC_j]=SOC_value;
			}
		}
		fclose(SOC_file);
	#endif
```

```
        host_to_node_int_2(SOC_size_i,SOC_size_j);
        host_to_node_real(SOC,(2*n_DATA));
}
DEFINE_SOURCE(A123_01,c,k,dS,eqn)
{
#if !RP_HOST
        real source1;
                source1 = HEAT[0];
                dS[eqn]=0.0;
        return source1;
#endif
}
DEFINE_SOURCE(A123_02,c,k,dS,eqn)
{
#if !RP_HOST
        real source2;
                source2 = HEAT[1];
                dS[eqn]=0.0;
        return source2;

#endif
}
DEFINE_SOURCE(A123_xx,c,k,dS,eqn)
{
#if !RP_HOST
        real source3;
                source3 = HEAT[2];
                dS[eqn]=0.0;
        return source3;
#endif
}
DEFINE_EXECUTE_AT_END(execute_at_end)
{
        #if !RP_NODE
                FILE *fp;
        #endif
        real t;
        real CURR_t=0.0;
        real SOC_t=0.0;
        int CELL_i;
        real VOL[n_CELL]={0};
        real TEMP_SUM[n_CELL]=[21];
        real TEMP_AV[n_CELL]=[21];
        real DUDT[n_CELL]=[21];
        real RIN[n_CELL]=[21];
        real QGEN[n_CELL]=[21];
        for (CELL_i=0; CELL_i<(ID_size); CELL_i++)
        {
                Domain *domain=Get_Domain(1);
                Thread *k=Lookup_Thread(domain,ID[CELL_i]);
                cell_t c;
                int CURR_k;
                int SOC_k;
                real TIME_min=0.0;
                real TIME_max=0.0;
                real CURR_min=0.0;
                real CURR_max=0.0;
```

```
		real SOC_min=0.0;
		real SOC_max=0.0;
		real Rin_Tmin_SOCmin=0.0;
		real Rin_Tmin_SOCmax=0.0;
		real Rin_Tmax_SOCmin=0.0;
		real Rin_Tmax_SOCmax=0.0;
		real Rin_T_SOCmin=0.0;
		real Rin_T_SOCmax=0.0;
		int l;
		int y1;
		int x1;
		real SOCmin=0.0;
		real SOCmax=0.0;
		real dUdTmin=0.0;
		real dUdTmax=0.0;
		real Tmin=0.0;
		real Tmax=0.0;
		#if !RP_NODE
			t=CURRENT_TIME;
		#endif
		host_to_node_real_1(t);
		if (t <= CURR[(CURR_size_i - 1)][0])
		{
			if (t <= CURR[0][0])
			{
				CURR_k = 0;
			}
			else
			{
				CURR_k = 1;
				while ((CURR_k < (CURR_size_i - 1)) & (t >=
CURR[CURR_k][0]))
				{
					CURR_k++;
				}
				CURR_k = (CURR_k - 1);
			}
			TIME_min = CURR[CURR_k][0];
			TIME_max = CURR[(CURR_k+1)][0];
			CURR_min = CURR[CURR_k][1];
			CURR_max = CURR[(CURR_k+1)][1];
			CURR_t = (CURR_min+(CURR_max-CURR_min)*(t-
TIME_min)/(TIME_max-TIME_min));
		}
		else
		{
			TIME_min = 0.0;
			TIME_max = 0.0;
			CURR_min = 0.0;
			CURR_max = 0.0;
			CURR_t = 0.0;
		}
		if (t <= SOC[(SOC_size_i - 1)][0])
		{
			if (t <= SOC[0][0])
			{
				SOC_k = 0;
```

```
                }
                else
                {
                        SOC_k = 1;
                        while ((SOC_k < (SOC_size_i - 1)) & (t >= SOC[SOC_k][0]))
                        {
                                SOC_k++;
                        }
                        SOC_k = (SOC_k - 1);
                }
                TIME_min = SOC[SOC_k][0];
                TIME_max = SOC[(SOC_k+1)][0];
                SOC_min = SOC[SOC_k][1];
                SOC_max = SOC[(SOC_k+1)][1];
                SOC_t = (SOC_min+(SOC_max-SOC_min)*(t-TIME_min)/(TIME_max-
TIME_min));
        }
        else
        {
                SOC_k = (SOC_size_i - 1);
                TIME_min = 0.0;
                TIME_max = 0.0;
                SOC_min = 0.0;
                SOC_max = 0.0;
                SOC_t = SOC[SOC_k][1];
        }
        #if !RP_HOST
                begin_c_loop_int(c,k)
                {
                        VOL[CELL_i] += C_VOLUME(c,k);
                        TEMP_SUM[CELL_i] +=C_T(c,k)*C_VOLUME(c,k);
                }
                end_c_loop_int(c,k)
                VOL[CELL_i] = PRF_GRSUM1(VOL[CELL_i]);
                TEMP_SUM[CELL_i] = PRF_GRSUM1(TEMP_SUM[CELL_i]);
                TEMP_AV[CELL_i] = (TEMP_SUM[CELL_i]/VOL[CELL_i]);
                if (SOC_t <= Coeftxt[0][0])
                {
                        l = 0;
                }
                else
                {
                        l = 1;
                        while ((l < (size_j-1)) & (SOC_t >= Coeftxt[l][0]))
                        {
                                l++;
                        }
                        l=l-1;
                }
                SOCmin=Coeftxt[l][0];
                SOCmax=Coeftxt[l+1][0];
                dUdTmin=Coeftxt[l][1];
                dUdTmax=Coeftxt[l+1][1];
                DUDT[CELL_i]=dUdTmin+(dUdTmax-dUdTmin)*(SOC_t-
SOCmin)/(SOCmax-SOCmin);
                if (SOC_t <= SOCrow[0])
                {
```

```
                        y1 = 0;
                }
                else
                {
                        y1 = 1;
                        while ((y1 < (size_n-1)) & (SOC_t >= SOCrow[y1]))
                        {
                                y1++;
                        }
                        y1 = y1-1;
                }
                SOCmin=SOCrow[y1];
                SOCmax=SOCrow[y1+1];
                if ((TEMP_AV[CELL_i]-273) <= Tcolumn[0])
                {
                        x1 = 0;
                }
                else
                {
                        x1 = 1;
                        while ((x1 < (size_m-1)) & ((TEMP_AV[CELL_i]-273) >=
Tcolumn[x1]))
                        {
                                x1++;
                        }
                        x1 = x1-1;
                }
                Tmin=Tcolumn[x1];
                Tmax=Tcolumn[x1+1];
                Rin_Tmin_SOCmin=DATA[x1][y1];
                Rin_Tmin_SOCmax=DATA[x1][y1+1];
                Rin_Tmax_SOCmin=DATA[x1+1][y1];
                Rin_Tmax_SOCmax=DATA[x1+1][y1+1];
                Rin_T_SOCmin=(Rin_Tmin_SOCmin-
Rin_Tmax_SOCmin)*((TEMP_AV[CELL_i]-273)-Tmax)/(Tmin-Tmax)+Rin_Tmax_SOCmin;
                Rin_T_SOCmax=(Rin_Tmin_SOCmax-
Rin_Tmax_SOCmax)*((TEMP_AV[CELL_i]-273)-Tmax)/(Tmin-Tmax)+Rin_Tmax_SOCmax;
                RIN[CELL_i]=(Rin_T_SOCmin-Rin_T_SOCmax)*(SOC_t-
SOCmax)/(SOCmin-SOCmax)+Rin_T_SOCmax;
                QGEN[CELL_i] =
(pow(CURR_t,2))*RIN[CELL_i]/1000+CURR_t*TEMP_AV[CELL_i]*DUDT[CELL_i]/1000;
                HEAT[CELL_i]=(QGEN[CELL_i]/2)/VOL[CELL_i];
        #endif
        node_to_host_int_1(CELL_i);
    node_to_host_real_3(t, CURR_t, SOC_t);
        node_to_host_real_6(VOL[CELL_i], TEMP_AV[CELL_i], DUDT[CELL_i],
RIN[CELL_i], QGEN[CELL_i], HEAT[CELL_i]);
        #if !RP_NODE
                Message("Cell = %d\n",(CELL_i+1));
                Message("Generation = %f\n", QGEN[CELL_i]);
                fp = fopen("GEN.txt", "a");
                fprintf(fp,"%d %f %f %f %f %f %f %f %f %f\n", (CELL_i+1), t, CURR_t,
SOC_t, VOL[CELL_i], TEMP_AV[CELL_i], DUDT[CELL_i], RIN[CELL_i], QGEN[CELL_i],
HEAT[CELL_i]);
                fclose(fp);
        #endif
```

```
        }
   node_to_host_real(HEAT,n_CELL);
        #if !RP_NODE
                Message("Current = %f\n",CURR_t);
                Message("SOC = %f\n",SOC_t);
        #endif
}
```

Moreover, for the simulations that have been carried out for the first analyzed application in terms of optimization, as it has been explained along the document a novel concept named *False Steady* has been introduced. For that purpose the following code has been defined. As it can be observed and in contrast than the previously developed code, in this case the entropic heat coefficient and internal resistance are not defined such as parameters, and instead of it the heat generation rate interpolation table has been introduced in function of the cell temperature (from 283 K to 323 K). For each power requirement level these values related to the heat generation rate changes.

```
#include "udf.h"
#include <stdio.h>
#define n_CELL 50
real ID[n_CELL]=[21];
real HEAT[n_CELL]=[21];
int ID_i;
int ID_size;
int ID_value;

float
Pavgtxt[9][2]={{283,0.534},{288,0.417},{293,0.383},{298,0.285},{303,0.285},{308,0.245},{313,0
.239},{318,0.206},{323,0.193}};
int size_j=9;

DEFINE_ADJUST(ID_input,d)
{

        #if !RP_NODE
                FILE *ID_file;
        #endif
        #if !RP_NODE
                ID_file= fopen("ID.txt","r");
                fscanf(ID_file,"%d\n",&ID_size);
                for (ID_i=0; ID_i<ID_size; ID_i++)
                {
                        fscanf(ID_file,"%d\n",&ID_value);

                        ID[ID_i]=ID_value;                }
                fclose(ID_file);
        #endif
        host_to_node_int_1(ID_size);
        host_to_node_real(ID,n_CELL);
}
DEFINE_SOURCE(A123b_01,c,k,dS,eqn)
{
```

```
#if !RP_HOST
	real source1;
		source1 = HEAT[0];
		dS[eqn]=0.0;
	return source1;
#endif
}

DEFINE_SOURCE(A123b_02,c,k,dS,eqn)
{
#if !RP_HOST
	real source2;
		source2 = HEAT[1];
		dS[eqn]=0.0;
	return source2;
#endif
}

DEFINE_SOURCE(A123b_xx,c,k,dS,eqn)
{
#if !RP_HOST

	real source3;
		source3 = HEAT[2];
		dS[eqn]=0.0;
	return source3;
#endif
}

DEFINE_EXECUTE_AT_END(execute_at_end)
{
	#if !RP_NODE
		FILE *fp;
	#endif
		int CELL_i;
	real VOL[n_CELL]={0};
	real TEMP_SUM[n_CELL]=[21];
	real TEMP_AV[n_CELL]=[21];
	real Pavg[n_CELL]=[21];

	for (CELL_i=0; CELL_i<(ID_size); CELL_i++)
	{
		Domain *domain=Get_Domain(1);
		Thread *k=Lookup_Thread(domain,ID[CELL_i]);
		cell_t c;
		int l;
		real Tmin=0.0;
		real Tmax=0.0;
		real Pavgmin=0.0;
		real Pavgmax=0.0;
		#if !RP_HOST
			begin_c_loop_int(c,k)
			{
				VOL[CELL_i] += C_VOLUME(c,k);
				TEMP_SUM[CELL_i] +=C_T(c,k)*C_VOLUME(c,k);
			}
			end_c_loop_int(c,k)
```

```
                        VOL[CELL_i] = PRF_GRSUM1(VOL[CELL_i]);
                        TEMP_SUM[CELL_i] = PRF_GRSUM1(TEMP_SUM[CELL_i]);

                        TEMP_AV[CELL_i] = (TEMP_SUM[CELL_i]/VOL[CELL_i]);


                        if (TEMP_AV[CELL_i] <= Pavgtxt[0][0])
                        {
                                l = 0;
                        }
                        else
                        {
                                l = 1;
                                while ((l < (size_j-1)) & (TEMP_AV[CELL_i]>= Pavgtxt[l][0]))
                                {
                                        l++;
                                }
                                l=l-1;
                        }
                        Tmin=Pavgtxt[l][0];
                        Tmax=Pavgtxt[l+1][0];
                        Pavgmin=Pavgtxt[l][1];
                        Pavgmax=Pavgtxt[l+1][1];

                        Pavg[CELL_i]=Pavgmin+(Pavgmax-Pavgmin)*(TEMP_AV[CELL_i]-
Tmin)/(Tmax-Tmin);

                        HEAT[CELL_i]=(Pavg[CELL_i]/(2*VOL[CELL_i]));
                #endif
                node_to_host_int_1(CELL_i);
        node_to_host_real_4(VOL[CELL_i], TEMP_AV[CELL_i], Pavg[CELL_i],
HEAT[CELL_i]); /*Resultados celda i*/

                        #if !RP_NODE
                        Message("Cell = %d\n",(CELL_i+1));
                        Message("Generation = %f\n", HEAT[CELL_i]);
                        fp = fopen("GEN.txt", "a");
                        fprintf(fp,"%d %f %f %f\n", (CELL_i+1), VOL[CELL_i],
TEMP_AV[CELL_i], HEAT[CELL_i]);
                        fclose(fp);
                #endif
        }
  node_to_host_real(HEAT,n_CELL);
 }
```

2.B DIFFERENTIAL, ALGEBRAIC AND DISCRETE EQUATION (DAE) SIMULATION TOOL

The generation model subroutine implemented in *Dymola/ TIL* simulation tool is described below. In Figure 2.1 is shown the schematic diagram of the heat generation model implemented in *Dymola/TIL* simulation tool based on the Eq.().

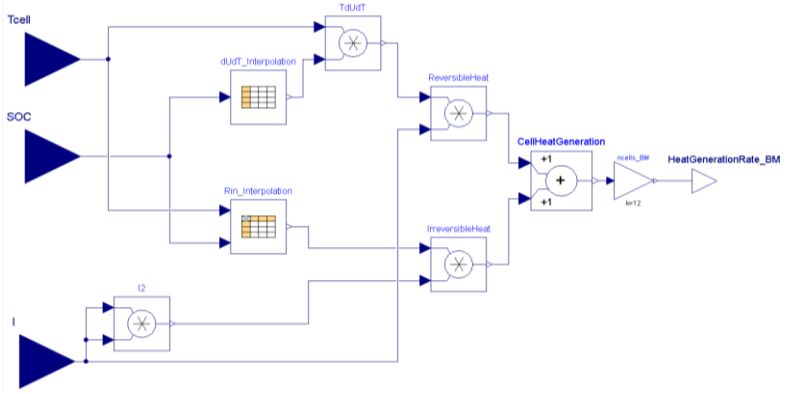

Figure 2.1 Schematic diagram of the heat generation model implemented in Dymola/TIL simulation tool

According to Eq. (), the actual cell temperature in Kelvin, the SOC value in % and the current rate in A are the inputs needed to estimate this value. The entropic heat generation $(\frac{\partial U^{avg}}{\partial T})$ and the internal resistance (R_{in}) are interpolated by means of look-up tables integrated in this simulation tool. As it can be seen in Figure 2.1, the entropic heat coefficient loo-up table as "dUdT_Interpolation", whereas the internal resistance look-up table is identified as "Rin_Interpolation". In Figure **2.2** (a) and (b) are shown the configuration windows related to the entropic heat coefficient an internal resistance, respectively.

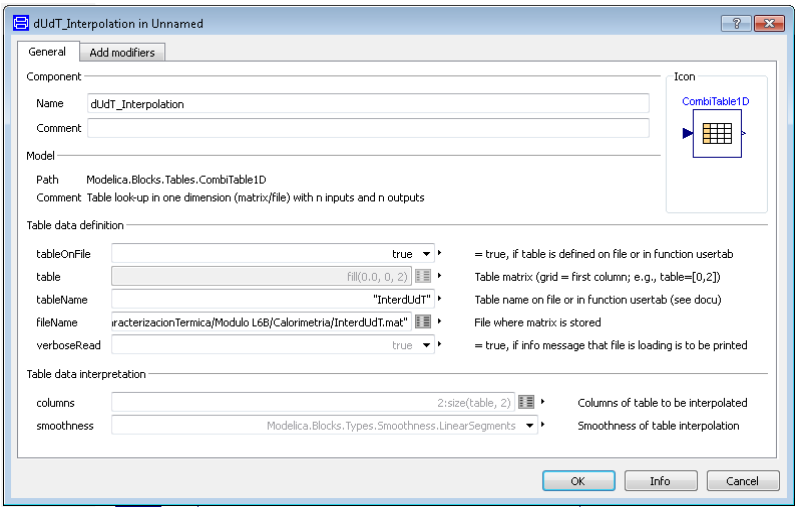

(a)

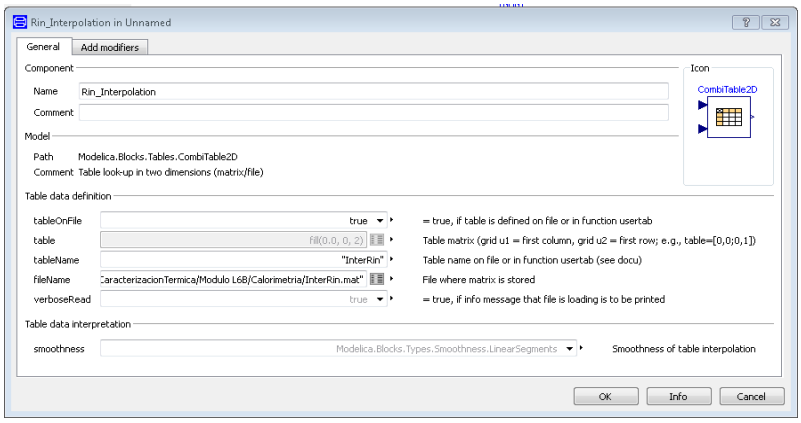

(b)

Figure 2.2 The look-up table configuration related to (a) dU/dT and (b) Rin.

For each parameter, a value table defined in Matlab is referenced in the configuration windows which are shown in Figure **2.2** (a) and (b).These value tables have been determinated experimentally. In the case of heat entropic coefficient, the correspondent values are function of *SOC* values, whereas the internal resistance values are dependent of cell temperature and *SOC*.

The values correspond to the entropic heat generation are shown in Figure **2.3** (a). As it can be seen in this case a lineal tendency of the values in function of *SOC* it does not exist, for *SOC* range from 10% to 35% and from 90% to 100% the heat entropic coefficient value is negative, whereas for *SOC* range from 35% to 90% are positive. In addition, the value table used for the interpolation in order to obtain the internal resistance is shown in Figure **2.3** (b). As it can be observed, a complete sweep regarding *SOC* values has been considered from 0% to 100%, whereas in terms of cell

temperature a scanning from 283.15 K to 333.15 K has been taken into account, every 10 Kelvin degress. It can be concluded analyzing these values that the internal resistance is higher, when the *SOC* value drops down and the temperature of the cell is low.

		dU/dT
SOC, %	11.2	-0.17787
	15.8	-0.1396
	34.5	-0.00825
	53.2	0.14603
	71.9	0.04324
	90.6	-0.02552
	95.3	-0.03924

(a)

		SOC, %												
		2.5	4.2	4.5	4.5	5.2	9.5	10.0	15.7	18.2	18.2	20.9	23.9	24.3
Tcell, K	283.15	7.4084	6.3612	6.1948	6.1873	5.7826	5.3663	5.3209	4.7848	4.5470	4.5414	4.2826	4.3231	4.3286
	298.15	3.9144	3.7483	3.7220	3.7208	3.6566	3.2398	3.1944	2.6576	2.6122	2.6111	2.5616	2.5078	2.5005
	313.15	2.0283	1.9549	1.9432	1.9427	1.9143	1.7300	1.7153	1.5415	1.4645	1.4626	1.4722	1.4825	1.4765
	323.15	1.5553	1.5206	1.5152	1.5149	1.5015	1.4146	1.4051	1.2475	1.1776	1.1782	1.2059	1.2360	1.2401
	333.15	1.1525	1.0366	1.0236	1.0230	0.9952	0.8814	0.8729	0.7992	0.7761	0.7756	0.7545	0.7351	0.7327

		SOC, %											
		31.2	36.6	36.7	36.7	40.6	42.1	42.9	43.2	44.5	55.0	55.1	57.7	60.6
Tcell, K	283.15	4.4226	4.1429	4.1367	4.1365	3.9304	3.8526	3.8199	3.8057	3.7454	3.8009	3.8018	3.8154	3.8307
	298.15	2.3756	2.2775	2.2753	2.2753	1.9977	2.0057	2.0094	2.0110	2.0178	2.0733	2.0742	2.0878	1.9976
	313.15	1.3731	1.2919	1.2901	1.2902	1.3448	1.3654	1.3750	1.3728	1.3633	1.2865	1.2851	1.2967	1.3096
	323.15	1.2026	1.0601	1.1725	1.1725	1.1508	1.1426	1.1387	1.1701	1.1300	1.0726	1.0738	1.0911	1.1105
	333.15	0.6974	0.6758	0.6753	0.6753	0.6617	0.6570	0.6548	0.6539	0.6501	0.6234	0.6230	0.6174	0.6115

		SOC, %											
		61.8	62.0	62.8	63.4	73.4	73.6	78.7	80.5	80.8	80.9	84.6	85.5	87.0
Tcell, K	283.15	3.8372	3.8382	3.8426	3.6851	3.5780	3.5754	3.5204	3.5010	3.4983	3.4972	3.4576	3.6001	3.5865
	298.15	2.0119	2.0142	2.0238	2.0298	2.1455	2.1483	2.2078	1.8452	1.8467	1.8472	1.8683	1.8734	1.8822
	313.15	1.3151	1.3141	1.3101	1.3076	1.2587	1.2575	1.3235	1.3468	1.3500	1.3471	1.2397	1.2131	1.1684
	323.15	1.1187	1.1201	1.1145	1.1109	1.0426	1.0456	1.1085	1.1307	1.1338	1.1350	1.0418	1.0188	0.9800
	333.15	0.6091	0.6087	0.6071	0.6061	0.5888	0.5884	0.5806	0.5780	0.5777	0.5775	0.5724	0.5712	0.5692

		SOC, %									
		87.3	94.2	94.5	94.6	95.1	95.2	96.0	97.0	98.0	99.0	100.0
Tcell, K	283.15	3.5840	3.5229	3.8180	3.5195	3.5149	3.5147	3.3375	3.3282	3.3190	3.3099	3.3009
	298.15	1.8838	1.9232	1.9249	1.9254	1.9283	1.9285	1.7749	1.7688	1.7628	1.7569	1.7510
	313.15	1.1600	1.1113	1.1092	1.1086	1.2151	1.1048	1.1729	1.1705	1.1681	1.1657	1.1634
	323.15	0.9818	1.0244	1.0262	1.0268	1.0299	1.0301	1.0247	1.0232	1.0217	1.0201	1.0186
	333.15	0.5688	0.5603	0.5600	0.5599	0.5593	0.5592	0.5404	0.5388	0.5372	0.5356	0.5341

(b)

Figure 2.3 The value table in order to obtain (a) the internal resistance and (b) Entropic Heat Coefficient .

Following the procedure explained up to now and using the values that have been shown in terms of heat entropic coefficient and internal resistance values, it has been

defined the heat generation model subroutine in *Dymola/TIL* simulation tool. The subroutine is shown below:

```
model HeatGenerationModel

  Modelica.Blocks.Math.Product IrreversibleHeat
    annotation (Placement(transformation(extent={{34,-38},{54,-18}},
                                         rotation=0)));
  Modelica.Blocks.Math.Product I2 annotation (Placement(transformation(extent={{-80,-60},
          {-60,-40}},          rotation=0)));
  Modelica.Blocks.Math.Product TdUdT annotation (Placement(transformation(
        extent={{-4,44},{16,64}},rotation=0)));
  Modelica.Blocks.Math.Product ReversibleHeat annotation (Placement(
      transformation(extent={{34,18},{54,38}}, rotation=0)));
  Modelica.Blocks.Math.Add CellHeatGeneration annotation (Placement(
      transformation(extent={{70,-8},{92,14}}, rotation=0)));
  Modelica.Blocks.Math.Gain ncells_BM(k=12) annotation (Placement(
      transformation(extent={{100,-4},{114,10}}, rotation=0)));
  Modelica.Blocks.Tables.CombiTable2D Rin_Interpolation(
    tableOnFile=true,
    tableName="InterRin",
    fileName=
      "D:/LEIREMARTIN/Tesis Leire/CaracterizacionTermica/Modulo L6B/Calorimetria/InterRin.
mat")
    annotation (Placement(transformation(extent={{-38,-24},{-18,-4}})));
  Modelica.Blocks.Tables.CombiTable1D dUdT_Interpolation(
    tableOnFile=true,
    tableName="InterdUdT",
    fileName="D:/LEIREMARTIN/Tesis Leire/CaracterizacionTermica/Modulo L6B/Calorimetria/In
terdUdT.mat")
    annotation (Placement(transformation(extent={{-38,24},{-18,44}})));
  Modelica.Blocks.Interfaces.RealInput SOC "Current SOC value"
    annotation (Placement(transformation(extent={{-132,-8},{-92,32}}),
      iconTransformation(extent={{-180,46},{-140,86}})));
  Modelica.Blocks.Interfaces.RealInput I "Current"
    annotation (Placement(transformation(extent={{-134,-102},{-94,-62}}),
      iconTransformation(extent={{-180,-86},{-140,-46}})));
  Modelica.Blocks.Interfaces.RealInput Tcell "Cell internal temperature"
    annotation (Placement(transformation(extent={{-132,28},{-92,68}}),
      iconTransformation(extent={{-180,12},{-140,52}})));
  Modelica.Blocks.Interfaces.RealOutput HeatGenerationRate_BM
    "Heat generation rate" annotation (Placement(transformation(extent={{128,-6},
        {146,12}}), iconTransformation(extent={{100,-18},{140,22}})));
equation
  connect(I2.y,IrreversibleHeat. u2) annotation (Line(points={{-59,-50},{-10,-50},
      {-10,-34},{32,-34}},     color={0,0,127}));
  connect(HeatGenerationRate_BM, ncells_BM.y) annotation (Line(
      points={{137,3},{114.7,3}},
      color={0,0,127},
      smooth=Smooth.None));
  connect(CellHeatGeneration.y, ncells_BM.u) annotation (Line(
      points={{93.1,3},{98.6,3}},
      color={0,0,127},
      smooth=Smooth.None));
  connect(SOC,Rin_Interpolation. u2)
                        annotation (Line(
```

```
    points={{-112,12},{-60,12},{-60,-20},{-40,-20}},
    color={0,0,127},
    smooth=Smooth.None));
  connect(SOC,dUdT_Interpolation. u[1]) annotation (Line(
    points={{-112,12},{-60,12},{-60,34},{-40,34}},
    color={0,0,127},
    smooth=Smooth.None));
  connect(I,I2. u1) annotation (Line(
    points={{-114,-82},{-90,-82},{-90,-44},{-82,-44}},
    color={0,0,127},
    smooth=Smooth.None));
  connect(I,I2. u2) annotation (Line(
    points={{-114,-82},{-90,-82},{-90,-56},{-82,-56}},
    color={0,0,127},
    smooth=Smooth.None));
  connect(Tcell, TdUdT.u1) annotation (Line(
    points={{-112,48},{-82,48},{-82,60},{-6,60}},
    color={0,0,127},
    smooth=Smooth.None));
  connect(Tcell, Rin_Interpolation.u1) annotation (Line(
    points={{-112,48},{-82,48},{-82,-8},{-40,-8}},
    color={0,0,127},
    smooth=Smooth.None));
  connect(dUdT_Interpolation.y[1], TdUdT.u2) annotation (Line(
    points={{-17,34},{-12,34},{-12,48},{-6,48}},
    color={0,0,127},
    smooth=Smooth.None));
  connect(Rin_Interpolation.y, IrreversibleHeat.u1) annotation (Line(
    points={{-17,-14},{-10,-14},{-10,-22},{32,-22}},
    color={0,0,127},
    smooth=Smooth.None));
  connect(I, ReversibleHeat.u2) annotation (Line(
    points={{-114,-82},{22,-82},{22,22},{32,22}},
    color={0,0,127},
    smooth=Smooth.None));
  connect(TdUdT.y, ReversibleHeat.u1) annotation (Line(
    points={{17,54},{22,54},{22,34},{32,34}},
    color={0,0,127},
    smooth=Smooth.None));
  connect(IrreversibleHeat.y, CellHeatGeneration.u2) annotation (Line(
    points={{55,-28},{62,-28},{62,-3.6},{67.8,-3.6}},
    color={0,0,127},
    smooth=Smooth.None));
  connect(ReversibleHeat.y, CellHeatGeneration.u1) annotation (Line(
    points={{55,28},{62,28},{62,9.6},{67.8,9.6}},
    color={0,0,127},
    smooth=Smooth.None));
  annotation (
    uses(Modelica(version="3.2.1")),
    Diagram(coordinateSystem(extent={{-120,-100},{160,80}}, preserveAspectRatio=
        false), graphics),
    Icon(coordinateSystem(extent={{-120,-100},{160,80}})));
end HeatGenerationModel;
```

Appendix 3

Cycler Programs of Experimental Tests

In this third appendix, the cycler programs that they have been used in order to carry out the experimental tests in laboratory environment with the constructed prototypes are shown.

In these cycler programs, the operation conditions in terms of electrical requirements are defined for each experimental test. They have been used in the fourth step of the proposed methodology, in order to validate the detailed thermal models by means of experimental data.

Following, the defined programms for each application can be seen.

3.A CASE STUDY I: VERTICAL ELEVATION APPLICATION

Test 1/ Test 2

BTS - 600 Test program: Lift_T8

Date/Time : 08/05/2015 12:15:24
Operator : Ikerlan

Version : V 1.600.395

Program : Lift_T8

Title : Test8

Step	Label	Procedure	Nominal Value	Limit	Action	Registration
/	*Introducir valores límite y condiciones de ensayo*					
1		SET	Vmin_cell = 2.4	log < 2.2	ERR 2	BPack
			Vmax_cell = 3.57	log > 3.6	ERR 2	1 sec
			Current = 2.5			
			CCCV = 0.125			
			Vcv_mod = 41.4			
			Vmax_mod = 43.2	> 43.2 V	ERR 2	
			Vmin_mod = 24.0	< 23.5 V	ERR 2	
2		PAU		5 min		
3		CHA	Current A	<= CCCV A		
			Vcv_mod V	log > Vmax_cell		
4		PAU		5 min		
5		DCH	Current A	0.4532 Ah		
				log <= Vmin_cell		
6		PAU		20 min		
7		SET	Timer1 = 240 min			
/	*Ciclos DCH/CH*					
8		BEG				
9		DCH	15.862 A	1.3596 Ah		
				log < 2.4		
10		CHA	6.798 A	1.3596 Ah		
				log >= 3.57		
11		PAU		20 ms		
				Timer1	GOTO END	
12		CYC	6*			
/	*Fin del ensayo*					
13	END	STO				

Test 3/ Test 4

BTS - 600 Test program: Lift_T2

Date/Time : 08/05/2015 12:14:39
Operator : Ikerlan

Version : V 1.600.395

Program : Lift_T2

Title : Test2

Step	Label	Procedure	Nominal Value	Limit	Action	Registration
!	*Introducir valores límite y condiciones de ensayo*					
1		SET	Vmin_cell = 2.4 Vmax_cell = 3.57 Current = 2.5 CCCV = 0.125 Vcv_mod = 41.4 Vmax_mod = 43.2 Vmin_mod = 24.0	log < 2.2 log > 3.6 > 43.2 V < 23.5 V	ERR 2 ERR 2 ERR 2 ERR 2	BPack 1 sec
2		PAU		5 min		
3		CHA	Current A Vcv_mod V	<= CCCV A log > Vmax_cell		
4		PAU		5 min		
5		DCH	Current A	0.9064 Ah log <= Vmin_cell		
6		PAU		20 min		
7		SET	Timer1 = 240 min			
!	*Ciclos DCH/CH*					
8		BEG				
9		DCH	6.798 A	0.4532 Ah log < 2.4		
10		CHA	2.266 A	0.4532 Ah log >= 3.57		
11		PAU		20 ms Timer1	 GOTO END	
12		CYC	5*			
!	*Fin del ensayo*					
13	END	STO				

Test 5

BTS - 600 Test program: Lift_T9

Date/Time : 08/05/2015 12:14:06
Operator : Ikerlan

Version : V 1.600.395

Program : Lift_T9

Title : Test9

Step	Label	Procedure	Nominal Value	Limit	Action	Registration
!	*Introducir valores límite y condiciones de ensayo*					
1		SET	Vmin_cell = 2.4	log < 2.2	ERR 2	BPack
			Vmax_cell = 3.57	log > 3.6	ERR 2	1 sec
			Current = 2.5			
			CCCV = 0.125			
			Vcv_mod = 41.4			
			Vmax_mod = 43.2	> 43.2 V	ERR 2	
			Vmin_mod = 24.0	< 23.5 V	ERR 2	
2		PAU		5 min		
3		CHA	Current A	<= CCCV A		
			Vcv_mod V	log > Vmax_cell		
4		PAU		5 min		
5		DCH	Current A	0.6798 Ah		
				log <= Vmin_cell		
6		PAU		20 min		
7		SET	Timer1 = 240 min			
!	*Ciclos DCH/CH*					
8		BEG				
9		DCH	11.33 A	0.9064 Ah		
				log < 2.4		
10		CHA	4.532 A	0.9064 Ah		
				log >= 3.57		
11		PAU		20 ms		
				Timer1	GOTO END	
12		CYC	6*			
!	*Fin del ensayo*					
13	END	STO				

3.B CASE STUDY II: URBAN ELECTRIC MINIBUS

Test 1 (FC)/ Test 4 (*AC*)

BTS - 600 Test program: Raal_T2

Date/Time : 26/04/2017 18:47:32
Operator : Ikerlan

Version : V 1.600.395

Program : Raal_T2

Title : Raal DOD20%60-40

Step	Label	Procedure	Nominal Value	Limit	Action	Registration
!	*Introducir valores limite y condiciones de ensayo*					
1		SET	Vmin_cell = 3.0	log < 2.98	ERR 2	BPack
			Vmax_cell = 4.15	log > 4.17	ERR 2	1 sec
			Current = 40.0	TypK > 55.0	ERR 3	
			CCCV = 2.0			
			Vmax_mod = 49.8	> 49.9 V	ERR 2	
			Vmin_mod = 37.2	< 37.1 V	ERR 2	
2		PAU		5 min		
3		DCH	Current A	3.0541 Ah		
				log <= Vmin_cell		
4		PAU		60 min		
5		SET	Timer1 = 480 min			
!	*Ciclos DCH/CH*					
6		BEG				
7		DCH	Current A	6.1082 Ah		
				log < 2.98		
8		CHA	Current A	6.1082 Ah		
				log >= 4.17		
9		PAU		20 ms		
				Timer1	GOTO END	
!	*Entry of nominal value 10* changed in step 10. New: 8 (Ikerlan)*					
10		CYC	10*			
!	*Fin del ensayo*					
11	END	STO				

Test 2 (FC)/ Test 5 (*AC*)

BTS - 600 Test program: Raal_T1

Date/Time : 26/04/2017 18:56:44
Operator : Ikerlan

Version : V 1.600.395

Program : Raal_T1

Title : Raal DOD30%6535

Step	Label	Procedure	Nominal Value	Limit	Action	Registration
!	*Introducir valores límite y condiciones de ensayo*					
1		SET	Vmin_cell = 3.0	log < 2.98	ERR 2	BPack
			Vmax_cell = 4.15	log > 4.17	ERR 2	1 sec
			Current = 40.0	TypK > 55.0	ERR 3	
			CCCV = 2.0			
			Vmax_mod = 49.8	> 49.9 V	ERR 2	
			Vmin_mod = 37.2	< 37.1 V	ERR 2	
2		PAU		5 min		
3		DCH	Current A	10.9347 Ah		
				log < 2.98		
4		PAU		30 min		
5		SET	Timer1 = 480 min			
!	*Ciclos DCH/CH*					
6		BEG				
7		DCH	Current A	9.3726 Ah		
				log < 2.98		
8		CHA	Current A	9.3726 Ah		
				log >= 4.17		
9		PAU		20 ms		
				Timer1	GOTO END	
!	*Entry of nominal value 10* changed in step 10. New: 7 (Ikerlan)*					
10		CYC	10*			
!	*Fin del ensayo*					
11	END	STO				

Test 3 (FC)/ Test 6 (*AC*)

BTS - 600 Test program: Raal_T1

Date/Time : 26/04/2017 18:46:05
Operator : Ikerlan

Version : V 1.600.395

Program : Raal_T1

Title : Raal DOD40%7030

Step	Label	Procedure	Nominal Value	Limit	Action	Registration
!	*Introducir valores límite y condiciones de ensayo*					
1		SET	Vmin_cell = 3.0	log < 2.98	ERR 2	BPack
			Vmax_cell = 4.15	log > 4.17	ERR 2	1 sec
			Current = 40.0	TypK > 55.0	ERR 3	
			CCCV = 2.0			
			Vmax_mod = 49.8	> 49.9 V	ERR 2	
			Vmin_mod = 37.2	< 37.1 V	ERR 2	
2		PAU		5 min		
3		SET	Timer1 = 480 min			
!	*Ciclos DCH/CH*					
4		BEG				
5		DCH	Current A	12.8892 Ah		
				log < 2.98		
6		CHA	Current A	12.8892 Ah		
				log >= 4.17		
7		PAU		20 ms		
				Timer1	GOTO END	
!	*Entry of nominal value 10* changed in step 8. New: 7 (Ikerlan)*					
8		CYC	10*			
!	*Fin del ensayo*					
9	END	STO				

References

1. *CAF, http://www.caf.net/.*

2. *Orona, http://www.orona-group.com/.*

3. *Quipplan, http://www.quipplan-mobility.com/.*

4. *Vectia, http://www.vectia.es/.*

5. *Ormazabal, http://www.ormazabal.com/es.*

6. *Iberdrola, https://www.iberdrola.es/.*

7. *Kim, M.H. and C.W. Bullard, Air-side thermal hydraulic performance of multi-louvered fin aluminum heat exchangers. International Journal of Refrigeration, 2002.* ***25****(3): p. 390-400.*

8. *Council Conclusions of 23/24 October 2014, www.consilium.europa.eu/uedocs/cms_data/docs/pressdata/en/ec/145397.pdf.*

9. *Roadmap to a Single European Transport Area – Towards a competitive and resource efficient transport system, 28March 2011, http://eur-lex.europa.eu/legal-content/EN/TXT/PDF/?uri=CELEX:52011DC0144&from=EN.*

10. *European-Comission: https://ec.europa.eu/transport/themes/research/horizon2020_en.*

11. Comission, E., *Horizon 2020. Work Programme 2016-2017 (11. Smart, green and integrated transport)*. July 2016, (European Commission Decision C(2016)4614 of 25 July 2016).

12. Eurelectric, E.f.E., *Electro-Mobility: A clear solution for sustainable transport and energy*. September 2015.

13. *SICC-E* Sistema de Inteligencia Competitiva del Cluster de Energía., *https://elperiodicodelaenergia.com/el-ayuntamiento-de-madrid-activara-la-restriccion-de-aparcar-en-la-zona-ser-a-no-residentes-por-alta-contaminacion/ (10/03/2017).*

14. *Estas son las 30 medidas del Plan A contra la contaminación del Ayuntamiento de Madrid*, in *El Confidential*. 2017: http://www.elconfidencial.com/espana/madrid/2017-03-13/carmena-contaminacion-30medidas_1347163/.

15. *SICC-E* Sistema de Inteligencia Competitiva del Cluster de Energía, *Gamesa logra su primer contrato para suministrar aerogeneradores en Tailandia https://elperiodicodelaenergia.com/gamesa-logra-su-primer-contrato-para-suministrar-aerogeneradores-en-tailandia/*. 2017.

16. Eurelectric, Electricity for Europe., *Smart charging: steering the charge, driving the change.* 2015.

17. European Comission., *Alternative fuels for sustainable mobility in Europe http://ec.europa.eu/transport/themes/urban/cpt_en*. 2017.

18. *European Comission: http://ec.europa.eu/transport/themes/urban/cpt_en.*

19. European Parliament, *Challenges for European Market for Electric Vehicles-Industry, Research and Energy.* 2010.

20. UBS, *Will solar, batteries and electric cars re-shape the electricity system?* August 2014.

21. Minority Report, vehicle.-to.-grid., http://360photography.in/?tag=creepy.

22. Georg Fuchs, et al., *Technology Overview on Electricity Storage*, in *Overview on the potential and on the deployment perspective of electricity storage technologies*. 2012, ISEA RWTH AACHEN.

23. *IEC International Electrotechnical Commision*. Electrical Energy Storage.

24. *Batteries 2020, http://www.batteries2020.eu/*.

25. Shriram Santhanagopalan, et al., *Design and Analysis of Large Lithium-Ion Battery Systems*.

26. Celina Mikolajczak, et al., *Lithium-Ion Batteries Hazard and Use Assessment*. 2011.

27. Battery University., http://batteryuniversity.com.

28. Languang Lu, et al., *A review on the key issues for lithium- ion battery management in electric vehicles.* Journal of Power Sources, 2013. **226**: p. 272-288.

29. Electropaedia., http://www.mpoweruk.com/lithium_failures.htm.

30. Sarasketa-Zabala, E., et al., *Calendar ageing analysis of a LiFePO4/graphite cell with dynamic model validations: Towards realistic lifetime predictions.* Journal of Power Sources, 2014. **272**: p. 45-57.

31. Sarasketa-Zabala, E., et al., *Cycle ageing analysis of a LiFePO4/graphite cell with dynamic model validations: Towards realistic lifetime predictions.* Journal of Power Sources, 2015. **275**: p. 573-587.

32. Pesaran, A.A., *Battery thermal models for hybrid vehicle simulations.* Journal of Power Sources, 2002. **110**(2): p. 377-382.

33. Xinhiao Xing, et al., *Battery Management Systems in Electric and Hybrid Vehicles.* Energies, 2011. **4**: p. 1840-1857.

34. *SLPB (Superior Lithium Polymer Battery) Technical Specification*. 2009: Kokam Co. Ltd, Research & Development Department.

35. Waldmann, T., et al., *Temperature dependent ageing mechanisms in Lithium-ion batteries – A Post-Mortem study.* Journal of Power Sources, 2014. **262**: p. 129-135.

36. Mahamud, R. and C. Park, *Reciprocating air flow for Li-ion battery thermal management to improve temperature uniformity.* Journal of Power Sources, 2011. **196**(13): p. 5685-5696.

37. Ahmad Pesaran, et al. *Tools for Designing Thermal Management of Batteries in Electric Drive Vehicles*. in *Large Lithium Ion Battery Technology & Application Symposia Advanced Automotive Battery Conference*. 2013. Pasadena, CA.

38. C.-W. Park, A.K.J., *Dynamic Thermal Model of Li-ion Battery for Predictive Behavior in Hybrid and Fuel Cell Vehicles.* SAE 2003-01-2286, 2003.

39. *Quallion LLC, https://www.ntsb.gov/news/events/Documents/2013_Lithium_Batteries_FRM-Panel1f-Visco.pdf.*

40. Guezennec, Y., *Thermal Analysis of Lithium-Ion Battery Packs and Thermal Management Solutions*, in *Graduate Program in Mechanical Engineering*. 2013, The Ohio State University.

41. Pesaran, A.A. *Battery Thermal Management in EVs and HEVs: Issues and Solutions*. in *Advanced Automotive Battery Conference*. 2001. Las Vegas, Nevada.

42. Jin, X., et al., *Researches on Modeling and Experiment of Li-ion Battery PTC Self-heating in Electric Vehicles.* Energy Procedia, 2016. **104**: p. 62-67.

43. *Hybrid and Electric Car Technology, http://www.twinkletoesengineering.info/hybrid_car.htm.*

44. Q. Wang, B.J., Q.F. Xue, H.L. Sun, B. Li, H.M. Zou a, Y.Y. Yan, Applied Thermal Engineering, 2014. **7**: p. 1-7.

45. Swanepoel, G., *Thermal management of Hybrid Electrical Vehicles Using Heat Pipes.* University of Stellenbosch, 2001.

46. Burban, G., et al., *Experimental investigation of a pulsating heat pipe for hybrid vehicle applications.* Applied Thermal Engineering, 2013. **50**(1): p. 94-103.

47. Rao, Z., et al., *Experimental investigation on thermal management of electric vehicle battery with heat pipe.* Energy Conversion and Management, 2013. **65**: p. 92-97.

48. Tran, T.-H., et al., *Experimental investigation on the feasibility of heat pipe cooling for HEV/EV lithium-ion battery.* Applied Thermal Engineering, 2014. **63**: p. 551- 558.

49. Al-Hallaj, S. and J.R. Selman, *A Novel Thermal Management System for Electric Vehicle Batteries Using Phase-Change Material* J. Electrochem. Soc, 2000. **174**(9): p. 3231-3236.

50. Al-Hallaj, S. and J.R. Selman, *Thermal modeling of secondary lithium batteries for electric vehicle/hybrid electric vehicle applications.* Journal of Power Sources, 2002. **110**(2): p. 341-348.

51. Khateeb, S.A., et al., *Thermal management of Li-ion battery with phase change material for electric scooters: experimental validation.* Journal of Power Sources, 2005. **142**(1–2): p. 345-353.

52. Javani, N., et al., *Modeling of passive thermal management for electric vehicle battery packs with PCM between cells.* Applied Thermal Engineering, 2014. **73**(1): p. 307-316.

53. Spal Autootive., http://www.spalautomotive.com.

54. *HEV Battery Testing Results 2013 Honda Civic Hybrid* 2013.

55. Zolot, M., A.A. Pesaran, and M. Mihalic, *Thermal Evaluation of Toyota Prius Battery Pack*, in *Future Car Congress*, N.R.E. Laboratory, Editor. 2002.

56. *GAS 2, The green is the new fast http://gas2.org/2016/01/22/ev-owners-expect-battery-upgrades/.*

57. *Green Hybrid, http://www.greenhybrid.com.*

58. *EVbus, http://evbud.com/news/143/.*

59. *Enggcyclopedia, http://www.enggcyclopedia.com/2012/01/typical-vapor-compression-refrigeration-cycle-vcr/.*

60. *ASHRAE Handbook: HVAC Systems and Equipment*. 2012.

61. D. R. Weber and R. M. Brisbane, *COOLING PLATE FOR LITHIUM-ION BATTERY PACK*. 2011.

62. Leonid C. Lev and N. Kondratyev, *COOLING SYSTEM FOR AUTOMOTIVE BATTERY*. 2013.

63. *Car and Driver, http://blog.caranddriver.com/2016-chevrolet-volt-drivetrain-details-quicker-new-engine-increased-range-and-battery-capacity/.*

64. *GM Volt, http://gm-volt.com/2013/05/03/volt-battery-thermal-management-system-in-the-hot-arizona-sun/.*

65. Peter Thomas Tennessen, J.C.W., Weston Arthur Hermann, *Extruded and Ribbed Thermal Interface for use with a Battery Cooling System* I. Tesla Motor, Editor. 2011.

66. Hybrid Drive, propuslsion systems (http://www.hybridrive.com).

67. HTTP://WWW.V-MODELL-XT.DE., *Part 1: Fundamental of the V-Modell*. 2004, BUNDESREPUBLIK DEUTSCHLAND.

68. Nieto, N., *A Model based Design of a Thermal Management System for a High Power Lithium-ion Battery Pack.* 2014, Tecnun, Universidad de Navarra.

69. Nieto, N., et al., *Thermal Modeling of Large Format Lithium-Ion Cells Batteries and Energy Storage* Journal of Electrochemical Society, 2013. **160**(2): p. A212-A217.

70. Nieto, N., et al., *Novel thermal management system design methodology for power lithium-ion battery.* Journal of Power Sources, 2014. **272**: p. 291-302.

71. Martín-Martín, L., et al., *Modeling based on design of thermal management systems for vertical elevation applications powered by lithium-ion batteries.* Applied Thermal Engineering, 2016. **102**: p. 1081-1094.

72. *Open FOAM, http://www.openfoam.com/.*

73. *Ansys Fluent, http://www.ansys.com/Products/Fluids/ANSYS-Fluent.*

74. *STAR CCM+, http://mdx.plm.automation.siemens.com/star-ccm-plus.*

75. Wang, T., K.J. Tseng, and J. Zhao, *Development of efficient air-cooling strategies for lithium-ion battery module based on empirical heat source model.* Applied Thermal Engineering, 2015. **90**: p. 521-529.

76. Jeon, D.H., *Numerical modeling of lithium ion battery for predicting thermal behavior in a cylindrical cell.* Current Applied Physics, 2014. **14**(2): p. 196-205.

77. Fan, L., J.M. Khodadadi, and A.A. Pesaran, *A parametric study on thermal management of an air-cooled lithium-ion battery module for plug-in hybrid electric vehicles.* Journal of Power Sources, 2013. **238**: p. 301-312.

78. Saw, L.H., et al., *Computational fluid dynamic and thermal analysis of Lithium-ion battery pack with air cooling.* Applied Energy, 2016. **177**: p. 783-792.

79. Yang, N., et al., *Assessment of the forced air-cooling performance for cylindrical lithium-ion battery packs: A comparative analysis between aligned and staggered cell arrangements.* Applied Thermal Engineering, 2015. **80**: p. 55-65.

80. Wang, T., et al., *Thermal investigation of lithium-ion battery module with different cell arrangement structures and forced air-cooling strategies.* Applied Energy, 2014. **134**: p. 229-238.

81. Jarrett, A. and I.Y. Kim, *Design optimization of electric vehicle battery cooling plates for thermal performance.* Journal of Power Sources, 2011. **196**(23): p. 10359-10368.

82. Huo, Y., et al., *Investigation of power battery thermal management by using mini-channel cold plate.* Energy Conversion and Management, 2015. **89**: p. 387-395.

83. *CoolSim, http://www.coolsimsoftware.com/*.

84. *CARNOT Matlab Toolbox, https://es.mathworks.com/matlabcentral/linkexchange/links/4321-carnot-toolbox-version-6-0-for-r2013b*.

85. *Thermolib Matlab Toolbox, https://es.mathworks.com/matlabcentral/linkexchange/links/4321-carnot-toolbox-version-6-0-for-r2013b*.

86. *TIL Suite, https://www.tlk-thermo.com/index.php/en/software-products/overview/38-til-suite*.

87. *KULI, http://kuli.magna.com/*.

88. *MapleSim, http://www.maplesoft.com/products/maplesim/index1a.aspx*.

89. Tummescheit, H., *Design and Implementation of Object-Oriented Model Libraries using Modelica*, in *Department of Automatic Control*. 2002, Lund Institute of Technology.

90. Lemke, N.C., *Untersuchung zweistufiger Flüssigkeitskühler mit dem Kältemittel CO2*, in *Forschungsberichte des Deutschen Kälte- und Klimatechnischen Vereins*. 2005: DKV, Stuttgart.

91. Ritcher, C.C., *Proposal of New Object-Oriented Equation-Based Model Libraries for Thermodynamic Systems*. 2008, TU Braunschweig.

92. Kiss, T., L. Chaney, and J. Meyer. *A New Automotive Air Conditioning System Simulation Tool Developed in MATLAB/Simulink*. in *SAE 2013 World Congress and Exhibition*. 2013.

93. Kiss, T., J. Lustbader, and D. Leighton. *Modeling of an Electric Vehicle Thermal Management System in MATLAB/Simulink*. in *SAE 2015 World Congress & Exhibition*. 2015. Detroit, Michigan.

94. Bouvy, C., et al. *Holistic Vehicle Simulation using Modelica – An Application on Thermal Management and Operation Strategy for Electrified Vehicles*. in *9th International Modelica Conference*. 2012. Munich, Germany.

95. Batteh, J., J. Gohl, and S. Chandrasekar. *Integrated Vehicle Thermal Management in Modelica: Overview and Applications*. in *10th International ModelicaConference*. 2014. Lund, Sweden.

96. Varchmin, A., M. Gräber, and J. Köhler. *Modeling and Validation of a Multiple Evaporator Refrigeration Cycle for Electric Vehicles*. in *11th International Modelica Conference*. 2015. Versalles, France.

97. TFischer et al. *Model-based Development of a Holistic Thermal Management System for an Electric Car with a High Temperature Fuel Cell Range Extender*. in *11th International Modelica Conference*. 2015. Versalles, France.

98. Thermo-Concept., http://www.thermoconcept-sarl.com/index.php/en/.

99. F. P. Incropera and D. P. DeWitt, *Fundamentals of Heat and Mass Transfer*, ed. t. Edition. 2006.

100. E. del Castillo, *Process Optimization, A statistical Approach*, ed. Springer. 2007.

101. Box, G.E.P. and Wilson. K. B., *On the Experimental Attainment of Optimum Conditions.* Journal of the Royal Statistical Society, 1951. **13**: p. 1-45.

102. *Minitab 17.0 Support, http://support.minitab.com/en-us/minitab/17/.*

103. Drake, S.J., et al., *Measurement of anisotropic thermophysical properties of cylindrical Li-ion cells.* Journal of Power Sources, 2014. **252**: p. 298-304.

104. Jeon, D.H. and S.M. Baek, *Thermal modeling of cylindrical lithium ion battery during discharge cycle.* Energy Conversion and Management, 2011. **52**(8–9): p. 2973-2981.

105. B.R. Hutchinson, G.D.R., *A multigrid method based on the additive correction strategy.* Numerical Heat Transfer, 1986. **9**: p. 511-537.

106. Patankar, S.V., *Numerical Heat Transfer and Fluid Flow*. Vol. 126-131. 1980: Hemisphere Publishing Corporation.

107. S.R. Mathur, J.Y.M., *A pressure-based method for unstructured meshes. Part B: Fundamentals.* Numerical Heat Transfer, 1997. **31**(2): p. 195-215.

108. J.H. Ferziger, M.P., *Computational Methods for Fluid Dynamics, third ed.* Vol. 154-217. 2002, Germany.

109. *Fluent Inc. F., 6.3 User's Guide*. 2006, Cavendish Court, Lebanon, NH 03766.

110. Bobbo, S., et al., *R1234yf as a substitute of R134a in automotive air conditioning. Solubility measurements in two commercial PAG oils.* International Journal of Refrigeration, 2014. **40**: p. 302-308.

111. Spatz, M. and B. Minor. *HFO-1234yf: A low GWP refrigerant for MAC*. in *VDA Alternative refrigerant. Winter Meeting. Saalfelden, Australia.* 2008.

112. *AMS Technologies, http://www.amstechnologies.com/es/home/*.

113. *EMP Powering the Future, http://www.emp-corp.com/*.

114. *RAAL complete cooling solutions, http://www.raal.ro/*.

115. *Masterflux, http://www.masterflux.com/*.

116. P.E. Bagnoli, C.C., M. Ciampi, E. Dallago, *Thermal Resistance Analysis by Induced Transient (TRAIT) Method for Power Electronic Devices Thermal Characterization- Part I: Fundamentals and Theory*. IEEE Transaction on Power Electronics, 1988. **13**(6).

117. P.E. Bagnoli, C.C., M. Ciampi, E. Dallago, *Thermal Resistance Analysis by Induced Transient (TRAIT) Method for Power Electronic Devices Thermal Characterization- Part II: Practice and Experiments.* IEEE Transaction on Power Electronics, 1988. **13**(6).

118. Kossel, R., *Objektorientierte Modellierung von W□arme□ubertragern in Modelica*. 2006, Studienarbeit, TU Braunschweig.

119. Ahlbrink, N., *Optimierung eines objektorientierten W□arme□ubertragers in Modelica*. 2007: Studienarbeit, TU Braunschweig.

120. Richter, C.C., *Proposal of New Object-Oriented Equation-Based Model Libraries for Thermodynamic Systems*. 2008, TU Braunschweig.

121. Mortada, S., et al., *Dynamic modeling of an integrated air-to-air heat pump using Modelica.* International Journal of Refrigeration, 2012. **35**(5): p. 1335-1348.

122. M. Gräber, et al., *Modeling of Heat Pumps with an Object- Oriented Model Library for Thermodyamic Systems*, in *MATHMOD 09*. 2009: Vienna.

123. V., G., *New equations for heat and mass transfer in turbulent pipe and channel flow.* International Chemical Engineering, 1976. **16**(2): p. 359-368.

124. Shah, M.M., *A general correlation for heat transfer during film condensation inside pipes.* International Journal of Heat and Mass Transfer, 1979. **22**(4): p. 547-556.

125. Steiner, D. and J. Taborek, *Flow Boiling Heat Transfer in Vertical tubes Correlated by an Asymtotic Model.* Heat Transfer Engineering 1992. **13**: p. 43-68.

126. Wang, C.C., et al., *Heat transfer and friction correlation for compact louvered fin-and-tube heat exchangers.* International Journal of Heat and Mass Transfer, 1998. **42**(11): p. 1945-1956.

127. Kim, M.-H. and C.W. Bullard, *Air-side thermal hydraulic performance of multi-louvered fin aluminum heat exchangers.* International Journal of Refrigeration, 2002. **25**(3): p. 390-400.

128. *VDI Heat Atlas, ed. e.S VDI_Buch*, ed. V. Gesellschaft. Düsseldorf, Germany.

129. Lee, J. and K.-S. Lee, *Flow characteristics and thermal performance in chevron type plate heat exchangers.* International Journal of Heat and Mass Transfer, 2014. **78**: p. 699-706.